

THE JOURNAL OF PHYSICAL CHEMISTRY

Volume 73, Number 2 February 1969

The Mechanism for Exchange between Aqueous Solutions and Deuterium Gas on Palladium Surfaces G. L. Holleck and Ted B. Flanagan	285
Proton Chemical Shifts and the Reactivity of Polynuclear Aromatic Hydrocarbons K. D. Bartle and D. W. Jones	293
Moving Boundary Measurement of Transference Numbers Paul Milios and John Newman	298
Sorption of Water Vapor and of Nitrogen by Genetic Variants of α_{s1} -Casein E. Berlin, B. A. Anderson, and M. J. Pallansch	303
Effect of Fast Internal Rotation on the Nitrogen-14 Nuclear Magnetic Resonance Relaxation Times of the Methylbenzyl Cyanides Daniel Wallach	307
Salting Out of Nonpolar Gases in Aqueous Potassium Hydroxide Solutions S. K. Shoor, R. D. Walker, Jr., and K. E. Gubbins	312
The Rate of Reaction of Methyl Iodide and Hydrazine in Aqueous Solution R. A. Hasty	317
Reactive Silica. I. The Formation of a Reactive Silica by the Thermal Collapse of the Methoxy Groups of Methylated Aerosil Claudio Morterra and M. J. D. Low	321
Reactive Silica. II. The Nature of the Surface Silicon Hydrides Produced by the Chemisorption of Hydrogen Claudio Morterra and M. J. D. Low	327
Thermophysical Properties of the Lanthanide Oxides. IV. Heat Capacities and Thermodynamic Properties of Thulium(III) and Lutetium(III) Oxides. Electronic Energy Levels of Several Lanthanide(III) Ions Bruce H. Justice, Edgar F. Westrum, Jr., Elfreda Chang, and Ray Radebaugh	333
Temperature-Dependent Electron Spin Resonance Studies. II. Cyclooctatetraene Anion Radical F. J. Smentowski and Gerald R. Stevenson	340
Heats of Mixing Aqueous Electrolytes. VI. Magnesium Chloride with Some Alkali Metal Chlorides R. H. Wood, J. D. Patton, and M. Ghamkhar	346
Thermodynamic Properties of Plutonium Nitride by Galvanostatic Potential Determination G. M. Campbell	350
Radiolysis of Solutions of Perfluorocarbons in <i>n</i> -Hexane L. A. Rajbenbach	356
Secondary Valence Force Catalysis. VIII. Catalysis of Hydrolysis of Methyl Orthobenzoate by Anionic Surfactants R. Bruce Dunlap and E. H. Cordes	361
Electronic Excitation Transfer from Pyrene to Perylene by a Very Weak Interaction Mechanism N. Mataga, H. Obashi, and T. Okada	370
The Vaporization Thermodynamics of Europium Monoxide John M. Haschke and Harry A. Eick	374
Energy Transfer in the Radiolysis of Gaseous Mixtures of Ethylene and Carbon Monoxide S. Russo, S. Munari, and E. Biagini	378
Lifetime of a Highly Soluble Dense Spherical Particle Daniel E. Rosner	382
Variation of the Lattice Parameter with Aluminum Content in Synthetic Sodium Faujasites. Evidence for Ordering of the Framework Ions E. Dempsey, G. H. Köhl, and D. H. Olson	387
Reactions of O(⁴ D) with Hydrocarbons in Liquid Argon W. B. DeMore	391
Production of Perchlorate and Chlorite Ions in Crystalline Potassium Chlorate Irradiated with Cobalt-60 γ Rays L. C. Brown and G. E. Boyd	396
Electrolyte-Solvent Interaction. XX. Picric Acid in Mixtures of Acetonitrile and Basic Solvents Alessandro D'Aprano and Raymond M. Fuoss	400
The Importance of Lone-Pair Electrons in the Intramolecular Potential Function of Group V Hydrides and Trihalides Shih-Tung King and John Overend	406
Pulse-Radiolysis Studies. XIV. Rate Constants for the Reactions of Hydrogen Atoms with Aromatic Compounds in Aqueous Solution P. Neta and Leon M. Dorfman	413

APPLIED KINETICS

and chemical
reaction
engineering

This is the third of a series of state-of-the-art books growing out of summer symposia sponsored jointly by I&EC and the Division of Industrial and Engineering Chemistry.

The 15 papers from the 1966 symposium which were published from September 1966 to June 1967 in *INDUSTRIAL AND ENGINEERING CHEMISTRY* are combined in this book.

Reaction engineering, with its focus on the chemical transformation itself, lays some claim to being the discipline that uniquely differentiates chemical engineering from other branches of engineering. The recently developing interest in reaction analysis has served to reorient chemical engineering research toward the reaction itself and increasingly to consider unit operations from the viewpoint of their interaction with the chemical transformation. This book offers much to the engineering researcher and reactor designer as well as the practicing chemical engineer.

Robert L. Goring and Vern W. Weekman of the Systems Research Division of Mobil Oil Corporation and co-chairmen of the symposium, contributed the introduction. Chapter titles and the authors appear below:

Mixing and Contacting in Chemical Reactors

Kenneth B. Bischoff

Kinetic Considerations in Surface Catalysis

John H. Sinfelt

Photochemical Reaction Engineering

A. E. Cassano, P. L. Silveston, and J. M. Smith

Reaction Mechanisms for Engineering Design

Hugh M. Hulburt and Y. G. Kim

Is Sophistication Really Necessary?

Rutherford Aris

Disguised Kinetics

James Wei

Surface Models in Heterogeneous Catalysis

Giuseppe Parravano

Yield in Chemical Reactor Engineering

James J. Carberry

Acetylene and Hydrogen from the Pyrolysis of Methane

John Happel and Leonard Kramer

Reaction Rate Modeling in Heterogeneous Catalysis

J. R. Kittrell and R. Mezaki

Segregation Effects in Pseudolaminar Flow Reactors

W. M. Edwards and D. I. Saletan

The Theory of Oscillating Reactions

Joseph Higgins

The Concept of Diffusion in Chemical Kinetics

Thor A. Bak and Edward R. Fisher

Stochastic Mixing Models for Chemical Reactors

F. J. Krambeck, R. Shinnar, and S. Katz

Turbulent Heat Transfer to a Nonequilibrium,

Chemically Reacting Gas

P. L. T. Brian and S. W. Bodman



To order, fill out the coupon below

AMERICAN CHEMICAL SOCIETY Dept. M

Special Issues Sales / 1155 Sixteenth Street, N. W. /
Washington, D. C. 20036

Please send _____ copies of **Applied Kinetics and Chemical Reaction**

Engineering at \$7.50 each.

224 pages (9 x 12) with index.

Clothbound.

An I&EC Reprint.

(3rd I&EC Division Summer Symposium)

Check enclosed (to American Chemical Society).

Send bill.

NAME _____

MAILING ADDRESS _____

CITY _____ STATE _____ ZIP CODE _____

SIGNATURE _____

Calculation of the Mean-Square Dipole Moments and Proton Fluctuation Anisotropy of Hemoglobin at Low Ionic Strength	William H. Orttung	418
A Nuclear Magnetic Resonance Study of the Association of Porphyrins in Chloroform Solution. Mesoporphyrin IX Dimethyl Ester and Its Nickel Chelate	Daryl A. Doughty and C. W. Dwiggin, Jr.	423
The Anodic Oxidation of Saturated Hydrocarbons. A Mechanistic Study	J. O'M. Bockris, E. Gileadi, and G. E. Stoner	427
Hindered Rotation in N-Methylthiourea	A. S. Tompa, R. D. Barefoot, and E. Price	435
Further Studies on the Decarboxylation of <i>n</i> -Hexylmalonic Acid in Polar Solvents	Louis Watts Clark	438

NOTES

The Crystal and Molecular Structure of Tris(diethyldithiocarbamato)cobalt(III)	Thomas Brennan and Ivan Bernal	443
A Reinvestigation of the Dielectric Constant of Water and Its Temperature Coefficient	Robert L. Kay, G. A. Vidulich, and Krishnahadi S. Pribadi	445
Photochemical Reactions of Fluorescein Dyes with H ₂ O ₂	Karl J. Youtsey and L. I. Grossweiner	447
Vibrational Spectra of the Hydrogen Dihalide Ions. V. BrHBr ⁻ at 20°K	J. C. Evans and G. Y-S. Lo	448
Two-Bond, Carbon-Proton Coupling in Halogenated Ethylenes	Frank J. Weigert and John D. Roberts	449
The Thermal Conductivity of Aqueous Solutions of Alkali Hydroxides	Zdenek Losenicky	451
A Proton Magnetic Resonance Solute-Solute Correlation. Solvent Interactions with the Sulfhydryl Proton	Sheldon H. Marcus and Sidney I. Miller	453
Nuclear Magnetic Resonance Spectra of Some Indole Salts	John F. Sebastian, Manfred G. Reinecke, and Harry W. Johnson, Jr.	455
The Photolysis of Ammonia at 2062 Å in the Presence of Ethylene	U. Schurath, P. Tiedemann, and R. N. Schindler	456
The Dielectric Properties of Pyridine Complexes with Dichloro- and Trichloroacetic Acids	S. R. Gough and A. H. Price	459

COMMUNICATIONS TO THE EDITOR

Charge Distribution in Some Alkanes and Their Mass Spectra	Vittoria Santoro and Giulio Spadaccini	462
Reply to "Charge Distribution in Some Alkanes and Their Mass Spectra"	J. C. Lorquet	463
Comment on the Paper "Charge Distribution in Some Alkanes and Their Mass Spectra"	Kozo Hirota, Yoshio Niwa, and Masao Yamamoto	464
Recoil Tritium Reactions with Methylsilanes	T. Tominaga, A. Hosaka, and F. S. Rowland	465
"Electrocapillary Curves" of Solid Metals Measured by Extensometer Instrument	T. R. Beck	466
Electron Injection into Zinc Oxide	Thomas Freund	468
Study of the Energetics of Ion-Molecule Reactions by Pulsed Ion Cyclotron Double Resonance	L. R. Anders	469

AUTHOR INDEX

- Anders, L. R., 469
 Anderson, B. A., 303
 Barefoot, R. D., 435
 Bartle, K. D., 293
 Beck, T. R., 466
 Berlin, E., 303
 Bernal, I., 443
 Biagini, E., 378
 Bockris, J. O'M., 427
 Boyd, G. E., 396
 Brennan, T., 443
 Brown, L. C., 396
 Campbell, G. M., 350
 Chang, E., 333
 Clark, L. W., 438
 Cordes, E. H., 361
 D'Aprano, A., 400
 DeMore, W. B., 391
 Dempsey, E., 387
 Dorfman, L. M., 413
 Doughty, D. A., 423
 Dunlap, R. B., 361
 Dwiggins, C. W., Jr., 423
 Eick, H. A., 374
 Evans, J. C., 448
 Flanagan, T. B., 285
 Freund, T., 468
 Fuoss, R. M., 400
 Ghamkhar, M., 346
 Gileadi, E., 427
 Gough, S. R., 459
 Grossweiner, L. I., 447
 Gubbins, K. E., 312
 Haschke, J. M., 374
 Hasty, R. A., 317
 Hirota, K., 464
 Holleck, G. L., 285
 Hosaka, A., 465
 Johnson, H. W. Jr., 455
 Jones, D. W., 293
 Justice, B. H., 333
 Kay, R. L., 445
 King, S.-T., 406
 Kuhl, G. H., 387
 Lo, G. Y.-S., 448
 Lorquet, J. C., 463
 Losenicky, Z., 451
 Low, M. J. D., 321, 327
 Marcus, S. H., 453
 Mataga, N., 370
 Milios, P., 298
 Miller, S. I., 453
 Morterra, C., 321, 327
 Munari, S., 378
 Neta, P., 413
 Newman, J., 298
 Niwa, Y., 464
 Obashi, H., 370
 Okada, T., 370
 Olson, D. H., 387
 Orttung, W. H., 418
 Overend, J., 406
 Pallansch, M. J., 303
 Patton, J. D., 346
 Pribadi, K. S., 445
 Price, A. H., 459
 Price, E., 435
 Radebaugh, R., 333
 Rajbenbach, L. A., 356
 Reinecke, M. G., 455
 Roberts, J. D., 449
 Rosner, D. E., 382
 Rowland, F. S., 465
 Russo, S., 378
 Santoro, V., 462
 Schindler, R. N., 456
 Schurath, U., 456
 Sebastian, J. F., 455
 Shoor, S. K., 312
 Smentowski, F. J., 340
 Spadaccini, G., 462
 Stevenson, G. R., 340
 Stoner, G. E., 427
 Tiedemann, P., 456
 Tominaga, T., 465
 Tompa, A. S., 435
 Vidulich, G. A., 445
 Walker, R. D., Jr., 312
 Wallach, D., 307
 Weigert, F. J., 449
 Westrum, E. F., Jr., 333
 Wood, R. H., 346
 Yamamoto, M., 464
 Youtsey, K. J., 447

THE JOURNAL OF PHYSICAL CHEMISTRY

Registered in U. S. Patent Office © Copyright, 1969, by the American Chemical Society

VOLUME 73, NUMBER 2 FEBRUARY 1969

The Mechanism for Exchange between Aqueous Solutions and Deuterium Gas on Palladium Surfaces

by G. L. Holleck and Ted B. Flanagan

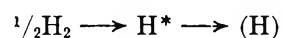
Chemistry Department, University of Vermont, Burlington, Vermont 05401 (Received November 17, 1967)

The isotopic exchange reactions occurring between D chemisorbed on palladium and solutions of H₂O have been investigated. The isotopic content of palladium specimens which had absorbed H and D from D₂-stirred solutions was determined by mass spectral analysis. In addition, the electrochemical exchange current was measured during the run by a galvanostatic pulse technique. It was found by comparing the exchange current calculated from the isotopic content of the specimen with the electrochemical exchange current that in very acid solutions an electrochemical exchange mechanism appears to be the only important mode of exchange, whereas, in other pH ranges, an additional exchange mechanism (catalytic) comes into play.

Introduction

It has been shown by a number of workers that H₂ is spontaneously absorbed by palladium from H₂-stirred aqueous solutions.¹ This has provided the basis of a convenient technique for the determination of the characteristics of absorption of hydrogen and deuterium by palladium and its alloys.² The slow step in the over-all rate of absorption from aqueous solutions is the transport of dissolved H₂ through the Brunner-Nernst layer up to the surface of the specimen.^{2,3} The electrode potentials of the specimens measured during this absorption process show that the chemical potential of the hydrogen atoms at the surface is closely equal to that in the metal layers immediately adjacent to the surface, *i.e.*, the chemisorption-absorption transition is rapid compared with, for example, internal diffusion.⁴ Thus chemisorbed hydrogen atoms, which subsequently become absorbed, do not pile up at the surface. Over an extensive range of hydrogen contents in palladium; *i.e.*, [H]/[Pd] = 0–0.58 (25°), the equilibrium H₂ pressure is small, ≤ 18 torr,⁵ as compared with 1 atm. A pressure of 1 atm of H₂ is most convenient for this technique and has been used in this work. Therefore, under these conditions, desorption can be neglected and

all of the H₂ which is transported up to the surface undergoes the reaction sequence



where H* and (H) represent chemisorbed and absorbed species, respectively. As expected from these considerations, the rate of absorption is constant from [H]/[Pd] = 0 to 0.58.² The hydrogen content can be followed by changes of electrical resistance of the specimen. The resistance of palladium alters markedly and is nearly linear over the two-phase region from $\alpha_{\text{max}} = 0.02$ to $\beta_{\text{min}} = 0.58$ (25°).⁶ This experimental technique, which

(1) C. A. Knorr and E. Schwartz, *Z. Elektrochem.*, **40**, 38 (1934); L. Kandler, C. A. Knorr, and M. Schwitzer, *Z. Phys. Chem. (Leipzig)*, **A180**, 281 (1937); J. P. Hoare and S. Schuldiner, *J. Phys. Chem.*, **61**, 399 (1959); T. B. Flanagan and F. A. Lewis, *Trans. Faraday Soc.*, **55**, 1400, 1409 (1959).

(2) *E.g.*, A. W. Carson, T. B. Flanagan, and F. A. Lewis, *Trans. Faraday Soc.*, **56**, 363, 371, 1311 (1960).

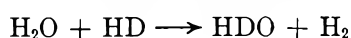
(3) R. J. Fallon and G. W. Castellan, *J. Phys. Chem.*, **64**, 4 (1960).

(4) J. W. Simons and T. B. Flanagan, *ibid.*, **69**, 3581 (1965).

(5) For a general review of the thermodynamics of the palladium-hydrogen system, see F. A. Lewis, "The Palladium-Hydrogen System," Academic Press, London, 1967.

(6) See, for example, T. B. Flanagan and F. A. Lewis, *Z. Phys. Chem. (Frankfurt am Main)*, **27**, 104 (1961).

has been used for absorption studies, offers a new approach for the investigation of hydrogenic isotopic exchange reactions which occur between chemisorbed hydrogenic species and aqueous solutions. It is well known that metal surfaces such as platinum or palladium catalyze the isotopic exchange between D_2 and many molecules containing light hydrogen.⁷ With reference to water, Farkas⁸ has investigated the H and D contents of unpalladized specimens (*i.e.*, palladium specimens which were not especially catalytically active) which were charged cathodically (1.2–20 mA/cm²) from aqueous mixtures of D_2O and H_2O . Farkas concluded that equilibrium between chemisorbed species, solution, and gas obtains because the separation factors observed were not far removed from those expected on the basis of the equilibrium constant for the reaction



His conclusion contains an element of uncertainty because the kinetic isotope effect might lead to a separation factor of comparable magnitude. In contrast to these experiments, where equilibrium was stated to have been established, he found that if palladium which had been presaturated with H spontaneously evolved molecular species in D_2O -enriched solutions, only H_2 was returned to the gas phase. Farkas explained these apparently contradictory results by assuming that in the latter case the hydrogen atom precursors to molecular hydrogen do not come into contact with solution. His results can also be explained if the observed separation factors were mainly kinetic, rather than equilibrium, and that exchange does not occur appreciably even if solution contact obtains.

More recently von Stackelberg and Jahns⁹ found on active, but unpalladized, palladium that H and D separation factors between metal, solution, and the gas phase could be obtained which were very close to those expected for equilibrium if the specimen was charged cathodically from H_2O - D_2O solutions at very low current densities (~ 1 mA/cm²) for long periods of time and then allowed to equilibrate further by sitting in the solution for at least 24 hr. By contrast, Flanagan¹⁰ has found, using active platinum-palladium alloys (unpalladized), that equilibrium was not established during cathodic charging from H_2O - D_2O solutions at low current densities for at least 24 hr.

Using a nonelectrochemical approach, Farkas and Farkas¹¹ found that isotopic exchange takes place between D_2 and H_2O on platinum in the gas phase and more slowly in solution. In this type of experiment, exchange is followed by the return of H_2 and HD to the gas phase. The amount of D_2 which is chemisorbed and then desorbed without exchanging cannot be measured. By contrast, in the technique to be employed here, where D_2 is spontaneously absorbed from H_2O solutions by palladium in the range of contents not exceeding the two-phase region, the chemisorbed D

which does not exchange can also be measured because it becomes absorbed. Of course, the D which has exchanged can be measured because it is absorbed as H. This system therefore offers the important advantage over the conventional approach to catalytic exchange studies in solution in that the fates of all species which have been chemisorbed are known.

The second motive of this research is to examine quantitatively the possibility that the principal mode of isotopic exchange in solution is electrochemical. Horiuti and Polanyi¹² and others⁷ have suggested such a possibility because, for example, in the platinum-catalyzed exchange between D_2 and H_2O solutions the rate is faster in acidic than in basic media.¹² More recently von Stackelberg⁹ has tacitly assumed that exchange occurs by an electrochemical mechanism and he has pointed out that if the cathodic charging of a palladium sample is carried out at ~ 1 mA/cm² then considerable equilibration will occur during charging because the exchange current is also of this magnitude. Also, Lauer and Vielstich¹³ have indicated that on rotating platinum electrodes the time for isotopic exchange equilibrium to be established between gas and liquid can be accounted for by the electrochemical exchange current. By contrast, Trusov and Aladzhalova¹⁴ measured the electrochemical exchange current and isotopic exchange on palladium diffusion membranes and concluded that a nonelectrochemical exchange mechanism is most important over all pH ranges. A detailed discussion of their paper, which is the one most closely related to the present work, will be given in the Discussion section, where it can be more fully related to the present research. An important motive of the present research is to resolve the discrepancy between the results of Trusov and Aladzhalova¹⁴ on the one hand and the suggestions of Vielstich¹³ and von Stackelberg⁹ on the other.

Experimental Section

Loops of palladium wire (15 cm long and 0.027 cm in diameter) were employed as specimens. These were fastened to special soft-glass holders so that only palladium was exposed to the solution.² The samples could be activated by prior anodic treatment or by palladization, *i.e.*, coating with palladium black electrolytically. The hydrogen-free electrical resistance, R_0 , was measured in distilled water (25.0°). The reaction

(7) G. C. Bond, "Catalysis by Metals," Academic Press, London, 1962.

(8) A. Farkas, *Trans. Faraday Soc.*, **33**, 552 (1937).

(9) M. von Stackelberg and W. Jahns, *Z. Elektrochem.*, **62**, 349 (1958).

(10) T. B. Flanagan, *J. Phys. Chem.*, **67**, 203 (1963).

(11) A. Farkas and L. Farkas, *Trans. Faraday Soc.*, **33**, 678 (1937).

(12) J. Horiuti and M. Polanyi, *Nature*, **132**, 819 (1933).

(13) This unpublished research is referred to in H. V. Buttler, W. Vielstich, and H. Barth, *Ber. Bunsenges. Phys. Chem.*, **67**, 650 (1963).

(14) G. Trusov and N. Aladzhalova, *Dokl. Akad. Nauk SSSR*, **130**, 370 (1960).

vessel was stirred vigorously with a magnetic stirrer and was continually saturated with either D₂ or H₂. The vessel was thermostated at 25.0 ± 0.2°.

The palladium wire specimens spontaneously absorbed both D and H (if isotopic exchange occurred), and the rate of total absorption was followed by changes in relative electrical resistance.^{6,15,16} The electrical resistance of palladium containing either solely H or D is not very different in the two-phase regions,^{6,15,16} and for the purposes of this research an average value was taken. The simultaneous presence of H and D did not introduce any anomalous effects into the electrical resistance; *i.e.*, the resistance appeared to be an average of the two values. For example, a sample which contained 77% D had a value of $R/R_0 = 1.36$ at $([H] + [D])/[Pd] = 0.32$; this value falls among the data in the literature given for pure $[H]/[Pd]$ and $[D]/[Pd]$ *vs.* relative resistance relationships.^{5,15,16} Simultaneous measurements of the electrode potential with respect to a reference electrode showed that the system was in the two-phase, (α, β) region. The relative resistance increased almost linearly with time during the runs, indicating that the rate of absorption was constant, as would be expected if the slow step were diffusion up to the surface.^{2,3}

After the attainment of H(D)/Pd contents in the range between 0.1 and 0.5, the specimen was quickly transferred to a vacuum system. The active palladium surface was still wet during this operation so that hydrogen loss was inhibited. The palladium was then degassed by passing an electric current through the specimen *in vacuo*. The isotopic composition of the collected gases was determined by mass spectral analysis.

For unpalladized samples there were no problems associated with the loss of hydrogen and the samples could be dried before evacuation. For some of the runs on unpalladized specimens, the isotopic content of the specimens was determined gravimetrically, and these results checked quite well with the mass spectral analysis.

The electrochemical exchange current was measured during an absorption run on a palladium specimen, and the same specimen was degassed at the end of the run; thus the isotopic content and the electrochemical exchange current were determined on the same specimen, and therefore problems of irreproducibility with respect to a comparison of the two quantities were minimized. In order not to perturb the isotopic content of the specimen appreciably, the electrochemical exchange current was determined quickly and only three or four times during the course of an absorption run (typically 1–3 hr in duration). A galvanostatic pulse was applied between the palladium specimen and a platinum electrode with a square-wave generator (Hewlett-Packard, Model 202A). The corresponding potential change with respect to a saturated calomel electrode was determined as a function of time with an oscilloscope

(Tektronix, Model 561A, dual trace). A Luggin capillary which connected the calomel electrode to the vessel was positioned adjacent to the sample.

This technique allows the charge-transfer overvoltage to be easily separated from the diffusion and IR -drop components.¹⁷ For low overvoltages the charge-transfer resistance is given by¹⁷

$$R_t = (d\eta/di)_{i=0} = RT/zF i_0 \quad (1)$$

where $z = 1$, i_0 is the electrochemical exchange current, and η is the charge-transfer overvoltage. It was demonstrated that the measurements were in the region of linear dependence of η upon i , so that routinely one measurement of η and i sufficed for a determination of i_0 . The square-wave pulse was applied generally in the range between 1 and 100 cps.

The solutions employed were 0.1 and 1.0 *N* HCl, H₂SO₄, NaOH, and mixtures of NaOH and H₂SO₄. Solutions comprised of mixtures of NaOH, HCl, and NaH₂PO₄ were also used such that the pH could be varied at a total ionic strength of 1 *m*. The HCl was Transistor grade (Mallinckrodt); all other reagents were analytical grade. The DCl was >99.5% isotopic purity (Merck Sharp and Dohme). The D₂O was 99.7% isotopic purity (Columbia Southern). Doubly distilled water was employed to make up solutions of the electrolyte in water of natural isotopic abundance. The palladium-wire specimens were 99.9% pure (Engelhard Industries, Inc). They were heated *in vacuo*, were treated with nitric acid, and then were palladized in a solution of Pd(NO₃)₂ using current densities of 10–30 mA/cm² for 1–3 min before an absorption run.

Results

Dependence of Isotopic Exchange upon Electrolyte and Surface Activity. For most runs it was found to be convenient to saturate H₂O solutions with D₂ (1 atm, 25°) since the solutions could then be readily altered. Over 100 runs were performed and typical results of the isotopic analyses of the final contents of the specimens are shown in Table I. The final $([H] + [D])/[Pd]$ ratios in the specimen before isotopic analysis were generally about 0.3, and it was found over the range between 0.1 and 0.5 that the observed isotopic ratio did not depend upon the final values of $([H] + [D])/[Pd]$. This is not unexpected because the essentially pure β phase, $([H] + [D])/[Pd] = 0.6$ exists on the surface of the specimen as H + D contents corresponding to the two-phase region are traversed. This is of great convenience for these studies because ample time is then available

(15) T. B. Flanagan, *J. Phys. Chem.*, **65**, 280 (1961).

(16) A. Sieverts and W. Danz, *Z. Phys. Chem. (Leipzig)*, **B38**, 46, 61 (1937).

(17) K. J. Vetter, "Elektrochemische Kinetik," Springer-Verlag, Berlin, 1961.

for measurements to be made under the invariant conditions which obtain during the absorption run.

Table I: Isotopic Contents from Palladium Specimens Containing H + D in the Two-Phase Region during Absorption of D₂ from Various H₂O Solutions (25°)

Soln	Activation of sample	[H], %	[D], %
1 N HCl	Anodized	10.4	89.6
1 N HCl	Anodized	11.2	88.8
H ₂ O	Anodized	14.7	85.3
H ₂ O	Anodized	12.1	87.9
0.1 N NaOH	Anodized	6.3	93.7
H ₂ O	Palladized	46.9	53.1
H ₂ O	Palladized	27.9	72.1
H ₂ O	Palladized	30.9	69.1
H ₂ O	Palladized	41.7	53.1
0.1 N NaCl	Palladized	21.5	78.5
	(anodic during run)		
0.1 N NaCl	Palladized	42.3	57.6
0.1 N KI	Palladized	6.7	93.4
0.1 N H ₂ SO ₄	Palladized	44.6	55.3
0.1 N H ₂ SO ₄	Palladized	50.2	49.8
0.1 N H ₂ SO ₄	Palladized	51.7	48.3
0.1 N H ₂ SO ₄	Palladized	53.8	46.1

The total rates of H + D absorption were found to be nearly constant and reproducible from run to run under conditions of maximum mechanical stirring. The surprising result should be noted (Table I) that little isotopic exchange occurs on active (for H₂ or D₂ absorption) but unpalladized specimens. A similar result is observed when D₂O solutions are saturated with H₂. Arguments about a lack of contact of the chemisorbed species with the solution cannot be reasonably applied here. Farkas' observations⁸ of the return of H₂ to the gas phase from D₂O-enriched solutions is consistent with these findings.

The total rate of H + D absorption for palladized specimens was generally equal to that of the unpalladized specimens. However, in contrast to unpalladized specimens, isotopic exchange is significant (Table I) for palladized specimens (large true surface areas). Although the rate of total H + D absorption was reproducible, exchange was plagued with some irreproducibility despite the many precautions which were exercised, *e.g.*, doubly distilled H₂O and preelectrolysis of the solution. The best reproducibility was obtained if the same specimen was employed for consecutive runs, as shown in the last four rows of Table I. Despite the irreproducibility in the data, the large number of runs performed allowed some trends in the results to be discerned.

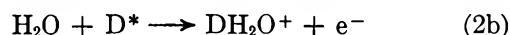
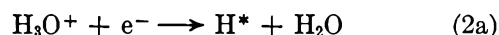
(a) The isotopic exchange is reduced if the specimen is made slightly anodic with respect to an inert electrode during the absorption run (this procedure should not be

confused with anodic activation of a specimen prior to a run).

(b) The isotopic exchange is greatest in concentrated acidic solutions.

(c) The isotopic exchange is greatly inhibited in the presence of strongly adsorbed species such as I⁻.

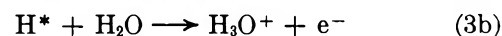
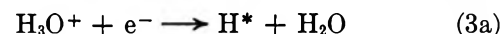
Relationship of Isotopic Exchange to the Measured Electrochemical Exchange Current. Results a and b indicate that an electrochemical process may be an important contributor to isotopic exchange. Previous workers have also suggested this possibility.^{9,12} In H₂O solutions which are saturated with D₂, the electrochemical mechanism which leads to isotopic exchange is



where the asterisk represents a chemisorbed species. If the electrode is made anodic during an absorption run, the rate of reaction 2a will be inhibited as observed (Table I). (The specimens were made only slightly anodic so that the total content, [H] + [D], was not seriously depleted.) In addition, the rate of reaction 2a should depend on (H⁺) as also observed.

In order to determine quantitatively the extent to which isotopic exchange occurs by an electrochemical process, electrochemical exchange currents were measured during an absorption run. During the absorption experiments a net current does not flow except during extremely brief periods when the electrochemical measurements are carried out (neglecting special experiments such as the "anodic" runs (Table I) which will no longer be referred to). In the following analysis the hypothesis will be made that isotopic exchange occurs exclusively by an electrochemical process, and the agreement or disagreement of the results with the hypothesis will confirm or negate it.

Reaction 2b must be balanced by an equal contribution arising from reaction 2a. If the specimen contains appreciable (H) arising from reactions 2a and b, then reaction 3b can also occur (balanced by reaction 3a).



This reaction does not lead to isotopic exchange. In the absence of a net current flow an equality of the rates must hold; *i.e.*, rate (2a) + rate (3a) = rate (2b) + rate (3b).

The electrochemical exchange current, *i*₀, has been measured during spontaneous absorption of D₂ from various H₂O solutions. This current is the sum of reactions 2a and 3a (proton discharge) and is equal to the sum of reactions 2b and 3b (deuterium and hydrogen atom ionization); analogous reactions represent the measured electrochemical exchange current in H₂-saturated D₂O solutions. The final isotopic content is determined when the run is completed, ([H] + [D])/[Pd] < 0.58.

The measured electrochemical exchange current, i_0 , which involves a sum of reactions 2 and 3 must be related to the isotopic exchange which is controlled only by reaction 2. From the changes of resistivity with time, a total rate of absorption can be determined. A typical value for this total, constant rate is 10^{16} molecules $\text{cm}^{-2} \text{sec}^{-1}$. In order for this rate of absorption to be achieved by electrolysis, the necessary current density must be 3.2 mA cm^{-2} . Since reappearance of molecular species arising from recombination of chemisorbed species can be neglected in the range of H + D contents employed here and since only H⁺ can be discharged from the D₂-saturated H₂O solutions, the following relationship between the fluxes passing through a plane, P, in the solution just above the chemisorbed layer (Figure 1) must hold. (Fluxes are expressed as current densities in the case of charged species or for molecular species as a current density representing an equivalent rate of absorption.)

$$[D]/[H] = (\bar{i}_{1/2D_2} - \bar{i}_{D^*})/(\bar{i}_{H^+} - \bar{i}_{H^*}) \quad (4)$$

where $\bar{i}_{1/2D_2}$ is the equivalent current density arising from the transport of D₂ up to the surface, \bar{i}_{H^+} is the proton discharge current density, \bar{i}_{H^*} and \bar{i}_{D^*} are the current densities due to the ionization of H* and D*, respectively, and [H] and [D] represent the percentages of H and D in the specimen at any total H + D content; the [D]/[H] ratio is invariant throughout the run so that the final ratio is the same as that at any time. Using the equality $\bar{i}_{H^*} + \bar{i}_{D^*} = \bar{i}_{H^+}$, eq 4 can be written

$$[D]/[H] = (\bar{i}_{1/2D_2} - \bar{i}_{D^*})/\bar{i}_{D^*} \quad (5)$$

Solving for \bar{i}_{D^*} yields

$$\bar{i}_{D^*} = \{[H]/([H] + [D])\} \bar{i}_{1/2D_2} \quad (6)$$

and

$$i_0^* = \bar{i}_{H^+} = \bar{i}_{D^*} + \bar{i}_{H^*} = \left\{ \frac{[H]}{[H] + [D]} \right\} \bar{i}_{1/2D_2} + \bar{i}_{H^*} \quad (7)$$

For the analogous situation of H₂ absorption from D₂O solutions we have

$$\bar{i}'_{H^*} = \left\{ \frac{[D]}{[H] + [D]} \right\}' \bar{i}'_{1/2H_2} \quad (8)$$

and

$$i_0^{*'} = \bar{i}_{D^{*'}} = \bar{i}_{H^{*'}} + \bar{i}_{D^{*'}} = \left\{ \frac{[D]}{[H] + [D]} \right\}' \bar{i}'_{1/2H_2} + \bar{i}_{D^{*'}} \quad (9)$$

where the primes refer to reactions in H₂-saturated D₂O solutions. The quantities i_0^* and $i_0^{*'}$ are defined by eq 7 and 9 and will be termed the calculated isotopic exchange currents. Since \bar{i}_{H^*} represents the same chemical reaction as \bar{i}_{D^*} except for the isotopic substitution of H* for D*, an expression for \bar{i}_{H^*} can be given in analogy to eq 6

$$\bar{i}_{H^*} = \left\{ \frac{[H]}{[H] + [D]} \right\} \alpha \left\{ \frac{[H]}{[D]} \right\} \bar{i}_{1/2D_2} \quad (10)$$

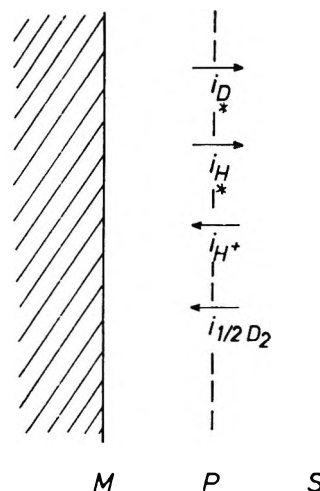


Figure 1. Schematic drawing of the fluxes obtaining at the electrode-solution interface during a run.

The additional factor $\alpha[H]/[D]$ is introduced to allow for the relative chance of ionization of an H* as compared with a D*, and α is an isotope effect for the ionization. Similar considerations apply for the evaluation of $\bar{i}_{D^{*'}}$ giving

$$\bar{i}_{D^{*'}} = \left\{ \frac{[D]}{[H] + [D]} \right\} \left\{ \frac{[D]}{\alpha[H]} \right\}' \bar{i}'_{1/2H_2} \quad (11)$$

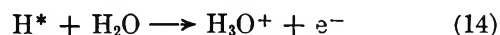
Inserting the expressions for \bar{i}_{H^*} and $\bar{i}_{D^{*'}}$ into eq 7 and 9, respectively, we obtain

$$i_0^* = \left\{ \frac{[H]}{[H] + [D]} \right\} \times \left[1 + \alpha \frac{[H]}{[D]} \right] \bar{i}_{1/2D_2} = i_0 \quad (12)$$

and

$$i_0^{*' } = \left\{ \frac{[D]}{[H] + [D]} \right\}' \times \left[1 + \left\{ \frac{[D]}{\alpha[H]} \right\}' \right] \bar{i}'_{1/2H_2} = i_0' \quad (13)$$

The unknown in these relationships is α . It is difficult to measure α experimentally because the slow step in the measurement must be unequivocally the ionization process. Recently Lauer and Vielstich¹⁸ cited evidence that they were able to achieve this when H and D ([D] = 150–2650 ppm) were removed anodically from palladium alloy electrodes. Their measured separation factors, when corrected for the relative solubilities in the alloys, represent the relative rates of



The values of α obtained ranged from 0.7 to 0.95.

Considering the spread in the values of α reported,¹⁸ it seems not unreasonable to choose $\alpha = 1$ as a starting point and then examine the consistency of this choice with the data of the present study. Table II shows the

(18) H. Lauer and W. Vielstich, *Ber. Bunsenges. Phys. Chem.*, **69**, 538 (1965).

values of i_0^* calculated on this basis from eq 12 in comparison to values of i_0 . It is noted that in strong acid solutions the two values are closely equal. If α were actually considerably greater than 1 (*i.e.*, >1.2), then the only way that i_0^* and i_0 could be nearly equal, as observed, would be for two effects to operate in opposite directions so that fortuitously $i_0 = i_0^*$. These two effects would be $\alpha > 1$ together with a significant nonelectrochemical mechanism which leads to isotopic exchange. This is unlikely since $i_0 = i_0^*$ (Table II) in both H_2SO_4 and HCl , and it is shown below that the magnitude of the nonelectrochemical mechanism (which does play a role in pH ranges other than strong acid) is very dependent upon the nature of the electrolyte. The data also suggest that α cannot be less than 0.85 in order for i_0 to equal i_0^* within the limit of experimental error (Table II).

Table II: Comparison of Exchange Currents Measured Electrochemically, i_0 , and Calculated, i_0^* , Using $\alpha = 1$ from Isotopic Contents of Specimens during Absorption of D_2 from Various H_2O Solutions by Palladized Palladium Containing H + D in the Two-Phase Region (25°)

Soln	i_0^* , mA/cm ²	i_0 , mA/cm ²
0.1 N H_2SO_4	7.16	6.1
0.1 N H_2SO_4	1.55	1.15
0.1 N H_2SO_4	2.86	3.3
0.1 N H_2SO_4	3.71	4.0
2.0 N H_2SO_4	12.4	11.5
1.0 N HCl	9.0	10.5
pH 5.8	4.42	0.6
0.1 N NaOH	4.88	0.23
1.0 N NaOH	7.02	0.42
1.0 N NaOH	11.4	0.40

The unlikely occurrence of two effects operating in opposite directions mentioned above can be ruled out from the simultaneous consideration of events occurring in D_2 -saturated H_2O solutions and H_2 -saturated D_2O solutions. The isotope effect operates in opposite directions for the calculation of i_0^* and $i_0^{*'} (eq 12 and 13); e.g., again if α is really greater than 1, then the assumption of $\alpha = 1$ leads to $i_0^* < i_0$ and $i_0^{*' > i_0'$ or alternatively if α is less than 1 then the assumption leads to $i_0^* > i_0$ and $i_0^* < i_0'$. The data eliminate values of α significantly greater than 1 but values of α much less than 1 are required to reconcile the data in D_2O (Table III). This discrepancy probably arises because it is an oversimplification to assume that α is the same in H_2O and in D_2O solutions. The data indicate that α is of the order of 0.2 in D_2O solutions.$

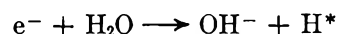
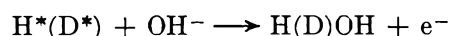
The results of Lauer and Vielstich¹⁸ and the data of the present study show that in H_2O solutions $\alpha \sim 1.0$. Furthermore, the hypothesis that isotopic exchange

occurs exclusively by an electrochemical mechanism is valid only in strong acid solutions.

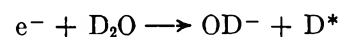
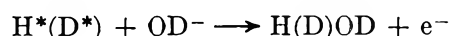
The same sample was employed for the H_2 -saturated D_2O runs as for the run listed in 1 N HCl (Table II); therefore, the absolute reproducibility should be comparable with that exhibited by the last four rows in Table I. A large isotopic effect exists in 1 N acidic solutions as shown by the relative values of i_0^* and $i_0^{*'}$ and i_0 and i_0' . The isotope effect clearly reflects the relative discharge rates of H_3O^+ and D_3O^+ . Thus even though H is initially chemisorbed onto the surface in 1 N DCl solutions, the value of i_0' is smaller by a factor of 10 than in the situation where D is initially chemisorbed onto the surface in HCl solutions. This suggests that the ionization step is forced to keep pace with the discharge step. If the reverse were true, then the values of i_0' and i_0 would be comparable.

In pH ranges other than those of strong acid $i_0 \neq i_0^*$, and another mechanism for isotopic exchange, which will be called the catalytic mechanism,¹⁴ must come into play. The ratio i_0/i_0^* is plotted in Figure 2 as a function of pH at a constant ionic strength. It can be seen that there is a rapid falloff from the limiting value of 1 to a low, very nearly constant value in the pH range from 7 to 12. When the ionic strength is increased at a constant pH, i_0/i_0^* decreases (Figure 2). This indicates that the electrochemical process is more easily blocked at the surface than the catalytic process.

In basic solutions the electrochemical exchange current arises from



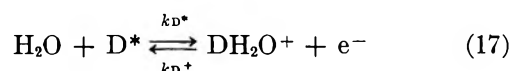
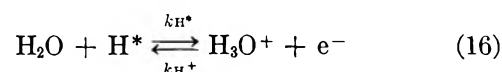
or



in D_2 -saturated H_2O solutions or H_2 -saturated D_2O solutions, respectively. There is only a small isotope effect for i_0 and i_0' in basic solutions but a rather large isotope effect for i_0^* and $i_0^{*'}$. The latter values arise principally from the catalytic mechanism.

Discussion

Since the magnitude of the isotope effect for the ionization step employed in the analysis of the data and reported elsewhere¹⁸ is perhaps of an unexpected magnitude, it is of interest to relate it to the more frequently investigated discharge step. In acidic H_2O solutions the ionization-discharge equilibrium can be given as



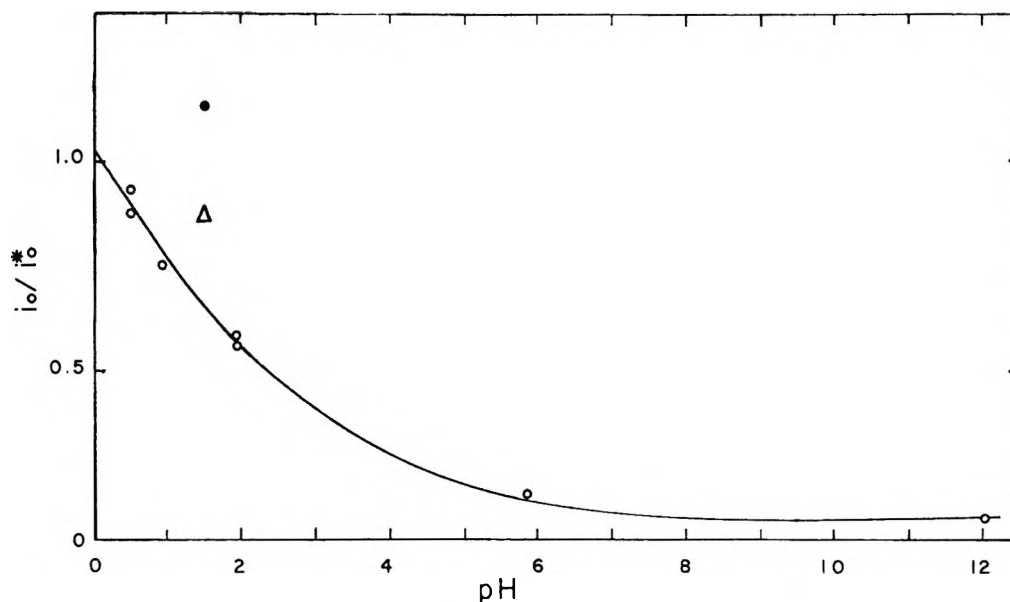
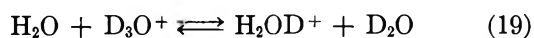


Figure 2. The ratio of electrochemical exchange current, i_0 , to the isotopic exchange current, i_0^* , as a function of pH in the two-phase region of palladium electrodes in aqueous solutions: O, values determined at a constant ionic strength of 1 *m* ($\text{H}_2\text{SO}_4 + \text{Na}_2\text{SO}_4$); ●, solution of 0.1 *N* HCl; Δ, solution of 0.1 *N* H_2SO_4 .

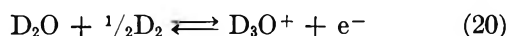
since these are both elementary rate processes

$$k_{\text{H}^*}/k_{\text{D}^*} = k_{\text{H}}K_{\text{H}}/k_{\text{D}}K_{\text{D}} \quad (18)$$

where K_{H} and K_{D} are the equilibrium constants for reactions 16 and 17, respectively. In the two-phase region of the hydrogen-palladium system K_{H} is known and K_{D} can be obtained from the addition of



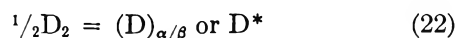
and



to give



ΔG° for reaction 21 can be obtained from the known ΔG° values for reactions 19¹⁹ and 20.¹⁹ Combination of reaction 21 with



gives the free energy change for reaction 17. (Since $(\text{D})_{\alpha/\beta}$ and D^* are at the same chemical potential, the free energy change for absorption of D_2 in the two-phase region may be employed for reaction 22⁵). This gives for eq 18

$$k_{\text{H}^*}/k_{\text{D}^*} = 0.13k_{\text{H}}/k_{\text{D}} \quad (23)$$

This shows that the ionization step would be expected to have a much lower isotope effect than the discharge process.

The catalytic mechanism giving rise to isotopic exchange is most likely a hydrogen-switch mechanism;

i.e., in D_2 -saturated H_2O solutions



An H atom attached to the water molecule and the D^* switch places simultaneously. Dissociatively adsorbed water molecules are probably not important intermediates for exchange, since liquid water is not dissociatively chemisorbed to any extent on similar metals such as platinum (25°).²⁰ The catalytic mechanism is suppressed in strong acid; it is not masked by experimental differences between i_0 and i_0^* because these differences are much smaller than the large values of i_0^* observed in neutral or basic solutions (Table II) where these large values of i_0^* arise from the catalytic reaction. The suppression of the catalytic mechanism may arise from a change in the nature of the double layer and the accompanying alteration in the type of dischargeable species as the pH is altered.

The research of Trusov and Aladzhilova¹⁴ yielded results apparently in disagreement with those found in this research; *i.e.*, they found that over the whole pH range the catalytic reaction was the most important. Their experimental approach was quite different from that employed here. A palladium diffusion membrane separated on one side a solution of natural isotopic abundance and on the other side 90% D_2SO_4 or KOD. The membrane was made cathodic until $[\text{H}]/[\text{Pd}] > 0.7$, and the isotopic ratio of the evolved gases on the diffusion side of the membrane (the enriched side) was

(19) M. Salmon and B. E. Conway, *Discussions Faraday Soc.*, **39**, 223 (1965).

(20) H. Chon, R. A. Fisher, E. Tomezsko, and J. G. Aston, *Actes Congr. Int. Catalyse*, **2**, Paris, 1960, 217 (1961).

determined. Overvoltages were measured on the same membrane in a completely separate set of experiments in light water of natural isotopic abundance. There are several sources of error in their experiments; for example, the use of only 90% isotopic purity means that H^+ will constitute almost half of the exchange current because of the large isotope effect for discharge.⁹ In addition, the measurement of exchange currents in light water and the utilization of these values for the interpretation of data obtained in 90% D_2SO_4 is not a valid procedure owing to the large variation in i_0 in passing from H_3O^+ to D_3O^+ solutions (Tables II and III). Since details were not given of the calculation of the isotopic exchange current (i_0^*), it is not possible to say if an attempt was made to correct for these errors.

Table III: Comparison of Exchange Currents Measured Electrochemically, i_0 , and Calculated, i_0^* , Using $\alpha = 1$ from Isotopic Contents of Specimens during Absorption of H_2 from Various D_2O Solutions by Palladized Palladium Containing $H + D$ in the Two-phase Region (25°)

Soln	i_0^* , mA/cm ²	i_0 , mA/cm ²
1.0 N DCl	0.66	1.2
1.0 N DCl	0.66	1.0
1.0 N DCl	0.31	0.5
0.1 N NaOD	0.64	0.17

It is not unlikely that the two different conclusions with regard to the exchange behavior in strong acid may result from the experimental conditions. In the

present experiments the chemisorbed species enter the palladium, whereas in their research¹⁴ the chemisorbed species are evolved as molecular species (with or without exchange). Different sites may be involved for these two processes, especially in view of the fact that the surface coverage was much greater in their experiments ($[H]/[Pd] > 0.7$).

The fact that isotopic exchange is small on unpalladized specimens in the various types of solution investigated here indicates that in, for example, D_2 -saturated H_2O solutions the total amount of D which is chemisorbed and then rapidly absorbed is not a decisive factor in isotopic exchange because the same flux passes through the apparent surfaces of both the palladized and unpalladized specimens—the rates of total absorption are comparable in both cases. The main difference between the two types of sample is that a palladized one has a larger active area which gives rise to greater isotopic exchange either by having a greater total steady-state amount of D on the surface, arising from the rapid absorption–chemisorption equilibrium, or by allowing the discharge step to occur more readily (in strong acid solutions). The latter appears to be the case, since ionization is forced to keep pace with the discharge step (see above). The reverse situation must be true for the catalytic mechanism, however, because a supply of D^* is needed for the hydrogen-switch mechanism.

Acknowledgments. The authors are grateful to the U. S. Atomic Energy Commission for financial support of this research.

Proton Chemical Shifts and the Reactivity of Polynuclear

Aromatic Hydrocarbons

by K. D. Bartle and D. W. Jones

School of Chemistry, University of Bradford, Bradford, England (Received February 27, 1968)

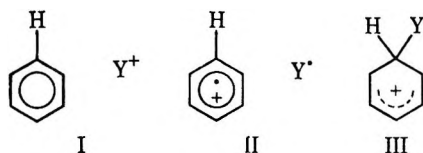
The apparently significant correlations in 22 alternant and 7 nonalternant hydrocarbons between pmr chemical shifts (δ) and the corresponding values of the LCAO index of free valence (F_r) have been investigated. They are found to arise as a fortuitous consequence of the geometry of these molecules so that, in a causative sense, δ is unrelated to F_r and hence to other molecular orbital indices of chemical reactivity. F_r can also be correlated with δ for the more distant CH_3 and CH_2CH_3 protons in substituted hydrocarbons. In general, F_r is larger for positions closer to ring centers because such positions are flanked by one or two ring-junction carbon atoms. Those chemical shifts in alternant hydrocarbons which deviate markedly from the δ vs. F_r regression line are well explained by ring-current theory.

Introduction

Proton magnetic resonance spectroscopy has been applied to the direct study of chemical reactivity in aromatic systems through determination of the nature and structure of substitution products as, for example, in the reactions of phenanthrene¹ and of dibenz[*b,f*]oxepin.² Recently, comparisons of reactivity in aromatic substitution reactions have been made with pmr chemical shifts^{3,4} (δ) and with esr hyperfine coupling constants.⁵ An interest both in the origin of pmr chemical shifts⁶ and in the carcinogenic properties of polynuclear aromatic hydrocarbons has led us to investigate reported correlations between δ and a number of Hückel LCAO indices for relative chemical reactivity in substitution reactions.

Choice of Molecular Orbital Reactivity Indices for Comparison

Many indices of intermolecular and intramolecular reactivity have been proposed and their applications to various classes of mechanism (*e.g.*, electrophilic and free radical) have been reviewed.⁷⁻¹⁰ Broadly, both well-established and more recently proposed indices may be grouped under one or other of two somewhat extreme quantum mechanical approaches: (i) isolated molecule methods, based on the initial states of the reaction, and (ii) localization methods, based on energy changes involved in the formation of the substitution transition-state complex. Thus for electrophilic substitution in, say, benzene, contributory hybrid I corresponds to approach i, while structures II and III, respectively, emphasize the transfer of charge and delocalization aspects of approach ii.



Greenwood and McWeeny⁹ ascribed the similarity in reactivity predictions made by superficially distinct indices, summarized by Streitwieser,⁷ to analytical properties of the equations from which the indices are derived. In particular, the close agreement between these indices and the experimental reactivities in alternant hydrocarbons arises^{8,11} because of a fortuitous correspondence between reactivity indices and the more fundamental energies of reaction and activation, ΔE . In favorable cases, differences in ΔE may be dominated by changes in the π -electron energy, E_π , as compared with changes in E arising from all other causes. Thus the reaction rate, k , relative to some standard such as benzene, at an alternant position r is given by⁸

$$-RT \ln (k/k_{\text{std}}) = 2\beta(F_r - F_{\text{std}}) \quad (1)$$

Here β , the LCAO resonance integral of the C-C bond,

- (1) P. M. G. Bavin, K. D. Bartle, and J. A. S. Smith, *Tetrahedron*, **21**, 1087 (1965).
- (2) P. M. G. Bavin, K. D. Bartle, and D. W. Jones, *J. Heterocyclic Chem.*, **5**, 327 (1968).
- (3) J. Kuthan, *Z. Chem.*, **6**, 150, 422 (1966).
- (4) J. Kuthan, *Collect. Czech. Chem. Commun.*, **33**, 1220 (1968).
- (5) C. P. Poole, Jr., and O. F. Griffith, *J. Phys. Chem.*, **71**, 3672 (1967).
- (6) K. D. Bartle and D. W. Jones, *Trans. Faraday Soc.*, **63**, 2868 (1967).
- (7) A. Streitwieser, Jr., "Molecular Orbital Theory for Organic Chemists," John Wiley & Sons, Inc., New York, N. Y., 1961, Chapter 11.
- (8) M. J. S. Dewar in "The Application of Wave Mechanical Methods to the Study of Molecular Properties," R. Daudel, Ed., Interscience Publishers, Ltd., London, 1965, p 65.
- (9) H. H. Greenwood and R. McWeeny, *Advan. Phys. Org. Chem.*, **4**, 73 (1966).
- (10) L. Salem, "The Molecular Orbital Theory of Conjugated Systems," W. A. Benjamin, Inc., New York, N. Y., 1966, Chapter 6.
- (11) F. Burkitt, C. A. Coulson, and H. C. Longuet-Higgins, *Trans. Faraday Soc.*, **47**, 553 (1951).

Table I: Scope and Sources of Chemical Shift Data^a

	Parent		Methyl derivative		Ethyl derivative	
	Hydrogen position	Ref	Methyl position	Ref	Ethyl position	Ref
Naphthalene	1, 2	24	1, 2	31, 37, 40	2	41
Anthracene	1, 2, 9	24	2, 9	31, 37, 41		
Phenanthrene	1-4, 9	25	1-4, 9	25, 31, 36, 37, 39, 42, 43	2, 3, 9	25, 42
Benz[a]anthracene	1-12	26	1-12	31, 39		
Benzo[c]phenanthrene	1-6	27	1, 3 ^b	44, 45		
Chrysene	1-6	28	5, 6	46		
Naphthacene	1, 2, 5	29				
Triphenylene	1, 2	6	1, 2	27, 47	2	51
Pyrene	1, 2, 4	24	1, 2, 4	27, 37, 43, 48		
Benzo[a]pyrene	8	29				
Benzo[e]pyrene	1-4, 9, 10	30				
Dibenz[a,c]anthracene	1-4, 9-11	30	10	31		
Dibenz[a,h]anthracene	7	29				
Dibenz[a,j]anthracene	7, 14	31				
Perylene	1-3	24	1	49	1-3	52
Pentaphene	5, 6, 13	29				
Picene	5, 6, 13	30				
Coronene	1	24	1	37, 43	1	43
Biphenyl	2-4	32	2, c 4 ^d	40, 50	2, 3	40
<i>p</i> -Terphenyl	2'	32				
Biphenylene	1, 2	33				
Acenaphthylene	1, 3-5	27				
Fluoranthene	1-3, 7, 8	15				
Benzo[k]fluoranthene	1-3, 7-9	15				
Benzo[ghi]fluoranthene	1-5	15				
Dibenzo[ghi,mno]fluoranthene	1	34				
Acepleiadylene	1, 2, 5-7	13				
Azulene	1, 2, 4-6	13, 35				

^a Alternant hydrocarbons, from naphthalene to biphenylene, are listed first, followed by nonalternants from acenaphthylene to azulene. Except for those marked with a superscript, all methyl derivatives are monomethyl; all ethyl derivatives are monoethyl. ^b 3,10-Dimethylbenzo[c]phenanthrene. ^c 2,2'-Dimethylbiphenyl. ^d 4,4'-Dimethylbiphenyl.

is closely related to ΔE , and F_7 , the free valence index, is an example of a type i index.

A chemical shift, δ , at a hydrogen atom is a measure of the total of shielding effects arising from the following, and possibly other, contributions: (1) diamagnetic circulations in the hydrogen atom, (2) paramagnetic circulations in the hydrogen atom, (3) σ -bond circulations on the attached carbon and other atoms, and (4) π -system circulations.

The q_π index (one of type i) is based on the LCAO π density at the carbon atom and may influence term 1 above, despite¹² insulation of hydrogen from carbon by σ bonds. While correlations between δ and q_π are well established for hydrocarbon ions,¹³ nitrogen heterocycles,¹⁴ certain nonalternant hydrocarbons,^{13,15} and substituted aromatic hydrocarbons,¹⁶ q_π is unity for all positions in unsubstituted alternant hydrocarbons according to HMO¹⁷ and some more realistic SCF theories,¹⁸ effects arising from changes in terms 1 and, *a fortiori*, 2, should therefore be small. Moreover, calculations on polycyclic hydrocarbons show⁶ that, if shifts are referred to the appropriate monocycle, the contributions from term 3 are also small.

Of the five indices with which Kuthan^{3,4} compared literature values of shieldings, only F_7 and π_{ii} are of type i; the self-polarizability, π_{ii} , is closely related to F_7 and reflects the ease with which the electron density distribution of the hydrocarbon is modified by the charge of the attacking reagent. The other indices considered by Kuthan were all variants of approach ii: Wheland localization energy, L or A_i ; Dewar reactivity, A_D ; and super-delocalizability, S , or S_i . Similarly, the esr hyperfine coupling constant, a_i , recently shown⁵ to be correlated with the intramolecular reactivity of phenanthrene, is a simple function of the frontier electron density, f_7 , and is therefore of type ii.

(12) A. D. Buckingham, *Can. J. Chem.*, **38**, 300 (1960).

(13) T. Schaefer and W. G. Schneider, *ibid.*, **41**, 966 (1963).

(14) P. J. Black, R. D. Brown, and M. C. Heffernan, *Aust. J. Chem.*, **20**, 1305 (1967).

(15) K. D. Bartle, D. W. Jones, and J. E. Pearson, *J. Mol. Spectrosc.*, **23**, 330 (1967).

(16) A. Zweig, J. E. Lancaster, and M. T. Neglia, *Tetrahedron*, **23**, 2577 (1967).

(17) C. A. Coulson and G. S. Rushbrooke, *Proc. Cambridge Phil. Soc.*, **36**, 193 (1940).

(18) J. A. Pople, *J. Phys. Chem.*, **61**, 6 (1957).

In view of the close numerical relationship between reactivity indices, it is necessary to investigate in detail only one of the five discussed by Kuthan.^{3,4} Of these, F_r has the merits of fairly ready calculation and more direct association (*via* eq 1) with the reaction rate than indices of type ii. Further, the arguments above suggest that, in polycyclic hydrocarbons, chemical shifts are dominated by effects arising from the π -electron distribution,¹⁹ of which F_r provides the most direct representation.

Calculations

Accordingly we have calculated correlations between δ and the free-valence index,²⁰ F_r , a descendant^{7,8} of Thiele's theory of residual affinity. In essence, F_r specifies the remaining ability of a carbon atom to form π bonds such that, for the r th atom in a hydrocarbon²¹

$$F_r = N_{\max} - N_r \quad (2)$$

where N_r is the sum of the HMO bond orders for all bonds to the r th atom, and the maximum, N_{\max} , is generally taken to be $\sqrt{3}$ even though it can be greater in certain cases.^{22,23}

Correlations have been tested (a) between mainly tabulated values of F_r and literature values of δ , referred to the appropriate monocycle, for 107 protons in 22 alternant and 7 nonalternant hydrocarbons^{6,13,15,24-36} and (b) between shifts δ_{CH_3} , $\delta_{CH_2CH_3}$, and $\delta_{CH_2CH_2}$ in 29 methyl- and 11 ethyl-substituted alternants^{25,27,31,36-52} and F_r values for the corresponding sites in the parent hydrocarbon. Any shift effects arising from successive substitution were eliminated by selecting data, where possible, from monosubstituted derivatives. Aromatic proton shifts were admitted only if they referred to singlets or were the result of complete (rather than first-order) analyses of spin systems. All values of δ included in Table I had been measured either at infinite dilution or at low concentration in a solvent expected to have small intermolecular interaction with the hydrocarbon.

For the (equivalent) perimeter positions of dibenzo-[*ghi,mno*]fluoranthene, F_r was calculated on the Bradford University ICT 1909 by means of an HMO program to be 0.450 on the basis of a planar molecule; a nonplanar configuration has recently been suggested.⁵³ For benzo[*k*]fluoranthene and benzo[*ghi*]fluoranthene, F_r values calculated by Zahradnik and Michl⁵⁴ were used; F_r values for all other compounds were taken from the tables of Coulson and Streitwieser.⁵⁵

Correlation (r) and regression (a and b) coefficients were calculated on the above computer for the equation

$$\delta = aF_r + b$$

for the following groups in turn: (a) aromatic protons: (1) nonsterically hindered protons of alternant hydrocarbons; (2) sterically hindered protons of alternant

hydrocarbons; (3) all nonalternant protons; and (4) protons of benzenoid rings in nonalternants; and (b) methyl and ethyl protons: (5) protons of nonsterically hindered methyl groups; (6) methylene protons of nonsterically hindered ethyl groups; and (7) methyl protons of the same compounds as group 6.

- (19) B. P. Dailey, *J. Chem. Phys.*, **41**, 2304 (1964).
- (20) B. Pullman and A. Pullman, *Progr. Org. Chem.*, **4**, 31 (1958).
- (21) C. A. Coulson, *Discussions Faraday Soc.*, **2**, 9 (1947).
- (22) W. M. A. Smit and D. H. W. de Boer, *Theor. Chim. Acta*, **5**, 358 (1966).
- (23) C. Finder, *J. Org. Chem.*, **32**, 1672 (1967).
- (24) N. Jonathan, S. Gordon, and B. P. Dailey, *J. Chem. Phys.*, **35**, 2443 (1962).
- (25) K. D. Bartle and J. A. S. Smith, *Spectrochim. Acta*, **A23**, 1689 (1967).
- (26) T. J. Batterham, L. Tsai, and H. Ziffer, *Aust. J. Chem.*, **13**, 1959 (1965).
- (27) K. D. Bartle and D. W. Jones, unpublished measurements.
- (28) J. D. Memory, G. W. Parker, and J. C. Halsey, *J. Chem. Phys.*, **45**, 3569 (1966).
- (29) R. H. Martin, N. Defay, F. Geerts-Evrard, and S. Delavarenne, *Tetrahedron*, **20**, 1073 (1964).
- (30) T. B. Cobb and J. D. Memory, *J. Chem. Phys.*, **47**, 2020 (1967).
- (31) P. Durand, J. Parello, N. P. Buu-Hoi, and L. Alais, *Bull. Soc. Chim. France*, 2438 (1963).
- (32) R. E. Mayo and J. H. Goldstein, *Mol. Phys.*, **9**, 301 (1966).
- (33) A. R. Katritzky and R. E. Reavill, *Rec. Trav. Chim. Pays-Bas*, **83**, 1230 (1964).
- (34) W. E. Barth and R. G. Lawton, *J. Amer. Chem. Soc.*, **88**, 380 (1966).
- (35) H. Spiessicke and W. G. Schneider, *Tetrahedron Lett.*, 468 (1961).
- (36) R. H. Martin, N. Defay, F. Geerts-Evrard, and H. Figeys, *Bull. Soc. Chim. Belges*, **73**, 199 (1964).
- (37) I. C. Lewis, *J. Phys. Chem.*, **70**, 1667 (1966).
- (38) F. F. Yew, R. J. Kurland, and B. J. Mair, *Anal. Chem.*, **36**, 943 (1964).
- (39) C. MacLean and E. L. Mackor, *Mol. Phys.*, **4**, 241 (1961).
- (40) American Petroleum Institute, Research Project 44, Agricultural and Mechanical College of Texas, College Station, Texas, 1960.
- (41) N. S. Bhacca, L. F. Johnson, and J. N. Shoolery, Varian Spectra Catalogue, Vol. I and II, Varian Associates, Palo Alto, Calif., 1962, 1964.
- (42) A. Cornu, J. Ulrich, and K. Persaud, *Chim. Anal.*, **47**, 357 (1965).
- (43) E. Clar, B. A. McAndrew, and M. Zander, *Tetrahedron*, **23**, 985 (1967).
- (44) R. Peter and W. Jenny, *Helv. Chim. Acta*, **49**, 2123 (1966).
- (45) R. H. Martin, N. Defay, and F. Geerts-Evrard, *Tetrahedron*, **21**, 2435 (1965).
- (46) D. Cagniant, *Bull. Soc. Chim. Fr.*, 2325 (1965).
- (47) K. D. Bartle, H. Heaney, P. Lees, and D. W. Jones, *Spectrochim. Acta*, **22**, 941 (1966).
- (48) R. H. Martin, R. Flammang, and M. Arboui, *Bull. Soc. Chim. Belges*, **74**, 418 (1965).
- (49) H. E. Zieger and E. M. Laski, *Tetrahedron Lett.*, 3801 (1966).
- (50) "Catalogue of N.M.R. Spectra," The Humble Oil and Refining Co., Baytown, Texas, 1959.
- (51) R. H. Martin, N. Defay, and F. Geerts-Evrard, *Tetrahedron*, **20**, 1091 (1964).
- (52) H. E. Zieger, *J. Org. Chem.*, **31**, 2977 (1966).
- (53) G. J. Gleicher, *Tetrahedron*, **23**, 4257 (1967).
- (54) R. Zahradnik and J. Michl, *Collect. Czech. Chem. Commun.*, **31**, 3442, 3453 (1966).
- (55) C. A. Coulson and A. Streitwieser, "Dictionary of π -Electron Calculations," Pergamon Press Ltd., London, 1965.

Table II, which summarizes values of r , a , and b , confirms a correlation between δ and F_r for alternant hydrocarbons. Although the value of r is lower than that reported,³ its statistical significance is high (a low numerical value in the per cent significance⁵⁶ column of Table II corresponds to a low probability that the correlation arises merely by chance). Despite the apparent statistical significance of these correlations, however, the argument below demonstrates that they are a fortuitous consequence of molecular geometry.

Discussion

In unsubstituted polynuclear hydrocarbons, carbon-carbon bonds may be classified⁵⁷ as NN, NJ, or JJ if, respectively, neither, one, or both carbon atoms are at ring junctions. Pairing of these bond types leads to a classification of carbon atoms, of which three can carry hydrogen atoms.

Table II: Correlation (r) and Regression (a and b) Coefficients for Relation^a $\delta = aF_r + b$

Group ^b	No. of protons	r	a	b	Significance level, %
1	58	-0.628	-7.32	2.73	0.1
2	18	-0.580	-8.69	2.47	2
3	31	-0.313	-3.79	1.29	10
4	22	-0.668	-5.43	1.91	0.1
5	29	-0.635	-4.52	1.61	0.1
6	11	-0.569	-6.11	2.33	10
7	11	-0.313	-1.48	0.52	...

^a For groups 1 and 5-7, the numbers of protons include one for the reference monocycle. ^b See the text.

The larger HMO orders for NN than NJ bonds lead to an increasing sequence of F_r ranges for nonhindered positions in alternants as follows: (a) non-*peri* (flanked by NN and NN), 0.393-0.420; (b) *peri* (flanked by NN and NJ), 0.428-0.473 (or 0.449-0.473 if special cases of biphenyl H(2), *p*-terphenyl H(2'), or biphenylene H(1) are excluded); and (c) *peri-peri* (flanked by NJ and NJ), 0.514-0.530.

Now geometry requires that (c) hydrogens are closer to more ring centers than are (b) hydrogens, which, in turn, are closer to more rings than (a) hydrogens. Consequently if, as will be expected for nonsterically hindered alternant positions, other shielding influences are small,⁶ any model dominated by proximity to ring currents (whether calculated by a simple dipole at the ring center⁵⁸ or by taking more explicit account of the π -electron distribution^{32,59-61}) will predict a trend of shifts: $\delta_c > \delta_b > \delta_a$. Observed shifts do, indeed, follow this prediction, and the correlation between δ and F_r is merely a manifestation of this, just as the further correlations reported by Kuthan^{3,4} are assured by the interrelation of reactivity indices.

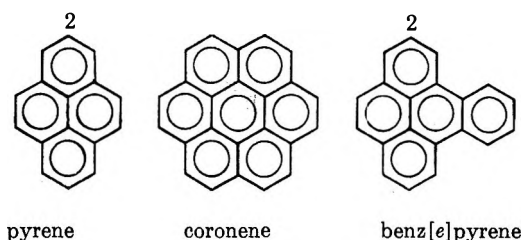
Support for the above argument is provided by those five shifts which deviate most from the calculated regression line. Table III shows that experimental deshieldings for coronene, for pyrene H(2), and for benz-

Table III: Comparison of Chemical Shifts Calculated from F_r , and by the Ring-Current Method, with Experimental Values

Proton	Calcd from $-7.32F_r + 2.73$	Shieldings from ring-current ^a	Ref	Exptl values	Ref
Coronene	-0.56	-1.66	<i>b</i>	-1.57	<i>e</i>
Pyrene H(2)	-0.15	-0.68	<i>b</i>	-0.72	<i>e</i>
Benz[e]pyrene H(2)	-0.17	-0.75	<i>c</i>	-0.67	<i>c</i>
Biphenylene H(1)	-0.41	0.62	<i>d</i>	0.64 ^e	<i>f</i>
Biphenylene H(2)	-0.35	0.52	<i>d</i>	0.77 ^e	<i>f</i>

^a Shieldings in parts per million with respect to benzene. ^b Reference 19. ^c Reference 30. ^d H. P. Figeys, *Chem. Commun.*, 495 (1967). ^e Reference 24. ^f Reference 33. ^g These assignments are not proven and may be reversed (H. P. Figeys, *Chem. Commun.*, 495 (1967)).

[e]pyrene H(2) are substantially greater than those calculated from the δ vs. F_r regression equation. For both types of proton in biphenylene, the above equation predicts deshieldings with respect to benzene instead of the large shieldings observed experimentally. On the other hand, shifts calculated from ring-current theory agree well with experiment for all five protons (Table III). Since coronene, pyrene, and benz[e]pyrene are compact platelike hydrocarbons, ring-current contributions to δ are larger than for the more open-



chain compounds which comprise the majority of alternants in Table I. F_r values, on the other hand, which reflect only the immediate environment of the carbon position, are typical of non-*peri* (pyrene and

(56) J. A. Fisher and F. Yates, "Statistical Tables," 6th ed, Oliver and Boyd, Edinburgh, 1963, p 63.

(57) D. W. J. Cruickshank, *Tetrahedron*, **17**, 155 (1962).

(58) J. A. Pople, *J. Chem. Phys.*, **24**, 1111 (1956).

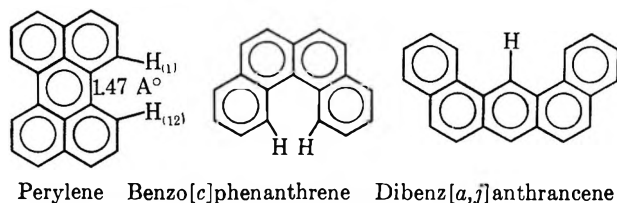
(59) J. S. Waugh and R. W. Fessenden, *J. Amer. Chem. Soc.*, **79**, 846 (1957).

(60) C. E. Johnson and F. A. Bovey, *J. Chem. Phys.*, **29**, 1012 (1958).

(61) D. G. Farnum and C. F. Wilcox, *J. Amer. Chem. Soc.*, **89**, 5379 (1967).

benz[e]pyrene) and *peri* (coronene) positions. Simple ring-current theory cannot explain why biphenylene protons resonate at higher field than those of benzene. Recently, Figeys⁶² has found that, for the four-membered ring in biphenylene, the reverse or paramagnetic current characteristic⁶³ of $4n$ π -systems more than outweighs the diamagnetic currents for the six-membered rings; thus both protons in biphenylene have a large net shielding compared with those of polyacene positions with similar F_r values.

Although the correlation between δ and F_r for alternant positions which are sterically hindered to varying degrees (Table II, row 2) appears to be significant, it also is fortuitous. Of those protons which are similarly hindered in "bay" situations and hence presumably subject to comparable σ -bond anisotropy-van der Waals influences, 11 are NN-NJ ($F_r = 0.439$ - 0.455) and 4 are NJ-NJ; as argued above, the latter are more deshielded and, for different reasons, have larger values of F_r (0.498 - 0.502). Of the three shifts which deviate most from the line, H(1) of perylene is less hindered than the other protons in group 2, owing to the long C-C bond,⁶⁴ while both H(1) of benzo[*c*]phenanthrene ("fjord") and H(14) of dibenz[*a,j*]anthracene (double "bay") are more hindered.



Chemical shifts of nonalternant hydrocarbons are only fairly significantly correlated with F_r (row 3, Table II); restriction of the values to benzenoid protons produces better correlation (row 4). Two factors make interpretation of these results more difficult than for alternants; first, nonuniform charge densities may make quite large shift contributions; second, the currents in rings containing fewer than six carbon atoms have not been calculated for all these compounds; for the cases where they have been calculated, these currents are diamagnetic.⁶⁶

F_r values for benzenoid positions in nonalternants also fall into three groups, corresponding to proximity to an increasing number of rings: (a) flanked by bonds NN and NN, 0.395 - 0.409 ; (b) flanked by bonds NN and NJ, 0.438 - 0.478 ; and (c) flanked by bonds NJ and NJ, 0.497 (one only).

Plots of δ for nonsterically hindered methyl and ethyl protons *vs.* F_r value at the same position in the unsubstituted parent hydrocarbon, together with the regression data in rows 5-7 of Table II, provide further support for the ring-current explanation of chemical shifts in polynuclears. Even though the CH_3 and CH_2CH_3 protons are separated from the aromatic carbon atoms

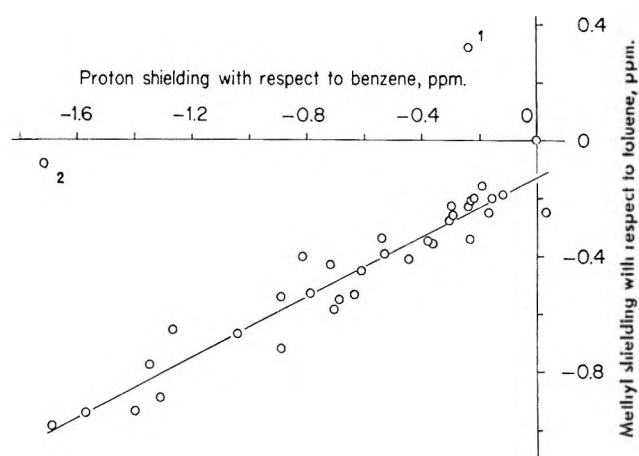


Figure 1. Graph of methyl shielding (parts per million relative to toluene) *vs.* proton shielding (parts per million relative to benzene). The regression line, $\delta_{CH_3} = 0.51\delta_H - 0.13$ is calculated with divergent points (1) 2,2'-dimethylbiphenyl, (2) 1-methylbenzo[*c*]phenanthrene) excluded.

Table IV: Correlation (r) and Regression (a and b) Coefficients for Relation $\delta_x = a\delta_H + b$

x^a	No. of compounds	r	a	b	Significance level %
Methyl	34	0.961	0.511	-0.130	0.1
CH_2 of ethyl	11	0.961	0.607	-0.049	0.1
CH_3 of ethyl	11	0.948	0.226	-0.043	0.1

^a x includes compounds listed in Table I except where specified in the text.

by two σ bonds, their shifts still correlate well with the π index, F_r . Moreover, those points which show greatest deviations from the regression lines are again well explained by ring-current theory. For 2-methylpyrene and ethyl- and methylcoronene, the same argument applies as was used with pyrene and coronene in Table III. In 2,2'-dimethylbiphenyl and 2-ethylbiphenyl, substituent groups are *shielded* since, as uv evidence suggests,⁶⁶⁻⁶⁸ they are held above the ring plane.

Although the deviations for ethylcoronene and 2-ethylbiphenyl evidently reduce the r value in the CF_2 - CH_3 graph of δ *vs.* F_r , the degree of correlation for both the CH_3 and CH_2CH_3 graphs is similar to these for aromatic protons (Table II). This is not unexpected in

(62) H. P. Figeys, *Chem. Commun.*, 495 (1967).

(63) J. A. Pople and K. G. Untch, *J. Amer. Chem. Soc.*, **88**, 4811 (1966).

(64) A. Camerman and J. Trotter, *Proc. Roy. Soc.*, **A279**, 629 (1964).

(65) J. A. Pople, *Mol. Phys.*, **1**, 175 (1958).

(66) G. H. Beaven, "Steric Effects in Conjugated Systems," H. B. Gray, Ed., Butterworth and Co. Ltd., London, 1958, p 22.

(67) G. H. Beaven and E. A. Johnson, "Conference on Molecular Spectroscopy," E. Thornton and H. W. Thompson, Ed., Pergamon Press, London, 1959, p 78.

(68) S. F. Mason, *Quart. Rev. (London)*, **15**, 287 (1961).

view of correlation between δ_{CH_3} and the corresponding unsubstituted δ_{H} noted earlier by MacLean and Mackor³⁹ for seven compounds and extended in Figure 1 to include additional methyl polynuclears; analogous plots can be made for CH_2 and CH_3 shifts in ethyl polynuclears. The regression data in Table IV have been calculated for all positions given in Table I, apart from the special cases in which the methyl group suffers shielding from its location above the ring plane.^{69,70} All three groups of shifts are highly significantly related to δ_{H} ; for CH_3 and CH_2CH_3 , the gradients (a) are

similar, while, for the CH_2CH_3 protons more remote from the ring centers, the gradient is lower.

Acknowledgments. We are grateful to Mr. R. L. Cureton, who provided a computer program for calculating regression parameters. This work was carried out during the tenure of an I.C.I. Fellowship by K. D. B.

(69) M. S. Newman and M. Wolf, *J. Amer. Chem. Soc.*, **74**, 3225 (1952).

(70) A. W. Johnson, *J. Org. Chem.*, **24**, 833 (1959).

Moving Boundary Measurement of Transference Numbers

by Paul Milios and John Newman

Inorganic Materials Research Division, Lawrence Radiation Laboratory, and Department of Chemical Engineering, University of California, Berkeley, California (Received March 8, 1968)

A moving-boundary system is analyzed, and an equation, valid for concentrated as well as dilute solutions, is obtained for the transference number. When the partial molal volume of the solvent is constant through the boundary, the equation reduces to the approximate equation now in common use. The cation transference number in 0.213 *M* NH_4NO_3 was experimentally determined at 25° and found to be 0.5140 ± 0.0024 .

Introduction

Moving-boundary measurements date back to the nineteenth century.¹ The two-salt boundary was analyzed in 1900 by the mathematician Weber.² In 1910, the chemist Lewis³ presented an analysis which corrected for the boundary movement caused by the electrode reaction. His equation was thought to be restricted to dilute solutions¹ until Bearman,⁴ in 1962, showed that it actually applies to systems in which the partial molal volumes are constant through the boundary—a slightly less stringent condition. No other theoretical progress has yet been made, and Lewis's equation is still used today.⁵ In the present work a more detailed analysis of the moving-boundary system yields an expression of more general validity for the transference number.

Analysis of the Two-Salt Boundary

Figure 1 shows the two-salt boundary at steady state. Solution A is composed of ions 1 and 3 and, being the lighter of the two solutions, is above solution B, which is composed of ions 2 and 3. The solvent is referred to by "O."

The equations necessary to describe the moving-boundary system are the continuity equation or material balance

$$\frac{\partial c_i}{\partial t} = -\frac{\partial c_i v_i}{\partial x} \quad (1)$$

an equation relating the current density to the fluxes

$$i = F \sum_i z_i c_i v_i \quad (2)$$

a statement of electroneutrality

$$\sum_i z_i c_i = 0 \quad (3)$$

and a flux or transport equation

$$c_i \frac{\partial \mu_i}{\partial x} = RT \sum_j \frac{c_i c_j}{c_T \mathfrak{D}_{ij}} (v_j - v_i) \quad (4)$$

where μ_i is the electrochemical potential and where $\mathfrak{D}_{ij} = \mathfrak{D}_{ji}$. These equations are discussed in detail by Newman.⁶

When the motion of the ions is referred to the solvent motion, the transference number (relative to the solvent velocity) is defined as the fraction of the current carried by an ion in a solution of uniform composi-

(1) D. A. MacInnes and L. G. Longworth, *Chem. Rev.*, **11**, 171 (1932).

(2) (a) H. Weber, *Sitzber. Deut. Akad. Wiss. Berlin*, 936 (1897); (b) H. Weber, "Die partiellen Differential-gleichungen der mathematischen Physik," Friedrich Vieweg und Sohn, Braunschweig, 1900, pp 481-506.

(3) G. N. Lewis, *J. Amer. Chem. Soc.*, **32**, 862 (1910).

(4) R. J. Bearman, *J. Chem. Phys.*, **36**, 2432 (1962).

(5) R. Haase, G. Lehnert, and H.-J. Jansen, *Z. Phys. Chem. (Frankfurt am Main)*, **42**, 32 (1964).

(6) J. Newman, *Advan. Electrochem. Electrochem. Eng.*, **5**, 87 (1967).

tion, that is

$$t_+ = \frac{z_+ c_+ (v_+ - v_0)}{z_+ c_+ (v_+ - v_0) + z_- c_- (v_- - v_0)} \quad (5)$$

for a solution of two ions. In terms of the transport properties this becomes

$$t_+ = \frac{z_+ \mathcal{D}_{+0}}{z_+ \mathcal{D}_{+0} - z_- \mathcal{D}_{-0}} \quad (6)$$

By an analysis similar to that of Weber, but with a transport eq 4 applicable in concentrated solutions, these equations can be manipulated to yield the exact relationships

$$t_1 = \frac{F}{i} \frac{z_3 c_3}{c_0} \Big|_{x=-\infty} [c_0 (v_0 - v_b)] \quad (7)$$

$$t_2 = \frac{F}{i} \frac{z_3 c_3}{c_0} \Big|_{x=+\infty} [c_0 (v_0 - v_b)] \quad (8)$$

where v_b is the velocity of the boundary, the subscript $x = -\infty$ indicates that c_3/c_0 must be evaluated in solution A above the boundary, and the subscript $x = +\infty$ indicates that c_3/c_0 must be evaluated in solution B below the boundary.

This derivation is effected by observing that the system is in a steady state in a coordinate frame which moves with the velocity v_b of the boundary. Equation 1 then becomes

$$c_i (v_i - v_b) = \text{constant} \quad (9)$$

for all species, and

$$v_1 = v_2 = v_b \quad (10)$$

since the concentrations c_1 and c_2 are zero either above or below the boundary. Equation 2 then gives

$$v_3 = v_b + i/z_3 c_3 F \quad (11)$$

The transport relation 4 for ions 1 and 3 now takes the forms

$$\frac{\partial \mu_1}{\partial x} = \frac{RT}{c_T} \left[\frac{c_0 (v_0 - v_b)}{\mathcal{D}_{10}} + \frac{c_3 (v_3 - v_b)}{\mathcal{D}_{13}} \right] \quad (12)$$

$$\frac{\partial \mu_3}{\partial x} = \frac{RT}{c_T} \left[\frac{c_0 (v_0 - v_b)}{\mathcal{D}_{30}} - \left(\frac{c_0}{\mathcal{D}_{30}} + \frac{c_2}{\mathcal{D}_{31}} + \frac{c_2}{\mathcal{D}_{32}} \right) (v_3 - v_b) \right] \quad (13)$$

The chemical potential μ_A of the neutral salt A is defined in terms of the ion electrochemical potentials as

$$\mu_A = v_1 \mu_1 + v_3^A \mu_3 = v_1 (\mu_1 - z_1 \mu_3 / z_3) \quad (14)$$

where $v_3^A = -z_1 v_1 / z_3$. Hence eq 11 and 12 yield

$$\frac{\partial \mu_A}{\partial x} = \frac{v_1 RT}{c_T} \left[(v_0 - v_b) \left(\frac{c_0}{\mathcal{D}_{10}} - \frac{z_1 c_0}{z_3 \mathcal{D}_{30}} \right) + (v_3 - v_b) \left(\frac{z_1 c_0}{z_3 \mathcal{D}_{30}} + \frac{z_1 c_1}{z_3 \mathcal{D}_{31}} + \frac{z_1 c_2}{z_3 \mathcal{D}_{32}} + \frac{c_3}{\mathcal{D}_{13}} \right) \right] \quad (15)$$

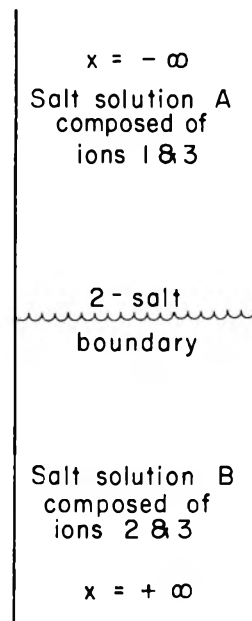


Figure 1. The 2-salt boundary.

As $x \rightarrow -\infty$, one approaches the region of uniform concentration of salt A above the boundary. Here $c_2 \rightarrow 0$ and $\partial \mu_A / \partial x \rightarrow 0$, and eq 15 becomes

$$\frac{v_0 - v_b}{v_3 - v_b} \Big|_{x=-\infty} = \frac{z_1 \mathcal{D}_{10}}{z_1 \mathcal{D}_{10} - z_3 \mathcal{D}_{30}} = t_1 \quad (16)$$

Equation 7 is then obtained by the elimination of $v_3 - v_b$ through eq 11. Equation 8 for t_2 in solution B can be derived in a similar manner by noting that $c_1 \rightarrow 0$ and $\partial \mu_B / \partial x \rightarrow 0$ as $x \rightarrow +\infty$.

It should be noted that eq 16 can be obtained directly from 5 since both equations apply to a medium containing two ion types and of uniform composition. Thus the steps from eq 11 on can be bypassed. These steps merely show that the modern theory of multicomponent diffusion is self-consistent with respect to the basic definition 5 of the transference number. Such a theory would be necessary for calculating the detailed concentration profiles in the two-salt boundary and the thickness of this boundary and for showing that the steady boundary is stable if the current is passed in one direction, but not if it is passed in the opposite direction. Incidentally, the thickness of the boundary can be shown to be inversely proportional to the current density, and, roughly speaking, the boundary is stable if the direction of current is such that

$$z_1 i t_1 < z_1 i t_2$$

i.e., the leading solution should have the higher conductivity. The detailed transport theory is not necessary if one is interested only in the conditions on the two sides of the sharp boundary. Similar situations are encountered in the treatments of a hydraulic jump and of a planar shock wave in a compressible gas.

Equations 7 and 8 are the principal result of the anal-

ysis of the two-salt boundary, and they immediately yield the Kohlrausch regulating function¹

$$\frac{t_1}{t_2} = \frac{[c_3/c_0]_{x=-\infty}}{[c_3/c_0]_{x=+\infty}} \quad (17)$$

This is identical with the relation derived by Smits and Duyvis⁷ in their criticism of work done separately by Bearman,⁴ Haase,⁸ and Spiro.⁹ If the concentration of the solution following the boundary does not initially satisfy the Kohlrausch regulating function, it will adjust itself so that it does. In this case a concentration boundary between the initial solution and that following the boundary will be left behind as the two-salt boundary progresses up or down the channel. This boundary between solutions of two different concentrations of the following ion has been studied optically by Longworth.¹⁰

The "Volume Correction." In eq 7 and 8, the term $c_0(v_0 - v_b)$ is the solvent flux relative to the boundary and is constant through the boundary. The application of these equations requires the determination of v_0 either above or below the two-salt boundary. Usually one electrode is selected with a well-defined reaction, and this electrode chamber is tightly closed so that the volume changes at the electrode can be assessed. Thus the system shown in Figure 1 must be expanded to include the closed electrode chamber. Figure 2 shows this arrangement with the two-salt boundary and a concentration boundary, formed as described in the preceding paragraph.

To illustrate the method of assessing volume effects,

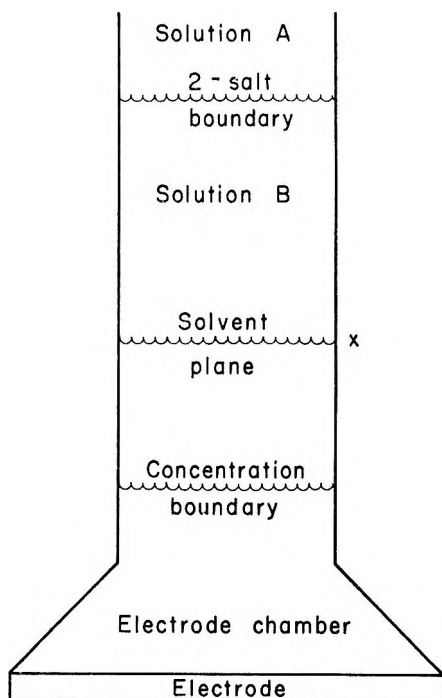


Figure 2. The closed electrode.

let the electrode reaction be that of metal dissolution, with the two-salt boundary progressing up the channel, so that solution A is the leading solution. This is the usual arrangement for determining t_1 . On account of the dissolution process, the concentration of solution B near the electrode will be higher than its initial value. The solvent velocity v_0 in the solution below the two-salt boundary can be calculated by means of material balances over the region below a plane x fixed in the solvent (see Figure 2), allowance being made for the dissolution of the anode, the concentration dependence of the density of solution B, and transference of ions across the solvent plane.

Consider a volume V_0 bounded by the electrode and by the plane x moving with the solvent velocity v_0 . This volume changes with time as

$$\frac{dV_0}{dt} = \frac{d}{dt} \int_{V_0} dV = -v_0 A - \frac{I}{z_+ F} \frac{M_a}{\rho_a} \quad (18)$$

where A is the cross-sectional area of the channel, I is the total current (negative for an anode), and M_a and ρ_a are the atomic weight and density of the anode. The first term on the right represents the displacement of the solvent plane, and the second term represents the volume rate of dissolution of the anode. Since the amount of solvent in the volume V_0 remains constant, a material balance on the solvent yields

$$\frac{d}{dt} \int_{V_0} c_0 dV = 0 \quad (19)$$

while a material balance on the electrolyte gives

$$\frac{d}{dt} \int_{V_0} c_+ dV = \frac{It_+}{z_+ F} - \frac{I}{z_+ F} \quad (20)$$

The first term on the right represents the transport of cations across the solvent plane, and the second term represents the contribution of cations due to dissolution of the anode.

An assumption is now made which allows for the explicit determination of the transference number. Assume that the density of solution B below the solvent plane at x is linearly related to its concentration

$$\rho_B = \alpha_B + \beta_B c_B \quad (21)$$

Since

$$\rho_B = M_B c_B + M_0 c_0 \quad (22)$$

this implies that

$$c_0 B = \alpha_B + \beta_B c_B = \alpha_B + \beta_B c_+ / \nu_+^B \quad (23)$$

(7) L. J. M. Smits and E. M. Duyvis, *J. Phys. Chem.*, **70**, 2747 (1966).

(8) R. Haase, *Z. Phys. Chem. (Frankfurt am Main)*, **39**, 27 (1963).

(9) M. Spiro, *J. Chem. Phys.*, **42**, 4060 (1965).

(10) L. G. Longworth, *J. Amer. Chem. Soc.*, **66**, 449 (1944).

where

$$a_B = \alpha_B/M_0; \quad b_B = (\beta_B - M_B)/M_0 \quad (24)$$

Equation 19 then becomes

$$a_B \frac{d}{dt} \int_{V_0} dV + \frac{b_B}{\nu_+^B} \frac{d}{dt} \int_{V_0} c_+ dV = 0 \quad (25)$$

Substitution of eq 18 and 20 then gives the desired relation for v_0

$$a_B v_0 A + \frac{a_B I}{z_+ F} \frac{M_e}{\rho_e} = \frac{b_B}{\nu_+^B} \frac{I}{z_+ F} (t_+ - 1) \quad (26)$$

or

$$v_0 = -\frac{i}{F} \left[\frac{M_e}{z_+ \rho_e} + \frac{1 - t_+}{z_+ \nu_+^B} \frac{b_B}{a_B} \right] \quad (27)$$

Finally, substitution of this equation into eq 7 with elimination of t_+ (here ion 2 is the cation reacting at the electrode) by means of eq 8 yields¹¹

$$t_1 = -a_B \frac{z_3 c_3}{c_0} \Big|_{x=-\infty} \left[\frac{FV}{It} + \frac{M_e}{z_2 \rho_e} + \frac{b_B}{z_2 \nu_2 a_B} \right] \quad (28)$$

where V is the volume through which the boundary moves when current I is passed for time t .

For eq 28 to be fruitfully applied to a system, eq 23 must be a good approximation. If the density of the following solution is given by

$$\rho = k_1 + k_2 c + k_3 c^{3/2} + k_4 c^2 \quad (29)$$

then the solvent concentration is

$$c_0 = e + fc + gc^{3/2} + hc^2 \quad (30)$$

where

$$\left. \begin{aligned} e &= k_1/M_0; & f &= (k_2 - M)/M_0 \\ g &= k_3/M_0; & h &= k_4/M_0 \end{aligned} \right\} \quad (31)$$

rather than eq 23. A least-squares fit of eq 23 to eq 30 over the concentration range of interest, from c to $(1 + \epsilon)c$, yields

$$a = e - \frac{1}{2} g c^{3/2} \left[1 + \frac{3}{4} \epsilon + \frac{1}{80} \epsilon^2 + 0(\epsilon^3) \right] - hc^2 \left(1 + \epsilon + \frac{1}{6} \epsilon^2 \right) \quad (32)$$

and

$$b = f + \frac{3}{2} g c^{1/2} \left[1 + \frac{1}{4} \epsilon + 0(\epsilon^2) \right] + 2hc \left(1 + \frac{1}{2} \epsilon \right) \quad (33)$$

where 0 indicates the order of neglected terms.

Application

If the following solution is initially prepared so that its concentration is less than that required by the Kohlrausch relation, eq 17, then eq 32 and 33 are immediately applicable with the initially prepared value of the

concentration equal to c and with ϵ equal to either ϵ_1 in the anode chamber or ϵ_2 across the concentration boundary, whichever is larger.

If the initially prepared following solution is of higher concentration than that required by the Kohlrausch relation, one can, with little error, approximate ϵ by $\epsilon_1 + \epsilon_2$ and take c to be the initially prepared concentration (rather than the lowest concentration of solution B present).

The value ϵ_2 due to the Kohlrausch adjustment must be experimentally minimized or measured. The part ϵ_1 due to the electrode reaction can be calculated from one of the following approximate equations.¹¹ For a uniform concentration in the anode chamber (an unlikely situation)

$$\epsilon_1 \approx V/U \quad (34)$$

where U is the volume of the anode chamber. If the anode can be treated as a vertical electrode with free convection

$$\epsilon_1 = \frac{1.62}{c} \left(\frac{It_-}{z_+ \nu_+ F D A_e} \right)^{0.8} \left(\frac{\nu D L}{g \beta} \right)^{0.2} \approx \frac{0.00932}{c} \left(\frac{I}{z_+ \nu_+ A_e} \right)^{0.8} \left(\frac{L}{\beta} \right)^{0.2} \quad (35)$$

where in the latter expression I is the current in mA, A_e is the effective electrode area in cm², c is in mol/l., L is the effective electrode height in cm, and $\beta = (1/\rho) d\rho/dc$ is in l./mol. The latter expression is based on a diffusion coefficient D of 10⁻⁵ cm²/sec, a transference number t_- of 0.5, a kinematic viscosity ν of 10⁻² cm²/sec, and a gravitational acceleration g of 10³ cm/sec².

For a horizontal electrode

$$\epsilon \approx \frac{1}{A_e} \sqrt{\frac{2IV}{\pi z_+ \nu_+ F D c}} \approx \frac{0.8}{A_e} \sqrt{\frac{IV}{z_+ \nu_+ c}} \quad (36)$$

where in the latter expression A_e is in cm², I is in mA, V is in cm³, c is in mol/l., and the value $t_- = 0.5$ has been assumed.

Discussion

Equations 7 and 8 are exact relations describing the two-salt boundary. Equation 28, relating the transference number to the experimentally measured quantities, depends additionally only on the very good approximation of a linear concentration dependence of the density of solution B over the range of concentrations encountered between the electrode and the two-salt boundary. Equation 28 is derived without ever referring to the details of the two-salt boundary itself. In particular, no assumptions are made concerning the partial molal volume of the solvent through the boundary or of the density variation within the boundary.

(11) P. Milios, "A Theoretical Analysis of the Moving Boundary Measurement of Transference Numbers," Master's Thesis, University of California, Berkeley, Sept 1967 (UCRL-17807).

For the system being analyzed, the equation of the type derived by Lewis^{1,3} is

$$t_1^L = -\frac{z_3 c_3(-\infty)}{1 - c_A \bar{V}_A} \left[\frac{FV}{It} + \frac{\bar{V}_e}{z_2} - \frac{\bar{V}_B}{z_2 \nu_2} \right] \quad (37)$$

It can be shown¹¹ that

$$t_1^L/t_1 = a_A/a_B = \bar{V}_{0B}/\bar{V}_{0A} \quad (38)$$

where a_A is given by an equation analogous to eq 23. Thus eq 28 reduces to a Lewis-type equation in the special case where the partial molal volume of the solvent is constant through the boundary, precisely the assumed situation in the derivation of the Lewis-type equation.

In the present analysis a consequence of the assumed concentration-density relationship below the two-salt boundary is that the partial molal volume of the solvent below the boundary is constant. The distinction to be made is that this consequence refers to "below" the boundary while the assumption associated with the Lewis-type equation refers to "through" the boundary. In the general case it is not necessary to consider the partial molal volume of the solvent in the analysis of the two-salt boundary.

In applications, eq 28 is not very sensitive to the value of ϵ , but it is of course better to keep ϵ small. For most situations encountered, eq 35 and 36 indicate that the use of a vertical anode results in an appreciably smaller value of ϵ_1 than a horizontal electrode. Then the linear approximation, eq 23, is better, and a_B is more accurately known. This should be expected since with a vertical electrode there is a tendency toward a uniform concentration in the anode chamber (the optimum case), while with the horizontal electrode stratified layers of solution form with very little mixing. Equation 36 suggests that an autogenic boundary (one formed with solution A initially adjacent to the electrode surface) should not be used since then ϵ_1 is very large—either A_0 is small or V is large—and the analysis is not applicable.

In the derivation of eq 28, it was assumed that ion 2 is the cation reacting at the electrode. If, on the other hand, the common ion 3 is positive, eq 28 should be replaced by

$$t_1 = a_B \frac{z_3 c_3}{c_0} \Big|_{z=-\infty} \left[-\frac{Fv_b}{i} - \frac{M_e}{z_3 \rho_e} \right] \quad (39)$$

where v_b and i now have opposite signs. If the boundary moves down the channel, eq 28 or 39 is still applicable, but now the concentration boundary is above the two-salt boundary, and ion 2 is the leading ion. If the electrode operates as a cathode, ϵ_1 should be taken to be negative.

The analysis treats an electrode involving metal dissolution or deposition. The analysis can be modified

to treat other cases with well-defined volume changes at the electrode.

The transference number of the leading ion can always be determined more accurately than that of the following ion, since the concentration is known. The transference number of the following ion can be calculated from eq 17 if the concentration difference across the concentration boundary is determined, say, in the manner of Longworth.¹⁰ The uncertainty in the concentration so determined must be added to the uncertainty in the transference number of the leading ion in order to determine the uncertainty in the following-ion transference number.

Experimental Section

The transference number of 0.213 *M* NH_4NO_3 at 25° was determined¹¹ with AgNO_3 as the following solution. A standard Tiselius cell with a closed vertical silver anode was used. Equation 32 was used to calculate a_B , with eq 35 being used to calculate ϵ_1 and ϵ_2 being measured by a Rayleigh interference optical method. All other procedures were standard methods for moving-boundary measurements.

Equation 28 yielded the result $t_+ = 0.5140 \pm 0.0024$. Other than the value $t_+ = 0.5130$ at 0.1 *M* determined by MacInnes and Cowperthwaite,¹² this is the only value measured for NH_4NO_3 . The value at infinite dilution, calculated from the limiting ionic mobilities of the ions,¹³ is 0.507.

Equation 17 was used to estimate the cation transference number of the following AgNO_3 solution. The result $t_+ = 0.467 \pm 0.009$ at a concentration of 0.195 *M* can be compared with the work of Haase, *et al.*,⁵ 0.4708 and 0.4723 (two determinations) at 0.1995 *M*, calculated from a Lewis-type equation. If reasonable values are assumed for the concentration range of the following solution used by Haase, his data can be re-evaluated with eq 28 to yield the results 0.4693 and 0.4708, respectively.

Summary

An equation for the transference number, applicable at high as well as low concentrations, was presented. The difference between the present equation and the approximate equation now in common use lies in the calculation of the volume changes which accompany transference number measurements.

The equation in common use was originally arrived at by an intuitive approach and accounts for volume changes across the two-salt boundary. Approximations are thus introduced which limit the usefulness of the equation to dilute solutions.

The present equation is derived from fundamental equations. It is seen that once a steady-state concen-

(12) D. A. MacInnes and I. A. Cowperthwaite, *Trans. Faraday Soc.*, **23**, 400 (1927).

(13) G. Milazzo, "Electrochemistry," Elsevier Publishing Co., Amsterdam, 1963.

tration profile is established in the two-salt boundary, no changes take place across the two-salt boundary which affect the determination of the transference number. Rather, the volume corrections are dependent only upon what takes place in the region from the electrode in the closed electrode assembly to, but not including, the two-salt boundary. The approximation is made that, in this region, the concentration of solvent is linear with respect to the concentration of solute, $c_0 = a + bc$. This approximation does not greatly limit the usefulness of the transference number equation.

Equations are presented which allow the calculation of the quantities a and b if the density of the solution is known as a function of concentration and the concentrations on both sides of the Kohlrausch concentration boundary are known. The transference number of 0.213 M NH_4NO_3 was measured at 25°.

Acknowledgment. This work was supported by the U. S. Atomic Energy Commission.

Nomenclature

a_B	Defined by eq 23
A	Area of channel, cm^2
A_e	Surface area of electrode, cm^2
b_B	Defined by eq 23
c_i	Concentration of species i , mol/cm^3
c_T	Total solution concentration, mol/cm^3
D	Diffusion coefficient of salt, cm^2/sec
\mathfrak{D}_{ij}	Diffusion coefficient for binary interactions, cm^2/sec
e, f, g, h	Defined by eq 30 and 31

F	Faraday's constant, 96,493 C/equiv
g	Acceleration of gravity, cm/sec^2
i	Current density, A/cm^2
I	Current, A
k_1, k_2, k_3, k_4	Defined by eq 29
L	Electrode height, cm
M_i	Molecular weight of substance i , g/mol
R	Universal gas constant, J/mol-deg
t	Time, sec
t_i	Transference number of species i
t_i^L	Transference number of species i as calculated using a Lewis-type volume correction, see eq 37
T	Temperature, °K
U	Volume of anode chamber, cm^3
v_b	Velocity of the two-salt boundary, cm/sec
v_i	Velocity of species i , cm/sec
V	Volume through which the two-salt boundary moves, cm^3
\bar{V}_i	Partial molal volume of component i , cm^3/mol
x	Distance variable, cm
z_i	Charge number of species i
β	Coefficient of expansion, cm^3/mol
ϵ	Range of concentrations of solution B present below the two-salt boundary, relative to the lowest concentration in that range
ϵ_1	Relative concentration range in electrode chamber
ϵ_2	Relative concentration change across concentration boundary
μ_i	Electrochemical potential of species i , J/mol
ν	Kinematic viscosity, cm^2/sec
ν_+, ν_-	Numbers of cations and anions produced by the dissociation of one molecule of electrolyte
ρ	Density of solution, g/cm^3
ρ_e	Density of electrode metal, g/cm^3

Sorption of Water Vapor and of Nitrogen by Genetic Variants of α_{s1} -Casein

by E. Berlin, B. A. Anderson, and M. J. Pallansch

Dairy Products Laboratory, Eastern Utilization Research and Development Division, Agricultural Research Service, U. S. Department of Agriculture, Washington, D. C. 20250 (Received April 15, 1968)

Water vapor sorption by dried preparations of α_{s1} -caseins A and C was measured at 24.2°. At lower relative pressures, both forms sorbed identical amounts of water, while at intermediate to higher relative pressures the A variant sorbed more water. A reproducible hysteresis loop was observed over the entire isotherm through two successive sorption-desorption cycles. Treatment of the H_2O sorption data and nitrogen adsorption data according to the Frenkel-Halsey-Hill isotherm equation allowed for clear distinction between the natures of the sorption processes involved with H_2O and N_2 .

Introduction

It is widely accepted that proteins sorb water vapor by binding water molecules to specific hydrophilic sites at lower relative humidities followed by condensation or multimolecular adsorption as the humidity increases.^{1,2} The nature of these hydrophilic sites has, however, been the subject of much research, and there is no general

agreement at present concerning the chemical groupings in proteins to which water is bound.³ The nature of these binding sites has been studied indirectly by com-

(1) L. Pauling, *J. Amer. Chem. Soc.*, **67**, 555 (1945).

(2) A. D. McLaren and J. W. Rowen, *J. Polym. Sci.*, **7**, 289 (1951).

(3) F. Haurowitz, "The Chemistry and Function of Proteins," 2nd ed, Academic Press, New York, N. Y., 1963, p 118.

paring the H₂O sorption capacity of proteins with that of chemically modified forms of the same proteins and more directly by using such techniques as infrared spectroscopy.^{4,5}

Chemical modifications of such proteins as keratin and casein have been related to changes in water vapor sorption isotherms for these proteins. Leeder and Watt⁶ used deamination techniques to demonstrate that the binding of water by amino groups constitutes a large percentage of the sorption capacity of keratin. Mellon, *et al.*,⁷ found that benzylation of amino groups reduced the water binding capacity of casein, particularly at low relative pressure. Kanagy and Cassel⁸ obtained similar results with collagen after deamination, acetylation, and esterification treatments.

Though these modification techniques have been used to determine the role of particular polar groups in water binding, some investigators⁶ have been concerned that these alterations of the protein by chemical reactions, particularly those which introduce new groups, may give effects other than the desired specific reaction. Therefore, more direct techniques which do not alter the protein studied are preferable.

The existence of different genetic polymorphs of α_{s1} -casein⁹ has made it possible for us to compare the water vapor sorption properties of two proteins which are almost identical chemically and physiologically. These polymorphs differ only slightly in electrophoretic mobility on starch gel¹⁰ and in amino acid composition.¹¹ By considering these protein forms, it is possible to study the effects of minor differences in amino acid composition of a protein upon its water vapor sorption properties without resorting to chemical modification of the protein.

This paper presents data for water vapor sorption and low-temperature nitrogen adsorption by two genetic variants of α_{s1} -casein.

Experimental Section

Samples of the genetic variants α_{s1} -casein A and α_{s1} -casein C, prepared by the method of Thompson and Kiddy,¹² were furnished by Dr. M. P. Thompson of the Eastern Regional Laboratory, U. S. Department of Agriculture, Philadelphia, Pa. Both protein preparations were dried by lyophilization.

Water vapor sorption by these proteins at 24.2° was determined gravimetrically. Samples of each of the proteins were subjected to two successive sorption-desorption cycles, and single adsorption runs were measured with additional samples of the caseins. These measurements were made using the Cahn RG recording electrobalance incorporated into a glass adsorption apparatus equipped with suitable accessories for outgassing the powders and controlling and monitoring water vapor pressure. Complete details of the apparatus and experimental technique have been presented in detail in a previous publication.¹³

Nitrogen adsorption, at -195°, was measured over the relative pressure range $0.1 < P/P_0 < 0.8$ by conventional volumetric techniques.

Results and Discussion

The water vapor sorption data yielded sigmoid type II isotherms as shown in Figures 1 and 2. Both α_{s1} -caseins displayed hysteresis loops over almost the entire relative pressure range, with the curves for the second sorption-desorption cycle essentially coinciding with those of the first cycle. The second cycle loop may be somewhat smaller for the α_{s1} -casein A (Figure 2) in the lower relative pressure range, while both loops are perfectly coincident for the α_{s1} -casein C (Figure 1). Excellent agreement was observed between data for initial sorption runs on different samples of the caseins.

The sorption legs only of these isotherms are compared in Figure 3. At lower relative pressure values, up to $0.25P_0$, the isotherms for the two α_{s1} -casein forms are almost exactly superimposable; however, at intermediate to higher relative pressures α_{s1} -casein A sorbed more H₂O than α_{s1} -casein C.

The difference in sorption capacity between the α_{s1} -caseins was not very great, yet it was a clearly reproducible difference. Rates of adsorption did not differ significantly for the two caseins, both normally requiring 8-12 hr for the attainment of equilibrium values at most points over the entire isotherm. Minimum equilibration periods of 24 hr, however, were allowed for all experimental points. Removal of sorbed H₂O after the first sorption-desorption cycle was more difficult with α_{s1} -casein A, requiring a room-temperature evacuation period of 7-10 days at 10^{-6} torr to reach the initial dry weight of the sample, while evacuation for 1-2 days sufficed with the C variant.

Studies of the amino acid composition of the genetically different α_{s1} -caseins A, B, and C by Gordon, *et al.*,¹¹ showed that α_{s1} -casein A is devoid of nine amino acid residues when compared with the B and C variants. Identification of proteolytic digests of the α_{s1} -caseins demonstrated¹⁴ that eight of these amino acids were sequentially deleted from the A variant. From our

(4) S. H. Ehrlich and F. A. Bettelheim, *J. Phys. Chem.*, **67**, 1954 (1963).

(5) M. Folman and D. J. C. Yates, *Trans. Faraday Soc.*, **54**, 1684 (1958).

(6) J. D. Leeder and I. C. Watt, *J. Phys. Chem.*, **69**, 3280 (1965).

(7) E. F. Mellon, A. H. Korn, and S. R. Hoover, *J. Amer. Chem. Soc.*, **69**, 827 (1947).

(8) J. R. Kanagy and J. M. Cassel, *J. Amer. Leather Chemists' Assoc.*, **52**, 248 (1957).

(9) M. P. Thompson, C. A. Kiddy, L. Pepper, and C. A. Zittle, *Nature*, **195**, 1001 (1962).

(10) C. A. Kiddy, J. O. Johnston, and M. P. Thompson, *J. Dairy Sci.*, **47**, 147 (1964).

(11) W. G. Gordon, J. J. Basch, and M. P. Thompson, *ibid.*, **48**, 1010 (1965).

(12) M. P. Thompson and C. A. Kiddy, *ibid.*, **47**, 626 (1964).

(13) E. Berlin, B. A. Anderson, and M. J. Pallansch, *ibid.*, in press.

(14) E. B. Kalan, R. Greenberg, and M. P. Thompson, *Arch. Biochem. Biophys.*, **115**, 468 (1966).

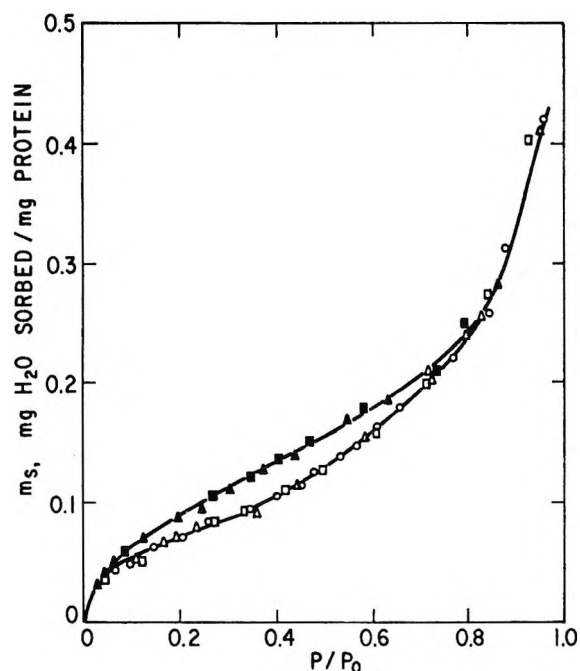


Figure 1. H_2O adsorption-desorption isotherms for α_{s1} -casein C at 24.2° : Δ , adsorption (first cycle); \blacktriangle , desorption (first cycle); \square , adsorption (second cycle); \blacksquare , desorption (second cycle); \circ , first adsorption isotherm on second sample.

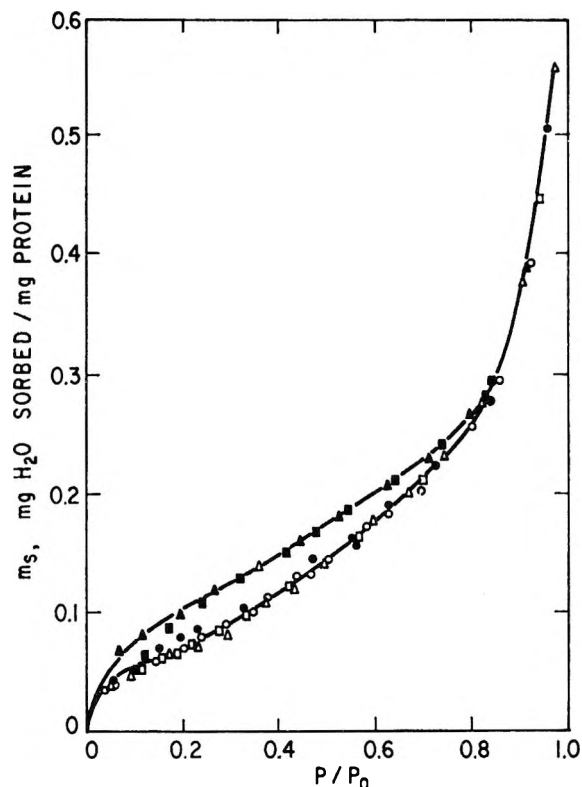


Figure 2. H_2O adsorption-desorption isotherms for α_{s1} -casein A at 24.2° : Δ , adsorption (first cycle); \blacktriangle , desorption (first cycle); \bullet , adsorption (second cycle); \blacksquare , desorption (second cycle); \circ , first adsorption isotherm on second sample; \square , first adsorption isotherm on third sample.

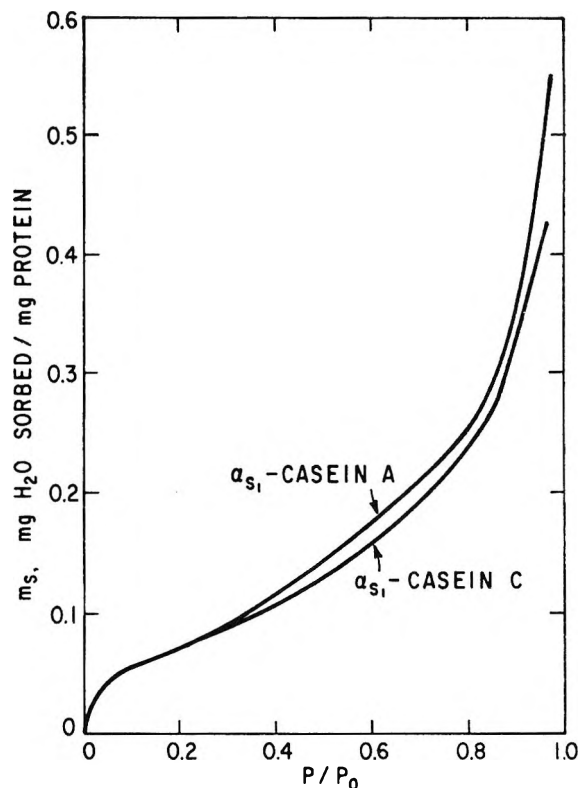


Figure 3. Comparison of H_2O adsorption isotherms for α_{s1} -caseins A and C.

data it is apparent that this peptide segment, which contains the nonpolar amino acids alanine, valine, two phenylalanines, and three leucines and the polar amino acid arginine, does not extensively affect the water binding capacity of these casein forms in the dry state. Thompson, *et al.*,¹⁵ however, reported that the loss of this segment of the molecule has profoundly affected its solubility in aqueous $CaCl_2$ solutions. At temperatures of 10 – 33° , α_{s1} -casein A remains soluble under conditions in which the B and C variants are totally insoluble. Thompson, *et al.*,¹⁵ suggested that the increased solubility of the A variant may be due to less extensive hydrophobic bonding and/or altered protein conformation in solution in the absence of these principally nonpolar amino acid residues. The data reported in this paper together with their solubility data, however, lead to the conclusion that this hydrophobic peptide segment as present α_{s1} -casein C must have a conformation on the surface of the molecule which influences its overall solubility.

There has been wide discussion in the literature^{1,16} concerning the applicability of the BET equation¹⁷ to

(15) M. P. Thompson, H. M. Farrell, Jr., and R. Greenberg, *Comp. Biochem. Physiol.*, in press.

(16) F. Stitt in "Fundamental Aspects of the Dehydration of Foodstuffs," Society of the Chemical Industry, London, England, 1953, p 67. (See also the original references cited in the discussion of sorption theories, p 72.)

(17) S. Brunauer, P. H. Emmett, and E. Teller, *J. Amer. Chem. Soc.*, **60**, 309 (1938).

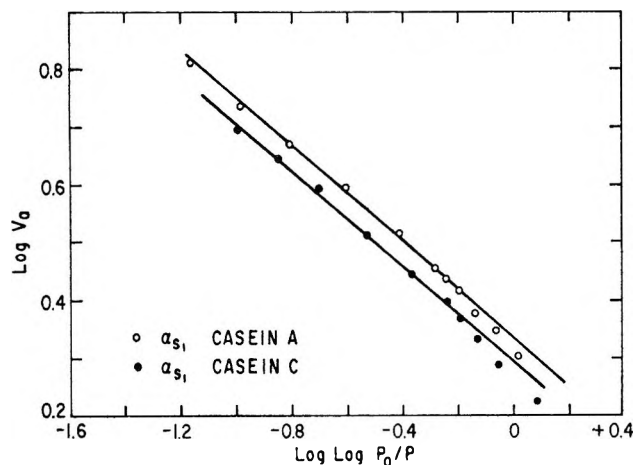


Figure 4. Frenkel-Halsey-Hill isotherm plots for N_2 adsorption at -195° on α_{s1} -caseins (V_a , volume adsorbed as cm^3/g).

the sorption of water vapor by dried proteins or other materials of biological origin. It has been pointed out¹⁸ that the significance of a BET monolayer with regard to vapor sorption in a swelling polymer network is questionable. Treatment of our data for H_2O and N_2 adsorption according to the isotherm equation of Frenkel,¹⁹ Halsey²⁰, and Hill²¹ (FHH) yielded information distinguishing between the sorption processes involved.

Data obtained from N_2 adsorption measurements yielded linear plots, as shown in Figure 4, in the relative pressure range predicted by Pierce²² for physical adsorption on surfaces with no unusual capillarity. It has been previously demonstrated that N_2 adsorption data for high polymers²³ and dried material of biological origin²⁴ do yield linear plots with the FHH isotherm equation. The plots in this paper have steeper slopes than the standard plot for nitrogen adsorption of Pierce.²² Hightower and Emmett²³ made similar observations with polyolefins. They attributed these deviations in slope to lowered heats of adsorption for N_2 as evidenced by the low C values, ranging from 11 to 48, which they obtained from their BET plots. We obtained a low C value of 32 for N_2 adsorption on α_{s1} -casein C; however, the α_{s1} -casein A data yielded a C value of 79.

When our water sorption data were plotted according to the FHH equation, wide deviations from linearity were observed, as shown in Figure 5. The linear portion of the curves shown in this figure correspond to a value of $r = 2.5$ in the FHH equation

$$\log \log (P_0/P) = r \log \theta$$

where θ corresponds to the fraction of surface coverage or any variable proportional to it such as volume or mass adsorbed. The value of 2.5 for the constant r is in agreement with that observed by Halsey²⁰ for the adsorption of H_2O on anatase at 25° . According to

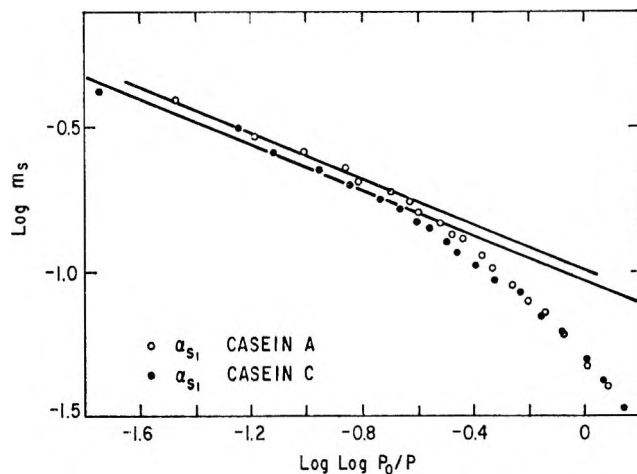


Figure 5. Frenkel-Halsey-Hill isotherm plots for H_2O vapor sorption on α_{s1} -caseins at 24.2° . Although similar results were obtained for all the H_2O sorption runs, only one set of data is shown for each variant for clarity in presentation.

Pierce,²² such a value of $r = 2.5$ should be standard for adsorption of water vapor on any adsorbent where strictly multilayer adsorption is occurring.

The linear portion of the FHH isotherm shown in the present paper can correspond to multilayer adsorption at higher relative pressures. However, the curved nature of the major portion of these FHH isotherms indicates that either capillary condensation is occurring in very fine pores or that the sorbent is undergoing swelling and physical changes as a result of the sorption process. Brandt and Budrys²⁵ have published similar curves for the sorption of various vapors by polypeptides, which they interpreted as indicating morphological changes in the peptides as a result of the sorption.

Any swelling occurring in the α_{s1} -caseins is, however, fully reversible through at least two sorption-desorption cycles as shown in Figures 1 and 2. These results are not necessarily at variance with those recently reported by Rao and Das²⁶ for native and denatured caseins. They showed that during a series of sorptions and desorptions of water vapor the hysteresis loop showed a tendency to decrease in size and finally disappear in subsequent cycles. Those authors, however, have pointed out that varietal differences in the proteins affect the

(18) F. A. Bettelheim, *J. Colloid Interfac. Sci.*, **23**, 301 (1967).

(19) J. Frenkel, "Kinetic Theory of Liquids," Oxford University Press, London, 1946.

(20) G. D. Halsey, *J. Chem. Phys.*, **16**, 931 (1948).

(21) T. L. Hill, *Advan. Catal.*, **4**, 212 (1952).

(22) C. Pierce, *J. Phys. Chem.*, **64**, 1184 (1960); C. Pierce and B. Ewing, *J. Amer. Chem. Soc.*, **84**, 4070 (1962).

(23) J. W. Hightower and P. H. Emmett, *J. Polym. Sci., Part A*, **2**, 1647 (1964).

(24) E. Berlin, H. R. Curran, and M. J. Pallansch, *J. Bacteriol.*, **86**, 1030 (1963).

(25) W. W. Brandt and R. S. Budrys, *J. Phys. Chem.*, **69**, 600 (1965).

(26) K. S. Rao and B. Das, *ibid.*, **72**, 1223 (1968).

tendency of the hysteresis loop to disappear in successive sorption-desorption cycles.

Nevertheless, the sharp contrast between the shapes of the FHH plots for N₂ and H₂O sorption of the α_{s1}-caseins further demonstrates the basic differences in the

types of interactions involved in H₂O and N₂ adsorption on dried proteins.

Acknowledgment. We wish to thank Dr. M. P. Thompson for the samples of α_{s1}-caseins A and C.

Effect of Fast Internal Rotation on the Nitrogen-14 Nuclear Magnetic Resonance Relaxation Times of the Methylbenzyl Cyanides

by Daniel Wallach¹

Department of Chemistry, Stanford University, Stanford, California (Received April 19, 1968)

It is shown that nmr can be used to study internal rotation which occurs at a rate comparable to the molecular rotation rate. Specifically, the nmr relaxation times of the ¹⁴N nucleus in 2-, 3-, and 4-methylbenzyl cyanide have been measured in the neat liquids and in *m*-xylene solutions. The relaxation times depend on both the rate of the molecular rotation and the rate of internal rotation of the CH₂CN group relative to the benzene ring. At 65°, for 3- or 4-MBC in the neat liquids, the calculated diffusion constants for the molecular and internal rotation are $D_M = 2.1 \times 10^{10} \text{ sec}^{-1}$ and $D_I = 4.4 \times 10^{10} \text{ sec}^{-1}$, respectively.

Introduction

Nuclei with spin $I > 1/2$ possess an electric quadrupole moment which interacts with the electric field gradient at the nucleus. In a liquid this interaction is time dependent, due to the molecular rotation, and therefore serves as a relaxation mechanism for the nuclear magnetic sublevels. Since the efficiency of this mechanism depends on the reorientation of the principal field gradient axes relative to a laboratory fixed frame, the measurement of the relaxation time can provide information about this reorientation.²

The principal field gradient axes are essentially fixed relative to the bond to the nucleus. If this bond direction reorients relative to the rest of the molecule, both this internal rotation and the overall molecular rotation can reorient the field gradient axes and thereby affect the relaxation time.³ Since these rotational processes compete with one another in reorienting the bond direction, the internal rotation rate must be at least comparable to the molecular rotation rate if its effect on the relaxation time is to be significant. For small molecules, then, the internal rotation rates of interest are on the order of 10¹⁰ Hz or faster. In order to investigate experimentally the effect of fast internal rotation on the relaxation time, the ¹⁴N relaxation times for 2-, 3-, and 4-methylbenzyl cyanide (MBC) have been measured. The ¹⁴N nucleus has a spin $I = 1$, and in these molecules the bond to that nucleus can reorient relative to the benzene ring about a single axis

of internal rotation (Figure 1). It is shown that the overall molecular rotation rates of the methylbenzyl cyanides are nearly identical. However, the internal rotation is expected to be significantly slower in 2-MBC than in 3- or 4-MBC. By comparing the relaxation times for these three molecules, it is then possible to separate the contributions of the molecular and internal rotations to the relaxation process.

Experimental Section

The measured line widths are displayed in Figures 2 and 3. The samples of 2-, 3-, and 4-MBC (Aldrich, research grade) and benzyl cyanide and *m*-xylene (Matheson Coleman and Bell, reagent grade), were used without further purification. The solutions with 50% by volume *m*-xylene were made up at room temperature and correspond to 53 mole % *m*-xylene (see Table I for the relevant densities).

The liquid samples were studied in a Varian 4-12 MHz TWL insert. The temperature was varied by a stream of air which first flowed past a heater sensor unit, driven by a V4343 Varian temperature control unit, and then through a "U" of glass tubing extending below the liquid level in the insert. The sample tem-

(1) Department of Chemistry, The Pennsylvania State University, University Park, Pa. 16802.

(2) A. Abragam, "The Principles of Nuclear Magnetism," Oxford University Press, London, 1961, Chapter VIII.

(3) D. Wallach, *J. Chem. Phys.*, **47**, 5258 (1967).

Table I

Molecule	Bp. °C ^a	Density, g/ml
2-MBC	244	1.0156 ^a (22°)
3-MBC	240-241	1.0022 ^a (22°)
4-MBC	242-243	0.9922 ^a (22°)
<i>m</i> -Xylene	139	0.8642 ^b (20°)

^a "Dictionary of Organic Compounds," Oxford University Press, New York, N. Y., 1965. ^b "Handbook of Chemistry and Physics," 44th ed, Chemical Rubber Publishing Co., Cleveland, Ohio, 1962.

perature, which was measured by a thermocouple placed directly in the liquid sample, though well above the radiofrequency receiver coil, varied less than $\pm 1^\circ$ during each experiment.

The resonances were observed using a Varian 4.33-MHz radiofrequency unit and probe. The reported line widths represent the full widths at half-height of the side bands formed by modulating the magnetic field at frequencies between 900 and 1400 Hz. These line widths are related to the T_2 relaxation times by

$$\Delta\nu = (\pi T_2)^{-1} \quad (1)$$

Each experimental point is the average of at least six measurements, and the uncertainties shown in Figures 2 and 3 represent the standard deviations of the measured line widths.

Qualitative Results

If it is assumed that the ^{14}N relaxation times for the methylbenzyl cyanides are due solely to the quadrupole interactions, and if it is further assumed that the field gradient at the nitrogen is symmetrical about the bond direction, then these relaxation times depend only on a single quadrupole coupling constant and on the molecular and internal reorientations. Both of these assumptions are expected to be quite good. The other relaxation mechanism most likely to be significant is that due to dipole-dipole interactions. However, the nitrogen relaxation times are on the order of a millisecond or some three orders of magnitude shorter than common relaxation times for protons, which have a much larger nuclear magnetic dipole moment than ^{14}N but no quadrupole moment. The asymmetry in the field gradient is only a second-order effect, due to deviations from cylindrical symmetry of the charge distribution around the bond to the nitrogen. It is also assumed that the ^{14}N quadrupole coupling constants are the same for all three methylbenzyl cyanides, since the position of the methyl group on the ring should have only a very small effect on the charge distribution around the nitrogen. Any differences in the relaxation times of the methylbenzyl cyanides must then be due to differences in the

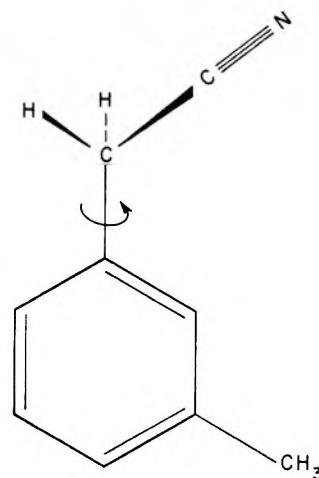


Figure 1. In 2-MBC, 3-MBC (shown above), and 4-MBC, both the internal rotation and the molecular rotation can reorient the direction of the bond to the nitrogen relative to the lab.

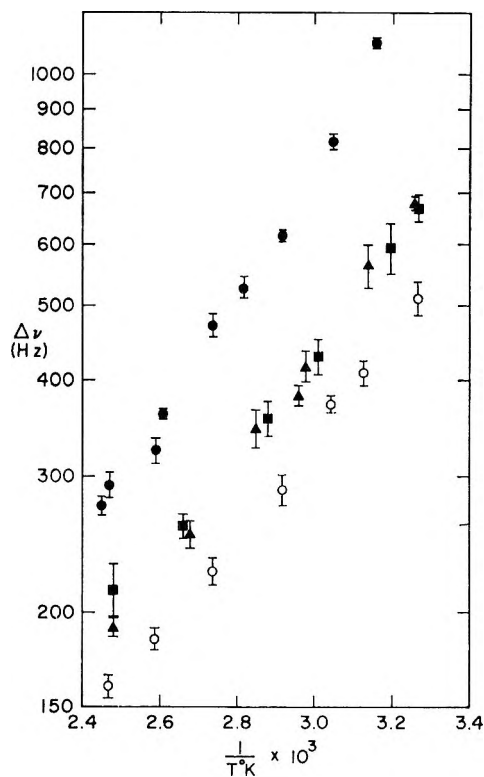


Figure 2. ^{14}N line widths in the neat liquids: ●, 2-MBC; ■, 3-MBC; ▲, 4-MBC; ○, benzyl cyanide.

molecular or internal reorientations. The exact dependence of the relaxation time on the reorientations cannot be specified unless the details of the reorientation processes are known. In general, the relaxation time depends on both the characteristics of the molecular and internal rotations in the free gas and on the way in which these rotations are affected by the intermolecular interactions in the liquid.

The ^{14}N relaxation times for 3- and 4-MBC are very

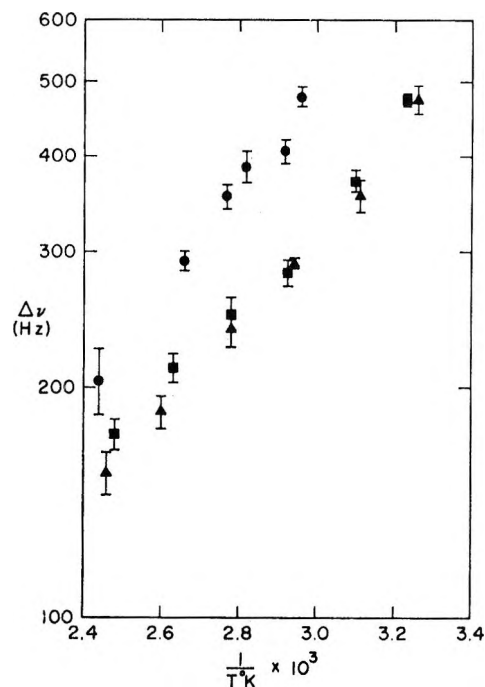


Figure 3. ^{14}N line widths in solutions with 50% by volume *m*-xylene: ●, 2-MBC; ■, 3-MBC; ▲, 4-MBC.

similar, as shown by Figures 2 and 3. It is possible, of course, that both the molecular and internal rotations change in going from 3-MBC to 4-MBC, but that the changes just compensate for one another in the relaxation times. However, it seems unlikely that this would occur over the entire temperature range studied, and in any case the molecular structures, densities, and boiling points of 3- and 4-MBC are very similar (Table I). It is more reasonable to conclude, then, that the molecular and internal rotations are both very nearly the same in the two molecules.

It is expected that the position of the methyl group on the ring should not have a large effect on the molecular rotation, and these results indicate that the effect is, in fact, quite negligible. Therefore, it is assumed that the molecular rotation of 2-MBC is also nearly the same as that of 3- and 4-MBC. However, the 3- and 4-MBC relaxation times are significantly longer than the corresponding 2-MBC relaxation times. This difference must then be due to differences in the internal rotations. Furthermore, the bond reorientation rates are all well within the "extreme narrowing" limit, so that a longer relaxation time implies a faster reorientation rate. It seems then that in particular the internal rotation in 3- and 4-MBC is faster than in 2-MBC. The observation that the temperature dependence of the 2-MBC relaxation times is larger than that of the 3- or 4-MBC relaxation times confirms that the rotation of the bond direction is more hindered in 2-MBC. This is certainly as expected, for one of the substituents adjacent to the CH_2CN group in 2-MBC is a relatively bulky methyl group rather than a proton. Finally,

the fact that the internal rotation affects the 3- and 4-MBC relaxation times at all implies that the internal rotation rates in those molecules must be at least comparable to their overall molecular rotation rates.³

The above conclusions apply equally to the neat liquids and the solutions with *m*-xylene. In addition, all the relaxation times in the *m*-xylene solutions are longer than the corresponding values for the neat liquids. This suggests that the reorientation rate of the CH_2CN group has increased in solution for all three methylbenzyl cyanides. However, in order to determine the separate changes in the molecular and internal rotation rates, it is necessary to have an explicit relation between the relaxation time and these rates.

Figure 2 also shows that the ^{14}N relaxation times of benzyl cyanide are about 25% longer than the corresponding 3- and 4-MBC relaxation times. This is reasonable, since the overall molecular rotation should be somewhat faster for the lighter benzyl cyanide than for 3- or 4-MBC, though neither this molecular rotation nor the internal rotation should differ too markedly between these molecules.

Calculations

In order to obtain an explicit expression for the ^{14}N relaxation time in terms of the rotation rates, it is necessary to make some simplifying assumptions about the rotational precesses. In particular, it is assumed that the molecular and internal rotations are independent, that the molecular rotation is diffusional and isotropic, so that it can be described by a single diffusion constant, and that the internal rotation is also diffusional and therefore can also be described by a diffusion constant. The equation for the ^{14}N relaxation time is then

$$1/T_2 = \frac{3\pi^2}{2} \left(\frac{e^2Qq}{h} \right)^2 \left[\frac{(3/4) \sin^4 \theta}{6D_M + 4D_I} + \frac{3 \sin^2 \theta \cos^2 \theta}{6D_M + D_I} + \frac{(1/4)(3 \cos^2 \theta - 1)^2}{6D_M} \right] \quad (2)$$

where e^2Qq/h is the ^{14}N quadrupole coupling constant in Hz, θ is the angle between the internal rotation axis and the bond to the nitrogen, and D_M and D_I are the diffusion constants for the overall molecular rotation and the internal rotation, respectively. The diffusion constants are defined by the equations⁴

$$D_M(\text{sec}^{-1}) = \frac{1}{2} \lim_{\Delta t \rightarrow 0} \frac{\langle \Delta \psi^2 \rangle}{\Delta t} \quad (3)$$

$$D_I(\text{sec}^{-1}) = \frac{1}{2} \lim_{\Delta t \rightarrow 0} \frac{\langle \Delta \phi^2 \rangle}{\Delta t} \quad (4)$$

(4) L. D. Favro, *Phys. Rev.*, **119**, 53 (1960). It is also common to define rotational diffusion constants as $D_M' = a^2 D_M$ and $D_I' = a^2 D_I$, where a is the molecular radius. With these definitions the quantities appearing in eq 2 would be D_M'/a^2 and D_I'/a^2 .

where $\Delta\psi$ is the angle through which the benzene ring has rotated in time Δt , $\Delta\phi$ is the angle through which the CH_2CN group has rotated relative to the ring, and the pointed brackets indicate an ensemble average. If the quadrupole coupling constants for the methylbenzyl cyanides are assumed to be the same as for acetonitrile in the gas phase, 4.4 MHz,⁵ and θ is taken as the tetrahedral angle, 109.5°, eq 2 becomes

$$\frac{1}{T_2} = \frac{170 \times 10^{12}}{6D_M + 4D_I} + \frac{85.0 \times 10^{12}}{6D_M + D_I} + \frac{31.8 \times 10^{12}}{6D_M} \quad (5)$$

The methylbenzyl cyanides are asymmetric and quite polar, so the overall molecular rotations should be hindered significantly by intermolecular interactions and may well be diffusional or close to diffusional. The internal rotation should also be affected to some extent by the intermolecular interactions, as the CH_2CN group is also quite asymmetrical. However, the molecular rotation will not be isotropic, since the molecules are asymmetric tops, and in the free gas, at least, the molecular and internal rotations are coupled. Of course it is still possible to use eq 5 to calculate values of D_M and D_I for the methylbenzyl cyanides, but D_M and D_I can no longer be defined exactly as in eq 3 and 4. Nevertheless, it seems reasonable to assume that D_M is still at least an approximate measure of the average molecular rotation rate, and similarly that D_I is still an approximate measure of the internal rotation rate.

Equation 5 can be applied to 2-MBC and to 3- or 4-MBC, giving two independent equations which contain as unknowns the one common molecular diffusion constant and two internal diffusion constants. If any one of these diffusion constants were known, it would be possible to evaluate the other two. Though none of the diffusion constants has been measured explicitly, there is evidence which suggests that the internal rotation in 2-MBC is sufficiently slower than the molecular rotation that it may be neglected. Dielectric relaxation measurements on benzyl cyanide in dilute benzene solution have shown that while there seems to be evidence for two relaxation processes, it is impossible to separate their contributions to the dielectric results.⁶ This implies that D_M and D_I are comparable for methylbenzyl cyanide, and the same should generally be true then for 3- and 4-MBC also. Therefore, if the internal rotation in 2-MBC were as much as a factor of 10 slower than in 3- or 4-MBC, it would be reasonable to ignore its contribution to the relaxation time. The most closely analogous data are from the xylenes. The barrier to internal rotation in σ -xylene is 2 kcal/mol,⁷ while in m - and p -xylene it is less than 1 kcal/mol,^{7a} and probably very close to the value for toluene, 0.014 kcal/mol.⁸ Even at 130°, the highest temperature of interest, the internal rotation in σ -xylene is then slower than that in m - or p -xylene by a factor of about $\exp(-E_a/RT) = 1/12$. It is assumed that the differ-

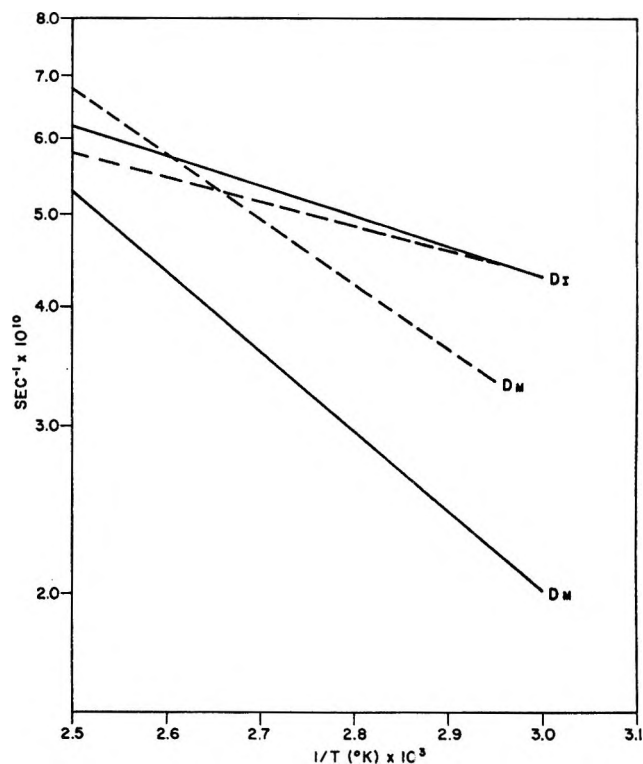


Figure 4. Molecular diffusion constants D_M for 2-, 3-, or 4-MBC and internal diffusion constants D_I for 3- or 4-MBC: ---, in the neat liquids; —, in 50% by volume m -xylene solutions.

ence between the internal rotation rates in 2-MBC and 3- or 4-MBC is at least this large.

When D_M is much larger than D_I , eq 5 reduces to

$$(T_2)^{-1} = (287 \times 10^{12})/6D_M \quad (6)$$

The values of the 2-MBC relaxation times are used in this equation to calculate values of D_M , and these values in turn are used in eq 5, together with the 3- and 4-MBC relaxation times, to calculate values of D_I for 3- and 4-MBC. The results for D_M and D_I are shown in Figure 4. The values of the relaxation times used in the calculations were taken from the least-squares lines through the 2-MBC results and the combined 3- and 4-MBC results, and it is estimated that the uncertainties in the diffusion constants due to the uncertainties in the experimental results are about $\pm 4\%$ for D_M and $\pm 15\%$ for D_I .

It is possible to predict qualitatively the way in which the molecular and internal rotation rates should change in going from the neat liquids to the m -xylene solutions. In size and shape, m -xylene is similar to the methylbenzyl cyanides. However, the dipole moment of

(5) W. J. Orville-Thomas, *Quart. Rev. (London)*, **11**, 162 (1957).

(6) C. P. Smyth in "Molecular Relaxation Processes," Academic Press, London, 1966.

(7) (a) K. S. Pitzer and D. W. Scott, *J. Amer. Chem. Soc.*, **65**, 803 (1943); (b) J. J. Rush, *J. Chem. Phys.*, **47**, 3936 (1967).

(8) H. D. Rudolph, H. Breizler, A. Jaeschke, and P. Wendling, *Z. Naturforsch.*, **22a**, 940 (1967).

m-xylene is only 0.37 D,⁹ while the dipole moments of the methylbenzyl cyanides will be similar to that of benzyl cyanide, which is 3.50 D.⁹ In fact, *m*-xylene was chosen as solvent to try to limit the effect of dilution to a reduction in the intermolecular dipole interactions. This should allow freer and therefore faster molecular rotation, but should have much less effect on the internal rotation, since the internal rotation re-orientates the dipole moment to only a limited extent in any case. The molecular diffusion constant should then increase, but the internal diffusion constant should not be greatly affected. This is in fact the observed behavior of D_M and D_I , respectively, which is at least consistent with the suggestion that D_M is a measure of the molecular rotation rate and D_I a measure of the internal rotation rate.

It is also possible to obtain information about the rotations by comparing the temperature dependences of the diffusion constants. The temperature dependence reflects both an average barrier to rotation and the fact that in the liquid the barrier itself may vary with temperature. However, if two rotational processes are sufficiently similar, it is reasonable to assume that the variation of the barrier with temperature is more or less the same in both cases. This assumption should certainly be valid in comparing the molecular rotation rates in the neat liquid and in *m*-xylene solution, and is probably valid even in comparing the molecular and internal rotation rates, since both rotations are affected generally by the same interactions. Activation energies obtained from the data in Figure 4 are displayed in Table II. The fact that D_M has a smaller temperature dependence in *m*-xylene solution than in the neat liquid indicates that the molecular rotation is less hindered in the solution. Table II also shows that apparently the internal rotation is less hindered than the molecular rotation in both the neat liquid and the solution. The same general behavior has been observed in a number of other molecules. Dielectric relaxation measurements on diphenyl ether,¹⁰ 2-naphthol,¹¹ and 2-naphthalenethiol¹¹ have shown that in each case the internal rotation rate varies very little, if at all, with temperature, while the temperature dependence of the molecular rotation rate is much more marked.

Table II: Activation Energies Calculated from the Data in Figure 4

Diffusion constant	Solvent	Activation energy, kcal/mol
D_M	Neat liquid	3.8
D_M	<i>m</i> -Xylene	3.1
D_I	Neat liquid	1.5
D_I	<i>m</i> -Xylene	1.2

The magnitudes of D_M and D_I for 3- and 4-MBC can be compared with values for similar molecules determined by dielectric measurements. In order to make this comparison, it is useful to review the significance of the parameters determined by the dielectric experiments. The interpretation of these experiments is based on very nearly the same assumptions used in deriving eq 2.¹² Though the original derivation allows for the possibility of anisotropic molecular rotation, the dielectric results are commonly interpreted in terms of just the two rotational parameters—a diffusion constant for the overall molecular rotation and a diffusion constant for the internal rotation. In terms of these diffusion constants, the relaxation times obtained from the dielectric experiments are¹²

$$(\tau_1)^{-1} = 2D \quad (7)$$

and

$$(\tau_2)^{-1} = D + D_I \quad (8)$$

Even though the dielectric results for benzyl cyanide cannot be rigorously separated into two correlation times, it is possible to obtain a most probable value of $\tau_1 = 19 \times 10^{-12}$ sec for the overall molecular rotation in dilute benzene solution at 20°. This corresponds to $D_M = 2.6 \times 10^{10}$ sec⁻¹, compared to the extrapolated value $D_M = 1.9 \times 10^{10}$ sec⁻¹ for the methylbenzyl cyanides in *m*-xylene solution at 20°. This agreement is certainly reasonable since the rotation in dilute benzene solution should be faster than in 50% *m*-xylene solution and since the overall molecular rotation of benzyl cyanide is in any case somewhat faster than that of the methylbenzyl cyanides.

Dielectric measurements have also been made on *p*-xylylene dicyanide. The internal rotation rate of the CH₂CN groups in this molecule should be comparable to the internal rotation rates in 3- and 4-MBC, since the molecules themselves are not too dissimilar and since in each case the CH₂CN group is adjacent to two protons on the ring. The value $\tau_2 = 8.9 \times 10^{-12}$ sec was obtained for *p*-xylylene dicyanide in benzene solution at 20°. If τ_1 for this molecule is assumed to be the same as for benzyl cyanide, the internal diffusion constant is $D_I = 8.6 \times 10^{10}$ sec⁻¹. This value should actually be somewhat smaller, since the molecular rotation of *p*-xylylene dicyanide is no doubt slower than that of benzyl cyanide. The values of D_I for 3- or 4-MBC, extrapolated to 20°, are $D_I = 3.4 \times 10^{10}$ sec⁻¹ for the neat liquids and $D_I = 3.6 \times 10^{10}$ sec⁻¹ for the *m*-xylene solutions. For comparison, the internal rotation rates differ by about 40% between benzyl chloride and *p*-

(9) C. P. Smyth, "Dielectric Behavior and Structure," McGraw-Hill Book Co., Inc., New York, N. Y., 1955.

(10) K. Bergmann, D. M. Roberti, and C. P. Smyth, *J. Phys. Chem.*, **64**, 665 (1960).

(11) F. K. Fong and C. P. Smyth, *ibid.*, **67**, 226 (1963).

(12) A. Budo', *Physik. Z.*, **39**, 706 (1938).

xylylene dichloride⁶ and by about 90% between methoxybenzene and *p*-dimethoxybenzene,⁶ and in both cases the monosubstituted molecule has the larger diffusion constant. Most of the discrepancy between the 3- or 4-MBC results and the *p*-xylylene dicyanide results is probably due then to the uncertainties in the calculated values of D_I in the two cases.

Summary

Internal rotation which reorients the field gradient axes of a quadrupolar nucleus relative to the rigid molecular framework, and which does so at a rate at least comparable to the rotation rate of the framework, has a direct effect on the nuclear relaxation time. If the molecular and internal rotation are assumed to be diffusional and uncoupled, an explicit expression for the

relaxation time in terms of the diffusion constants can be obtained. Then, if an independent measure of the molecular rotation rate is available, the relaxation time can be used to calculate the rate of the internal rotation. The results obtained in this way for 3- and 4-MBC are physically reasonable and are in fair agreement with the results for similar molecules obtained by dielectric relaxation measurements.

Acknowledgments. The author wishes to acknowledge particularly the assistance and encouragement of Professor John D. Baldeschwieler and helpful discussions with W. T. Huntress. The support of the National Institutes of Health under Grant GM 14752-01 and the National Science Foundation under Grant GP 4924-x are also gratefully acknowledged.

Salting Out of Nonpolar Gases in Aqueous Potassium Hydroxide Solutions¹

by S. K. Shoor, R. D. Walker, Jr., and K. E. Gubbins

Department of Chemical Engineering, University of Florida, Gainesville, Florida 32601 (Received May 2, 1968)

The solubilities of helium, hydrogen, oxygen, argon, methane, sulfur hexafluoride, and neopentane in aqueous KOH solutions have been measured for the temperature range 25–80°. For oxygen and hydrogen, data are also reported at 100°. The experimental method used involved stripping the dissolved gas from solution using a carrier gas stream, and subsequent analysis of this stream by gas chromatography. The results of these investigations for oxygen and hydrogen are in good agreement with those of most previous workers. Partial molal heats of solution are calculated from the temperature dependence of the solute activity coefficient, and the electrolyte concentration dependence of this quantity is used to calculate salting-out coefficients.

Large salting-out effects are observed in potassium hydroxide solutions, both because of the nature of the ions involved and the high ionic strengths that may be encountered. Experimental studies of salt effects should include solubility measurements for a series of nonelectrolytes in water and electrolyte solutions, over a range of temperatures as well as electrolyte concentrations. In this way enthalpies and entropies of solution may be obtained in addition to activity coefficients; such comprehensive data may be used to test theories of the salting-out effect.^{2,3} Several previous studies of the solubility of oxygen and hydrogen in potassium hydroxide solutions have been reported.^{4–8} No previous studies of solubilities in potassium hydroxide solutions seem to have been made for the other gases reported here, namely, helium, argon, methane, sulfur hexafluoride, and neopentane.

The solute gases chosen for study in the present work are composed of nonpolar molecules which are spherical or globular in shape and are of widely varying sizes. The temperature range covered (25–80° in most cases)

is sufficient for estimates of enthalpies and entropies of solution to be made. The gas solubilities to be measured were in the range 10⁻⁵ to 10⁻⁸ mol fraction. Manometric and volumetric methods of determining gas solubilities are not well suited to concentrations as low as these,^{9,10} and therefore the concentration of dissolved gas was determined by gas chromatographic analysis.

(1) These studies were supported by the National Aeronautics and Space Administration under Grant No. NGR10-005-022. Reprint requests should be addressed to K. E. Gubbins.

(2) F. A. Long and W. F. McDevitt, *Chem. Rev.*, **51**, 119 (1952).

(3) B. E. Conway, *Ann. Rev. Phys. Chem.*, **17**, 503 (1966).

(4) G. Geffcken, *Z. Phys. Chem. (Leipzig)*, **49**, 257 (1904).

(5) M. B. Knaster and L. A. Apel'baum, *Russ. J. Phys. Chem.*, **38**, 120 (1964).

(6) P. Ruetschi and R. F. Amli, *J. Phys. Chem.*, **70**, 718 (1966).

(7) R. E. Davis, G. L. Horvath, and C. W. Tobias, *Electrochim. Acta*, **12**, 287 (1967).

(8) K. E. Gubbins and R. D. Walker, *J. Electrochem. Soc.*, **112**, 469 (1965).

(9) M. W. Cook and D. N. Hanson, *Rev. Sci. Instrum.*, **28**, 370 (1957).

(10) R. Battino and H. L. Clever, *Chem. Rev.*, **66**, 395 (1966).

Experimental Section

Materials. Minimum purities for the gases used were as follows: helium and argon, 99.99%; hydrogen, 99.9%; oxygen, 99.6%; neopentane and methane, 99.0%; and sulfur hexafluoride, 98.0%. Potassium hydroxide solutions were prepared from specially distilled (all glass-Teflon still) and degassed water. The method of degassing water was similar to that employed by Clever, *et al.*¹¹ Potassium hydroxide pellets used for preparing aqueous solutions were Baker Analyzed reagent grade and contained a maximum of 1% K_2CO_3 . To minimize carbon dioxide absorption, bottles containing potassium hydroxide solution were fitted with glass bulbs containing ascarite.

Preparation of Gas Solutions. Saturated solutions of the gas in the electrolyte were prepared by bubbling the gas at a flow rate of 30 ml/min through a set of presaturators and then through a sample (usually about 250 ml) of the potassium hydroxide solution, contained in a 500-ml round-bottomed flask. The gas was dispersed through the solution by a fritted disk, and a time of 30 min was found to be sufficient to attain equilibrium. Before withdrawing a sample, the bubbling was stopped, and an atmosphere of the solute gas was placed over the surface of the solution. Gas leaving the saturating vessel was bubbled through a second vessel containing the solution under study, to avoid the possibility of contamination from atmospheric air.

Attainment of equilibrium is of prime importance for equilibrium solubility determinations and was checked by withdrawing samples after different intervals of saturation time and analyzing the dissolved gas. The equilibrium solubility was taken as the value measured when at least three samples withdrawn at different times gave the same result within the limits of experimental error. This process was repeated for gas flow rates in the range 10–60 ml/min, and it was found that gas flow rate did not affect the measured solubility value. Supersaturation was guarded against by the following procedure. A sample of the solution prepared in the manner described above was removed and analyzed. Bubbling of the gas was stopped and the solution was maintained under an atmosphere of the solute gas. Samples of the solution were analyzed over a time period of 48 hr, and the results were compared with the original values. No measurable supersaturation effect was observed in these experiments.

Samples were withdrawn from the saturating vessel by means of a gas-tight Hamilton syringe. The samples were withdrawn extremely slowly so that at no stage of the sampling process was the flask or syringe placed under reduced pressure. Several samples were taken and rejected before final sampling was made. As a check on the procedure of sampling and degassing, blank samples consisting of potassium hydroxide solution saturated with carrier gas were injected into the

chromatograph. No peak was obtained, indicating that negligible contamination with atmospheric or other gases occurred.

For experiments at temperatures of 80° and below, two presaturators containing the KOH solution studied were used. For experiments at 100° additional presaturators were necessary. In order to check that the solute gas stream contacting the sample was fully presaturated, samples of exit gas were analyzed for water vapor. In addition, the concentration of potassium hydroxide in the solution contained in the saturation flask was checked at the end of the experiment.

The whole assembly, consisting of presaturators and saturating vessel, was completely immersed in a constant-temperature bath controlled to $\pm 0.05^\circ$. Thermometers checked for accuracy against the National Bureau of Standards calibrated thermometers were used for measuring the temperature.

Analysis of Dissolved Gas. The experimental method used for the gas solubility measurements has been previously described in detail by Gubbins, Carden, and Walker.¹² It involved removal of the dissolved gas from a 20-ml sample of the saturated solution by stripping with chromatograph carrier gas, followed by gas chromatographic analysis. The chromatograph peaks obtained by this procedure were slightly wider and less symmetrical than those obtained by injecting a gas sample directly into the chromatograph sampling port. However, this peak broadening was not sufficient to result in significant loss of accuracy or precision. All analyses were made using a thermal conductivity detector. Helium was used as a carrier gas for all solute gases except hydrogen and helium, for which nitrogen was used as carrier.

In determining the solubilities of sulfur hexafluoride and neopentane in 31.6 wt % potassium hydroxide solution, the amount of dissolved gas was found to be too small to obtain accurate results by the above method. For these systems a modified procedure¹³ was used in which the gas from a 200-ml sample of solution was collected before analysis in a tube immersed in liquid nitrogen. This procedure enabled large samples to be used without loss of accuracy due to broadening of chromatographic peaks.

The chromatograph was calibrated by injecting an accurately measured volume of pure dry gas. For those gases where accurate literature values of the solubility in water at 25° were available, the calibration was checked by carrying out the above procedure on a water sample. The relationship of the amount of dissolved gas to the instrument response was checked and was

(11) H. L. Clever, R. Battino, J. H. Saylor, and P. M. Gross, *J. Phys. Chem.*, **61**, 1078 (1957).

(12) K. E. Gubbins, S. N. Carden, and R. D. Walker, *J. Gas Chromatog.*, **3**, 98 (1965).

(13) S. K. Shoor, Ph.D. Thesis, University of Florida, Gainesville, Fla., 1968.

Table I: Activity Coefficients, $\gamma_1 = x_1^\circ/x_1$ for Gases Dissolved in KOH Solutions

[KOH], wt %	C_s^a	γ_1					[KOH], wt %	C_s	γ_1					
		25°	40°	60°	80°	100°			25°	40°	60°	80°	100°	
		O ₂							H ₂					
0.00	0.00	1.00	1.00	1.00	1.00	1.00	0.00	0.00	1.00	1.00	1.00	1.00	1.00	
5.00	0.92	1.53	1.54	1.45	1.35	...	5.00	0.92	1.36	1.28	1.32	1.33	...	
13.50	2.67	3.06	2.87	2.58	2.50	...	9.00	1.70	1.71	1.64	1.74	1.81	...	
23.00	5.00	8.15	7.24	6.30	5.73	...	19.50	4.12	3.50	3.29	3.58	3.65	...	
31.61	7.35	20.1	17.8	15.6	14.4	...	32.40	7.60	...	8.70	9.16	9.04	...	
40.70	10.12	70.1	53.3	45.3	40.1	38.4	38.00	9.27	15.3	
50.65	13.75	230	...	162	143	141	41.40	10.37	20.1	20.4	21.4	21.8	21.9	
56.50	16.20	338	52.40	14.35	72.0	73.7	76.7	75.4	82.6	
							56.50	16.20	108	
		He							SF ₆					
0.00	0.00	1.00	1.00	1.00	1.00		0.00	0.00	1.00	1.00	1.00	1.00		
5.00	0.92	1.39	1.36	1.39	1.44		5.00	0.92	2.15	1.97	1.88	1.73		
9.00	1.70	1.75	1.73	1.96	1.89		13.50	2.67	7.44	6.53	5.88	4.91		
19.00	3.99	3.57	3.71	3.59	3.77		23.00	5.00	43.2	31.9	26.6	22.6		
32.40	7.60	13.1	12.7	13.0	13.7		31.6	7.35	234	146	112	84.2		
		Ar							CH ₄					
0.00	0.00	1.00	1.00	1.00	1.00		0.00	0.00	1.00	1.00	1.00	1.00		
5.00	0.92	1.56	1.48	1.40	1.32		5.61	1.03	1.66	1.51	1.48	1.39		
13.50	2.67	3.18	2.81	2.59	2.48		13.90	2.77	3.64	3.14	2.83	2.50		
23.0	5.00	7.68	6.93	5.85	5.57		23.50	5.13	10.2	8.08	6.90	6.22		
31.61	7.35	14.5	13.4		31.61	7.35	26.7	19.8	16.7	14.4		
32.40	7.60	22.8		40.70	10.12	100	63.4	49.6	38.0		
40.70	10.15	30.0									
41.40	10.37	70.3	58.2	46.1	...									
		C(CH ₃) ₄												
0.00	0.00	1.00	1.00	1.00	1.00									
5.61	1.03	2.18	2.17	2.64	1.94									
13.90	2.77	8.91	7.87	6.80	5.94									
23.50	5.13	56.1	42.0	33.0	28.6									
31.61	7.35	288	220	158	138									

^a Molarity of KOH measured at 25°.

found to be linear within the limits of the experimental error.

Results

Consider a nonideal liquid solution in contact with a vapor phase. For any component i

$$f_i^g = f_i^l \quad (1)$$

where superscripts g and l refer to the gas and liquid phases, respectively, and f_i is the fugacity of i . Subscripts 1, 2, and 3 will be used to denote the solute gas, water, and potassium hydroxide, respectively. The standard state chosen for the solute gas is the pure solute in a hypothetical liquid state which is defined by reference to the behavior of this component at infinite dilution in pure water, that is

$$\lim_{\substack{x_1 \rightarrow 0 \\ x_2 = 0}} f_1^\circ = K_1^\circ x_1^\circ \quad (2)$$

where K_1° is Henry's law constant for the gas in pure

water, f_1° is the fugacity of dissolved gas, and x_1° is the liquid-phase mole fraction. The fugacity of the gas dissolved in the electrolyte solution using this standard state is

$$f_1^l = K_1^\circ \gamma_1 x_1 \quad (3)$$

where γ_1 and x_1 are the activity coefficient and mole fraction in the electrolyte solution, respectively. For the systems studied here the values of x_1 are low enough that Henry's law should be a good approximation. The term $K_1^\circ \gamma_1$ in eq 3 should then be a constant, dependent only on temperature and electrolyte concentration. If eq 1 and 3 are combined

$$P y_1 = K_1^\circ \gamma_1 x_1 \quad (4)$$

where y_1 and P are the gas-phase mole fraction and total pressure, respectively. Since the pressure involved is about 1 atm, the gas-phase fugacity has been replaced by partial pressure in eq 3.

Experimental solubilities were determined at a partial pressure ($P - p$) of solute gas, where p is the vapor

Table II: Solubility of Gases in Water at 1 Atm of Partial Pressure^a

Solute gas	10 ⁵ x ₁ ^o (1)							
	25°		40°		60°		80°	
	This work	Lit.	This work	Lit.	This work	Lit.	This work	Lit.
O ₂ ^b	2.25	2.279	1.90	1.868	1.60	1.591	1.44	1.455
H ₂ ^b	1.43	1.415	1.29	1.329	1.30	1.307	...	1.322
He ^{c,d}	0.67	0.682	0.67	0.674	0.72	0.718	0.80	...
Ar ^{c,d}	2.53	2.480	2.00	1.942	1.68	1.671	1.52	...
SF ₆ ^e	0.40	0.406	2.74	...	2.20	...	1.91	...
CH ₄ ^b	2.48	2.421	1.90	1.915	1.62	1.596	1.44	1.461
C(CH ₃) ₄ ^f	1.01	1.02	0.69	0.683	0.48	...	0.43	...

^a Literature value (from footnote b) of $x_1^o(1)$ for O₂ at 100° equals 1.424×10^{-5} ; literature value (from footnote b) of $x_1^o(1)$ for H₂ at 100° equals 1.342×10^{-5} . ^b N. A. Lange, Ed., "Handbook of Chemistry," 10th ed, McGraw-Hill Book Co., Inc., New York, N. Y., 1961, pp 1099-1101. ^c T. J. Morrison and N. B. Johnstone, *J. Chem. Soc.*, **76**, 3441 (1954). ^d A. Lannung, *J. Amer. Chem. Soc.*, **52**, 68 (1930). ^e H. L. Friedman, *ibid.*, **76**, 3294 (1954). ^f D. F. Wetlaufer, S. K. Malik, L. Stoller, and R. L. Coffin, *ibid.*, **86**, 508 (1964).

pressure of the electrolyte solution. Solubility values for a partial pressure of 1 atm of solute were calculated from these data by assuming Henry's law to apply. From eq 4 and the corresponding equation for the gas dissolved in pure water

$$\gamma_1 = \frac{x_1^o(1)}{x_1(1)} \quad (5)$$

where $x_1^o(1)$ and $x_1(1)$ are mole fractions in water and electrolyte solution, respectively, at 1 atm of partial pressure. In deriving eq 5 Henry's law is assumed, so that γ_1^o is unity.

Activity coefficients calculated from eq 5 are presented in Table I. Each value is the mean of four or more replicate measurements. The standard deviation from the arithmetic mean for replicate measurements ranged from approximately 1% at the highest concentrations (mole fractions in the region of 10^{-5}) to about 5% for the lowest solubilities measured (10^{-7} to 10^{-8} mol fraction). Table II shows measured solubility values in water and compares them with values from the literature. In most cases the agreement is better than 2%.

No previous studies of the solubility in potassium hydroxide solutions of helium, argon, sulfur hexafluoride, methane, and neopentane seem to have been reported. However, several studies have been made for oxygen and hydrogen. Geffcken⁴ measured solubilities of oxygen and hydrogen at 15 and 25° in solutions 0-1.4 M in KOH, and Knaster and Apel'baum⁵ made similar measurements at 21, 45, and 75° for KOH concentrations up to 10 M. Ruetschi and Amlie⁶ have measured solubilities of hydrogen for KOH concentrations up to 10 M at 30°, while Davis, *et al.*,⁷ recently reported oxygen solubilities at 0, 25, and 60° for KOH concentrations to 12 M. Measurements for oxygen at 25° have been reported by Gubbins and Walker.⁸

To facilitate the comparison of the results of the present investigation with those of previous workers, the data for oxygen and hydrogen at 25° have been plotted in Figures 1 and 2 in the form of a semi-logarithmic plot. This type of plot has been used since most electrostatic theories of salting out predict a linear relationship between the logarithm of the activity coefficient and the molar concentration of electrolyte at moderate electrolyte concentrations.²

Figure 1 reveals that the 25° oxygen solubility values obtained in this work agree within 2 and 5% with those obtained by Geffcken⁴ and Davis, *et al.*,⁷ respectively. The experimental results of these investigators are distributed on both sides of the solid line of Figure 1. The agreement with the results of Knaster and Apel'-

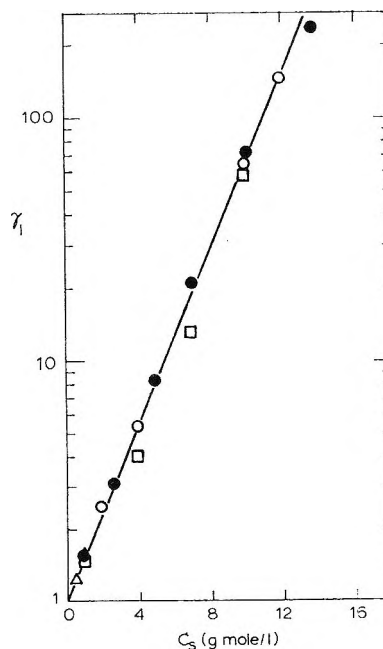


Figure 1. Activity coefficients of oxygen as a function of KOH concentration at 25°: ●, this work; ○, Davis, *et al.*;⁷ △, Geffcken;⁴ □, Knaster and Apel'baum.⁵

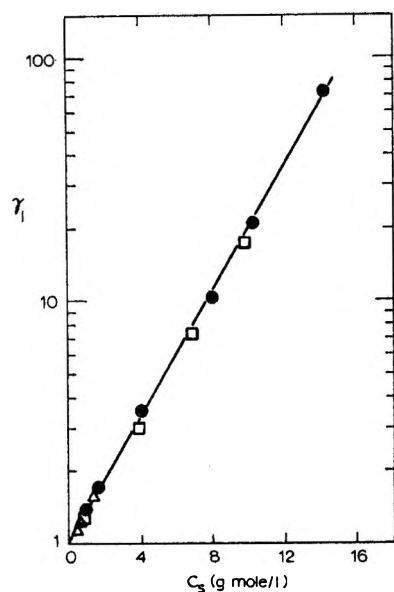


Figure 2. Activity coefficients of hydrogen as a function of KOH concentration at 25°: ●, this work; △, Geffcken;⁴ □, Knaster and Apel'baum.⁵

baum⁵ is good (about 10%) at very low and very high concentrations. However, at intermediate concentrations the disagreement is more pronounced, the results of Knaster and Apel'baum falling consistently below the solid line. Previous solubilities reported by Gubbins and Walker⁸ agree well with the present data for concentrations up to 8 M but deviate somewhat at the highest concentrations. At temperatures other than 25°, only the data of Knaster and Apel'baum and Davis, *et al.*, are available for comparison. The agreement of the results reported here with those of Knaster and Apel'baum⁵ at 40 and 60° is of the same general nature as at 25°. Close agreement is found between the present measurements at 60° and those of Davis, *et al.*⁷

Figure 2 shows that hydrogen solubilities obtained in this work at 25° are in good agreement with those of other workers. Agreement with the results of Geffcken⁴ is within 2% and with those of Knaster and Apel'baum⁵ is within 10%. For dilute KOH solutions, the reported results agree within 3% with those of Ruetschi and Amlie.⁶ However, the values of activity coefficients obtained by them are consistently lower than those reported here, and these discrepancies are as large as 10% for the higher KOH concentrations. At temperatures of 40 and 60°, the agreement between the reported results and those of Knaster and Apel'baum⁵ is also within 10%.

Discussion

In dilute electrolyte solutions the expression for the activity coefficient of a dissolved nonelectrolyte becomes

$$\log \gamma_1 = k_s C_s \quad (6)$$

Table III: Salting-Out Coefficients for KOH Solutions

Gas	k_s				
	25°	40°	60°	80°	100°
He	0.015	0.015	0.015	0.015	...
H ₂	0.129	0.129	0.129	0.129	0.129
Ar	0.179	0.168	0.158	0.148	...
O ₂	0.180	0.168	0.159	0.155	0.155
CH ₄	0.197	0.176	0.164	0.154	...
SF ₆	0.326	0.297	0.278	0.262	...
C(CH ₃) ₄	0.340	0.316	0.299	0.285	...

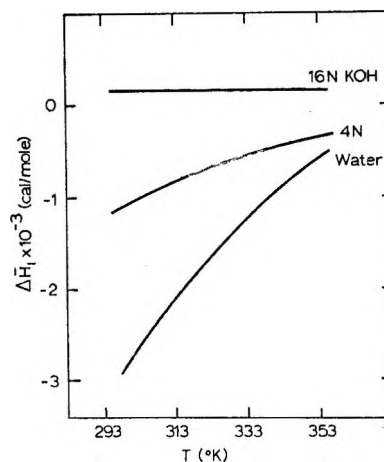


Figure 3. Partial molal heats of solution for oxygen.

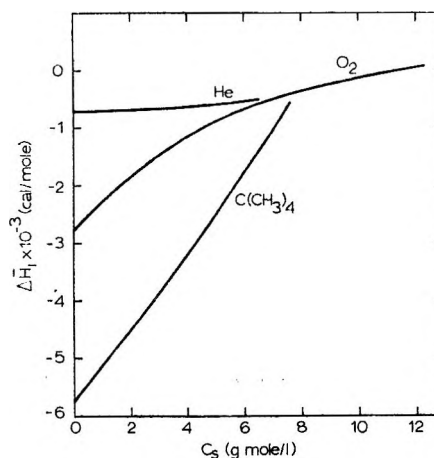


Figure 4. Partial molal heats of solution as a function of KOH concentration at 25°.

where k_s is the salting coefficient and C_s is the molar concentration of the salt. This equation was proposed empirically by Setchenow¹⁴ and on theoretical grounds by Debye and McAulay.¹⁵ Plots of $\log \gamma_1$ vs. C_s were found to be linear within experimental error as predicted by eq 6 over the entire range of KOH concentrations for the systems studied (see Figures 1 and 2).

(14) A. Setchenow, *Z. Phys. Chem. (Leipzig)*, **4**, 117 (1889).

(15) P. Debye and J. McAulay, *Physik. Z.*, **26**, 22 (1925).

Values of the salting-out coefficient are shown in Table III. The salting-out effect is large for all solutes studied, being the largest for neopentane and the smallest for helium. The effect increases as the molecular size increases. Theoretical equations for the salting coefficient involve parameters which are neither readily available nor easily calculated,² and quantitative comparison of theory and experiment is difficult.

The activity coefficients in Table I may be used to calculate partial molal enthalpies and entropies of solution from the equations

$$\left[\frac{\partial \ln (\gamma_1 K_1^\circ)}{\partial T} \right]_{P,C.} = -\frac{\Delta \bar{H}_1}{RT^2} \quad (7)$$

$$\Delta \bar{S}_1 = \frac{\Delta \bar{H}_1}{T} \quad (8)$$

where $\Delta \bar{H}_1 = \bar{H}_1 - H_1^\circ$ is the enthalpy change when 1

mol of gas in the ideal gas state is transferred to the dissolved state, the temperature, pressure, and electrolyte concentration being kept constant. $\Delta \bar{S}_1$ is the corresponding entropy change for this process. A typical plot of the partial molal heat of solution is that for oxygen and is shown in Figure 3. Similar behavior is observed for the other gases. In dilute KOH solutions the partial molal heats of solution are large and negative for the large solute molecules (sulfur hexafluoride and neopentane), and the absolute values decrease with decrease in molecular size, being less than 1 kcal/g-mol in the case of helium. The $\Delta \bar{H}_1$ values become less negative as the KOH concentration increases; this effect is greatest for the large molecules and is only very small in the case of helium. These trends are shown for three of the solutes in Figure 4. As seen from eq 8, the trends observed for partial molal entropies of solution will be similar to those for partial molal enthalpies of solution.

The Rate of Reaction of Methyl Iodide and Hydrazine in Aqueous Solution^{1,2}

by R. A. Hasty^{3,4}

Air Pollution Chemistry Section, Atmospheric Resources Department, Environmental and Life Sciences Division, Pacific Northwest Laboratory, Battelle Memorial Institute, Richland, Washington (Received May 15, 1968)

The rate of reaction of methyl iodide with hydrazine in aqueous solution was investigated from 24.6 to 64.6°, from 0.03 to 1.5 *M* hydrazine, and at *ca.* 3×10^{-8} *M* methyl iodide. The high volatility of methyl iodide in aqueous solution was utilized to follow the reaction. The rate of reaction was determined from the sum of the two processes, sparge removal and reaction. The rate of reaction was independent of hydroxide ion concentration and first order with respect to both methyl iodide and hydrazine concentrations. At 25°, the second-order reaction rate constant was 1.1×10^{-3} l. mol⁻¹ sec⁻¹ and the activation energy was 20.2 kcal/mol.

Introduction

The rate of removal of methyl iodide from a gas phase by absorption and reaction with sprays has been the subject of several recent studies. Unlike the removal of iodine by reactive sprays, the process is not limited by the gas-phase mass-transfer resistance. The removal process in the case of methyl iodide is a combination of the partition between vapor and liquid, diffusion into the liquid, and reaction in the liquid. The partition coefficient for the range of concentration of interest (*ca.* 10^{-8} g-mol/l.) has been reported.⁵ The total process, *i.e.*, the rate of removal of methyl iodide from the gas phase by aqueous alkaline hydrazine solutions, has also been reported.⁶ The rate of reaction of methyl iodide with a variety of nucleophilic reagents has been reported.⁷⁻¹² In this paper is reported the kinetics of

the reaction of methyl iodide and hydrazine in aqueous solution.

- (1) This paper is based on work performed under U. S. Atomic Energy Commission Contract AT(45-1)-1830.
- (2) Presented at the 23rd Northwest Regional Meeting of the American Chemical Society, Portland, Ore., June 1968.
- (3) Senior Research Scientist, Air Pollution Chemistry Section, Pacific Northwest Laboratory, Division of Battelle Memorial Institute, Richland, Wash.
- (4) Address correspondence to Department of Chemistry, Montana State University, Bozeman, Mont.
- (5) R. A. Hasty, *Can. J. Chem.*, **46**, 1643 (1968).
- (6) R. A. Hasty, *J. Chem. Eng. Data*, **13**, 134 (1968).
- (7) E. A. Moelwyn-Hughes, *Proc. Roy. Soc.*, **A196**, 540 (1949).
- (8) A. Slator, *J. Chem. Soc.*, **85**, 1286 (1904).
- (9) B. W. Marshall and E. A. Moelwyn-Hughes, *ibid.*, 7119 (1965).
- (10) R. H. Bathgate and E. A. Moelwyn-Hughes, *ibid.*, 2642 (1959).
- (11) E. A. Moelwyn-Hughes, *ibid.*, 779 (1938).
- (12) R. A. Ogg, *J. Amer. Chem. Soc.*, **60**, 2000 (1938).

Experimental Section

A Varian Model 1527B gas chromatograph with an electron-capture detector was used in this study. The remainder of the chromatographic system is described elsewhere.^{5,6}

Chemicals. Methyl iodide and 95% hydrazine were obtained from Eastman Organic Chemicals and were used without further purification. Stock solutions of hydrazine were prepared by dilution of the 95% hydrazine. Solutions were analyzed for hydrazine by the direct iodate method (using solvent) described by Audrieth.¹³ Methyl iodide stock solutions (ca. 10^{-4} g-mol/l.) were prepared by dilution of a saturated aqueous solution of methyl iodide at room temperature. There was appreciable change in the concentration of methyl iodide in the stock solution over a 24-hr period so that a fresh stock solution was prepared for each series of experiments. Nitrogen (99.97%) was used both as the carrier gas for the gas chromatograph and as the sparge gas in the experiments.

Kinetic Measurements. The reaction cell shown in Figure 1 was employed to study the reaction between hydrazine and methyl iodide. A 50–100- μ l volume of a stock solution of methyl iodide was delivered through the injection port to the aqueous hydrazine solution (170 ml) in the jacketed cell. The temperature of the cell was maintained by circulation of water from a constant-temperature bath. Aliquots of the sparge gas (normally 30 μ l) were taken from the sampling port at 1-min intervals for at least one half-life and then at 3- to 5-min intervals until the gas-phase concentration was approximately 10% of the extrapolated initial concentration. The flow rate of the sparge gas was controlled by the pressure drop across a microregulating valve and was measured with a soap bubble meter before and after each experiment. The flow rate was constant within 3% or less of the average. The results from a typical experiment are shown in Figure 2. The peak height is directly proportional to the concentration of methyl iodide in the sparge gas. The methyl iodide which exits from the reaction cell initially increases then exponentially decreases. No deviation from the exponential decrease was observed within the error of the experimental measurement.

After methyl iodide has been sparged from the system, the flow rate was changed and the experiment was repeated. A series of at least four experiments were performed to calculate the reaction rate constant of methyl iodide in solution.

Analysis of solution for hydrazine was performed after the last experiment of the series had been completed.

Development of Equations. Wiewiorowski¹⁴ derived a set of equations utilizing the sparging of the unreacted volatile component as a means of determination of both the reaction velocity and the solubility of oxygen in molten sulfur. The method was modified and was applied to the reaction of methyl iodide with hydrazine.

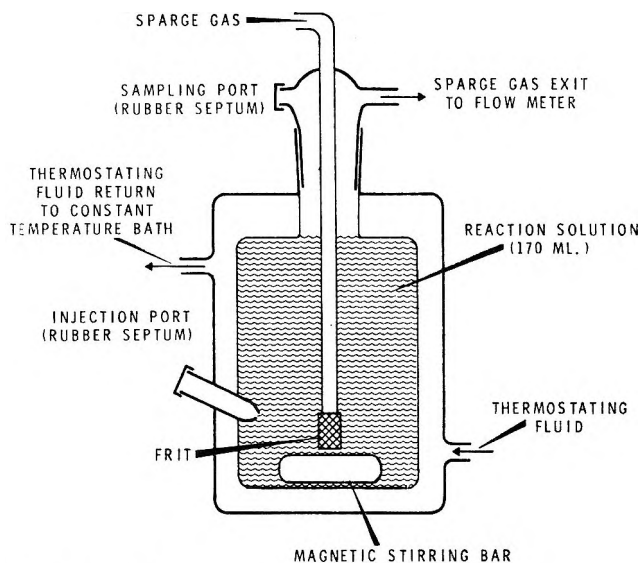


Figure 1. The reaction cell.

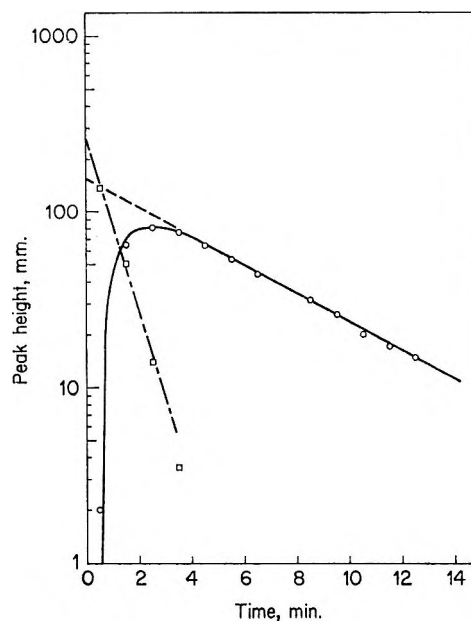


Figure 2. A typical sparge experiment, peak height for methyl iodide as a function of time (30- μ l aliquots at $4\times$ attenuation, $34.70 \pm 0.01^\circ$, 14.6 ± 0.2 -ml/min flow rate of sparge gas, 0.758 M hydrazine, 0.053 N sodium hydroxide, and 3×10^{-8} M methyl iodide): \circ , the observed peak height; \square , the difference between the extrapolated and observed peak heights. $(k_{\text{obsd}})^{-1} = 5.34$ min; $A_s = 9069$ (amount of methyl iodide sparged from cell, arbitrary unit).

The rate of disappearance of methyl iodide is the sum of the rate of sparge removal and the rate of reaction in the solution. Both the rate of sparge removal and the rate of reaction are first order with respect to the methyl iodide concentration. The expression for the rate of

(13) L. F. Audrieth and B. A. Ogg, "The Chemistry of Hydrazine," John Wiley & Sons, Inc., New York, N. Y., 1951, p 157.

(14) T. K. Wiewiorowski and B. L. Slaten, *J. Phys. Chem.*, **71**, 3014 (1957).

disappearance of methyl iodide is given by

$$-\frac{dC}{dt} = k_{\text{obsd}}C = (k_r + k_s)C \quad (1)$$

where k_{obsd} is the experimentally observed rate of decrease of methyl iodide, k_s and k_r are the first-order reaction rate constants for sparging and reaction, and C is the concentration of methyl iodide in the solution. The concentration of methyl iodide in solution and thus the rate of change of the concentration of methyl iodide in the gas is also given by eq 1, when C_g is substituted for C .

Integrating eq 1 and setting the boundary conditions of the initial concentration of methyl iodide equal to C_g^0 gives the time-dependent value of C_g . The amount of methyl iodide sparged from the solution, A_s , is given in eq 2. This is obtained by integration of the amount of methyl iodide which leaves the reaction cell. The result is

$$A_s = \frac{(dV/dt)C_g^0}{k_r + k_s} \quad (2)$$

where dV/dt is the flow rate of sparge gas. Similarly, the total amount of methyl iodide, A_0 , is obtained if no reaction had occurred

$$A_0 = \frac{(dV/dt)C_g^0}{k_s} \quad (3)$$

Combining eq 2 and 3 and substituting for k_s yields eq 4, which will be used to determine the reaction rate constant.

$$\frac{1}{k_{\text{obsd}}} = \frac{1}{k_r} - \frac{1}{k_r} \left(\frac{A_s}{A_0} \right) \quad (4)$$

The experiment is complicated by a volume of gas above the solution in which the sparge gas must mix before it can exit from the reaction vessel. This is seen in Figure 2 in the first few minutes of observations when the concentration of methyl iodide is increasing. Mixing is treated in a similar manner, and the concentration of methyl iodide which is measured is shown to be

$$C_g = C_g^0(e^{-k_{\text{obsd}}t} - e^{-k_2t}) \quad (5)$$

where k_2 is a constant related to the mixing of the sparge gas with the gas in the volume above the solution. The integration to obtain the amount sparged from the solution is treated as before in order to obtain

$$A_s = C_g^0(dV/dt) \left(\frac{1}{k_{\text{obsd}}} - \frac{1}{k_2} \right) \quad (6)$$

Results and Discussion

From a series of experiments at a given set of conditions, the observed rate of change of methyl iodide and the amount of methyl iodide sparged from the cell is determined for four or more flow rates. By variation of the flow rate over a range of values usually from *ca.* 8 to

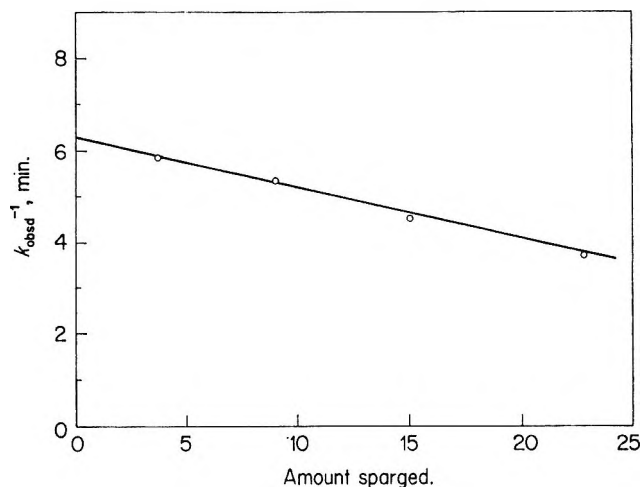
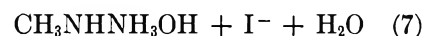


Figure 3. $(1/k_{\text{obsd}})$ as a function of the amount of methyl iodide sparged from cell ($34.70 \pm 0.04^\circ$, $0.758 M$ hydrazine, $0.053 N$ sodium hydroxide, $3 \times 10^{-8} M$ (initial) methyl iodide, $k_r(\text{extrapolated}) = 0.159 \text{ min}^{-1}$).

60 ml/min, sufficient data are obtained to permit extrapolation by use of eq 4. An example of one series of experiments is shown in Figure 3 for a $0.758 M$ hydrazine and $0.053 N$ sodium hydroxide solution at $34.70 \pm 0.04^\circ$, where sufficient methyl iodide was added to give an initial concentration of methyl iodide of $3 \times 10^{-8} M$. The rate constant for the reaction of methyl iodide with hydrazine in the solution from the extrapolation is 0.159 min^{-1} . Some difficulty was encountered for low flow rates, which was evidenced by lower values of the observed rate of decrease of the methyl iodide concentration than predicted from the values at higher flow rates. The cause of this difficulty has not yet been identified.

Results obtained for solutions where the hydrazine concentration was varied are shown in Table I. These results demonstrate the direct dependence of the rate on the hydrazine concentration as would be assumed for the displacement reaction shown in the equation



Because the methyl iodide is at very low concentrations,

Table I: Reaction Rate of Methyl Iodide in $0.0530 N$ Sodium Hydroxide Solution (34.7° , *ca.* $3 \times 10^{-8} M$ CH_3I)

Hydrazine concn, <i>M</i>	Reaction rate constant, min^{-1}	$10^3 \times$ second-order reaction rate constant, $\text{l. mol}^{-1} \text{ sec}^{-1}$
0.174	0.0382	3.65
0.374	0.0735	3.27
0.758	0.159	3.49
1.51	0.32	3.53
		Av 3.5 ± 0.2

the reaction is not expected to proceed to 1,1-dimethylhydrazine as in the reaction at higher concentrations.¹⁶ The rate of reaction was not dependent on the hydroxide ion concentration, unlike the case of the rate of the reaction of hydrazine and iodine.¹⁶ The effect of hydroxide or hydrogen ion concentration on the reaction rate is shown in Table II.

Table II: Effect of Hydroxide and Chloride Concentration at 34.77°

[N ₂ H ₄], M	[OH ⁻], N	[NaCl], M	k _r , min ⁻¹
0.758	0.053	0	0.159
0.76	0.026	0	0.153
0.75	0.026	0.05	0.159
0.754	7 × 10 ⁻⁵	0.053	0.148

Similarly the reaction rates at 49.3 and 24.56° were first order with respect to the hydrazine concentration. The reaction rate as a function of the hydrazine concentration at three temperatures is shown in Figure 4.

The nonzero intercept of the data at 49.3 and 64.7° (not shown in Figure 4) is indicative of the methyl iodide reaction with the solvent. The extrapolated value of k_r at 49.3° from Figure 4 is 2 × 10⁻⁴ sec⁻¹ and is in reasonable agreement with the calculated^{7,17} rate of hydrolysis, 6 × 10⁻⁵ sec⁻¹. The rate law for the disappearance of methyl iodide then becomes

$$-\frac{d[\text{CH}_3\text{I}]}{dt} = k_1[\text{H}_2\text{O}][\text{CH}_3\text{I}] + k_2[\text{OH}^-][\text{CH}_3\text{I}] + k_h[\text{N}_2\text{H}_4][\text{CH}_3\text{I}] \quad (8)$$

where k₁ and k₂ are the rate constants of hydrolysis by water and hydroxide ion and k_h is the rate constant for the reaction with hydrazine.

The second-order reaction rate constants at 64.7, 49.3, 34.7, and 24.6° are 0.064, 0.015, 0.0035, and 0.0011 l. mol⁻¹ sec⁻¹, respectively, with an uncertainty of ca. 8%. The activation energy is 20.2 ± 0.4 kcal/mol.

The activation energy for the reaction of methyl iodide and hydrazine does not differ greatly from that for reactions between methyl iodide and a number of anions in aqueous solution. The activation energy, preexponential term, bimolecular reaction rate constant, and nucleophilic constant for various reactions with methyl iodide are compared in Table III. The bimolecular reaction rate constant is directly proportional to the nucleophilic constant, E_n. (The nucleophilic constant, E_n, is a nonkinetic parameter which is calculated from the half-cell potential for the oxidative dimerization, E°: 2N₂H₄ → N₄H₈²⁺ + 2e⁻ (E_n = E° + 2.60).) Unfortunately, the value of E_n defined by Edwards¹⁸ cannot be calculated for all nucleophiles. From

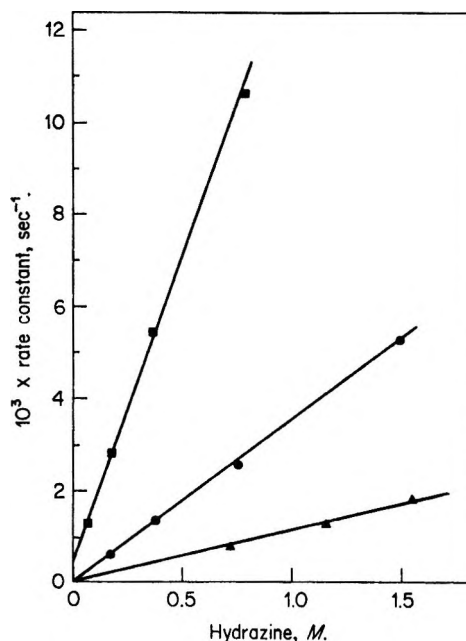


Figure 4. The pseudo-first-order rate constant as a function of hydrazine concentration (0.053 N sodium hydroxide): ■, at 49.3°; ●, at 34.7°; ▲, at 24.6°.

the correlation in Table III and bimolecular reaction rate constant for the reaction of methyl iodide with hydrazine, the nucleophilic constant for hydrazine is determined to be 2.1 ± 0.1. The reactivity of hydrazine toward methyl iodide is high in comparison to the rates of most anion-methyl iodide reaction rates. The availability of an unshared pair of electrons on the nucleophile thus appears more of a factor in determining the reaction rate than does the charge or absence of a charge on the nucleophile. (It would be interesting to examine the relative reaction rate of methyl iodide with respect to the phenoxide, thiophenoxide, and selenophenoxide ions to see the effect of expansion on the orbitals occupied by the unshared electron pair.)

The reaction of methyl iodide with nucleophiles (see Table III) gives preexponential terms which are large in comparison to the "normal" value for bimolecular reactions (ca. 10¹¹ l. mol⁻¹ sec⁻¹). This high preexponential term becomes even more apparent when the steric limitations of the reaction are considered. The nucleophile must approach the methyl iodide from the opposite side of the carbon atom in relation to the iodide in order for the collision to result in a reaction. The application of collision theory as developed for gases and applied to solution kinetics is only a rough approximation of the process which occurs in solution.

(15) Reference 13, p 30.

(16) K. K. Sengupta and S. K. Sengupta, *Z. Phys. Chem.* (Frankfurt am Main), **45**, 378 (1965).

(17) E. A. Moelwyn-Hughes, *Proc. Roy. Soc.*, **A220**, 386 (1953).

(18) J. O. Edwards, *J. Amer. Chem. Soc.*, **76**, 1540 (1954).

Table III: Comparison of Reaction Rates of Nucleophiles toward Methyl Iodide

Nucleophile	Nucleophilic constant	Bimolecular reaction rate constant, l. mol ⁻¹ sec ⁻¹	Activation energy, kcal mol ⁻¹	Preexponential term, l. mol ⁻¹ sec ⁻¹	Ref
F ⁻	-0.27	7.08 × 10 ⁻⁸	25.2 ± 0.5	2.08 × 10 ¹¹	10
H ₂ O	0	1.4 × 10 ^{-9^b}	28.4 ^c	1 × 10 ¹²	17
Cl ⁻	1.24	3.30 × 10 ⁻⁶	21.97 ± 0.34	4.16 × 10 ¹⁰	11
Br ⁻	1.51	4.16 × 10 ⁻⁶	19.31 ± 0.50	6.00 × 10 ⁹	11
OH ⁻	1.65	6.36 × 10 ⁻⁶	22.22 ± 0.23	1.24 × 10 ¹²	7
SCN ⁻	1.83	3.58 × 10 ⁻⁴	19.95 ± 0.40	1.49 × 10 ¹¹	20
I ⁻	2.06	4.71 × 10 ⁻⁴	17.58 ± 0.20	0.93 × 10 ¹⁰	12
CN ⁻	2.04	5.76 × 10 ⁻⁴	20.47 ± 0.12	6.01 × 10 ¹¹	9
S ₂ O ₈ ²⁻	2.52	2.84 × 10 ⁻²	18.88	2.01 × 10 ¹²	7
N ₂ H ₄	<i>a</i>	1.1 × 10 ⁻³	20.2 ± 0.4	1.7 × 10 ¹²	This work

^a Not available. ^b Calculated from unimolecular hydrolysis rate constant. ^c Calculated between 30.03 and 38.10°. The activation energy goes through a minimum at approximately 60°. The term in column 5 was calculated at 25° assuming $E_A(25^\circ) = 28.4$ kcal/mol.

In summary, our understanding of the factors which influence the rate of reaction of this simple displacement reaction is unsatisfactory. Changes in the hydration of the reactants,^{9,10} formation of bonds in the reaction intermediate,¹⁹ nucleophilicity of the reactants,¹⁸ and influence of the solvent viscosity on the preexponential term²⁰ have been considered in models which attempt to predict reaction rates and/or activation energies. None of these factors are by themselves sufficient to produce

an adequate model. The relative contribution of each factor in a single model has not yet been accomplished.

Acknowledgments. The author wishes to thank Mrs. S. Sutter for her assistance in performing the experiments.

(19) C. G. Swain and E. R. Thornton, *J. Amer. Chem. Soc.*, **84**, 817 (1962).

(20) G. C. Lalor and E. A. Moelwyn-Hughes, *J. Chem. Soc.*, 2201 (1965).

Reactive Silica. I. The Formation of a Reactive Silica by the Thermal Collapse of the Methoxy Groups of Methylated Aerosil

by Claudio Morterra and M. J. D. Low¹

Department of Chemistry, New York University, New York, New York 10458 (Received June 18, 1968)

The degassing of methylated Aerosil silica was studied by infrared spectroscopic techniques. The surface methoxy groups were quite stable and were removed only very slowly at temperatures up to 600°. At higher temperatures, however, the removal of methoxy groups became very rapid. The methoxy groups cracked, and the silica surface was drastically modified. Surface silanol and silane groups were formed. Also, the spectra indicate that hydrocarbonic surface species were formed which were acetylenic in nature and which showed extreme stability to degassing. Silane and other groups were only slowly removed at 830°; their removal resulted in the formation of a silica surface exhibiting unusually high reactivity. A possible mechanism is discussed.

It is well known that silicas can react with methanol, and that the resulting methylated surfaces are unusually stable.² The surface Si-O-CH₃ groups are removed only very slowly by pumping at temperatures up to approximately 600°. Degassing at higher temperatures, however, leads to rapid changes.³ Essen-

tially, the thermally induced collapse of the methoxy groups results in a drastically altered surface. The

- (1) To whom inquiries should be directed.
- (2) (a) E. Borello, A. Zecchina, and C. Morterra, *J. Phys. Chem.*, **71**, 2938 (1967), and references therein; (b) M. J. D. Low and Y. Harano, *J. Res. Inst. Hokkaido Univ.* (Anniversary Vol.), in press.
- (3) C. Morterra and M. J. D. Low, *Chem. Commun.*, 203 (1968).

new adsorbent produced in this manner, termed "reactive silica" for brevity, exhibits interesting properties which differentiate it from "normal" degassed silica, including an exceptionally high activity for chemisorption.

The present paper deals with the surface species formed in the preparation of reactive silica, as studied by infrared spectroscopic techniques. The reactivity of the new surface will be described elsewhere.

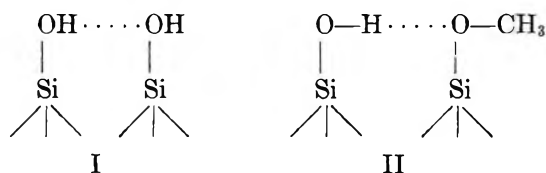
Experimental Section

Samples for spectroscopic study were prepared by compressing approximately 85 mg of Aerosil silica⁴ in a steel die at 35–40 kg/cm². The resulting pellet (approximately 40 mg/cm²) was mounted in a cell similar to that described by Peri and Hannan⁵ connected to a conventional vacuum system capable of 10⁻⁵ to 10⁻⁶ Torr. The sample was exposed to 70 Torr of methanol at 350°. Nearly all of the surface hydroxyls of the silica were replaced by methoxy groups by this treatment after about 20 hr.^{2b} The methylated sample was then degassed as required.

A Perkin-Elmer Model 621 spectrophotometer fitted with a Reeder⁶ thermocouple was used to record spectra. Scale expansions were frequently used to observe small spectral changes and to study weak or sharp bands. In the various figures, %*T* is per cent transmittance and *D* is optical density.

Results and Discussion

Demethoxylation. Methylated samples were subjected to degassing under various conditions. As noted earlier,² the spectra showed that the surface Si–O–CH₃ groups were very stable to outgassing until quite high temperatures were reached. However, if the outgassing was carried out much above 600°, even relatively small increases in temperature markedly changed the decomposition rate of the methoxy groups. Such heating of methylated silica caused the desorption of water and methanol in the early stages of decomposition and the evolution of several hydrocarbons (mainly methane, ethylene, and acetylene), water, formaldehyde, CO, and H₂, in the later stages.⁷ The initial stages thus involved the elimination of water and methanol from surface structures^{2a} such as I and II



followed by a cracking of the Si–O–CH₃ groups. The changes in the infrared spectra occurring during the pyrolysis were complex, and are summarized as follows.

When a methylated sample was degassed, the bands² due to the C–H stretching vibrations of the methoxy groups declined in intensity. An example of the

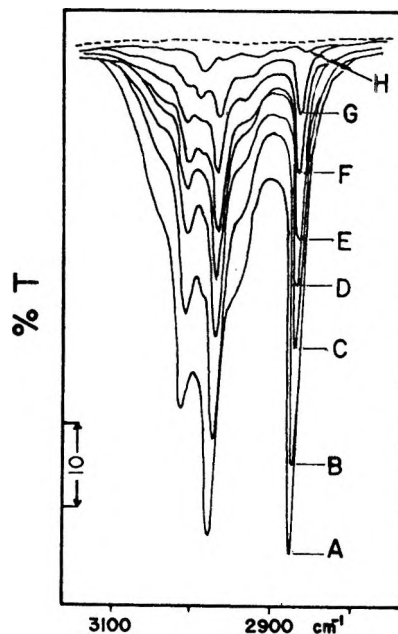


Figure 1. Effect of outgassing at 750° on methylated aerosil: broken line, background. The sample was degassed at the following times in minutes: A, 0; B, 1; C, 2; D, 3; E, 5; F, 9; G, 16; H, 40.

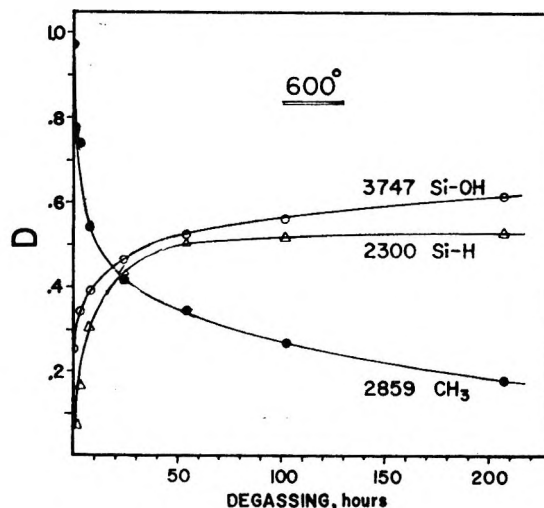


Figure 2. Degassing at 600°.

changes observed at 750° is given in Figure 1. The changes were similar at other degassing temperatures and differed only in rate. The decline of the prominent 2859-cm⁻¹ C–H band with degassing time for three temperatures is shown in Figures 2, 3A, and 4A. The time required to remove the methoxy groups completely at 750° varied from 30 min to about 2 hr depending on the degree of methylation. Demethylation was com-

(4) Aerosil 2491/380, Degussa Inc., Kearny, N. J.

(5) J. B. Peri and R. B. Hannan, *J. Phys. Chem.*, **64**, 1526 (1960).

(6) C. M. Reeder Co., Detroit, Mich.

(7) Experiments of E. Borello, *et al.*, at the University of Turin.

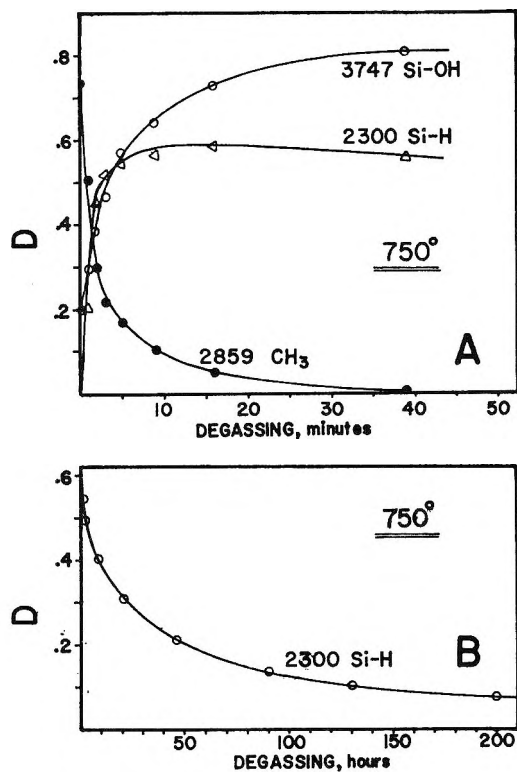


Figure 3. Degassing at 750°.

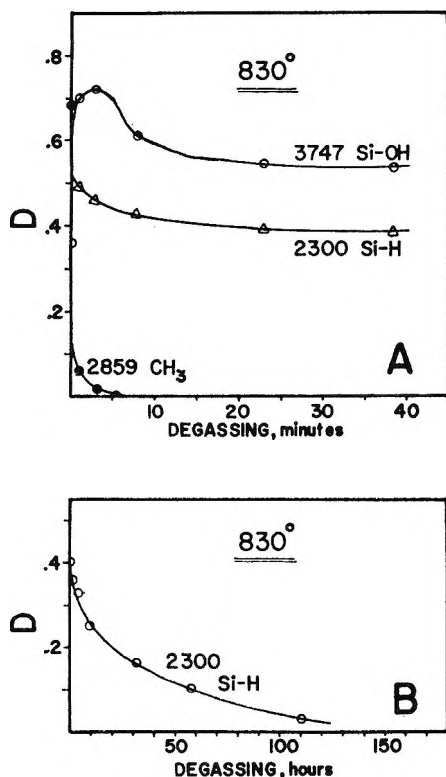


Figure 4. Degassing at 830°.

plete in a few minutes above 800° but required several days at 600°. The decline of the C-H bands was accompanied by changes in other spectral regions.

Hydroxyl Formation. With spectra of silicas, a band

near 3747 cm^{-1} , hereafter termed the Si-OH band, is generally attributed to "free" or isolated surface silanol groups. In the present study, the intensity of the Si-OH band increased upon degassing, the increases closely following the decreases of the C-H bands. The changes occurring at three temperatures are shown in Figures 2, 3A, and 4A. The Si-OH band which was formed was quite sharp ($\Delta\nu_{1/2} \sim 10 \text{ cm}^{-1}$) and perfectly symmetrical, indicating that the newly formed silanols were completely free of both inter- and intramolecular interactions. Subsequent to the complete removal of the methoxy groups, the Si-OH band decreased slowly upon further degassing at 750° or higher. It was not feasible to observe the decrease in the Si-OH band at 600° because the removal of methoxy groups was incomplete even after 10 days.

The formation of the surface silanols could arise through the rupture of the C-O bonds of the Si-O-CH₃ groups, with subsequent abstraction of hydrogen from the gaseous pyrolysis products. The formation of large numbers of hydroxyls would recreate some structures of type I, which would then be immediately destroyed at high temperatures to yield water molecules. The occurrence of such processes would agree with the observation of water in the gas phase during both early and late stages of pyrolysis.

Surface Silane. The pyrolysis of the methoxy groups led to the formation of a strong and broad band near 2280 cm^{-1} . The intensity of the latter increased rapidly until the number of methoxy groups was quite small ($D \leq 0.1$), and declined very slowly thereafter. The band, hereafter termed the 2300- cm^{-1} band, shifted to 2300 cm^{-1} after several hours of degassing. Changes of that band with continued degassing are shown in Figures 2-5. At temperatures around 600° the growth of the 2300- cm^{-1} band was not complete even after 200 hr. At 830°, however, the growth was very rapid and the decline of the band occurred even in the first few minutes of degassing.

The 2300- cm^{-1} band was clearly brought about by an Si-H stretching vibration, as suggested by the spectral position of the band^{8,9} and demonstrated by the formation of an analogous band near 1650 cm^{-1} when methanol-*d*₄ was used in the surface methylation.³ The simplest assignment of the 2300- cm^{-1} band would be to the Si-H stretching vibration of a grouping consisting of an hydrogen atom bonded to an Si atom of the SiO₂ surface or to an Si atom of a small aggregate or "island" of silicon. The latter hypothesis must be rejected because others have studied the adsorption of hydrogen on pure silicon and observed the Si-H band at quite different frequencies.¹⁰ Also, the position of the 2300-

(8) E. A. V. Ebsworth, "Volatile Silicon Compounds," The Macmillan Co., New York, N. Y., 1963.

(9) L. J. Bellamy, "The Infrared Spectra of Complex Molecules," John Wiley and Sons, 2nd ed, New York, N. Y., 1963.

(10) G. E. Becker and G. W. Gobeli, *J. Chem. Phys.*, **38**, 2942 (1963).

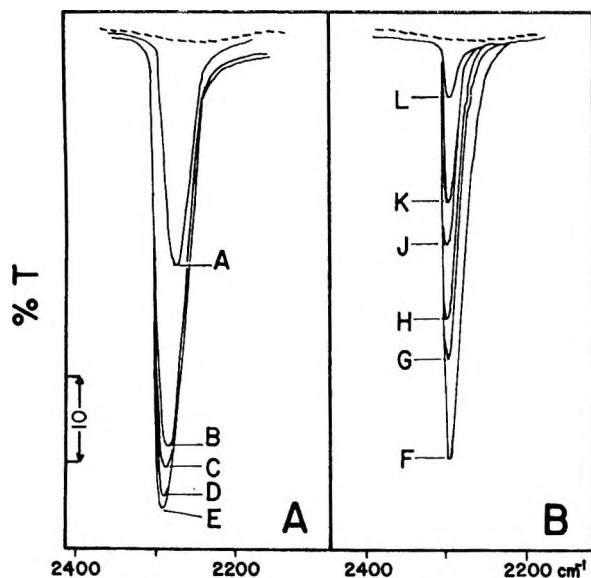


Figure 5. Changes of the silane band at 750°: broken line, background. Part A, outgassing time in minutes: A, 1; B, 2; C, 3; D, 5; E, 16; part B, outgassing time in hours: F, 2; G, 18; H, 27; J, 42; K, 66; L, 130.

cm^{-1} band is rather high in comparison to those of Si-H stretching bands of many silanes.¹¹ Absorptions at such high wave numbers have only been observed when several electronegative atoms were bonded to the Si-H structure, or when the Si atom was part of a polysiloxanic structure.¹¹ The present surface compound is analogous to the latter, if it is supposed that the hydrogenated Si atom is still a part of the silica surface. The assignment of the 2300- cm^{-1} band to a surface silane, with the Si atom being a part of the silica surface, would therefore appear to be a reasonable one. However, this is an oversimplification, on the basis of the observed reactions of the reactive Aerosil. These, and the nature of the species responsible for the 2300- cm^{-1} absorption, will be discussed in the paper following.

The shape and changes of the 2300- cm^{-1} band at 750° are shown in Figure 5. The continuous shift of the band position, both during the formation and the decline of the band, toward higher wave numbers as well as the narrowing of the band during the decline, suggest that the Si-H bond varied over a wide range of energies, possibly as a consequence of surface surroundings of quite different polarity. The grouping of lesser stability, namely those least hydridic in nature, would be formed first and cause absorption at the lower frequencies. Such species would also be the first removed, and their removal would lead to a shift in the band position and a narrowing of the band. The existence of interactions between the groups which give rise to the low wave number absorption would seem to be excluded, because it seems quite unlikely that interacting groups would be the first ones to form, weakly interacting or entirely free groups being formed later.

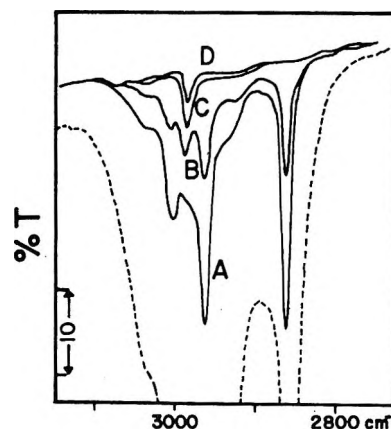


Figure 6. Formation and decrease of the 2983- cm^{-1} band at 750°: broken line, methylated sample. The outgassing times were: A, 5 min; B, 15 min; C, 3 hr; D, 13 hr.

The formation of the surface silane structures during the high-temperature outgassing appears to be connected with the breaking of the Si-O bond of the Si-O-CH₃ groups, followed by reaction with the hydrogen of the products of the pyrolysis. The nature of the latter is uncertain. Also, the slow elimination of the silane grouping, as shown in Figures 3, 4, and 5B, does not lead to the formation of infrared-active species on the surface. However, the final degassing leads to a silica exhibiting unusually and unexpectedly high activity. Aerosil which has been subjected to a methylation-demethylation cycle as described is termed "reactive silica." Its reactive properties will be described in a subsequent paper.

Surface Hydrocarbon. A small band was formed at 2983 cm^{-1} during the last stages of the pyrolysis, *e.g.*, Figure 6. This band was always very weak and was hardly observable in the 600° experiment. The 2983- cm^{-1} band was not found when deuteriomethanol was used, but an extremely weak band was then observed at 2237 cm^{-1} . This indicates that a hydrogen-containing species was involved and, in view of the spectral position of the band, the 2983- cm^{-1} band is attributed to the C-H stretching of an otherwise unidentified surface hydrocarbon structure. The latter was quite stable to outgassing at 750° (Figure 6), but declined and completely disappeared at 800–850° in several hours. This unusually high stability and the time at which the band was formed suggest that the species causing it were formed at surface sites at which other highly stable species were formed which gave rise to absorptions at 3311 and 2070 cm^{-1} .

Surface Acetylide. Two bands were formed which were quite sharp although weak, and were stable in position at 3311 and 2070 cm^{-1} . The two bands appeared and disappeared together, and are consequently as-

(11) A. L. Smith and N. C. Angelotti, *Spectrochim. Acta*, **15**, 412 (1959).

cribed to the same species. Also, they seem to be connected with the elimination of silane groups rather than with the disappearance of methoxy groups. The bands, and their behavior on degassing, are shown in Figures 7 and 8. The absorptions are ascribed to the C—H stretching and the C≡C stretching vibrations of a surface C≡C—H structure, respectively. The observed frequencies of the bands are in good agreement with those expected for an asymmetric acetylene which has a mass much greater than a hydrogen at one end of the molecule.¹² Also, using deuteriomethanol, the band attributed to C≡C was shifted to 1936 cm⁻¹, as would be expected for a deuterioacetylene;¹² using tenfold ordinate scale expansion, a weak band was observed at 2588 cm⁻¹ which can be assigned to the C—D stretch of the deuterated acetylenic structure.¹²

It is difficult to explain the formation of such an unusual surface species and also its great stability to outgassing at high temperature. The acetylenic molecule could be bonded to the surface either through an oxygen atom (structure III) or directly to a silicon atom (structure IV). However, the rapid decomposition of methoxy groups, involving the scission of Si—O and O—C bonds, suggests that a structure such as III would not

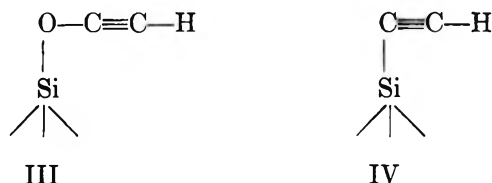


exhibit the extraordinarily high stability which was observed. Rather, structure IV is indicated. The observed higher stability of the Si—C bonds in comparison to that of the O—C bond¹³ would explain the stability of IV, and thus lends some support for the assignment.

Comparison of Figures 7B, 3A, and 4A shows that IV was mainly formed when methoxyl groups were no longer present on the surface and when the gaseous products of the pyrolysis had been pumped away. The initial, increasing parts of the curves of Figure 7B seem to be connected with the initial, steep decline of the Si—H curves of Figures 3B and 4B, thus pointing to a relation between the elimination of surface silane and the formation of surface acetylene. The following mechanism is suggested. It is postulated that reactive sites of the type formed by the elimination of the silane are created in the initial stages of the decomposition of the methoxy groups. Some of these sites can then chemisorb hydrocarbon from the gas phase to produce a structure responsible for the weak but stable band observed at 2983 cm⁻¹. Some of the sites could also be suitably spaced to hold an acetylene (or ethylene) molecule to yield, after a dehydrogenation step, a structure such as V.

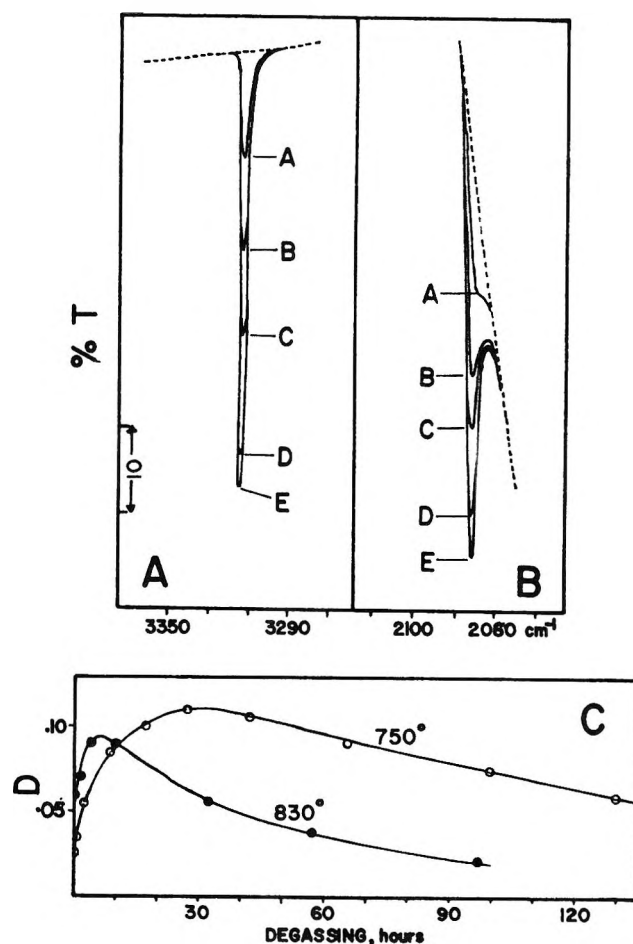
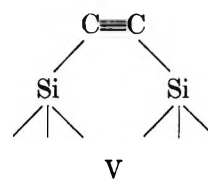


Figure 7. Effect of outgassing on surface acetylene: parts A, B: degassing at 830°; broken line, background. The degassing times in minutes were: A, 2; B, 5; C, 20; D, 90; E, 240; part C: optical density of the 3311-cm⁻¹ band as a function of degassing time at 750 and 830°.

The C≡C stretching of V would not be observed because of the symmetry of the structure. During the slow decomposition of the 2300-cm⁻¹ silane some of the hydrogen atoms formed could react with the bridges of structure V, thus leading to the formation of structure IV and the 3311- and 2070-cm⁻¹ bands (see the increasing portions of the curves of Figure 7B). The acetylenic structure IV would then be slowly eliminated (decreasing parts of the curves of Figure 7B), probably through the reaction of IV with additional hydrogen with subsequent desorption of acetylene. The reactive

(12) D. J. C. Yates and P. J. Lucchesi, *J. Chem. Phys.*, **35**, 243 (1961).

(13) Reference 8, p 82 ff.

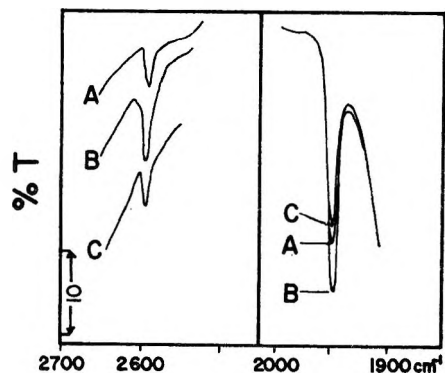


Figure 8. Effect of degassing at 830° on deuterioacetylene. The outgassing times in hours were: A, 1; B, 16; C, 40.

sites, unsaturated silicon atoms discussed in a subsequent paper, would be regenerated by this description process.

The above mechanism receives some support from the observation that the acetylenic structure IV can be eliminated by reaction with hydrogen. The process is quite slow at 450° but is faster at higher temperatures. Hydroxyls were not formed during this reaction, thus again excluding structure III, and surface hydrocarbons were not formed. At these temperatures (450–550°) the sites could also react with hydrogen and contribute to the formation of a band at 2227 cm^{-1} . This will be discussed elsewhere.

The surface silicon acetylide was also quite stable toward oxygen and water vapor. The reaction with oxygen started at 350–400° and proceeded very slowly, more than 10 hr being required for the complete oxidation at such temperature. The oxidation rate increases with increasing temperatures. Water vapor had no effect on

Table I: Summary of Bands

3747		Isolated Si—OH
3032		
2996		Surface
2958		Si—O—CH ₃
2929		
2857		
3311	C—H	Surface acetylide Structure IV
2070	H—C≡C—	
2588	C—D	
1936	D—C≡C—	
2983	C—H	Unidentified sur-
2237	C—D	face species
2300	Si—H	(SiH ₂ ; see part
1650	Si—D	II)

the 3311- and 2070- cm^{-1} bands at room temperature or at temperatures up to 400°. This is further evidence in favor of structure IV and against structure III, because one would expect the latter to be more reactive to water in analogy to the reaction of methoxy groups with water to yield surface hydroxyls.¹⁴ Note also that the species responsible for the small 2983- cm^{-1} band showed an even greater stability to oxygen, being oxidized only at temperatures as high as 500–600°. For a summary of the bands, see Table I.

Acknowledgment. Support from the National Center for Air Pollution Control is gratefully acknowledged.

(14) L. H. Little, "Infrared Spectra of Adsorbed Species," Academic Press, New York, N. Y., 1967, p 244 ff.

Reactive Silica. II. The Nature of the Surface Silicon Hydrides

Produced by the Chemisorption of Hydrogen^{1a}

by Claudio Morterra and M. J. D. Low^{1b}

Department of Chemistry, New York University, New York, New York 10453 (Received June 18, 1968)

The pyrolysis of the methoxy groups of methylated Aerosil silica leads to the production of surface Si-OH and SiH₂ groups, as indicated by infrared absorptions at 3747 and near 2300 cm⁻¹, respectively. Prolonged outgassing causes the elimination of hydrogen from these groups and leads to the formation of surface Si radicals. Experiments with electron spin resonance confirm this mechanism. The radical is very reactive and permits the dissociative chemisorption of hydrogen at temperatures as low as 25°. A second surface silane, Si-H, is also formed, but is not stable above 550°. Adsorbed water does not interact extensively with the surface silanes. The latter are stable to oxygen up to 350°. The nature of the surface, the surface species, and their interactions, are discussed.

It is well known that molecular hydrogen is not chemisorbed by silica surfaces. The physical adsorption of hydrogen on Vycor glass has been observed,² the adsorption causing an activation of the H-H stretching vibration at 4131 cm⁻¹, and atomic hydrogen is bound to Vycor but apparently without producing any infrared-active species.^{3a} However, a material^{3b} resulting from the pyrolysis of methylated Aerosil has been found to chemisorb molecular hydrogen and to do so at room temperature. The present paper is concerned with the interactions of this "reactive silica" and molecular hydrogen, studied mainly by means of infrared spectroscopic techniques, and with the probable nature of the silicon hydrides which were formed on the silica surface.

Experimental Section

The preparation and some surface properties of reactive silica have been described elsewhere, as have most of the experimental methods used in these studies.^{3b}

Hydrogen, or deuterium, was purified by diffusion through hot palladium. H₂O and D₂O were purified by alternate freezing and thawing *in vacuo*. Oxygen was prepared by the thermal decomposition of KMnO₄. Electron spin resonance (esr) measurements were carried out with a Varian Model V4502 spectrometer. Separate samples were used for esr and infrared measurements. Samples used for esr study were confined in a quartz tube of the type normally used for esr work and were subjected to the methylation, degassing, and other steps, under the same conditions as were employed for the preparation of samples used for infrared study. Infrared spectra were recorded with a Perkin-Elmer Model 621 spectrophotometer, using scale expansions as required. In the various figures, *D* is optical density and %*T* is per cent transmittance. Temperatures are in °C.

Results and Discussion

Reaction with Hydrogen. When a sample of reactive silica was exposed to hydrogen, usually at a pressure of 30 Torr, a sharp and perfectly symmetrical band (termed the 2227-cm⁻¹ band) was produced at positions ranging from 2225 to 2230 cm⁻¹. The band was produced at temperatures ranging from 25 to 550°. An example is shown in Figure 1. Such a band, implying that an interaction had occurred between the reactive silica and molecular hydrogen, has not been observed so far for normal silicas when exposed to hydrogen under any condition.

Exposure of reactive silica to deuterium produced an analogous band near 1624 cm⁻¹, the isotope shift thus indicating that a hydrogenous species was involved responsible for the 2227-cm⁻¹ band. This result, the spectral position of the band,^{4,5} and reasoning^{1b} identical with that used for the assignment of a band near 2300 cm⁻¹ to a surface silane, lead to the assignment of the 2227-cm⁻¹ band to the silicon-hydrogen stretching vibration of a surface silane.

Throughout the following presentation and discussion the surface silane absorbing near 2300 cm⁻¹ will be termed species A and that responsible for the 2227-cm⁻¹ band will be termed species B.

Outgassing a de-methoxylated sample at 830-850° caused a slow decrease of the 2300-cm⁻¹ band of species A, as described earlier,^{3b} and simultaneously brought

(1) (a) For part I, see ref 3b; (b) to whom inquiries should be directed.

(2) N. Sheppard and D. J. C. Yates, *Proc. Roy. Soc.*, **A238**, 69 (1956).

(3) (a) M. J. D. Low and E. Argano, *J. Vacuum Sci. Techn.*, **3**, 324 (1966); (b) C. Morterra and M. J. D. Low, *J. Phys. Chem.*, **73**, 321 (1969).

(4) E. A. V. Ebsworth, "Volatile Silicon Compounds," The Macmillan Co., New York, N. Y., 1963.

(5) L. J. Bellamy, "The Infrared Spectra of Complex Molecules," John Wiley and Sons, 2nd ed, New York, N. Y., 1963.

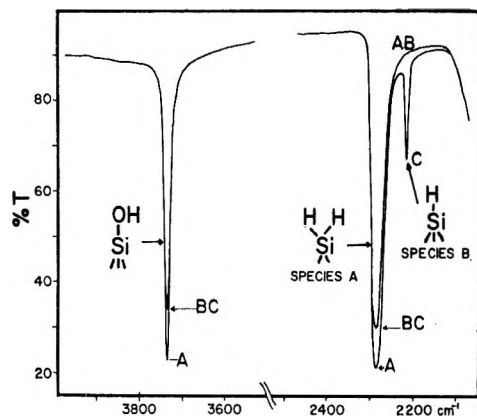


Figure 1. Reaction with hydrogen. Aerosil was methylated and then activated by high-temperature degassing (spectrum A), degassed at 830° for 15 hr (spectrum B), and was then exposed to 30 Torr of hydrogen at room temperature for 10 hr (spectrum C).

about an increase in the reactivity of the silica. Such behavior is illustrated by Figure 2. Part A of Figure 2 shows portions of the spectra recorded after degassing a reactive silica sample at 830° for various times and then exposing it to hydrogen at 350°. Part B of Figure 2 summarizes such data and shows the optical density of the 2300-cm⁻¹ band to decrease linearly with increases of the 2227-cm⁻¹ band. In spite of the facts that the 2300-cm⁻¹ band was quite broad, asymmetric, and shifted slightly in position, and that data of different experiments and samples were used, the plot is satisfactory. Such results indicate that the formation of species B was connected with the surface sites formed through the elimination of species A.

Species B was formed very slowly at room temperature, possibly because of the difficulty of dissociating H₂ on the surface. More than 2 days was usually required for the reaction to form species B to be complete at 25–30°. The process was faster at higher temperatures and was completed in several hours at 350° and in about 2 hours at 500°. However, species B were not stable above 550°. They were removed quite slowly on degassing at 600° and were eliminated in a few minutes at 650–750°. The surface again became active to hydrogen after such a removal of species B, but the full activity was not restored. The band intensities were restored, but the room temperature reaction was not observed, and reactions at higher temperature were slower, after an adsorption-desorption cycle.

The surface silanol groups were not affected by the formation of species B (Figure 1), but significant changes occurred if a sample was heated in hydrogen after the formation of species B had occurred. Some spectra showing such effects are shown in Figure 3. Spectra such as those show that the silanol groups which were formed were perfectly "free" or isolated on the surface, because the 3747-cm⁻¹ Si-OH band did not exhibit a

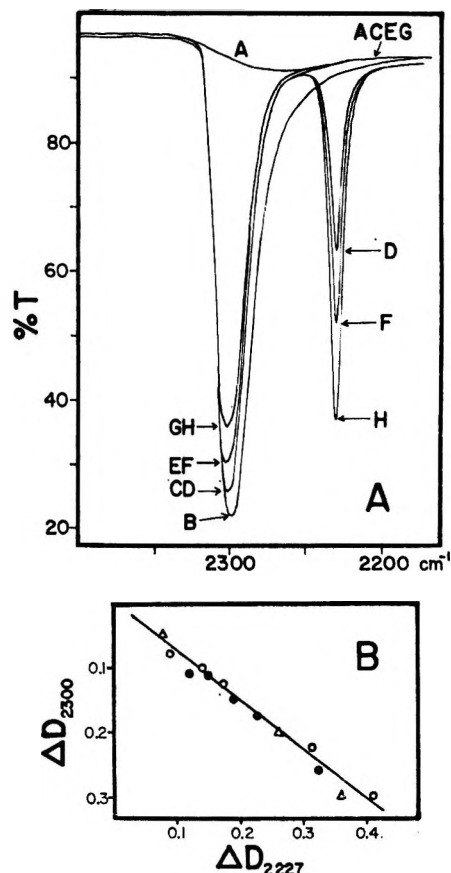
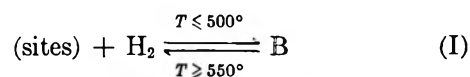


Figure 2. Effect of outgassing. An Aerosil sample was methylated, heated, and then exposed to hydrogen after various degassings. Part A: A, background; B, after demethylation at 750° for 3 hr; C, after degassing at 830° for 15 hr; D, after exposure to hydrogen at 350° for 3 hr; E, after degassing at 830° for 9 hr; F, after exposure to hydrogen at 350° for 3 hr; G, after degassing at 830° for 19 hr; H, after exposure to hydrogen at 350° for 3 hr. Part B shows the changes in the optical densities of the 2300 and 2227 cm⁻¹ bands, obtained from various experiments such as those of part A.

spectral shift, asymmetry, or broadening. At the same time, the band of species A increased and shifted its maximum to lower wave numbers and broadened on its low wave number side. Also, at the end of the reaction with hydrogen at high temperature, both the intensities and shapes of the 3747- and 2300-cm⁻¹ bands were much like those observed before the reaction. After a complete reaction cycle there was usually a small increase of the 3747-cm⁻¹ band and a small decrease of the 2300-cm⁻¹ band. These small changes could have been caused by an oxygen contaminant of the 10⁻⁵ to 10⁻⁶ Torr vacuum used.

The various results suggest the occurrence of several reactions, including a reversible reaction I



There appeared to be several simultaneous effects

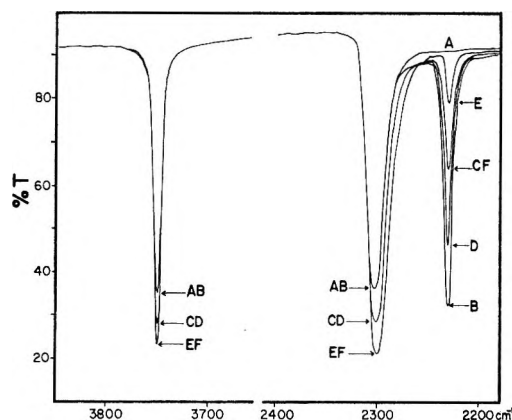
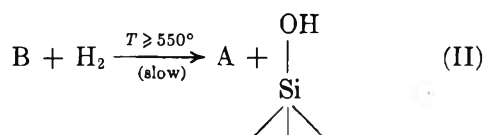


Figure 3. Heating in hydrogen. The sample was demethylated and degassed at 830° for 36 hr (spectrum A) and was then heated in 30 Torr of hydrogen at the following temperatures and times in hours: B, 450°, 2; C, 700°, 0.5; D, 450°, 2; E, 700°, 1.5; F, 450°, 2.

when species B were heated in hydrogen. The faster of these is taken as the desorption process of reaction I; it would be slower than under vacuum because of the presence of hydrogen in the gas phase. A second slower reaction would lead to the regeneration of hydroxyls and the formation of species A, as shown by the increase of the 3747- and 2300-cm⁻¹ bands when a sample was heated in hydrogen (Figure 3). This process is taken as



However, results such as those of Figure 3 clearly show that reaction II was not the only one occurring when species B was heated in hydrogen above 500°. The observed decrease of the 2227-cm⁻¹ band (*e.g.*, spectra C and E, Figure 3) appear to have been caused by two different effects, because the band of species B was partially restored when the sample was heated in hydrogen at 450° (spectra D and F, Figure 3).

The effects observed when a sample exhibiting species B was heated in an evacuated and isolated cell, *i.e.*, in a static vacuum, were in between those observed on heating in a hydrogen atmosphere or in a dynamic vacuum, *i.e.*, under degassing conditions. The fast, reversible desorption step of reaction I occurred, much like that found on degassing under dynamic conditions. However, an increase of the bands of species A and silanols was not observed or occurred only to a very small extent, probably because the pressure of hydrogen produced during the desorption was too small to permit reaction II to occur to a significant extent.

The various observations lead to the following conclusions. (a) The surface silanols and the silane spe-

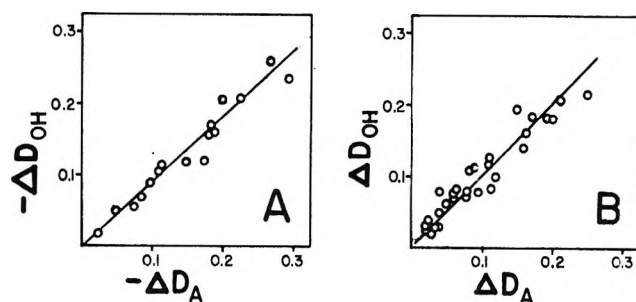
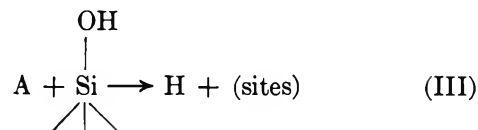


Figure 4. Relation of the 3747- and 2300-cm⁻¹ bands: part A, decreases of the optical densities of the two bands on outgassing at 830°; part B, increases of the optical densities of the two bands when samples reacted with hydrogen at temperatures above 550°.

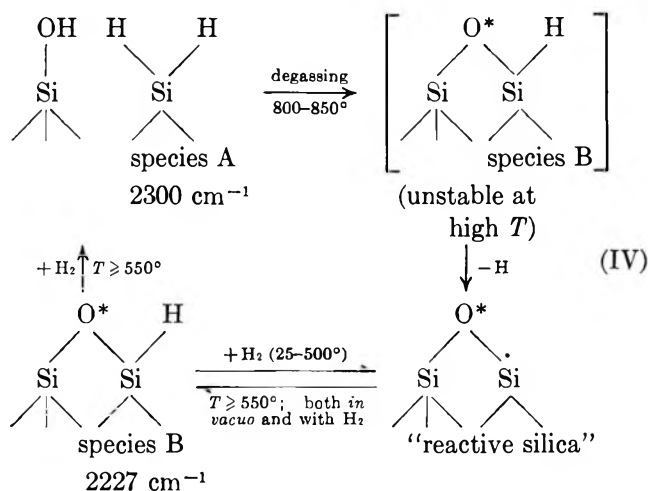
cies A were not destroyed independently upon outgassing at high temperatures. The removal of these groups was related and is attributed to a reaction III.



Support for this comes from the linear relation between the decrease of the optical density of the 3747-cm⁻¹ band ($-\Delta D_{\text{OH}}$) and that of the 2300-cm⁻¹ band ($-\Delta D_A$) shown in Figure 4A. (b) Reaction III between the surface silanols and silane A led to a new surface species which was reversible to hydrogen at high temperatures. The number of silanol and silane A groups which were formed through reaction II was almost the same as that eliminated through reaction III upon outgassing. Reaction II can thus be taken as the reverse of reaction III. Support for this comes from the linear relation between the increase of the optical densities of the two bands shown in Figure 4B and the similarity of the slopes of the two plots of Figure 4. The small difference in slopes accounts for the observation that the silanol band was slightly increased and the species A band slightly decreased after a complete cycle. (c) The preparation of the reactive silica (reaction III) led to the production of a surface site which reacted with hydrogen above 500° (reaction II) and also at lower temperatures to form a surface silane which was different in structure from species A. The results of an esr study, carried out with samples prepared and treated under conditions identical with those used for infrared studies, showed that a strong, sharp singlet at $g \sim 2.002$ was produced during the activation of the reactive silica. The singlet absorption was quenched by hydrogen. The results thus suggest that the sites responsible for reaction I were surface radicals.

The most reasonable explanation of the described effects is the following. Species A is a silane in which two hydrogen atoms are bonded to a surface silicon atom. Species B is a simple surface Si-H structure.

Outgassing at 800–850° causes the slow elimination of the hydrogen of silanol and silane A groups, leading to the formation of a very strained siloxane bridge and silane B. The siloxane bridge is stable to hydrogen up to 500° but reacts reversibly at higher temperatures. The silane B is not stable at high temperature and, as soon as it is formed, eliminates hydrogen and produces an unsaturated silicon atom bearing a spare electron. This esr-active structure is the "site" and is responsible for the extraordinary reactivity of the reactive silica. The silane B is restored by reaction with hydrogen at temperatures ranging from 25 to 500°. The esr singlet disappears during this reaction, indicating that the spare electron has been coupled. All these reactions are summarized in scheme IV.



Species A absorbs at higher frequencies than species B, as is usually observed for the case of disilanes.^{6,7} An Si-H₂ structure may be expected to exhibit two stretching fundamentals corresponding to the symmetrical and antisymmetrical modes. Such a doublet was never found in the present spectra, but this does not seriously detract from the credibility of the assignment. Even in very simple silanes the difference between the two modes is rather small⁸ and, as soon as the substitution of silanes becomes more complex, the doublet of disilanes is reduced to a single band.^{9,10} Analogously, the asymmetry and changing position of the 2300-cm⁻¹ band would indicate that the bonding of the species on the surface was complex, so that a doublet would not be resolvable. Additional evidence for the present assignment could come from the observation of the Si-H deformations, but these lie in a spectral region where the silica is opaque.

Isotopic Exchange. Both species A and B could be exchanged with deuterium. Some results are shown in Figure 5. The exchange reactions began to occur only at 450–500° and were quite slow in that range, especially for the conversion of species A (e.g., spectrum B, Figure 5A). The exchange rates increased very much between 500 and 600°, but species B began to be destroyed at these temperatures. The exchange of

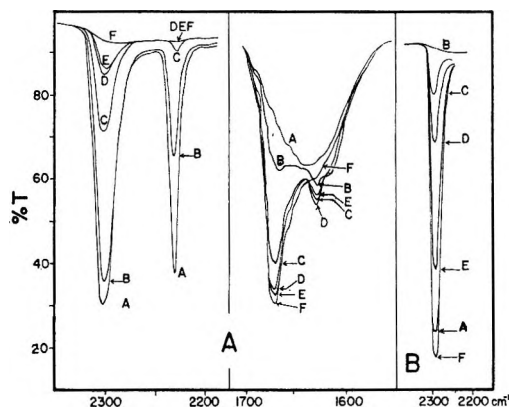


Figure 5. Isotopic exchange of surface silanes. Parts A: the hydrogenated sample (spectrum A) was exposed to 30 Torr of D₂ at the following temperatures and periods in hours: B, 500°, 11; C, 600°, 1; D, 600°, 3; E, 600°, 15; F, 700°, 1. Part B: the hydrogenated sample (spectrum A) reacted with D₂ to remove the 2300-cm⁻¹ band (spectrum B) and was then exposed to 30 Torr of H₂ at the following temperatures and periods in hours: C, 550°, 3; D, 550°, 15; E, 630°, 2; F, 700°, 1.

species A and the desorption of species B were complete at 700°. The effect of isotopic substitution on the extinction coefficients is particularly evident for species B. The band near 1624 cm⁻¹, corresponding to the deuterated species B, was quite weak. Also, the ratio of the intensities of the two bands of the normal species was no longer maintained for the deuterated species. If a deuterated sample was heated in hydrogen, it was not possible to restore the bands of species A and B to the intensities originally found with the sample prior to the deuteration, because the use of temperatures above 550° had partially transformed species A to species B (reaction II). An example of the increased intensity of the 2300-cm⁻¹ band after a complete exchange cycle is shown by spectra A and F of Figure 5B.

Heating a hydrogenated specimen in D₂O vapor caused the well-known conversion of Si-OH to Si-OD groups. However, neither species A nor B could be exchanged with D₂O at temperatures up to 400°.

The band near 1665 cm⁻¹ exhibited the same asymmetry and changeable position as those of the comparable 2300-cm⁻¹ band. Also, the more stable groups, absorbing at higher frequencies, appeared to exchange at a faster rate. A similar effect was observed in the

(6) N. B. Colthup, L. H. Daly, and S. E. Wiberly, "Introduction to Infrared and Raman Spectroscopy," Academic Press, New York, N. Y., 1964.

(7) R. N. Kniseley, V. A. Fassel, and E. E. Conrad, *Spectrochim. Acta*, **15**, 651 (1959).

(8) K. E. Lawson, "The Infrared Absorption of Inorganic Compounds," Reinhold Publishing Corp., New York, N. Y., 1961.

(9) C. Newman, S. R. Polo, and M. K. Wilson, *Spectrochim. Acta*, **15**, 793 (1959).

(10) E. A. V. Ebsworth, M. Onyszchuck, and N. Sheppard, *J. Chem. Soc.*, 1453 (1958).

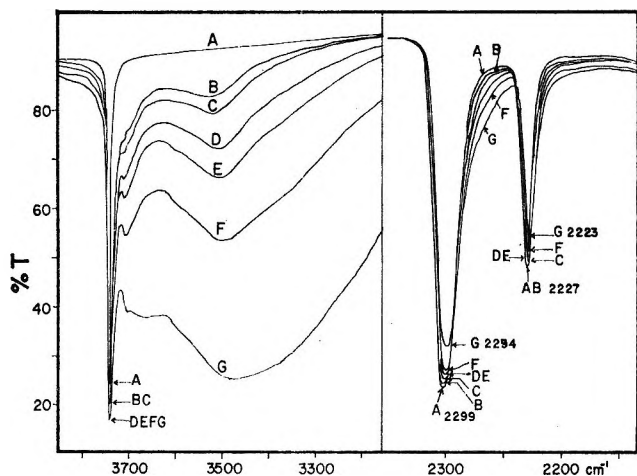


Figure 6. Water adsorption. The hydrogenated sample (spectrum A) was exposed to water vapor at room temperature at the following pressures in Torr: B, 1; C, 3; D, 5; E, 8; F, 15; G, approximately 30.

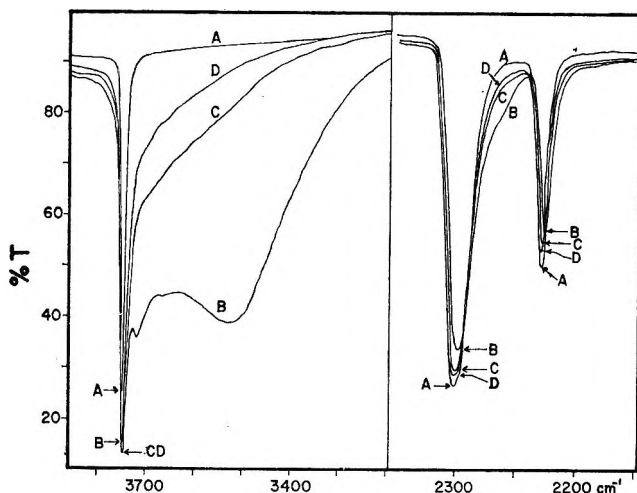


Figure 7. Water desorption. The hydrogenated sample (spectrum A) was exposed to approximately 30 Torr of water vapor for 12 hr and degassed at room temperature for 12 hr (spectrum B) and was then degassed at 300° for 30 min (spectrum C), and at 400° for 3 hr (spectrum D).

“back exchange” of a deuterated sample when exposed to hydrogen (Figure 5B). The shift of the band of species A toward lower wave numbers upon exchange is particularly evident. Such effects would seem to exclude, at least for the present system, the theory¹¹ that higher frequencies of a silane band of a silicon specimen corresponded to internal and consequently more dispersed and less interacting groups. Such structures should be expected to react slowly and be the last to exchange, in contradiction to the present observations, but an explanation of these differences in exchange rates is not evident.

The asymmetry of the 1665-cm⁻¹ band, its changing position, the superposition of a broad band of the silica,

and the poor transmittance did not permit the resolution of the doublet of Si-D₂ groups, in spite of the wider splitting usually observed for the deuterated species.^{7,9} Also, new absorptions for the stretching vibrations of partially exchanged groups, Si-HD, were not observed. This, however, was not surprising, because the partial substitution of hydrogen with deuterium has little effect on the stretching frequencies of even quite simple gaseous silanes.^{12,13} In fact, the Si-H stretching vibration is known to be scarcely affected by mass and other effects.^{6,14}

Water Adsorption. Hydrogen bonding of Si-H structures has not been reported and is thought to be very weak.¹⁴ The present results tend to confirm this opinion. Some spectra showing the effects of water sorption are shown in Figures 6 and 7.

The adsorption of water caused pronounced changes in the O-H region but had very little effect on the bands of the two silane species. The latter decreased slowly in intensity, and the band maxima shifted slightly to lower wave numbers, with increasing water adsorption (Figure 6). Also, “tailing” developed on the low wave number side of each band. In general, the effects were weak and were more pronounced with the species A band than with the species B band.

Degassing at room temperature for several hours removed weakly bound water but did not produce any changes in the silane bands. This is shown, for example, by spectra G of Figure 6 and B of Figure 7. Initially, the silane bands of the two samples had roughly the same intensities (spectra A, Figures 6 and 7), and were then diminished equally by water adsorption (spectrum G, Figure 6, spectrum B, Figure 7). The pronounced, broad adsorption in the 3600-3200-cm⁻¹ region of spectrum G, however, indicated the presence of much more weakly bound water than in spectrum B. Such effects indicate that little if any of the physically adsorbed water was bound to and affected the surface silanes. Degassing at 300°, however, caused a drastic decrease of the “tailing,” shifted the silane bands to higher wave numbers, and increased their intensities, but the starting conditions were not completely restored. A 300° degassing eliminated the broad band centering near 3520 cm⁻¹ and the small band near 3715 cm⁻¹.

The changes of the silane bands could be brought about either by the bridged water molecules responsible for the 3520-cm⁻¹ absorption¹⁵ or by clusters of hydrogen-bonded hydroxyls formed by the rehydration of the

(11) G. E. Becker and G. W. Gobeli, *J. Chem. Phys.*, **38**, 2942 (1963).

(12) J. H. Meal and M. K. Wilson, *ibid.*, **24**, 385 (1956).

(13) S. R. Polo and M. K. Wilson, *ibid.*, **22**, 1559 (1954).

(14) A. L. Smith and M. G. C. Angelotti, *Spectrochim. Acta*, **15**, 412 (1959).

(15) M. L. Hair, “Infrared Spectroscopy in Surface Chemistry,” Marcel Dekker, Inc., New York, N. Y., 1967.

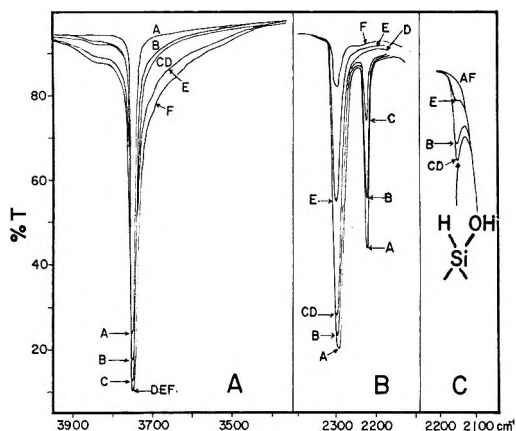


Figure 8. Oxidation of surface silanes. The hydrogenated specimen (spectrum A) was heated in 140 Torr of oxygen at the following temperatures and times in hours: B, 350°, 0.5; C, 350°, 1; D, 350°, 15; E, 500°, 0.5; F, 500°, 15.

silica surface. The fact that the shapes of the silane bands were not restored when the bridged water was removed by degassing at 300° would point to the importance of the hydroxyl clusters. However, vicinal hydroxyls were still abundant after a 300° degassing as shown, for example, by the tailing on the low wave number sides of the silanol bands of spectra C and D of Figure 7. Also, the importance of bridged water is supported by the observation that the tailing of the silane bands occurred under conditions where the surface rehydration was absent or very small (spectra B and C, Figure 6) so that the effects of hydroxyl clusters would be absent or negligible. However, it seems likely that there is merely a formal distinction between the two mechanisms. The interaction of the silane groups with hydroxylated species would occur only when a tightly bonded polar layer is built up on the surface, and it is unimportant whether the layer is made up of silanols or water molecules strongly bonded through two or three hydrogen bondings.

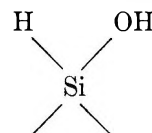
It is important that neither of the surface silane species was hydrolyzed by water vapor, unlike the situation sometimes found with simple or substituted silanes.⁴ There was no change in the silane bands up to 400°, but the silanes were quickly eliminated when a sample was heated in water vapor at 600–650°. However, it is probable that the high-temperature reaction was not a hydrolysis but an oxidation. In fact, appreciable amounts of Si–OH groups were formed when a hydrogenated sample was heated in D₂O vapor. A great excess of D₂O was used, so that only Si–OD groups should have been observed if a simple hydrolysis reaction had occurred.

The silanes did not exchange with D₂O. Also, the perturbations of the silane bands by adsorbed water were quite small. The absence of significant interactions would indicate that the surface silane groupings were hydrophobic and similar in nature to silicon hy-

dride, the silanic hydrogen atoms being electronegative in character.

Reaction with Oxygen. Both surface silanes exhibited a good stability to oxygen, reactions starting only at temperatures of about 350°. The species B were slowly but completely oxidized at 350° (Figure 8B), while only a fraction of the species A were destroyed. Temperatures above 350° were required to oxidize species A completely. This behavior confirms both the lesser stability of the silane species B, as already observed throughout the course of degassing experiments, and also the heterogeneous nature of the silane species A. In some of the experiments none of the species A was oxidized at 350–400°, thus indicating that the outgassing process had already eliminated the more weakly bonded groups. Also, as would be expected of heterogeneous groups as discussed above, the destruction of species A began with a decrease in absorption on the low wave number side of the 2300-cm⁻¹ band, causing a narrowing and a shift of its maximum to higher wave numbers (Figure 8B).

A new small band was formed at 2147 cm⁻¹ when the reaction between oxygen and species A began at temperatures ranging from 350 to 420°. The 2147-cm⁻¹ band, shown in Figure 8C, is attributed to the Si–H stretching vibration of the structure



formed at the first step of the oxidation of species A. The formation of the 2147-cm⁻¹ band lends further support to the assignment made earlier for the 2300-cm⁻¹ band. When the oxidation of species A started at temperatures above 420°, or when the temperature was increased after the completion of reactions at 350–420°, the 2147-cm⁻¹ band either was not formed at all or, if formed, was eliminated very rapidly. Such behavior is consistent with the reported instability¹⁶ of structures such as =SiH(OH).

The oxidation of the silanes resulted in the formation of surface hydroxyl groups, as shown by the changes in the 3900–3400-cm⁻¹ regions of spectra such as those of Figure 8A. The oxidation caused an increase in intensity of the Si–OH band, shifted its maximum from 3747 to 3732 cm⁻¹, increased the half-width from ~10 to ~30 cm⁻¹, led to asymmetry on the low wave-number side, and brought about a weak broad tailing between 3700 and 3500 cm⁻¹ (Figure 8A). Such results indicated the occurrence of inter- or intramolecular interactions, the latter being the most likely. This opinion is supported by experiments with deuterated samples.

A fully hydrogenated sample was treated with D₂O until the Si–OH groups had been almost completely

(16) J. B. Peri, *J. Phys. Chem.*, **70**, 2937 (1966).

converted to Si-OD groups. This exchange process did not affect the silane species A and B. The specimen was then heated in oxygen. The resulting destruction of the silanes led to the formation of Si-OH groups, the spectral changes observed being like those described above; the spectra in the O-H region were much like those shown in Figure 8A. However, in such oxidation experiments there was no change, or only a small modification, of the intensity and shape of the 2761-cm⁻¹ band of Si-OD groups. It is thus concluded that the oxidation led only to the formation of localized hydroxyl groups, water molecules not being formed because exchange was not observed, and also that the interactions producing the new shape of the 3742-cm⁻¹ band were more of an intra- than intermolecular nature, because the hydroxyls already present on the surface were not involved at all.

One would expect the oxidation of species A to lead

to the formation of geminal hydroxyls, and the above results and conclusions are not at variance with this. On the other hand, it seems surprising that such geminal hydroxyls gave rise to interactions which were so weak that the Si-OH band after the oxidation reaction was not much different from that caused solely by isolated silanols. However, such behavior is congruent with Peri's conclusion,¹⁶ based upon work with ordinary silica, that geminal hydroxyls are probably not hydrogen bonded to their partners because a five- or six-membered ring is normally needed for intramolecular hydrogen bonding.

Acknowledgment. Support by grants from the National Center for Air Pollution Control and the Communicable Disease Center are gratefully acknowledged. We thank Dr. G. Underwood for fruitful discussions and help with the esr experiments.

Thermophysical Properties of the Lanthanide Oxides. IV. Heat Capacities and Thermodynamic Properties of Thulium(III) and Lutetium(III) Oxides. Electronic Energy Levels of Several Lanthanide(III) Ions¹

by Bruce H. Justice, Edgar F. Westrum, Jr.,² Elfreda Chang, and Ray Radebaugh

Department of Chemistry, University of Michigan, Ann Arbor, Michigan 48104 (Received June 23, 1968)

The heat capacities of thulium(III) and lutetium(III) oxides were measured from 6 to 350°K. The electronic heat capacity associated with the Tm(III) ion is resolved from the total heat capacity values for the two oxides and that of gadolinium(III) oxide. Several low-lying energy levels for the Tm(III) ion arising from crystal field splitting of the ground term (⁶H₆) of Tm(III) ion and of related lanthanide(III) ions are discernible. The observed heat capacity values yield for C_p , $S^\circ - S^\circ_{T'}$, and $(G^\circ - H^\circ_{T'})/T$ 24.32, 26.28, and -12.22 cal/(mol °K) at 298.15°K for Lu₂O₃ with $T' = 0^\circ\text{K}$ and 27.90, 33.15, and -16.41 for Tm₂O₃ with $T' = 10^\circ\text{K}$. The latter values are extended to a 0°K reference point by estimating a magnetic contribution below 10°K.

Introduction

This paper extends and broadens the earlier studies³⁻⁵ on the thermophysical properties of the lanthanide oxides by providing thermal capacity data on thulium(III) and lutetium(III) oxides. Since both oxides crystallize with cubic symmetry as the C-type isomorph,^{6,7} this endeavor supplements knowledge of gradual change in the lattice heat capacity for cubic oxides with increasing atomic number obtained from a combination of the heat capacity curves for gadolinium and ytterbium oxides, by providing data on diamagnetic lutetium oxide with a ¹S₀ ground state. The inter-

polated lattice heat capacity results in a reasonable accounting of the electronic heat capacities of the intervening cubic paramagnetic oxides. Moreover, exten-

(1) This research was supported in part by the U. S. Atomic Energy Commission.

(2) To whom correspondence concerning this paper should be addressed.

(3) B. H. Justice and E. F. Westrum, Jr., *J. Phys. Chem.*, **67**, 339 (1963).

(4) B. H. Justice and E. F. Westrum, Jr., *ibid.*, **67**, 345 (1963).

(5) E. F. Westrum, Jr., and B. H. Justice, *ibid.*, **67**, 659 (1963).

(6) L. Pauling, *Z. Krist.*, **69**, 415 (1929).

(7) R. S. Roth and S. J. Schneider, *J. Res. Nat. Bur. Stand.*, **64**, 309 (1960).

sion of the interpolation scheme to the lattice heat capacity of the hexagonal oxides enhances the correlation between the observed spectrum and the (re)-derived electronic heat capacity. Both calorimetric and spectroscopic investigations involved A-type hexagonal isomorphs^{7,8} in which the heptacoordinated magnetic ions occupy equivalent lattice sites.

Since thermal measurements on lanthanum(III) and on neodymium(III) oxides and deduced crystal field splitting of the ground electronic level of the former were reported,³ the spectrum of Nd(III) ion in a lanthanum(III) oxide host has been observed by Henderson, *et al.*⁹ They report five crystal field lines for the ground state ($^4I_{9/2}$) at 0, 23, 84, 253, and 496 cm^{-1} . The first two excited levels are in excellent accord with corresponding values deduced from heat capacity data alone³ (0, 21, 81, and 400 cm^{-1}), and the center of density of the higher levels also corresponds. However, the interpretation of the electronic heat capacity data^{4,5} of the cubic gadolinium(III), dysprosium(III), holmium(III), and erbium(III) oxides was hampered by the lack of spectral data. These cubic lattices have two nonequivalent types of cation sites.¹⁰ Three-quarters of the cations have C_2 symmetry and each is surrounded by six anions at the corners of a cube with the two missing anions at the ends of a face diagonal. The remaining cations possess C_{3i} symmetry, in which each cation is similarly surrounded except that the missing anions are at the ends of a body diagonal. The spectra reported for Dy(III),¹¹ Er(III),^{12,13} and Tm(III)¹³ ions with C_2 symmetry in yttrium(III) oxide or in single crystal lanthanide(III) oxides together with heat capacity data for Gd_2O_3 ,⁴ Dy_2O_3 ,⁵ Er_2O_3 ,⁵ Tm_2O_3 , and Lu_2O_3 permit derivation of the lattice heat capacity for any of the cubic oxides from Gd_2O_3 to Lu_2O_3 and energy levels for the C_{3i} ions in Dy_2O_3 , Er_2O_3 , and Tm_2O_3 .

Thus, thermal measurements on thulium and lutetium oxides provide correlations of lattice heat capacity contributions for C-type oxides and electronic heat capacity contributions from ions on both types of sites. The measurements on thulium oxide afford a further opportunity for correlation of electronic heat capacity with the highly degenerate Tm(III) ion (3H_6) and further insight into the effect of the two-site structure of the C-type oxides on their energy levels.

Experimental Section

Thulium(III) and Lutetium(III) Oxide Samples. Finely divided (about 300 mesh) samples of the two lanthanide(III) oxides were loaned to us by Professor F. H. Spedding, Director of the Ames Laboratory of Iowa State University. The samples, with reported purities greater than 99.97%, were placed in alundum crucibles and fired in air within a muffle furnace at 900°. After cooling to room temperature, the samples were loaded into the calorimeter in a nitrogen-filled

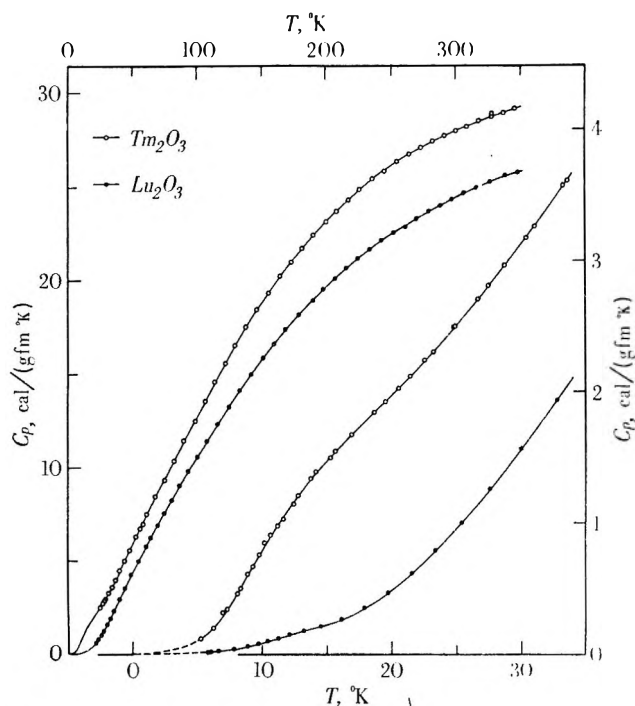
drybox. A pressure of about 100 Torr (at 300°K) of helium exchange gas facilitated thermal equilibration. The masses of thulium and lutetium oxide taken for measurement were 124.261 and 127.202 g *in vacuo*; molecular weights of 385.88 and 397.98 g were used. Powder patterns of the calorimetric samples showed C-type cubic structures with the accepted lattice constants.

Cryostat and Calorimeter. Measurements were made in the Mark II cryostat, which is similar to that described by Westrum and McCullough,¹⁴ by use of the quasiadiabatic technique.¹⁵ A capsule-type, platinum-resistance thermometer (laboratory designation A-5) calibrated by the National Bureau of Standards (NBS) from 10 to 90°K on their provisional scale and above 90°K on the International Temperature Scale was used. Below 10°K a provisional scale¹⁶ was adopted. Measurements of mass, resistance, potential, and time were made with devices whose calibrations are traceable to standards of NBS. The heat capacity of the gold-plated, copper calorimeter (laboratory designation W-28) was determined in a separate series of measurements. The calorimeter-heater-thermometer assembly contributed about 7% of the total apparent heat capacity at 10°K, 50% at 80°K, and decreased gradually to 40% at 350°K for thulium(III) oxide. Corresponding percentages for the lutetium(III) oxide are 40, 56, and 45. Corrections were made for slight differences in amounts of helium, grease, and solder between the calibration determination and the measurements on the samples. Crystallographic densities¹⁷ of 8.84 and 9.30 g/cc for Tm_2O_3 and Lu_2O_3 , respectively, were used in making buoyancy corrections.

Results and Discussion

Heat Capacities and Thermal Functions for Thulium and Lutetium Oxides. The observed heat capacities for thulium and lutetium oxides are presented in Table I in chronological order so that temperature increments of the individual points can usually be inferred from

- (8) R. M. Douglass and E. Staritzky, *Anal. Chem.*, **28**, 552 (1956).
- (9) J. R. Henderson, M. Muramoto, and J. B. Gruber, *J. Chem. Phys.*, **46**, 2515 (1967).
- (10) L. Pauling and M. D. Shappell, *Z. Krist.*, **75**, 128 (1930).
- (11) J. R. Henderson, M. Muramoto, T. M. Henderson, and J. B. Gruber, *J. Chem. Phys.*, **47**, 5097 (1967).
- (12) P. Kisliuk, W. F. Krupke, and J. B. Gruber, *ibid.*, **40**, 3606 (1964).
- (13) J. B. Gruber, W. F. Krupke, and J. M. Poindexter, *ibid.*, **41**, 3363 (1964).
- (14) E. F. Westrum, Jr., G. T. Furukawa, and J. P. McCullough, "Adiabatic Low-Temperature Calorimetry," in "Experimental Thermodynamics," J. P. McCullough and D. W. Scott, Ed., Butterworth and Co., Ltd., London, 1968.
- (15) E. F. Westrum, Jr., J. B. Hatcher, and D. W. Osborne, *J. Chem. Phys.*, **21**, 419 (1953).
- (16) H. J. Hoge and F. G. Brickwedde, *J. Res. Nat. Bur. Stand.*, **22**, 351 (1939).
- (17) D. H. Templeton and C. H. Dauben, *J. Amer. Chem. Soc.*, **76**, 5237 (1954).


 Figure 1. Heat capacities of Tm_2O_3 and Lu_2O_3 .

differences in adjacent mean temperatures. The observed apparent heat capacities have been adjusted for curvature with a Taylor series expansion of the true heat capacity about the mean temperature (\bar{T}) of the measurement.¹⁸ The curvature adjustment is then given by

$$C_p - \frac{\Delta H}{\Delta T} = - \sum_{n=1}^{\infty} \left(\frac{\partial^{2n} C_p}{\partial T^{2n}} \right) \frac{(\Delta T)^{2n}}{(2n+1)! 2^{2n}}$$

If it is assumed that the temperature derivatives of C_p and $\Delta H/\Delta T$ are equal, the derivatives in the infinite sum can be easily calculated from an analytical formulation of the apparent heat capacity. These adjustments were always considerably smaller than experimental precision. The data are given in terms of the defined thermochemical calorie (4.1840 J) and ice point (273.15°K). Heat capacities for both compounds are displayed in Figure 1. The heat capacities and derived thermodynamic functions at selected temperatures are presented in Table II. The probable error in the heat capacity is less than 0.1% above 30°K; that in the other functions is about 0.1% above 100°K. Below these temperatures the error increases somewhat due to the decreasing sensitivity of the thermometer and adiabatic shield thermocouples.

Resolution of the Electronic Heat Capacities in Lanthanide(III) Oxides. Electronic heat capacities, C_{el} , are here derived by procedures used formerly³ except that the lattice heat capacity contribution is interpolated linearly in terms of atomic number between

Table I: Heat Capacities of Lutetium(III) and Thulium(III) Oxides^a

$T, ^\circ K$	C_p	$T, ^\circ K$	C_p	$T, ^\circ K$	C_p
Lutetium(III) Oxide (Lu_2O_3)					
6.03	0.019	35.59	2.343	168.18	17.33
5.77	0.016	39.51	2.908	178.62	18.15
6.61	0.025	43.97	3.552	189.02	18.92
7.80	0.041	48.84	4.254	197.26	19.46
8.85	0.060	54.08	4.979	206.20	20.07
9.68	0.078	60.12	5.799	215.17	20.61
10.42	0.098	63.46	6.249	224.10	21.12
11.20	0.119	68.93	6.923	233.03	21.62
12.10	0.143	74.37	7.559	242.05	22.09
13.18	0.172	79.86	8.250	251.11	22.51
14.49	0.210	86.04	9.018	260.13	22.87
16.10	0.267	92.86	9.782	269.18	23.24
17.87	0.351	99.91	10.545	278.22	23.63
19.67	0.465	107.53	11.381	287.32	23.95
21.53	0.613	115.90	12.294	296.53	24.27
23.41	0.788	124.54	13.221	305.83	24.58
25.39	0.997	133.00	14.102	315.34	24.89
27.57	1.254	141.60	14.956	325.96	25.19
30.02	1.564	150.46	15.793	337.75	25.54
32.75	1.934	159.36	16.58	347.35	25.70

 Thulium(III) Oxide (Tm_2O_3)

Series I		17.40	1.728	39.66	4.466
			19.48	1.926	43.42
300.10	27.94	21.43	2.120	47.42	5.567
308.91	28.26	23.18	2.306	51.98	6.234
318.17	28.53	24.87	2.498	57.24	6.970
327.46	28.74	26.67	2.709		
336.58	28.90	28.69	2.962	Series V	
		31.02	3.260		
Series II		33.58	3.609	55.05	6.664
		36.41	4.013	60.80	7.494
254.71	26.31			67.17	8.393
263.59	26.68	Series IV		74.17	9.324
272.70	27.03			81.46	10.351
281.75	27.38	5.26	0.12	89.20	11.429
290.76	27.67	6.21	0.20	97.46	12.470
299.82	27.93	7.24	0.34	105.63	13.522
308.96	28.18	8.31	0.50	113.46	14.517
318.10	28.44	9.23	0.67	121.48	15.522
327.22	28.63	10.14	0.85	129.69	16.515
336.31	28.87	11.16	0.980	137.88	17.478
345.39	29.07	12.38	1.147	146.32	18.40
		13.73	1.339	155.01	19.31
Series III		15.21	1.497	163.76	20.17
		16.88	1.671	172.47	20.97
6.94	0.32	18.65	1.843	181.18	21.71
8.07	0.46	20.49	2.028	189.87	22.41
8.87	0.61	20.47	2.024	198.70	23.07
9.75	0.76	22.54	2.240	207.53	23.69
10.61	0.91	24.77	2.486	216.63	24.27
11.59	1.03	27.43	2.806	225.79	24.82
12.76	1.21	30.36	3.173	235.04	25.36
14.11	1.391	33.24	3.567	244.36	25.79
15.58	1.549	36.23	3.983	253.63	26.23

^a Units: cal, mol, °K.

(18) N. S. Osborn, H. F. Stimson, T. S. Sligh, Jr., and C. S. Cragoe, *Nat. Bur. Stand. Sci. Papers*, 20, 65 (1924).

Table II: Thermodynamic Functions of Lutetium(III) and Thulium (III) Oxides^a

T	C_p	S°	$H^\circ - H^\circ_0$	$-(G^\circ - H^\circ_0)/T$	T	C_p	$S^\circ - S^\circ_{10^\circ\text{K}}$	$H^\circ - H^\circ_{10^\circ\text{K}}$	$-(G^\circ - H^\circ_{10^\circ\text{K}})/T$
Lutetium(III) Oxide (Lu_2O_3)					Thulium(III) Oxide (Tm_2O_3)				
5	0.011	0.003	0.014	0.000	10	0.804	0.000	0.000	0.000
10	0.077	0.022	0.172	0.005	15	1.480	0.462	5.816	0.075
15	0.225	0.080	0.906	0.019	20	1.976	0.958	14.490	0.234
20	0.489	0.176	2.614	0.046	25	2.515	1.455	25.68	0.428
25	0.955	0.332	6.147	0.086	30	3.128	1.967	39.75	0.642
30	1.563	0.558	12.395	0.145	35	3.810	2.499	57.07	0.869
35	2.257	0.850	21.92	0.224	40	4.514	3.046	77.58	1.107
40	2.980	1.199	35.01	0.324	45	5.226	3.619	101.93	1.354
45	3.704	1.592	51.72	0.442	50	5.942	4.207	129.85	1.610
50	4.416	2.019	72.03	0.578	55	6.658	4.807	161.35	1.873
60	5.780	2.946	123.08	0.895	60	7.371	5.417	196.4	2.143
70	7.064	3.934	187.4	1.258	70	8.778	6.659	277.2	2.699
80	8.280	4.958	264.1	1.656	80	10.153	7.921	371.9	3.273
90	9.444	6.001	352.8	2.081	90	11.496	9.195	480.2	3.860
100	10.569	7.054	452.9	2.525	100	12.808	10.474	601.7	4.457
110	11.666	8.113	564.1	2.985	110	14.091	11.755	736.2	5.063
120	12.739	9.174	686.1	3.457	120	15.341	13.035	883.4	5.674
130	13.787	10.236	818.8	3.937	130	16.549	14.311	1042.9	6.289
140	14.798	11.295	961.7	4.425	140	17.704	15.580	1214.2	6.908
150	15.761	12.349	1114.6	4.918	150	18.793	16.839	1396.8	7.528
160	16.66	13.395	1276.8	5.415	160	19.81	18.085	1590	8.149
170	17.50	14.431	1447.6	5.915	170	20.75	19.315	1793	8.769
180	18.27	15.453	1626.6	6.417	180	21.62	20.526	2005	9.389
190	18.99	16.460	1812.9	6.919	190	22.42	21.716	2225	10.007
200	19.65	17.452	2006.1	7.421	200	23.16	22.885	2453	10.621
210	20.29	18.426	2206	7.922	210	23.84	24.032	2688	11.233
220	20.89	19.384	2412	8.421	220	24.48	25.156	2929	11.840
230	21.45	20.325	2623	8.918	230	25.06	26.257	3177	12.443
240	21.98	21.249	2841	9.413	240	25.60	27.336	3431	13.041
250	22.47	22.156	3063	9.904	250	26.09	28.390	3689	13.634
260	22.91	23.046	3290	10.393	260	26.53	29.42	3952	14.22
270	23.31	23.918	3521	10.878	270	26.93	30.43	4220	14.80
273.15	23.43	24.190	3595	11.030	273.15	27.05	30.74	4305	14.99
280	23.68	24.773	3756	11.359	280	27.30	31.42	4491	15.38
290	24.04	25.610	3995	11.836	290	27.64	32.38	4765	15.95
298.15	24.32	26.281	4192	12.222	298.15	27.90	33.15	4992	16.41
300	24.39	26.431	4237	12.309	300	27.95	33.32	5043	16.51
310	24.72	27.236	4482	12.777	310	28.25	34.24	5324	17.07
320	25.03	28.026	4731	13.242	320	28.52	35.15	5508	17.62
330	25.30	28.801	4983	13.701	330	28.75	36.03	5895	18.16
340	25.54	29.560	5237	14.157	340	28.96	36.89	6183	18.70
350	25.76	30.303	5494	14.607	350	29.16	37.73	6474	19.23

^a Units: cal, mol, °K.

Gd_2O_3 and Lu_2O_3 . The two assumptions (a) that the electronic levels reported for Gd(III) ion in cubic Gd_2O_3 ⁴ represent the electronic heat capacity of Gd_2O_3 and (b) that the C_2 and C_{3i} ions have identical levels with an overall splitting of about 10 cm^{-1} are still inherent. The latter is a reasonable consequence of the small second-order interaction of the crystal field with "spin only" ions of the $^8\text{S}_{7/2}$ ground state. However, the discussion of Abraham, *et al.*,¹⁹ who cite Wybourne's²⁰ discouraging endeavor to derive a theoret-

ical description of the splitting of S-state ions should be noted. This procedure results in substantially identical lattice heat capacities for Gd_2O_3 and Lu_2O_3 from 5 to 10°K . A further implicit assumption is that the variation of the increment, $C_p - C_v$, is compensated across the series; hence, subtracting the lattice con-

(19) M. M. Abraham, L. A. Boatner, C. B. Finch, E. J. Lee, and R. A. Weeks, *J. Phys. Chem. Solids*, **28**, 81 (1967).(20) B. G. Wybourne, *Phys. Rev.*, **148**, 317 (1966).

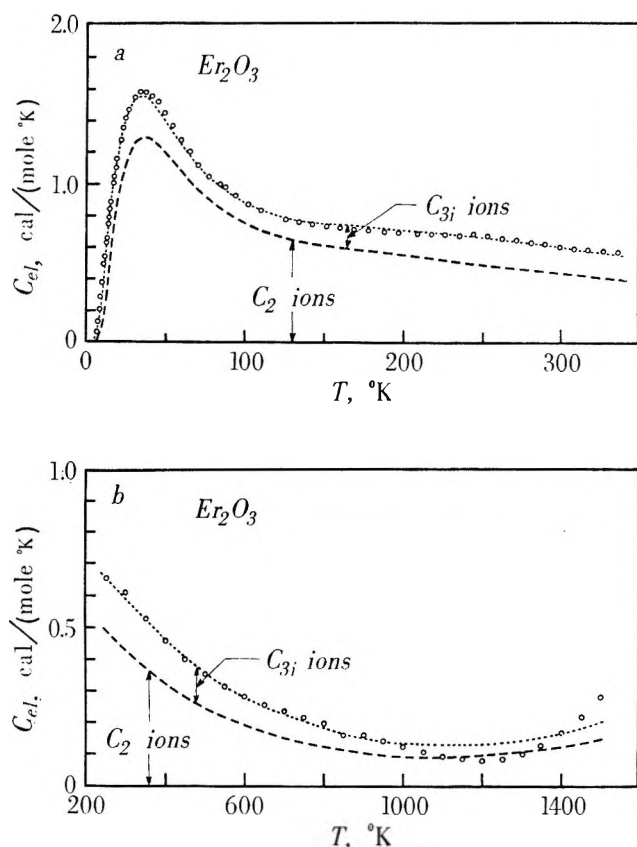


Figure 2. Schottky anomalies for Er(III) ion in Er_2O_3 . In Figure 2a the circles represent data from this laboratory.⁶ The dashed curves represent the calculated electronic heat capacity of the C_2 ions based on the spectroscopic data of Kisliuk, *et al.*,¹² and Gruber, *et al.*,¹³ the dotted curve shows total electronic heat capacity by adding the contribution for the C_{3i} levels in Table V. In Figure 2b the circles represent heat capacities from enthalpy increment determinations of Pankratz and King,²³ and the curves have the same significance.

tribution from the apparent heat capacity yields the true C_{e1} at constant volume as shown in Figure 2.

The Electronic Heat Capacity of Er(III) Ion. Contributions to C_{e1} based on spectroscopic levels reported for the C_2 -type ions in erbium(III) oxide,^{12,13} consisting of doublets at 0, 39, 76, 89, 158, 258, 495, and 500 cm^{-1} , are represented by dashed curves in Figure 2. Figure 2a depicts C_{e1} for the low-temperature region. These values summarized in Table III were derived by subtracting the lattice contribution given in Table IV from the apparent heat capacities. The C_{e1} remaining after removal of the contributions from the C_2 ions is attributed to the levels in the C_{3i} ions. The levels and their degeneracies (shown in Table V) are deduced in part from the position and magnitude of the Schottky peaks in the observed C_{e1} (for separations of less than 100 cm^{-1}) and in part from the splittings of the ground-state term by fourth- and sixth-order terms of cubic crystal fields.²¹ The levels thus derived are doublets at 0, 12, 50, 55, 150, and 450 cm^{-1} and a quartet at 550 cm^{-1} . These correspond most closely to the levels in a

Table III: Experimental Electronic Heat Capacities for Lanthanide(III) Ions and Lanthanide(III) Oxides^a

T	Nd(III)	Dy(III)	Er(III)	Tm(III)
5	0.202	0.056	0.032	0.048
10	0.783	0.128	0.494	0.360
25	0.817	0.598	1.407	0.764
50	0.675	0.874	1.430	0.742
100	0.544	0.986	0.882	1.018
150	0.560	1.258	0.720	1.360
200	0.58	1.44	0.69	1.60
250	0.53	1.47	0.65	1.67
300	0.50	1.40	0.60	1.65
350	0.49	1.30	0.54	1.58

^a Units: cal, mol, °K.

Table IV: Lattice Heat Capacity Contribution for Some Lanthanide(III) Oxides^a

T	Nd_2O_3	Dy_2O_3	Er_2O_3	Tm_2O_3
5	0.005	0.011	0.011	0.011
10	0.076	0.083	0.080	0.079
25	1.213	1.039	1.006	0.989
50	5.255	4.530	4.484	4.461
100	12.593	11.084	10.878	10.775
150	17.94	16.525	16.219	16.066
200	21.56	20.44	20.12	19.96
250	23.98	23.15	22.88	22.75
300	25.67	25.03	24.77	24.64
350	26.93	26.35	26.13	26.02

^a Units: cal, mol, °K.

Table V: Electronic Levels for C_{3i} Ions in Lanthanide(III) Oxide^a

Dy(III):	0(2), 42(2), 200(2), 450(2), 600(2), 700(2), 950(4), [3700](14), ¹¹ [6100](12), ¹¹ [7700](10), ¹¹ [8100](12), ¹¹ [9200](8), ¹¹ [9300](10) ¹¹
Er(III):	0(2), 12(2), 50(2), 55(2), 150(2), 450(2), 550(4), [6660](14), ^{12,13} [10300](12) ^{12,13}
Tm(III):	0(1), 600(3), 1050(2), 2500(7), ¹³ [6500](9) ¹³

^a Degeneracies are indicated in parentheses; values in cm^{-1} . Values in square brackets are mean values selected to represent other Russell-Saunders states of the ground multiplet.

cubic field with a ratio of sixth- to fourth-order terms (V_6/V_4) of -0.25 . The Γ_8 level is split to 12 and 50 (or 55) cm^{-1} , and the second Γ_8 level is split to 150 and 450 cm^{-1} . The C_{e1} data require levels at 12, 50, and 55 cm^{-1} ($\pm 10\%$ of ΔE). The uncertainties in the upper levels can probably reach 20% due to the relative magnitude of the lattice heat capacity and the consequent insensitivity of the electronic heat capacity at temperatures corresponding to levels above 100 cm^{-1} .

(21) J. A. White, *J. Phys. Chem. Solids*, **23**, 1787 (1962).

It is interesting, but not surprising, that C_{3i} levels are quite similar to C_2 levels. Concern^{4,5} about the magnitude of error introduced by adsorption of helium exchange gas on the samples below 10°K was probably overly conservative. Effects associated with the onset of antiferromagnetism²² and poor thermal equilibration may have been mistakenly attributed to helium adsorption in view of the present excellent accord of the known spectral data and the derived lattice heat capacity. The only significant deviation of theoretical and observed electronic heat capacities is found below 35°K. This is probably associated with the removal of the Kramers degeneracy of the Er(III) ion by ordering. The measured entropy increment from 10 to 298.15°K⁶ of 33.81 cal/(mol °K) correlates well with the value of 33.71 cal/(mol °K) calculated from the energy levels plus the lattice contribution. Moreover, the electronic heat capacity of the Er(III) ion, derived from high-temperature enthalpy data for Er₂O₃,²³ Gd₂O₃,²⁴ and Lu₂O₃²⁵ using a treatment similar to that employed for the low temperatures, gives excellent agreement with the heat capacity calculated from the observed spectra and proposed levels as shown in Figure 2b. The practical entropy of Er₂O₃ at 298.15°K is calculated as 37.2 ± 0.1 cal/(mol °K) using the lattice entropy extrapolated below 10°K, the given levels, and the $2R \ln 2$ entropy units removed by antiferromagnetic ordering. This compares with 36.6 cal/(mol °K) reported previously.⁵

The Electronic Heat Capacity of Dy(III) Ion. The contributions of the levels reported for the C_2 ions in dysprosium(III) oxide¹¹ consisting of doublets at 0, 74, 261, 355, 505, 602, 746, and 1080 cm^{-1} are shown as dashed curves in Figure 3. Again the excess C_{e1} (cf. Table III) obtained by the same procedure described for erbium(III) ion is ascribed to the C_{3i} ions. The levels which best fit these data are doublets at 0, 42, 200, 450, 600, and 700 cm^{-1} and a quartet at 900 cm^{-1} . The level at 42 cm^{-1} is readily apparent in the C_{e1} data of Figure 3. If the first four proposed states of the ion are from splitting two quartets at about 125 and 525 cm^{-1} in a slightly perturbed cubic field, then the model given by White²¹ with a potential ratio (V_6/V_4) of -0.30 most nearly applies. Uncertainties in the levels would be similar to those given for Er(III) ion. Here, too, the adsorption of helium exchange gas may not have been a significant contribution in the values published below 10°K. The only significant deviation of the theoretical C_{e1} from the calorimetric value occurs below 25°K. This is probably a consequence of the tail of the antiferromagnetic²⁶ transition removing $2R \ln 2$ units of entropy associated with the Kramers degeneracy of the ground crystal field state in dysprosium(III) oxide. The high temperature C_{e1} of the Dy(III) ion derived from enthalpy data²⁶ for this oxide does not agree as well with the calculated heat capacity as does that of Er(III) ion, but the agreement is still within the

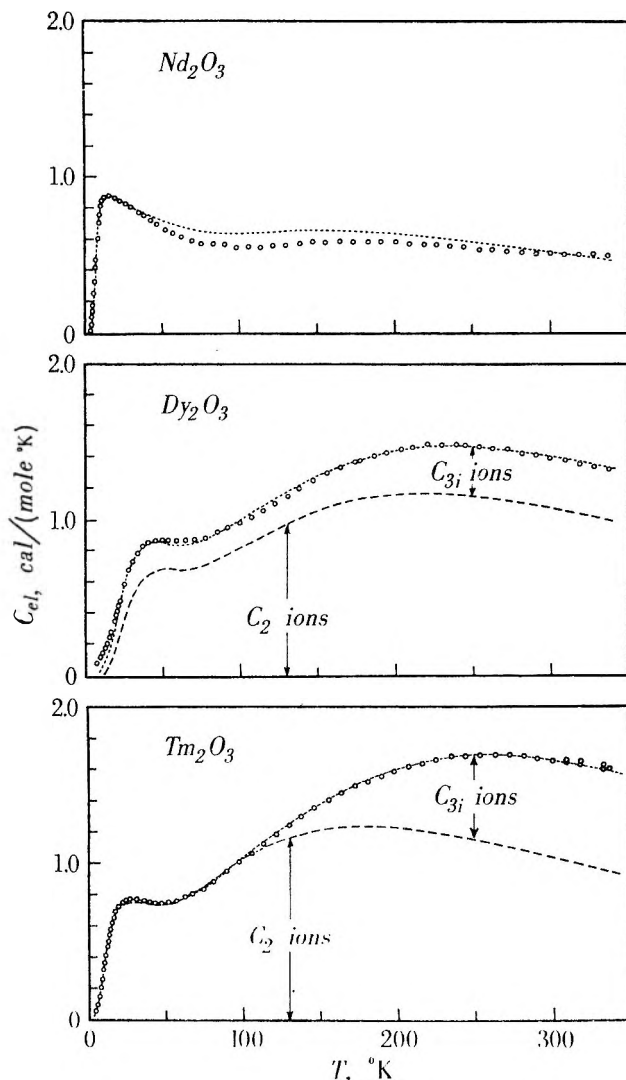


Figure 3. Schottky anomalies for the Dy(III), Tm(III), and Nd(III) ions in Ln₂O₃. The dashed curve is the electronic heat capacity of C_2 ions derived from the levels discussed in the text. The dotted curve is the total electronic heat capacity, *i.e.*, the sum of the C_{e1} contributions from the C_2 and C_{3i} ions. The points are calculated from the original heat capacity data and the appropriate lattice heat capacity curve as described in the text.

experimental error of the heat capacity derived from the enthalpy increment data. The observed entropy increment from 10 to 298.15°K was reported as 33.06 cal/(mol °K) while the sum of lattice and electronic en-

(22) M. K. Wilkinson, W. C. Koehler, E. O. Wollan, and J. W. Cable, *Bull. Am. Phys. Soc.*, **2**, 127 (1957).

(23) L. B. Pankratz and E. G. King, U. S. Bureau of Mines, Report of Investigations No. 6175, U. S. Department of the Interior, Mines Bureau, Pittsburgh, Pa., 1963.

(24) L. B. Pankratz, E. G. King, and K. K. Kelley, U. S. Bureau of Mines, Report of Investigations No. 6033, U. S. Department of the Interior, Mines Bureau, Pittsburgh, Pa., 1962.

(25) L. B. Pankratz and K. K. Kelley, U. S. Bureau of Mines, Report of Investigations No. 6248, U. S. Department of the Interior, Mines Bureau, Pittsburgh, Pa., 1963.

(26) H. Bonrath, K. H. Hellwege, K. Nicolay, and G. Webre, *Phys. Kondensierten Mat.*, **4** (5), 382 (1966).

properties gives 32.99 cal/(mol °K). This work therefore confirms the previously reported value of 35.8 ± 0.1 cal/(mol °K) for the practical entropy at 298.15°K.

The Electronic Heat Capacity of Tm(III) Ion. The levels given by Gruber, *et al.*,¹³ for the C_2 ions ($3/4$ of the total cations present in Tm_2O_3) are singlets at 0, 30.7, 89.3, 219.0, 230.3, 340.0, 382.4, 435.7, 488.4, (680.1), 692.3, 788.5, and 769.9 cm^{-1} . These generate, perhaps fortuitously, a C_{e1} equal to the total C_{e1} observed below 110°K within experimental error (which is probably more reliable than C_{e1} derived by subtracting the lattice heat capacity from the measured values). The data of Table V are consistent with a triplet at 600 cm^{-1} , a doublet at 1050 cm^{-1} , and seven levels near 2500 cm^{-1} . This fits White's²¹ potential term ratio (V_6/V_4) of -0.20 . The sensitivity of this analysis is not high because of relatively high energies of the C_{3i} levels. Some credibility is lent to the unexpectedly high levels by the high-temperature enthalpy data on thulium(III) oxide of Pankrantz and King²³ although the correlation is not as good as for erbium(III) ion. The existence of the C_{3i} levels so far removed from the C_2 levels is further authenticated by Kalvius'²⁷ Mössbauer spectra of thulium(III) oxide. He found the energy of electric interaction of the nuclear spin levels with 4f electrons in the C_2 ions to be 8×10^{-7} eV and that for the C_{3i} ions to be 1.9×10^{-6} eV and implied that the C_{3i} 4f electrons are about twice as energetic as the C_2 4f electrons.

The entropy increment observed from 10 to 298.15°K is 33.15 cal/(mol °K) while that calculated from the interpolated lattice curve and the deduced levels is 33.18 cal/(mol °K). The practical entropy of Tm_2O_3 at 298.15°K is calculated as 33.4 ± 0.1 cal/(mol °K) by extrapolating the lattice and electronic heat capacity functions to 0°K. This extrapolation assumes that the ground states for all ions are singlets. Some support for this is provided by magnetic susceptibility data given by Brown and Hubbard²⁸ over the range 1.3 to 4.2°K. They assert that no ordering occurs in Tm_2O_3 , Dy_2O_3 , and Gd_2O_3 . In the case of Dy_2O_3 ²⁵ and Gd_2O_3 ²⁹ this appears contrary to other evidence.

Reevaluation of Neodymium(III) Oxide Electronic Heat Capacity. The success of the foregoing treatment of cubic oxides suggests that the linear extrapolation scheme may be extended with a somewhat looser approximation to the hexagonal (A-type) oxides. The lattice heat capacity of neodymium(III) oxide is now approximated by adjusting that of lanthanum(III) oxide by $3/7$ of the increment between the cubic gadolinium(III) and lutetium(III) oxides. This new lattice heat capacity for neodymium(III) oxide is shown in Table IV, together with that derived for the other oxides treated in this paper. Until other evidence for the variation in heat capacity with atomic numbers can be obtained for A-type oxides, the value for neody-

mium(III) oxide must be somewhat provisional, but better than the original estimate of using lanthanum(III) oxide without adjustment. The resulting C_{e2} of Nd(III) ion is given in Table III and shown in Figure 3 as points based at the mean temperatures of the experimental determinations on lanthanum(III) oxide. The theoretical curve is in this instance based on the spectroscopic levels of Henderson, *et al.*,⁹ and agrees well with the thermal value, but trends below the data points near 350°K as a consequence of the fact that Henderson, *et al.*, do not report levels for the other states of the ground multiplet ($4I_{11/2}$, $4I_{13/2}$, $4I_{15/2}$). Above 300°K, C_{e1} would have contributions from these levels which probably range from 2000 to 6000 cm^{-1} , if the spectral data of Chang³⁰ for the Nd(III) ion in an yttrium(III) oxide host are indicative. The practical entropy of Nd_2O_3 at 298.15°K remains at 37.9 cal/mol °K as reported earlier.³

Gibbs Energy of Formation of Thulium(III) and Lutetium(III) Oxides. The enthalpies of formation for thulium(III) oxide³¹ and lutetium(III) oxide³² are reported from static oxygen combustion experiments leading to values of -451.4 ± 1.4 and -448.9 ± 1.4 kcal/mol. Holley, *et al.*,³³ have reviewed the heat capacity determinations of thulium and lutetium metals and found S°_{298} values of 17.80 ± 0.05 and 12.18 ± 0.05 cal/(g-atom °K). The entropy derived by these authors is based on work by Lounasmaa,³⁴ Dreyfus, *et al.*,³⁵ Lounasmaa and Sundström,³⁶ and by Jennings, *et al.*³⁷ Similarly, the tabulated entropy for lutetium is based on measurements by Lounasmaa³⁸ and Jennings, *et al.*³⁹ The entropy of $O_2(g)$ at 298.15°K is taken from the tabulation of Wagman, *et al.*,⁴⁰ and is 48.996 cal/(mol °K). From these data one obtains

(27) M. Kalvius, *Z. Naturforsch.*, **17a**, 248 (1962).

(28) R. E. Brown and W. M. Hubbard, U. S. Department of Commerce Clearing House, Technical Information AD 627224, 1965, pp 31-42 [*cf. Chem. Abstr.*, **65**, 161b (1966)].

(29) W. F. Giaque and J. W. Stout, *J. Amer. Chem. Soc.*, **61**, 1342 (1939).

(30) N. C. Chang, *J. Chem. Phys.*, **44**, 4044 (1966).

(31) E. J. Huber, Jr., E. L. Head, and C. E. Holley, Jr., *J. Phys. Chem.*, **64**, 379 (1960).

(32) E. J. Huber, Jr., E. L. Head, and C. E. Holley, Jr., *ibid.*, **6-**, 1768 (1960).

(33) C. E. Holley, Jr., E. J. Huber, Jr., and F. B. Baker in "Progress in the Science and Technology of the Rare Earths," L. Eyring, Ed., Pergamon Press, London, 1968.

(34) O. V. Lounasmaa, *Phys. Rev.*, **134A**, 160 (1964).

(35) B. Dreyfus, B. B. Goodman, A. Lacaze, and G. Trolliet, *Compt. Rend.*, **253**, 1764 (1961).

(36) O. V. Lounasmaa and L. J. Sundström, *Phys. Rev.*, **150**, 399 (1966).

(37) L. D. Jennings, E. Hill, and F. H. Spedding, *J. Chem. Phys.*, **34**, 2082 (1961).

(38) O. V. Lounasmaa, *Phys. Rev.*, **133**, 219 (1964).

(39) L. D. Jennings, R. E. Miller, and F. H. Spedding, *J. Chem. Phys.*, **33**, 1849 (1960).

(40) D. D. Wagman, W. H. Evans, I. Halow, J. B. Parker, S. M. Bailey, and R. H. Schumm, U. S. National Bureau of Standards Technical Note 270-1, "Selected Values of Chemical Thermodynamic Properties," U. S. Government Printing House, Washington, D. C. 20402, 1965.

$\Delta G_f^\circ_{298.15}$ of $\text{Tm}_2\text{O}_3(\text{c})$ to be -428.8 ± 1.5 kcal/mol and $\Delta G_f^\circ_{298.15}$ for $\text{Lu}_2\text{O}_3(\text{c})$ to be -427.6 ± 1.5 kcal/mol.

Acknowledgment. The authors are grateful for the partial support of the United States Atomic Energy

Commission and to Professor F. H. Spedding and the Ames Laboratory of Iowa State University for the loan of calorimetric samples of both oxides. They further acknowledge the technical assistance of Dr. John C. Trowbridge in making the measurements.

Temperature-Dependent Electron Spin Resonance Studies. II.¹

Cyclooctatetraene Anion Radical

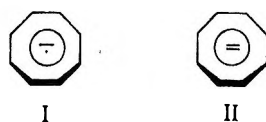
by F. J. Smentowski and Gerald R. Stevenson

Department of Chemistry, Texas A & M University, College Station, Texas 77843 (Received April 25, 1968)

The cyclooctatetraene (COT) anion radical (I) has been formed by the alkali metal reduction of COT in liquid ammonia. Ion pairing affects the esr spectra of the anion radical I, influencing the line widths of the individual hyperfine splittings, the activation energy of the line-broadening process, and the spin concentration. The dependence of the hyperfine line width of the cyclooctatetraenide salts is $\text{Li}^+ > \text{Na}^+ > \text{K}^+$, the reverse order of that found in ether solvents. For the COT-NH₃-K system, the radical(s) observed are dependent upon the ratio of COT to its dianion (II). Equilibrium constants for the disproportionation (eq 3) in liquid ammonia have been measured. Factors affecting the direction of reaction 3 are considered.

Introduction

Ion pairing has been found to play a predominant role in solution chemistry.² Current developments have been stimulated by csr,^{3,4} conductance,⁵ and optical⁶ studies. Much of the esr work on ion-pairing phenomena has recently been reviewed.⁷ Studies^{8,9} of the cyclooctatetraene (COT) anion radical (I) in



tetrahydrofuran (THF) and 1,2-dimethoxyethane (DME) have given some insight into ion pairing on these systems. Since details of the preparation of anion radicals in liquid ammonia are now available,¹⁰ it was of interest to study the system COT-NH₃-metal. Anion radicals of various organic substrates have been prepared by electrolytic reduction in liquid ammonia.¹¹ COT has been reduced electrolytically in liquid ammonia, giving nine lines with $a_{\text{H}} = 3.28$ G.¹¹

Experimental Section

Adequate safety precautions must be considered, since the esr sample tubes of these ammonia systems are at approximately 11 atm at 30°.

COT was purchased from Chemical Procurement

Laboratories, Inc. and was degassed and distilled under high vacuum before use. The anion radicals were pre-

- (1) Part I: F. J. Smentowski and G. R. Stevenson, *J. Amer. Chem. Soc.*, **89**, 5120 (1967). The present article is also part II of the series Anion Radicals in Liquid Ammonia (Part I: F. J. Smentowski and G. R. Stevenson, *ibid.*, **90**, 4661 (1968)).
- (2) (a) E. Grunwald, *Anal. Chem.*, **26**, 1696 (1954); (b) S. Winstein, E. Clippinger, A. H. Fainberg, and G. C. Robinson, *J. Amer. Chem. Soc.*, **76**, 2597 (1954); (c) S. Winstein and G. C. Robinson, *ibid.*, **80**, 169 (1958).
- (3) (a) N. M. Atherton and S. I. Weissman, *J. Amer. Chem. Soc.*, **83**, 1330 (1961); (b) P. J. Zandstra and S. I. Weissman, *ibid.*, **84**, 4408 (1962); (c) F. C. Adam and S. I. Weissman, *ibid.*, **80**, 1518 (1958).
- (4) (a) A. H. Reddoch, *J. Chem. Phys.*, **43**, 225 (1965); (b) N. Hirota and R. Kreilick, *J. Amer. Chem. Soc.*, **88**, 614 (1966); (c) R. Chang and C. S. Johnson, *ibid.*, **88**, 2238 (1966); (d) N. Hirota, *ibid.*, **90**, 3603 (1968); (e) N. Hirota, R. Carraway, and W. Schook, *ibid.*, **90**, 3611 (1968); A. M. Hermann, A. Rembaum, and W. R. Carper, *J. Phys. Chem.*, **71**, 2661 (1967).
- (5) (a) P. Chang, R. V. Slates, and M. Szwarc, *J. Phys. Chem.*, **70**, 3180 (1966); D. N. Bhattacharyya, C. L. Lee, J. Smid, and M. Szwarc, *ibid.*, **69**, 112 (1965); (c) C. Carvajal, K. J. Tolle, J. Smid, and M. Szwarc, *J. Amer. Chem. Soc.*, **87**, 5548 (1965).
- (6) (a) T. E. Hogen-Esch and J. Smid, *ibid.*, **88**, 307, 318 (1966); (b) T. E. Hogen-Esch and J. Smid, *ibid.*, **87**, 669 (1965); (c) J. Smid, *ibid.*, **87**, 655 (1965).
- (7) (a) N. Hirota, *J. Phys. Chem.*, **71**, 127 (1967); (b) M. C. R. Symons, *ibid.*, **71**, 172 (1967); (c) N. Hirota, *J. Amer. Chem. Soc.*, **89**, 32 (1967).
- (8) F. J. Smentowski and G. R. Stevenson, *J. Amer. Chem. Soc.*, **89**, 5120 (1967).
- (9) H. L. Strauss, T. J. Katz, and G. K. Fraenkel, *ibid.*, **85**, 2360 (1963).
- (10) (a) F. J. Smentowski and G. R. Stevenson, *ibid.*, **90**, 4661 (1968); (b) H. J. Chen and M. Bersohn, *Mol. Phys.*, **13**, 573 (1967).
- (11) (a) D. H. Levy, Ph.D. Thesis, University of California, 1965; (b) D. H. Levy and R. Myers, *J. Chem. Phys.*, **41**, 1062 (1964); **42**, 3731 (1965); **43**, 3063 (1965); **44**, 4177 (1966).

pared by reduction of COT with the alkali metal-liquid ammonia solution.^{10a}

Activation energies were determined from the slope of $\ln(\text{line width})$ vs. $1/RT$ plots.¹² Line widths were measured between the extrema in the first-derivative spectrum. In the linear region of the $\ln(\text{line width})$ vs. $1/RT$ plot, all hyperfine components of the same system gave the same line width. Spectra of each system were run at several different metal and COT concentrations to verify that the energy of activation for the line broadening is independent of the concentration of the dianion. The concentration of the dianion was low enough that a visible amount of the dianion salt did not precipitate out of solution. For the system COT-NH₃-K, kinetics for the line-broadening process were determined as described previously.⁸ Equilibrium constants for the disproportionation (reaction 3) were measured by comparison of the spin concentration of the ammonia system to that of the system COT-THF-Li, where the equilibrium constant is known.^{9,13}

The spectra were recorded using the X band of a Varian V-4502-15 esr spectrometer with a 12-in. magnet. Temperature was controlled within $\pm 1^\circ$ by a Varian V-4557 variable-temperature controller. A copper-constantan thermocouple was used to calibrate the variable-temperature controller. Coupling constants and line widths were taken directly from the calibrated chart paper.

Results

Three systems (COT-NH₃-metal) were studied, where the metal is lithium, sodium, or potassium. Ion pairing affects the esr spectra of I, even in liquid ammonia, influencing the line widths of the individual hyperfine splittings, the activation energy of the line-broadening process, and the spin concentration. For all systems studied, successive additions of metal to 10^{-2} M COT leads to a wider line in the slow-exchange region and a narrower line in the fast-exchange region. Because of precipitate formation, spectral measurements were not possible for $>10^{-2}$ M concentrations of I and II. Over the linear range of the $\ln(\text{line width})$ vs. $1/RT$ plot (Figures 1-3) the same activation energy is obtained for different amounts of metal added. For the three systems it was found that the activation energy of the line-broadening process over the linear range of the $\ln(\text{line width})$ vs. $1/RT$ plot was independent of the dianion II concentration. The dependence of the hyperfine line width of the cyclooctatetraenide salts is $\text{Li}^+ > \text{Na}^+ > \text{K}^+$ when the spin concentration in these systems is $\leq 10^{-5}$ M.

Figure 4 is a plot of the relative spin concentration vs. T , varying the counterion. Table I gives the equilibrium constants of the disproportionation (reaction 3) for the three systems at 22° .

For the COT-NH₃-K system, the radical(s) ob-

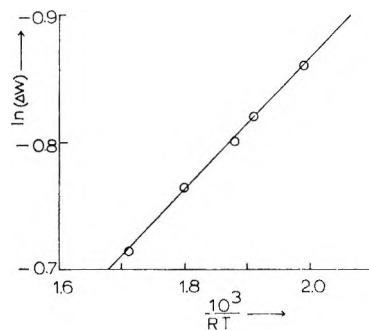


Figure 1. Plot of $\ln(\text{line width})$ vs. $10^3/RT$ for the system COT-NH₃-Li (0.05 M COT-0.05 M Li) in the region of fast exchange.

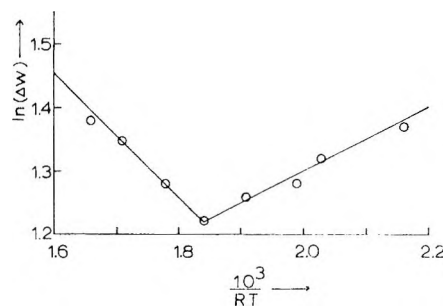


Figure 2. Plot of $\ln(\text{line width})$ vs. $10^3/RT$ for the system COT-NH₃-Na (0.136 M COT-0.060 M Na) in the region of fast exchange.

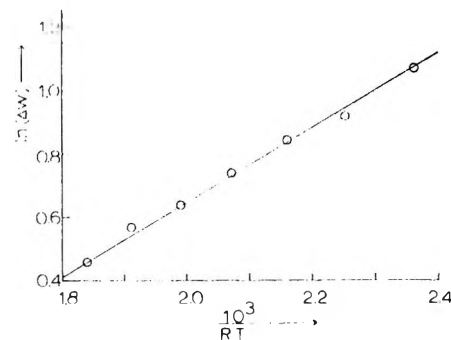


Figure 3. Plot of $\ln(\text{line width})$ vs. $10^3/RT$ for the system COT-NH₃-K (0.055 M COT-0.06 M K) in the region of slow exchange.

served are dependent upon the ratio of COT to K. No metal splitting is observed in any of these systems.

COT-NH₃-Li. Fast-exchange conditions (one line) prevail at room temperature for all lithium systems, except for very low concentrations (approximately 10^{-4} M) of lithium when nine lines can be observed. The activation energy for those factors affecting the line width in this system is 1.1 kcal/mol over the temperature range -70 to 10° . The spin concentration of this system increases by a factor of 2.2 over the inter-

- (12) (a) R. L. Ward and S. I. Weissman, *J. Amer. Chem. Soc.*, **79**, 2086 (1957); (b) M. T. Jones and S. I. Weissman, *ibid.*, **84**, 4269 (1962); (c) W. L. Reynolds, *J. Phys. Chem.*, **67**, 2866 (1963); (c) E. deBoer and C. MacLean, *J. Chem. Phys.*, **44**, 1334 (1966).
 (13) T. J. Katz, *J. Amer. Chem. Soc.*, **82**, 3784, 3785 (1960).

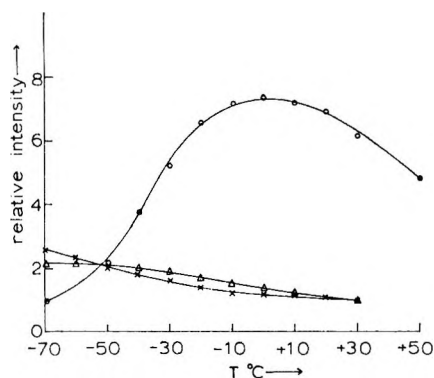


Figure 4. Plot of temperature *vs.* the relative intensity of the esr signal for liquid NH_3 systems: O, K reduction; X, Na reduction; Δ , Li reduction. Intensity is the esr line height times the line width squared.

Table I: Equilibrium Constants at 22° for the Disproportionation for Various COT Alkali Metal Systems

Solvent	Metal	K_{eq}	Ref
NH_3	K	$(1.4 \pm 1) \times 10^{-6}$	This work
NH_3	Na	$(2.5 \pm 2) \times 10^{-2}$	This work
NH_3	Li	$(7 \pm 5) \times 10^{-1}$	This work
THF	K	3.4×10^{-9}	9
THF	Li	9×10^{-9}	9
DMF	Electrolytic ^a	10^4	18
DMSO	Electrolytic ^a	10^4	18

^a Carrier electrolyte, tetra-*n*-propylammonium perchlorate.

val -70 to 30° . K_e for the disproportionation (reaction 3) for the lithium system is $(7 \pm 5) \times 10^{-1}$, greater than the sodium or potassium systems.

COT-NH₃-Na. There are several activation energies observed for those factors affecting the line width in this system (Figure 2). The activation energy for the lower temperatures is 0.50 kcal/mol. At the higher temperatures, a "negative" activation energy of 1.0 kcal/mol is observed. Fast-exchange conditions prevail for sodium systems when the dianion concentration is greater than 10^{-3} M. At lower concentrations of the dianion II, nine lines can be observed. The spin concentration of this system increases by a factor of 2.6 over the interval -70 to 30° . K_e for the disproportionation (reaction 3) for the sodium system is $(2.5 \pm 2) \times 10^{-2}$.

COT-NH₃-K. For this system, nine lines are always observed, even for high (*e.g.*, 0.05 M) concentrations of dianion II. The activation energy for those factors affecting the line width in this system is 0.60 kcal/mol. Comparing the line widths of the potassium system with the other metal systems, the line for the potassium salt is much narrower than the line for the sodium or lithium systems. The spin concentration of this system increases by a factor of 8 over the interval -70 to 30° . This variation is larger than that ob-

served for the lithium or sodium systems. K_e for the disproportionation (reaction 3) for the potassium system is $(1.4 \pm 1) \times 10^{-6}$. Table II gives a representative series of systems used to calculate K_e . Two different radicals are observed for this system for the concentration of II from 10^{-3} to 5×10^{-2} M. At the lower limit of dianion concentrations, I was not observed by esr spectroscopy. At the upper limit, II precipitated from solution. For high concentrations of metal ($(K) > 6(\text{COT})$) radical 1 ($a_H = 3.28 \pm 0.01$ G) is found. For low concentrations of metal ($(K) < 1/2(\text{COT})$), radical 2 ($a_H = 3.30 \pm 0.01$ G) is found. Table III summarizes this information on the two radicals. Between these limits, the two radicals exist, superimposed on each other (Figure 5). In both radicals 1 and 2 all nine lines are equivalent.

Table II: Disproportionation Constant for the COT-NH₃-K System, 22° (Representative Data)

Sample	$[\text{COT}]^a$	$10^{-3}[\text{COT}^{2-}]^a$	$[\text{COT}^{1-}]^a$	$10^6 K_e$
I	0.04	4.9	0.05	1.2
II	0.10	4.2	0.038	0.46
III	0.038	1.9	0.004	2.5

^a Molar equilibrium concentration.

Table III: Dependence of the Radical(s) Observed on the Ratio of COT to Its Dianion for the COT-NH₃-K System at 22°

$[\text{COT}]^a / [\text{K}]^b$	$[\text{COT}]^a$	$[\text{K}^+]^c$	$[\pi^{2-}]^c$	$[\pi]^c$	Radical obsd
1.3	0.30	0.20	0.10	0.20	1
7.7	0.10	0.013	0.0065	0.099	2
0.9	0.053	0.061	0.03	0.023	1
1.1	0.033	0.030	0.015	0.018	1
8.3	0.048	0.058	0.029	0.019	2
1.4	0.083	0.060	0.030	0.053	1
2.2	0.103	0.046	0.023	0.080	1, 2
4.4	0.203	0.046	0.023	0.180	1, 2
6.6	0.303	0.046	0.023	0.280	2
8.8	0.403	0.046	0.023	0.380	2
8.0	0.064	0.008	0.004	0.060	2
16.3	0.13	0.008	0.004	0.13	2
23.7	0.19	0.008	0.004	0.19	2
1.1	0.013	0.012	0.006	0.012	1
4.9	0.19	0.039	0.020	0.17	1, 2

^a Initial COT concentration, M. ^b Initial K concentration, g-atoms/l. ^c Equilibrium concentration, M.

For the system COT-NH₃-K, kinetics for the line-broadening process were attempted. However, the concentration of II could not be varied over a large enough range to obtain meaningful results for either radical 1 or 2.

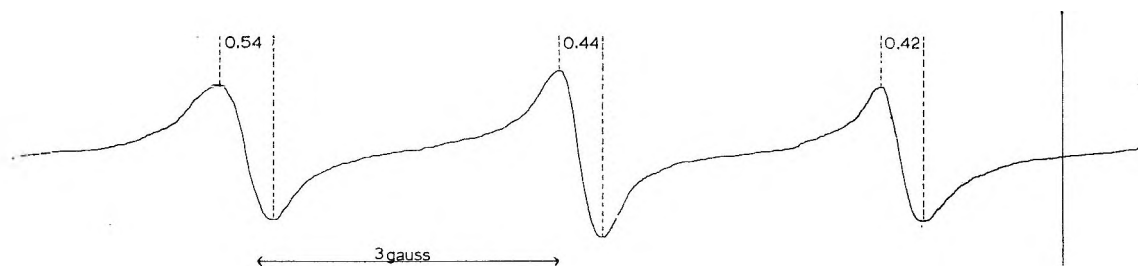


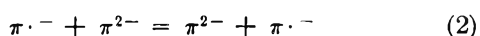
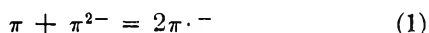
Figure 5. Three center lines of the esr spectrum of the system COT-NH₃-K. The numbers between the dotted lines are the line widths in gauss.

COT-NH₃-Ca. A spectrum of nine lines ($a_H = 3.2$ G) was observed for this system. The calcium salt of II was very insoluble. Thus studies similar to those made for the alkali metal systems were not possible.

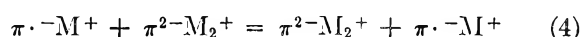
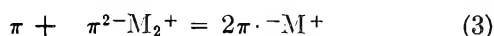
Discussion

Only recently have esr studies of anion radicals in liquid ammonia been made. Levy and Myers have electrolytically reduced a number of hydrocarbons and nitrobenzene derivatives in liquid ammonia to their anion radicals.^{11,14} Katz and Talcott have electrolytically reduced bicyclo[6.1.0]-2,4,6-nonatriene in ammonia.¹⁵ More recently hydrocarbons and related derivatives have been reduced with liquid ammonia alkali metal to their anion radicals.¹⁰ Because of the influence of ion pairing on esr spectra,^{3,7,8} it is of interest to determine if ion pairing is present in the higher dielectric solvent, ammonia. In ammonia, the effects of ion pairing on some esr spectral parameters of the nitrobenzene anion radical (III) appear to be minor.^{10a} The coupling constants of III were independent of counterion, temperature, or added electrolyte. Similarly, the coupling constant of I is slightly dependent upon the counterion and temperature. In contrast, line width and disproportionation parameters of I, as measured by esr spectroscopy, are very sensitive to changes in ion pairing.

The anion radical I, which undergoes disproportionation (eq 1) and electron transfer (eq 2) (where $\pi = \text{COT}$)¹³ is influenced by the effects of ion pairing^{8,9}

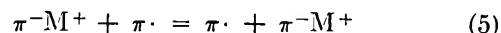


such that eq 1 and 2 are replaced by eq 3 and 4, where $\pi^{2-}\text{-M}_2^+$ and $\pi\text{-M}^+$ represent all forms of the ions from tight ion pairs and/or higher agglomerates^{7c} to dissociated ions.²



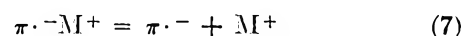
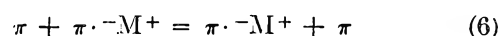
We now consider the effects of ion pairing on the activation energy of the line-broadening process of anion radical I. If the concentration of dianion II is varied,

the same activation energy is derived for a particular system COT-NH₃-metal. However, a different activation energy is obtained if the system is changed (*i.e.*, COT-NH₃-Li *vs.* COT-NH₃-Na). Similar behavior was noted for the systems COT-DME-metal and COT-THF-metal, where the metal is lithium, sodium, potassium.⁸ Likewise, Jones and Weissman^{12b} have observed the independence of the activation energy on the concentration of π^- for the electron transfer in eq 5, where π is tris-*p*-nitrophenylmethyl.



They also found the activation energy for this electron transfer was solvent and counterion dependent. Further evidence for ion pairing for the system COT-NH₃-Na is the occurrence of two activation energies (Figure 2), one "negative" for systems with high concentrations of metal. Weissman and Zandstra^{3b} observed this behavior for the systems naphthalene-solvent-metal. The current explanation^{7a} for this anomaly is the occurrence of different equilibrium concentrations of ion pairs for different temperatures. This explanation for our system is suggested by the identification of two different radicals, radicals 1 and 2 in the potassium systems (Figure 5). Two radicals were not observed for the lithium or sodium systems, since even at moderate concentrations of metal, fast-exchange conditions prevail.

Several mechanisms could be responsible for line broadening of I in liquid ammonia. The five most likely possibilities are given by eq 3, 4, 6, 7, and 8. In



eq 4, the lines of the anion radical I are broadened by the dianion II, while in eq 6 they are broadened by COT. In eq 7, equilibration between differently solvated ion pairs is responsible for the line broadening of I, while in eq 8 solvated electron broadening of I occurs.

(14) D. H. Levy and R. Myers, *J. Chem. Phys.*, **41**, 1062 (1964); **42**, 3731 (1965); **43**, 3063 (1965); **44**, 4177 (1966).

(15) T. J. Katz and C. Talcott, *J. Amer. Chem. Soc.*, **88**, 4732 (1966).

Electron transfer from the anion radical to the neutral molecule (eq 6) is not considered likely for the ammonia systems. For the systems COT-THF-K,¹³ COT-THF-Li,¹³ and COT-DME-Na,⁸ this electron transfer was shown to be slow relative to electron transfer from the dianion (eq 4). Apparently the similar geometries of I and II favor electron transfer (eq 4) over eq 6, the latter involves different geometries and energy states of COT and I. The predominance of eq 4 over eq 6 is also favored for other COT-solvent-M systems.¹⁶

Similarly, equilibration between ion pairs (eq 7)^{4e} as a line-broadening mechanism does not seem likely for most systems COT-solvent-M (where solvent = THF, DME, or NH₃ and M = Li, Na, or K). An increase in the concentration of II for every one of these systems leads to increased line broadening. For higher concentrations of II, a system would have more ion pairs or agglomerates, resulting in a slower rate of ion pair equilibration (eq 7).^{4e} Likewise, for the only one of the nine systems exhibiting metal splitting, *i.e.*, COT-THF-Na,⁹ all components of the alkali metal splitting have the same line width, indicating the absence of 7 as a line-broadening mechanism for this system. Also a kinetic study⁸ of the system COT-DME-Na indicated a first-order dependence upon the dianion concentration and the anion radical concentration. Such kinetic dependence for equilibrium (eq 7) seems unlikely, though not impossible.

Line broadening from the disproportionation (eq 3) was not present for the systems COT-DME-Na, COT-THF-Li, and COT-THF-K as determined from kinetic studies.^{8,13} For all systems except those with high concentrations of anion radical I, *i.e.*, COT-Li-NH₃ and COT-Na-NH₃, disproportionation broadening is unlikely.

Finally, the ease with which liquid ammonia forms a solvated electron¹⁷ might lead one to believe that solvated electron broadening (eq 8) is present in the



ammonia systems. For systems with high concentrations of II, it appears as if hyperfine splitting line broadening from eq 8 plays a minor role. We have no direct evidence that the anion radical I in the ammonia systems is dianion broadened. Results from ether solvents^{8,9} and possibly DMF (dimethylformamide) and DMSO (dimethyl sulfoxide)¹⁸ indicate I is dianion broadened. This along with a broadening of hyperfine splitting components for greater concentrations of II in ammonia and ether solvents, and the identical activation energy (for a particular system) for various concentrations of II in these solvents, makes it seem the anion radical I is dianion broadened in ammonia also. If eq 8 were the major source of line broadening, one would observe a broader line as more metal is added to the system, along with the free-electron line. This is not observed.

In ammonia, the dependence of the hyperfine splitting line width of the cyclooctatetraenide salts is $\text{Li}^+ > \text{Na}^+ > \text{K}^+$. In the ether solvents DME and THF the reverse order prevails⁸: $\text{K}^+ > \text{Na}^+ > \text{Li}^+$. Conductance studies¹⁹ of anion radicals indicated this same relative order of cation migration in the ether solvents, with the small cation coordinating to the solvent to form an immobile ion. Also for systems undergoing the electron transfer (eq 5), it appears this transfer is faster for the dissociated ion than for the ion-paired anion radical.²⁰ However, addition of water to aprotic solvents has in some instances²¹ led to a decrease in the electron-transfer rate. At this point, further details of the electron transfer for these cyclooctatetraene systems cannot be given. Electron transfer for simpler systems²² is complex.

What is most surprising are the results obtained for the equilibrium constants for the disproportionation (eq 3), given in Table I. All three systems, lithium, sodium, and potassium, give higher concentrations of anion radical I than the ether solvents THF and DME. Comparing the two systems COT-THF-Li and COT-NH₃-Li, the K_e 's differ by 100,000,000! The anion radical I appears to be favored over the dianion II for the system COT-NH₃-electrode,¹¹ but the equilibrium constant was not determined. Allendoerfer and Rieger¹⁸ have observed a similar dramatic shift in K_e of the disproportionation (eq 3) for the dissociated ions for the systems COT-DMF-electrode and COT-DMSO-electrode. They suggest that the shift in equilibrium (eq 3) in going from DMF and DMSO to ethereal solvents is due to the formation of a strong alkali metal-dianion complex. For the six systems COT-solvent-M, where solvent = THF, DME, or NH₃ and M = Li or Na, an increase in the dielectric constant of the solvent (*i.e.*, lowering of the temperature of a particular system or changing the solvents) together with a small cation favors the anion radical. Similarly, from Table I, the concentration of I is greater for those systems with solvents of high dielectric constant. In solvents of low dielectric constant, aromatic hydrocarbon dianions are more highly associated with alkali

(16) F. J. Smentowski and G. R. Stevenson, submitted for publication in *J. Amer. Chem. Soc.*

(17) (a) W. L. Jolly and C. J. Hallada, "Non-aqueous Solvent Systems," T. C. Waddington, Ed., Academic Press, New York, N. Y., 1965, p 1; (b) G. Lepoutre and M. J. Sienko, "Metal-Ammonia Solutions," Benjamin, New York, N. Y., 1964.

(18) R. D. Allendoerfer and P. H. Rieger, *J. Amer. Chem. Soc.*, **87**, 2336 (1965).

(19) (a) R. V. Slates and M. Szwarc, *J. Phys. Chem.*, **69**, 4124 (1965); (b) P. Chang, R. V. Slates and M. Szwarc, *ibid.*, **70**, 3180 (1966).

(20) (a) R. Chang and C. S. Johnson, Jr., *J. Amer. Chem. Soc.*, **88**, 2338 (1966); (b) J. E. Harriman and A. H. Maki, *J. Chem. Phys.*, **39**, 778 (1963).

(21) T. Layoff, T. Miller, R. N. Adams, A. Horsfield, and W. Procter, *Nature*, **205**, 382 (1965).

(22) (a) R. A. Marcus, "Annual Review of Physical Chemistry," Vol. 15, H. Eyring, C. J. Christensen, and H. S. Johnston, Ed., Annual Reviews Inc., Palo Alto, Calif., 1964; (b) R. A. Marcus, *J. Chem. Phys.*, **43**, 2654 (1965).

metal ions than the corresponding monoanions.²³ No further relationship between the above-mentioned factors and the thermodynamic functions^{9,24} affecting K_e can be made. The greater stability of the COT dianion II over the anion radical for systems such as COT-DME-Li has been widely quoted as an application of the Hückel $4n + 2$ rule. However, the system COT-NH₃-Li gives approximately equal concentrations of anion radical I and the dianion II. HMO calculations show the anion radical I and the dianion II have the same resonance energies. Approximate SCF-MO calculations²⁵ using the Pople-Santry-Segal method²⁶ show the anion radical I to be much more stable, 110 kcal/mol, than the dianion II. However, these calculations do not consider solvation effects.

Summary and Conclusions

Even in ammonia, a solvent having a reasonably high dielectric constant, ion pairing is a major factor in the variation of some of the physical properties of anion radical I. For the alkali metal systems in liquid ammonia, the major source of line broadening appears to be electron transfer from dianion II to anion radical I. The activation energy of the electron transfer between dianion II and anion radical I is not as dependent upon the counterion as it is in either solvents. The line widths of the individual hyperfine splittings are a logarithmic function of the temperature (Figures 1 and 2) and are somewhat dependent upon the counterion. Again, the variation of spin concen-

tration with temperature, solvent, and counterion is indicative of the influence of ion pairing on the disproportionation (eq 3). The dielectric constant of the solvent and its coordinating ability for the cation are important in determining the rate of electron transfer between the anion radical I and its dianion II. These factors are also important in determining the direction of the disproportionation (eq 3).

Acknowledgment. The authors are indebted to Professor B. J. Zwolinski for helpful discussion. The authors thank the National Aeronautics and Space Agency for Fellowship support to G. R. Stevenson. The esr spectrometer was made available by the National Science Foundation Grant GP-3767. Support from the Research Council of Texas A & M University is gratefully acknowledged. Time for machine calculations was made available by the Data Processing Center of Texas A & M University. Acknowledgment is made to the donors of The Petroleum Research Fund, administered by the American Chemical Society, for partial support of this research.

(23) (a) G. J. Hoijtink and P. H. van der Meij, *Z. Phys. Chem.* (Frankfurt am Main), **20**, 1 (1959); (b) G. J. Hoijtink, E. de Bcer, P. H. van der Meij, and W. P. Weijland, *Rec. Trav. Chim.*, **75**, 487 (1956).

(24) G. R. Stevenson, Ph.D. Thesis, Texas A & M University, 1969.

(25) F. J. Smentowski, B. D. Faubion, and R. M. Hedges, submitted for publication in *J. Chem. Phys.*

(26) (a) J. A. Pople, D. P. Santry, and G. A. Segal, *J. Chem. Phys.*, **43**, S129 (1965); (b) J. A. Pople and G. A. Segal, *ibid.*, **43**, S.36 (1965); (c) J. A. Pople and G. A. Segal, *ibid.*, **44**, 3289 (1966).

Heats of Mixing Aqueous Electrolytes. VI. Magnesium Chloride

with Some Alkali Metal Chlorides¹

by R. H. Wood, J. D. Patton,² and M. Ghamkhar

Department of Chemistry, University of Delaware, Newark, Delaware (Received July 12, 1968)

The heats of mixing aqueous solutions of magnesium chloride with the chlorides of lithium, sodium, potassium, and cesium at constant ionic strength have been measured at 25° and ionic strengths of 0.5 to 3.0. The magnitudes of the heats of mixing are similar to the magnitudes of the heats of mixing two alkali chlorides. At the lower concentrations RTh_0 becomes more positive. A trend to plus infinity for RTh_0 is expected from the limiting law. If the contributions of oppositely charged ions are estimated and subtracted from the heat of mixing, the sign of the remainder correlates reasonably well with the properties of the water structure around the two cations. This observation extends the correlation to charge-asymmetrical mixtures.

Introduction

Recent work on the heats of mixing electrolyte solutions has mostly been confined to charge-symmetrical mixtures, that is, mixtures of salts of the same charge type.³⁻¹⁰ For these mixtures it has been shown that pairwise interactions of like-charged ions are generally more important than triplet interactions^{7-9a} and that a set of equations for predicting the heat content or free energy of many component mixtures can be derived using this information.^{9a} The equations are accurate for mixtures of three salts.^{9a} Further work has shown that the structure of the water around the ions is the important factor in determining the sign of the heat of mixing.⁹ The purpose of the present investigation was to collect data on a representative charge-asymmetrical mixture and to see in what ways the conclusions and theories developed on the basis of charge-symmetrical mixtures are affected by the charge asymmetry.

Experimental Section

The details of the experimental procedure have been given elsewhere.¹¹ Potassium, sodium, and magnesium chloride were Fisher Certified reagents and no impurity was greater than 0.01%. Cesium chloride (99.9%) was obtained from Kawecki Chemical Co. Lithium chloride (99.7%) was furnished *gratis* by Foote Mineral Co. The LiCl and CsCl were analyzed for impurities by flame spectrophotometry and found to contain 0.01% or less alkali metal or alkaline earth impurities. Stock solutions were prepared using deionized distilled water and the concentration determined gravimetrically with AgNO₃. Operating solutions whose concentrations were accurate to 0.1% were prepared by weight dilution of the stock solutions.

Heat of mixing was measured in a twin calorimeter which has been described previously.^{8,12} Errors in the measured heat of mixing due to hydrolysis and

neutralization were reduced to a negligible level by adjusting the pH of all operating solutions to 4.0-5.0 prior to use. Heat of dilution errors due to slight differences in the concentrations of the solutions were calculated to be no larger than the standard deviation of the data. Errors arising from impurities in the reagents are negligible.

Results and Discussion

The experimental data were fitted by the method of least squares to the equation

$$\Delta H_m \text{ (cal/kg of solvent)} = RTI^2y(1 - y)[h_0 + (1 - 2y)h_1] \quad (1)$$

where I is the molal ionic strength, y is the ionic strength fraction of magnesium chloride, h_0 is a measure of the magnitude of the interaction, and h_1 is a measure of the skew of the interaction. The heats of mixing were measured in the ranges $y = 0-0.2$ and $y = 0.8-1.0$.

(1) Presented at the Middle Atlantic Meeting of the American Chemical Society, Feb 2, 1968.

(2) E. I. du Pont de Nemours and Co., Inc., Wilmington, Del.

(3) T. F. Young and M. B. Smith, *J. Phys. Chem.*, **58**, 716 (1954).

(4) T. F. Young, Y. C. Wu, and A. A. Krawetz, *Discussions Faraday Soc.*, **24**, 37, 77, 80 (1957).

(5) J. H. Stern and A. A. Passchier, *J. Phys. Chem.*, **67**, 2420 (1963).

(6) J. H. Stern and C. W. Anderson, *ibid.*, **68**, 2528 (1964).

(7) Y. C. Wu, M. B. Smith, and T. F. Young, *ibid.*, **69**, 1868, 1973 (1965).

(8) R. H. Wood and R. W. Smith, *ibid.*, **69**, 2974 (1965).

(9) (a) R. H. Wood and H. L. Anderson, *ibid.*, **70**, 992, 1877 (1966);

(b) R. H. Wood and H. L. Anderson, *ibid.*, **71**, 1869, 1871 (1967).

(10) M. S. Stakhanova, M. Kh. Karapetyants, I. V. Bazlova, and K. K. Vlasenko, *Russ. J. Phys. Chem.*, **40**, 553, 1000 (1966).

(11) J. D. Patton, Ph.D. Thesis, University of Delaware, 1968. The results for the MgCl₂-KCl mixture and all of the three salt mixtures containing sodium chloride are incorrect due to errors in the concentrations of the solutions.

(12) H. S. Jongenburger and R. H. Wood, *J. Phys. Chem.*, **69**, 4231 (1965).

Table I: Heat of Mixing, MgCl₂-MCl

Salt pair	Ionic strength	RTh_0^a	RTh_1	N^b
LiCl-MgCl ₂	0.5	5 ± 2	-2.5 ± 2	4
	1	-1.8 ± 0.2	-1.3 ± 0.2	15
	2	-8.7 ± 0.2	-0.3 ± 0.2	8
	3	-12.75 ± 0.04	-0.76 ± 0.06	15
NaCl-MgCl ₂	0.5	189 ± 2	-6 ± 2	14
	1	172.5 ± 0.9	-12 ± 1	14
	2	138.8 ± 0.4	-15 ± 1	16
	3	113.6 ± 0.6	-18 ± 1	14
KCl-MgCl ₂	0.5	108 ± 2	-8 ± 4	15
	1	86.7 ± 0.6	-4 ± 1	8
	2	54.0 ± 0.2	-3.1 ± 0.4	7
	3	31.7 ± 0.3	-1.5 ± 0.6	6
CsCl-MgCl ₂	0.5	73 ± 2	-2.5 ± 4	8
	1	19.0 ± 0.4	2 ± 1	12
	2	-23.7 ± 0.5	2.7 ± 0.8	7
	3	-49.6 ± 0.1	9.6 ± 0.2	14

^a Units are calories per kilogram of solvent per ional squared. ^b Number of experimental points.

The results together with the number of data points are given in Table I. Any points that differed from the least-squares fit by more than about twice the standard deviation were rejected.

An examination of the results in Table I shows that RTh_0 , which ranges from -50 to 190, is of the same order of magnitude for these mixtures as for the mixtures of the alkali metal halides which range from 85 to -195.7. This is somewhat surprising since in these mixtures the concentration of chloride ion changes during the mixing so that oppositely charged pairwise interactions contribute to heat of mixing. The result is that Young's rule³ (which is equivalent to assuming $RTh_0 = 0$) is about as good an approximation for these mixtures as for the alkali halides.

One of the most striking things about the values of RTh_0 plotted in Figure 1 is that they all turn toward more positive values at low concentrations. This is in contrast to the results for charge-symmetrical mixtures^{13,14} where the curves are relatively flat. Friedman predicted that for charge-asymmetrical mixtures RTg_0 (the free-energy analog of RTh_0) would go to $-\infty$ as $\ln I$ when I approaches zero. This is a limiting law and is independent of the model. It depends only on the properties of the solvent and the charge types of the electrolytes. The derivation of the limiting-law coefficient for both RTg_0 and RTh_0 starts with eq 17.8 of Friedman¹³

$$\frac{G^{\text{ex}} - DHLL}{RT} = -\frac{1}{3V} \left[\frac{n_3}{n_2} \right]^2 A^2 I^2 \ln I + O(I^2) \quad (2)$$

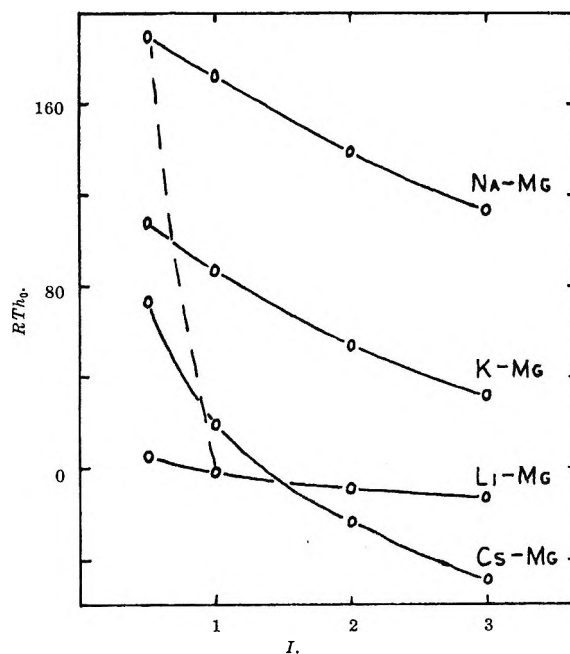


Figure 1. RTh_0 vs. molal ionic strength for alkali metal chloride-magnesium chloride mixtures. The limiting law is indicated by a dashed line.

applied to a mixing experiment to give

$$\Delta_m \left(\frac{G^{\text{ex}}}{RT} \right)_v - \Delta_m \left(\frac{DHLL}{RT} \right)_v = \frac{-A^2}{3V} \Delta_m \left(\frac{n_3^2}{n_2^2} \right) I^2 \ln I + \dots \quad (3)$$

(13) H. L. Friedman, "Ionic Solution Theory," Interscience Publishers, New York, N. Y., 1962, p 244.

(14) H. L. Friedman, *J. Chem. Phys.*, **32**, 1134 (1960).

where the symbolism is Friedman's. The change in the Debye-Hückel limiting law (*DHLL*) is zero and for a mixture of a 1-1 electrolyte with a 2-1 electrolyte $\Delta_m(n_3^2/n_2^2) = y^2$, where y is the ionic strength fraction of 2-1 electrolyte. This gives

$$G^{\text{ex}}/RT = -(A^2/3V)y^2I^2 \ln I + \dots \quad (4)$$

which is used to calculate ΔG^{ex} for the mixing

$$\Delta_m G^{\text{ex}} = (A^2/3V)RTI^2y(1-y) \ln I \quad (5)$$

but by definition

$$\Delta_m G^{\text{ex}} = y(1-y)I^2RTg_0 \quad (6)$$

so that

$$g_0 = (A^2/3V) \ln I \quad (7)$$

and this is the limiting law for free energy. Using Friedman's eq 18.54¹³

$$h_0 = -T[\partial g_0/\partial T] \quad (8)$$

gives

$$h_0 = -(TA^2/3V)\left(\frac{1}{d} \frac{\partial d}{\partial T} - \frac{3}{D} \frac{\partial D}{\partial T} - \frac{3}{T}\right) \ln I \quad (9)$$

For water at 25° the numerical values are

$$g_0 = 1.05 \log I; \quad RTh_0 = -633 \log I \quad (10)$$

The limiting law is shown as a dashed line in Figure 1. An eventual trend toward $+\infty$ is predicted by the limiting law. The values of RTh_0 do increase as the concentration decreases but there is no sign of quantitative approach to the limiting law. This is not surprising at ionic strengths of 0.5 and higher. The free energy measurements of alkaline earth chloride-alkali metal chloride mixtures generally do not show the corresponding decrease in RTg_0 as the concentration decreases, even at $0.75I$.^{15,16} Friedman has shown that HCl-AlCl₃ mixtures do show the expected trend.¹³

The interactions between two ions which contribute to a charge-asymmetric mixture with a common ion have been calculated by Friedman¹⁷

$$-g_{02}/2 = \left(\frac{B(1,1,0)}{z_1 z_2 (z_1 - z_3)(z_2 - z_3)}\right) - \left(\frac{B(2,0,0)}{z_1^2 (z_1 - z_3)^2}\right) - \left(\frac{B(0,2,0)}{z_2^2 (z_2 - z_3)^2}\right) + \frac{z_1 - z_2}{z_3(z_1 - z_3)(z_2 - z_3)} \left[\left(\frac{B(0,1,1)}{z_2(z_2 - z_3)}\right) - \left(\frac{B(1,0,1)}{z_1(z_1 - z_3)}\right) - \left(\frac{(z_1 - z_2)B(0,0,2)}{z_3(z_1 - z_3)(z_2 - z_3)}\right) \right] \quad (11)$$

where for a NaCl-MgCl₂ mixture $z_1 = z(\text{Mg}^{2+}) = +2$, $z_2 = z(\text{Na}^+) = +1$, and $z_3 = z(\text{Cl}^-) = -1$. The

cluster integrals, $B(x,y,z)$, are integrals involving (x) magnesium ions, (y) sodium ions, and (z) chloride ions. Thus, for this kind of mixture, all possible pairs of ions contribute. For a charge-symmetric mixture z_1 is equal to z_2 and the last three terms in eq 11 cancel so that only cation-cation pair terms are left. It has been shown earlier that the sign of the heat of mixing could be correlated with the effect of the ions on the water structure for common-ion, charge-symmetric mixtures.⁹ The rule is that two structure-making ions or two structure-breaking ions give a positive value of RTh_0 whereas mixing a structure-maker with a structure-breaker gives a negative RTh_0 . Since the ion-pair interactions are the major contributors to these mixings, it is the heat effect of the cation-cation interactions which correlates with the water structure (the first three terms of eq 11). Thus, a similar correlation of the present results for charge-asymmetric mixtures is not expected. The results in Table I confirm this expectation.

In 1935 Guggenheim¹⁸ derived an equation for mixed electrolytes which, when applied to the present case,¹⁹ gives

$$RTh_0 = \frac{2.303RT^2}{3} \left[\frac{1}{3} \frac{\partial B_{\text{MgCl}_2}}{\partial T} - \frac{\partial B_{\text{MCl}}}{\partial T} \right] \quad (12)$$

where the B terms are the interaction coefficients of the anion-cation pairs.¹⁹ Values of $\partial B/\partial T$ at low concentration were taken from Lewis and Randall¹⁹ and the calculated values of RTh_0 are given in Table II. The values of RTh_0 calculated from Guggenheim's equation are not very close to the experimental values. This is expected because the like-charged ion interactions in eq 11 ($B(1,1,0)$, $B(2,0,0)$, $B(0,2,0)$, and $B(0,0,2)$) are ignored. The calculation is interesting because it gives a rough estimate²⁰ of the cation-anion interaction terms ($B(1,0,1)$ and $B(0,1,1)$) of eq 11. A comparison of the calculated and experimental values of RTh_0 in Table II shows that the neglected terms are about as large as the cation-anion interactions. Guggenheim's new equation²¹ includes like-charged ion interactions but is not applicable to charge-asymmetric mixtures.

It might be expected that the cation-cation inter-

(15) (a) R. A. Robinson and V. E. Bower, *J. Res. Nat. Bur. Stand.*, **69A**, 19, 439 (1965); **70A**, 313 (1966); (b) R. A. Robinson and A. K. Covington, *ibid.*, **72A**, 239 (1968).

(16) J. N. Butler and R. Huston, *J. Phys. Chem.*, **71**, 4479 (1967).

(17) H. L. Friedman, ref 13, eq 18.36.

(18) E. A. Guggenheim, *Phil. Mag.*, **19**, 588 (1935).

(19) G. N. Lewis and M. Randall, "Thermodynamics," 2nd ed, revised by K. S. Pitzer and L. Brewer, McGraw-Hill Book Co., Inc., New York, N. Y., 1961, Chapter 25 and Appendix 4.

(20) This is a rough estimate because the contributions of like-charged ion interactions to the properties of the pure electrolytes are ignored.

(21) E. A. Guggenheim, *Trans. Faraday Soc.*, **62**, 3446 (1966).

Table II: Comparison of Experimental and Calculated $RT h_0$ Using Guggenheim's Equation

Salts	Ionic strength	$RT h_0$, ^{a,b} calcd	$RT h_0$, exptl	$\frac{RT h_0}{RT h_0}$ (exptl) - (calcd)
LiCl-MgCl ₂	0.5	-76	5	81
	1.0	-76	-1.8	74
	2.0	-76	-8.7	67
	3.0	-76	-12.75	63
NaCl-MgCl ₂	0.5	53	189	136
	1.0	53	172.5	120
	2.0	53	138.8	86
	3.0	53	113.6	61
KCl-MgCl ₂	0.5	68	108	40
	1.0	68	86.7	19
	2.0	68	54.0	-14
	3.0	68	31.7	-36
CsCl-MgCl ₂	0.5	178	73	-105
	1.0	178	19.0	-159
	2.0	178	-23.7	-202
	3.0	178	-49.6	-228

^a Guggenheim's equation applied to heats of mixing predicts that $RT h_0$ is independent of concentration. ^b These values are calculated from heats of dilution and should be accurate to about ± 10 .

actions in a charge-asymmetric mixture would obey the water-structure correlation. These interactions can be estimated in the following manner to see if the

structure rule holds. The limiting law is neglected and the oppositely-charged ion interactions ($B(1,0,1)$ and $B(0,1,1)$) are estimated from Guggenheim's equation (eq 12). The difference between the experimental $RT h_0$ and that calculated by eq 21 should then be equal to the like-charged pair interaction plus any triplet interactions. If the triplet interactions are small, as they are for the alkali halides, and if the Cl^- , Cl^- interaction is small ($B(0,0,2)$) then the structural correlation should hold. In Table II the last column shows the value of $RT h_0$ when the oppositely charged pairwise interactions are subtracted. The rule predicts that the LiCl-MgCl₂ and NaCl-MgCl₂ mixings (structure-maker, structure-maker) should have a positive $RT h_0$ and the KCl-MgCl₂ and CsCl-MgCl₂ should have a negative $RT h_0$. The prediction is correct except for the KCl-MgCl₂ mixings at low concentration. This failure may be due to the neglect of the limiting-law contribution to $RT h_0$ which requires that all $RT h_0$ for 1-1 with 2-1 electrolyte mixtures goes to $+\infty$ as I approaches zero. Considering all of the approximations involved, it would not be surprising if the prediction were not correct. Data on a wide variety of systems will be needed to test whether the sign prediction is generally valid for 2-1 with 1-1 mixtures.

Acknowledgments. The authors gratefully acknowledge the support of this work by the Office of Saline Water, U. S. Department of the Interior. The authors also wish to thank Miss Nalini Bhatt for help with the calorimetric measurements.

Thermodynamic Properties of Plutonium Nitride by Galvanostatic Potential Determination¹

by G. M. Campbell

Los Alamos Scientific Laboratory, University of California, Los Alamos, New Mexico 87544 (Received July 19, 1968)

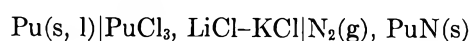
A galvanostatic technique has been developed for the determination of equilibrium potentials in fused salts. The technique makes it possible to measure the emf of metal-metal ion couples without requiring the presence of the metal for long periods of time. This has obvious advantages, especially in the case of very reactive metals where surface impurities are difficult to eliminate by the usual techniques. The technique was used to obtain direct measurements on the cell $\text{Pu}(s, l)|\text{PuCl}_3, \text{LiCl-KCl}|\text{N}_2(g), \text{PuN}(s)$ over the temperature range 714–1032°K. The reaction of Pu with N_2 at these temperatures precludes obtaining the emf by other methods. Over this temperature range, at 1 atm N_2 the emf is $E = 7.90071 - 2.31690 \times 10^{-2}T + 2.517855 \times 10^{-5}T^2 - 9.1644 \times 10^{-9}T^3 (\pm 0.003)$ V. Above the melting point of Pu (913°K) the standard free energy of formation of PuN is $-\Delta G^\circ_T = 73.8 - 0.0225T$ kcal/mol of PuN. From the condition $S^\circ_{298}(\text{PuN}) - S^\circ_{298}(\text{Pu}) = S^\circ_{298}(\text{UN}) - S^\circ_{298}(\text{U})$ the estimate $-\Delta H^\circ_{298} = 72.5$ kcal/mol is made. Theoretical development of the technique is included.

Introduction

The importance of emf determination for obtaining thermodynamic information has recently been re-emphasized.² It should be recognized, however, that the technical difficulties involved in ascertaining the chemical equilibrium represented by any stable emf are still in need of improvement. The difficulty of detecting side reactions which have an indeterminate effect on the results is one of the principal uncertainties in any emf determination. The galvanic potential at the electrode-electrolyte interface is affected by the gradual buildup of impurities over extended periods of time, especially if the electrode surface is easily oxidized.

Experience in this laboratory has indicated that at temperatures above the melting point of Pu (913°K), slow side reactions of Pu with LiCl-KCl eutectic cause conditions leading to electronic conduction between electrodes in any cell containing them. This was indicated by the presence of a linear iR component in the voltammetric trace using a W microelectrode. Since it is necessary to allow considerable time to reach chemical equilibrium at any particular temperature when a solid alloy is used as an electrode, it is often impossible to make direct measurements of the Pu alloy *vs.* pure Pu metal by using a semipermanent Pu(l) electrode.³ Indirect measurements using a reference substitute are time consuming and must necessarily lead to results of lower accuracy.

A galvanostatic technique which virtually eliminates these difficulties has been developed for determinations made in high-temperature electrochemical cells. The technique was used to determine the Pu-Pu³⁺ potential in the cell



at temperatures ranging from 714 to 1032°K. Since N_2 is known to react with Pu throughout this temperature range, no direct measurements are possible by the usual technique. Emf measurements have previously been made in this laboratory by an indirect method.⁴ Since the technique involved the use of a liquid junction and a solid Pu electrode, it was necessary to restrict the measurements to a very limited temperature range. The galvanostatic technique has made it possible to eliminate the liquid junction and otherwise minimize the technical difficulties which had existed. Rather than depend on a semipermanent reference electrode, this technique makes use of a W microelectrode upon which Pu³⁺ is reduced to Pu by passing a constant current between the W microelectrode and a third electrode. By reversing the current, the Pu is immediately re-oxidized. The entire time for reduction and oxidation is completed in a few seconds. Since the concentration of Pu³⁺ at the microelectrode surface is a function of electrolysis time and current, by making use of diffusion theory and monitoring the potential between the microelectrode and the PuN electrode, the desired potential is obtained. In effect an "in situ" electrode is formed and the depletion of the electroactive species is counteracted by anodic dissolution such that a calculated time is used to estimate local return to the bulk concentration at the electrode-electrolyte interface. It is necessary of course to assume that the activity of Pu metal reduced onto the W electrode is the same as that of a semi-

(1) This work was performed under the auspices of the U. S. Atomic Energy Commission.

(2) O. Kubaschewski, "Thermodynamics of Nuclear Materials, 1967," IAEA, Vienna, 1968.

(3) G. M. Campbell, L. J. Mullins, and J. A. Leary, ref 2, pp 75-88.

(4) G. M. Campbell and J. A. Leary, *J. Phys. Chem.*, **70**, 2703 (1966).

permanent Pu electrode. This is not true at times near the beginning of the reduction process or the end of the oxidation process. Experiments in which a semi-permanent Pu electrode was used as a reference indicated, however, that this condition was met during the stripping process as the Pu^{3+} concentration gradient approached zero for stripping times of 1 sec or longer. This was also found to be true for the U- U^{3+} couple. The microelectrode used in these experiments was a W wire 0.04 cm in diameter dipping about 1 cm into the melt. The thermal emf of Ta *vs.* W was determined by placing two electrodes in position and substituting Al metal (mp 659.7°) for the electrolyte.

Spectro pure N_2 gas at a carefully measured pressure was maintained in the cell at all times during the experiments. When significant amounts of PuN were produced during the short period of reduction and stripping a characteristic wave in the time-potential trace was observed near the equilibrium potential of the PuN reference. Since the number of electrons per equivalent for the stripping of Pu and of PuN is the same, the total Pu reduced was easily accounted for. The amount of PuN produced during the period of an average scan time was negligible at temperatures below about 1000°K. Above this temperature significant amounts of PuN were produced. In all cases the PuN stripping time was small compared to that of pure Pu.

Galvanostatic Potential Determination

The electrochemical technique often referred to as chronopotentiometry or the galvanostatic technique has been used for the determination of diffusion coefficients of electroactive species in a liquid, the determination of its concentration, and studies related to electrode processes. To the author's knowledge, the technique has not previously been used to determine equilibrium potentials. Since the technique is described adequately in the literature,⁵ a complete explanation will not be given here. Three electrodes are involved when using the technique: (a) a microelectrode at which the electroactive species is reduced or oxidized, also called the working electrode; (b) a counterelectrode through which the current is passed to complete the circuit with the microelectrode, serving as the anode when the microelectrode is the cathode and vice versa; and (c) a reference electrode which is at equilibrium with the electrolyte and undisturbed by the passage of a current. While a direct current of constant magnitude is passed through the circuit formed by the current source, the microelectrode, and the counterelectrode, the emf between the microelectrode and the reference electrode is measured as a function of time and is recorded. The potential of the microelectrode is a function of the activities of the reduced and oxidized forms of the electroactive species at the electrode surface. As one of these forms is depleted to an activity approaching zero,

a break is observed in the potential *vs.* time trace. To find the equilibrium potential it is necessary to determine the emf of Pu metal in equilibrium with Pu^{3+} in solution at a time when the Pu^{3+} activity is equal to the Pu^{3+} activity in equilibrium with a semipermanent PuN electrode. In this case the semipermanent PuN electrode is made the reference electrode. First Pu^{3+} is reduced onto the microelectrode by electrolysis with a current of constant magnitude. At a planar electrode the concentration of Pu^{3+} decreases during reduction, assuming no other reducible species is present, and is given by⁶

$$C_{(x,t)} = C^0 - \frac{2i_1 t_1^{1/2}}{3FD^{1/2}\pi^{1/2}} \exp\left(-\frac{x^2}{4Dt_1}\right) + \frac{i_1 x}{3FD} \operatorname{erfc}\left(\frac{x}{2D^{1/2}t_1^{1/2}}\right) \quad (\text{I})$$

For a definition of symbols, see Appendix A.

An expression for the concentration after current reversal is arrived at by using eq I and the relation

$$D\left(\frac{\partial C}{\partial x}\right)_{x=0} = -\frac{i_2}{3F} \quad (\text{II})$$

as boundary conditions for Fick's second law

$$\frac{\partial C_{(x,t_2)}}{\partial t_2} = D \frac{\partial^2 C_{(x,t_2)}}{\partial x^2} \quad (\text{III})$$

This results in the relation⁷

$$C_{(0,t_2)} = C^0 - \frac{2}{3FD^{1/2}\pi^{1/2}} \times (i_1 t_1^{1/2} - i_1 t_2^{1/2} - i_2 t_2^{1/2}) \quad (\text{IV})$$

The times of electrolysis of Pu^{3+} during reduction can be measured by observing the break in the potential-time trace (Figure 1). To avoid the possibility of a difference in the current efficiency during the two processes, the relationship

$$i_1 t_1 = i_2 t_2 \quad (\text{V})$$

is used. The only assumption necessary is that all the Pu^{3+} plated out is subsequently stripped from the electrode. Combining (IV) and (V), the concentration during the stripping process is then

$$C_{(0,t_2)} = C^0 - \frac{2i_2}{3FD^{1/2}\pi^{1/2}} \times \left(\frac{T_2}{t_1^{1/2}} - \frac{T_2 t_2^{1/2}}{t_1} - t_2^{1/2}\right) \quad (\text{VI})$$

(5) M. Paunovic, *J. Electroanal. Chem.*, **14**, 447 (1967).

(6) P. Delahay, "New Instrumental Methods in Electrochemistry," Interscience Publishers, New York, N. Y., 1954, p 180.

(7) See Appendix B for the development of eq IV.

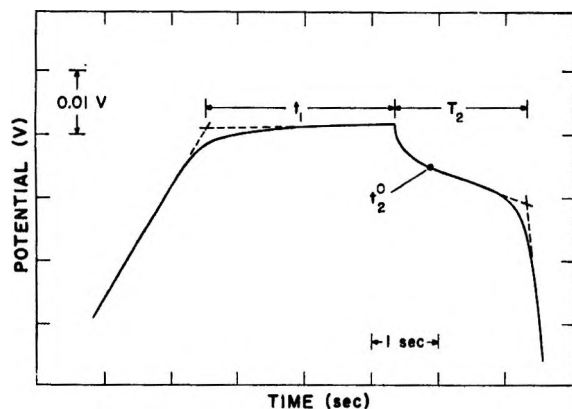


Figure 1. Chronopotentiogram of the type used to measure equilibrium potentials.

and

$$C_{(0,t_2)} = C^0$$

when

$$t_2^0 = t_1 \left(\frac{T_2}{t_1 + T_2} \right)^2 \quad (\text{VII})$$

Since t_2^0 is independent of current, the relative values of t_1 and T_2 can be changed by using a constant current of different magnitude for each of the two processes. It should be noted that eq I is valid only as long as the concentration, $C_{(0,t_1)}$, at the electrode surface is finite. This means that the current must be reversed before the chronopotentiometric transition time of the reduction process is reached. The best results are achieved when the reducing current is as small as possible to prevent a large concentration gradient from developing at the electrode surface. This is especially true for electrodes whose geometry differs greatly from a planar surface.

The foregoing equations are based on the conditions found for diffusion to a planar surface. The solution for the case of cylindrical diffusion has also been derived for chronopotentiometry⁸ but is more complex and depends on a knowledge of the diffusion coefficient, D , which is a function of temperature. However, the two approaches give results in which significant differences are observed only when the volumes containing the concentration gradient at the electrode surface become significantly different. In our case the currents used were sufficiently small (always considerably below the voltammetric diffusion limiting current) that the concentration gradient and therefore the volume containing them remained small. This was indicated by the relatively slow change of potential with time during the stripping process. The rate was usually of the order of 0.015 V/sec.

The electrode geometry problem is more easily avoided for equilibrium potential determination than in most other instances. When the technique of chronopotentiometry is used for determination of concentra-

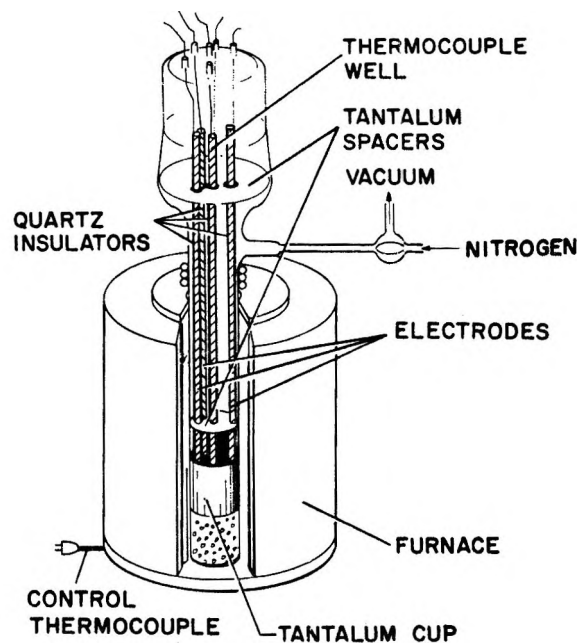


Figure 2. Electrochemical cell.

tion, for example, the solute concentration must approach zero at the transition time. Consequently, the volume containing the concentration gradient is usually considerably different for the case of cylindrical as compared to that for planar electrodes. When the technique is used for emf determination at high temperatures, however, the solute concentration at the electrode surface need vary little from the bulk concentration. Consequently, the volume containing the concentration gradient is nearly the same for planar as for cylindrical electrodes. This was verified experimentally by making galvanostatic determinations against a Pu(I) reference electrode, over the temperature range of these experiments. Agreement was always within ± 0.002 V. Stripping times used were between 1 and 2.3 sec. Electrodeposition times were between 3 and 7 sec. Similar experiments on the U-U³⁺ couple at the same temperatures gave similar results.

Experimental Section

Equipment. 1. Apparatus and Materials. The cell used for emf determinations is diagrammed in Figure 2. The quartz container was surrounded by an electrically grounded nickel tube to provide shielding against stray electric fields. The quartz container, 18 in. deep and 1⁷/₈ in. in diameter, was positioned so that the lower 9 in. was inside the tube furnace. A Cu cooling coil placed around the container above the furnace kept the cell top at a moderate temperature at all times.

The electrolyte was contained in a Ta cup 2.5 in. deep and 1.5 in. in diameter. The PuN reference elec-

(8) D. G. Peters and J. J. Lingane, *J. Electroanal. Chem.*, **2**, 1 (1961).

trode was made by clamping a doughnut-shaped sintered pellet of PuN between W washers at the end of a Ta rod. Nitrogen content in the PuN was 0.99 atom of N to 1 atom of Pu. X-Ray powder diffraction analysis indicated that the material was single-phase PuN, with $a_0 = 4.9055 \text{ \AA}$. Spectroscopically pure N_2 was maintained at a carefully measured pressure in the cell.

The W microelectrode, or working electrode, was made by suspending a 0.04-cm diameter W wire from a 3-mm i.d. quartz tube so that the wire was immersed to a depth of about 1 cm in the electrolyte. The quartz tube extended to within about 1 in. of the electrolyte and served as an electrical insulator from the other electrodes which were placed inside similar quartz tubes.

The auxiliary electrode was made by melting Pu metal into a $1/2$ in. diameter by $1/2$ in. deep TaC coated Ta cup attached to the end of a $1/8$ -in. Ta rod. In addition to serving to carry current, this electrode helped maintain the purity of the electrolyte. Reaction with N_2 reduced the Pu activity on the electrode surface and prevented electronic conduction from developing in the cell.

A chromel-alumel thermocouple calibrated against the melting point of NBS pure Zn and Al metals was used in all temperature measurements. The thermocouple was inserted into a $1/8$ -in. diameter Ta tube which was closed at one end and immersed in the molten electrolyte.

Electric contacts for electrodes and thermocouples were directed through Kovar seals at the top of the cell. This made it possible to evacuate the cell and flush with N_2 to remove gaseous impurities from the cell.

2. *Procedure.* The initial preparation of the LiCl-KCl electrolyte was similar to that described by Laitinen, *et al.*⁹

After treatment with HCl, the eutectic mixture was repeatedly equilibrated with Pu metal and filtered, until voltammetric analysis indicated the desired purity was obtained.

All cell parts except the electrodes were assembled and outgassed overnight at 800° . After cooling, the electrodes and electrolyte were added and the cell repeatedly evacuated and flushed with N_2 as the temperature was slowly raised. The temperature was controlled with a Minneapolis Honeywell "Pyr-O-Vane" controller.

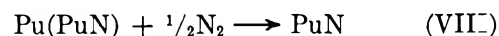
The emf between the PuN reference electrode and the Pu auxiliary electrode was monitored continuously on a Sargent Model MR recorder. Chronopotentiograms were recorded periodically on a second Sargent Model MR recorder. A constant current source of conventional design, built by the LASL instruments group, produced direct currents ranging from about 200 to $630 \mu\text{A}$ in magnitude. The current from this source was passed through a 10-ohm resistor before and after the potential *vs.* time trace was recorded. The chart

speed of the recorder during the electrolysis period was 1 in./sec. After measuring the Pu plating and stripping periods, the time during stripping at which the Pu^{3+} concentration at the microelectrode surface was equal to the bulk concentration was calculated using eq VII. By bucking the recorder circuit with the potential from a Minneapolis Honeywell potentiometer until the recorder pen was located at the indicated chart position, the emf was read from the potentiometer. This made it possible to make each measurement using a standard calibrated Weston cell as a reference potential. At least three chronopotentiograms were recorded at each PuN equilibrium with the current at a new setting each time. Regardless of the variation in plating and stripping times and in current, the measured emf usually varied less than 2 mV. In cases where the Pu plated on the microelectrode reacted to produce a significant amount of PuN, as indicated by a break in the potential-time trace near the PuN reference potential, the stripping time for the PuN was added to the stripping time of Pu to arrive at the total stripping time T_2 . The stripping time for PuN was determined independently of that for pure Pu to avoid error due to double-layer charging. The time was measured by drawing tangents to either side of the inflections in the curve (Figure 1) and taking the intersection of the tangent lines as starting and ending times.

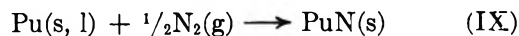
After the emf was determined at one temperature setting, the temperature was raised or lowered by about 20° . At least 24 hr was allowed for the PuN reference electrode to reach a new equilibrium.

Results

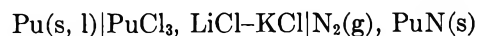
Since N_2 is known to react with Pu over the range of temperatures of these experiments, the cell reaction is properly written as



However, it is unlikely that the solubility of PuN in Pu is great enough to cause a significant difference in the emf at these temperatures. For this reason the results will be treated as if the cell reaction were



and the schematic representation of the cell is



Pu(l) is of course saturated with N_2 . The concentration of PuCl_3 in the three cells was 0.338, 0.166, and 0.112 mol %. The correction for the thermal emf of Ta *vs.* W was

$$E = -5.7240 \times 10^{-3} + 1.1966 \times 10^{-5}T + 2.9652 \times 10^{-9}T^2 \quad (\text{X})$$

(9) H. A. Laitinen, W. S. Ferguson and R. R. Osteryoung, *J. Electrochem. Soc.*, **104**, 516 (1957).

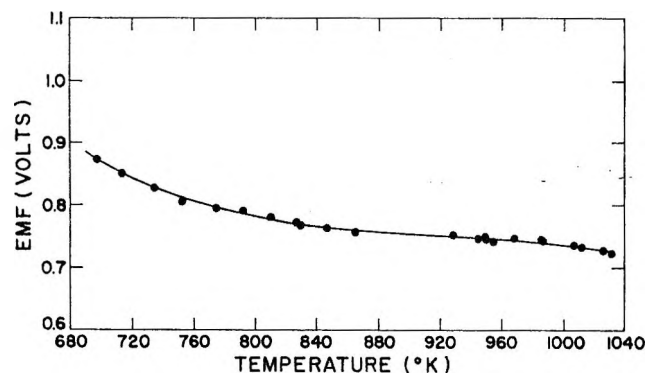


Figure 3. Emf vs. temperature over the range 714 to 1032°K at 1 atm N_2 for the cell $Pu(s,l) | PuCl_3, LiCl-KCl | N_2(g), PuN(s)$.

where E is in volts and T is in °K. Since Ta was the negative pole, the thermal emf was added to the measured galvanic emf. After correcting the N_2 pressure to 1 atm by using the equation

$$E_{(1 \text{ atm})} = E_{(\text{measd})} - \frac{2.3RT}{3F} \log p^{1/2}_{(\text{measd})} \quad (\text{XI})$$

the emf is plotted vs. temperature in Figure 3. N_2 pressures measured were between 0.686 and 0.786 atm. The least-squares line is represented by the equation

$$E = 7.90071 - 2.31690 \times 10^{-2}T + 2.517855 \times 10^{-5}T^2 - 9.1644 \times 10^{-9}T^3 (\pm 0.003) \text{ V} \quad (\text{XII})$$

with T in °K.

The results of previous experiments by the indirect method⁴ gave 0.8745 (± 0.005) V for the emf at 700°K. From the present experiments the emf at this temperature is 0.8765 (± 0.003) V, which is in good agreement.

The greatest phase change of Pu in this temperature range is the solid to liquid at 913°K. Since this involves only about 1 eu no change in the emf plot is detectible.

In the region of ϵ Pu(749-913° K) a least-squares analysis of the data gives

$$E = 1.1644 - 4.663 \times 10^{-4}T (\pm 0.0016) \text{ V} \quad (\text{XIII})$$

Above the melting point of Pu(913° K) the least-squares line from the two cells is (Figure 4)

$$E = 1.0672 - 3.258 \times 10^{-4}T (\pm 0.0025) \text{ V} \quad (\text{XIV})$$

The decrease in emf with increasing temperature below the melting point of Pu is larger than can be accounted for by consideration of the known thermodynamic properties of the constituents. It seems likely that in the lower temperature range the emf includes a component that is not related to the free-energy change

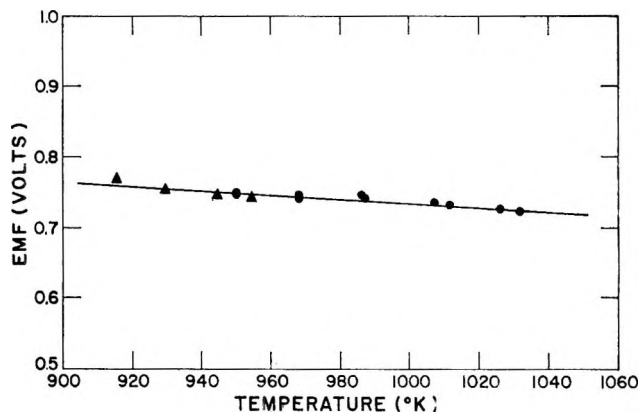


Figure 4. Emf vs. temperature above the melting point of Pu at 1 atm N_2 for the cell $Pu(l) | PuCl_3, LiCl-KCl | N_2(g), PuN(s)$.

in the Pu- N_2 reaction. This probably results because the surface of the PuN pellet is not in equilibrium with the center of the pellet at these temperatures.

Using the data above the melting point of Pu

$$-\Delta G^{\circ}_T = 73.8 - 0.0225T \text{ kcal/mol} \quad (\text{XV})$$

for reaction IX.

By combustion calorimetry, Lapage¹⁰ found $-\Delta H = 70.2 \pm 1.5$ kcal/mol at 298° K for reaction IX. Using the UN data of Godfrey,¹¹ the U data of Hultgren,¹² the Pu data of Rand¹³ and the relation $C_p(\text{PuN}) = C_p(\text{UN}) - C_p(\text{U}) + C_p(\text{Pu})$, $(H_{1000} - H_{298})\text{PuN} = 8.5887$ kcal/mol and $(S_{1000} - S_{298})\text{PuN} = 14.9$ eu.

This gives $-\Delta H_{1000} = 72.35$ and is within experimental error of the intercept of eq XV. Equation XV then leads to $-\Delta G^{\circ}_{298} = 71.6 - 0.0185T$ kcal/mol and $S^{\circ}_{298}(\text{PuN}) = 17.6$ eu. This compares with $S^{\circ}_{298}(\text{UN}) = 14.97$ eu. If the condition that $S^{\circ}_{298}(\text{PuN}) - S^{\circ}_{298}(\text{Pu}) = S^{\circ}_{298}(\text{UN}) - S^{\circ}_{298}(\text{U})$ is used, $S^{\circ}_{298}(\text{PuN}) = 16.17$ eu and from emf data $-\Delta H^{\circ}_{298} = 72.5$ kcal/mol. Recently, vapor pressure measurements of PuN have led to an estimate of $-\Delta H^{\circ}_{298} = 72.9$ kcal/mole.¹⁴

Summary

A galvanostatic technique has been used to determine the equilibrium potential of the Pu-Pu³⁺ couple in fused LiCl-KCl. This technique was found to have

(10) R. Lapage and J. L. Bunce, *Trans. Faraday Soc.*, **63**, 1889 (1967).

(11) R. G. Godfrey, J. A. Woolley, and J. M. Leitnaker, "Thermodynamic Functions of Nuclear Materials: UC, UC₂, UO₂, ThO₂, and UN," ORNL-TM-1596 (1966).

(12) R. Hultgren, R. L. Orr, P. D. Anderson, and K. K. Kelley, "Selected Values of Thermodynamic Properties of Metals and Alloys," John Wiley & Sons, Inc., New York, N. Y., 1963.

(13) M. H. Rand, IAEA 4, Special Issue No. 1 Plutonium, Vienna, 1966.

(14) R. A. Kent and J. A. Leary, "Mass Spectrometric Studies of Plutonium Compounds at High Temperatures. I. The Heats of Vaporization of Gold and Plutonium and the Heat of Decomposition of Plutonium Mononitride." Los Alamos Scientific Laboratory Report No. LA-3902 (1968).

several advantages over that of using a semipermanent Pu electrode. The technique works equally well whether the reduced form of Pu on a W microelectrode is liquid or solid. The technique has also been used to determine the equilibrium potential of the U-U³⁺ couple in the same electrolyte and has been equally successful.

It is unlikely that the technique will work well in all media especially at low temperatures since it is mandatory that the overpotential for oxidation or reduction of the electroactive species at the microelectrode be negligible. It should have rather general application to high temperature measurements, however.

Acknowledgments. The author wishes to express thanks to J. A. Leary for his encouragement throughout the work and to M. W. Shupe for fabricating the PuN pellets. Analytical work was done by K. S. Bergstresser and N. L. Koski, who made the Pu and N₂ analysis of the PuN pellets, C. W. Bjorkound, who did the X-ray diffraction analysis, and G. M. Matlack, who was responsible for the radiochemical analysis for Pu in the electrolyte.

Appendix A

Definitions of Symbols

- C* Concentration in mol/cm³
- C*(*x, t*) Concentration at a distance, *x*, from the electrode at time, *t*
- C*⁰ Concentration in the bulk of the electrolyte
- D* Diffusion coefficient of depolarizing agent in cm²/sec
- erfc(*y*) Compliment of the error function, (1 - erf(*y*))
- erf(*y*) $2/\pi \int_0^y \exp(-z^2) dz$
- F* Faraday's constant (96,492 C/equiv)
- i*₁ Current density at the electrode surface during the reduction process in A/cm²
- i*₂ Current density at the electrode surface during the stripping process in A/cm²
- n* The number of electrons involved in the electrode reaction
- t*₁ Total time of electrodeposition of Pu on the microelectrode measured from the inflection of the potential time curve to the time of current reversal (sec)
- t*₂ Electrode stripping time measured from the time of current reversal (sec)
- T*₂ Total electrode stripping time measured from time of current reversal until the inflection in the time *vs.* potential plot (sec)
- t*₂⁰ Time at which the concentration of Pu³⁺ at the electrode surface is equal to the concentration in the bulk of the solution

Appendix B

Equation IV was derived in the following manner. The Laplace transform of eq III is¹⁵

$$-U_{(x,0)} + s\bar{U}_{(x,s)} = D \frac{d^2 \bar{U}_{(x,s)}}{dx^2} \quad (1)$$

By defining

$$U_{(x,t_2)} = C_{(x,t_2)} - C^0 + F(C, x, t_1) \quad (2)$$

where from eq I

$$F(C, x, t_1) = \frac{2i_1 t_1^{1/2}}{nFD^{1/2}\pi^{1/2}} \exp\left(-\frac{x^2}{4Dt_1}\right) - \frac{i_1 x}{nFD} \operatorname{erfc}\left(\frac{x}{2D^{1/2}t_1^{1/2}}\right) \quad (3)$$

we have for *t*₂ = 0, *U*(*x,0*) = 0. Equation 1 then has a solution of the form

$$\bar{U}_{(x,s)} = \alpha \exp\left(-\frac{s^{1/2}x}{D^{1/2}}\right) + \beta \exp\left(\frac{s^{1/2}x}{D^{1/2}}\right) \quad (4)$$

Since *U*(*x, t*) and consequently $\bar{U}_{(x,s)}$ have in general a finite value for very large values of *x* (i.e. for *x* → ∞), the constant β is equal to zero and only the first term should be retained.

From eq 2 we have

$$\frac{\partial U_{(x,t_2)}}{\partial x} = \frac{\partial C_{(x,t_2)}}{\partial x} + \frac{\partial F(C, x, t_1)}{\partial x} \quad (5)$$

but

$$\left(\frac{\partial C_{(x,t_2)}}{\partial x}\right)_{x=0} = -\frac{i_2}{nFD}; \quad \left(\frac{\partial F(C, x, t_1)}{\partial x}\right)_{x=0} = -\frac{i_1}{nFD}$$

and the transform of (5) is

$$\left(\frac{\partial \bar{U}_{(x,s)}}{\partial x}\right)_{x=0} = -\frac{i_2}{nFDs} - \frac{i_1}{nFDs} \quad (6)$$

From eq 4

$$\left(\frac{\partial \bar{U}_{(x,s)}}{\partial x}\right)_{x=0} = -\frac{s^{1/2}}{D^{1/2}}\alpha \quad (7)$$

so

$$\alpha = \frac{i_1}{nFD^{1/2}s^{3/2}} + \frac{i_2}{nFD^{1/2}s^{3/2}} \quad (8)$$

$$\bar{U}_{(x,s)} = \left(\frac{i_1}{nFD^{1/2}s^{3/2}} + \frac{i_2}{nFD^{1/2}s^{3/2}}\right) \exp\left(-\frac{xs^{1/2}}{D^{1/2}}\right) \quad (9)$$

$$\bar{U}_{(0,s)} = \frac{i_1}{nFD^{1/2}s^{3/2}} + \frac{i_2}{nFD^{1/2}s^{3/2}} \quad (10)$$

The transform of (10) is

$$U_{(0,t_2)} = \frac{2i_1 t_2^{1/2}}{nFD^{1/2}\pi^{1/2}} + \frac{2i_2 t_2^{1/2}}{nFD^{1/2}\pi^{1/2}} \quad (11)$$

From eq 2

$$C_{(0,t_2)} = C^0 - \frac{2i_1 t_1^{1/2}}{nFD^{1/2}\pi^{1/2}} + \frac{2i_1 t_2^{1/2}}{nFD^{1/2}\pi^{1/2}} + \frac{2i_2 t_2^{1/2}}{nFD^{1/2}\pi^{1/2}} \quad (12)$$

(15) R. V. Churchill, "Modern Operational Mathematics in Engineering," McGraw-Hill Book Co. Inc., New York, N. Y., 1944.

Radiolysis of Solutions of Perfluorocarbons in *n*-Hexane

by L. A. Rajbenbach

Soreq Nuclear Research Centre, Yavne, Israel (Received July 23, 1968)

The radiolytic yields of hydrogen and hydrogen fluoride in dilute solutions of perfluorocarbons in *n*-hexane were determined, as well as the yields of cyclohexene and bicyclohexyl in solutions of perfluorocyclobutane in cyclohexane. The larger perfluoroalkane molecules, beginning with C₄F₁₀, were found to depress the hydrogen yield. The reduction in hydrogen yield was accompanied by formation of HF. The ability of perfluoroalkanes to reduce the hydrogen yield is correlated with data on resonant attachment of thermal electrons to some of these solutes in the gas phase. The decrease in hydrogen yield in the presence of unsaturated perfluorocarbon solutes is attributed to electron scavenging. Possible mechanisms for the formation of HF are discussed. The low yield of HF in the presence of unsaturated solutes is explained as being due to the ability of perfluoroolefin anions to extract protons from molecular solvent cations. The absence of any effect of perfluoroalkane solutes on the yield of olefins from the corresponding alkane solvent is interpreted as confirming the assumption that charge neutralization reactions between molecular cations and electrons do not lead to the formation of molecular hydrogen.

Introduction

The presence of small amounts of solutes in liquid hydrocarbons can change the course of radiation decomposition of the solvent by other than the normally expected secondary radical reactions. It has been recognized for some time that certain solutes in hydrocarbon solutions are capable of capturing electrons, thus interfering with the radiolytic decomposition of the solvent, which occurs partly *via* a charge neutralization reaction between molecular solvent cations and electrons. Hydrogen is the most important final product of the radiolysis of normal alkanes. Thus the effect of solutes on the hydrogen yield, barring of course hydrogen atom scavengers, could serve as a measure of the interaction of electrons with the solute. The conversion of electrons to negative ions by the addition of electron-scavenging solutes is known to reduce solvent decomposition drastically.

In an earlier article,¹ preliminary results were reported on the reduction of the radiolytic hydrogen yield from cyclohexane and *n*-hexane by several perfluoroalkane solutes. It should be noted that perfluoroalkanes would not be expected to exhibit any direct reactivity toward hydrogen atoms for the following reasons. Perfluoromethane is inert to hydrogen atoms² and the primary CF bond strength has been estimated to remain constant in the homologous series of normal perfluoroalkanes.³ The secondary CF bond strength, at least in *c*-C₄F₈ (152 kcal/mol),⁴ appears to be higher than in CF₄ (122 kcal/mol).⁵ In the present work this study was expanded to include a number of additional solutes, among them perfluorinated olefins. An attempt was made to correlate the gas-phase cross-section data for electron attachment by perfluorocarbons with the decrease in radiolytic hydrogen yield

in solutions. An attempt was also made to correlate this decrease with the fate of the solute molecules.

Experimental Section

Materials. *n*-Hexane (Phillips research grade) was shaken overnight with one-tenth its volume of concentrated sulfuric acid and was stored over anhydrous sodium carbonate. CF₄, C₂F₆, C₃F₈, C₄F₈-2, *c*-C₄F₈, C₄F₁₀ (Peninsular Chemresearch Co., Gainesville, Fla.), and N₂O (Matheson Co.) were dried over phosphorus pentoxide and were purified by distillation.

Procedure. The sample preparation techniques were the same as those used previously.⁶ Irradiation of 4- and 7-ml samples was carried out at room temperature with a ⁶⁰Co source (Gammacell 200, Atomic Energy of Canada Ltd.) at a dose rate of 3.1 × 10¹⁷ eV ml⁻¹ min⁻¹. After irradiation the samples were connected to a vacuum line and were thoroughly degassed at 77°K. The gases were transferred by means of a Toepler pump into a calibrated volume and the pressure was measured on a McLeod gauge. The gases were then transferred to a gas sampler and were analyzed by gas chromatography. A 2-m column of 50–100-mesh molecular sieve (Linde 5A) was used to separate the compounds. In order to measure the yield of HF the irradiated degassed samples were transferred under vacuum into a bulb containing a 5-ml aqueous solution

(1) L. A. Rajbenbach, *J. Amer. Chem. Soc.*, **88**, 4275 (1966), and references contained therein.

(2) J. R. Dacey and H. W. Hodgkins, *Can. J. Res.*, **B28**, 173 (1950).

(3) W. M. Bryant, *J. Polym. Sci.*, **56**, 277 (1962).

(4) M. M. Bibby and G. Carter, *Trans. Faraday Soc.*, **59**, 2445 (1963).

(5) C. R. Patrick, *Advan. Fluorine Chem.*, **2**, 17 (1961).

(6) L. A. Rajbenbach and U. Kaldor, *J. Chem. Phys.*, **47**, 242 (1967), and references contained therein.

Table I: γ Radiolysis of Perfluorocarbon Solutions in *n*-Hexane

Solute	Concn, mM	$G(\text{H}_2)^a$	$G(\text{HF})^a$	$K_{\text{N}_2\text{O}}^b$
	0	4.7		<i>c</i>
CF ₄	22	...	<0.05	<i>c</i>
	108	...	<0.05	<i>c</i>
C ₂ F ₆	54.5	4.7	<0.05	<i>c</i>
	109	4.6	<0.05	<i>c</i>
C ₃ F ₈	55	4.7	<0.05	<i>c</i>
	120	4.5	<0.05	
<i>n</i> -C ₄ F ₁₀	55	4.3	0.2	0.1
	123	4.1	0.4	
<i>n</i> -C ₆ F ₁₂	25	3.9	0.6	0.15
	50	3.7	0.7	
<i>n</i> -C ₈ F ₁₄	30	3.6	1.0	0.4
	60	3.1	1.4	
<i>c</i> -C ₄ F ₈	13	3.9	0.9	0.9
	55	2.9	1.7	
	151	2.6	1.9	
<i>c</i> -C ₆ F ₁₂	14	4.0	1.4	0.9
	52	3.0	1.7	1.0
<i>c</i> -C ₈ F ₁₄ CF ₃	24	3.3	1.2	1.0
	48	3.0	1.5	
<i>c</i> -C ₆ F ₁₀	47	3.1	0.4	0.9
	95	2.5	0.4	
<i>c</i> -C ₈ F ₁₀	55	2.8	0.7	0.9
	95	2.6	0.8	
C ₄ F ₈ -2	27	3.6	0.25	0.7
	54	3.1	0.40	

^a Total dose, 9.6×10^{19} eV ml⁻¹. ^b Total dose, 1.1×10^{19} eV ml⁻¹. Calculated from expression A. N₂O concentrations were approximately 5×10^{-3} M each. The decrease in N₂ yield was in all cases $\sim 50\%$. ^c No decrease in $G(\text{N}_2)$ observed.

Table II: Effect of Hexene-1 on Radiolytic HF Yield from 0.3 M Solutions of Perfluorocyclobutane in *n*-Hexane

Hexene-1 concn, mM	$G(\text{HF})^a$
0	2.3
20	2.2
38	2.1
76	1.9

^a Total dose, 2×10^{20} eV ml⁻¹.

of NaOH (10^{-2} M). The bulb was sealed and shaken mechanically for 0.5 hr. The aqueous phase was then separated and analyzed for fluorine photometrically using a modified zirconium-alizarin reagent.⁷ Liquid products were determined by gas chromatography.

Results

The yields of radiolytic hydrogen and hydrogen fluoride from solutions of perfluorinated hydrocarbons in *n*-hexane are shown in Table I. At a dose of 9.6×10^{19} eV ml⁻¹ the yield of hydrogen from pure hexane was found to be $G(\text{H}_2) = 4.7$. The determinations were

made at this dose because of difficulties in determining the HF yield at shorter irradiations. The presence of the small amounts of hexenes, formed in radiolysis, while slightly depressing the hydrogen yield in pure hexane (extrapolated to zero dose, $G(\text{H}_2)_0$), were found to have almost no effect on the yield of hydrogen fluoride (see Table II).

It can be seen from Table I that CF₄, C₂F₆, and C₃F₈ have no effect on the yield of H₂ and that no HF is formed in these solutions. However, thereafter there is a steady decrease in the hydrogen yield, accompanied by the formation of HF, as the size of the perfluoroalkane molecules increases, the perfluorocycloalkanes being particularly effective. The decrease in hydrogen yield is almost equivalent to the yield of HF. In the case of perfluorounsaturated solutes, the yield of HF was found to be considerably smaller than the decrease in the hydrogen yield.

The results of electron capture competitive experiments carried out in solutions of *n*-hexane containing N₂O and perfluorocarbons are also presented in Table I. The $K_{\text{N}_2\text{O}}$ values shown in the table were obtained from the expression⁸

$$K_{\text{N}_2\text{O}} = \frac{\Delta G(\text{N}_2)[\text{N}_2\text{O}]}{G(\text{N}_2)[\text{S}]} \quad (\text{A})$$

This expression does not take into account the possibility that N₂ may be formed by excitation transfer from the solvent to N₂O. However, at the low N₂O concentration used in these determinations excitation transfer to N₂O would not appear to be significant.⁹ In the derivation of expression A there is also no provision for the possibility of electron transfer from the anions of one solute, prior to their decomposition, to competing solute molecules. Qualitatively a considerable decrease in the yield of N₂ from the solution of N₂O in the presence of a second solute may be taken as an indication of electron capture by that solute.

The effect of perfluorocarbons on the yield of congruent olefins in alkane solutions was also measured. For this purpose cyclohexane was chosen as the solvent, since no isomeric olefins are formed in it, thus facilitating the analyses. In Table III the effect of varying the concentration of perfluorocyclobutane on the radiolytic yield of cyclohexene and bicyclohexyl solutions is shown. The results clearly show the absence of any effect of the solute on the yield of olefins. A similar observation was made by Sagert,¹⁰ who found that the radiolytic formation of cyclohexene is not affected by the presence of perfluorocyclohexane in concentrations up to 0.25 M of solute.

(7) S. Megregian and F. J. Maier, *J. Amer. Water Works Assoc.*, **44**, 239 (1952).

(8) V. W. Sherman, *J. Chem. Soc., A*, 599 (1966).

(9) (a) R. A. Holroyd, *J. Phys. Chem.*, **72**, 759 (1968); (b) A. Hcrowsitz and L. A. Rajbenbach, *J. Chem. Phys.*, **48**, 4278 (1968).

(10) W. H. Sagert, *Can. J. Chem.*, **46**, 95 (1968).

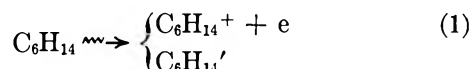
Table III: Effect of Varying the Concentration of Perfluorocyclobutane in Cyclohexane on the Radiolytic Yield of Cyclohexene and Bicyclohexyl

<i>c</i> -C ₄ F ₈ concn, <i>M</i>	<i>G</i> (cyclohexene) ^a	<i>G</i> (bicyclohexyl) ^a
15	3.1	1.6
30	3.0	1.7
60	2.8	1.8
120	2.8	1.9

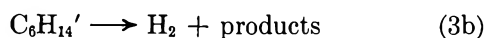
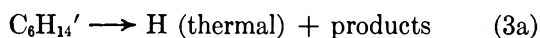
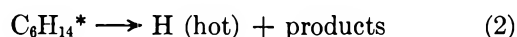
^a Total dose, 3×10^{19} eV ml⁻¹.

Discussion

The Effect of Solutes on Hydrogen Formation. In the radiolysis of saturated hydrocarbons the primary products are excited molecules and positive ions accompanied by an equivalent number of electrons. In the case of *n*-hexane the initial step can be written



Hydrogen molecules can be produced from these products by three separate processes (we use Dyne's¹¹ notation, writing C₆H₁₄* for C₆H₁₄⁺ + e)



The neutralization reaction between a molecular cation and an electron is assumed to yield predominantly hot hydrogen atoms,⁶ as shown in reaction 2. It should be noted that the excited species C₆H₁₄' in reactions 3a and b does not necessarily represent a single excited state. The hot and thermal hydrogen atoms produced in reactions 2 and 3a yield H₂ by hydrogen abstraction from the solvent



The presence of perfluoroalkanes would not be expected to interfere with reaction 4, since, as already mentioned, they are assumed not to be reactive toward hydrogen. It also seems unlikely that the perfluoroalkanes interfere with the precursor of the thermal hydrogen, *i.e.*, C₆H₁₄' in reaction 3a, on the basis of the following. In our previous work on the radiolysis of *n*-hexane containing perfluorocyclobutane, we found that the addition of hexene-1, an efficient hydrogen atom scavenger, and benzene further depresses the yield of hydrogen. We interpreted this as confirming the presence of thermal hydrogen atoms, presumably formed by reaction 3a, and concluded that C₆H₁₄' is

not subject to deexcitation by perfluorocyclobutane. (However, in view of the evidence¹² presented recently on the interaction of photochemically generated excited cyclohexane molecules with cyclohexene and benzene, one cannot exclude the possibility that some of the observed decrease in the hydrogen yield in our system upon addition of the unsaturates may be due to the interaction of C₆H₁₄' with benzene and hexene-1.) Assuming that other perfluoroalkanes also do not deexcite C₆H₁₄', we conclude that the main mode of action of these solutes is to interfere with reaction 2, the neutralization reaction. It should be mentioned here that if reaction 2 yielded molecular hydrogen, which would of course be accompanied by an equivalent amount of the corresponding olefin, the yields of these products would be affected by the presence of the solutes. The fact that the yield of cyclohexene from cyclohexane remained constant when perfluorocyclobutane was added (Table III) supports the assumption that this product is not formed in reaction 2 and that the main source of molecular hydrogen is reaction 3b.

There are two possibilities for the interference with reaction 2, the charge neutralization reaction. One is a charge transfer from the solvent molecular cation to the solute, but this is not plausible because of the high ionization potential of the perfluoroalkanes. The other possibility, electron capture by perfluoroalkanes, would seem to be quite probable.¹

The absence of any effect of CF₄, C₂F₆, and C₃F₈ on the radiolytic hydrogen yield from hexane and on N₂ formation, as compared with the definite effects of the higher molecular weight solutes, fits the pattern observed in gas-phase reactions, between electrons and perfluoroalkanes. The bombardment of CF₄ by low-energy electrons did not yield negative ions,¹³ as indicated by mass spectrometric analysis. In another mass spectrometric study¹⁴ of thermal electron attachment to C₂F₆, C₃F₈, C₄F₁₀, and *n*-C₆F₁₄, it was found that only the last compound yields molecular anions. The absence of the parent ions in these mass spectrometric studies indicates that their lifetime is less than 1 μsec. Young,¹⁵ using a microwave cavity resonance technique, obtained the rate constants 8.8×10^{-12} and 8.8×10^{-8} ml/molecule sec, for the electron attachment to perfluoropropane and perfluoromethylcyclohexane, respectively, further indicating the low affinity of C₃F₈ for thermal electrons.

In the gas phase, electron capture by a molecule results in the formation of a negative ion with internal energy equal to the electron affinity of the compound

(11) P. J. Dyne, *Can. J. Chem.*, **43**, 1080 (1965).

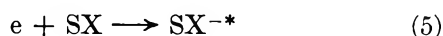
(12) J. Y. Yang, F. M. Servedia, and R. A. Holroyd, *J. Chem. Phys.*, **48**, 1331 (1968).

(13) V. M. Hickman and D. Berg, *ibid.*, **29**, 517 (1958).

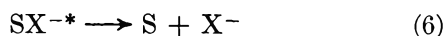
(14) H. L. Greenhaus, Ph.D. Thesis, Rensselaer Polytechnic Institute, Troy, N. Y., 1965.

(15) C. E. Young, Ph.D. Thesis, University of California, Berkeley, Calif., 1966.

formed



where *SX* denotes a solute molecule. The excess energy of the ion may be dissipated by a dissociative process



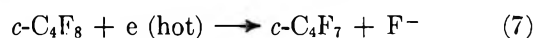
but in the case of perfluoroalkanes this reaction would not seem to be plausible thermodynamically and the ion will more probably lose an electron again unless it is stabilized by collision or emission of radiation. In small molecules such as CF₄, C₂F₆, and C₃F₈ the autoionization is apparently very rapid. The fact that the parent anions of more complex symmetrical perfluorocyclo carbons have been observed in a mass spectrometer may be because it presumably takes a relatively long time before the whole energy of the metastable ion SX^{-*} is concentrated randomly in one electron, leading to its detachment.

Turning now to our results, we observe that the depression of the radiolytic hydrogen yield by perfluoroalkane solutes becomes noticeable in *n*-C₄F₁₀ and increases gradually in *n*-C₅F₁₂ and *n*-C₆F₁₄, being especially pronounced in the case of cyclic perfluoroalkanes. We could interpret these results as implying that the initially formed metastable negative ions of small perfluoroalkane molecules are not collisionally deactivated by the solvent and that they autoionize before charge recombination can take place. In this case the presence of a solute would not be expected to have any effect on the radiolytic decomposition of the solvent. In the case of the larger perfluoroalkane solutes, the "long" lifetime (>10⁻⁸ sec) of the negative ion permits charge neutralization to occur between it and the molecular solvent cation, thus removing the latter and reducing the hydrogen yield of reaction 2. The fact that at a solute concentration of (4–5) × 10⁻² *M* *c*-C₄F₈, C₄F₈-2, *c*-C₇F₁₄, *c*-C₆F₆, and *c*-C₅F₁₂ depress the radiolytic hydrogen yield to the same extent would imply that these solutes all have the same ability to form negative ions which can engage in charge recombination with the solvent cations (however, their respective rate constants for electron attachment are not necessarily identical). As already mentioned, the perfluoroalkanes display similar effectiveness, both in reducing H₂ yield and in affecting the N₂ yield in solutions containing N₂O, as the cyclic saturated solutes, indicating that they operate by a similar mechanism, *i.e.*, by capturing electrons. This view is supported by some very recent mass spectrometric studies¹⁶ on thermal electron attachment to perfluoropropane, where the negative parent ion C₃F₆⁻ has been observed.

The Formation of HF. The formation of HF as a major product in the radiolysis of solutions of the large size perfluoroalkanes starting with C₄F₁₀ and to a

lesser degree in solutions of unsaturated perfluoroalkanes is somewhat puzzling. The fact that the decrease in hydrogen yield is balanced by an almost equal formation of HF would seem superficially to indicate that hydrogen atoms abstract fluorine from the solutes and that only in the case of CF₄, C₂F₆, and C₃F₈ such reactions do not occur. This assumption would imply that the CF bond in the higher homologs and the cyclic compounds is weaker than in CF₄. However, it has been shown⁶ that addition of increasing concentrations of hexene-1, an effective hydrogen atom scavenger, to a 3.7 mol % solution of perfluorocyclobutane in *n*-hexane results in a continuing decrease of hydrogen yield. The decrease in hydrogen reaches a *G* value of 1.4, which corresponds to the entire thermal hydrogen yield in *n*-hexane as reported by other laboratories.¹⁷ This means that the perfluorocyclobutane cannot have reacted with any of the thermal hydrogen atoms. Furthermore, the formation of HF is almost unaffected by the addition of hexene-1 (see Table II), supporting the view that thermal atoms are not involved in the formation of HF. The possibility of hot hydrogen atoms preferentially attacking the solute is hardly plausible, in view of the far greater quantities of solvent present.

The electrons generated initially in reaction 1 can be expected to be formed with several electronvolts of excess energy. Such subexcitation electrons could conceivably lead to the following reactions resulting in the formation of HF



However, in dilute solute solutions the subexcitation electrons would be expected to be moderated to thermal energies before they could interact with solute molecules.

Another argument against a subexcitation electron reaction with the solutes is that such electrons would not be expected to discriminate between the unreactive smaller perfluoroalkanes and the larger reactive ones, especially since it is known that there is little difference in the appearance potential of F⁻ from C₃F₈ (1.7 eV), C₄F₁₀ (1.8 eV), *c*-C₄F₈ (1.8 eV), and C₆F₁₁CF₃ (1.7 eV).¹⁸

As stated in the previous section, dissociative electron capture by solute reaction 7 would not be expected to occur with thermal electrons, as the CF bond strength in perfluoroalkanes considerably exceeds the electron affinity of the fluorine atom.

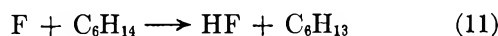
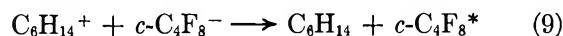
One could consider the possibility of HF formation by the neutralization reaction between the solvent mo-

(16) C. Lifshitz and R. Grajower, private communication.

(17) (a) R. A. Holroyd, *J. Phys. Chem.*, **70**, 1341 (1966); (b) G. Meisner and A. Henglein, *Ber. Bunsenges. Phys. Chem.*, **69**, 264 (1965).

(18) M. M. Bibb and G. Carter, *Trans. Faraday Soc.*, **62**, 2637 (1966).

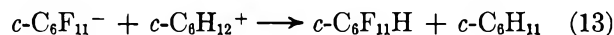
lecular cation and the solute anion, the neutralization energy being localized in the solute molecule



An alternative mechanism for HF formation, which we consider to be more plausible, involves the splitting off of a fluorine atom from the solute anion followed by reaction 11. In the mass spectrometric study of thermal electron attachment to perfluoromethylcyclohexane, the ion $\text{C}_7\text{F}_{13}^-$ was observed in considerable yield along with the parent negative ion.¹⁹ In the liquid phase, scission of a fluorine atom from a molecular negative ion of a perfluoroalkane molecule would be facilitated if the solvent participated in the transition state of the splitting process. The formation of a new HF bond, taking place simultaneously with the fission of the existing CF bond, could provide the extra driving force for such a reaction.

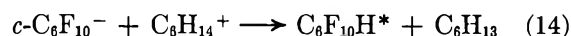
It is noteworthy that Sagert¹⁰ in his study on the radiolysis of solutions of $c\text{-C}_6\text{F}_{12}$ in $c\text{-C}_6\text{H}_{12}$ has observed the formation of $c\text{-C}_6\text{F}_{11}\text{H}$. From Sagert's data one can derive that $G(\text{C}_6\text{F}_{11}\text{H})$ equals approximately 2 at a solute concentration of $5 \times 10^{-2} M$. At a similar concentration of $c\text{-C}_6\text{F}_{12}$ in n -hexane we found that $G(\text{HF}) = 1.7$. This correspondence between the yields of $\text{C}_6\text{F}_{11}\text{H}$ and HF suggests that at least at low solute

concentration the formation of $\text{C}_6\text{F}_{11}\text{H}$ may be due to the reactions



One might thus expect that whenever HF has been found in the systems studied in this work there is a corresponding formation of a liquid solute product in which one fluorine atom is replaced by hydrogen.

The fact that the yield of HF is considerably lower in the presence of unsaturated perfluoroolefins requires some comment. A possibility is that, instead of undergoing the above reactions, the perfluoroolefin anions might extract a proton from the solvent molecular cation



Fluoroolefin carbanions are indeed known to extract protons efficiently from available sources.²⁰ The fluorinated excited radical formed in reaction 14 might still split off an F atom, leading to the eventual formation of HF, but it is more likely that CH bond fission will occur in view of the greater strength of CF bonds. Thus one would expect a lower yield of HF.

(19) L. H. James and G. Carter, *J. Electron. Control*, **13**, 213 (1962). These authors actually assigned a value of 1.2 eV for the appearance potential of $\text{C}_7\text{F}_{14}^-$. In a more recent study this value was found to be close to 0.0 eV (see R. K. Assundi and J. D. Craggs, *Proc. Phys. Soc.*, **83**, 611 (1964)).

(20) R. D. Chambers and R. H. Mobbs, *Advan. Fluorine Chem.*, **4**, 50 (1965).

Secondary Valence Force Catalysis. VIII. Catalysis of Hydrolysis of Methyl Orthobenzoate by Anionic Surfactants¹

by R. Bruce Dunlap and E. H. Cordes²

Contribution No. 1642 from the Department of Chemistry, Indiana University, Bloomington, Indiana 47401
(Received July 25, 1968)

A survey of the effect of 21 anionic surfactants on the kinetics of hydrolysis of methyl orthobenzoate in slightly acidic aqueous solution generates the following generalizations concerning the catalytic efficiencies of these species: (i) catalytic efficiency is decreased as the anionic group is moved away from the terminus of the hydrocarbon-like chain; (ii) catalytic effectiveness decreases as the head group is changed from sulfate to sulfonate to oxyethyl or substituted oxyethyl sulfate; and (iii) although catalytic efficiency varies with the nature of the head groups, surfactants possessing two anionic sites tend to be more effective catalysts than those possessing one. Increasing concentrations of nonionic and zwitterionic surfactants cause modest decreases in the rate of hydrolysis of methyl orthobenzoate. Ethanol, 1-butanol, 1-heptanol, and 1-decanol, in increasing order of effectiveness, are inhibitors of the sodium dodecyl sulfate catalyzed hydrolysis of methyl orthobenzoate. For a series of *para*-substituted methyl orthobenzoates, catalysis of hydrolysis by sodium dodecyl sulfate becomes more important as the electron-donating ability of the polar substituent increases.

Introduction

Previous studies concerning catalysis of hydrolysis of methyl orthobenzoate by anionic surfactants, particularly sodium dodecyl sulfate, have established several features of this process. First, the catalyzed reaction occurs within the micellar phase formed by association of the surfactant molecules.³ This conclusion is required by the observation that the profile of rate constant against surfactant concentration parallels the extent of incorporation of orthoester into the micellar phase³ and by the observation that it is possible to saturate the micellar phase with excess substrate.^{4,5} Second, catalysis of orthoester hydrolysis is most marked for those substrates which are most hydrophobic in character.⁴ Third, the catalyzed reaction is markedly susceptible to inhibition by cations.^{3,6} The implications of these and other observations for the understanding of surfactant-catalyzed orthoester hydrolysis have been discussed in detail.^{3,7} Rather little effort has been expended in terms of understanding those structural features of the surfactant molecules which make them effective as catalysts for methyl orthobenzoate hydrolysis. Herein, we report the results of the survey of some 24 anionic, nonionic, and zwitterionic surfactants as catalysts for this reaction.

Experimental Section

Methyl orthobenzoate was synthesized and purified as previously described.⁸ Methyl ortho-*p*-methoxybenzoate, methyl ortho-*p*-methylbenzoate, and methyl ortho-*p*-chlorobenzoate were synthesized and purified by Mr. Karl Koehler according to the methods of McElvain and Venerable and Kwart and Price.^{8,9} Methyl ortho-*p*-fluorobenzoate was kindly donated by

Professor R. W. Taft. Sodium dodecyl sulfate was the best grade available from Distillation Products Industries and was employed without further purification. Sodium 1-hexadecyl sulfate and sodium dodecyl sulfonate were obtained from Mann Research Laboratories. Dr. F. Puschel of the Institute for Fat Chemistry, Berlin, kindly donated samples of 2-hexadecyl, 3-hexadecyl, and 5-hexadecyl sodium sulfates.¹⁰ Sodium 2-oleoxy-1-methylethyl sulfate,¹¹ sodium 2-hexadecyloxy-1-methylethyl sulfate,¹² sodium 2-hexadecyloxy-1-ethylethyl sulfate,¹² sodium 2-hexadecyloxyethyl sulfate,¹² disodium 2-sulfooctadecyl sulfate,¹³ disodium 2-sulfoethyl- α -sulfo palmitate,¹⁴ disodium 2-sulfoethyl- α -sulfo stearate,¹⁴ disodium 2-sulfo-2-butyltetradecano-

(1) Supported by Grant AM-08232-04 and AM-08232-05 from the National Institutes of Health.

(2) Career Development Awardee of the National Institutes of Health, Grant K3GM10-248-02. Fellow of the Alfred P. Sloan Research Foundation.

(3) R. B. Dunlap and E. H. Cordes, *J. Amer. Chem. Soc.*, **90**, 4395 (1968).

(4) M. T. A. Behme, J. G. Fullington, R. Noel, and E. H. Cordes, *ibid.*, **87**, 266 (1965).

(5) J. G. Fullington and E. H. Cordes, *Proc. Chem. Soc.*, 224 (1964).

(6) L. R. Romsted, R. B. Dunlap, and E. H. Cordes, *J. Phys. Chem.*, **71**, 4581 (1967).

(7) R. B. Dunlap, Ph.D. Thesis, Indiana University, 1968.

(8) S. M. McElvain and J. T. Venerable, *J. Amer. Chem. Soc.*, **72**, 1661 (1950).

(9) H. Kwart and M. B. Price, *ibid.*, **82**, 5123 (1960).

(10) F. Puschel, *Tenside*, **3**, 71 (1966).

(11) J. K. Weil, A. J. Stirton, and E. B. Leardi, *J. Amer. Oil Chemists' Soc.*, **44**, 522 (1967).

(12) J. K. Weil, A. J. Stirton, and M. V. Nunez-Ponzoa, *ibid.*, **43**, 603 (1966).

(13) A. J. Stirton, F. D. Smith, and J. K. Weil, *ibid.*, **42**, 114 (1965).

(14) A. J. Stirton, R. G. Bistline, J. K. Weil, W. C. Ault, and E. W. Maurer, *ibid.*, **39**, 128 (1962).

Table I: The Effect of the Concentration of Several Isomeric Hexadecyl Sulfates on Second-Order Rate Constants for the Hydrolysis of Methyl Orthobenzoate^a

Surfactant	Temp, °C	Concn, M	$10^{-6}k_2$, $M^{-1} \text{ min}^{-1}$
1-Hexadecyl sodium sulfate $\text{CH}_3(\text{CH}_2)_{14}\text{CH}_2\text{OSO}_3^- \text{Na}^+$	45	0.000	0.0298
		0.0001	0.0338
		0.0004	0.293
		0.0008	0.522
		0.0012	0.844
		0.002	1.15
		0.003	1.50
		0.004	1.78
		0.006	2.56
0.008	2.38		
2-Hexadecyl sodium sulfate $\text{CH}_3(\text{CH}_2)_{13}\text{CHCH}_3$ $\text{OSO}_3^- \text{Na}^+$	40	0.000	0.0188
		0.0005	0.086
		0.001	0.21
		0.002	0.54
		0.004	0.89
		0.008	1.20
		0.015	1.49
		0.0225	1.27
		0.030	1.25
0.0375	1.21		
3-Hexadecyl sodium sulfate $\text{CH}_3(\text{CH}_2)_{12}\text{CHCH}_2\text{CH}_3$ $\text{OSO}_3^- \text{Na}^+$	40	0.000	0.020
		0.0005	0.080
		0.001	0.23
		0.002	0.55
		0.004	0.88
		0.008	1.20
		0.015	1.59
		0.0225	1.24
		0.030	0.91
0.0375	1.21		
5-Hexadecyl sodium sulfate $\text{CH}_3(\text{CH}_2)_{10}\text{CHCH}_2\text{CH}_2\text{CH}_2\text{CH}_3$ $\text{OSO}_3^- \text{Na}^+$	40	0.000	0.017
		0.001	0.048
		0.002	0.130
		0.004	0.26
		0.008	0.44
		0.015	0.50
		0.030	0.56
0.045	0.53		

^a All reactions carried out in aqueous solution containing 0.01 M sodium phosphate buffer, pH 6.4, with an initial concentration of methyl orthobenzoate near $5 \times 10^{-6} M$.

ate,¹⁵ disodium 2-sulfo-2-methyloctadecanoate,¹⁵ sodium hexyl- α -sulfolargonate,¹⁶ sodium methyl- α -sulfolalmitate,¹⁷ sodium butyl- α -sulfolalmitate,¹⁷ and sodium methyl- α -sulfofostearate¹⁷ were generous gifts of Dr. A. J. Stirton and Dr. J. K. Weil of Eastern Regional Research Laboratory, Agricultural Research Service, Philadelphia, Pa. Dimethyldodecylphosphine oxide, sodium 2-dodecylbenzenesulfonate, dimethyldodecylammonium propanesulfonate, and dimethyldodecylammonium acetate were kindly provided by the Miami Valley Laboratories of Procter & Gamble, Inc. All other chemicals were of reagent grade and were used without

further purification. Glass-distilled water was employed throughout.

Kinetic measurements were carried out spectrophotometrically with a Zeiss PMQ II spectrophotometer equipped with a heatable cell holder through which water from a thermostated bath was continuously circulated. With surfactants having critical micelle concentrations near or below 0.001 M, such as the hexadecyl sulfate isomers or the oxyethylene sulfates, it was necessary to utilize 5-cm path length cells in order to avoid substrate inhibition of methyl orthobenzoate hydrolysis; the initial methyl orthobenzoate concentration under the preceding conditions was either 5×10^{-6} or $6 \times 10^{-5} M$ (1% ethanol). Hydrolysis of methyl orthobenzoate was followed by observing the appearance of methyl benzoate at 228 or 273 μ , respectively, depending on the nature of the surfactant. With the other surfactants, 1-cm path length cells were used and the initial concentration of methyl orthobenzoate was either 5×10^{-5} or $2 \times 10^{-4} M$ (3% ethanol) depending on whether the formation of methyl benzoate was followed at 228 or 273 μ . Hydrolysis of *p*-Cl-, *p*-H-, *p*-CH₃-, and *p*-OCH₃-substituted methyl orthobenzoates in the presence of sodium dodecyl sulfate was followed by observing the appearance of the substituted methyl benzoate at 242, 228, 241, and 256 μ , respectively. First-order rate constants were obtained from plots of $\text{OD}_\infty - \text{OD}_t$ against time in the usual way; second-order rate constants were obtained by dividing the first-order constants by the activity of the hydrated proton. Values of pH were determined with a Radiometer PHM 4c pH meter utilizing an internal glass electrode for measurements at 25° and a thermostated external glass electrode for those at 40°.

Results and Discussion

Factors considered to be important for the understanding of the catalysis of hydrolysis of methyl orthobenzoate by anionic surfactants have been considered in some detail in a previous publication³ and certain of the important points have been summarized in the Introduction. The hydrolysis of methyl orthobenzoate proceeds with rate-determining cleavage of a carbon-oxygen bond (which may be preceded by or concerted with proton transfer to the orthoester) passing through a transition state with substantial carbonium ion character and yielding the corresponding carbonium ion as an intermediate.¹⁸ The surfactant-dependent reaction is considered to occur at or near the double layer within the hydrodynamic shear surface of

(15) W. C. Ault, T. J. Micich, A. J. Stirton, and R. J. Bistline, *J. Amer. Oil Chemists' Soc.*, **42**, 233 (1965).

(16) A. J. Stirton, R. G. Bistline, J. K. Weil, and W. C. Ault, *ibid.*, **39**, 55 (1962).

(17) A. J. Stirton, R. G. Bistline, E. A. Barr, and M. V. Nunez-Ponzoa, *ibid.*, **42**, 1078 (1965).

(18) E. H. Cordes, *Progr. Phys. Org. Chem.*, **4**, 1 (1967).

Table II: The Effect of the Concentration of Several Substituted Oxyethylene Sulfates on Second-Order Rate Constants for Hydrolysis of Methyl Orthobenzoate^a

Surfactant	Temp, °C	Concn, M	10 ⁻⁶ k ₂ , M ⁻¹ min ⁻¹
Sodium 2-oleyloxy-1-methylethyl sulfate $\text{CH}_3(\text{CH}_2)_7\text{CH}=\text{CH}(\text{CH}_2)_7\text{CH}_2\text{OCH}_2\text{CHOSO}_3^-\text{Na}^+$ <div style="margin-left: 150px;"> $\begin{array}{c} \\ \text{CH}_3 \end{array}$ </div>	40	0.000	0.018
		0.0001	0.027
		0.0004	0.037
		0.0008	0.12
		0.0012	0.17
		0.002	0.21
		0.003	0.27
		0.004	0.27
		0.006	0.36
Sodium hexadecyloxyethyl sulfate $\text{CH}_3(\text{CH}_2)_{14}\text{CH}_2\text{OCH}_2\text{CH}_2\text{OSO}_3^-\text{Na}^+$	40	0.000	0.018
		0.0001	0.025
		0.0004	0.053
		0.0008	0.13
		0.0012	0.18
		0.002	0.23
		0.003	0.32
		0.004	0.35
		0.006	0.44
Sodium 2-hexadecyloxy-1-methylethyl sulfate $\text{CH}_3(\text{CH}_2)_{14}\text{CH}_2\text{OCH}_2\text{CHOSO}_3^-\text{Na}^+$ <div style="margin-left: 150px;"> $\begin{array}{c} \\ \text{CH}_3 \end{array}$ </div>	40	0.000	0.015
		0.0001	0.018
		0.0004	0.031
		0.0008	0.093
		0.0012	0.11
		0.003	0.21
		0.004	0.25
		0.006	0.33
		0.008	0.36
Sodium 2-hexadecyloxy-1-ethylethyl sulfate $\text{CH}_3(\text{CH}_2)_{14}\text{CH}_2\text{OCH}_2\text{CHOSO}_3^-\text{Na}^+$ <div style="margin-left: 150px;"> $\begin{array}{c} \\ \text{CH}_2\text{CH}_3 \end{array}$ </div>	40	0.000	0.02
		0.0004	0.060
		0.0008	0.088
		0.0012	0.12
		0.002	0.20
		0.003	0.26
		0.004	0.33
		0.006	0.35
0.008	0.41		

^a All reactions carried out in aqueous solution containing 0.01 M sodium phosphate buffer, pH 6.4, and an initial concentration of methyl orthobenzoate near 5×10^{-6} M.

the micellar structures. Thus the principal factor responsible for catalysis of orthoester hydrolysis by anionic surfactants is probably the electrostatic stabilization of the developing carbonium ion in the transition state.

In Tables I-V are collected second-order rate constants for the hydrolysis of methyl orthobenzoate in slightly acidic aqueous solutions as a function of the concentration of (i) hexadecyl sodium sulfate isomers, (ii) substituted oxyethylene sulfates, (iii) surfactant dianions, (iv) α -sulfo-surfactant esters, and (v) substituted dodecyl anions. In the case of each surfactant, catalysis is observed and begins near the critical micelle

concentration (cmc) of the particular compound. The results obtained with the 1-hexadecyl, 2-hexadecyl, 3-hexadecyl, and 5-hexadecyl sodium sulfates, presented in Table I, demonstrate that the efficiency of these catalysts decreases as the anionic head group becomes further removed from the end of the hexadecyl chain; this relationship is manifest in the decreasing order of the maximum rate increase, 86, 74, 79, and 33, with the 1-, 2-, 3-, and 5-hexadecyl sodium sulfates, respectively. Actually, the maximum rate increases observed are not quite directly comparable, since the kinetics with the first of these surfactants was, for reasons of solubility, studied at 45° while that for the others was studied at

Table III: The Effect of the Concentration of Several Surfactant Dianions on Second-Order Rate Constants for Hydrolysis of Methyl Orthobenzoate

Surfactant	Temp, °C	Concn, M	$10^{-6}k_2$, $M^{-1} \text{ min}^{-1}$
Disodium 2-sulfooctadecyl sulfate ^a $\text{CH}_3(\text{CH}_2)_{15}\text{CHCH}_2\text{OSO}_3^- \text{Na}^+$ $\begin{array}{c} \\ \text{SO}_3^- \text{Na}^+ \end{array}$	25	0.000	0.0044
		0.001	0.0051
		0.004	0.091
		0.008	0.46
		0.015	0.61
		0.030	0.50
		0.045	0.42
		0.075	0.28
Disodium 2-sulfoethyl- α -sulfo palmitate ^b $\begin{array}{c} \text{O} \\ \\ \text{CH}_3(\text{CH}_2)_{12}\text{CH}_2\text{CHCOCH}_2\text{CH}_2\text{SO}_3^- \text{Na}^+ \\ \\ \text{SO}_3^- \text{Na}^+ \end{array}$	25	0.000	0.0049
		0.005	0.012
		0.010	0.063
		0.015	0.094
		0.030	0.12
		0.045	0.11
		0.060	0.094
		0.075	0.086
Disodium 2-sulfoethyl- α -sulfo stearate ^b $\begin{array}{c} \text{O} \\ \\ \text{CH}_3(\text{CH}_2)_{14}\text{CH}_2\text{CHCOCH}_2\text{CH}_2\text{SO}_3^- \text{Na}^+ \\ \\ \text{SO}_3^- \text{Na}^+ \end{array}$	25	0.000	0.005
		0.001	0.070
		0.005	0.11
		0.010	0.16
		0.015	0.18
		0.030	0.15
		0.045	0.13
		0.075	0.11
Disodium 2-sulfo-2-butyltetradecanoate ^c $\begin{array}{c} \text{CH}_2\text{CH}_2\text{CH}_2\text{CH}_3 \\ \\ \text{CH}_3(\text{CH}_2)_{10}\text{CH}_2\text{CCOO}^- \text{Na}^+ \\ \\ \text{SO}_3^- \text{Na}^+ \end{array}$	40	0.000	0.018
		0.0025	0.040
		0.005	0.11
		0.015	0.54
		0.020	0.65
		0.040	1.2
Disodium 2-sulfo-2-methyloctadecanoate ^c $\begin{array}{c} \text{CH}_3 \quad \text{O} \\ \quad // \\ \text{CH}_3(\text{CH}_2)_{14}\text{CH}_2\text{C}-\text{CO}^- \text{Na}^+ \\ \\ \text{SO}_3^- \text{Na}^+ \end{array}$	40	0.000	0.019
		0.0008	0.066
		0.0016	0.17
		0.0032	0.37
		0.0048	0.62
		0.0064	0.79

^a Carried out in 0.01 M acetate buffer, 80% base, at an initial concentration of methyl orthobenzoate near 5×10^{-5} M. ^b Carried out in 3% aqueous ethanol containing 0.01 M acetate buffer, 80% base, at an initial concentration of methyl orthobenzoate near 2×10^{-4} M. ^c Carried out in 0.01 M sodium phosphate buffer, pH 6.4, at an initial concentration of methyl orthobenzoate near 6×10^{-5} M. Solutions contained 1% ethanol.

40°. Previous work has established that maximal rate increases for catalysis of methyl orthobenzoate hydrolysis by alkyl sulfates decrease with increasing temperature.³ Maximal rate increases for these reactions have been shown to increase with increasing alkyl chain length of the surfactant.³ In this regard, it is interesting to note that the catalytic efficiencies of the

isomeric hexadecyl sulfates can be approximately accounted for in terms of the length of the longest alkyl chain emanating from the sulfate group. Thus the maximal rate increase for the 3 isomer, 79-fold, is similar to that observed for the tetradecyl sulfate, 81-fold,³ at the same temperature. Similarly, the maximal rate increase for the 5 isomer, 33-fold, is similar to that

observed for the dodecyl sulfate, 41-fold,³ at this temperature.

With substituted oxyethylene compounds (Table II) the rate increases are near 20-fold for each surfactant studied in comparison with the 86-fold rate increase found with 1-hexadecyl sodium sulfate; substitution of the oxyethylene moiety with a methyl or ethyl group does not change the effect of the catalyst significantly. The observed rate increases are probably not quite the maximal ones, since the rate constants continue to increase slightly with increasing surfactant concentration. However, the limitations of availability of these surfactants preclude measurements in more concentrated solutions. At any event, it seems quite unlikely that any of these compounds would prove as effective as 1-hexadecyl sulfate as catalyst for this reaction.

The effects of several surfactant dianions on rate constants for methyl orthobenzoate hydrolysis are given in Table III and Figure 1. Disodium 2-sulfooctadecyl sulfate is the most effective catalyst (maximal rate increase, 139-fold) yet encountered for methyl orthobenzoate hydrolysis. Comparison of these data with those for the surfactant esters, disodium 2-sulfoethyl- α -sulfoalmitate and disodium 2-sulfoethyl- α -sulfoleostearate, is complicated, since higher orthoester concentrations were employed with the latter two surfactants and since the reactions involving the latter surfactants were carried out in the presence of about 3% ethanol (see below). Previous work has established that if the orthoester concentration employed is too high, inhibition of the reaction can occur.⁵ Thus, even though inhibition by substrate and ethanol is involved, the preceding surfactants, containing two sulfonate groups per molecule, gave maximum rate increases of 24- and 36-fold, respectively. Disodium 2-sulfo-2-butyltetradecanoate and disodium 2-sulfo-2-methyloctadecanoate, surfactants which contain sulfonate and carboxylate groups in close proximity, yielded rate increases of 60- and 40-fold, respectively. These are certainly not the maximal rate increases that might have been observed at 25°, since their solubility properties required their study at 40° and, even at this temperature, we were not able to employ concentrations high enough to achieve maximal rates. Thus disodium 2-sulfo-2-methyloctadecanoate causes a 40-fold rate increase at 40° and at a concentration of only 0.0064 *M*; were one able to examine this surfactant under optimal conditions, it might well prove to be the most effective of those studied.

In Table IV, data for several α -sulfo-surfactant esters illustrate that the effects of increasing the ester chain length from methyl to *n*-butyl results in a decrease in the catalytic efficiency of the surfactant. On the other hand, lengthening the hydrophobic portion of the surfactant results in larger rate increases. Studies on the acid hydrolysis of these and similar surfactants parallel the trends cited above.^{12,13,16,17,19}

Table IV: The Effect of the Concentration of Several α -Sulfo-Surfactant Esters on Second-Order Rate Constants for Hydrolysis of Methyl Orthobenzoate^a

Surfactant	Temp., °C	Concn., <i>M</i>	10 ⁻⁶ <i>k</i> ₂ , <i>M</i> ⁻¹ min ⁻¹
Sodium hexyl- α -sulfoelargionate $\begin{array}{c} \text{O} \\ \\ \text{CH}_3(\text{CH}_2)_6\text{CHCOCH}_2(\text{CH}_2)_4\text{CH}_3 \\ \\ \text{SO}_3^-\text{Na}^+ \end{array}$	40	0.000	0.019
		0.005	0.018
		0.010	0.036
		0.015	0.048
		0.030	0.083
		0.050	0.077
Sodium methyl- α -sulfoalmitate $\begin{array}{c} \text{O} \\ \\ \text{CH}_3(\text{CH}_2)_{13}\text{CHCOCH}_3 \\ \\ \text{SO}_3^-\text{Na}^+ \end{array}$	40	0.000	0.016
		0.00025	0.020
		0.001	0.043
		0.0025	0.091
		0.005	0.152
		0.010	0.23
Sodium propyl- α -sulfoalmitate $\begin{array}{c} \text{O} \\ \\ \text{CH}_3(\text{CH}_2)_{13}\text{CHCOCH}_2\text{CH}_2\text{CH}_3 \\ \\ \text{SO}_3^-\text{Na}^+ \end{array}$	40	0.000	0.020
		0.00025	0.024
		0.001	0.039
		0.0025	0.073
		0.005	0.12
		0.010	0.19
Sodium butyl- α -sulfoalmitate $\begin{array}{c} \text{O} \\ \\ \text{CH}_3(\text{CH}_2)_{13}\text{CHCOCH}_2\text{CH}_2\text{CH}_2\text{CH}_3 \\ \\ \text{SO}_3^-\text{Na}^+ \end{array}$	40	0.000	0.021
		0.00025	0.026
		0.001	0.040
		0.0025	0.067
		0.005	0.11
		0.010	0.17
Sodium methyl- α -sulfoleostearate $\begin{array}{c} \text{O} \\ \\ \text{CH}_3(\text{CH}_2)_{13}\text{CHCOCH}_3 \\ \\ \text{SO}_3^-\text{Na}^+ \end{array}$	40	0.000	0.021
		0.00025	0.030
		0.001	0.071
		0.0025	0.13
		0.005	0.22
		0.010	0.29

^a All reactions studied in aqueous solutions containing 1% ethanol and 0.01 *M* sodium phosphate buffer, pH 6.4, and a initial concentration of methyl orthobenzoate of 3×10^{-5} *M*.

The results collected in Table V for three sodium dodecyl anions indicate maximum increases in rate constants for methyl orthobenzoate hydrolysis of approximately 41-, 52-, and 23-fold for sodium dodecyl sulfate, sodium 2-dodecylbenzenesulfonate, and sodium dodecyl sulfonate, respectively. Comparison of the data for sodium 2-dodecylbenzenesulfonate catalyzed reactions in 0.01 *M* acetate buffer, 80% base at an initial concentration of methyl orthobenzoate near 2×10^{-4} *M* (3% ethanol) with those run in 0.01 *M*

(19) A. J. Stirton, *J. Amer. Oil Chemists' Soc.*, **39**, 490 (1962).

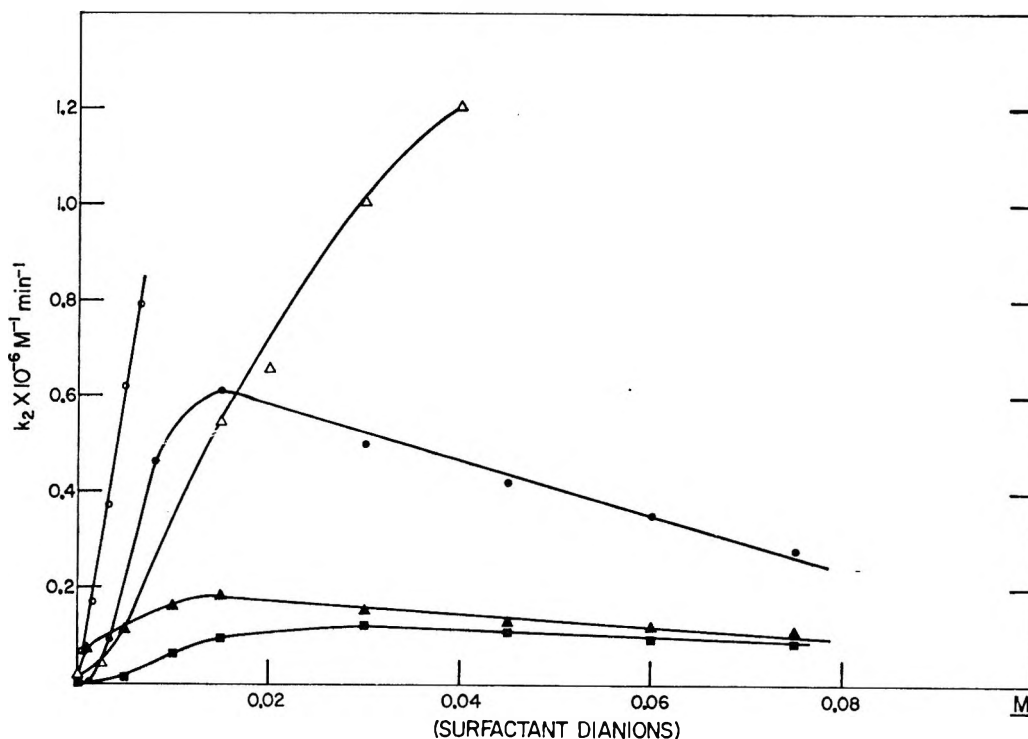


Figure 1. Second-order rate constants for hydrolysis of methyl orthobenzoate in aqueous solution plotted against the concentration of disodium 2-sulfo-2-methyloctadecanoate (O), disodium 2-sulfo-2-butyltetradecanoate (Δ), disodium 2-sulfooctadecyl sulfate (\bullet), disodium 2-sulfoethyl- α -sulfostearate (\blacktriangle), and disodium 2-sulfoethyl- α -sulfopalmitate (\blacksquare). See Table III for details.

sodium phosphate buffer, pH 6.4, at an initial concentration of methyl orthobenzoate near $6 \times 10^{-5} M$ (1% ethanol) reveal much smaller rate increases for the former experiments which are probably the combined result of substrate and ethanol (see below) inhibition of the surfactant-catalyzed reaction.^{4,6}


As revealed by the data of Tables I–V, rate constants for methyl orthobenzoate hydrolysis decrease somewhat at concentrations of anionic surfactants above those at which maximal catalysis is obtained. Similar behavior has been previously observed for this reaction in the case of sodium dodecyl sulfate and is the consequence of inhibition by the counterions of the surfactants.^{3,6}

The variation of second-order rate constants for methyl orthobenzoate hydrolysis with increasing concentrations of the nonionic surfactant, dimethyldodecylphosphine oxide, and of the two zwitterionic surfactants, dimethyldodecylammonium propanesulfonate and dimethyldodecylammonium acetate, indicates modest inhibition of the reaction by each of the surfactants (Table VI). These results are consistent with the notion that the fraction of substrate bound by these surfactants and, thus, protected from hydrolysis increases with increasing concentration of the micellar species. That the rate of hydrolysis of methyl orthobenzoate is less in a nonionic micellar phase than in

water is not unexpected, since (i) the electrostatic stabilization which accounts for catalysis with the anionic surfactants is absent and (ii) decreasing medium polarity is known to retard the rate of orthoester hydrolysis.¹⁸ Therefore, the inhibition is probably a medium effect arising from stabilization of the ground state, the orthoester in the micellar phase and the hydrated proton in the bulk phase, relative to the transition state, the developing carbonium ion in the micellar phase compared with the same reaction occurring in water. It is likely that similar considerations apply to the reactions in the presence of the zwitterionic surfactants. Cationic surfactants are also known to inhibit the hydrolysis of methyl orthobenzoate,⁴ and, although extensive quantitative information is not available, the inhibition seems to be somewhat greater than in the cases of nonionic and zwitterionic surfactants.

In Table VII second-order rate constants for the hydrolysis of methyl orthobenzoate in the presence of 0.01 M sodium dodecyl sulfate solutions at 25° are collected as a function of the concentration of ethanol, 1-butanol, 1-heptanol, 1-decanol, and dimethyldodecylphosphine oxide. As is apparent from this table and Figure 2, the extent of inhibition of the surfactant-catalyzed reaction becomes greater as the concentration of alcohol is increased. Further, the effectiveness of the alcohol at any given concentration as an inhibitor

Table V: Effect of Concentration of Sodium Dodecyl Anions on Second-Order Rate Constant for Hydrolysis of Methyl Orthobenzoate

Surfactant	Temp, °C	Concn, M	$10^{-4}k_2$, $M^{-1} \text{ min}^{-1}$
Sodium dodecyl sulfate ^a $\text{CH}_3(\text{CH}_2)_{10}\text{CH}_2\text{OSO}_3^-\text{Na}^+$	40	0.001	0.0182
		0.004	0.0202
		0.008	0.0270
		0.012	0.552
		0.018	0.700
		0.024	0.774
		0.036	0.668
		0.048	0.668
		0.060	0.602
		0.072	0.583
		0.084	0.534
		0.096	0.496
Sodium 2-dodecylbenzene-sulfonate ^b $\text{CH}_3(\text{CH}_2)_{10}\text{CHCH}_3$  SO_3^-Na^+	40	0.000	0.018
		0.001	0.141
		0.0025	0.342
		0.005	0.590
		0.010	0.856
		0.015	0.928
		0.025	0.864
		0.040	0.909
Sodium 2-dodecylbenzene-sulfonate ^c	40	0.000	0.015
		0.001	0.066
		0.002	0.136
		0.004	0.215
		0.008	0.344
		0.012	0.423
		0.018	0.404
		0.024	0.406
		0.036	0.372
		Sodium dodecyl sulfonate ^a $\text{CH}_3(\text{CH}_2)_{10}\text{CH}_2\text{SO}_3^-\text{Na}^+$	39.1
0.005	0.0188		
0.010	0.0372		
0.015	0.201		
0.030	0.335		
0.045	0.397		
0.060	0.392		
0.075	0.354		

^a Carried out in 0.01 M acetate buffer, 80% base, at an initial concentration of methyl orthobenzoate near 5×10^{-5} M.

^b Carried out in 1% aqueous ethanol containing 0.01 M sodium phosphate buffer, pH 6.4, at an initial concentration of methyl orthobenzoate near 6×10^{-5} M. ^c Carried out in 3% aqueous ethanol containing 0.01 M acetate buffer, 80% base, at an initial concentration of methyl orthobenzoate near 2×10^{-4} M.

increases with increasing length of the carbon chain of the alcohol molecule. As an example, 1-decanol at a concentration of 7.9×10^{-5} M inhibits the reaction about twofold. The inhibition of the sodium dodecyl sulfate dependent hydrolysis of methyl orthobenzoate by these nonionic additives may be the consequence of one or all of the following factors: (i) increase in the cmc of the anionic surfactant²⁰ (particularly in the

Table VI: The Effect of the Concentration of Selected Nonionic and Zwitterionic Surfactants on Second-Order Rate Constants for Hydrolysis of Methyl Orthobenzoate at 25^oa

Surfactant	Concn, M	$10^{-4}k_2$, $M^{-1} \text{ min}^{-1}$
Dimethyldodecylphosphine oxide $\text{CH}_3(\text{CH}_2)_{10}\text{CH}_2\text{P}(\text{CH}_3)_2\text{O}$	0.000	0.0048
	0.0005	0.0049
	0.002	0.0046
	0.006	0.0042
	0.01	0.0038
	0.02	0.0031
Dimethyldodecylammonium propane-sulfonate $\text{CH}_3(\text{CH}_2)_{10}\text{CH}_2\text{N}(\text{CH}_3)_2\text{CH}_2\text{CH}_2\text{CH}_2\text{SO}_3^-$	0.000	0.0050
	0.0005	0.0049
Dimethyldodecylammonium acetate $\text{CH}_3(\text{CH}_2)_{10}\text{CH}_2\text{N}(\text{CH}_3)_2\text{CH}_2\text{COO}^-$	0.000	0.0048
	0.0005	0.0048
	0.002	0.0048
	0.006	0.0044
	0.01	0.0040
	0.02	0.0033
	0.04	0.0025

^a All reactions carried out in solutions containing 0.02 M acetate buffer, 50% base, and an initial concentration of methyl orthobenzoate near 5×10^{-5} M.

case of ethanol and 1-butanol inhibition) thus lowering the concentration of micelles in the solution and hence the fraction of the orthoester in the micellar phase,²¹ (ii) displacement of methyl orthobenzoate from the micellar phase by the additives, or (iii) lessening of the electrostatic stabilization of the transition state. There exists no basis for distinguishing between these factors or for assigning relative weights to them at this time. Our results do contrast with those for acid-catalyzed hydrolysis of micellated sodium dodecyl sulfate.^{21,22} The modest rate increases for this reaction observed upon the addition of long-chain alcohols or nonionic surfactants have been interpreted in terms of increasing effective charge resulting from a lowered dielectric constant at the micellar surface²² or in terms of increasing charge density resulting from increased surfactant ionization.²¹ Regardless of the correct explanation, it

(20) M. F. Emerson and A. Holtzer, *J. Phys. Chem.*, **71**, 3320 (1967).

(21) B. W. Barry and E. Shotton, *J. Pharm. Pharmacol.*, **19**, 785 (1967).

(22) V. A. Motsavage and H. B. Kostenbauder, *J. Colloid Sci.*, **18**, 603 (1963).

Table VII: Effect of Several Additives on the Second-Order Rate Constants for the Sodium Dodecyl Sulfate Catalyzed Hydrolysis of Methyl Orthobenzoate at 25^o,^b

Additive	Concn, M	10 ⁻⁴ k ₂ , M ⁻¹ min ⁻¹
Ethanol	0.001	2.05
	0.005	1.96
	0.010	2.01
	0.015	2.00
	0.030	2.00
	0.060	1.93
	0.090	1.76
	0.12	1.76
	0.18	1.69
	0.24	1.51
1-Butanol	0.001	1.87
	0.005	1.85
	0.010	2.01
	0.015	1.62
	0.030	1.58
	0.060	1.38
	0.090	1.07
	0.12	0.88
	0.18	0.64
	0.24	0.46
1-Heptanol	0.0002	1.77
	0.0004	1.77
	0.0008	1.77
	0.0012	1.68
	0.0016	1.65
	0.002	1.63
	0.003	1.51
	0.004	1.34
	0.006	1.24
1-Decanol	2 × 10 ⁻⁸	1.84
	4 × 10 ⁻⁸	1.88
	6 × 10 ⁻⁸	1.83
	1 × 10 ⁻⁶	1.76
	2 × 10 ⁻⁶	1.70
	3 × 10 ⁻⁶	1.49
	4 × 10 ⁻⁶	1.43
	6 × 10 ⁻⁶	1.31
7.9 × 10 ⁻⁶	1.07	
Dimethyldodecylphosphine oxide	0.000	1.87
	0.0005	1.47
	0.002	1.02
	0.006	0.46
	0.010	0.30
	0.020	0.12
	0.030	0.084
	0.035	0.057

^a All reactions carried out in 0.01 M sodium dodecyl sulfate, 0.02 M acetate buffer, 50% base, and an initial concentration of methyl orthobenzoate near 5 × 10⁻⁵ M.

is clear that the influence of nonionic additives on sodium dodecyl sulfate hydrolysis and on sodium dodecyl sulfate dependent methyl orthobenzoate hydrolysis are distinct.

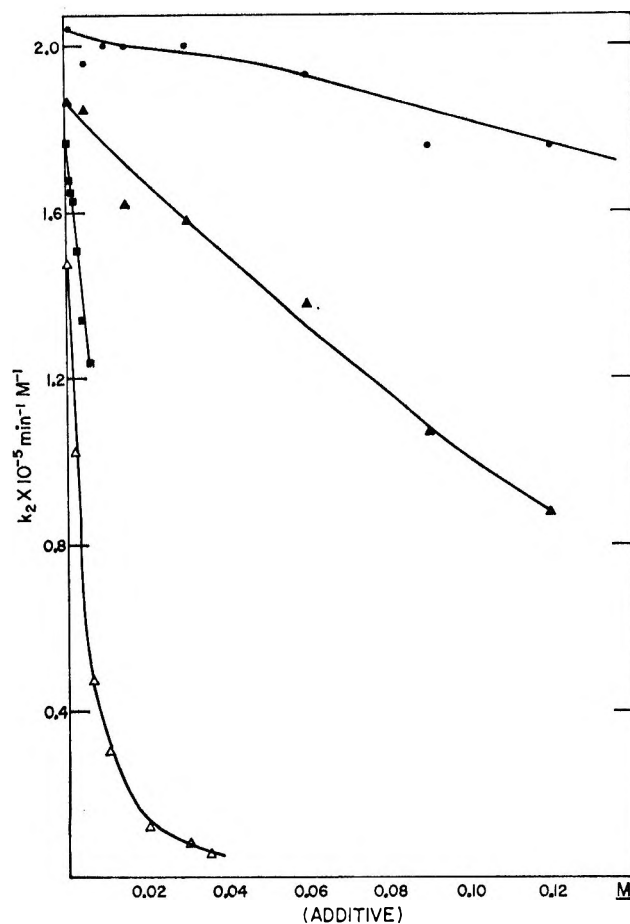


Figure 2. Second-order rate constants for the hydrolysis of methyl orthobenzoate in aqueous solution of 0.01 M sodium dodecyl sulfate at 25° plotted against the concentration of ethanol (●), 1-butanol (▲), 1-heptanol (■), and dimethyldodecylphosphine oxide (Δ). See Table VII for details.

In Table VIII, second-order rate constants for hydrolysis of a series of five *para*-substituted methyl orthobenzoates are collected as a function of the concentration of sodium dodecyl sulfate. In each case, catalysis of hydrolysis by the anionic surfactant is observed and in each case the catalysis is maximal near 0.03 M surfactant. There exists a significant trend toward increased catalysis as the electron-donating power of the polar substituent is increased and reaches a maximum of 115-fold with the *p*-methoxy derivative. Looked at in a slightly different way, this result requires that the Hammett ρ value for hydrolysis of methyl orthobenzoates in the presence of 0.03 M sodium dodecyl sulfate be greater than that for this reaction in water. Rate constants for methyl orthobenzoate hydrolysis in both solvent systems are well correlated by the ordinary σ substituent constants.⁹ Least-squares analysis of the data of Table VIII yields values of σ for the reactions in water and in the presence of 0.03 M sur-

Table VIII: The Effect of Concentration of Sodium Dodecyl Sulfate on Second-Order Rate Constants for Hydrolysis of a Series of *para*-Substituted Methyl Orthobenzoates^{a, b}

<i>p</i> -Substituted methyl orthobenzoates	[Sodium dodecyl sulfate], <i>M</i>	$10^{-6}k_2$, $M^{-1} \text{ min}^{-1}$
<i>p</i> -Cl	0.000	0.0014
	0.008	0.0951
	0.012	0.113
	0.020	0.102
	0.030	0.107
	0.040	0.088
	0.050	0.076
	0.070	0.066
	0.090	0.060
<i>p</i> -F	0.000	0.00317
	0.004	0.00339
	0.008	0.0861
	0.012	0.143
	0.020	0.165
	0.030	0.175
	0.040	0.174
	0.050	0.156
	0.070	0.146
0.090	0.142	
<i>p</i> -H	0.000	0.0045
	0.004	0.0050
	0.008	0.128
	0.012	0.250
	0.018	0.318
	0.024	0.351
	0.036	0.345
	0.048	0.357
	0.060	0.348
	0.072	0.314
	0.084	0.311
0.096	0.274	
<i>p</i> -CH ₃	0.000	0.0089
	0.004	0.0098
	0.008	0.486
	0.012	0.770
	0.020	0.856
	0.030	0.850
	0.040	0.779
	0.050	0.762
	0.070	0.660
0.090	0.595	
<i>p</i> -OCH ₃	0.000	0.011
	0.004	0.012
	0.008	0.610
	0.012	1.00
	0.020	1.20
	0.030	1.26
	0.040	1.20
	0.050	1.14
	0.070	0.970
0.090	0.850	

^a All *para*-substituted methyl orthobenzoates were studied in reaction mixtures at 25° containing 0.01 *M* acetate buffer, 80% base, and an initial concentration of orthoester, 5×10^{-5} *M*.

^b Methyl ortho-*p*-chlorobenzoate and methyl ortho-*p*-fluorobenzoate reaction mixtures contained 0.3% ethanol.

factant of -2.0 and -2.5 , respectively.²³ Thus the transition state for hydrolysis of substituted methyl orthobenzoates is reached somewhat later along the reaction coordinate for the reaction in the micellar phase compared with that in the aqueous phase. This is not a trivial observation. The considerations of Hammond,²⁴ Leffler,²⁵ and Swain and Thornton²⁶ suggest that stabilization of the transition state for methyl orthobenzoate hydrolysis by an electron-donating polar substituent should cause it to be reached *earlier* along the reaction coordinate (note that no evidence for such an effect, which would manifest itself in a nonlinear Hammett plot, has been obtained for this reaction presumably reflecting that this change is too small to be detected with the limits of accuracy of our measurements). Why, then, does stabilization of the transition state for this reaction by electron donation through space from the charged surface of the micelle cause it to be reached *later* along the reaction coordinate? Perhaps both points are best understood in terms of the following simple argument. Considering first the case of electron donation from a polar substituent, we note that the stabilizing effect is exerted directly on the developing carbonium ion and not on the entire transition state structure (which includes the leaving alcohol as well). Thus the degree of stabilization of the transition state by the polar substituent will increase with increasing carbon-oxygen bond cleavage, *i.e.*, with increasing motion along the reaction coordinate. The effect of increasing stabilization as a product state is reached is to move the maximum of the free energy curve (*i.e.*, the structure of the transition state) toward the reactant state. This accords with the considerations noted above. In contrast to this situation, electron donation from the micellar surface will be felt by the transition state as a whole, including the leaving alcohol which bears some positive charge. From a purely electrostatic point of view, one expects the stabilization to be greatest for the protonated (or partially protonated) orthoester, for which the positive charge is concentrated, and to decrease with increasing movement along the reaction coordinate which is accompanied by charge delocalization. Hence, in this case, stabilization decreases with increasing carbon-oxygen bond cleavage. The effect of decreasing stabilization as the product state is reached is to move the transition state along the reaction coordinate toward the product state. This accords with the observations recorded in this work.

(23) The value of ρ cited for the reaction in water is actually derived from a more extensive collection of data accumulated by Mr. K. Koehler in this laboratory. The single points in water contained in Table VIII are in reasonable agreement with expected values based on Koehler's data.

(24) G. S. Hammond, *J. Amer. Chem. Soc.*, **77**, 334 (1955).

(25) J. E. Leffler, *Science*, **117**, 340 (1953).

(26) C. G. Swain and E. R. Thornton, *J. Amer. Chem. Soc.*, **84**, 817 (1962).

While the details of these arguments have yet to be fully worked out, they do suggest a novel manner of looking at the whole question of the relationship of transition state structure to those variables which affect reactivity including variation in polar substituent, solvent, ionic strength, and the like.

Finally, we wish to note that catalysis of orthoester hydrolysis by anionic surfactants may be rather directly related to catalysis of glycoside hydrolysis by the enzyme, lysozyme. In the first place, it seems quite likely that the basic features of the mechanism of orthoester and glycoside hydrolysis are similar.²⁷ In the second place, recent speculations on the mechanism of action of this enzyme based on detailed X-ray diffraction studies of the enzyme and enzyme-substrate complexes include facilitation of substrate protonation and electrostatic stabilization of a developing carbenium ion as important catalytic functions of the enzyme.²⁸ These are, of course, precisely those functions

served by the anionic surfactants in the catalysis of orthoester hydrolysis.

Acknowledgment. We thank Dr. F. Püschel, Institute für Fettchemie der Deutschen Akademie der Wissenschaften, Berlin-Adlershof, DDR, for his gift of the isomeric hexadecyl sulfates, Dr. A. J. Stirton and Dr. J. K. Weil, Eastern Regional Research Laboratory, Agricultural Research Service, Philadelphia, Pa., for their generous donation of numerous surfactants, and Dr. Ted Logan and Dr. Lawrie Benjamin, Miami Valley Laboratories of Procter & Gamble Co., Cincinnati, Ohio, for their helpful discussions and the gifts of several surfactants. We also express our appreciation to Dr. R. W. Taft for his gift of methyl ortho-*p*-fluorobenzoate.

(27) C. A. Vernon, *Proc. Roy. Soc.*, **B167**, 389 (1967).

(28) C. C. F. Blake, L. N. Johnson, G. A. Mair, A. C. T. North, D. C. Phillips, and V. R. Sarma, *ibid.*, **B167**, 378 (1967).

Electronic Excitation Transfer from Pyrene to Perylene

by a Very Weak Interaction Mechanism^{1a}

by N. Mataga,^{1b} H. Obashi, and T. Okada

Department of Chemistry, Faculty of Engineering Science, Osaka University, Toyonaka, Osaka, Japan
(Received July 26, 1968)

The singlet-singlet electronic excitation transfer from pyrene to perylene in high polymer matrices has been investigated by measuring the fluorescence decay curve of pyrene using the nanosecond-flash light for excitation. The results of measurements in polymethyl methacrylate and polystyrene clearly showed that the excitation transfer occurred by the dipole-dipole coupling of the very weak interaction mechanism, and Förster's formula for the fluorescence decay curve in the case of fixed donors and acceptors was accurately satisfied. Although polystyrene has low-lying π -electronic energy levels compared to polymethyl methacrylate, the possibility of the indirect coupling through the π -electronic states of polystyrene was excluded.

Introduction

A large number of investigations has been performed to elucidate the mechanism of long-range intermolecular electronic excitation transfer.² The investigations by Bowen and Brocklehurst^{3a} as well as Bowen and Livingston^{3b} on the excitation transfer from 1-chloroanthracene to perylene in liquid solvents and in the rigid glass at 77°K indicated the long-range excitation transfer which is approximately independent of the solvent viscosity, in accordance with Förster's theory.^{2,4} Their measurements, however, were neither very accurate nor quantitative.

Melhuish⁵ studied the excitation transfer from 9-

methylanthracene to perylene in liquid solvents of various viscosities and also in polymethyl methacrylate

(1) (a) A preliminary report has been published: N. Mataga, H. Obashi, and T. Okada, *Chem. Phys. Letters*, **1**, 133 (1967). (b) To whom correspondence should be addressed.

(2) Th. Förster: (a) "Fluoreszenz Organischer Verbindungen," Vandenhoeck and Ruprecht, Göttingen, 1951; (b) *Discussions Faraday Soc.*, **27**, 7 (1959); (c) "Comparative Effect of Radiation," M. Burton, J. J. Kirby-Smith, and J. L. Magee, Ed., John Wiley & Sons, New York, N. Y., 1960, p 300; (d) "Modern Quantum Chemistry," O. Sinanoglu, Ed., Part III, Academic Press, New York, N. Y., 1965, p 93.

(3) (a) E. J. Bowen and B. Brocklehurst, *Trans. Faraday Soc.*, **51**, 774 (1955); (b) E. J. Bowen and R. Livingston, *J. Amer. Chem. Soc.*, **76**, 6300 (1954).

(4) Th. Förster, *Ann. Phys.*, **2**, 55 (1948).

(5) W. H. Melhuish, *J. Phys. Chem.*, **67**, 1681 (1963).

(PMMA). He concluded that the rate constant for energy transfer was strongly dependent on solvent viscosity and the rate constant in PMMA was a little smaller than that calculated by Förster's formula for dipole-dipole coupling, whereas its value in liquid solvent extrapolated to zero fluidity agreed with the calculated value.

We have made a detailed investigation on the excitation transfer from pyrene to perylene in fluid solvents by observing the fluorescence decay time of pyrene at various solvent viscosities and temperatures.⁶ The results have been analyzed by the method proposed by Yokota and Tanimoto⁷ to solve approximately the diffusion equation which includes the effect of the excitation transfer depending on the energy donor-acceptor distances. This analysis has shown that the observed rate of the energy transfer agrees exactly with that calculated by using Förster's formula.

In the present report, we shall show further that the excitation transfer in the same system, pyrene-peryene, fixed in high polymer matrices occurs by the dipole-dipole resonance and Förster's mechanism is exactly satisfied. Although Bennett⁸ has already made a similar measurement of the excitation transfer from pyrene to Sevron yellow L (a dye molecule) in cellulose acetate, we are concerned here with the case where both the energy donor and acceptor are aromatic hydrocarbon molecules.

Experimental Section

(a) *Apparatus and Measurements.* Fluorescence spectra were measured by using an Aminco-Bowman spectrophotofluorometer which is calibrated to obtain correct quantum spectra. Absorption spectra were measured by a Cary 15 spectrophotometer. The fluorescence quantum yield of pyrene in high polymer matrix which is necessary to calculate the critical transfer distance (eq 1) was determined by using an ethanol solution of pyrene as a standard.

The fluorescence decay curves were measured by an apparatus similar to the one described elsewhere.⁹ The exciting light pulse and the emission pulse were passed through appropriate filters so as to excite pyrene at 320 m μ , where the molar extinction coefficient ϵ (pyrene) $\approx 30 \times \epsilon$ (peryene), and to take out only the emission of pyrene. The measurements were made at room temperature as well as at 77° K.

(b) *Materials and Preparation of Specimens.* Pyrene was chromatographed on alumina and silica gel using *n*-hexane for elution, in a dark place. Chromatographed pyrene was sublimated under vacuum and zone-refined. Perylene was chromatographed on alumina and silica gel in a dark place using a mixed solvent of *n*-hexane and benzene (6:4 in volume) for elution. After recrystallization from the mixed solvent, it was sublimated under vacuum.

Methyl methacrylate (MMA) was shaken with an aqueous solution of sodium hydroxide (5%) several times, washed with water, dried over sodium sulfate anhydride or magnesium sulfate, and immediately after it was passed through a column of activated silica gel, it was distilled in an atmosphere of nitrogen under reduced pressure. The method of purification of styrene was quite similar to that of MMA.

Solid solutions of pyrene and/or perylene in PMMA were prepared by polymerizing the MMA solutions of pyrene and/or perylene as follows. The MMA solution in a glass tube was deaerated carefully by an ordinary evacuating system with an oil diffusion pump and a rotary pump. The deaerated solution was polymerized at 40° for 24 hr at first. Then the temperature of the system was raised gradually to 80°. It took over 8 hr for this temperature change. After it was polymerized at 80° for 24 hr, the system was cooled gradually. It took over 24 hr until the solution was cooled to room temperature. It was confirmed by means of absorption spectrometry that no decomposition of the solutes occurred during the polymerization.

If the polymerization is not complete, the solid solutions show the strong fluorescence of the pyrene excimer. The excimer fluorescence appears also when the solid solution is cracked in the course of polymerization. We have used clear glassy solutions polymerized completely of which no excimer fluorescence can be observed.

The polystyrene (PST) solution was prepared by the procedure similar to the case of PMMA solution. Namely, the deaerated styrene solution was polymerized at 60° for 24 hr followed by a further 72 hr at 90°. We have prepared both solid solutions polymerized with the addition of azobisisobutyronitrile as an initiator and polymerized without it.

Of course, the polymerization is followed by the volume decrease of the solution. We have determined the extent of the volume change and calibrated the concentrations of the solutes after the polymerization has been completed.

Results and Discussion

In Figure 1, the fluorescence and absorption spectra of pyrene and perylene, respectively, in PMMA at room temperature are indicated. The spectra in PST are quite similar to those in PMMA although the former spectra are a little shifted to red compared to the latter spectra. From these spectra, the integral, $\int_0^\infty f_Q^D(\bar{\nu}) \epsilon^A(\bar{\nu}) d\bar{\nu} / \bar{\nu}^4$, where $f_Q^D(\bar{\nu})$ represents the fluorescence

(6) M. Tomura, E. Ishiguro, and N. Mataga, *J. Phys. Soc. Japan* **22**, 1117 (1967).

(7) M. Yokota and O. Tanimoto, *ibid.*, **22**, 779 (1967).

(8) R. G. Bennett, *J. Chem. Phys.*, **41**, 3037 (1964).

(9) N. Mataga, M. Tomura, and H. Nishimura, *Mol. Phys.*, **9**, 367 (1965).

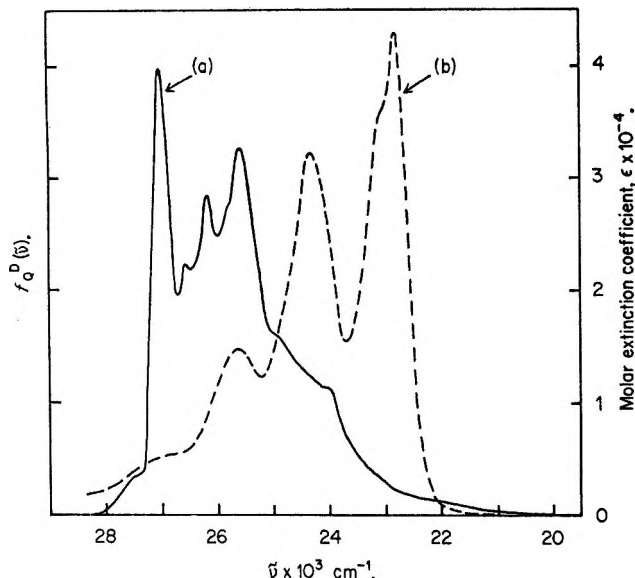


Figure 1. Fluorescence quantum spectrum of pyrene and absorption spectrum of perylene in PMMA at room temperature: (a) pyrene; (b) perylene.

quantum spectrum of pyrene normalized to unity and $\epsilon^A(\bar{\nu})$ is the molar extinction coefficient of perylene, can be evaluated. The observed values for this integral were 3.4×10^{-14} in the case of PMMA solution and 2.7×10^{-14} for the PST solution at room temperature.

According to Förster, the critical transfer distance R_0 in centimeters is given by

$$R_0 = \left[\frac{9000(\ln 10)\kappa^2 Q_F^D}{128\pi^5 n^4 N} \int_0^\infty f_Q^D(\bar{\nu}) \epsilon^A(\bar{\nu}) \frac{d\bar{\nu}}{\bar{\nu}^4} \right]^{1/6} \quad (1)$$

where n is the refractive index of the medium, N is Avogadro's number, κ is the orientation factor for the transition moments of donor and acceptor, respectively, and Q_F^D is the fluorescence quantum yield of the donor. According to our measurements, $Q_F^D \approx 0.70$ in PMMA and $Q_F^D \approx 0.65$ in PST at room temperature. The refractive indices of the solid solvents are given as $n(\text{PMMA}) \approx 1.49$ and $n(\text{PST}) \approx 1.60$. For the completely random distribution of acceptors in the ground state, the mean-square value of κ will take the value $2/3$. By using these values of the parameters, R_0 can be calculated as, $R_0 = 38 \pm 0.8 \text{ \AA}$ in PMMA and $R_0 = 34 \pm 0.7 \text{ \AA}$ in PST at room temperature. According to the measurement by Melhuish,¹⁰ Q_F^D in PMMA is 0.61. If we use this value, $R_0 \approx 37 \text{ \AA}$ in PMMA.

Some typical results of the fluorescence decay curve measurements are shown in Figures 2a, b and 3a, b. The fluorescence decay curves of pyrene in PMMA as well as those in PST are accurately exponential with τ_D (mean decay time of pyrene fluorescence) ≈ 380 nsec at room temperature when perylene is absent in the solution. In the case of PMMA solution, we have made measurements also at 77°K. In this case, $\tau_D \approx 520$

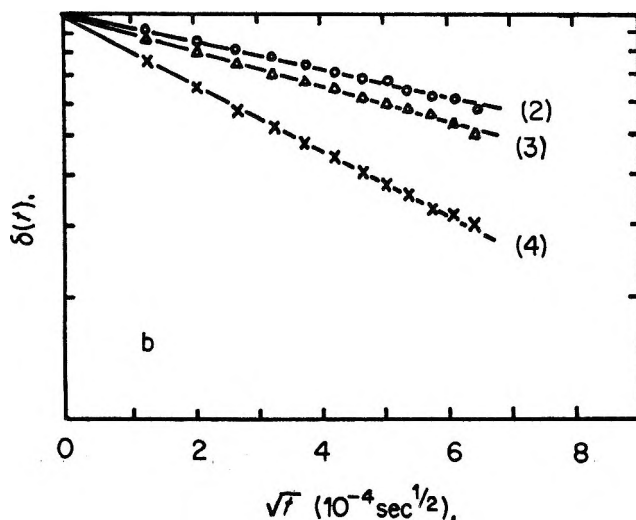
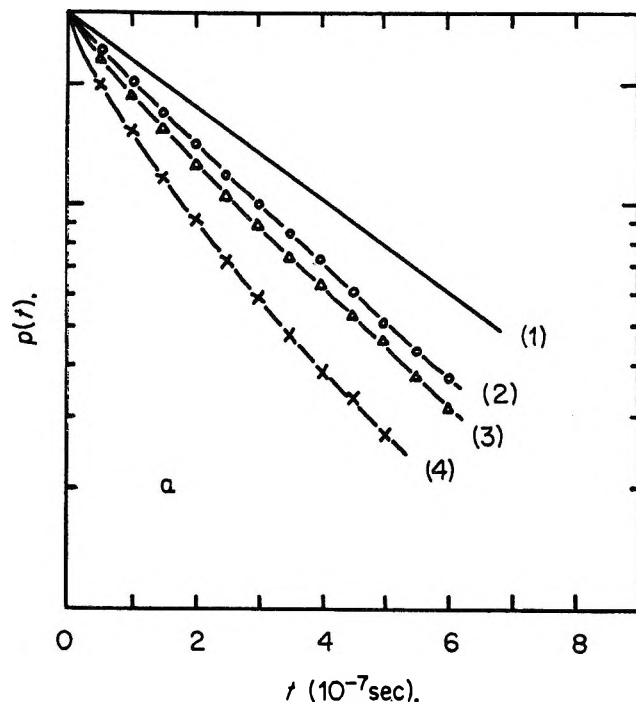


Figure 2. (a) $\log \rho(t)$ vs. t relation in PMMA at room temperature; (b) $\log \delta(t)$ vs. $t^{1/2}$ relation in PMMA at room temperature. Concentrations of donor (C_D) and acceptor (C_A), respectively: (1) pyrene only; (2) 5.5×10^{-3} and $2.3 \times 10^{-3} M$; (3) 8.4×10^{-3} and $3.5 \times 10^{-3} M$; (4) 1.4×10^{-2} and $5.8 \times 10^{-3} M$. No initiator was added in the preparation of specimens.

nsec. This increase of the τ_D value at 77°K seems to indicate a little decrease of the radiationless transitions at 77°K even if the molecule is fixed in the high polymer matrix.

(10) W. H. Melhuish, *J. Opt. Soc. Am.*, **54**, 183 (1964).

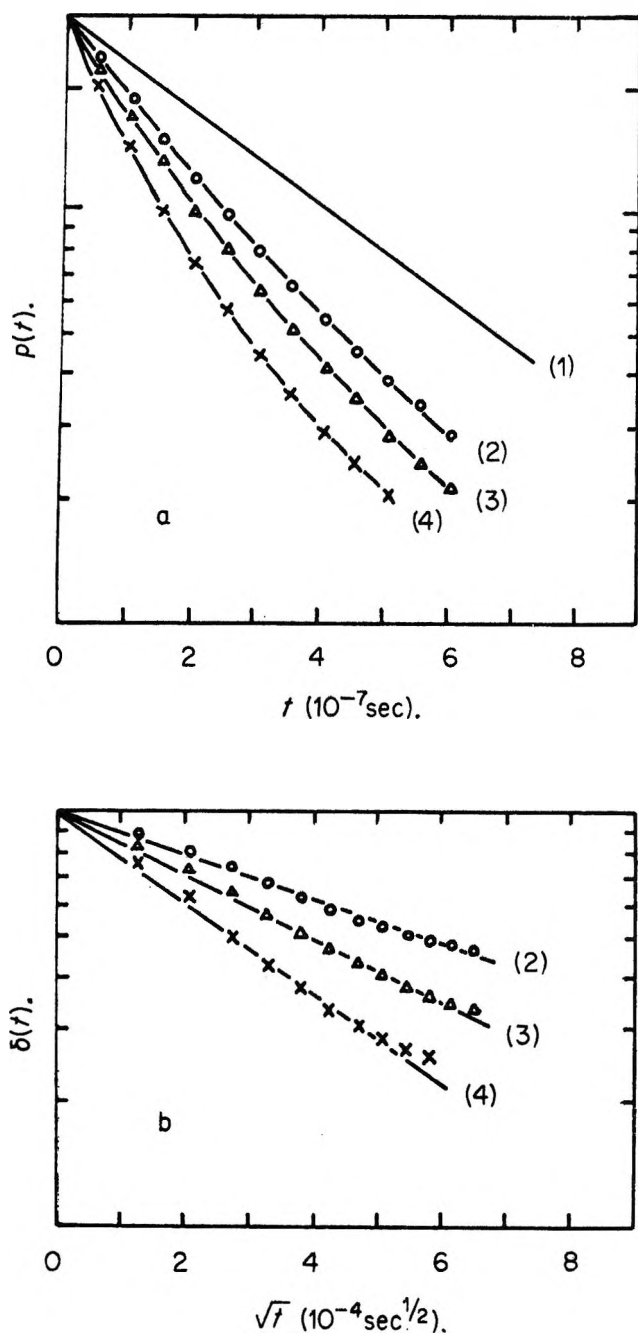


Figure 3. (a) $\log \rho(t)$ vs. t relation in PST at room temperature; (b) $\log \delta(t)$ vs. $t^{1/2}$ relation in PST at room temperature. Concentrations of donor (C_D) and acceptor (C_A), respectively: (1) pyrene only; (2) 7.0×10^{-3} and 2.9×10^{-3} M; (3) 1.04×10^{-2} and 4.4×10^{-3} M; (4) 1.74×10^{-2} and 7.3×10^{-3} M. No initiator was added in the preparation of specimens.

When perylene is present in the solid solutions, the observed fluorescence decay curves of pyrene can be well fitted to eq 2 as is shown in Figures 2 and 3

$$\rho(t) = \exp[-t/\tau_D - 2(C_A/C_0)(t/\tau_D)^{1/2}]$$

$$\delta(t) = \exp[-2(C_A/C_0)(t/\tau_D)^{1/2}] \quad (2)$$

where C_A is the concentration of the acceptors and C_0 is the critical concentration related to R_0 by the equation,

$C_0 = (3/2 \pi^{1/2} N_A' R_0^3)$, where N_A' is the number of acceptor molecules per millimole.

In the present work, the ratio (C_D/C_A), where C_D is the concentration of pyrene, was kept constant and the total concentration was varied. In the case of PMMA solutions, two series of specimens with (C_D/C_A) = 2.38 and (C_D/C_A) = (1/5.88) were examined while (C_D/C_A) = 2.31 and 1.88 in the case of PST solutions. It has been confirmed that τ_D value in the absence of perylene is approximately independent of the C_D value and the fluorescence decay curve of pyrene in the presence of perylene depends only on C_A for all specimens we have examined, in accordance with eq 2.

The R_0 values obtained from the fluorescence decay curves in PMMA at room temperature are given in Table I. Thus, the observed value of the critical transfer distance is given as, $R_0 = 36 \pm 2 \text{ \AA}$. Therefore, the R_0 value calculated by using eq 1 agrees completely with the observed value within the experimental error. The R_0 value observed at 77°K was a little larger than that at room temperature ($R_0 \approx 39 \text{ \AA}$). Although we have used the same C_A value as in the case of the evaluation at room temperature, the C_A value at 77°K may be a little larger than the value at room temperature because of the volume contraction at low temperature. Therefore, the true R_0 value at 77°K will be a little smaller than 39 Å, thus, being rather close to the value obtained at room temperature.

Table I: R_0 Values for PMMA Solid Solutions at Room Temperature

$C_D \times 10^{-3} M$	$C_A \times 10^{-3} M$	$R_0, \text{ \AA}$
0.46	2.7	39
0.68	4.0	37
0.90	5.3	35
1.13	6.7	34
5.5	2.3	35
8.4	3.5	34
14	5.8	35

The observed R_0 values for PST solutions are given in Table II. The observed value, $R_0 = 37 \pm 1 \text{ \AA}$, appears to be somewhat larger than the value calculated by using eq 1. However, it does not seem to be plausible that this small difference between the two R_0 values is very significant. Certainly, the difference may be within the limits of experimental accuracy in view of some uncertainties involved in the experiment. For example, there might be some inhomogeneities in the distribution of donor and acceptor molecules in the PST matrix which may realize preferential orientations of donor and acceptor on the polymer chains to some extent.

Thus, the present results clearly show that the long-range excitation transfer from pyrene to perylene occurs

Table II: R_0 Values for PST Solid Solutions at Room Temperature

$C_D \times 10^{-3} M$	$C_A \times 10^{-3} M$	$R_0, \text{\AA}$
a. Without the Addition of the Initiator		
7.0	2.9	39
10.4	4.4	38
17.4	7.3	36
b. With Addition of the Initiator		
7.1	3.8	38
9.4	5.0	37
11.8	6.2	37

by means of the very weak interaction mechanism and the interaction is due to the dipole-dipole term in the expansion of the interaction hamiltonian into the multipole-multipole interaction terms. Therefore, in the pyrene-perylene system, Förster's mechanism of dipole-dipole coupling is verified accurately both in solid as well as in fluid solutions.

The electronic interaction between the energy donor and acceptor molecules which is responsible for the excitation transfer is not limited to the direct interaction between the donor and the acceptor but also the indi-

rect interactions *via* the virtual excited states of the intervening solvent molecules might be effective for the transfer. Robinson and coworkers¹¹ suggested such a mechanism for the triplet-triplet excitation transfer in solid solution in view of very efficient triplet excitation transfer in the crystal of aromatic hydrocarbons. One may expect similar circumstance also for singlet-singlet excitation transfer in the pyrene-perylene-PST system since the energy difference between the fluorescence levels of PST and pyrene is not very large and there should be some interactions between the π -electron systems of PST and solute molecules in addition to the quite long fluorescence lifetime of pyrene.

The possibility of the transfer by indirect interaction was excluded, however, by the experimental study on the triplet-triplet excitation transfer for several systems in the rigid glass at 77°K.¹² Furthermore, as we have described already, the examination on the pyrene-perylene system in PST does not show any indication of the indirect coupling effect. There is no essential difference between the experimental result in PST matrix and that in PMMA matrix.

(11) H. Sternlicht, G. C. Nieman, and G. W. Robinson, *J. Chem. Phys.*, **38**, 1326 (1963).

(12) S. Siegel and H. Judeikis, *ibid.*, **41**, 648 (1964).

The Vaporization Thermodynamics of Europium Monoxide

by John M. Haschke and Harry A. Eick

Department of Chemistry, Michigan State University, East Lansing, Michigan 48823 (Received July 29, 1968)

Europium monoxide prepared by the reduction of the oxide chloride with lithium hydride has been studied by the target collection Knudsen effusion technique and found to vaporize according to the reaction $4\text{EuO(s)} \rightarrow \text{Eu}_3\text{O}_4\text{(s)} + \text{Eu(g)}$ (1), over the temperature range 1334–1758°K. At 1546°K, $\Delta H^\circ_T = 75.91 \pm 0.94$ kcal/gfw and $\Delta S^\circ_T = 28.66 \pm 0.61$ eu. Heat capacity data for EuO(s) have been estimated, and second- and third-law enthalpies for reaction 1 are presented. For EuO(s), $\Delta H_f^\circ_{298} = -145.2 \pm 4.1$ kcal/gfw, $\Delta G_f^\circ_{298} = -139.0 \pm 4.1$ kcal/gfw, and $S^\circ_{298} = 15.0 \pm 3.0$ eu.

Introduction

The well-characterized lower oxides of europium (EuO and Eu₃O₄) are the only reported lanthanide lower oxides whose existence has not been questioned.¹ Because of its ferromagnetic behavior, europium monoxide has been examined extensively. However, as we have noted previously in a study of Eu₃O₄,² the only thermochemical values reported for europium oxide phases are the enthalpy of formation and high-temperature heat capacity of Eu₂O₃ and the enthalpy of forma-

tion of EuO, all of which were obtained calorimetrically. Westrum³ has also estimated the absolute entropy of these phases.

Along with samarium and ytterbium, divalent europium often behaves chemically like the alkaline earths

(1) G. Brauer, H. Baernighausen, and N. Schultz, *Z. Anorg. Allg. Chem.*, **356**, 46 (1967).

(2) J. M. Haschke and H. A. Eick, *J. Phys. Chem.*, **72**, 4235 (1968).

(3) E. F. Westrum, Jr., *Advances in Chemistry Series*, No. 71, American Chemical Society, Washington, D. C., 1967.

and unlike the other lanthanides. This behavior has been discussed in a report of the vaporization of ytterbium dicarbide,⁴ which like europium, samarium, and the alkaline earths, vaporizes to gaseous metal and graphite. The vaporization behavior of the alkaline earths has been examined,^{5,6} and gaseous oxides are significant vapor species. Although europium monoxide might be expected to vaporize analogously, the presence of a higher oxide, Eu_3O_4 , might alter the vaporization pattern. The present investigation was initiated in an effort to characterize the vaporization mode of the monoxide and establish more firmly its thermodynamics through completion of the thermochemical cycles between Eu_2O_3 , Eu_3O_4 , and EuO .

Experimental Section

Preparative. Europium monoxide was prepared by an adaptation of the method reported by Baernighausen.⁷ Europium oxide chloride, which was prepared by a technique described previously,² was combined in a 1:2 stoichiometric ratio with LiH (Metal Hydrides Inc., Beverly, Mass.). The blended reactants were inserted in an outgassed nickel crucible under argon atmosphere, and were heated subsequently by induction in a water-cooled Vycor vacuum system in which the residual pressure was 10^{-6} to 10^{-7} Torr. The reaction temperature was increased slowly to 900° such that the system pressure never exceeded 10^{-3} Torr. Heating was continued for approximately 5–6 hr, by which time the pressure had decreased to the residual value, an indication that the loss of H_2 , LiCl , and excess LiH was essentially complete. The sample was removed, crushed, and reheated at 1000° for 2 hr to remove completely occluded LiCl . The final product was a reddish brown crystalline phase.

Analytical. The europium oxide phase was analyzed by both chemical and crystallographic techniques. Metal analysis was effected by hydrolysis of weighed specimens and subsequent ignition at 900° to the sesquioxide. X-Ray powder diffraction patterns of the polycrystalline phases and solid vaporization products were obtained with a Hagg-type Guinier camera using $\text{Cu K}\alpha_1$ radiation (λ 1.54051 Å) with a KCl internal standard ($a_0 = 6.29300 \pm 0.00009$ Å).

Vaporization. One europium monoxide sample was subjected to weight-loss vaporization measurements. A weighed specimen was heated for 1-hr increments to constant weight by induction at 1100 – 1200° . Molybdenum effusion cells were used for this and for all subsequent vaporization experiments. The equilibrium vapor species of the monoxide were also analyzed mass spectrometrically with a Bendix Time-of-Flight mass spectrometer, Model 12-107, at 1100 – 1450° with a 20–70-eV ionizing electron beam. The appearance potential for europium was obtained by the linear extrapolation technique using mercury as a reference.

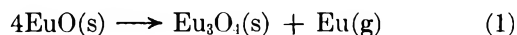
Target collection Knudsen effusion measurements over the temperature range 1060 – 1485° and analysis of the condensed effusate by X-ray fluorescence spectroscopy were performed as described previously.^{2,4}

The effusion cells, constructed with knife-edged orifices, were of two designs. The first was a symmetrical type which consisted of identical sample (internal height = internal diameter) and temperature cavities, while the second, an unsymmetrical design, had only a sample cavity with a blackbody hole (depth $> 10 \times$ radius) drilled perpendicularly into its base. Orifice areas, determined as described previously,² were 8.0×10^{-4} and 42.5×10^{-4} cm^2 for the symmetrical type and 60.5×10^{-4} for the unsymmetrical design. The cells were charged with 0.3–0.4 g of EuO and 0.05–0.10 g of Eu_3O_4 .

Results

Both chemical and crystallographic results confirmed the presence of the monoxide. Metal analysis of the composite sample (formed by the combination of three independent preparations) used in the vaporization experiments, together with standard deviation, indicated 90.38 ± 0.34 wt % Eu (90.47% calcd) or $\text{EuO}_{1.008 \pm 0.004}$. The invariant X-ray powder diffraction patterns, indexable on cubic symmetry, yielded a lattice parameter ($a_0 = 5.1437 \pm 0.0018$) agreeing within standard deviation with previously reported values.^{7,8} X-Ray diffraction patterns of the solid vaporization products indicated the presence of only EuO and Eu_3O_4 during the vaporization measurements which were extended to a bulk solid composition of $\text{EuO}_{1.25}$.

The combination of X-ray powder diffraction, weight loss, and mass spectrometric data indicates vaporization according to the equation



Weight loss measurements indicate 99.1% of theoretical change for reaction 1. Only Eu_3O_4 was present in the final weight loss product. The mass spectrometric results yielded only masses attributable to europium (151 and 153) over the entire temperature range. The observed appearance potential for europium (5.9 eV) is in agreement with the reported value (5.67 eV).⁹ Four independent vaporization experiments were performed with the composite analyzed sample. The linear least-

(4) J. M. Haschke and H. A. Eick, *J. Phys. Chem.*, **72**, 1697 (1968).

(5) R. F. Porter, W. A. Chupka, and M. G. Inghram, *J. Chem. Phys.*, **23**, 1347 (1955).

(6) M. G. Inghram, W. A. Chupka, and R. F. Porter, *ibid.*, **23**, 2-59 (1955).

(7) H. Baernighausen, *J. Prakt. Chem.*, **34** (4), 1 (1966).

(8) H. A. Eick, N. Baenziger, and L. Eyring, *J. Amer. Chem. Soc.*, **78**, 5147 (1956).

(9) R. W. Kiser, "Introduction to Mass Spectrometry and Its Applications," Prentice-Hall, Inc., Englewood Cliffs, N. J., 1965.

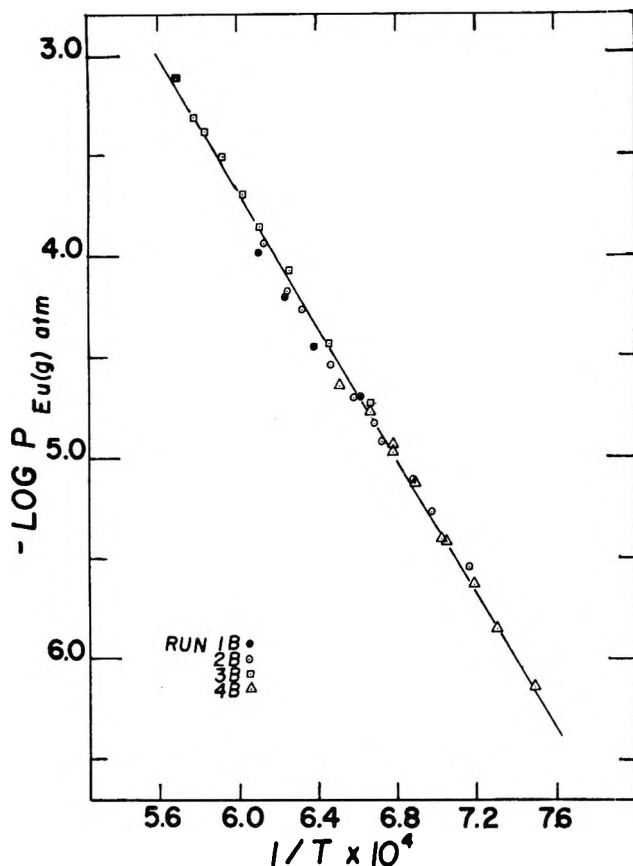


Figure 1. Pressure of gaseous europium in equilibrium with europium monoxide.

squares fit of the 34 $\log P_{\text{Eu}}$ vs. $1/T$ data points presented in Figure 1 is described with standard deviation as

$$2.303R \log P_{\text{Eu(atm)}} = \frac{(-75,910 \pm 940)}{T} + (28.66 \pm 0.61)$$

for $1334 < T < 1758$ °K. From this equation the following thermodynamic data, together with their standard deviations, are calculated for reaction 1: $\Delta H^{\circ}_{1546} = 75.91 \pm 0.94$ kcal/gfw and $\Delta S^{\circ}_{1546} = 28.66 \pm 0.61$ eu. These data have been corrected to 298°K by use of enthalpy and entropy data published for gaseous europium,¹⁰ and estimated for the tetroxide² and the monoxide. The high-temperature heat capacity for the monoxide was approximated as

$$Cp_{\text{EuO}} = 0.5Cp_{\text{Eu}_2\text{O}_3} - 0.5Cp_{\text{oxygen}}$$

The heat capacity equation for B-Eu₂O₃¹¹ and Kopp's approximation for oxygen in solids¹² were employed to give

$$Cp_{\text{EuO}} = 12.54 + (2.08 \times 10^{-3})T$$

$$(H^{\circ}_T - H^{\circ}_{298}) = (12.54)T + (1.04 \times 10^{-3})T^2 - 3830$$

$$(S^{\circ}_T - S^{\circ}_{298}) = 12.54 \ln T + (2.08 \times 10^{-3})T - 72.06$$

The corrected values obtained, with the listed error indicating the composite of the standard deviation and the estimated error in the reduction, are $\Delta H^{\circ}_{298} = 80.3 \pm 2.0$ kcal/gfw and $\Delta S^{\circ}_{298} = 33.9 \pm 1.3$ eu.

The second-law enthalpy for reaction 1 has been combined with the enthalpies of formation of gaseous europium¹⁰ and the tetroxide,² to yield for europium monoxide $\Delta H^{\circ}_{f, 298 \text{ EuO}} = -145.2 \pm 4.1$ kcal/gfw. The error limit in this value reflects a sum of standard deviation and estimated error in data reduction which includes an allowance for a possible 3 kcal error in the Eu₂O₃ data used to obtain the Eu₃O₄ enthalpy. In like manner, the entropy change for reaction 1 has been combined with published data^{2,10} to yield $\Delta S^{\circ}_{f, 298 \text{ EuO}} = -20.7 \pm 3.0$ eu. These values give $\Delta G^{\circ}_{f, 298 \text{ EuO}} = -139.0 \pm 4.1$ kcal/gfw. The absolute entropy of solid EuO calculated from the entropy of europium gas,¹⁰ Eu₃O₄,² and the second-law entropy change is $S^{\circ}_{298 \text{ EuO}} = 15.0 \pm 3.0$ eu.

A third-law enthalpy change has been calculated using free-energy functions published for gaseous europium¹⁰ and approximated for Eu₃O₄² and EuO, using the previously described high-temperature approximations. The value for $S^{\circ}_{298} = 48.6$ eu² was employed in calculating the free-energy functions of Eu₃O₄. Since no independent experimental value for S°_{298} is available for EuO, Westrum's approximated value (16.3 eu)³ was employed. This calculation yielded a value of $\Delta H^{\circ}_{298} = 72.64 \pm 0.59$ kcal/gfw, with a 1.5–2.0 kcal temperature trend evident in the data. However, when free-energy functions based on $S^{\circ}_{298 \text{ EuO}} = 15.0$ eu were employed, a value of $\Delta H^{\circ}_{298} = 80.00 \pm 0.42$ kcal/gfw was obtained with no noticeable temperature trend.

Discussion

As we have noted previously, similarities of the divalent lanthanides and the alkaline earths are numerous. However, an important difference between the two is the existence of trivalent lanthanide ions. The importance of this tripositive state is exemplified in the present investigation. Use of strontium⁵ or barium⁶ monoxide as a model would indicate that the principle mode of vaporization should be to the gaseous monoxide. The stability of the Eu₃O₄ phase, which has gaseous europium as the principal equilibrium vapor species in the Eu₃O₄-Eu₂O₃ two-phase region, forces europium to be the only gaseous product in the EuC-Eu₃O₄ two-phase region.

(10) R. Hultgren, R. L. Orr, P. D. Anderson, and K. K. Kelley, "Supplement to Selected Values of Thermodynamic Properties of Metals and Alloys," private communication, R. Hultgren.

(11) L. B. Pankratz, E. G. King, and K. K. Kelley, U. S. Bureau of Mines Report of Investigations, No. 6033, U. S. Department of the Interior, Mines Bureau, Pittsburgh, Pa., 1962.

(12) G. N. Lewis and M. Randall, revised by K. S. Pitzer and L. Brewer, "Thermodynamics," 2nd ed, McGraw-Hill Book Co., Inc., New York, N. Y., 1961.

Analogies between the EuO and Eu_3O_4 systems other than vaporization mode per se are worthy of comment. As in the vaporization of Eu_3O_4 , no evidence for crucible interaction was detected, nor would any be anticipated. Another interesting observation is the close correspondence between ΔS°_T measured for the two vaporization processes, both of which involve a solid europium oxide as reactant and as product in equilibrium with gaseous europium: $\Delta S^\circ_T = 28.2$ eu for Eu_3O_4 and 28.7 eu for reaction 1. These entropy values should be of equal magnitude, if identical vapor species were involved.

The entropy of europium monoxide and the third-law calculation have presented some interesting points. Westrum³ has estimated the sum of lattice and magnetic contributions to the entropy of EuO to be 16.3 eu, while the second-law result obtained in the present measurements is 15.0 ± 3.0 eu. These values agree within standard deviation, but the 3.0 eu uncertainty arises mainly from a large estimated error in Eu_3O_4 data and may not reflect a true uncertainty. Although the discrepancy does not appear to be great, the coefficients of reaction 1 are such that a 1.3 eu difference in S°_{298} of EuO gives rise to a 8.0 kcal difference in the third-law enthalpy. The observation that the third-law value (72.6 kcal/gfw) obtained by using $S^\circ_{298 \text{ EuO}} = 16.3$ is several kilocalories less than the second-law value (75.9 kcal/gfw) at the median temperature (1546°K), indicates that this estimated entropy value is in error. However, the third-law enthalpy (80.0 kcal/gfw) obtained from the free-energy functions based on $S^\circ_{298} = 15.0$ for EuO agrees within 0.3 kcal with the second-law ΔH°_{298} . The absence of a temperature trend in the latter calculation is reflected in the lower standard deviation. Perhaps Westrum's estimate of 4.2 eu for the magnetic contribution to EuO^3 is too large since the use of this value to approximate the contribution of Eu(II) in Eu_3O_4 results in an S°_{298} which is 0.9 eu larger than the experimental value.

Consistency of the present thermodynamic data with previous measurements and with anticipated trends is evident. The calculated enthalpy of formation (-145.2 kcal/gfw) agrees exactly with the calorimetric value of Burnett and Cunningham.¹³ This value fits well in the correlation of ionic radii of the divalent alkaline earths¹⁴ with their enthalpies of formation¹⁵ pre-

sented in Table I. The entropy of formation (-20.7 eu) is in agreement with the values reported for other MO phases¹⁵: SrO (-24.5 eu), SnO (-23.2 eu), and BaO (-23.8 eu). Similarly, the S°_{298} value for EuO is consistent with that of other monoxide phases, when their mass differences are considered: SrO (13.0 eu), SnO (13.5 eu), EuO (15.0 eu), and PbO (16.1 eu).

The present investigation has essentially completed the thermodynamics of the europium-oxygen system.

Table I: The Correlation of Divalent Metal Radii and Enthalpy of Formation of the Monoxides

MO	M ²⁺ radius, Å	$\Delta H_f^\circ_{298}$, kcal/gfw
CaO	0.99	-151.9
EuO	1.12	-145.2
SrO	1.13	-141.1
BaO	1.35	-133.5

By combining the calorimetrically determined enthalpy of formation for Eu_2O_3 ¹⁶ with our data for Eu_3O_4 and EuO, we have obtained exactly the calorimetric enthalpy of formation reported previously for EuO. The Eu_3O_4 data and the present results should be re-evaluated as better thermochemical values for Eu_2O_3 become available. Data with lower uncertainties would be an obvious result. However, the agreement attained in the cycle suggests that the equilibrium measurements, the estimated heat capacities, and the related thermochemical values for both Eu_3O_4 and EuO are quite accurate.

Acknowledgment. The support of the U. S. Atomic Energy Commission (COO-716-031) and the assistance of Donald W. Werner in mass spectrometric analysis are gratefully acknowledged.

(13) J. L. Burnett and B. B. Cunningham, U. S. Atomic Energy Commission Report, UCRL-11126 (1964).

(14) L. Pauling, "The Nature of the Chemical Bond," 3rd ed, Cornell University Press, Ithaca, N. Y., 1960.

(15) F. D. Rossini, D. D. Wagman, N. H. Evans, S. Levine, and I. Jaffe, National Bureau of Standards Circular 500, U. S. Government Printing Office, Washington, D. C., 1952.

(16) E. J. Huber, G. C. Fitzgibbons, and C. E. Holley, *J. Phys. Chem.*, **68**, 2720 (1964).

Energy Transfer in the Radiolysis of Gaseous Mixtures of

Ethylene and Carbon Monoxide^{1a}

by S. Russo,^{1b} S. Munari, and E. Biagini

Centro Nazionale di Chimica delle Macromolecole, Sez. V, Genoa; Istituto di Chimica Industriale, Università, Genoa, Italy
(Received July 29, 1968)

We have carried out a set of gas chromatographic analyses for the radiolysis products of irradiated ethylene-carbon monoxide mixtures. The dependence of $G_{C_2H_2}$, G_{H_2} , and G_{CO_2} on their respective feed compositions suggests the presence of an energy transfer process from CO to C₂H₄. A kinetic scheme for the formation rates of acetylene and hydrogen, based on the energy transfer, agrees with the experimental results and enables us to determine the behavior of the initiation rate for the copolymerization.

Introduction

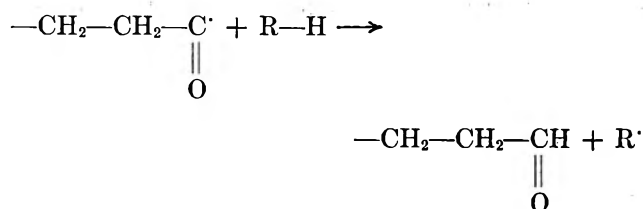
In recent years, two of the present authors have carried out a detailed study on the radiation-induced copolymerization of ethylene and carbon monoxide at room temperature.²⁻⁵

By comparing the copolymerization rate data with the cryoscopic molecular weights of a few polyketones, we found that the ratio R_p/\bar{M}_n (proportional to the number of growing chains) did not change directly with the feed composition.⁵ Unfortunately, due to the total insolubility of copolymers with high $-C-$ content,



we were not able to obtain a complete pattern of the molecular weights but only limited data.

In spite of the paucity of data, we can reasonably suppose that the trend in the number of growing chains corresponds to a similar behavior of the initiation rates. In fact, we can easily exclude the possibility of an appreciable chain transfer effect, proportional to the number of carbonyl groups in the main chain, as such an effect would be likely to occur in accordance with the reaction



with formation of an aldehydic function at the end of the chain. An ir analysis of our copolymer⁶ did not indicate the presence of any aldehydic group.

As the initiation rate does not exhibit a linear dependence on the initial mixture composition, we can suppose, on the assumption that the polymerization initiating species are supplied only by ethylene molecules, that in the radiation-induced copolymerization of

ethylene and carbon monoxide an energy transfer reaction is present.

To test the correctness of this hypothesis, we carried out gas chromatographic analyses of the radiolysis products, which also can be altered by energy transfer processes.

Experimental Section

Research grade ethylene and carbon monoxide, supplied by Phillips and SIO, respectively, were used. Gas chromatographic controls confirmed their high grade of purity. The oxygen content was <5 ppm for ethylene, <10 ppm for carbon monoxide. Aluminum cylinders 250 mm long with an internal diameter of 10 mm (20 ml volume) were used as reaction vessels. Stainless steel was avoided due to the phenomenon of "poisoning." Before every run, the vessels were purged with inert gas and evacuated to 2×10^{-5} Torr. Then, by cooling with liquid nitrogen, the vessels were filled with 5.35×10^{-2} mol of mixture, according to the technique previously described.^{2a} A 500 Ci ⁶⁰Co source was used for the irradiation at room temperature ($D = 3.63 \times 10^{20}$ eV/g; $I = 1386$ rad/min, measured with acetylene dosimeter).

After irradiation, the gases were analyzed with a Varian Aerograph 90 P-3 gas chromatograph, provided with thermal conductivity detector (helium as carrier gas; a column $1/4$ in. o.d., 2 ft long, filled with activated

(1) (a) Work performed under the financial sponsorship of the Consiglio Nazionale delle Ricerche; presented in part at "X Congresso Nazionale della Società Chimica Italiana, sez. XVI, Chimica delle Macromolecole, Padova 1968." (b) Department of Chemical Engineering, State University of Raleigh, Raleigh, N. C.

(2) (a) S. Munari, S. Russo, and C. Rossi, Proceedings, 2nd Tihany Symposium on Radiation Chemistry, Akadémiai Kiadó, Budapest, 1967, p 501 ff; (b) S. Russo and S. Munari, "Atti del Convegno di Chimica delle Radiazioni e dei Radioelementi, Roma," 1967, in press.

(3) S. Russo and S. Munari, *J. Polymer Sci.*, B5, 827 (1967).

(4) S. Munari, S. Russo, and F. Vigo, *ibid.*, B6, 23 (1968).

(5) S. Russo and S. Munari, to be published.

charcoal 30–60 mesh; temperature of 160°; 1 ml gas sampling). Under these conditions there was a good separation of H₂, CO, CH₄, CO₂, C₂H₂, and C₂H₄. Only for hydrogen has it been impossible to obtain a quantitative evaluation, owing to its low concentration and the use of helium as carrier gas.

Therefore, to obtain a better evaluation of the H₂ content, a second series of analyses was carried out, using a 3 ft long, 1/4 in. o.d. column, filled with 30–60 mesh silica gel (room temperature, nitrogen as carrier gas, sampling of 5 ml of gas).

For all the gases, except hydrogen, the correction factors quoted in the literature were used. For hydrogen, as is well known,⁶ the use of a correction factor is often incorrect, and therefore we used a direct calibration, employing mixtures of H₂ and C₂H₄ of known concentrations. The experimental conditions were strictly constant and the same as those used for the analyses of the various irradiated samples.

Results

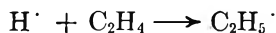
In Figures 1, 2, and 3, the trends of *G* values are reported for acetylene, hydrogen, and carbon monoxide, respectively, as functions of the initial mixture composition. (*The absorbed energy has been evaluated, taking in account the different electronic density of the two components.*) We can observe that all these three most important radiolysis products deviate sharply from the dotted lines, which represent the linear relationship between the corresponding *G*'s and the feed composition, without energy transfer. The nature of these deviations suggests that the energy transfer proceeds mainly from carbon monoxide to ethylene.

We have also carried out radiolysis experiments on ethylene alone, varying the total monomer concentration from 0.120×10^{-3} to 2.675×10^{-3} mol/cm³. No appreciable variation of *G* values for hydrogen and acetylene was found.

In contrast, the radiolysis of pure carbon monoxide showed a significant dependence of *G*_{CO₂} on the CO total concentration in the range from 1.338×10^3 to 2.675×10^{-3} mol/cm³.

Discussion

It is now generally accepted^{7,8} that the radiation-polymerization of ethylene at room temperature starts mainly by addition of a hydrogen atom (primary radiolysis product) to an ethylene molecule



The subsequent steps of propagation consist in additions of ethylene molecules to the radical C₂H₅·.

The energy required for breaking a C–H bond and starting the polymerization has been evaluated as less than 5 eV.^{9,10} The lowest excited energy levels of ethylene are the triplet states at 4.6 and 6.4 eV.¹¹

The energy level diagram of carbon monoxide¹² shows

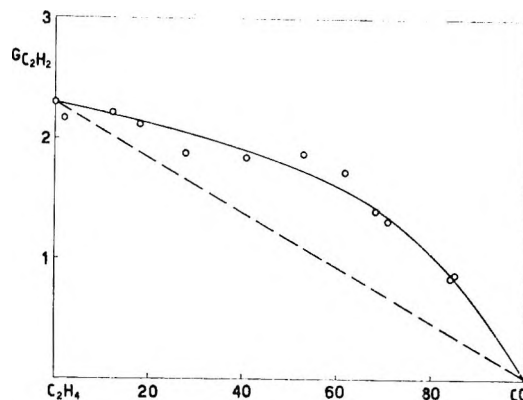


Figure 1. *G* values of acetylene formation in mixtures of carbon monoxide and ethylene.

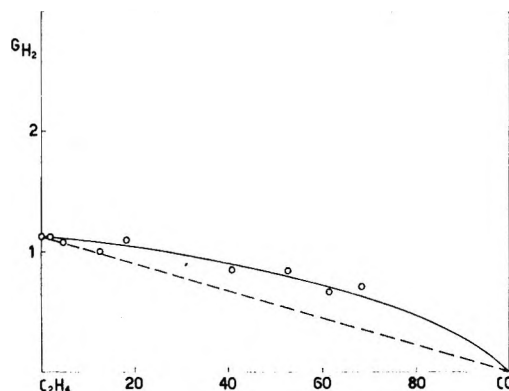


Figure 2. *G* values of hydrogen formation in mixtures of carbon monoxide and ethylene.

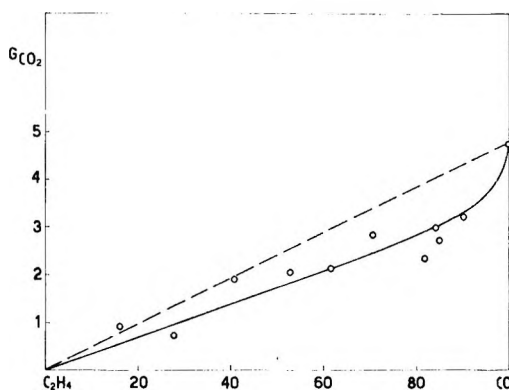


Figure 3. *G* values of carbon dioxide formation in mixtures of carbon monoxide and ethylene.

that the lowest triplet states (at 6.031, 6.928, and 7.721 eV) are situated at energies in excess of the energy

(6) See, for instance, G. Castello, E. Biagini, and S. Munari, *J. Chromatog.*, **20**, 447 (1965).

(7) G. G. Meisels, *J. Amer. Chem. Soc.*, **87**, 950 (1965).

(8) H. Mitsui, S. Machi, M. Hagiwara, and T. Kagiya, *J. Polymer Sci.*, **A1**, **5**, 1073 (1967).

(9) M. Szwarc, *Chem. Rev.*, **47**, 75 (1950).

(10) A. G. Harrison and F. P. Lossing, *J. Amer. Chem. Soc.*, **82**, 519 (1960).

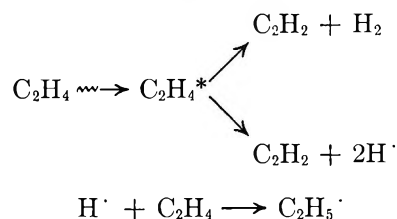
(11) R. S. Mulliken, *J. Chem. Phys.*, **33**, 1596 (1960).

(12) S. Dondes, P. Hartek, and H. Von Weyssenhoff, *Z. Naturforsch.*, **19a**, 13 (1964).

value of the C-H bond in ethylene. These considerations make reasonable the direction of energy transfer we have found to occur.

It is well known⁸ that the gaseous products of room temperature high-pressure ethylene radiolysis are hydrogen and acetylene, with some small amounts of methane and propane (the former probably produced from ethylene through ionic mechanisms^{7,13,14}).

The formation process of H_2 ^{15,16} and C_2H_2 ^{14,16,17} is also a measure of the initiation stage of C_2H_4 radiopolymerization,⁸ so that it is possible to represent in a single scheme the reactions

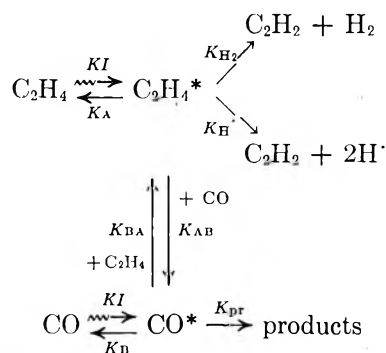


The carbon monoxide radiolysis gives carbon dioxide and a solid polymer. The composition of the latter depends on the reaction temperature and irradiation dose rate.^{12,18-24} At room temperature, the CO radiolysis may be represented by the stoichiometric equation²⁴



The kinetic scheme suggested for the formation of carbon dioxide is rather complex.^{12,24} The G_{CO_2} value depends—as our results also indicated—on the total CO concentration.

The whole reaction scheme for the system C_2H_4 -CO may be represented, on the basis of the general equations reported by Nikitina and Bagdasarian²⁵ for a binary system with energy transfer, in the following way



Let us assume that the energy transfer processes occur more quickly than the other reactions. Then

$$K_{AB}[C_2H_4^*][CO] = K_{BA}[CO^*][C_2H_4]$$

Applying steady-state conditions for the excited species $C_2H_4^*$ and CO^* , the rate of acetylene formation

is given as

$$R_{C_2H_2} = (K_{H_2} + K_H)[C_2H_4^*] = \frac{KI \frac{K_{H_2} + K_H}{K_A + K_{H_2} + K_H} ([C_2H_4] + [CO])}{1 + \frac{(K_B + K_{pr})K_{AB}[CO]}{(K_A + K_{H_2} + K_H)K_{BA}[C_2H_4]}} \quad (1)$$

The ratio $K_{H_2} + K_H / K_A + K_{H_2} + K_H$ represents the probability of acetylene formation from an ethylene molecule in an excited state; $K_{BA} / K_B + K_{pr}$ and $K_{AB} / K_A + K_{H_2} + K_H$ represent, respectively, the probabilities of excitation energy transfer relative to the sum of the probabilities of collisional deactivation and disruption of the excited states. Let us call P_{AB} and P_{BA} these probabilities; then eq 1 becomes

$$R_{C_2H_2} = \frac{K_1 I [C]}{1 + \frac{P_{AB}}{P_{BA}} \frac{1}{x}} \quad (2)$$

where

$$K_1 = K \frac{K_{H_2} + K_H}{K_A + K_{H_2} + K_H}; \quad [C] = [C_2H_4] + [CO]; \quad x = \frac{[C_2H_4]}{[CO]}$$

P_{AB}/P_{BA} represents the relative probability of energy transfer from A to B with respect to transfer from B to A.

Equation 2 may be written as

$$\frac{1}{R_{C_2H_2}} = \frac{1}{K_1 I [C]} + \frac{P_{AB}/P_{BA}}{K_1 I [C]} \frac{1}{x} \quad (3)$$

which is a straight line equation.

Similarly, for hydrogen we have

$$R_{H_2} = \frac{K_2 I [C]}{1 + \frac{P_{AB}}{P_{BA}} \frac{1}{x}} \quad (4)$$

(13) G. G. Meisels and T. J. Sworski, *J. Phys. Chem.*, **69**, 2867 (1965).

(14) G. G. Meisels, *J. Chem. Phys.*, **42**, 2328 (1965).

(15) M. C. Sauer and L. M. Dorfman, *J. Phys. Chem.*, **66**, 322 (1962).

(16) G. G. Meisels and T. J. Sworski, *ibid.*, **69**, 815 (1965).

(17) H. Okabe and J. R. McNesby, *J. Chem. Phys.*, **36**, 601 (1962).

(18) R. E. Woodley, Report HW-31929, Hanford Works, Richland, Wash., 1954.

(19) R. E. Woodley, Report HW-20142, Hanford Works, Richland, Wash., 1955.

(20) P. S. Rudolph and S. C. Lind, *J. Chem. Phys.*, **32**, 1572 (1960).

(21) A. C. Stewart and H. T. Bowlden, *J. Phys. Chem.*, **64**, 212 (1960).

(22) P. S. Rudolph and S. C. Lind, *J. Chem. Phys.*, **33**, 705 (1960).

(23) S. C. Lind, "Radiation Chemistry of Gases," Reinhold Publishing Corp., New York, N. Y., 1961, p 112.

(24) A. R. Anderson, J. V. F. Best, and M. J. Willett, *Trans. Faraday Soc.*, **62**, 595 (1966).

(25) T. S. Nikitina and Kh. S. Bagdasarian, "Sbornik Rabot po Radiatsionnoi Khimii," Academy of Sciences of the USSR, Moscow, 1955, p 183 ff.

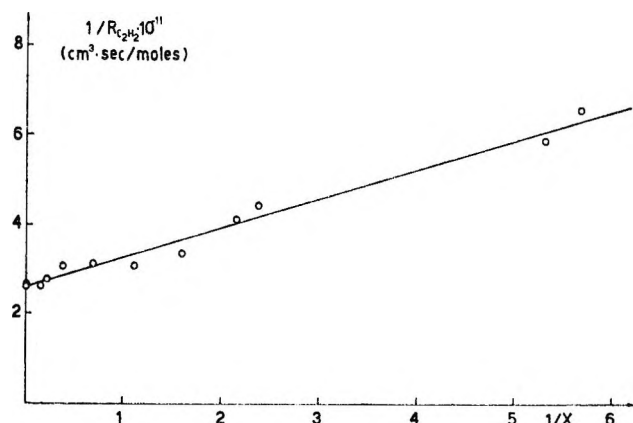


Figure 4. Reciprocal of the rate of acetylene formation as a function of the molar ratio $[\text{CO}]/[\text{C}_2\text{H}_4]$.

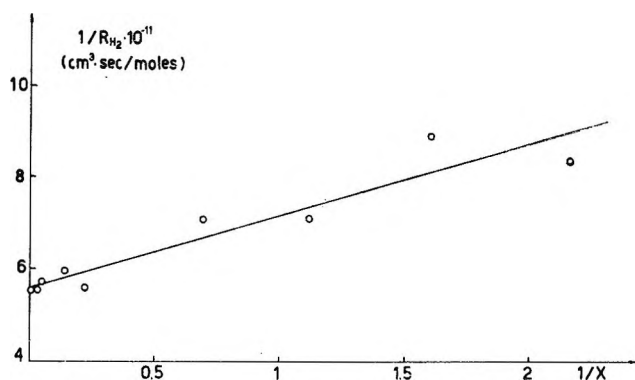


Figure 5. Reciprocal of the rate of hydrogen formation as a function of the molar ratio $[\text{CO}]/[\text{C}_2\text{H}_4]$.

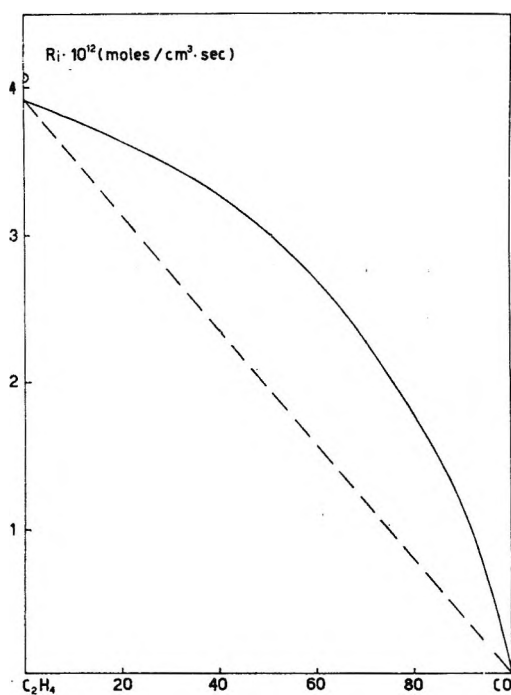


Figure 6. Calculated behavior of the initiation rate for the copolymerization of ethylene and carbon monoxide.

where

$$K_2 = K \frac{K_{H_2}}{K_A + K_{H_2} + K_H}$$

$K_{H_2}/K_A + K_{H_2} + K_H$ represents the probability of formation of hydrogen molecules from an excited ethylene molecule, from which

$$\frac{1}{R_{H_2}} = \frac{1}{K_2 I [C]} + \frac{P_{AB}/P_{BA}}{K_2 I [C]} \frac{1}{x} \quad (5)$$

The initiation rate in the copolymerization may be represented in the following manner

$$R_i = R_{H\cdot} = 2K_{H\cdot} [C_2H_4^*] = \frac{K_3 I [C]}{1 + \frac{P_{AB}}{P_{BA}} \frac{1}{x}} \quad (3)$$

where

$$K_3 = K \frac{2K_{H\cdot}}{K_A + K_{H_2} + K_H}$$

the ratio $2K_{H\cdot}/K_A + K_{H_2} + K_H$ representing the probability of formation of hydrogen atoms, *i.e.*, growing chains, from an excited molecule of ethylene. Thus we obtain

$$\frac{1}{R_i} = \frac{1}{R_{H\cdot}} = \frac{1}{K_3 I [C]} + \frac{P_{AB}/P_{BA}}{K_3 I [C]} \frac{1}{x}$$

and also observe that

$$K_1 = K_2 + K_3/3$$

In Figures 4 and 5 we have reported the behavior of $1/R_{C_2H_2}$ and $1/R_{H_2}$ as functions of $1/x$. We can see that the experimental values obey eq 3 and 4. For acetylene, K_1 is equal to 0.641×10^{-10} (rad^{-1}), P_{BA}/P_{AB} to 3.471. For hydrogen, K_2 is 0.325×10^{-10} (rad^{-1}), and P_{BA}/P_{AB} has the value 3.081.

The fairly good agreement between the two values of P_{BA}/P_{AB} ($\Delta = 12.7\%$; mean value: 3.276), besides demonstrating the correctness of our kinetic scheme, supports the presence of an energy transfer reaction from carbon monoxide to ethylene.

We could not use the results related to the carbon dioxide yields because its production, as we indicate above, occurs following a more complicated scheme, which does not enable us to obtain the value of P_{BA}/P_{AB} .

Furthermore, it is possible to sketch (Figure 6) the behavior of the initiation rate for the radiation-induced copolymerization of ethylene and carbon monoxide, under our experimental conditions, on the basis of the values $P_{BA}/P_{AB} = 3.276$ and $K_3 = 0.632 \times 10^{-10}$ (rad^{-1}).

The R_i value for the ethylene radiopolymerization, obtained from the experimental values of yields and number-average molecular weights (assuming a termination by coupling) is 4.08×10^{-12} mol/cm³ sec, in good agreement with the one calculated from our curve (3.92×10^{-12} mol/cm³ sec).

Acknowledgments. The authors wish to thank Professor C. Rossi for his helpful suggestions.

Lifetime of a Highly Soluble Dense Spherical Particle¹

by Daniel E. Rosner

*AeroChem Research Laboratories, Inc., Subsidiary of Sybron Corporation,
Princeton, New Jersey 08540 (Received August 5, 1968)*

The lifetime of an isolated spherical solute particle in a solvent is expressed in closed form, simultaneously incorporating the major effects of (i) limitations to solute escape by molecular diffusion, (ii) nonzero interfacial velocities for highly soluble solute-solvent systems, and (iii) kinetic limitations to atom (-ion-molecule) detachment at the solute-solvent interface. Illustrative calculations are displayed in compact form and well-known results are recovered in the extremes of sparing solubility, infinite interfacial rate constant, or interface kinetics-controlled dissolution. Assumptions and approximations underlying the general phenomenological expression (and each of its more familiar limiting forms) are reviewed and criteria governing its domain of validity are indicated.

I. Introduction

The classical problem of the lifetime of a dissolving quasi-spherical particle in an isothermal solvent plays a central role in the design of equipment for dissolving powdered materials² and the relevant theory is often applied in research to estimate fundamental transport properties³ (e.g., solute-solvent diffusion coefficients). Not surprisingly, simple approximate relations for the effective particle lifetime are available only in certain limiting cases,⁴ perhaps the best known of which correspond to (i) external solute diffusion control or (ii) rate control due to interface atom (-ion-molecule) detachment kinetics. Especially for small particles,⁵ simultaneous consideration of rate limitations due to both solute escape *via* diffusion and interface kinetics is necessary. However, until now this has been accomplished only for the case of sparingly soluble systems, using a method first exploited by Berthoud and Valetton.⁶ Unfortunately, this "resistance additivity" method breaks down for systems of appreciable solubility because it fails to account for the distortion of solute concentration profiles and radial convection associated with rapid recession of the solid-liquid interface.⁷ In the present paper it is shown that a potentially useful closed-form expression for the particle lifetime can be obtained even for highly soluble systems. We conclude with a brief discussion of the assumptions underlying this general result.

II. Extended Quasi-Stationary Model

In keeping with our objectives, we consider the dissolution of an isolated sphere of pure solute (see Figure 1) subject to the following set of simplifying assumptions.⁸

A1. The interface kinetics are well described by a reversible first-order rate law of the Berthoud form: $v_s = k(\rho/\rho_s)(c_{sat} - c_w)$, where the rate constant⁹ k is nominally the same at all positions on the sphere surface. Here $(c_{sat} - c_w)$ represents the prevailing

undersaturation at the liquid-solid interface, using solute *mass fraction* as the concentration variable.

A2. The physical properties of the solution (density, ρ , effective Fick diffusion coefficient, D , etc.) are replaced by appropriate (constant) mean values and the solute-solution system is considered to be isothermal.

A3. The instantaneous concentration field surrounding the dissolving sphere is approximated by the steady-state concentration field surrounding a (fictitious) spherical solid of the same size, through which solute is being artificially forced at a mass rate equal to the instantaneous rate of dissolution. This is an extended form of the now-familiar quasi-stationary

(1) Supported by the Propulsion Division of the U. S. Air Force Office of Scientific Research under Contract AF 49(638)-1654; originally issued as AeroChem TP-178, July 1968.

(2) See, e.g., the early work of A. W. Hixson and collaborators, *Ind. Eng. Chem.*, **23**, 923, 1002, 1160 (1931); **33**, 478 (1941); for a recent survey, see P. H. Calderbank in "Mixing—Theory and Practice," V. W. Uhl and J. B. Gray, Ed., Vol. II, Academic Press, New York, N. Y., 1967, pp 1-114.

(3) Analogous to the recent bubble dissolution studies of I. M. Krieger, G. W. Mulholland, and C. S. Dickey, *J. Phys. Chem.*, **71**, 1123 (1967).

(4) See, e.g., E. A. Moelwyn-Hughes, "Physical Chemistry," 2nd rev ed, Pergamon Press, Oxford, 1964, and "The Kinetics of Reactions in Solution," 2nd ed, Oxford University Press, London, 1947, p 374 ff. See section V of the present paper for a discussion of the underlying assumptions.

(5) Of course, regardless of *initial* size, at some point in the life span of a dissolving particle it will become small enough so that solute-solvent molecular diffusion does not limit the rate of further dissolution.

(6) A. Berthoud, *J. Chim. Phys.*, **10**, 624 (1912); J. J. P. Valetton, *Z. Krist.*, **59**, 135, 335 (1924); **60**, 1 (1924).

(7) D. E. Rosner, *Int. J. Heat Mass Transfer*, **9**, 1233 (1966).

(8) Discussion of the validity of these assumptions is postponed until section V.

(9) k is here treated as a phenomenological coefficient to be determined from experiment. For *a priori* estimates of k based on microscopic models, see W. K. Burton, N. Cabrera, and F. C. Frank, *Phil. Trans. Roy. Soc. (London)*, **A243**, 299 (1951), and F. C. Frank, "Growth and Perfection of Crystals," John Wiley and Sons, Inc., New York, N. Y., 1958. The present model is readily extended to embrace phenomenological dissolution rate laws which are *non-linear* in the prevailing undersaturation, $(c_{sat} - c_w)$, at the liquid-solid interface [see section V, footnote 23].

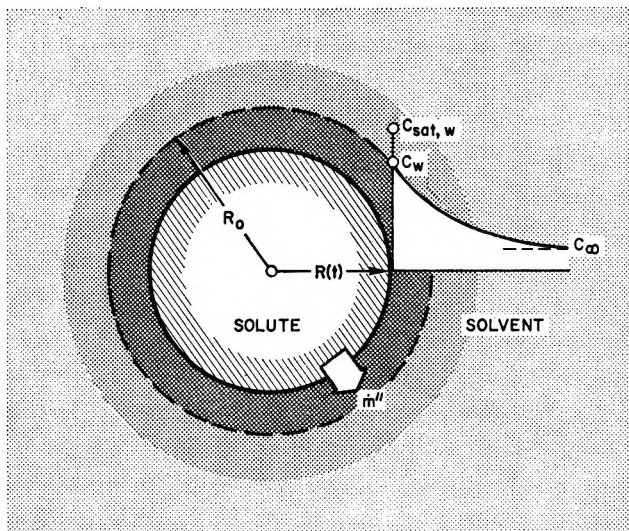


Figure 1. Configuration and notation; dissolution of an isolated spherical particle.

(QS) approximation (the extension being necessary to account for the principal effects of interface motion).

A4. The initial particle radius R_0 is very large compared to the particle radius at which the saturation concentration c_{sat} becomes strongly particle-size dependent.¹⁰ Thus, over most of the particle lifetime, c_{sat} is essentially constant (independent of instantaneous particle size and, therefore, time).

A5. Solute transport by convection due to (i) relative motion between the particle and bulk solvent or (ii) buoyant diffusion boundary layers is neglected. The concentration field surrounding the particle is assumed to be spherically symmetric at all times.

III. Analysis

Let us consider solute mass fluxes in and out of a (locally) flat control volume moving in such a way as to always straddle a unit area of receding solute surface (Figure 2). On the solid solute side of this moving "pillbox" control volume, solute enters at the rate \dot{m}'' . Relative to this control volume, solute escapes on the

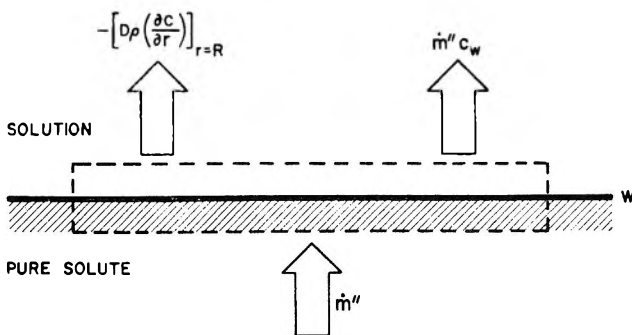


Figure 2. Solute mass balance at moving liquid-solute interface.

liquid side both by "convection" and by molecular diffusion. Thus, in the absence of solute mass accumulation within the control volume, the solute mass balance equation at the liquid-solid interface becomes

$$-D\rho\left(\frac{\partial c}{\partial r}\right)_{r=R} + \dot{m}''c_w = \dot{m}'' \tag{1}$$

where use has been made of Fick's first law for the diffusion contribution. According to the extended quasi-stationary assumption (A3) we introduce¹¹

$$-\frac{D\rho}{1-c_w}\left(\frac{\partial c}{\partial r}\right)_{r=R} = \frac{D\rho}{R} \ln\left[1 + \frac{c_w - c_{\infty}}{1 - c_w}\right] \tag{2}$$

Combining eq 1 and 2 with the first-order interface kinetics expression (A1) provides an implicit equation for the quasi-steady solute concentration c_w established at the surface of instantaneous radius R

$$k(c_{sat} - c_w) = \frac{D}{R} \ln\left[1 + \frac{c_w - c_{\infty}}{1 - c_w}\right] \tag{3}$$

However, the dissolution mass flux \dot{m}'' is related to the rate of particle surface recession by

$$\rho_S \frac{dR}{dt} = -\dot{m}'' \tag{4}$$

so that the radius-time history of the dissolving particle is completely defined by the result of combining eq 1 and 4, viz.

$$-\rho_S \frac{dR}{dt} = \frac{D\rho}{R} \ln\left[1 + \frac{c_w - c_{\infty}}{1 - c_w}\right] \tag{5}$$

together with the $c_w(R)$ relation defined implicitly by eq 3.

To obtain a general, closed-form expression for the time t_{life} it takes a particle to go from initial radius R_0 to final radius $R(t_{life}) = 0$, it is first convenient to introduce the following dimensionless variables and parameters

$$\mathcal{R} \equiv R/R_0 \quad (\text{normalized particle radius}) \tag{6}$$

$$\tau \equiv 2(\rho/\rho_S)(Dt/R_0^2) \ln(1 + B) \tag{7}$$

(dimensionless time)

$$B \equiv \frac{c_{sat} - c_{\infty}}{1 - c_{sat}} \quad (\text{effective solubility parameter}) \tag{8}$$

$$\eta \equiv \frac{c_{sat} - c_w}{c_{sat} - c_{\infty}} \tag{9}$$

(dimensionless interfacial undersaturation)

(10) See, e.g., J. W. Mullen, "Crystallization," Butterworth and Co. Ltd., London, 1961, p 33 ff.

(11) See, e.g., (a) D. B. Spalding, "Some Fundamentals of Combustion," Butterworth and Co. Ltd., London, 1955; (b) D. B. Spalding, "Convective Mass Transfer," McGraw-Hill Book Co., New York, N. Y., 1963; and (c) J. M. Lommel and B. Chalmers, *Trans. AIME*, 215, 499 (1959).

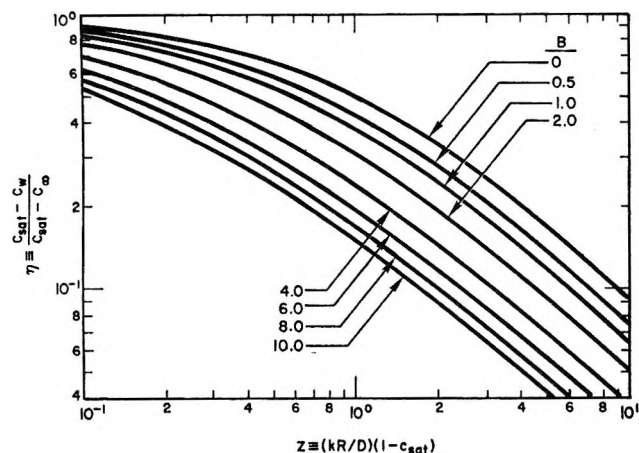


Figure 3. Relation between dimensionless undersaturation at interface and dimensionless first-order rate constant (cf. eq 12) for highly soluble systems.

$$z \equiv [kR(t)/D](1 - c_{sat}) \quad (\text{dimensionless rate constant}) \quad (10)$$

Then eq 5 becomes

$$\frac{d\mathcal{R}^2}{d\tau} = - \left[1 - \frac{\ln(1 + B\eta)}{\ln(1 + B)} \right] \quad (11)$$

and eq 3 becomes an implicit relation for $\eta(z; B)$, viz.

$$z = \frac{1}{B\eta} \ln \left(\frac{1 + B}{1 + B\eta} \right) \quad (12)$$

(see Figure 3). At time $t = 0$, η takes on the value η_0 related to z_0 by eq 12. Since (from their definitions) $z/z_0 = \mathcal{R}$, eq 12 is equivalent to the following $\mathcal{R}(\eta; \eta_0, B)$ relation

$$\mathcal{R} = \frac{\eta_0 \ln \left(\frac{1 + B}{1 + B\eta} \right)}{\eta_0 \ln \left(\frac{1 + B}{1 + B\eta_0} \right)} \quad (13)$$

To obtain the dimensionless particle lifetime τ_{life} from eq 11 and 13, it now proves convenient to eliminate the normalized particle size \mathcal{R} from eq 11 in favor of η (with the help of eq 13) and then integrate between the limits of η_0 and 1 (since eq 12 reveals that $\eta \rightarrow 1$ when $z \rightarrow 0$). The closed-form result

$$\tau_{life} = \frac{\ln(1 + B)}{\ln \left(\frac{1 + B}{1 + B\eta_0} \right)} \left\{ 1 + (B\eta_0)^2 + \frac{B\eta_0^2[(1/\eta_0) - B \ln(1/\eta_0) - 1]}{\ln \left(\frac{1 + B}{1 + B\eta_0} \right)} \right\} \quad (14)$$

is seen to simultaneously embody the effects of finite interfacial kinetics (via $\eta_0(z_0)$, see Figure 3) and exten-

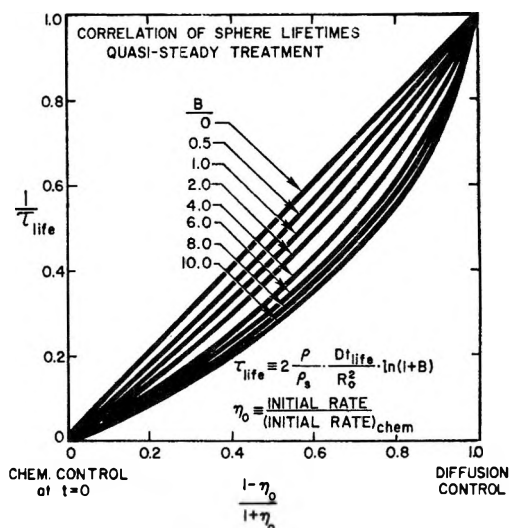


Figure 4. Correlation of dense particle lifetimes for highly soluble systems in region of mixed control (cf. eq 14).

sive solubility (via $B > 0$). Consideration of the special cases of eq 14 (see below) suggests the concise representation shown in Figure 4, in which $1/\tau_{life}$ is shown plotted against $(1 - \eta_0)/(1 + \eta_0)$ with B as a parameter (in the range $0 \leq B \leq 10$). This abscissa has the property of mapping the entire region of mixed control (from initial interface kinetics control to initial diffusion control) onto the interval from zero to unity. Similarly, the reciprocal lifetime $1/\tau_{life}$ also varies between zero and unity.¹² With regard to limiting behavior, it is easy to show that the $1/\tau_{life}$ curves in Figure 4 have the slopes

$$\frac{B}{(1 + B) \ln(1 + B)} \text{ for } \frac{1 - \eta_0}{1 + \eta_0} \rightarrow 0 \quad (15)$$

and

$$\frac{B}{\ln(1 + B)} \text{ for } \frac{1 - \eta_0}{1 + \eta_0} \rightarrow 1 \quad (16)$$

which can be used to express $1/\tau_{life}$ in simple form for particles which (initially) are either near interface kinetics control or near diffusion control, respectively. For arbitrary η_0 but in the limit of sparing solubility,¹³ B is small ($B \ll 1$); hence we may use expansions of the form

$$\ln(1 + B) = B[1 - (B/2) + \dots] \quad (17)$$

to demonstrate that eq 14 exhibits the small B behavior

$$\frac{1}{\tau_{life}} = \frac{1 - \eta_0}{1 + \eta_0} [1 - \eta_0 B + \dots] \quad (18)$$

(12) This immediately implies the useful lower bound $\tau_{life} \geq 1$.

(13) Or for c_∞ near c_{sat} . Note that if particle interaction effects become important for the dissolution of collections of particles, the effects of nonzero B would tend to vanish during the latter stages of the process.

Thus, in the limit $B \rightarrow 0$, the reciprocal lifetime approaches the straight line of unit slope [when plotted against $(1 - \eta_0)/(1 + \eta_0)$] shown in Figure 4.

IV. Discussion

The limiting cases of eq 14, which motivated our choice of variables, are comparatively well known. Thus, if $(kR_0/D)(1 - c_{\text{sat}})$ is so large that the prevailing undersaturation (at the interface) η is small during most of the particle's lifetime, then eq 11 immediately reveals that $-dR^2/d\tau$ will be nearly unity, which leads immediately to the result: $\tau_{\text{life}} \rightarrow 1$. In terms of our original variables¹¹

$$t_{\text{life}} \approx \frac{1}{2} \frac{\rho_s R_0^2}{\rho D \ln(1+B)} \frac{1}{D} \text{ for } \frac{kR_0}{D}(1 - c_{\text{sat}}) \gg 1 \quad (19)$$

indicating a lifetime which increases as the *square* of the initial radius (or the ^{2/3} power of the initial mass). Conversely, if the particle dissolution is initially chemically controlled [*i.e.*, $(kR_0/D)(1 - c_{\text{sat}}) \ll 1$], then chemical control will prevail over the entire particle lifetime. In this extreme, τ_{life} becomes very large but the product $\tau_{\text{life}}(1 - \eta_0)$ remains finite. When η_0 is near unity, eq 12 reveals that $(1 - \eta_0) \approx (1 + B)z_0$. Combining these findings with eq 14, we find $\tau_{\text{life}} \approx (2/z_0)[\ln(1+B)]/B$ or—in terms of our original variables

$$t_{\text{life}} \approx \frac{\rho_s R_0}{k\rho(c_{\text{sat}} - c_\infty)} \text{ for } \frac{kR_0}{D}(1 - c_{\text{sat}}) \ll 1 \quad (20)$$

In this limit the lifetime is seen to increase *linearly* with initial radius (or as the cube root of initial mass). Equation 14, which is valid for *arbitrary* $(kR_0/D)(1 - c_{\text{sat}})$, must therefore be regarded as a rational interpolation formula between eq 19 and 20.

In the limit of sparing solubility $\tau_{\text{life}} \rightarrow (1 + \eta_0)/(1 - \eta_0)$ for mixed control and eq 12 reveals

$$\eta_0 \rightarrow \frac{1}{1 + z_0} \quad (21)$$

Combining these two results and reverting to physical variables leads to the following "series resistance" (or "additive time") form for the particle lifetime

$$t_{\text{life}} = \underbrace{\frac{1}{2} \frac{\rho_s R_0^2}{\rho D} \frac{1 - c_{\text{sat}}}{c_{\text{sat}} - c_\infty}}_{t_{\text{diff}}} + \underbrace{\frac{\rho_s R_0}{k\rho(c_{\text{sat}} - c_\infty)}}_{t_{\text{chem}}} \quad (22)$$

equivalent to that developed by Berthoud,⁶ Frisch and Collins,¹⁴ and others.¹¹ Equation 14 may be regarded as the generalization of this relation to the case of appreciable solubility.

The magnitude of the solubility effect for typical cases can be calculated from the present results, with the help of a compilation of representative values of the parameter B . Interestingly enough, if the ambient

solvent is solute-free (*i.e.*, if $c_\infty = 0$), then eq 8 reveals that B is numerically equal to the solubility of the solute expressed in grams of solute per gram of solvent (*i.e.*, 10^{-2} times the conventionally reported solubility, which is based on 100 g of solvent). Some representative solubilities (based on ref 10 and 15) of solid salts and acids in pure water near 20° are given in Table I.

Table I: Some Values^{10,15} of the Saturation Parameter B for Solid Dissolution in Pure Water^a

Compound	Formula	B
Silver nitrate	AgNO ₃	2.22
Silver bromide	AgBr	0.000000084
Potassium iodide	KI	1.44
Potassium sulfate	K ₂ SO ₄	0.1111
Sodium chloride	NaCl	0.360
Benzoic acid	C ₆ H ₅ COOH	0.0029
Anhydrous ^b calcium sulfate	CaSO ₄	0.0020
Antimony trichloride	SbCl ₃	9.315
Sucrose	C ₁₂ H ₂₂ O ₁₁	2.04
Urea	NH ₂ CONH ₂	1.05
Barium chloride	BaCl ₂	0.357

^a At 20°. ^b The present theory is readily extended to the dissolution of hydrated solutes "S·xH₂O" for which the solute mass fraction is $c_s = M_s/(M_s + 18x)$ where M_s is the molecular weight of the anhydrous solute. One then substitutes $m''c_s$ for m'' in eq 1, $(c_s - c_w)$ for $(1 - c_w)$ in eq 2, 3, and 5, and $(c_s - c_{\text{sat}})$ for $(1 - c_{\text{sat}})$ in eq 8 and 10 and interprets ρ_s as the density of the *hydrated* particle. Since solubility is given in terms of grams of *anhydrous* salt per 100 grams of solvent, B can be obtained directly from the tabulated solubility by multiplication with $(10^{-2}/c_s)$ when $c_\infty = 0$.

At first sight, the effect of extensive solubility on predicted particle lifetimes would appear (in Figure 4) to be greatest for mixed control. However, this is a consequence of the absorption of the parameter B in the ordinate. In fact, the solubility effect is greater for $\eta \rightarrow 0$ [*i.e.*, large $(kR_0/D)(1 - c_{\text{sat}})$], as reference to the limiting forms (eq 19 and 20) suggests. For example, consider the "moderately soluble" case of NaCl(s) dissolution in pure 20° water ($B = 0.36$). Neglect of the solubility effect in this case (all other things being equal) would underestimate t_{life} by some 17% in the diffusion limit, but this error becomes vanishingly small in the limit of interface kinetics control.

V. Validity of the Model

While most of the approximations exploited herein have been discussed elsewhere (in different con-

(14) H. L. Frisch and F. C. Collins, *J. Chem. Phys.*, **20**, 1797 (1952); **21**, 2158 (1953).

(15) "Handbook of Chemistry and Physics," C. D. Hodgman, R. C. Weast, and S. M. Selby, Ed., Chemical Rubber Publishing Co., Cleveland, Ohio.

texts),¹⁶⁻¹⁸ it is prudent to briefly reconsider them to avoid applying the principal result (eq 14) in unreasonable physicochemical situations.

The quasi-stationary approximation obviously breaks down for very short times¹⁹ since it takes time to initially establish a zone of solute-enriched solution around the particle. However, it is intuitively clear that, during this initial transient, an insignificant change in particle radius will occur if solute molecules are packed in the solid much more densely than in the saturated solution (*i.e.*, if $\rho_s \gg \rho_{c_{sat}}$). Indeed this inequality not only guarantees that the initial transient will be short compared to t_{life} , but when $c_{sat} = O(1)$, it also ensures the accuracy of the extended QS approximation at later times.²⁰

Since surface free energy and charge modify c_{sat} for sufficiently small particles¹⁰ (high interface curvature), it is necessary to restrict eq 14 to cases for which $c_{sat} =$ constant during most of the particle's lifetime. Considering only the effect of surface free energy σ (analogous to surface "tension" of a liquid) in the diffusion limit (for sparing solubility), this implies³ $R_0 \gg 4\sigma/(n_s kT)$ —a condition equivalent to the statement that the initial particle radius should be very large compared to the critical radius of a solute "germ" or embryo needed to nucleate a supersaturated solution (usually of the order of 10–100 Å).

In practice, the condition that k be nominally constant over the surface of the particle (imposed in order that the particle remain spherical during the course of the dissolution) implies either that the particle be vitreous or, if crystalline, be comprised of crystallites of size negligible compared to R_0 , with negligible preferential grain boundary attack. Assumption 5 implies that the Reynolds number (based on settling velocity) and the Grashof number (dimensionless bouyancy group) both be small (see, *e.g.*, ref 11a, b for relevant correlation formulas).

If the heat of solution (Q per unit mass of solute) is nonzero, then even an initially isothermal system will develop temperature gradients as the dissolution proceeds (*i.e.*, the particle surface temperature will depart from T_∞ by an amount which allows the heat generated/absorbed at the liquid interface to be conducted away/to the surface through the adjacent solution). However, consideration of this QS energy balance reveals that a *sufficient* condition for the neglect of this thermal effect is

$$\left| Q \left(\frac{D\rho}{\lambda} \right) \left(\frac{dB}{dT} \right) \right| \ll 1 \quad (23)$$

where λ is the thermal conductivity of the solution. This condition is usually adequately satisfied,²¹ *e.g.*, for NaCl(s)–H₂O(l) at $\approx 20^\circ$, the left-hand side of the inequality (23) is about 5×10^{-5} .

Finally, we come to the assumption of constant (mean) properties in nondilute systems (*cf.* A2). While necessary to achieve the simple general results presented, there is no question that breakdown of this assumption (*e.g.*, due to the concentration dependence of density and diffusion coefficient) will limit the accuracy with which eq 14 can be applied in particular cases. These additional complications, which frequently accompany nondiluteness,²² will ultimately necessitate more exact variable property calculations for particular solute–solvent systems. However, eq 14 now provides a readily evaluated reference condition which in many cases should correctly predict the dominant effects of extensive solubility on particle lifetimes under conditions of mixed control.²³

Acknowledgments. It is a pleasure to acknowledge the computational assistance of Mrs. L. Paul and the helpful comments of Drs. M. Epstein, A. R. Cooper, Jr., R. J. Leonard Jr., R. Prober, and S. C. Kurzius.

(16) See, *e.g.*, (a) A. R. Cooper, Jr., *J. Chem. Phys.*, **38**, 284 (1963); (b) A. R. Cooper, Jr., *Trans. Faraday Soc.*, **58**, 2468 (1962); (c) D. W. Readey and A. R. Cooper, Jr., *Chem. Eng. Sci.*, **21**, 917 (1966); (d) K. B. Bischoff, *ibid.*, **18**, 711 (1963).

(17) J. R. Philip, *J. Atmos. Sci.*, **22**, 196 (1965); see also G. Luchak and G. O. Langsroth, *Can. J. Res.*, **A28**, 574 (1950).

(18) F. A. Williams, *J. Chem. Phys.*, **33**, 133 (1960).

(19) The subscript zero appearing in our previous analysis identified symbols *formally* evaluated at zero time *within the quasi-steady approximation*. In diffusion limited systems of sparing solubility, the transient will die out at a time large enough to ensure $(\pi Dt)^{1/2} \gg R_0$. For example, the dissolution rate falls within 10% of the QS value when $(\pi Dt)^{1/2} = 10R_0$ or, in the present notation when $\tau > 64(\rho_{sat}/\rho_s)$. Accordingly, this latter quantity must be small compared with $\tau_{life} \geq 1$. When B is not small, and the system is diffusion limited, a rough estimate of the initial transient period can be made using the one-dimensional transient dissolution analysis of Cooper.^{16b} Generally, one anticipates that the principal effect of this initial transient is equivalent to some shift in the effective starting radius of the particle or a corresponding shift in the time scale. However, a detailed treatment of this transient is beyond the scope of this paper.

(20) When $\rho_s \rightarrow \rho$ concentration profile distortion is due largely to the receding boundary *per se* (not true radial convection relative to an observer fixed in space) and is overestimated by our extended-QS approximation at large values of the saturation parameter B . However, for sufficiently small values of B (say, $B < 2$), boundary recession or equivalent true radial convection produce nearly identical profile distortion. This observation, which is the basis of A3, coupled with the $\beta \rightarrow \eta$ transformation, enables the closed-form solution, eq 14, to be obtained. A3 and eq 14 can be further generalized to more accurately include *arbitrary* solvent/solute density ratios, ρ/ρ_s . Fortunately, a closed form QS result is still possible (which reproduces eq 14 in the limit $\rho/\rho_s \rightarrow 0$) (*cf.* M. Epstein and D. E. Rosner, in preparation).

(21) In part because the effective Fick diffusivity is usually much smaller than the thermal diffusivity of the solution. In aqueous systems this diffusivity ratio is typically of the order of 10^{-2} . By way of contrast, thermal effects in liquid–vapor systems will often prevent direct application of the present results to the closely related problem of droplet evaporation into a background gas.

(22) See, *e.g.*, A. Emanuel and D. R. Olander, *Int. J. Heat Mass Transfer*, **7**, 539 (1964).

(23) If the interface kinetics are well described by a nonlinear power law: $v_B \propto (c_{sat} - c_w)^n$ where $n \neq 1$ (*cf.* *e.g.*, R. F. Strickland-Constable, "Kinetics and Mechanism of Crystallization," Academic Press, London, 1968, p 25) then the present approach leads to an expression of the form $\tau_{life} = fct(\eta_0, B, n)$, involving only a numerical quadrature to determine τ_{life} for any value of the exponent n .

Glossary of Symbols

B	Solubility parameter; eq 8
c	Mass fraction of solute
D	Effective Fick diffusion coefficient
k	Berthoud first-order rate constant
k	Boltzmann constant
(l)	Liquid
\dot{m}''	Mass flux across solid-liquid interface
M	Molecular weight
n	Number density (per unit volume)
Q	Heat of solution (per gram of solute)
R	Particle radius
\mathcal{R}	R/R_0 ; normalized particle radius
r	Radial coordinate
(s)	Solid
t	Time
T	Absolute temperature
v_s	Recession velocity of interface, $= \dot{m}''/\rho_s$
x	Moles of water (of hydration) per mole of solute
z	$(kR/D)(1 - c_{sat})$; dimensionless rate constant; eq 10

Greek Symbols

η	Dimensionless local undersaturation; eq 9
λ	Thermal conductivity of solution; eq 23
ρ	Density
σ	Surface free energy
τ	Dimensionless time; eq 7

Miscellaneous

O()	Order of magnitude symbol
------	---------------------------

Subscripts

chem	Chemically controlled (interface kinetics)
diff	Diffusion controlled
S	Pertaining to solute
life	Life (of dissolving particle)
w	At liquid-solid interface
sat	Saturated
0	Evaluated at $t = 0$
∞	Far from particle surface

Variation of the Lattice Parameter with Aluminum Content in Synthetic Sodium Faujasites. Evidence for Ordering of the Framework Ions

by E. Dempsey, G. H. K uhl, and D. H. Olson

Mobil Research and Development Corporation, Research Department, Central Research Division, Princeton, New Jersey 08540 (Received August 8, 1968)

A plot of crystal lattice parameter against silicon:aluminum ratio for a range of hydrated sodium X- and Y-zeolites shows two distinct breaks at silicon:aluminum ratios near 1.4:1 and 2:1. A similar plot for dehydrated calcium materials published earlier by Breck and Flanigen shows similar breaks. It is suggested that the breaks are related to phase changes occurring in the materials as the silicon-aluminum ordering changes.

Introduction

Although the framework structures of at least 25 zeolites are known, information concerning the ordering of silicon and aluminum ions in the framework has been reported for only a handful of these structures. Such information is vital for the development of any detailed theory of crystallization or reaction mechanisms. At this time, no concrete experimental data have been presented pertaining to the ordering of silicon and aluminum ions in faujasite-type zeolites. During the course of an accurate determination of the variation of the cubic lattice parameter with aluminum content in hydrated sodium faujasites, we noted distinct discontinuities in what was expected to be a continuous linear relationship. The experimental data and their possible implications concerning silicon-aluminum ordering is discussed.

Experimental Section

All of the sodium synthetic faujasites used in this study were of high quality, as judged by their chemical analyses, X-ray scattering power, and sorption capacity for water and cyclohexane. The X-ray measurements were made on a Siemens X-ray diffractometer equipped with a scintillation counter, pulse-height analyzer, and strip-chart recorder. A scan speed of 0.25°/min was used with a 2-cm/min chart speed. Before the measurements were made, the samples were equilibrated for 16 hr in a 75% r.h. constant-humidity cabinet. The cubic lattice parameters, a_0 , were measured using the double scanning diffractometry technique,¹ which minimizes 0 2 θ errors. In most instances, four diffraction peaks in the 50–60° 2 θ (Cu) range were measured and the

(1) H. W. King and L. F. Vassamillet, *Advan. X-Ray Anal.*, **5**, 78 (1962).

resulting values of a_0 were averaged. The precision of the a_0 values is estimated to be ± 0.005 Å. Because extrapolation techniques were not employed, this value represents the relative accuracy of the a_0 values.

Results

The lattice parameters found are summarized in Table I, along with the corresponding $\text{SiO}_2:\text{Al}_2\text{O}_3$ molar ratios and the number of Al atoms per unit cell. Three lattice parameters larger than any included in the table were also found, but since there was a proportion of A zeolite admixed with the faujasite material in these samples, it was impossible to determine the number of Al atoms per unit cell for the faujasite alone. The largest of the three lattice parameters was 25.132 Å.

Table I: Lattice Parameters, Sorption Capacity, and Aluminum Content of Sodium Synthetic Faujasites

[SiO ₂]/ [Al ₂ O ₃]	Sorption, g/100 g—		No. of Al atoms/unit cell	a_0
	H ₂ O	Cyclo C ₆		
2.45	29.9	17.1	86.2	24.996
2.47	30.1	18.0	85.9	24.983
2.56	29.6	19.2	84.2	24.968
2.73	31.0	19.8	81.2	24.931
2.81	28.6	17.4	79.8	24.943
3.02	31.6	18.3	76.5	24.913
3.18	29.3	18.5	74.1	24.883
3.35	30.7	18.9	71.8	24.845
3.55	32.4	19.2	69.2	24.834
3.74	31.5	19.4	66.9	24.798
3.85	31.9	19.0	65.6	24.823
3.95	30.4	18.8	64.5	24.810
4.34	30.3	18.3	60.6	24.763
4.52	33.0	20.7	58.9	24.752
4.86	29.4	19.7	56.0	24.709
5.32	29.5	19.2	52.5	24.655
5.45	27.8	17.8	51.5	24.674
5.54	29.0	20.5	50.9	24.675
5.59	29.4	20.1	50.6	24.673
5.83	28.9	18.6	49.0	24.669

In Figure 1, the values for a_0 are plotted as a function of the number of Al atoms per unit cell. Since the lattice parameter of 25.132 Å fits on this plot at a $\text{SiO}_2:\text{Al}_2\text{O}_3$ molar ratio of very close to 2.0, it is included. Two, if not three, discontinuities are apparent in Figure 1. Two approximately parallel straight lines may be drawn in the ranges 96–80 and 66–52 Al atoms/unit cell. At about 80 and 66 Al atoms/unit cell, distinct breaks occur. The data points between these two compositions also form a straight line but of a somewhat different slope from the lines in the other regions.

Breck and Flanigen² found two discontinuities in a similar plot using dehydrated calcium zeolites having a faujasite structure. Their data are shown in Figure 2. The breaks, in the regions 79–76 and 64–60 Al atoms/

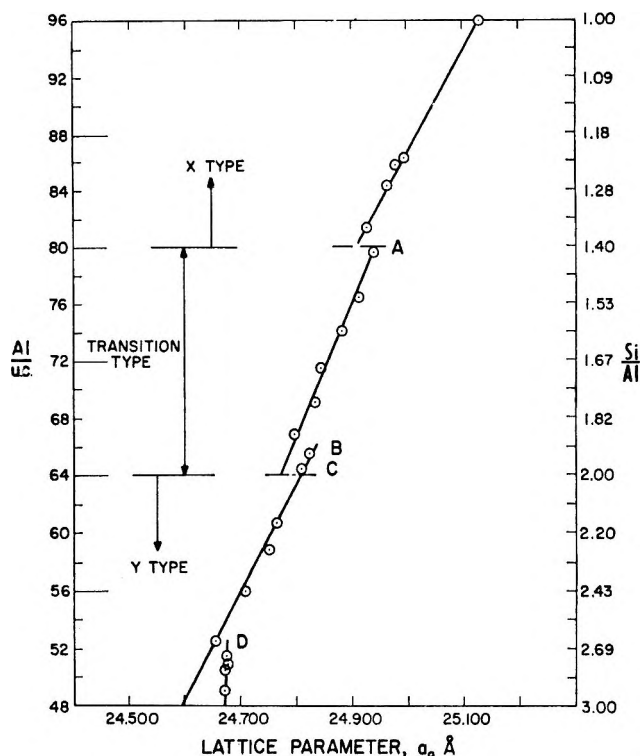


Figure 1. The number of Al atoms per unit cell and the Si:Al ratio vs. a_0 for hydrated synthetic sodium faujasites (bars on the left-hand side denote theoretical model compositions).

unit cell, are in good agreement with the points of discontinuity in Figure 1.

In Figure 1, at 52 Al atoms/unit cell, another discontinuity is observed. Since the probable lower limit of 48 Al atoms/unit cell is being approached, it is conceivable that the samples below 52 Al atoms/unit cell in Figure 1 contain amorphous silica; the small variation in the lattice parameter shown for the last four points of Figure 1 suggests that an increasing amount of amorphous silica may occur in these samples as we go to lower Si:Al ratios. A corresponding discontinuity does not occur in Figure 2.

Discussion

The existence of at least two distinct breaks in the plot of aluminum atoms per unit cell (equivalent to the number of sodium cations per unit cell) vs. lattice parameter (Figure 1) implies that at least three different faujasite phases may be occurring across the range of Si:Al variation. The approximate agreement between the results described above (relating to water-loaded sodium faujasites) and those shown in Figure 2 (relating to dehydrated calcium faujasites) suggests that the different phase regions do not result from variation in the cation distribution as the cationic content of the zeolites varies with the Si:Al ratio. Rather, the breaks

(2) D. W. Breck and E. M. Flanigen in "Molecular Sieves," Society of Chemical Industry, London, p 47 1968.

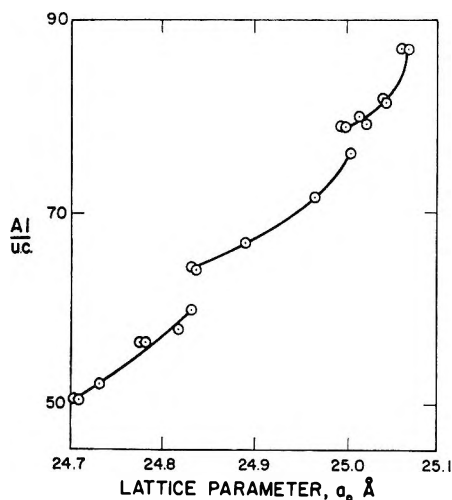


Figure 2. The relation between the cell constant, a_0 , and the Si:Al ratio of dehydrated forms of calcium-exchanged X- and Y-zeolites. The degree of calcium exchange is greater than 85 mol % for all zeolite samples. Dehydration carried out by heating in air at 400° for 16 hr.² (From Breck and Flanigen, ref 2.)

in the plot must be connected with changes that occur in the $\text{SiO}_2\text{-AlO}_2$ framework structure of the zeolites. Clearly if silicon and aluminum ions occur at random over the zeolite framework, the ideal space group $\text{Fd}\bar{3}\text{m}$ should apply to all faujasite materials regardless of the Si:Al ratio, and the plot of Figure 1 should show a single straight line having no breaks. The breaks must then correspond to transitions from one type of silicon-aluminum ordering to another.

In the past few years, calculations have been made of the electrostatic properties of ionic models of faujasite materials.³ At the time the models were set up, the generally accepted view of faujasite structures held that the silicon and aluminum ions were disordered relative to each other. In order to make reliable calculations, however, it was necessary to set up *ordered* models of the structures. This was done in a way that was consistent with the assumed ionic nature of the materials, and is described in ref 3. It turns out that the description of the zeolite models in ref 3 and the Summary and Discussion of that paper contain the substance of an explanation of Figure 1; for the moment, this explanation must be considered tentative.

Starting out from the idealized 1:1 material in which the silicon and aluminum ions alternate regularly throughout the structure (according to Löwenstein's rule), we see that (with suitable and plausible positioning of the exchangeable cations) the structure can be divided into identical units having zero net charge and dipole moment. The smallest unit obeying these criteria is the double sodalite unit having a center of symmetry at the center of the hexagonal prism linking the two sodalite units. We thus consider all faujasite-type materials as being formally constructed of identical

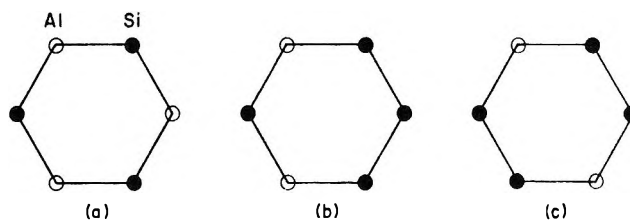


Figure 3. The arrangement of Al and Si ions in faujasite six rings for: (a) Si:Al = 1:1 (X-zeolite, *meta*); (b) Si:Al = 1.18:1 (Y-zeolite, *meta* form); (c) Si:Al = 2:1 (Y-zeolite, *para* form).

centrosymmetric double sodalite units placed at the points of a fcc lattice. If we now go from the 1:1 material to higher silicon:aluminum ratios, preserving our zero net charge and dipole moment criteria, we can set up faujasite models having the following Si:Al ratios: 1:1, 1.18:1, 1.4:1, 1.67:1, 2:1, 2.43:1, 3:1. These ratios are marked on the left side of Figure 1.

The 1:1 material has a very high symmetry: the space group $\text{Fd}\bar{3}$ is strictly applicable and all silicon and aluminum ion sites are equivalent to each other. All six rings have the *a-meta* form (see Figure 3a). (Hexagons in the sodalite units (formed of six -MO- pairs, where M is Al or Si) are called site-I or site-II six rings, depending upon whether they form part of a hexagonal prism or part of the supercage structure.)

Going to the 1.18:1 material involves replacing one Al ion per sodalite cage by a Si ion, ensuring that the two changes made in a typical double sodalite cage are at positions that are inverse with respect to each other. Since all Al ions are initially equivalent, it is immaterial which centrosymmetric pair of ions is exchanged. The important points are that this process generates two *b-meta* six rings per sodalite cage (Figure 3b) and that *no subsequent rearrangement of the Al and Si ions is possible*.

Taking the next step, exchanging two more Al ions for Si ions at inverse positions with respect to the center of symmetry of the double sodalite cage to produce the 1.4:1 ratio, creates two more *b-meta* rings per sodalite cage. Now we have to choose the position of the Al ions more carefully, since none of the ions in a 1.18:1 sodalite cage is equivalent to any other one. Clearly the second change, $\text{Al}\rightarrow\text{Si}$, has to be made as far as possible in the sodalite cage from the first one, and again it turns out that no subsequent rearrangement of the Si and Al ions will lower the energy. Since all we have done in going from the 1:1 through the 1.18:1 to the 1.4:1 material is to change Al ions to Si ions without further rearrangement, we can say that up to and including the 1.4:1 material the order is typical of the 1:1 structure. It may be appropriate to reserve the designation X-zeolite for materials obeying this criterion.

(3) E. Dempsey in "Molecular Sieves," Society of Chemical Industry, London, 1968, p 293.

Making two more Al→Si changes in our unit, at inverse points, produces the 1.67:1 material and two more *b-meta* rings per sodalite cage. Having made the change at the energetically most favorable position, however, we find that now a rearrangement of the Si and Al ions will diminish the electrostatic energy. (For practical reasons changes in repulsive energy have not been calculated, but the changes in repulsive energy should operate with, rather than against, the electrostatic energy changes.) The result of the redistribution of Si and Al ions is to create six rings of the *para* type (Figure 3c). Now we have moved away from the typical 1:1 order. The limit for the pure 1:1 order type, characterized by having all site-I and -II six rings of the *meta* forms and designated *Im*, *IIm*, is the 1.4:1 ratio. It is just at this point that Figure 1 shows its first break, point A. The "mixed" quality of the 1.67:1 material may be illustrated by the designation *Im*, *IImp*, site-II six rings having both the *meta* and *para* forms.

The next step, to the 2:1 material, permits a further rearrangement, after the two Al→Si changes have been made, with the creation of two more *para* rings. Now we have the situation (see the Discussion in ref 3 and Table I of that paper) in which all site-I six rings are *meta* and all site-II six rings are *para*, designated *Im*, *IIp*. Furthermore (see Table IV of ref 3), all site II's appear to be equivalent. This suggests that at the 2:1 composition a new symmetrical structure appears, which we have designated Y. The region between Si:Al > 1.4:1 and Si:Al < 2:1 appears to have the character of a transition region between the X and Y phases.

The second break in Figure 1 occurs close to the 2:1 Si:Al point but not quite at it. It is difficult to speculate about this since the models used have only the discrete Si:Al molar ratios indicated above and in Figure 1. It may be that materials near the end of the transition range in Figure 1 anticipate the structure existing at and beyond Si:Al = 2:1. In some support of this, it should be observed that the material of point

B has a composition that may be represented as being 2:1 with one in every five sodalite cages containing an extra Al ion.

A detailed analysis of the situation for the 2.43:1 and 3:1 materials has not been carried out. An examination of the models shows, however, that for the 2:1 material two diametrically opposing square faces of every sodalite cage carry two Al ions (the remainder carry only one each). Clearly, to achieve the optimum reduction in electrostatic energy on going to Si:Al = 2.43:1, an Al ion on one of these squares has to be replaced by a silicon ion, and then, to reach the 3:1 ratio, an Al ion has to be replaced in the remaining square carrying two Al ions. After making each of these changes, it appears that further reduction of energy cannot be achieved by rearranging the Si and Al ions. This is equivalent to saying that the 2.43:1 and 3:1 materials properly belong to the same phase region as the 2:1 material and that neither defines a new phase.

At this stage, it seems pointless to speculate on the apparent discontinuity at D in Figure 1, beyond the comments made in the Results section; the model discussed has no explanation of the discontinuity.

In summary, the form of Figures 1 and 2 implies that in zeolites having the faujasite structure the silicon and aluminum ions are ordered rather than disordered. The existence of the breaks in the figures is probably related to changes in the nature of the silicon-aluminum ordering as the Si:Al ratio is varied; the position of the breaks lends support to the particular ordered models described earlier.³ The fact that the section of Figure 1 between points A and B has a greater slope than the other two sections, which are approximately parallel, may be evidence for the proposed "transition" nature of zeolites in this range.

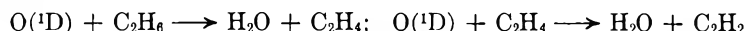
Acknowledgment. We wish to thank G. T. Kerr and G. R. Landolt for supplying us with some of the zeolite samples used in this study.

Reactions of O(¹D) with Hydrocarbons in Liquid Argon¹

by W. B. DeMore

Jet Propulsion Laboratory, California Institute of Technology, Pasadena, California 91103 (Received August 12, 1968)

Photolysis of O₃ (2537 Å) in dilute solutions in liquid argon has been used to study the reactions of O(¹D) with several hydrocarbons and also C₂F₄. In the case of the alkanes, the major products were the corresponding alcohols formed by insertion of O(¹D) into the C—H bonds in an indiscriminate manner. Reactions involving removal of two H atoms occurred to the extent of about 3% of the overall reactions of O(¹D) with both alkanes and alkenes



For ethane and the higher alkanes, there was no evidence for the production of radicals which could be scavenged by O₂, unlike previous results with H₂ and CH₄. The relative rates of O(¹D) attack on alkanes were found to be proportional to the number of C—H bonds present, but independent of the type. The evidence was that the C=C bond is attacked five times as rapidly as a C—H bond.

Introduction

In the present work O₃ photolysis in liquid argon has been used to study the reaction of O(¹D) with several hydrocarbons and also with C₂F₄. These studies are an extension of previous work on the reactions of O(¹D) with H₂^{2a} and CH₄.^{2b} The new work, together with previous results, provides information on the relative rates of attack by O(¹D) on different compounds in liquid argon and also on the relative rates of attack at different sites within a particular molecule. Information has also been obtained in regard to the primary reaction paths and products.

Results from earlier work point to important differences in the reactions of O(¹D) and O(³P) with hydrocarbons. Castellion and Noyes³ and Murad and Noyes⁴ studied the photolysis of N₂O—C₂H₆ mixtures and found that it was necessary to postulate the reaction



in order to account for the quantity of C₂H₄ in the products. The complete mechanism could not be elucidated because of the complexity of the system and the difficulty in distinguishing effects due to O(¹D) and O(³P). Yamazaki and Cvetanović⁵ approached the latter problem by studying the effects of added electronic deactivators in the photolysis of N₂O—C₃H₈ mixtures. They showed that a major reaction was indiscriminate insertion of O(¹D) into the C—H bonds, giving ROH-type products. Products corresponding to H abstraction from the C₃H₈ and fragmentation of excited ROH compounds were also found. Another primary reaction path which has been identified for O(¹D) is the elimination of molecular H₂^{2b}



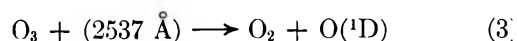
All of the above O(¹D) reaction paths can be envisaged as occurring *via* an excited ROH* intermediate

formed by the insertion reaction. If so, it is not clear at the present time whether the lifetime of the intermediate is sufficient for complete equipartition of the reaction exothermicity.

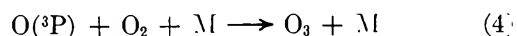
The only previous work on the reaction of O(¹D) with olefins seems to be that of Sato and Cvetanović,⁶ who studied the addition of O(¹D) to 1-butene. An increased yield of α-butene oxide, relative to the O(³P) case, was taken as evidence that O(¹D) adds directly to the C=C double bond to form the epoxide.

Experimental Section

The approach used has been previously described² and is reviewed here only briefly. Mixtures of O₃ and the hydrocarbon were dissolved in liquid argon at 87°K and were irradiated at 2537 Å. Typical concentrations were [O₃] = 5 × 10⁻⁴ M and [RH] = 0.1 M. Under these conditions O₃ serves as a source of O(¹D) by the process



which has a quantum yield near unity.⁷ Any O(³P) that appears in the reaction mixture by deactivation of O(¹D) can be scavenged by O₂



(1) This paper presents the results of one phase of research carried out at the Jet Propulsion Laboratory, California Institute of Technology, under Contract No. NAS7-100, sponsored by the National Aeronautics and Space Administration.

(2) (a) W. B. DeMore, *J. Chem. Phys.*, **47**, 2777 (1967); (b) W. B. DeMore and O. F. Raper, *ibid.*, **46**, 2500 (1967).

(3) G. A. Castellion and W. A. Noyes, Jr., *J. Amer. Chem. Soc.*, **79**, 290 (1957).

(4) E. Murad and W. A. Noyes, Jr., *ibid.*, **81**, 6405 (1959).

(5) H. Yamazaki and R. J. Cvetanović, *J. Chem. Phys.*, **41**, 3703 (1964).

(6) S. Sato and R. J. Cvetanović, *Can. J. Chem.*, **36**, 1668 (1958)

(7) W. B. DeMore and O. F. Raper, *J. Chem. Phys.*, **44**, 1780 (1966)

In most cases other reactions of $O(^3P)$ are too slow at $87^\circ K$ to compete with reaction 4, even at the lowest O_2 concentrations experimentally attainable. One exception is the addition of $O(^3P)$ to olefins, in which case excess O_2 must be added to completely scavenge the $O(^3P)$. Fortunately, the $O(^3P)$ can be effectively scavenged at O_2 concentrations which are too small to affect appreciably the $O(^1D)$ steady-state concentration. The reason for this is that $O(^3P)$ scavenging depends on the ratio O_2/C_2H_4 and $O(^1D)$ deactivation depends on the ratio O_2/Ar . Since Ar is present in great excess over C_2H_4 , large values of the former ratio can be obtained while maintaining small values for the latter ratio. Quantitative measurements of the efficiency of $O(^3P)$ scavenging by O_2^8 permit a correction to be made for any small residual contribution of $O(^3P)$ reaction to the overall quantum yield of O_3 disappearance.

With complete $O(^3P)$ scavenging by O_2 , the quantum yields of O_3 disappearance, Φ_{O_3} , are then given by

$$1/\Phi_{O_3} = \frac{k_r + k_d}{k_r} + \frac{k_{Ar}}{k_r[\text{substrate}]} \quad (5)$$

In eq 5, k_d denotes the rate constant for $O(^1D)$ deactivation by the added substrate, k_{Ar} represents solvent deactivation, and k_r is the rate constant for $O(^1D)$ reaction with the substrate.

Alcohol products were analyzed mainly on an 8-ft Porapak Q column at 140° . Ethylene in the presence of excess ethane was analyzed on an 8-ft Porapak S column at 40° , using H_2 flame ionization detection. Acetylene in the presence of ethylene was analyzed on an 8-ft Porapak T column at 70° . The latter column, at 140° , was found to give good CH_2O analyses. Formaldehyde analysis, which is usually unreliable in gas-phase work, is facilitated in the low-temperature, liquid work because the product is frozen out as soon as formed, and does not stand in the gaseous state. Determination of the CH_2O/CH_3OH product ratio from the reaction of $O(^1D)$ with CH_4 gave results which agreed very well with previous results^{2b} obtained by a mass spectrometric analysis.

Research grade hydrocarbons were used, and in most cases these were further purified by gas chromatography. Blanks were run in all cases to ensure that impurities did not interfere with product analyses. The C_2F_4 was a product of Peninsular ChemResearch, Inc., and was purified only by vacuum fractionation.

The nonphotochemical rate of O_3 decomposition in the presence of dissolved alkanes was zero. However, a slight spurious reaction between O_3 and the alkanes did occur either during sample preparation or product separation. The major product of this reaction in the case of C_2H_6 was CH_3CHO . The amount of product formed in this way was not more than 5–10% of the photochemical product.

Ozonolysis of olefins was a problem in the present

experiments. Rate measurements showed that ozonolysis of C_2H_4 and C_2F_4 was negligibly slow compared to the photochemical reaction rates. However, for higher olefins ozonolysis was more rapid and a quantitative study of the $O(^1D)$ reactions with these olefins was not possible.

Results

Relative Rate Measurements. Figure 1 shows the quantum yields of O_3 disappearance plotted according to eq 5. Previous results for H_2 , CH_4 , and O_3 are included for comparison. The intercepts are approximately identical and have values close to unity, showing that in each case deactivation of $O(^1D)$ by the substrate is not a major process compared to reaction. (As was shown in the CH_4 experiments,^{2b} a small fraction of deactivation may occur.) Since the slopes in Figure 1 are inversely proportional to the rate constants, k_r , the rates can be placed on a relative basis. The results, normalized relative to the O_3 rate constant as unity, are shown in Table I.

Products. As in the case of CH_4 , the major products for reaction of $O(^1D)$ with the alkanes were the corresponding alcohols formed by insertion into the C–H bonds. These products accounted for at least 75% of the O_3 decomposed. Olefins corresponding to removal of 2 H atoms from the alkane were produced, in yields of about 3%. In the case of C_2H_6 , the C_2H_4 product was identified chromatographically in the product analysis. Additional evidence for the presence

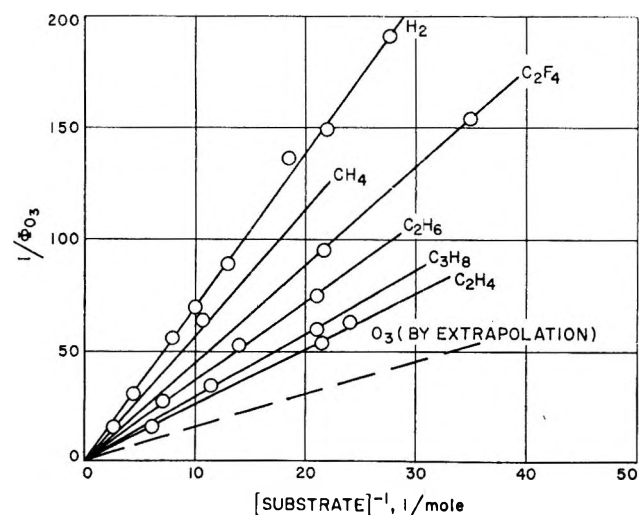


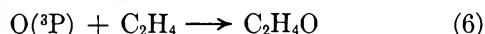
Figure 1. Quantum yields of O_3 disappearance as a function of substrate concentration. Previous data for H_2 , CH_4 , and O_3 are included for comparison. The O_3 quantum yields are obtained by comparing the rate of O_3 photolysis in a given hydrocarbon solution with the rate of O_3 photolysis in a solution of O_3 dissolved in liquid N_2 . The O_3 quantum yield in the latter solution is 0.018 ± 0.002 (O. F. Raper and W. B. DeMore, *J. Chem. Phys.*, **40**, 1053 (1964).

(8) W. B. DeMore, unpublished work.

Table I: Rates of O(¹D) Reactions Relative to O₃

Substrate	Relative rate (normalized to O ₃ = 1)
H ₂	0.232
CH ₄	0.267
C ₂ H ₆	0.445
C ₂ F ₄	0.370
C ₃ H ₈	0.570
C ₂ H ₄	0.610
O ₃	1.000

of C₂H₄ was the appearance of ethylene oxide among the products, by the reaction



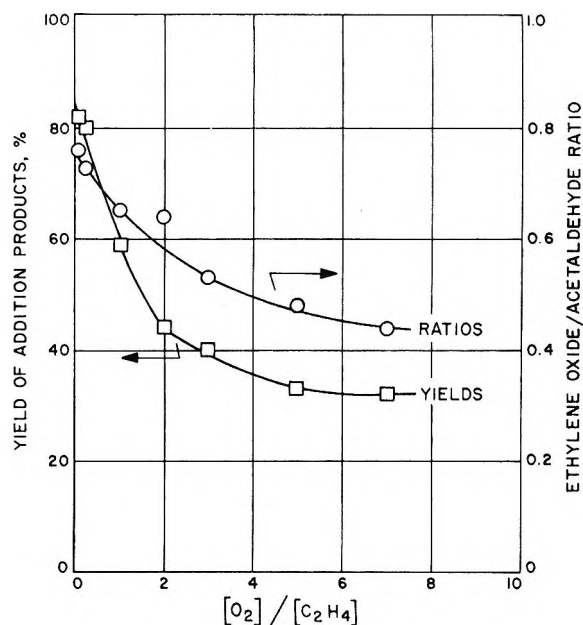
It was established that ethylene oxide was not a primary product of the O(¹D) reaction by the fact that small amounts of added O₂ eliminated ethylene oxide from the products, but did not reduce the C₂H₄ yield. Formation of propylene and isobutylene in the reactions of O(¹D) with propane and isobutane, respectively, was inferred from the appearance of the corresponding epoxides among the products.

Molecular H₂ was also detected as a product of the alkane reactions. The yield, however, was only about 1%, compared to 10% found in the reaction of O(¹D) with CH₄. Acetaldehyde was present among the products in about 10-fold excess over the H₂, but most of the aldehyde undoubtedly was formed by the previously mentioned nonphotochemical O₃-C₂H₆ reaction which occurred during either mixture preparation or product separation.

The ratios of the isomeric alcohols formed by O(¹D) reaction with different C-H bonds in C₃H₈ and *i*-C₄H₁₀ are shown in Table II. In each case the product ratios show very nearly indiscriminate insertion of O(¹D) into the different C-H bonds. As shown in the Discussion section, the relative rate measurements given in preceding paragraphs are also consistent with equal

Table II: Ratios of Isomeric Alcohols Formed by O(¹D) Insertion in C-H Bonds of Propane and Isobutane in Several Experiments

Propane ratio <i>n</i> -C ₃ H ₇ OH/ <i>i</i> -C ₃ H ₇ OH	Isobutane ratio <i>i</i> -C ₄ H ₉ OH/ <i>t</i> -C ₄ H ₉ OH
3.3	8.9
3.0	8.5
3.0	8.3
3.2	9.0
3.2	
2.9	
Average: 3.2	Average: 8.7
Statistical: 3.0	Statistical: 9.0


 Figure 2. Effect of O₂ on the yield and ratio of addition products in the reaction of O(³P) with C₂H₄.

rates of attack by O(¹D) on all C-H bonds, including those of ethylene.

In the ethylene experiments, the possible participation of O(³P) reactions must be considered. At an O₂/C₂H₄ ratio of 7:1, the scavenging of O(³P) by O₂ is sufficiently complete so that less than 20% of the reaction is due to O(³P) and the remainder is due to O(¹D). Under these conditions the products were CH₃CHO, ethylene oxide (EO), CH₂O, H₂, and C₂H₂. The ratio of EO to CH₃CHO was 0.44, and together the addition products EO and CH₃CHO accounted for 32% of the decomposed O₃. The CH₂O yield was comparable to that of CH₃CHO. The H₂ yield was about 6-7%, and the C₂H₂ yield was 1-3%.

At lower O₂/C₂H₄ ratios the extent of O(³P) reaction increases until at very low ratios virtually all of the products are due to O(³P). Therefore it is possible to compare the O(³P) and O(¹D) products under nearly identical conditions. Figure 2 shows that the combined EO and CH₃CHO yields increased to about 85% in the limit of pure O(³P) reaction, and the ratio EO/CH₃CHO increased to 0.75. The yields of CH₂O and H₂ declined by a factor of about 2, and the C₂H₂ disappeared entirely. It appears, therefore, that C₂H₂ is formed only by O(¹D) whereas the other products are formed to some extent by both O(¹D) and O(³P).

The products of the O(¹D) reaction with C₂F₄ were not determined because of the slowness of the photochemical reaction. Infrared analysis of the O(³P) products showed only CF₂O, as found in the case of the gas phase reaction.⁹ The possible products perfluoro-

(9) D. Saunders and J. Heicklen, *J. Amer. Chem. Soc.*, **87**, 2088 (1965).

ethylene oxide, CF_3CHO , and the cyclo- C_3F_6 were not present in detectable amounts.

Tests for Radical Production in the Alkane Reactions.

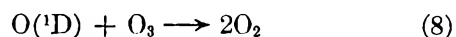
Formation of radicals by reactions such as



can be detected by observing the effect of added O_2 on the quantum yield of O_3 disappearance, Φ_{O_3} . If scavengeable radicals are produced, then the ratio $\Phi_{\text{O}_3}(\text{unscavenged})/\Phi_{\text{O}_3}(\text{scavenged})$ has a value greater than unity because unscavenged radicals attack O_3 . By this method the formation of radicals was demonstrated in the reactions of $\text{O}(^1\text{D})$ with H_2^{2a} and CH_4^{2b} . It was of interest, therefore, to determine if reaction of $\text{O}(^1\text{D})$ with higher alkanes would also give radicals or if on the other hand the radical fission process would be suppressed by virtue of the increased degrees of freedom in the presumed ROH^* intermediate. Several experiments of this type with ethane and propane were carried out in which Φ_{O_3} was measured at $\text{O}_2/\text{O}_3 \gg 1$ (the scavenged case) and at $\text{O}_2/\text{O}_3 \ll 1$ (the unscavenged case). In both cases the quantum yields were identical within an experimental uncertainty of about 5%. The conclusion therefore is that the efficiency of production of scavengeable radicals diminishes with increasing size of the alkane. It should be noted that in the foregoing discussion the words "scavenged" or "unscavenged" refer to radicals and not to $\text{O}(^3\text{P})$, because in all of the alkane solutions $\text{O}(^3\text{P})$ disappears only by combination with O_2 . Experiments of this type were not possible in the case of C_2H_4 because excess O_2 is required to scavenge $\text{O}(^3\text{P})$, and therefore effects due to radical scavenging would be masked.

Discussion

The data of Table I summarize the relative rates of $\text{O}(^1\text{D})$ attack on a variety of substrates. The most rapid reaction observed is that with O_3



An important question then arises as to what factors determine the reactivity of a given substrate. In this connection two significant relationships can be pointed out on the basis of Table I. First, the relative rate data for all the alkanes can be accurately represented by an average relative reactivity *per C—H bond* of 0.071 ± 0.004 . This shows that the alkane reactivities depend only on the number of C—H bonds present in the molecule, regardless of the type and strength of the bonds. Second, it may be shown that if the observed reactivity of C_2F_4 is taken to represent the C=C reactivity, then the relative reactivity of C_2H_4 can be represented quite accurately as the sum of the reactivities of four C—H bonds and one C=C bond. These results are summarized in Table III, and are based on $R(\text{CH}) = 0.071$ and $R(\text{C}=\text{C}) = 0.37$. The indication therefore is that the C=C bond is five times more reactive to $\text{O}(^1\text{D})$ than a C—H bond.

Table III: Bond Additivity of Reaction Rates

Compound	Bonds	Relative reactivity	
		Calcd	Obsd
CH_4	4CH	0.28	0.27
C_2H_6	6CH	0.43	0.44
C_3H_8	8CH	0.57	0.57
C_2H_4	4CH + 1C=C	0.65	0.61

The very nearly statistical distributions of isomeric alcohols shown in Table II give further indication that the rate of $\text{O}(^1\text{D})$ insertion into C—H bonds is independent of the bond type. Similar results were found in the gas phase reaction of $\text{O}(^1\text{D})$ with propane⁶ and the gas phase reaction of $\text{S}(^1\text{D})$ with propane and isobutane.¹⁰ Singlet CH_2 , which reacts in a parallel manner, apparently shows some preferential insertion into C—H bonds in the order tertiary > secondary > primary.¹¹ Interpretation of the CH_2 results is complicated by the difficulty of ascertaining that the inserting particle is fully thermalized, and also that the triplet CH_2 does not intervene.¹¹ The former problem also arises in the present work. There is no doubt, on the other hand, that all of the insertion products are due to $\text{O}(^1\text{D})$, because $\text{O}(^3\text{P})$ does not react with the alkanes under the present experimental conditions.

An additional similarity between $\text{O}(^1\text{D})$ and singlet CH_2 is found in the relative rates of addition to C=C and C—H insertion. Values for this ratio reported for CH_2 usually are 10 or greater,¹² which may be compared to the ratio of 5 found in the present work for $\text{O}(^1\text{D})$. These results again seem to indicate that $\text{O}(^1\text{D})$ is somewhat less discriminate than CH_2 .

The production of scavengeable radicals in the reactions of $\text{O}(^1\text{D})$ with various alkanes can be correlated with the expected lifetime of an ROH^* intermediate. The experimental results were that, for the $\text{O}(^1\text{D})$ - H_2 reaction, dissociation of the intermediate HOH^* to $\text{H} + \text{OH}$ was virtually complete, even in liquid argon. With CH_4 , the radical dissociation of CH_3OH^* occurred to the extent of about 30%. In the present work, reaction of $\text{O}(^1\text{D})$ with C_2H_6 or C_3H_8 gave no evidence of radical formation at all. Table IV gives the results of some classical RRK calculations for radical fission of the various ROH^* intermediates. These calculations, while approximate, show that dissociation of HOH^* can easily be more rapid than collisional deactivation, which in solution should occur at a rate of 10^{11} - 10^{12} sec⁻¹. The calculations of Table IV also show that partial dissociation of CH_3OH^* is possible, and further that radical dissociation of $\text{C}_2\text{H}_5\text{OH}^*$

(10) A. R. Knight, O. P. Strausz, and H. E. Gunning, *J. Amer. Chem. Soc.*, **85**, 2349 (1963).

(11) B. M. Herzog and R. W. Carr, Jr., *J. Phys. Chem.*, **71**, 2688 (1967).

(12) H. M. Frey, *Progr. Reaction Kinetics*, **2**, 131 (1964).

Table IV: Estimated Radical Dissociation Rates of Vibrationally Excited Alcohols Formed by Reaction of O(¹D) with Alkanes^a

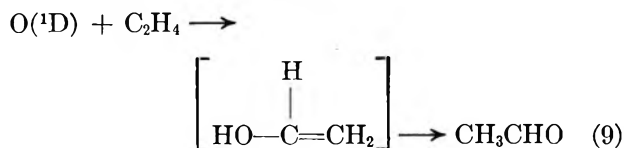
Reaction	log <i>A</i> (sec ⁻¹) ^b	<i>E_a</i> ^c	<i>E</i> * ^d	<i>s</i> ^e	log <i>k</i> (sec ⁻¹)
H ₂ O* → H + OH	14	119	163	1.8	13.6
CH ₃ OH* → CH ₃ + OH	14	91	135	7.2	11.0
CH ₃ OH* → CH ₃ O + H	14	102	135	7.2	10.2
C ₂ H ₅ OH* → C ₂ H ₅ + OH	14	91	141	12.6	8.8
C ₂ H ₅ OH* → CH ₃ + CH ₂ OH	14	83	141	12.6	9.5

^a Rates calculated from the RRK expression $k = A((E^* - E_a)/E^*)^{s-1}$. ^b Assumed values. ^c Taken as equal to the strength of the bond broken. Some of the values are uncertain by 1–2 kcal/mol. ^d Taken as equal to the exothermicity of the insertion reaction. ^e The assumed value $s = 0.6(3n - 6)$ was used.

should be too slow to occur in solution. Both of these calculations are in agreement with the experimental results. These results seem to indicate that the radical-producing reactions involve an intermediate which is susceptible to collisional deactivation.

Observation of olefin formation in the reaction of O(¹D) with the alkanes confirms the earlier conclusion of Noyes and coworkers^{3,4} that removal of two H atoms is a primary reaction path. While contributing only a few per cent to the overall reaction in solution, this reaction may be much more important in the gas phase if it also involves the intermediate ROH*. Formation of HC≡CH in the reaction of O(¹D) indicates that the reaction is quite general for O(¹D), but not O(³P). This property may be useful for detecting the presence of O(¹D) in reaction systems.

The present results for C₂H₄ unfortunately do not provide much information on the details of the initial reaction of O(¹D) with the C=C bond. The ratio of ethylene oxide to acetaldehyde was lower for the O(¹D) reaction than for the O(³P) reaction. However, in the case of O(¹D) the observed ratio probably did not reflect the initial product distribution, for two reasons. First, account must be taken of the fact that O(¹D) attacks the C–H bonds, a probable reaction being



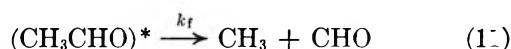
Therefore it is necessary to correct the CH₃CHO yield

for the amount arising from reaction 9. As shown above, reaction of O(¹D) with the C–H bonds of C₂H₄ accounts for about 40% of the total reaction. When the latter amount is deducted from the CH₃CHO yield the resulting C₂H₄O/CH₃CHO ratio is approximately unity. A second correction would have to be made for the CH₃CHO formed by isomerization of the initially excited EO



The energy of C₂H₄O* is 130 kcal/mol, and by means of RRK calculations for EO similar to those of Benson,¹³ the rate *k_i* for that energy is found to be 10^{12.2} sec⁻¹. This is equal to or greater than the collisional deactivation rate of 10^{11.6±0.5} sec⁻¹, so that it must be presumed that even if all the initial reaction gave EO, some CH₃CHO would have been formed by isomerization.

The CH₃CHO product of reaction 10 can have as much as 157 kcal/mol of vibrational energy if no collisional deactivation occurs in intervening steps leading to its formation. Thus it is necessary to consider the fission reaction



By an RRK calculation similar to the above, the estimated rate *k_f* is 10^{12.1} sec⁻¹, again sufficiently rapid to occur in liquid argon. Reaction 11 probably accounts, at least in part, for the decline in total yield of the addition products shown in Figure 2.

(13) S. W. Benson, *J. Chem. Phys.*, **40**, 105 (1964).

Production of Perchlorate and Chlorite Ions in Crystalline Potassium

Chlorate Irradiated with Cobalt-60 γ Rays¹

by L. C. Brown and G. E. Boyd

Oak Ridge National Laboratory, Oak Ridge, Tennessee 37830 (Received August 15, 1968)

The production of perchlorate and chlorite ions in crystalline KClO_3 irradiated with ^{60}Co γ rays at *ca.* 30° was demonstrated by infrared absorption measurements. Quantitative determinations of the concentration of ClO_4^- ions in the solid were performed, and the results were compared with chemical analyses for perchlorate in aqueous solutions of the irradiated solid. The concentrations of ClO_4^- in solution and in the crystal were found equal within experimental error. Accordingly, the hypothesis that the perchlorate observed in solution was produced by the hydrolysis of Cl_2O_6 assumed to be present in the solid was unnecessary. Radiolytic yields for the species Cl^- , ClO^- , ClO_2^- , and ClO_4^- were obtained. The concentrations of the first three species appeared to increase linearly with the absorbed dose to a dose as great as 4.4×10^{23} eV (mol of KClO_3)⁻¹; the concentration of ClO_4^- ion, however, increased less rapidly than linearly at large doses. Interesting similarities between the radiolytic and thermal decompositions of the alkali metal chlorates were noted.

A knowledge of the identities and concentrations of the species formed in inorganic crystals by energetic ionizing radiations is essential to an understanding of the radiation chemistry of solids. Spectroscopic methods have proved useful in this connection, particularly in investigations with crystals containing oxyanions. With the alkali metal and alkaline earth chlorates, for example, esr studies on irradiated NaClO_3 ,² KClO_3 ,³ and $\text{Ba}(\text{ClO}_3)_2$ ³ have shown ClO_2 and ClO_3 to be present at low temperatures. Absorption measurements in the visible and ultraviolet have been employed⁴ to assign the color centers in irradiated KClO_3 to the species ClO_2 , ClO_2^- , ClO^- , and O_3^- , respectively. Infrared absorption measurements have been applied⁵ in an unsuccessful search for ClO_4^- ion in X-irradiated KClO_3 . A small peak at 1113 cm^{-1} , not present in the unirradiated compound, was observed, but its absorption was too small for it to be considered as reliable evidence for perchlorate ion. Heal therefore postulated that the ClO_4^- ion observed by himself and others⁶ in aqueous solutions of irradiated solid potassium chlorate was produced by the hydrolysis of Cl_2O_6 assumed to be formed and trapped in the crystal. This hypothesis has been reiterated by McCallum and coworkers^{7,8} to account for their observation of perchlorate ion in aqueous solutions of crystalline NaClO_3 , KClO_3 , and $\text{Ba}(\text{ClO}_3)_2$ irradiated with ^{60}Co γ rays. In an elaboration of this hypothesis it has been assumed^{2b} that Cl_2O_6 is formed in the solid by the dimerization of ClO_3 . Recently, the detection of ClO_4^- ion by infrared absorption measurements on a single crystal of KClO_3 irradiated with X-rays and subjected to thermal bleaching has been reported.⁹

Infrared absorption measurements were employed in this research to demonstrate the production of ClO_2^-

and ClO_4^- ions in γ -ray irradiated crystalline KClO_3 at room temperature. Further, the concentration of ClO_4^- ion in the solid was determined by quantitative infrared analysis. The irradiated crystals were dissolved in water, and the concentration of perchlorate ion also was determined by a quantitative chemical method. A comparison of the concentrations in the crystal with those determined in aqueous solution showed that, within experimental error, all the ClO_4^- ion in solution was present originally within the irradiated solid. It does not seem to be necessary, therefore, to assume that any perchlorate in solution was produced by the hydrolysis of species such as Cl_2O_6 , ClO_3 , etc.

Experimental Section

Sample Preparation. Reagent grade KClO_3 was recrystallized from hot aqueous solution and the samples for irradiation were prepared by freeze-drying^{10,11} dilute solutions (0.25 M) of the recrystallized salt. The freeze-dried KClO_3 contained in sealed glass bottles

- (1) Research sponsored by the U. S. Atomic Energy Commission under contract with the Union Carbide Corp.
- (2) (a) F. T. Gamble, *J. Chem. Phys.*, **42**, 3542 (1965); (b) P. F. Patrick and F. P. Sargent, *Can. J. Chem.*, **46**, 1818 (1968).
- (3) R. W. Holmberg, Oak Ridge National Laboratory Report, ORNL-3320, 1962, pp 106, 107.
- (4) C. Ramasastry and S. B. S. Sastry, *J. Phys. Chem. Solids*, **29**, 399 (1968).
- (5) H. G. Heal, *Can. J. Chem.*, **37**, 979 (1959).
- (6) L. J. Sharman and K. J. McCallum, *J. Chem. Phys.*, **23**, 597 (1955).
- (7) C. E. Burchill, cited by P. F. Patrick and K. J. McCallum, *Nature*, **194**, 766 (1962).
- (8) C. E. Burchill, P. F. Patrick, and K. J. McCallum, *J. Phys. Chem.*, **71**, 4560 (1967).
- (9) V. Hovi and V. Räsänen, *Ann. Acad. Sci. Fenn., Ser. A*, **VI**, 228 (1967).
- (10) T. Y. Toribara and V. Distefano, *Anal. Chem.*, **26**, 1519 (1954).
- (11) H. Tai and A. L. Underwood, *ibid.*, **29**, 1430 (1957).

was irradiated in air, although one sample was radiolyzed in an evacuated (<0.1 Torr) glass ampoule. Confirmation of the anhydrous nature of the preparations was given by the infrared spectra which revealed no absorption at 1627 cm^{-1} (ν_2) nor in the range $3000\text{--}4000\text{ cm}^{-1}$ (ν_1 and ν_3) where strong vibrational water bands occur. The irradiations were conducted at constant geometry in a ^{60}Co γ -ray source where the equilibrium temperature was *ca.* 30° and the dose rate, as measured by a Fricke dosimeter ($G(\text{Fe}^{3+}) = 15.6$), was $1.08 \times 10^{20}\text{ eV min}^{-1}$ (mol of KClO_3) $^{-1}$. The ratio of the numbers of electrons per gram in KClO_3 and H_2O was employed to establish the dose absorbed by the former compound. Thus, $\text{dose}(\text{KClO}_3) = 0.882\text{ dose}(\text{H}_2\text{O})$. The irradiated crystals were stored in a Dry Ice bath at -78° until analysis.

Perchlorate Ion Determination in Solid KClO_3 . Standards prepared by freeze-drying dilute aqueous mixtures of $\text{KClO}_3 + \text{KClO}_4$ of known composition were used in the construction of an analytical calibration curve. The KClO_3 concentration in these solutions was kept low (*ca.* 0.25 M) so that this salt would not recrystallize before the water froze into a rigid ice matrix. It was reasoned that standards with a random distribution of KClO_4 within an amorphous KClO_3 lattice would be obtained, and that such standards would be more representative of radiolyzed KClO_3 than if solid KClO_4 and KClO_3 were ground together or if they were recrystallized from hot aqueous solution together. Electron microscopy of the freeze-dried KClO_3 revealed a finely divided solid composed of cylindrical crystalline particles *ca.* $0.5\ \mu$ in diameter and $3\text{--}6\ \mu$ in length.

Infrared measurements were obtained with a Beckman IR-12 double-beam infrared spectrophotometer operated in the double beam mode with dry air in the reference beam. Transmission spectra of Nujol mulls, suspended between two flat KBr plates, were recorded from 450 cm^{-1} to 1200 cm^{-1} . Daily adjustments of the spectrophotometer were made at a standard wavelength (1000 cm^{-1}) and a constant slit width (0.8 mm) so that the automatic slit program would be constant for both standards and samples.

Nujol mulls were prepared by mixing a 25-mg portion of sample with 4 drops of dry Nujol (dried over freshly cut sodium metal) in a clean, dry, mullite mortar until the solid had been completely wetted and a paste had been formed. The particle size in the freeze-dried sample (see above) was so small that mulls which yielded high quality spectra (see Figure 1) could be prepared directly without grinding. This property of freeze-dried solid KClO_3 was essential because pressure-induced annealing of radiolytically formed species has been observed in alkaline earth halate systems.¹²

Peak absorption intensities were determined by a straight "base-line" method.¹³ The ν_4 asymmetric vibrational absorbance of chlorate ion¹⁴ at 493 cm^{-1}

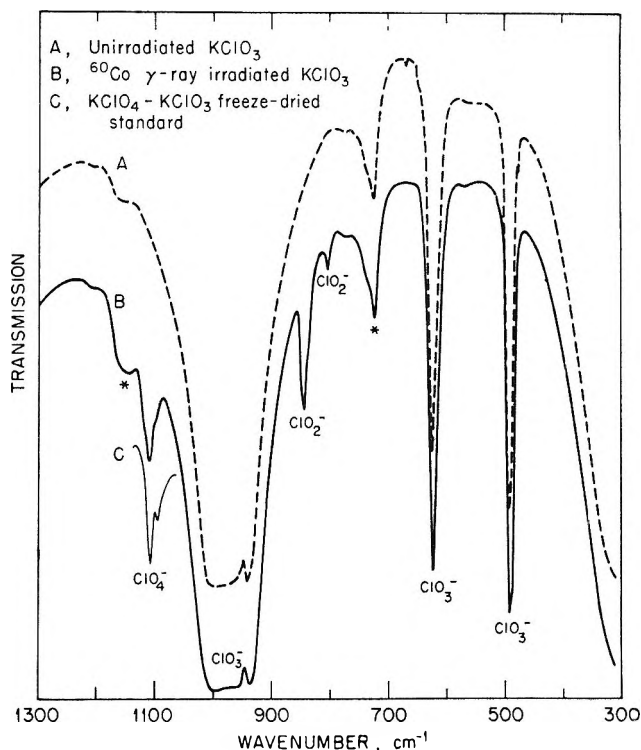


Figure 1. Infrared absorption by crystalline KClO_3 at room temperature. (Asterisks denote Nujol absorbancies.)

was employed as an internal standard. A calibration curve was constructed by plotting the ratios of the absorbancies of the perchlorate ion's ν_3 vibration (1103 cm^{-1} in a KClO_3 lattice) to the chlorate ion's ν_4 vibration against the mole % of KClO_4 in the standards (see Figure 2).

Perchlorate Ion Determination in Aqueous Solution. Aqueous solutions of irradiated KClO_3 were prepared by dissolving weighed portions of the salt in dilute H_2SO_3 solutions. These solutions contained sufficient H_2SO_3 to convert all reducible oxychlorine anions (all except ClO_4^-) to chloride ion. Excess H_2SO_3 was decomposed by heating the solutions on a steam bath.

Perchlorate ion was determined by the crystal violet solvent extraction-absorption spectrophotometry method of Uchikawa.¹⁵ A calibration curve was obtained which agreed well with Uchikawa's data, and it was verified that the interference of Cl^- ion on the extraction of the crystal violet perchlorate ion-pair complex could be compensated by preparing reagent blanks of equivalent Cl^- concentration.

Cl^- , ClO^- , and ClO_2^- Analyses. Chloride, ClO^- , and ClO_2^- ions were determined by potentiometric micro-

(12) M. Khare and S. R. Mohanty, *Radiochim. Acta*, **8**, 63 (1967).

(13) W. J. Potts, "Chemical Infrared Spectroscopy," Vol. I, John Wiley & Sons, New York, N. Y., 1963, pp 165-170.

(14) G. N. Krynavow and C. J. H. Schutte, *Spectrochim. Acta*, **21**, 1947 (1963).

(15) S. Uchikawa, *Bull. Chem. Soc., Jap.*, **40**, 798 (1967).

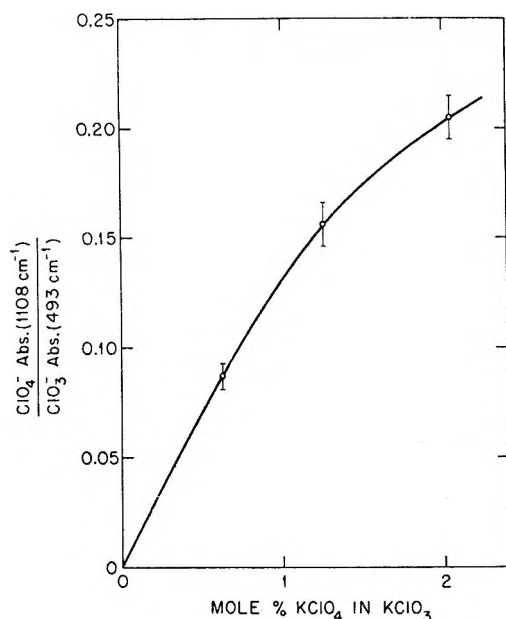


Figure 2. Calibration curve for the determination of KClO_4 in a KClO_3 matrix by infrared absorption techniques.

titrations. Chloride ion was assayed by dissolving weighed portions of irradiated KClO_3 in 0.01 M borax solution⁵ and titrating with 0.100 M Ag^+ . Hypochlorite and ClO_2^- ions were determined by an adaptation of Andersen and Madsen's¹⁶ methods for BrO^- and BrO_2^- . Weighed portions of sample were dissolved in 0.3 M NaHCO_3 and titrated with 0.0100 N arsenous acid. Osmium tetroxide catalyst was added after the ClO^- end point had been reached and the titration of ClO_2^- completed. Chlorine dioxide would also be reduced by titration with arsenous acid and would contribute to the ClO^- end point, but, owing to the nature of the KClO_3 samples (see footnote c, Table II), no attempt was made to determine ClO_2 independently.

Results

The results from the ClO_4^- analyses of ^{60}Co γ -ray irradiated KClO_3 are summarized in Table I. The errors quoted are standard deviations and include uncertainties in the calibration curves and in the analyses of the irradiated salt. The precision of the Nujol mulling procedure and the infrared spectrophotometry, as revealed by Figure 2, was approximately 7%. The accuracy of the crystal violet extraction data was much higher (see ref 15 for a calibration curve and discussion of accuracy).

The G values (*i.e.*, molecules produced per 100 eV absorbed) for Cl^- , ClO^- , ClO_2^- , and ClO_4^- are given in Table II. The errors quoted are standard deviations which represent the precision of the chemical analyses only. The G values for Cl^- , ClO^- , and ClO_2^- agree well with the values of Burchill, Patrick, and McCallum,⁸ who observed a linear concentration-dose

Table I: Comparison of KClO_4 Content of ^{60}Co γ -Ray Irradiated KClO_3 as Measured by Ir Analysis of Solid and by Chemical Analysis of Aqueous Solution

Sample	Dose, eV (mol of KClO_3) ⁻¹ $\times 10^{-23}$	Mol % KClO_4 in crystal (ir)	Mol % KClO_4 in aq solution of crystal (chemical)	Radiolytic yield, $G(\text{ClO}_4^-)^b$
1	3.22	0.48 ± 0.05	0.55 ± 0.01	1.03 ± 0.02
2 ^a	4.37	0.57 ± 0.06	0.70 ± 0.02	0.97 ± 0.03
3	4.42	0.65 ± 0.06	0.69 ± 0.01	0.94 ± 0.02
4	14.0	1.96 ± 0.20	1.89 ± 0.06	0.81 ± 0.03

^a Sample irradiated at reduced pressure (<0.1 Torr). ^b Computed from the more precise aqueous solution analyses, column 4, this table.

dependence to a dose of 1.2×10^{23} eV (mol of KClO_3)⁻¹. It therefore appears that this linearity extends to a dose as great as 4.4×10^{23} eV (mol of KClO_3)⁻¹; however, as is known from the results of Heal,⁵ the concentrations of ClO^- and ClO_2^- become nonlinear, and in fact independent of the dose, for doses greater than 10×10^{23} eV (mol of KClO_3)⁻¹. The G value for ClO_4^- ion at a dose of 4.4×10^{23} (*cf.* Table II) appears to be perceptibly lower than at 1.2×10^{23} eV (mol of KClO_3)⁻¹, and this can be explained by the nonlinear dose dependence of the perchlorate ion formation as revealed by column 5, Table I.

Discussion

Three new peaks were observed in the infrared spectrum of ^{60}Co γ -ray irradiated KClO_3 which were not present in the spectrum of unirradiated KClO_3 (*cf.* spectra B and A, respectively, Figure 1). The two new peaks at lower frequency (*i.e.*, 806 and 844 cm^{-1}) can be attributed to ClO_2^- and definitely prove the existence of ClO_2^- in the irradiated solid matrix. Measurements with crystalline NaClO_2 in a dry Nujol mull showed peaks at 806 and 835 cm^{-1} , while investigations¹⁷ with aqueous solutions of this compound have demonstrated absorptions at 790 (ν_1), 400 (ν_2), and 840 (ν_3) cm^{-1} , respectively. The new peak at higher frequency (maximum absorbancy at 1108 cm^{-1}) can be assigned to the ν_3 vibration of ClO_4^- and was used for the quantitative determination of the concentration of this ion. The frequency of the only other infrared active ClO_4^- absorbancy (ν_4 vibration at *ca.* 630 cm^{-1}) nearly coincides with the ν_2 of ClO_3^- (*ca.* 620 cm^{-1}), thereby resulting in complete overlap of the peaks. For this reason, the ν_4 vibrational absorbency of ClO_3^- at 493 cm^{-1} was chosen as the internal standard peak for the analysis.

The inserted portion of a spectrum (trace C, Figure 1) shows the structural features of ClO_4^- in a typical

(16) T. Andersen and H. E. L. Madsen, *Anal. Chem.*, **37**, 49 (1965).
 (17) J. P. Mathieu, *Compt. Rend.*, **234**, 2272 (1952).

Table II: Yields of Chlorine-Containing Species Produced by ^{60}Co γ Irradiation of Crystalline KClO_3

Sample	Dose, eV (mol of KClO_3) ⁻¹ $\times 10^{-23}$	$G(\text{Cl}^-)$	$G(\text{ClO}^-)^c$	$G(\text{ClO}_2^-)$	$G(\text{ClO}_4^-)^b$
2 ^a	4.37	1.55 ± 0.05	0.32 ± 0.01	2.08 ± 0.03	0.97 ± 0.03
3	4.42	1.65 ± 0.05	0.32 ± 0.01	2.05 ± 0.03	0.94 ± 0.02
Average	4.4	1.60 ± 0.07	0.32 ± 0.02	2.06 ± 0.04	0.96 ± 0.04
Lit. ⁸ value	≤ 1.2	1.64 ± 0.09	0.27 ± 0.04	2.07 ± 0.07	1.13 ± 0.06

^a See footnote a, Table I. ^b Calculated from analysis of aqueous solutions. ^c These data presented as $G(\text{ClO}^-)$ may contain a slight contribution from $G(\text{ClO}_2)$. Due to the strong $\text{ClO}_2(\text{g})$ odor of the irradiated samples and to the close agreement between these values and Burchill, *et al.*,⁸ values, it is felt that the great majority of the ClO_2 escaped from the finely divided samples before dissolution for analysis.

freeze-dried KClO_4 - KClO_3 standard (2.05 mol % KClO_4 in KClO_3 for this case). The remainder of the spectrum was identical with spectrum A and has been omitted for clarity. The two partially resolved peaks (1108 and 1095 cm^{-1}) are caused by different chlorine isotopes¹⁴ and show the resolution possible using a freeze-dried solid for the preparation of a mull. The slight loss of resolution of the 1108- cm^{-1} peak in spectrum B may have been caused by radiation damage in the solid (spectrum B represents sample no. 4, Table I, which was exposed to a dose of 14.0×10^{23} eV (mol of KClO_3)⁻¹). Samples exposed to lower doses yielded spectra with ClO_4^- peaks structurally indistinguishable from the peaks obtained with standards of comparable ClO_4^- content. No shift in frequency of the ClO_4^- peak was observed, as might have been expected if the ClO_4^- ion's lattice environment in the standard and in the sample had been appreciably different. The foregoing facts were considered sufficient evidence that (1) the freeze-dried KClO_4 - KClO_3 standards were truly representative of the γ -ray irradiated solid KClO_3 and (2) the calibration curve developed from the standards may be employed for a quantitative determination of ClO_4^- in the irradiated solid KClO_3 matrix.

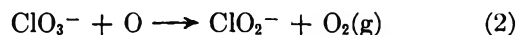
The data in Table I show that the amount of ClO_4^- found in the aqueous solutions was equal, within experimental error ($\pm ca. 10\%$), to the amount of ClO_4^- in the solid KClO_3 matrix before dissolution. This result indicates that no appreciable amounts ($\leq 10\%$ of the ClO_4^- formed) of unstable species which would hydrolyze to ClO_4^- (*e.g.*, Cl_2O_6 or ClO_3) are trapped in the solid KClO_3 matrix at room temperatures. It is further suggested that the Cl_2O_6 which Heal⁵ postulated "solely from the absorption spectra of crystals" does not exist and that the absorption peak he observed at 450 $\text{m}\mu$ was caused by ozonide ion, O_3^- . Evidence for O_3^- in crystalline halates has been obtained by many authors.^{4,18-22} This species would fit Heal's absorption peak, including even the fine structure he observed

at -196° , which is characteristic of O_3^- as observed in liquid ammonia solution.²³

The radiolytic and thermal decompositions²⁴ of the alkali metal chlorates are sufficiently alike to deserve comment. Appreciable yields of ClO_4^- and Cl^- ions and O_2 gas are produced in both reactions; however, in the thermolysis neither hypochlorite nor chlorite is observed, presumably because of their instability at the elevated temperatures required for the decomposition of chlorate ion. The yield of ClO_4^- ion in both reactions is significantly larger in KClO_3 than in NaClO_3 , suggesting that the addition of an oxygen atom by ClO_3^- ion is favored in the potassium salt. Formation of perchlorate by oxygen atom transfer during radiolysis



however, is not supported by the yield data (Table II) which show that the amount of chlorite formed is twice that for perchlorate. The yield of chlorite would be enhanced, however, by the abstraction reaction with oxygen atoms from the radiolysis



which would compete for oxygen atoms with the addition reaction



An additional supply of oxygen atoms will be produced

(18) P. W. Atkins, J. A. Brivati, N. Keen, M. C. R. Symons, and P. A. Trevalion, *J. Chem. Soc.*, 4785 (1962).

(19) C. Ramasastry, S. B. S. Sastry, Y. V. G. S. Murti, and J. Sobhanadri, *J. Phys. Soc. Jap.*, 19, 770 (1964).

(20) C. Ramasastry and S. B. S. Sastry, *ibid.*, 20, 2303 (1965).

(21) T. Andersen, J. R. Byberg, and K. J. Olsen, *J. Phys. Chem.*, 71, 4129 (1967).

(22) F. T. Gamble, *J. Chem. Phys.*, 47, 1193 (1967).

(23) A. J. Kacmarek, J. M. McDonough, and I. J. Solomon, *Inorg. Chem.*, 1, 659 (1962).

(24) M. M. Markowitz, D. A. Boryta, and H. Stewart, Jr., *J. Phys. Chem.*, 68, 2282 (1964).

by the decomposition of ClO_2^- (and ClO^-) at elevated temperatures thereby forming more ClO_4^- ion by reaction 3. This expectation is supported by the observation²⁴ that the residue from the thermal decomposition of KClO_3 at 566° contains 65.2% KClO_4 . The decomposition of ClO_2^- ion evidently occurs perceptibly even at much lower temperatures. Thermal bleaching experiments⁹ with X-ray irradiated KClO_3 have shown that additional ClO_4^- ion is produced on heating for as little as 1 hr at 150° , and further that the amount of ClO_2^- ion in the solid is decreased.

The nonlinearity of the increase in the concentration of perchlorate with dose (Table I) may be a consequence

of the decomposition of this ion by radiation. In the radiolysis of the pure, crystalline alkali metal perchlorates at room temperature, an initial yield for the decomposition of perchlorate, $G_0(-\text{ClO}_4^-) = 3.83$, was observed.²⁵ The primary product was chlorate which was formed with $G_0(\text{ClO}_3^-) = 2.99$.

Acknowledgment. It is a pleasure to acknowledge and thank M. M. Murray, Analytical Chemistry Division, and H. W. Morgan, Physics Division, for their interest and assistance during this research.

(25) L. A. Prince and E. R. Johnson, *J. Phys. Chem.*, **69**, 359 (1965).

Electrolyte-Solvent Interaction. XX. Picric Acid in Mixtures of Acetonitrile and Basic Solvents¹

by Alessandro D'Aprano² and Raymond M. Fuoss

Sterling Chemistry Laboratory of Yale University, New Haven, Connecticut 06520 (Received August 23, 1968)

The conductance of picric acid has been measured in the following mixed solvents: water-ethanol (WE), acetonitrile-ethanol (AE), acetonitrile-methanol (AM), and acetonitrile-water (WA). Association constants K_A were calculated from the data. In solvents WA and WE, K_A increases with decreasing dielectric constant D , but the $\log K_A - D^{-1}$ curves are sharply concave upward. In solvents AE and AM, association decreases with decreasing dielectric constant. Both characteristics conflict completely with theory based on electrostatic control of ion association. The assumption that four molecules of base ROH ($R = \text{H}, \text{CH}_3$, or C_2H_5) react with one molecule of picric acid, one to give the cation ROH_2^+ and three to solvate the three nitro groups of the picrate ion, leads to a conductance equation to which the data conform. The constant $K_B = [\text{ROH}_2^+][\text{X}^-]/[\text{HPi}][\text{ROH}]^4$, where X^- denotes the solvated picrate ion, is 2.5×10^{-5} for picric acid in water-acetonitrile, 4.0×10^{-7} in acetonitrile-methanol or acetonitrile-ethanol, and 0.4 in water-ethanol.

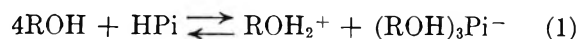
Picric acid is practically a nonconductor in acetonitrile, an aprotic solvent, and the solution is almost colorless. In water and the alcohols, however, the solutions are highly conducting and deep yellow. In order to investigate the reaction between picric acid and solvents which are basic relative to it, conductances were determined for solutions of picric acid in the following mixed solvents: acetonitrile-water, acetonitrile-methanol, acetonitrile-ethanol, and water-ethanol. The conductance increases sharply on the first addition of basic solvent to acetonitrile and continues to increase (at fixed picric acid concentration) as the content of basic solvent increases, regardless of whether the dielectric constant increases or decreases. This behavior is in marked contrast to that of normal electrolytes in mixed solvents and shows that more than electrostatics is involved. The conductance data nevertheless conform

to the familiar concentration function $\Lambda(c)$, which is based on long-range interionic forces and pairwise association of anions and cations. The data were therefore analyzed, in order to obtain limiting conductances and association constants; the latter are designated by K_A , *i.e.*, conductometric association constants, to distinguish them from K_A , the conventional ion-pair association constant whose logarithm increases linearly with reciprocal dielectric constant, D . The observed constant K_A must, of course, contain K_A as a factor, but our results show that it also contains a factor which is very sensitive to the concentration $[\text{ROH}]$ of basic sol-

(1) Acknowledgment is made for the support of this work by the Office of Saline Water, U. S. Department of the Interior, under Contract No. 14-01-0001-1308.

(2) On leave of absence from the University of Palermo, Palermo, Italy.

vent in the acetonitrile ($R = H, CH_3, \text{ or } C_2H_5$). Empirical analysis showed the presence of a factor in K_A which varies with the fourth power of $[ROH]$, which suggests that one molecule of base neutralized the acid to give the cation ROH_2^+ and that three more molecules solvated the three nitro groups of the anion. A conductance function based on normal long-range forces between free ions and a mass-action equilibrium describing the reaction



was derived; the observed results are in complete conformity with the theoretical equations. Further work is in progress; we expect to find three molecules of base necessary for dinitrophenols, two for *p*-nitrophenol, and one for acids whose anions do not solvate by ROH.

Experimental Section

Picric acid was recrystallized twice from ethanol, was vacuum dried at 40° for 2 days, and was stored over phosphorus pentoxide in a desiccator. Acetonitrile was stirred with calcium hydride³ for 3–5 days at room temperature and was then pumped through a sintered filter in a closed system into a flask containing phosphorus pentoxide. After standing overnight it was fractionally distilled from the pentoxide. All transfers were made by dry air or nitrogen pressure, and all openings to the air were protected by drying tubes. The vapor phase chromatogram of the acetonitrile, using a Chromosorb 102 column at 225° , was a single peak, with a very small blip at the water location corresponding to not more than 50 ppm of water. Methanol (Fisher's Spectraanalyzed grade) and ethanol (U. S. Industrial Chemical Co., absolute) were used as received. Water was from the laboratory still, specific conductance about $(1-2) \times 10^{-6}$ mho. All solutions were prepared by weight; volume concentrations (c , equiv/l.) of picric acid were calculated using solvent density. (With only a few exceptions, c was less than $0.005 N$). Considerable cooling was observed when water, methanol, or ethanol was added to acetonitrile.

Solvent properties are summarized in Table I. The first column gives identifying numbers for the water-acetonitrile (WA), water-ethanol (WE), acetonitrile-ethanol (AE), and acetonitrile-methanol (AM) mixtures used for the conductance measurements; w is the weight per cent of acetonitrile for mixtures containing that solvent and the weight per cent of ethanol in the WE systems. Dielectric constants, D , were measured at 1 Mc, using the General Radio Model 716-CS1 bridge and a stainless steel cell.⁴ Viscosities were measured in an Ubbelohde viscometer (water time, 473.1 sec at 25°), and densities were measured in a 20-ml Sprengel pycnometer. The last three columns give, respectively, density (ρ), viscosity (η), and solvent conductance (σ_0). In the systems containing water, no correction was made for solvent conductance, on the assumption

Table I: Properties of Solvents

No.	w	D	ρ	100η	$10^6\sigma_0$
Water-Acetonitrile					
1WA	0.00	78.54	0.9971	0.8903	1.66
2WA	22.08	69.22	0.9580	0.9745	1.33
3WA	53.60	53.96	0.8833	0.729	0.90
4WA	66.48	48.30	0.8543	0.597	0.64
5WA	75.91	44.53	0.8311	0.503	0.59
6WA	85.16	41.07	0.8098	0.424	0.54
7WA	90.24	39.21	0.7981	0.387	0.38
8WA	95.08	37.60	0.7882	0.361	0.17
9WA	97.08	36.89	0.7857	0.355	0.11
10WA	99.32	36.25	0.7799	0.349	0.04
Water-Ethanol					
1WE	66.02	39.44	0.8730	2.126	0.61
2WE	76.66	34.29	0.8480	1.860	0.53
3WE	84.02	30.94	0.8301	1.653	0.52
4WE	90.00	28.20	0.8140	1.466	0.49
5WE	96.08	26.07	0.7961	1.256	0.55
6WE	97.11	25.60	0.7937	1.223	0.48
7WE	98.09	25.18	0.7911	1.183	0.53
8WE	99.10	24.70	0.7880	1.139	0.54
Acetonitrile-Ethanol					
1AE	97.94	35.60	0.7771	0.347	0.16
2AE	89.79	34.55	0.7768	0.351	0.19
3AE	78.15	32.94	0.7796	0.366	0.34
4AE	70.48	31.96	0.7806	0.382	0.55
5AE	50.31	29.50	0.7827	0.453	0.83
6AE	29.82	27.41	0.7844	0.591	0.74
7AE	8.47	25.21	0.7850	0.885	0.61
8AE	0.00	24.30	0.7851	1.101	0.47
Acetonitrile-Methanol					
1AM	94.67	35.81	0.7771	0.340	0.44
2AM	90.66	35.64	0.7784	0.337	0.51
3AM	73.49	35.12	0.7812	0.336	0.66
4AM	0.00	32.63	0.7866	0.545	1.45

that the latter was due mainly to dissolved carbon dioxide; the dissociation of carbonic acid would be suppressed by the much stronger picric acid.

Most of the conductance measurements were made in an erlenmeyer-type cell⁴ with the constant 0.51361 determined by the Lind-Zwolenik-Fuoss (LZF)⁵ method by using aqueous solutions of potassium chloride. For systems which would give a resistance greater than about 20,000 ohms in this cell, a cell with a constant 0.038757 was used; the constant was determined by comparison with the first, using dilute aqueous sodium bicarbonate solutions. The bridge used has already been described.⁴ Resistances were measured at 2, 5, and 10 kHz and were extrapolated to infinite frequency

(3) J. F. Coetzee, G. P. Cunningham, D. K. McGuire, and G. R. Padmanabhan, *Anal. Chem.*, **34**, 1139 (1962).

(4) J. E. Lind, Jr., and R. M. Fuoss, *J. Phys. Chem.*, **65**, 999 (1961).

(5) J. E. Lind, Jr., J. J. Zwolenik, and R. M. Fuoss, *J. Amer. Chem. Soc.*, **81**, 1557 (1959).

after correcting for lead resistance and decade box errors.

For most of the systems, the dilution method was used. The solvent was pumped into the cell by dry air pressure, and after its resistance (parallel to 100,000 ohms) was determined, a sample of picric acid was weighed in. The cell was then placed in an oil thermostat at $25 \pm 0.003^\circ$; after temperature equilibrium, the resistance was measured. Then the cell was taken out, wiped, and washed. A portion of solvent was pumped in, and after thorough mixing, the cell plus the contents were weighed, then back to the thermostat, and so on. However, in systems high in acetonitrile (9WA, 10WA, 1-4AE, and 1-3AM), the dilution method could not be used, because the conductance changed slowly with time.⁶ For these systems, a batch of solvent was made up. To a weighed portion in the cell, already at temperature equilibrium, picric acid was weighed in. The resistance was measured at 2 kHz every 3 min for about 0.5 hr and was extrapolated back to zero time. For the next concentration, a fresh solution was made from another portion of the solvent and another sample of picric acid. This method, while tedious, avoids the errors of accumulative aging. In the solvents with lower acetonitrile contents, where the solution conductances were much higher, the conductance was perfectly steady; either the reactions producing the drift did not occur at higher water or alcohol contents or they went very quickly to completion, or else (and this seems most likely) the reactions were still going on, but any change in their contribution to the total conductance was too small to be observed.

The conductance data for the 30 systems studied are summarized in Tables II and III, where Λ is the equivalent conductance and c is the molarity of picric acid and where the systems are identified by the code in the first column of Table I. Several methods were used to derive the limiting conductance Λ_0 and the association constant K_A , depending on the magnitude of K_A . For systems 1-8WA and 1-8WE, the three-parameter equation⁷

$$\Lambda = \Lambda_0 - Sc^{1/2}\gamma^{1/2} + E'c\gamma \ln c\gamma + Jc\gamma - K_A c\gamma f^2 \Lambda \quad (2)$$

was used first. For the range of concentrations covered by our data, association was undetectable for systems 1-4WA and 1-4WE, so the data were reanalyzed using the two-parameter equation

$$\Lambda = \Lambda_0 - Sc^{1/2} + E'c \ln c + Jc \quad (3)$$

which is the limiting form of eq 2 when K_A is small or when γ is near unity.⁸ Systems 1-5WE were also analyzed using the empirical $c^{3/2}$ equation⁹

$$\Lambda = \Lambda_0 - Sc^{1/2} + E'c \ln c + Ac + Bc^{3/2} \quad (4)$$

The values of limiting conductance obtained by the three methods agreed within 0.1%. For picric acid in

Table II: Conductance of Picric Acid in Water-Acetonitrile and Water-Ethanol Mixtures at 25°

10%	A	10%	A	10%	A
1WA		7WA		3WE	
9.306	372.51	4.192	112.96	5.297	52.09
15.246	371.42	6.925	103.62	8.439	51.86
22.677	370.34	11.579	92.78	12.380	51.58
29.568	369.56	17.683	83.27	18.249	51.00
35.582	368.84	27.072	73.59	31.023	49.93
2WA		8WA		4WE	
7.239	280.25	6.749	46.46	5.370	46.08
12.302	279.70	11.092	37.81	7.771	45.62
19.232	279.33	17.339	31.20	11.060	45.21
33.635	278.16	27.285	25.52	15.435	44.84
		37.346	22.13	25.571	44.08
3WA		9WA		5WE	
5.364	185.52	12.662	13.02	5.651	41.89
9.860	183.99	22.814	9.81	9.215	40.70
16.199	182.60	38.163	7.63	13.328	39.55
22.895	181.42	48.203	6.82	18.649	38.24
36.753	179.47	70.162	5.55	28.002	36.38
4WA		10WA		6WE	
5.604	153.96	8.583	1.083	4.724	41.36
9.674	152.47	17.267	0.751	7.288	40.21
14.052	151.01	25.953	0.603	10.264	38.99
20.194	149.18	35.434	0.521	14.943	37.35
27.459	147.35	46.319	0.454	24.546	34.79
5WA		1WE		7WE	
5.573	137.29	4.490	76.10	4.355	40.23
9.069	135.03	7.087	76.02	6.788	38.66
13.599	132.54	10.281	75.96	9.561	37.07
19.849	129.61	14.927	75.87	14.295	34.86
30.640	125.48	27.143	75.27	24.029	31.62
6WA		2WE		8WE	
4.746	126.93	5.294	60.73	5.066	36.96
8.177	121.15	8.405	60.55	8.018	34.04
11.885	116.30	12.066	60.42	11.930	31.19
16.648	111.24	18.312	60.05	17.272	28.43
26.614	103.20	30.432	59.13	26.529	25.22

water, the three-parameter equation gave $\delta = 4.76$ for the contact distance. For the other systems where this equation was used, values of 1.0-3.6, with rather large uncertainty, were obtained; in our range of concentrations, the linear term was so small a fraction of the total conductance that no reliable δ value could be derived from it. For systems 5-8WA and 5-8WE, the three-

(6) A. D'Aprano and R. M. Fuoss, *J. Phys. Chem.*, **73**, 223 (1969).

(7) See eq 2.4, R. M. Fuoss, L. Onsager, and J. F. Skinner, *ibid.*, **69**, 2581 (1965) (Λ is the equivalent conductance, Λ_0 is the limiting conductance, c is the molarity, $1 - \gamma$ is the fraction associated to pairs, K_A is the conductimetric association constant, f is the Debye-Hückel activity coefficient, J is the empirical parameter, and S and E' are theoretical coefficients).

(8) See eq 2.1, R. M. Fuoss, L. Onsager, and J. F. Skinner, *ibid.*, **69**, 2581 (1965).

(9) R. M. Fuoss and K. L. Hsia, *Proc. Nat. Acad. Sci. U. S. A.*, **57**, 1550; **58**, 1818 (1967).

Table III: Conductance of Picric Acid in Acetonitrile-Ethanol and Acetonitrile-Methanol Mixtures at 25°

10 ⁴ c	Δ	10 ⁴ c	Δ	10 ⁴ c	Δ
1AE		5AE		1AM	
6.915	0.485	4.540	45.28	13.21	1.480
20.891	0.288	7.827	36.92	26.43	1.079
29.343	0.248	11.231	31.98	40.52	0.880
33.507	0.231	16.444	27.33	51.92	0.788
54.351	0.184	25.458	22.69	74.00	0.661
2AE		6AE		2AM	
11.651	4.117	5.304	49.87	19.28	3.181
17.248	3.383	8.591	42.29	42.05	2.183
26.755	2.725	12.205	37.17	62.61	1.792
32.746	2.468	18.122	31.93	77.36	1.621
46.247	2.080	31.023	25.72	93.86	1.474
3AE		7AE		3AM	
11.085	13.16	5.776	41.91	12.06	21.00
18.499	10.34	9.088	35.95	20.59	16.39
29.168	8.32	13.836	30.86	28.63	14.05
33.391	7.79	21.554	26.03	40.73	11.90
44.213	6.82	32.197	22.18	49.65	10.84
4AE		8AE		4AM	
7.916	22.79	6.267	31.15	5.141	82.67
14.205	17.72	10.785	25.74	7.651	73.00
27.066	12.81	15.840	22.22	10.831	64.82
31.998	11.85	22.759	19.20	16.392	55.69
37.664	10.98	38.266	15.52	25.632	46.82

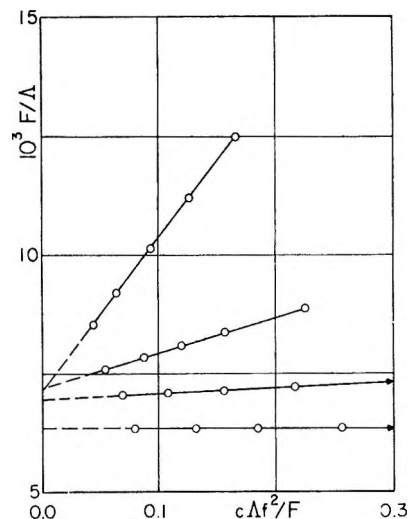
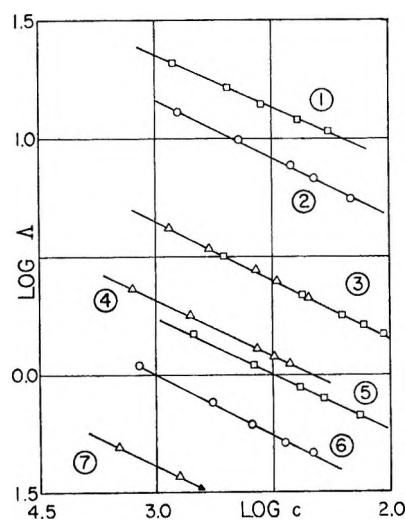
parameter equation gave nontrivial values of association constants. Since the range of concentration was kept low, we also used a simpler limiting form¹⁰ of eq 2

$$\Lambda = \gamma(\Lambda_0 - Sc^{1/2}\gamma^{1/2}) \quad (5)$$

in which the linear and $c \ln c$ terms (of opposite sign) are neglected; eq 5 was applied to data for systems 4-8WA, 5-8AE, and 4AM. Typical $F/\Lambda - c\Delta f^2/F$ plots are shown in Figure 1; the intercept is $1/\Lambda_0$ and the slope is K_A/Λ_0^2 . For the acetonitrile-rich systems 9WA, 10WA, 1-4AE, and 1-3AM, association was so high that extrapolation to zero concentration was impossible. For these systems, a plot of $\log \Lambda$ against $\log c$ was linear, with slope equal to -0.5 , as shown in Figure 2. Using the Arrhenius approximation $\gamma = \Lambda/\Lambda_0$ (i.e., neglecting the effects of long-range electrostatic forces), the mass-action equation reduces to

$$c\Lambda^2 = \Lambda_0^2/K_A \quad (6)$$

which predicts a slope of -0.5 for the log-log plots and calls for constancy of the $c\Lambda^2$ product. By a short extrapolation of plots of Walden product $\Lambda_0\eta$ against mole fraction of acetonitrile, values of Λ_0 could be estimated for these systems, and then from the average of $c\Lambda^2$ for a given system, the corresponding association constant was calculated. A summary of the derived constants is given in Table IV. The method used to

Figure 1. Determination of Λ_0 and K_A for systems 7WA (top), and 6WA, 5WA, and 4WA (bottom).Figure 2. Conductance plots for: 1, 3AM; 3, 2AM; 5, 1AM; 2, 9WA; 6, 10WA; 3, 2AE; 4, 4AE; 7, 1AE. (Line 4 ordinate is $\log \Lambda - 1.0$.)**Table IV:** Derived Constants

No.	Λ_0	K_A	No.	Λ_0	K_A
1WA ³	376.9	...	6WE ²	45.6	45
2WA ³	283.7	...	7WE ²	45.6	150
3WA ³	189.4	...	8WE ²	47.8	610
4WA ⁵	159.1	6	1AE ⁶	(150)	1.28×10^8
5WA ⁵	144.3	26	2AE ⁶	(144)	1.04×10^8
6WA ⁵	139.9	150	3AE ⁶	(134)	8.99×10^4
7WA ⁵	140.3	630	4AE ⁶	(127)	3.66×10^4
8WA ⁵	147.1	1.06×10^4	5AE ⁵	108.7	7.74×10^3
9WA ⁶	(148)	1.00×10^6	6AE ⁵	108.7	5.10×10^3
10WA ⁶	(151)	2.36×10^7	7AE ⁵	90.9	4.84×10^3
1WE ⁴	77.0	...	8AE ⁵	74.1	5.83×10^3
2WE ⁴	62.0	...	1AM ⁶	(160)	8.24×10^6
3WE ⁴	53.8	...	2AM ⁶	(159)	1.26×10^6
4WE ⁴	48.4	...	3AM ⁶	(158)	4.45×10^4
5WE ²	45.8	...	4AM ⁶	156.3	3.96×10^3

(10) R. M. Fuoss, *J. Amer. Chem. Soc.*, 57, 488 (1935).

evaluate the constants is shown by the superscripts on the system symbols in the table; for example, 4AE⁶ means that eq 6 was used for system 4 in the acetonitrile-ethanol series. Limiting conductances in parentheses are values estimated by Walden's rule.

Discussion

In the case of ionophores, the formation of ion pairs is controlled by electrostatic forces, *i.e.*, by ionic charge ϵ , center-to-center distance at contact a , and dielectric constant D , for a system represented by rigid charged spheres of diameter a in a dielectric continuum. For this model¹¹

$$K_A = K_0 \exp(\epsilon^2/aDkT) = K_0 e^b \quad (7)$$

and a plot of the logarithm of the association constant against the reciprocal dielectric constant is linear with a positive slope. Many examples of systems describable by eq 7 are known, such as the alkali halides in dioxane-water mixtures of dielectric constant below about 25.^{4,9,12} Figure 3 is a plot of $\log K_A$ against $1/D$ for the data of Tables II and III. Most briefly described, the curves do not conform to eq 7 at all: they are not linear, but strongly curved, and two of them have negative slopes instead of positive. In the case of the acetonitrile-water and ethanol-water systems, decreasing dielectric constant does indeed increase the association but the slopes are not constant and are much greater than would correspond to any reasonable value of a in eq 7. For the acetonitrile-methanol and acetonitrile-ethanol systems, association decreases as D decreases, precisely the opposite of what electrostatics would require. The WA curve appears to be approaching from the left a vertical asymptote at 0.0278, the reciprocal of the dielectric constant of acetonitrile, while the AE and AM curves approach it from the right. Clearly, another mechanism controls association in all these examples.

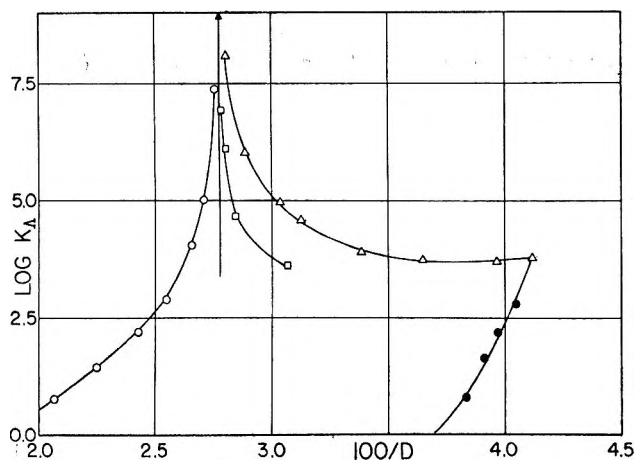


Figure 3. Association constants for picric acid in water-acetonitrile (O), acetonitrile-methanol (□), acetonitrile-ethanol (Δ), and water-ethanol (●) mixtures.

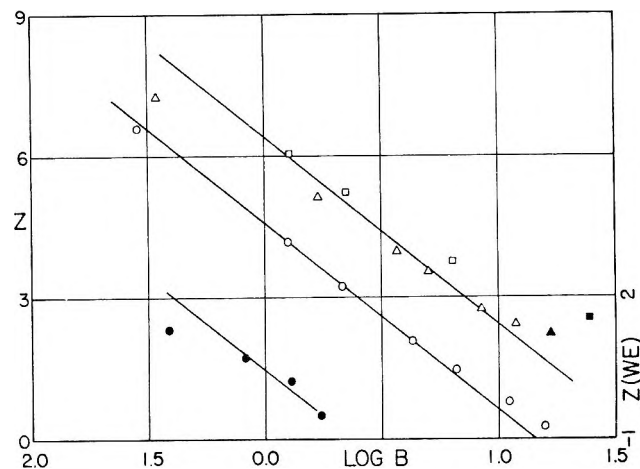
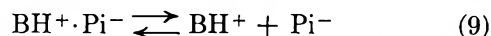
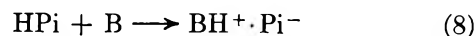


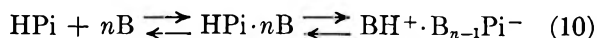
Figure 4. Test of eq 22. The symbols have the same meaning as in Figure 3.

Picric acid is practically a nonconductor in pure acetonitrile; Kolthoff¹³ has shown by measurements in buffered solutions that its pK is 11.0; in other words, acetonitrile is an extremely weak base with respect to picric acid. This value would give a point at 11.0 in Figure 4, indicated by the arrow and the abscissa corresponding to pure acetonitrile. (The conductances previously reported in the literature for picric acid in acetonitrile⁶ are actually the conductances of solutions of unknown concentration of ammonium picrate, produced by the reaction of the picric acid with traces of ammonia deriving from hydrolysis of the solvent.) Both water and the alcohols are much stronger bases than acetonitrile; we might expect them to react in our mixtures (where the base is far in excess over the picric acid) to give a complex which would rearrange to an ion pair, which then dissociates. Stated another way, picric acid is an ionogen in acetonitrile, which produces a conducting ionic species on addition of base. But if the reactions were simply



electrostatics should control and the curves of Figure 3 should still be linear with a positive slope. Obviously, reactions 8 and 9 do not describe the observed results.

Consider a reversible reaction between molecular picric acid and base, followed or accompanied by solvation, to give a complex which can rearrange to an ion pair which then behaves normally, *i.e.*, conforms to eq 2. Let B denote water, methanol, or ethanol; then the reactions



(11) R. M. Fuoss, *J. Amer. Chem. Soc.*, **80**, 5059 (1958).

(12) K. L. Hsia and R. M. Fuoss, *ibid.*, **90**, 3055 (1968).

(13) I. M. Kolthoff and M. K. Chantooni, *ibid.*, **87**, 4428 (1965).

are described by the mass-action equations

$$K_S = [\text{BH}^+ \cdot \text{X}^-] / [\text{HPi}]B^n \quad (12)$$

$$K_A = [\text{BH}^+ \cdot \text{X}^-] / [\text{BH}^+][\text{X}^-] \quad (13)$$

where X^- represents $\text{B}_{n-1}\text{Pi}^-$, B is the activity of base, and the bracketed symbols indicated the activities of the corresponding species. The constant K_S actually combines the three reaction constants for (1) the neutralization of picric acid by base B , (2) the solvation of $B \cdot \text{HPi}$ by a base, and (3) the rearrangement of $B \cdot \text{HPi} \cdot (n-1)B$ to $\text{BH}^+ \cdot \text{B}_{n-1}\text{Pi}^-$. Not excluded would be the sequence neutralization (1), rearrangement (2), and solvation (3) or other permutations of processes 1-3. There is no point in trying to resolve K_S into its factors, because conductance can only determine the lumped constant. The constant K_A is the normal association constant for the ion pair formed between the protonated base and the solvated anion $\text{B}_{n-1}\text{Pi}^-$. If α , β , and γ represent concentrations relative to the stoichiometric total picric acid of the species molecular picric acid HPi , complex $\text{HPi} \cdot nB = (\text{BH}^+ \cdot \text{X}^-)$, and solvated picrate ion X^- , mass balance requires that

$$\alpha + \beta + \gamma = 1 \quad (14)$$

and electroneutrality requires that

$$[\text{X}^-] = [\text{BH}^+] = c\gamma f \quad (15)$$

Combining the above equations by eliminating α and β , we obtain the quadratic in γ

$$cf^2K_A(1 + 1/K_S B^n)\gamma^2 + \gamma - 1 = 0 \quad (16)$$

if we approximate activities in eq 12 by concentrations. If the coefficient of $c\gamma^2$ in eq 16 is represented by A , the solution is

$$\gamma = [(1 + 4Ac)^{1/2} - 1] / 2Ac \quad (17)$$

This has precisely the same form as the solution of the ion-pair quadratic, where A is $K_A f^2$. The conducting species here are BH^+ and X^- ; their conductance at low concentrations is given by eq 2, the usual conductance equation, where the conductometric association constant K_A is the coefficient of $cf^2\gamma^2$ in eq 16; therefore, the observed association constant K_A is given by

$$K_A = K_A[1 + (1/K_S B^n)] \quad (18)$$

$$= K_0 e^b [1 + (1/K_S B^n)] \quad (19)$$

that is, K_A is the electrostatic pair constant multiplied by a factor which depends on the base concentration and K_S . A study of the association constants K_A of Table IV suggested that $K_S B^n$ was very small compared with unity; neglecting 1 in the quantity in brackets in eq 19 and taking logarithms gives

$$\log K_A \approx \log K_0 + 0.434b - \log K_S - n \log B \quad (20)$$

Defining a variable Z by

$$Z = \log K_A - \log K_0 - 0.434b \quad (21)$$

we see that the hypothesis represented by reactions 10 and 11 requires that

$$Z = -\log K_S - n \log B \quad (22)$$

This means that a plot of Z against the logarithm of the molar concentration of the base (water or alcohol) in the acetonitrile-base systems should be linear, with a slope n which specifies the number of molecules of base involved in eq 10 and with an intercept at $B = 1$ which determines K_S , the solvation constant. Figure 4 is such a plot for picric acid in the various mixed solvents and in methanol and ethanol. For K_0 , the theoretical¹¹ excluded-volume factor $4\pi N a^3 / 3000 = 0.002453 \bar{a}^3$ was used, with $\bar{a} = 4.8$, and $0.434b$ was set equal to $50.5D$, corresponding to the same value of \bar{a} . The points for the water-acetonitrile systems lie on a line with slope equal to 4.0 over a range of six decades in K_S . The alcohol-acetonitrile points can also be averaged by a line of slope 4; the points corresponding to 100% alcohol (solid square and triangle in Figure 4) are high but these systems are not mixtures.¹⁴ The AM points lie perhaps a little higher than the AE points, but within the experimental error, the difference is not significant; since the active group is the hydroxyl, we would expect methanol and ethanol to be quite similar in base strength and much weaker than water. From the intercepts at $\log B = 0$, we find that $K_S = 2.5 \times 10^{-5}$ for the water-acetonitrile systems and 4.0×10^{-7} for the alcohol-acetonitrile systems.

These results show that four molecules of base are involved in reaction 10, which of course suggests that one molecule neutralizes the active hydrogen of picric acid to form H_3O^+ or ROH_2^+ and that three more molecules solvate the three nitro groups of the anion, by hydrogen bonding to the negative oxygens. As might be expected on this basis, water with two protons gives a more stable complex than the alcohols. (One factor in K_S is the dissociation constant of the complex B_3Pi^- .) Dispersion forces due to delocalization of electronic oscillators in the picrate ion¹⁵ also contribute to the stability of the complex.

A similar analysis for the water-ethanol systems might appear to be hopelessly complicated, because two solvating species are competing for four reaction sites. However, given the factor of over 100 favoring water, we may test the hypothesis that in these mixtures the ethanol acts as an inert solvent, like acetonitrile in the other mixtures. The solid circles in Figure 4 (ordinates to the right) are points calculated on this

(14) Our value of K_A for picric acid in methanol corresponds to $pK_A = 3.60$, in fair agreement with the value of 3.80, H. Goldschmidt and H. Aarflot, *Z. Phys. Chem. (Leipzig)*, **A117**, 317 (1925). For ethanol, we have a value of $pK_A = 3.76$. From the rate of formation of diethyl acetal in absolute ethanol, catalyzed by picric acid, $pK_A = 4.0$, A. J. Deyrup, *J. Amer. Chem. Soc.*, **56**, 60 (1934).

(15) E. Grunwald and E. Price, *ibid.*, **86**, 4517 (1964).

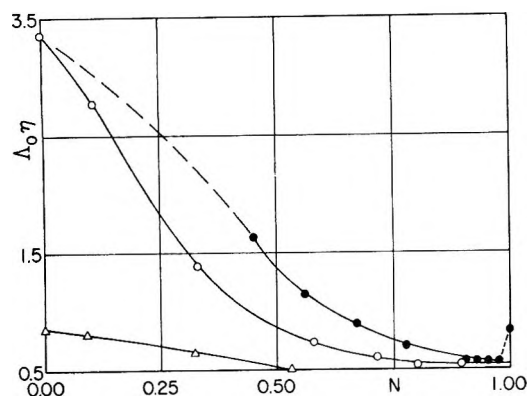


Figure 5. Walden products for picric acid in mixed solvents. The symbols have the same meaning as in Figure 3.

basis; the line is drawn with a slope of 4. Except for the point for the lowest water concentration (0.90%, where experimental errors are large), the assumption that water solvates picric acid in ethanol in the same way as in acetonitrile seems verified ($K_s = 0.4$). It would be interesting to extend the water-ethanol and water-acetonitrile curves to the pure-water point, which lies off-scale to the left and down on Figure 3; pK_a for picric acid in water¹⁶ is 0.2–0.3.

Finally we consider the mobilities. Figure 5 is a plot of the Walden product $\Lambda_0\eta$ against the mole fraction of acetonitrile (or ethanol, in the case of the water-ethanol mixtures). The product is abnormally high in the two mixtures containing water, on account of the added conductivity due to proton jumps in the water-rich systems. The product is also high in ethanol (0.815) compared with the value of about 0.5 in solvent mixtures where proton jumps cannot occur. The abrupt drop which appears on the initial addition of water to picric acid in ethanol confirms the result that water forms a more stable solvate with the picrate ion than does ethanol and suggests that the ethanol complex is somewhat labile, exchanging solvate ethanol with free ethanol rather easily, so that the migrating species is effectively the bare anion. The dependence of mobility on composition is much smaller in the acetonitrile-ethanol system, where proton jumps contribute little to conductance beyond 0.5 mol fraction of acetonitrile.

(16) The value of 0.3 was obtained from R. G. Bates and G. Schwarzenbach, *Experientia*, 10, 482 (1954), and the value of 0.2 was obtained from G. Kortüm and H. Wilski, *Z. Phys. Chem. (Frankfurt am Main)*, 2, 256 (1954).

The Importance of Lone-Pair Electrons in the Intramolecular

Potential Function of Group V Hydrides and Trihalides^{1a}

by Shih-Tung King^{1b} and John Overend

Molecular Spectroscopy Laboratory, School of Chemistry, University of Minnesota, Minneapolis, Minnesota 55455
(Received August 23, 1968)

A potential function for XY_3 molecules is described in which the nonbonded interaction between the Y atoms and the lone pair on the central X atom is included as a pseudo-Urey-Bradley force constant. Numerical values of this interaction parameter are determined for a range of molecules where X is a group V atom and Y is H, F, Cl, Br, or I. The lone-pair, Y force is attractive when Y = H and repulsive in the remaining cases.

Introduction

Pariseau, Wu, and Overend have shown that the Urey-Bradley force field (UBFF) can be modified to take into account the forces between the hydrogen atoms and the lone pair of electrons in the ammonia molecule.^{2a} These forces, represented as Urey-Bradley interactions, enter the internuclear potential energy through the factoring of the kinetic and potential energy matrices, and contribute in this way to the vibrational frequencies of the molecule. It is therefore pos-

sible, in principle, to determine the magnitude of the forces between the lone pair and the hydrogens from the vibrational frequencies by adjusting the force constants in the internuclear potential. In their treatment of the problem, however, Pariseau, Wu, and Overend^{2a} did

(1) (a) Based on a dissertation submitted by S-T. King in partial fulfillment of the requirements for the degree of Ph.D. (b) Chemical Physics Research Laboratory, The Dow Chemical Co., Midland, Mich.

(2) (a) M. Pariseau, E. Wu, and J. Overend, *J. Chem. Phys.*, 39, 217 (1963); (b) J. Overend and J. R. Scherer, *ibid.*, 33, 446 (1960).

not adjust the force constants associated with the lone pair of electrons since the relationships between these force constants and the ones in the working symmetry coordinates are nonlinear and cannot be handled in the usual formalism of perturbation theory.^{2b} Rather, they used the model described above to select certain non-Urey-Bradley force constants with which to augment the basic UBFF and later interpreted these non-Urey-Bradley force constants in terms of the lone-pair interactions.

Curtis and Muirhead³ have applied a similar procedure to NF_3 molecule. Because there are only four observed frequencies which can be used for NF_3 , they cannot uniquely determine more than four force constants from the observed frequencies. Only a range of values was estimated for each force constant.

We have now programmed a "stepwise adjustment" algorithm which allows the refinement of force constants, even though they be curvilinearly related to the working force constants. We have reexamined the hydrides of the group V elements and have extended the treatment to the group V halides. We present here the results of these calculations.

The Potential Energy Function

The primitive force field is written, in terms of the coordinates defined in Figure 1, as

$$2V = \sum_{i=1}^3 [2K_r' \Delta r_i + K_r (\Delta r_i)^2 + 2H_{\alpha'} \Delta \alpha_i + H_{\alpha} (\Delta \alpha_i)^2 + 2F_{\alpha'} q_{\alpha_i}^0 \Delta q_{\alpha_i} + F_{\alpha} (\Delta q_{\alpha_i})^2] + 2K_e' \Delta \xi + K_e (\Delta \xi)^2 + \sum_{i=1}^3 [2H_{\beta'} \Delta \beta_i + H_{\beta} (\Delta \beta_i)^2 + 2F_{\beta'} q_{\beta_i}^0 \Delta q_{\beta_i} + F_{\beta} (\Delta q_{\beta_i})^2] \quad (1)$$

The first six terms arise from the molecular skeleton and represent forces between the nuclei; the last six terms are the interactions of the nuclei with the lone pair of

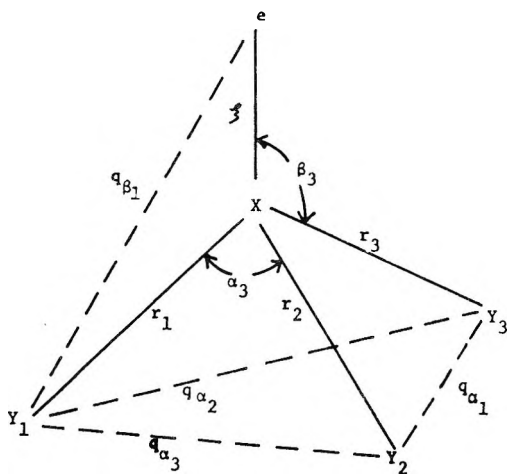


Figure 1. Internal coordinates used for the XY_3 molecule with the lone pair of electrons indicated by e.

electrons, taken as a point mass. Symmetry coordinates are defined as

$$S_1^{(a)} = 3^{-1/2}(\Delta r_1 + \Delta r_2 + \Delta r_3) \\ S_2^{(a)} = 3^{-1/2}(\Delta \alpha_1 + \Delta \alpha_2 + \Delta \alpha_3) \\ S_3^{(a)} = \Delta \xi$$

$$S_4^{(a)} = a(\Delta \alpha_1 + \Delta \alpha_2 + \Delta \alpha_3) + b(\Delta \beta_1 + \Delta \beta_2 + \Delta \beta_3)$$

$$S_1^{(e,a)} = 2^{-1/2}(\Delta r_2 - \Delta r_3)$$

$$S_2^{(e,a)} = 2^{-1/2}(\Delta \alpha_2 - \Delta \alpha_3)$$

$$S_3^{(e,a)} = 2^{-1/2}(-\Delta \beta_2 + \Delta \beta_3)$$

$$S_1^{(e,b)} = 6^{-1/2}(2\Delta r_1 - \Delta r_2 - \Delta r_3)$$

$$S_2^{(e,b)} = 6^{-1/2}(2\Delta \alpha_1 - \Delta \alpha_2 - \Delta \alpha_3)$$

and

$$S_3^{(e,b)} = 6^{-1/2}(-2\Delta \beta_1 + \Delta \beta_2 + \Delta \beta_3) \quad (2)$$

where $a = 2 \sin \alpha (\cos^2 \beta - \cos \alpha) (\cos \alpha - 1)$, $b = 2 \sin \beta \cos \beta (1 - \cos \alpha)^2$ are coefficients in the redundant coordinate S_4 . Although these symmetry coordinates are not orthogonal, the definition does separate exactly the coordinates of the lone pair and allows the coordinates and momenta of the lone pair to be split out of the Hamiltonian. Moreover, when this is done, the remaining symmetry coordinates, $S_1^{(a)}$, $S_2^{(a)}$, $S_1^{(e,a)}$, $S_2^{(e,a)}$, $S_1^{(e,b)}$, and $S_2^{(e,b)}$ are the symmetry coordinates usually written for a pyramidal XY_3 molecule.

The treatment of the potential energy is described fully in ref 2a. Briefly, the UBFF of the primitive model shown in Figure 1 is set up and the Urey-Bradley redundancies are removed to give a 9×9 matrix \mathbf{F} in the coordinates defined in Figure 1. After removing the coordinates and the momenta associated with the lone pair, we obtain an \mathbf{F} matrix which is factored into two 2×2 blocks. The elements of the first block, used with the coordinates $S_1^{(a)}$ and $S_2^{(a)}$ are

$$\mathbf{F}_{11}^{(a)} = F_{rr} + 2F_{rr'} - 3(F_{\xi r})^2/F_{\xi\xi} \quad (3)$$

$$\mathbf{F}_{12}^{(a)} = 2F_{r\alpha'} - (a/b)F_{r\beta} + 3(a/b)F_{\xi r}F_{\xi\beta}/F_{\xi\xi} \quad (4)$$

$$\mathbf{F}_{22}^{(a)} = F_{\alpha\alpha} + 2F_{\alpha\alpha'} - 4(a/b)F_{\alpha\beta'} + (a/b)^2(F_{\beta\beta} + 2F_{\beta\beta'}) - 3(a/b)^2(F_{\xi\beta})^2/F_{\xi\xi} \quad (5)$$

and the elements of the second block, used with the coordinates $S_1^{(e)}$ and $S_2^{(e)}$ are

$$\mathbf{F}_{11}^{(e)} = F_{rr} - F_{rr'} - (F_{r\beta})^2/F_{\beta\beta} - F_{\beta\beta'} \quad (6)$$

$$\mathbf{F}_{12}^{(e)} = -F_{r\alpha'} + F_{\alpha\beta'}F_{r\beta}/(F_{\beta\beta} - F_{\beta\beta'}) \quad (7)$$

$$\mathbf{F}_{22}^{(e)} = F_{\alpha\alpha} - F_{\alpha\alpha'} - (F_{\alpha\beta'})^2/(F_{\beta\beta} - F_{\beta\beta'}) \quad (8)$$

The F' in eq 3-8 represents the interaction between the internal coordinates with different subscripts. For

(3) E. C. Curtis and J. S. Muirhead, *J. Phys. Chem.*, **70**, 3330 (1966).

example, $F_{\alpha\beta}'$ is element in \mathbf{F} matrix for $\Delta\alpha_i$ and $\Delta\beta_j$, $i \neq j$. These matrix elements are used with an ordinary symmetrized \mathbf{G} matrix for the calculation of normal coordinates and vibrational frequencies. The procedure is straightforward and is carried out with standard computer programs.

Since the relationships in eq 3-8 are nonlinear, difficulties arise if we wish to adjust the parameters in the primitive force field (*i.e.*, the parameters in eq 1) to the vibrational frequencies using the customary first-order perturbation approach. Pariseau, Wu, and Overend avoided this problem by using the lone-pair model to suggest relationships between the elements of \mathbf{F} , and did not attempt to adjust the primitive force constants. In the present work we have used, instead of the least-squares adjustment, a stepwise procedure based on an algorithm described by Powell,⁴ and in this way have been able to determine numerical values for the force constants defined in eq 1.

Group V Trihydrides

In our simple model, we think of the primary interaction between the lone pair and the remainder of the molecule as a coulombic interaction with the hydrogen nuclei; this interaction is expressed in the force constant F_β . The other force constants H_β (lone-pair-bending) and κ (tension of the tetrahedral angle⁵) are considered to be of secondary importance; setting them equal to zero corresponds to neglecting the forces, over and above the coulombic forces which oppose the bending of the lone-pair orbital from its symmetrical configuration. K_e may be thought of as the effective stretching force constant of the lone pair, *i.e.*, as $\partial^2 V / \partial \xi^2$ when the lone pair of electrons is pulled off the central nucleus. It seems reasonable that the value of K_e be quite large and we have, as a first approximation, set it equal to infinity. We did explore the effect on the other force constants of varying K_e . Numerical results are given in Table I, and in Figure 2 we show plots of the refined force constants of NH_3 as a function of the assumed value of K_e . Our conclusion is that the assumption $K_e = \infty$ does not significantly affect the values of the other force constants determined in the present study. The total number of force constants was reduced further⁶ by setting $F_{\alpha'} = -1/10 F_\alpha$ and $F_{\beta'} = -1/10 F_\beta$.

The force constants K_r (X-H bonding), H_α (HXH bending), F_α (H, H interaction), and F_β were adjusted to fit the eight harmonic frequencies of XH_3 and XD_3 given in ref 2a. The results are displayed in Tables I and II. The calculated frequencies differ from the observed ones by less than 1%.

It is not clear what should be used for the effective distance of the lone pair from the parent atom. We have carried out calculations using the Bohr radius of the H atom (0.54 Å) and the covalent bond distance of the center atom. We show both sets of results in

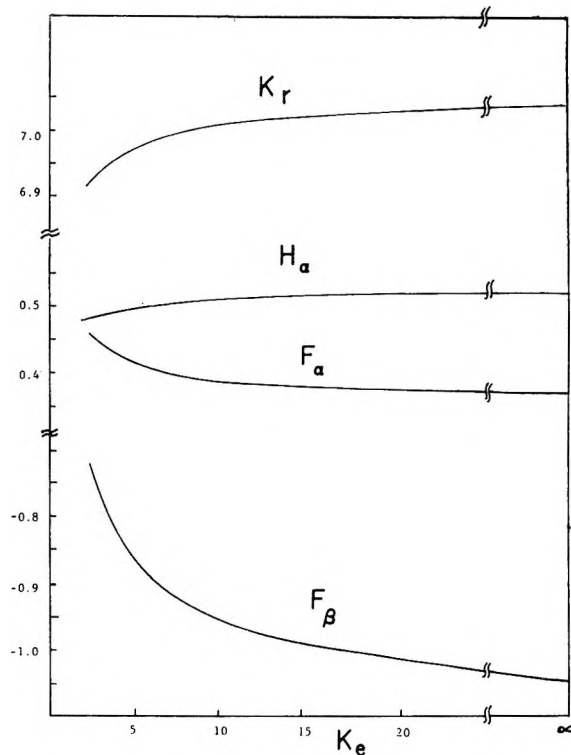


Figure 2. NH_3 , values of force constants K_r , H_α , F_α , and F_β as functional of the assumed value of K_e . $H_\beta = \kappa = 0$; ξ , the distance of the lone pair from the nitrogen nucleus, is taken to be 0.54 Å. Units: K_e , K_r , F_α , and F_β in $\text{mdyn } \text{Å} / (\text{radian})^2$, H_α in $\text{mdyn } \text{Å} / (\text{radian})^2$.

Table I. However, we prefer the second assumption and have used this in most of the present work.

If, as seems reasonable, the H atom in the XH_3 molecule has a partial positive charge,⁷ the interaction between the lone pair of electrons and the hydrogen nucleus is attractive and the force constant F_β has negative values. The results of our calculation are consistent with this; *cf.* Table I. The value of F_β changes from about -1.0 to -0.1 $\text{mdyn}/\text{Å}$ as we change X from N to Sb.

It is interesting to examine the numerical relationship between the force constant F_β and the spectroscopic data from which the force constants are determined. The change in each vibrational frequency, corresponding to a 0.1 $\text{mdyn}/\text{Å}$ change in K_r , F_α , and F_β or a 0.1 $\text{mdyn } \text{Å} / (\text{radian})^2$ change in H_α , is given in Table III. In each molecule, the antisymmetric deformation ν_4 does not depend on F_β ; the reason is obvious when one considers that the normal coordinate corresponds mainly to the symmetry coordinate $S_2^{(e)}$ in which the

(4) M. J. D. Powell, *Computer J.*, **7**, 155, 303 (1965).

(5) B. Crawford, Jr., and J. Overend, *J. Mol. Spectrosc.*, **12**, 307 (1964).

(6) Y. Morino, K. Kuchitsu, and T. Shimanouchi, *J. Chem. Phys.*, **20**, 726 (1952).

(7) V. Schomaker and C. S. Lu, *J. Amer. Chem. Soc.*, **72**, 1182 (1950).

Table I: Force Constants of Group V Hydrides, Adjusted to Fit the Harmonic Frequencies of XH_3 and XD_3 in Ref 2^a

Molecules	K_r , mdyn/Å	$H\alpha$, mdyn Å/ (radian) ²	$F\alpha$, mdyn/Å	$F\beta$, mdyn/Å	ξ , Å	$q\beta$, Å
$K_e = 3.0$ mdyn/Å						
NH_3 , ND_3	6.946	0.487	0.451	-0.757	0.54	1.3138
PH_3 , PD_3	3.277	0.455	0.295	-0.381	0.54	1.7703
AsH_3 , AsD_3	2.936	0.595	0.076	-0.219	0.54	1.8780
SbH_3 , SbD_3	2.334	0.427	0.119	-0.245	0.54	2.0643
$K_e = \infty$						
NH_3 , ND_3	7.048	0.524	0.361	-1.061	0.54	1.3138
PH_3 , PD_3	3.314	0.477	0.273	-0.468	0.54	1.7703
AsH_3 , AsD_3	2.946	0.606	0.067	-0.240	0.54	1.8780
SbH_3 , SbD_3	2.348	0.441	0.110	-0.275	0.54	2.0643
NH_3 , ND_3	7.040	0.540	0.324	-0.966	0.6	1.3566
PH_3 , PD_3	3.282	0.551	0.198	-0.283	1.1	2.2163
AsH_3 , AsD_3	2.920	0.671	0.014	-0.107	1.21	2.4157
SbH_3 , SbD_3	2.315	0.529	0.053	-0.124	1.41	2.7626

^a The force constants and the quantities of ξ and $q\beta$ are defined in Figure 1 and eq 1.

Table II: Group V Hydrides. Harmonic Frequencies (in cm^{-1}) Compared with (i) Those Calculated Using the Force Constants in Table I and (ii) Those Calculated Using a Simple UBFF ($\Delta\nu\%$ = $(\nu_{obsd} - \nu_{calcd}) \times 1000/\nu_{obsd}$)

i	XH_3			XD_3			
	ν_{obsd}	$\Delta\nu\%$ (i)	$\Delta\nu\%$ (ii)	ν_{obsd}	$\Delta\nu\%$ (i)	$\Delta\nu\%$ (ii)	
NH_3	1	3506	0.12	-3.33	2495	-0.12	-3.79
	2	1021.5	-0.94	-7.64	792.6	0.99	-5.37
	3	3577	-0.35	3.56	2651.6	0.36	4.41
	4	1691	0.07	10.65	1225	-0.10	10.34
PH_3	1	2448	-0.39	-1.64	1760	0.41	-0.98
	2	1045	0.39	-2.27	759	0.41	-2.92
	3	2390	-0.02	2.70	...	-0.38	2.35
	4	1153	0.11	3.19	822	-0.08	3.00
AsH_3	1	2209.2	-0.01	0.23	1571.2	0.01	0.10
	2	973.3	0.13	-1.01	696.3	-0.13	-1.14
	3	2225.8	0.08	-0.07	1582.4	-0.08	-0.26
	4	1012	-0.04	1.09	718.6	0.04	1.19
SbH_3	1	1989	0.07	-0.11	1409	-0.07	-0.33
	2	796	-0.07	-2.22	569	0.07	-2.00
	3	1975	-0.05	0.19	1404	0.05	0.27
	4	845	-0.07	2.29	600	0.07	2.44

motion of the hydrogen atoms is on a circle passing through their equilibrium positions and in this normal coordinate the hydrogen nuclei remain at almost constant distance from the lone pair. The strongest dependence on $F\beta$ is shown by ν_1 and ν_2 , the totally symmetric stretching and deformation modes, and it is these frequencies which principally determine $F\beta$.

In Table II, we also show the percentage errors in the frequencies when the basic UBFF is used without the extra force constant $F\beta$. The large percentage errors, compared with those obtained when $F\beta$ is admitted, clearly show that the introduction of $F\beta$ makes a substantial improvement in the potential function and suggest that the forces associated with the lone

pair do have a significant effect on the vibrational spectrum.

The present values of $F\beta$ may be compared with those expected from the electron hydrogen atom potential derived by Gorin, Walter, and Eyring^{8,9}

$$V_H = -\frac{e^2}{a_0} \left[1 + \frac{a_0}{r} \right] \exp \left[\frac{-2r}{a_0} \right]$$

where e is the electronic charge, a_0 is the Bohr radius, and r is the distance of the electron from the hydrogen

(8) E. Gorin, J. Walter, and H. Eyring, *J. Chem. Phys.*, **6**, 824 (1938).

(9) W. J. Kauzmann, J. E. Walter, and H. Eyring, *Chem. Rev.*, **26**, 370 (1940).

Table III: The Sensitivity of the Vibrational Frequencies to the Force Constants in Table I (The Change in Each Frequency, in cm^{-1} , Corresponding to an Increase in Each Force Constant of 0.1, in Appropriate Units, Is Given.)

	i	K_r	H_α	F_α	F_β
NH ₃	1	24.46	0.04	64.46	19.42
	2	0.85	107.21	32.36	26.61
	3	25.55	0.20	12.08	5.19
	4	0.02	120.48	51.30	0.00
ND ₃	1	17.65	0.01	44.51	14.80
	2	0.58	81.57	25.09	19.94
	3	18.84	0.83	7.16	3.82
	4	0.00	87.03	38.04	0.00
PH ₃	1	34.60	0.18	80.32	26.49
	2	1.03	77.01	58.05	26.82
	3	36.11	0.01	15.58	10.08
	4	0.13	73.99	72.71	0.04
PD ₃	1	24.94	0.02	55.12	19.88
	2	0.65	56.36	43.44	19.18
	3	26.00	0.00	10.14	7.26
	4	0.07	52.83	52.44	0.02
AsH ₃	1	38.27	0.00	80.89	31.22
	2	0.03	71.39	78.92	21.39
	3	38.09	0.00	14.52	11.00
	4	0.00	71.06	85.89	0.00
AsD ₃	1	27.25	0.01	56.15	22.66
	2	0.01	51.17	57.22	15.13
	3	27.13	0.01	9.91	7.83
	4	0.00	50.44	61.18	0.00
SbH ₃	1	42.15	0.05	92.85	33.01
	2	0.30	68.33	86.53	29.04
	3	42.52	0.00	17.26	12.43
	4	0.03	66.55	98.92	0.01
SbD ₃	1	29.95	0.02	65.02	23.72
	2	0.20	48.76	62.12	20.60
	3	30.21	0.00	11.96	8.83
	4	0.02	47.18	70.27	0.00

nucleus. The force constant F_β is just the second derivative of V_H , *i.e.*

$$F_\beta = \frac{\partial^2 V_H}{\partial r^2} = -\epsilon^2 \left[\frac{4}{a_0} + \frac{4}{ra_0} + \frac{4}{r^2} + \frac{2a_0}{r^3} \right] \exp \left[\frac{-2r}{a_0} \right]$$

The factor of ϵ is to take account of the effective number of electrons in the lone-pair orbital. Ideally, it should be 2 but may be less due to distortion of the electron distribution in the hydrogen orbital or the partial delocalization of the lone pair. In Figure 3, $(\partial^2 V_H / \partial r^2)$ is plotted against $r = q_\beta$ for different values of ϵ . The values of F_β for NH₃, PH₃, AsH₃, and SbH₃ are also shown in this plot. Even though the uncertainty is probably quite high, particularly for the heavier molecules where F_β makes a smaller contribution to the frequencies, the points do fall pleasingly close to the theoretical line.

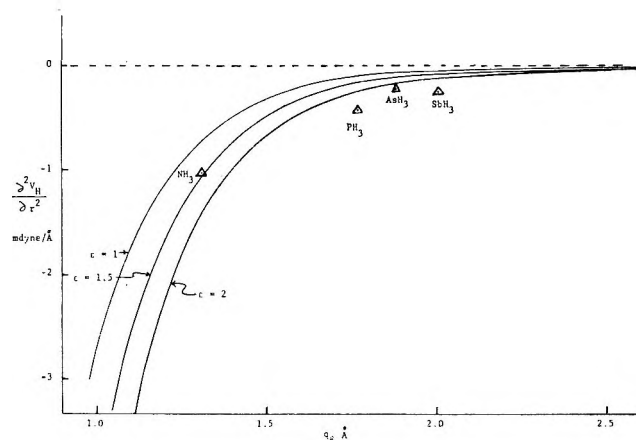


Figure 3. Plot of hydrogen-electron force constant, F_β vs. q_β for the group V trihydrides.

Group V Trihalides

The model taken for the potential energy of the halides XY_3 is the same as previously taken for the hydrides. In this case there are no isotopic frequency data and only four force constants (K_r , H_α , F_α , and F_β) can be determined. We make the assumptions, as previously checked for NH₃, $K_e = \infty$ and $H_\beta = \kappa = 0$. Since reliable estimates of the harmonic frequencies are not available, we have adjusted the force constants to the observed frequencies (Table V). Several starting sets of force constants were tried; all converged either to the values given in Table IV or to apparently unreasonable values.

Table IV: Force Constants of Group V Halides, Adjusted to Fit the Observed Frequencies Given in Table V

Molecule	K_r , mdyn/ \AA	H_α , mdyn \AA / (radian) ²	F_α , mdyn/ \AA	F_β , mdyn/ \AA	ξ , \AA	r_{eY} , \AA
NF ₃	2.746	0.364	1.559	1.496	0.6	1.717
PF ₃	3.913	0.288	0.809	1.520	1.1	2.263
PCl ₃	1.795	0.092	0.499	0.600	1.1	2.729
PBr ₃	1.725	-0.227	0.524	0.378	1.1	2.848
PI ₃	1.277	-0.251	0.384	0.295	1.1	3.078
AsF ₃	3.010	0.548	0.306	1.465	1.21	2.495
AsCl ₃	1.591	0.406	0.228	0.544	1.21	2.945
AsBr ₃	1.393	0.084	0.286	0.412	1.21	3.080

The positive values of F_β in Table IV are interpreted as evidence of a repulsive force between the halogen atoms and the lone pair, in contrast with the situation in the hydrides where the interaction is attractive. The attractive force in the hydrides must originate in the incomplete screening of the proton implying an effective residual positive charge resident on the hydrogen nucleus. The apparent repulsive force between the lone pair and the halogens in the group V

halides suggests that the halogen atom carries an effective negative charge, a result which is consistent with the electronegative character of the halogens. The value of F_β for NF_3 (1.496 mdyn/Å) is much lower than the calculated value from Slater-type orbitals by Curtis and Muirhead³ (3.65 mdyn/Å; $\bar{N} = 0.2$), but the F...F repulsive force constant for NF_3 in Table IV ($F_\alpha = 1.559$ mdyn/Å) falls into the range estimated by Curtis and Muirhead³ (1.0 ~ 1.9 mdyn/Å).

The comparisons between the observed frequencies and the calculated frequencies with or without the lone-pair interaction are given in Table V. The tests of the sensitivity of the vibrational frequencies to the dif-

ferent force constant are given in Table VI. The results are similar to that of the hydrides.

NHF₂ and NDF₂

Estimates of the vibrational frequencies of NHF₂ and NDF₂ are available,¹⁰ and the geometry has been determined.¹¹ It therefore appeared feasible and useful to test the lone-pair potential function on this molecule.

The procedure is similar to that used for the more symmetrical molecules and will not be described in any detail. Table VII shows the force constants of NHF₂, which has a different set of internal coordinates than that of more symmetrical molecules, *i.e.*, α is the HNF

Table V: Observed Frequencies Compared with (i) Those Calculated with the Lone-Pair Interaction (Table IV), $\Delta\nu\% = (\nu_{\text{obsd}} - \nu_{\text{calcd}}) \times 100/\nu_{\text{obsd}}$ and (ii) Those Calculated with a Simple UBFF

	<i>i</i>	$\nu_i(\text{obsd}),$ cm ⁻¹	$\Delta\nu_i\%$ (i)	$\Delta\nu_i\%$ (ii)
NF ₃ ^a	1	1031	-1.14	8.74
	2	642	3.97	8.38
	3	907	1.75	-4.37
	4	497	-2.81	-7.39
PF ₃ ^b	1	892	-4.97	4.43
	2	487	6.56	17.72
	3	860	4.12	-3.02
	4	344	-3.06	-9.03
PCl ₃ ^c	1	511	-2.23	6.66
	2	258	3.66	9.64
	3	484	2.04	-4.18
	4	190	-1.69	-6.97
PBr ₃ ^c	1	380	-1.32	7.30
	2	162	1.72	7.64
	3	400	0.92	-3.64
	4	116	-1.17	-4.31
PI ₃ ^c	1	303	0.05	8.00
	2	111	-0.01	5.04
	3	325	0.00	-4.91
	4	79	0.03	-4.82
AsF ₃	1	707	-1.55	
	2	341	4.70	
	3	644	1.89	
	4	273	-1.20	
AsCl ₃ ^c	1	405	-1.05	
	2	194	1.80	
	3	370	1.52	
	4	158	-0.56	
AsBr ₃ ^c	1	[284] ^d	-1.58	
	1	128	1.52	
	3	275	1.27	
	4	98	-0.48	

^a E. L. Pace and L. Pierce, *J. Chem. Phys.*, **23**, 1248 (1955).

^b L. Dayenette, *J. Chim. Phys.*, **58**, 487 (1961). ^c See F. A. Miller and W. K. Baer, *Spectrochim. Acta*, **17**, 112 (1961).

^d Estimated from $(\nu_1 + \nu_4) = 382$ cm⁻¹.

Table VI: The Sensitivity of the Vibrational Frequencies to the Different Force Constant (The Frequency changes When Each Force Constant Is Increased by 0.1.)

	<i>i</i>	K_r	H_α	F_α	F_β
NF ₃	1	7.50	5.30	7.77	11.68
	2	0.02	14.74	13.82	2.16
	3	13.21	4.52	1.09	3.15
	4	0.00	14.58	12.71	0.00
PF ₃	1	6.63	1.74	8.41	8.89
	2	0.05	12.41	15.86	3.66
	3	9.25	0.82	1.50	2.22
	4	0.03	15.17	15.82	0.01
PCl ₃	1	8.02	2.16	8.31	12.09
	2	0.01	8.86	17.83	3.50
	3	11.74	1.19	1.10	2.88
	4	0.03	9.17	16.72	0.01
PBr ₃	1	6.97	3.25	5.62	12.82
	2	0.00	7.11	14.92	3.48
	3	10.82	1.88	0.64	2.60
	4	0.03	6.56	13.29	0.01
PI ₃	1	7.40	3.93	5.44	14.81
	2	0.00	5.47	14.91	2.67
	3	12.02	2.13	0.75	2.29
	4	0.02	5.10	12.67	0.00
AsF ₃	1	7.02	0.56	11.97	7.83
	2	0.19	9.78	17.10	3.34
	3	9.17	0.22	2.71	2.10
	4	0.01	14.19	18.20	0.00
AsBr ₃	1	7.79	0.75	18.63	9.61
	2	0.05	7.59	18.63	2.89
	3	10.08	0.32	1.90	2.58
	4	0.01	8.49	18.00	0.00
AsCl ₃	1	6.15	1.19	6.64	9.10
	2	0.01	5.68	14.80	2.73
	3	8.75	0.68	0.85	2.15
	4	0.01	6.03	14.20	0.00

(10) J. J. Comeford, D. E. Mann, L. J. Schoen, and D. R. Lide, Jr., *J. Chem. Phys.*, **38**, 461 (1963).

(11) D. R. Lide, *ibid.*, **38**, 456 (1963), reports $r_{\text{NF}} = 1.400$ Å, $r_{\text{NH}} = 1.026$ Å, $\angle_{\text{FNF}} = 102.9^\circ$, $\angle_{\text{NHF}} = 99.8^\circ$.

angle, β is the FN-lone-pair angle, δ is the HN-lone-pair angle, and γ is the FNF angle. Two sets of UBFC were determined. The first set, shown in Table VII, column (i), were obtained when all the force constants associated with the lone pair were set equal to zero; they correspond to a treatment with a simple UBFF. The second column of Table VII (ii) shows the force constants resulting from a calculation in which the nonbonded interactions with the lone-pair electrons are taken into account. The calculated frequencies corresponding to the two sets of force constants are compared with the observed frequencies in Table VIII. Including the lone-pair force constants does improve considerably the agreement between observed and calculated frequencies; however, there remain some relatively large discrepancies, especially in the hydrogen deformation frequencies ν_2 and ν_5 . We believe that

Table VII: Force Constants of NHF_2 Adjusted to Fit All Vibrational Frequencies of NHF_2 and NDF_2 , and Are in the Same Units as Shown in Table I (Values Shown in Parentheses Were Constrained in the Adjustment.)

Force constant	NHF_2		NH_3^a	NF_3^b
	(i)	(ii)		
K_H	4.786	4.583	7.040	
K_F	3.003	2.865		2.746
H_α	0.203	0.167		
H_γ	1.832	1.022		3.364
F_α	1.315	1.283		
F_γ	0.088	0.641		1.559
K_e	(0)	(∞)	(∞)	(∞)
H_β	(0)	(0)		(0)
H_δ	(0)	(0)	(0)	
F_β	(0)	0.721		1.496
F_δ	(0)	-0.933	-0.966	
	(0)	(0)		

^a From Table I. ^b From Table IV.

Table VIII: NHF_2 and NDF_2 . Observed Frequencies (in cm^{-1}) Compared with Frequencies Calculated Using the Two Sets of Force Constants in Table VII

		Obsd ^a frequency	Calcd frequency (i)	Calcd frequency (ii)	
NHF_2	ν_1	3193	3237	3211	
	a'	ν_2	1307	1193	1260
		ν_3	972	907	981
		ν_4	500	482	496
	a''	ν_5	1424	1510	1465
		ν_6	888	886	884
NDF_2	ν_1	(2333) ^b	2343	2332	
	a'	ν_2	1008	955	1023
		ν_3	972	874	926
		ν_4	(500) ^b	480	493
	a''	ν_5	1042	1096	1065
		ν_6	888	886	883

^a Reference 10. ^b Estimated in ref 10.

these stem from neglect of stretch bend interaction force constants which play a larger role in NHF_2 on account of the proximity of δ_{NH} and ν_{NF} .¹²

The numerical values of the force constants found for NHF_2 differ somewhat from the corresponding values in NH_3 and NF_3 . Most obviously, K_H is quite a bit lower in NHF_2 than in NH_3 , but this is expected in a UBFF where, in the case of NHF_2 , there are large contributions to the effective CH-stretching force constant from the HF nonbonded interactions. Even the lone-pair fluorine interaction is smaller in NHF_2 than that of NF_3 , but the lone-pair hydrogen interaction is about the same as in NH_3 .

Conclusions

The new and more exact calculations of the force constants of the group V hydrides reinforce the previous conclusions:^{2a} that the protons are attracted by the lone pair of electrons and that this attractive force makes a significant contribution to the intramolecular potential energy. Similarly, it is to be concluded that there is a significant positive force constant associated with the interactions between the halogen atoms and the lone pair in the group V halides, and that this force constant decreases as we move down the periodic table. The positive sign of the force constant implies that, at distances close to geometrical equilibrium, repulsive forces are important though one cannot rule out the possibility of some attraction at greater distances.

The large values of the interactions in NH_3 and NF_3 suggest that these forces may be important in determining geometrical structure and possibly chemical reactivity. Schomaker and Lu⁷ have found that the electric moment of NF_3 is very small (0.2 D) compared to NH_3 (1.46 D) but the NF_3 bond angle ($102^\circ 30'$) is smaller than that of NH_3 ($106^\circ 47'$). These relative structures can easily be rationalized in terms of the interactions of the hydrogen and fluorine atoms with the lone pair. Because of the lone-pair electron on the nitrogen atom, the electric moment of NF_3 is reduced and the electric moment of NH_3 is enhanced. On the other hand, the smaller FNF angle in NF_3 is due to the repulsive force between lone-pair and F atoms, and the larger HNH angle in NH_3 is due to the attractive force between lone-pair and H atoms.

The present model for the potential function is unwieldy in the tetratomic case. One cannot suggest seriously that it be used for larger molecules.

Acknowledgment. We are grateful for financial support from the U. S. Army Research Office, Durham, under Contract DA-31-124-ARO-D-415.

(12) Such interactions would have a much smaller effect in the symmetrical molecules since the stretching and bending modes are, in that case, well separated.

Pulse-Radiolysis Studies. XIV. Rate Constants for the Reactions of Hydrogen Atoms with Aromatic Compounds in Aqueous Solution¹

by P. Neta and Leon M. Dorfman

Department of Chemistry, The Ohio State University, Columbus, Ohio (Received August 19, 1968)

Absolute rate constants have been determined for the addition of hydrogen atoms to aromatic compounds in water by observation of the formation rate curves of the cyclohexadienyl radicals. The values of these rate constants for the compounds studied are: C_6H_5COOH , 1.00×10^9 ; C_6H_5CN , 0.68×10^9 ; $C_6H_5NO_2$, 1.04×10^9 ; $C_6H_5SO_3H$, 0.82×10^9 ; $C_6H_5CH_2COOH$, 1.01×10^9 ; $C_6H_5COCH_3$, 1.10×10^9 ; $p\text{-Cl-C}_6\text{H}_4\text{COOH}$, 1.13×10^9 ; $p\text{-NO}_2\text{-C}_6\text{H}_4\text{COOH}$, 0.98×10^9 ; $p\text{-OH-C}_6\text{H}_4\text{COOH}$, $1.45 \times 10^9 M^{-1} \text{sec}^{-1}$ at 25° . The uncertainty in these values is about $\pm 15\%$. The specific rate constant for the reaction of hydrogen atoms with methanol, determined by competition kinetics with several of these compounds, is $1.6 \times 10^6 M^{-1} \text{sec}^{-1}$ at 25° . The isotope effect for the reaction of H and D atoms with two of these compounds was found to be $k_H/k_D = 1.32 \pm 0.05$ for C_6H_5COOH and $C_6H_5SO_3H$.

Introduction

Among the many reactions of the primary species (OH , e_{aq}^- , and H) formed in irradiated water, those for which absolute rate constants are at present least extensively known are the reactions of the hydrogen atom. Of some dozen specific rate constants for H-atom reactions determined by direct observation in fast reaction studies, most involve reactions with inorganic species such as oxygen,² several metal ions,³⁻⁶ and the hydroxide ion.⁷ Only a few are known for reactions of organic compounds,⁸⁻¹² mostly with aromatic molecules.

It has now been shown for several aromatic compounds that the cyclohexadienyl radicals formed by H-atom addition¹⁰⁻¹³ have an intense uv absorption band similar to that of the hydroxycyclohexadienyl radical.¹⁴⁻¹⁶ Thus the formation of the H-adduct free radical in pulse radiolysis may be used in the direct determination of the specific rate constants for such reactions, if the solution contains a scavenger, such as deuteriomethanol¹⁰ which removes the OH radical without reacting extensively with the H atom. This paper presents absolute rate constants for the addition of hydrogen atoms to nine aromatic compounds. We have also determined, by competition kinetics with several of these compounds, the rate constant for the reaction of H atoms with methanol.

Experimental Section

Absolute rate constants for the hydrogen atom reactions with aromatic compounds have been determined from the formation curves of the cyclohexadienyl radicals. It has been shown^{8,11,13,16} that both the H adduct and OH adduct of the same aromatic compound have similar absorption spectra. Thus, we have used the already known wavelength maxima for H adducts^{8,13,16} and OH adducts^{15,16} to follow the formation of the cyclohexadienyl radical.

The detailed technique in use with a Varian V-7715A electron linear accelerator has been described.¹⁷ These methods, with some modifications, are similar to those of our earlier work.^{14,18} Electrons of 3.5-4 MeV energy were used with a pulse duration of 0.1 to 0.4 μsec . The pulse current was generally in the range 310-330 mA. Although precise dosimetry was not explicitly needed for the interpretation of the present work, it was known from earlier investigations,^{13,15} using a modified Fricke dosimeter, that the 0.1- μsec

(1) Based on work supported by the U. S. Atomic Energy Commission.

(2) (a) S. Gordon, E. J. Hart, and J. K. Thomas, *J. Phys. Chem.*, **63**, 1262 (1964); (b) J. P. Sweet and J. K. Thomas, *ibid.*, **68**, 1363 (1964).

(3) J. H. Baxendale, E. M. Fielden, and J. P. Keene, *Proc. Roy. Soc.*, **A286**, 320 (1965).

(4) J. H. Baxendale, J. P. Keene, and D. A. Stott in "Pulse Radiolysis," J. H. Baxendale, M. Ebert, J. P. Keene, and A. J. Swallow, Ed., Academic Press, New York, N. Y., 1965, p 107.

(5) J. H. Baxendale, E. M. Fielden, and J. P. Keene, ref 4, p 207.

(6) K. D. Asmus and P. L. T. Bevan in "The Chemistry of Ionization and Excitation," G. R. A. Johnson and G. Scholes, Ed., Taylor and Francis Ltd., London, 1961, p 253.

(7) M. S. Matheson and J. Rabani, *J. Phys. Chem.*, **69**, 1324 (1965).

(8) K. D. Asmus, A. Henglein, M. Ebert, and J. P. Keene, *Ber. Bunsenges. Phys. Chem.*, **68**, 657 (1964).

(9) J. Rabani, W. A. Mulac, and M. S. Matheson, *J. Phys. Chem.*, **69**, 53 (1965).

(10) M. C. Sauer, Jr., and B. Ward, *ibid.*, **71**, 3971 (1967).

(11) E. J. Land and M. Ebert, *Trans. Faraday Soc.*, **63**, 1181 (1967).

(12) K. D. Asmus, B. Cercek, M. Ebert, A. Henglein, and A. Wigger, *ibid.*, **63**, 2435 (1967).

(13) R. Wander, P. Neta, and L. M. Dorfman, *J. Phys. Chem.*, **72**, 2946 (1968).

(14) L. M. Dorfman, I. A. Taub, and R. E. Bühler, *J. Chem. Phys.*, **36**, 3051 (1962).

(15) P. Neta and L. M. Dorfman, "Radiation Chemistry. I." *Advances in Chemistry Series*, No. 81, American Chemical Society, Washington, D. C., 1968, p 222.

(16) B. Chutny, *Nature*, **213**, 593 (1967).

(17) W. D. Felix, B. L. Gall, and L. M. Dorfman, *J. Phys. Chem.*, **71**, 384 (1967).

(18) M. S. Matheson and L. M. Dorfman, *J. Chem. Phys.*, **32**, 1870 (1960).

pulse used gives a dose of 6×10^{16} eV/g. The initial H-atom concentration in most of this work is thus about 3×10^{-6} M.

The detection system used was as described.¹⁷ The irradiation cells were 2 cm long (using a double pass of the analyzing light beam), 1.2 cm high, and 0.8 cm deep in the direction of the electron beam. The electron beam had a diameter of about 1.5 cm at the point of incidence on the cell wall.

Solutions, at pH 1 which was adjusted with sulfuric acid, were transferred into cells similar to those described.¹⁷ These consisted of a solution bulb (50 ml), a waste bulb (25 ml), and the irradiation cell (1.9 ml), the assembly of which could be connected to a vacuum line through a Teflon stopcock. The solution was first frozen in liquid nitrogen, evacuated, and then thawed. This procedure was repeated two more times. This method was used to prevent evaporation of solutes or water. It was found to reduce the oxygen concentration to 2×10^{-7} M or lower, as determined by gas chromatography.

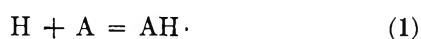
A fresh solution was used for each irradiation. Six irradiations could be done with each batch of solution. Four or five different concentrations were generally used to determine the absolute rate constant for the reaction of H atoms with a given aromatic compound.

The concentration range covered for each aromatic compound was at least threefold. Depending upon the rate constant, these concentrations varied from 3×10^{-4} to 2×10^{-3} M. Higher concentrations were used for several compounds, and these results will be discussed. Deuteriomethanol was used as a scavenger for hydroxyl radicals. The concentration of CD₃OD varied from 400 to 800 times that of the aromatic compound depending upon the rate constants for reaction of the latter with H and OH. The concentration ratio of CD₃OD to aromatic compound was kept constant through the entire concentration range of the aromatic reactant.

The materials used were either Baker Analyzed Reagent, if available, or Baker Grade. Deuteriomethanol was obtained from Merck Sharp and Dohme. Deuterium oxide, used in some experiments concerned with isotope effects, was obtained from City Chemical Corp. and had a nominal deuterium content of at least 99.5%. Both the water and the deuterium oxide were triply distilled.

Results and Discussion

The elementary reactions which are pertinent to the interpretation of the data are

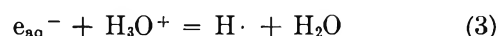


the rate constant of which is to be determined from the formation curve of the cyclohexadienyl radical, AH·, where A is the aromatic compound. At sufficiently

high pulse intensity and low concentration of A, there may be some competition for H atoms from the association reaction



for which¹⁹ $2k_2 = 3.0 \times 10^{10} \text{ M}^{-1} \text{ sec}^{-1}$ at 25°. Thus, with the 0.1-μsec pulse, $k_1 = 1 \times 10^9$ and $[\text{A}] = 5 \times 10^{-4}$ M, the lowest concentration used, the initial value for the ratio $k_1[\text{A}]/k_2[\text{H}] = 5.6$, so that more than 83% of the H atoms react by (1). At the higher concentrations used this exceeds 95%. An appropriate correction has been made with the use of an analog computer. The H-atom formation, as a primary species as well as by reaction of e_{aq}⁻



is instantaneous with respect to the subsequent kinetics.

The hydroxyl radical is removed by reaction with CD₃OH



for which $k_4 = 4.1 \times 10^8 \text{ M}^{-1} \text{ sec}^{-1}$ judging from the deuterium isotope effect²⁰ and the value of the rate constant for the reaction with methanol as determined by competition kinetics.¹⁵ The concentration conditions may be arranged to make the rate of the concurrent reaction



very small. But it may not be completely negligible, depending upon the ratio $k_4[\text{CD}_3\text{OH}]/k_5[\text{A}]$. Thus, for benzoic acid,¹³ with $[\text{CD}_3\text{OH}]/[\text{A}] = 400$, this ratio has the value 27, so that only 3.6% of the hydroxyl radicals react by (5).

There may also be a very slight occurrence of the reaction



for which²¹ $k_6 = 8 \times 10^4 \text{ M}^{-1} \text{ sec}^{-1}$, but this is relatively unimportant. Thus, for benzoic acid, at the concentration ratio $[\text{CD}_3\text{OH}]/[\text{A}] = 400$ and $k_1 = 1 \times 10^9 \text{ M}^{-1} \text{ sec}^{-1}$, 97% of the H atoms react by (1). Thus it is clear that of the foregoing elementary processes, reaction 1 is almost the exclusive reaction and the concurrent reactions, (2), (5), and (6), which are of lesser importance, may be taken into account with an analog computer treatment of the data.

The relative importance of the addition reaction of the hydroxydeuteriomethyl radical



(19) H. A. Schwarz, *J. Phys. Chem.*, **67**, 2827 (1963).

(20) M. Anbar, D. Meyerstein, and P. Neta, *J. Chem. Soc.*, **13**, 742 (1966).

(21) M. Anbar and D. Meyerstein, *J. Phys. Chem.*, **68**, 3184 (1964).

is more difficult to assess, but it appears to be very much slower than reaction 1, as has been suggested by Sauer and Ward.¹⁰ This seems to be borne out, not only by the kinetics of this investigation but also by our previous determination¹³ of the molar extinction coefficient for the radical $\text{HC}_6\text{H}_5\text{COOH}$ where agreement is obtained with the use of N_2O as a scavenger for e_{aq}^- and with CD_3OH as a scavenger for OH , two totally different methods, in the latter of which the nonoccurrence of reaction 7 is important to the interpretation. This conclusion is further confirmed by the following experiment combining the use of N_2O to convert the hydrated electron to OH , and methanol to convert OH to $\cdot\text{CH}_2\text{OH}$. A solution of benzoic acid at $7.2 \times 10^{-4} M$ at pH 3.0, containing N_2O at 3.4 atm, was irradiated and the formation of the carboxyhydroxycyclohexadienyl radical observed at $347 m\mu$ as previously described.^{13,15} A similar solution containing $0.2 M \text{CH}_3\text{OH}$ was treated identically. Only a very slight absorption was detected in this solution over several microseconds with the ratio of the optical density in the latter experiment to that in the former being 0.10. This is in accord with formation of only the H adduct in the presence of CH_3OH , the ratio being equal to $G_{\text{H}}/(G_{e_{\text{aq}}^-} + G_{\text{OH}} + G_{\text{H}})$. The experiment was also repeated at 327 and 367 $m\mu$. It seems clear, then, that the hydroxymethyl radical does not add to the aromatic ring over the time scale of our rate determinations, or that the adduct free radical formed does not absorb in this region of the spectrum, a less likely explanation.

Finally, the association reaction



occurs, but at a rate that is not significant to the foregoing kinetics. Thus for the association reaction of the H adduct of benzene¹⁰ or the OH adduct of benzoic acid,¹³ the half-time with the $0.1\text{-}\mu\text{sec}$ pulse would be approximately 300 μsec , almost two orders of magnitude longer than for any of reactions 1 through 6.

The experimental rate constants have been corrected for the small effect of reactions 2, 5, and 6 in the determination of k_1 . The extent of this correction was calculated using an Electronics Associates Inc. Type TR-20 analog computer.

This correction was determined by using the analog computer curves for the benzoic acid system as a representative set, with $k_1 = 1.0 \times 10^9$ and with the cited values for k_2 , k_4 , k_5 , and k_6 along with the appropriate concentrations for all reactants. From a plot of the first-order form of these computer rate curves, the combined effect of reactions 5 and 6 in the determination of k_1 under our conditions was found to be +5%. This correction is constant, and was applied to all the aromatic compounds. The effect of reaction 2 upon the value for the rate constant ranges from 0 to +9%, depending upon the values of $[\text{A}]$ and k_1 . This correc-

tion, the magnitude of which depends upon the value of $k_1[\text{A}]/k_2[\text{H}]$ for each compound, was applied to all cases. In addition, a somewhat smaller correction was made for the occurrence of the competitive reaction $\text{H} + \cdot\text{CD}_2\text{OH}$ without resorting to the computer analysis. Taking the rate constant for this reaction as comparable to k_2 , the correction would range from 0 to +4.5%. Thus a total correction of -5% to -18.5% was applied to the experimental rate constants determined directly from the formation rate curves. This correction is included in the rate constants given in Table I. In addition, the overall fit of the rate data to the computer curves was demonstrated for the case of benzoic acid.

The individual rate curves were all found to fit very well to a first-order rate law, as may be seen in Figure 1 which shows a plot of $\log(D_\infty - D_t)$ vs. time, where D is the optical density. The rate constant is determined from the expression

$$k_1 = -2.303 \times \text{slope}/[\text{A}]_0 \quad (9)$$

which is derived from the integrated form of the differ-

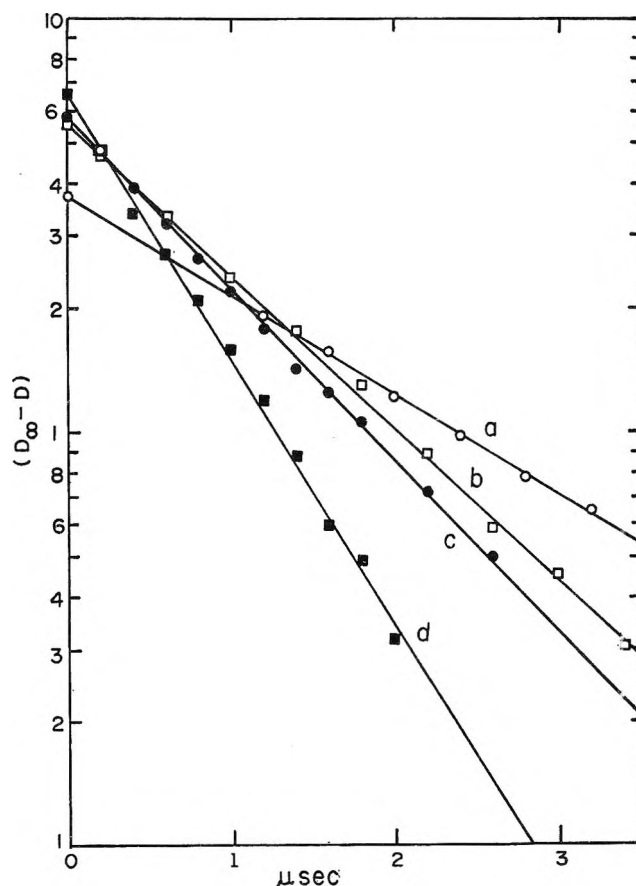


Figure 1. First-order plot of formation curves of the H adduct free radical of benzoic acid showing $\log(D_\infty - D_t)$ vs. time in microseconds. The benzoic acid concentrations are: a, $5 \times 10^{-4} M$; b, $7 \times 10^{-4} M$; c, $1.0 \times 10^{-3} M$; and d, $1.5 \times 10^{-3} M$.

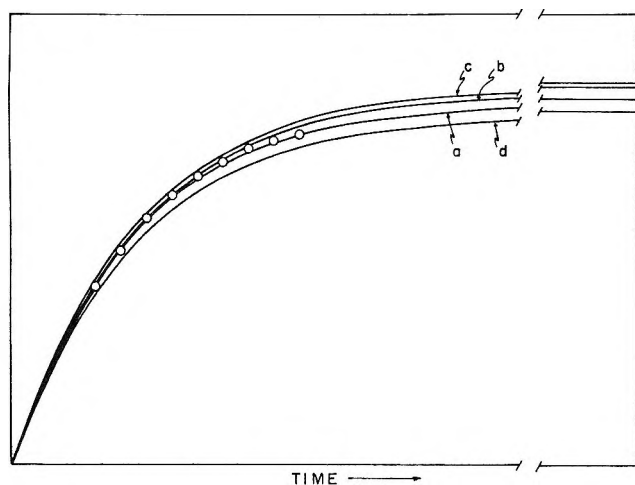


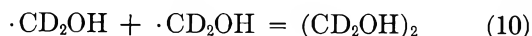
Figure 2. Analog computer curves for the rate of formation and the experimental points for a sample run. The relative optical density is plotted against time. The individual curves represent the following cases: a, reactions 1, 2, 5, and 6 included; b, reactions 1, 2, and 5 only with the rate of (6) taken to be zero; c, reactions 1, 5, and 6 only with the rate of (2) taken to be zero; d, reactions 1, 2, and 6 only with the rate of (5) taken to be zero.

ential rate expression, as has been discussed.²² The quality of fit of rate data for an individual run to the analog computer curves is shown in Figure 2 for benzoic acid.

The data in Table I show reasonably good constancy over the concentration range which is threefold or fourfold for each compound. Each value in the table is an average of five or six runs.

The extent to which reaction 7 might occur represents a possible complication of the system since a similarly absorbing species would be formed concurrently. The good linearity of the first-order plots, together with our earlier work on the extinction coefficient of the carboxycyclohexadienyl radical,¹³ seems to show that there is no significant occurrence of reaction 7 in the concentration region shown. This is further confirmed by the competition kinetics with methanol (see below) which provide good agreement with kinetic data referred to the reaction of H atoms with silver ions.⁶ We are thus in agreement with the conclusion of Sauer and Ward.¹⁰

At sufficiently high concentration of A, reaction 7 might occur to an appreciable extent, but would be in competition with the association reaction



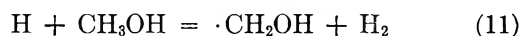
for which k_9 is probably $2 \times 10^9 \text{ M}^{-1} \text{ sec}^{-1}$ or higher judging from the value of the association rate constant for α -ethanol radicals.²³ If there is indeed a competition between (9) and (7), it should be found that k_1 is decreased at higher [A] because of the concurrence of reaction 7. This is, in fact, found to be the case, as for benzoic acid, where an increase in concentration of A

Table I: Absolute Rate Constants for the Reactions of Hydrogen Atoms with Aromatic Compounds

Compound	Concn, $M \times 10^4$	Absolute rate constant, $M^{-1} \text{ sec}^{-1} \times 10^{-9}$	Average
$\text{C}_6\text{H}_5\text{COOH}$	5	0.96	1.00 ± 0.15
	7	1.04	
	10	0.99	
	15	1.00	
$\text{C}_6\text{H}_5\text{CN}$	5	0.73	0.68 ± 0.10
	10	0.70	
	15	0.69	
	20	0.63	
	25	0.65	
$\text{C}_6\text{H}_5\text{NO}_2$	5	1.10	1.04 ± 0.15
	10	1.07	
	15	0.95	
$\text{C}_6\text{H}_5\text{SO}_3\text{H}$	5	0.85	0.82 ± 0.13
	10	0.87	
	12	0.78	
	15	0.76	
$\text{C}_6\text{H}_5\text{CH}_2\text{COOH}$	5	1.26	1.01 ± 0.15
	10	1.07	
	12	0.93	
	15	0.90	
	20	0.88	
$\text{C}_6\text{H}_5\text{COCH}_3$	5	1.22	1.10 ± 0.17
	10	1.19	
	12	1.08	
	15	1.01	
	20	1.00	
$p\text{-Cl-C}_6\text{H}_4\text{COOH}$	3	1.21	1.13 ± 0.20
	5	1.04	
$p\text{-NO}_2\text{C}_6\text{H}_4\text{COOH}$	5	1.07	0.98 ± 0.15
	10	0.95	
	15	0.91	
$p\text{-OH-C}_6\text{H}_4\text{COOH}$	3	1.48	1.45 ± 0.20
	5	1.30	
	7	1.48	
	10	1.55	

from 1.5×10^{-3} to $4 \times 10^{-3} \text{ M}$ results in a decrease in the apparent value of k_1 from 1.0×10^9 to $0.7 \times 10^9 \text{ M}^{-1} \text{ sec}^{-1}$.

Four of these compounds were used as reference reactions in determining the rate constant for the reaction



by competition kinetics. The data are shown in Table II. Methanol competes with A for both OH radicals

(22) L. M. Dorfman and M. S. Matheson, *Progr. Reaction Kinetics*, **3**, 237 (1965).

(23) L. M. Dorfman and I. A. Taub, *J. Amer. Chem. Soc.*, **85**, 2370 (1963).

and H atoms, but the ratio $k_{\text{OH}+\text{CH}_3\text{OH}}/k_{\text{H}+\text{CH}_3\text{OH}}$ is very much greater than $k_{\text{OH}+\text{A}}/k_{\text{H}+\text{A}}$. Thus the competition for H atoms could be determined from the observed optical density of both $\cdot\text{AH}$ and $\cdot\text{AOH}$, in the absence and presence of methanol, as a function of the ratio $[\text{CH}_3\text{OH}]/[\text{A}]$. In order to determine the relative contribution of $\cdot\text{AH}$ and $\cdot\text{AOH}$ to the measured optical density, oxygen, at 1.5 atm, was added to the degassed, methanol-free solution to scavenge 97% of the H atoms.

Table II: Rate Constant for the Reaction of Hydrogen Atoms with Methanol Determined by Competition Kinetics

Reference aromatic compound	$[\text{CH}_3\text{OH}]/[\text{A}]$	$k_{\text{H}+\text{CH}_3\text{OH}},$ $M^{-1} \text{ sec}^{-1}$ $\times 10^{-6}$
$\text{C}_6\text{H}_5\text{COOH}$	100-1000	1.7
$\text{C}_6\text{H}_5\text{CN}$	100-800	1.7
$\text{C}_6\text{H}_5\text{NO}_2$	100-800	1.5
<i>p</i> -OH- $\text{C}_6\text{H}_4\text{COOH}$	400-1800	1.6

This method for the determination of $k_{\text{H}+\text{X}}$ is useful, in this simple, direct form only in cases for which $k_{\text{OH}+\text{X}}/k_{\text{H}+\text{X}}$ is very large, say greater than 100.

The concentration of A used was 5×10^{-4} to 1×10^{-3} M, and the concentration of methanol added was 100 to 1800 times [A], as given in Table II. Six separate concentration ratios were used to obtain the straight line resulting from a plot of D/D' against $[\text{CH}_3\text{OH}]/[\text{A}]$, where D and D' represent the optical densities, in the absence and presence, respectively, of methanol in accord with the equation

$$D/D' = 1 + \frac{k_{\text{H}+\text{CH}_3\text{OH}}[\text{CH}_3\text{OH}]}{k_{\text{H}+\text{A}}[\text{A}]} \quad (12)$$

From the slope, $k_{\text{H}+\text{CH}_3\text{OH}}/k_{\text{H}+\text{A}}$ is determined. The separate values are in excellent agreement although the values of $k_{\text{H}+\text{A}}$ for the aromatic compounds used ranged from 0.7×10^9 to 1.5×10^9 $M^{-1} \text{ sec}^{-1}$. This agreement, together with the excellent agreement between our value for $k_{\text{H}+\text{CH}_3\text{OH}}$ and the value of 1.6×10^6 $M^{-1} \text{ sec}^{-1}$ determined relative to the reaction of H atom with silver ion,⁶ further justified neglecting reaction 7 in the foregoing determination of the values for k_1 .

It should be noted that our value of k_1 for nitrobenzene is substantially lower than that determined¹² with

the use of thallos ion as an OH scavenger. We examined this use of thallos ion and find a reaction of Ti^+ with H atom, which would explain the discrepancy.

We have also determined the deuterium isotope effect in the reaction of H and D atoms with two aromatic compounds. Solutions were made up in D_2O , using regular benzoic acid, sodium benzenesulfonate, and sulfuric acid, to give a deuterium content higher than 95%. The rate constant for D atoms was measured in a comparable way to H atoms. With 1.0×10^{-3} and 1.5×10^{-3} M benzoic acid the isotope effect was $k_{\text{H}+\text{A}}/k_{\text{D}+\text{A}} = 1.32 \pm 0.05$. The possibility that this effect is due to the occurrence of a COOD group on the aromatic ring instead of COOH was checked by using sodium benzenesulfonate instead of benzoic acid. This compound is ionized even at pH 1 and thus the reacting aromatic species is the same in H_2O and D_2O . The isotope effect was again 1.3. In order to check the possibility of a solvent effect, the rate constants for the reaction of benzoate ions and benzenesulfonate ions with OH and OD radicals have been measured in H_2O and D_2O , respectively, by the method previously described.¹⁵ No isotope effect was found in this case, thus suggesting that the possibility of a solvent effect contribution to the value of 1.3 determined for $k_{\text{H}+\text{A}}/k_{\text{D}+\text{A}}$ is unlikely.

The C-D bond energy is greater than that of the C-H bond.²⁴ Thus, if this bond formation were a rate-determining factor in the reaction of hydrogen atoms with the aromatic nucleus, the isotope effect should be in the opposite direction to that observed. Nor can the effect result from the difference in diffusion rates of H in H_2O and D in D_2O . It is evident from the fact that the rate constants for $\text{H} + \text{O}_2$ and $\text{H} + \text{H}$ are fully an order of magnitude greater than the values of k_1 determined here that the latter cannot be diffusion controlled. It would appear that the effect is in accord with the suggestion that the rate-determining step in reaction 1 is the electrophilic attack of the hydrogen atom on the aromatic nucleus.

Acknowledgment. We are indebted to Mrs. Rosemary Wander for carrying out the experiment which confirmed the nonreactivity of the hydroxymethyl radical in aromatic addition. This work was supported by the U. S. Atomic Energy Commission.

(24) E. A. Halevi, *Progr. Phys. Org. Chem.*, **1**, 109 (1963).

Calculation of the Mean-Square Dipole Moment and Proton Fluctuation

Anisotropy of Hemoglobin at Low Ionic Strength¹

by William H. Orttung

Department of Chemistry, University of California, Riverside, California (Received August 23, 1968)

The mean-square dipole moment and proton fluctuation anisotropy of horse oxy hemoglobin at low ionic strength have been calculated from the Kirkwood-Shumaker and extended Tanford-Kirkwood theories. Site coordinates were taken from a model built according to Perutz' 1965 description. Results are presented for the pH range 4.5-9.0. The mean moment is considerably more sensitive to the parameters and approximations used than is the fluctuation moment, and the correlation averages were found to make a significant contribution to the fluctuation moment. The anisotropy of the fluctuations is appreciable and varies with pH. Calculations for met hemoglobin and for hypothetical models of deoxy and human oxy hemoglobin are also presented. Good agreement was obtained with data for horse oxy hemoglobin, and small but unexplained discrepancies with the available data were noted for the other modifications.

At low ionic strength, the dielectric constant of a protein solution is largely determined by the charges bound to the protein molecules. A single molecular parameter, the root-mean-square (rms) dipole moment, may be deduced from measurements at low frequencies and studies of the frequency dependence may yield information about the relaxation times associated with certain degrees of freedom of the molecule. The pertinent available data on hemoglobin may be briefly summarized.

Oncley² measured a low frequency dielectric increment, $\Delta D/g$, of 0.33 per g/l. and a single relaxation time of 8.4×10^{-8} sec for horse carboxyhemoglobin solutions at 25°. No frequency dependence was observed below 500 kHz to the lowest frequency measured (25 kHz). In a more recent study at 15° and a frequency of 1 MHz, Takashima³ reported dielectric increments of 0.25, 0.35, and 0.58 for horse oxy, carboxy, and met hemoglobin, respectively. Goebel and Vogel⁴ studied met hemoglobin solutions between 100 kHz and 10 MHz and also reported pH dependence near the isoionic point. They obtained a dielectric increment of 0.34 at 25° and a pH dependence of approximately +0.1 per pH unit at pH 7. Hanss and Banerjee⁵ found that no observable change occurred in the dielectric increment or relaxation of horse or human hemoglobin in the range 0-100% oxygenation, and that the dielectric increment of human hemoglobin was significantly smaller than that of horse hemoglobin (0.28 vs. 0.32).

Oncley² used the Clausius-Mosotti equation to estimate an rms dipole moment of 470 D for horse carboxyhemoglobin, and attributed the dielectric dispersion to rotational relaxation in the applied field. Kirkwood and Shumaker⁶ pointed out that proton fluctuations among the available binding sites make a major contribution to the rms dipole moment of proteins. In order

to test the Kirkwood-Shumaker theory, Takashima⁷ collected data on the pH dependence of the dielectric increment and dispersion of ovalbumin and bovine serum albumin solutions. However, a quantitative test of the theory is not possible until the site coordinates are known for these proteins.

Lumry and Yue⁸ considered recent data on the kinetics of proton transfer processes and concluded that proton redistribution rates in the neutral pH region should be very slow relative to the 100 kHz to 1 MHz frequencies used in dielectric measurements. However, it does not follow that proton fluctuations do not contribute to the dielectric increment in this frequency range. At a given instant of time, all possible fluctuations exist on different molecules in the solution between the electrodes. When a high-frequency field is applied, each fluctuation acts as a rigid moment and the dispersion reflects only the rotational relaxation. The lack of observed dispersion below 500 kHz and the calculated magnitudes of the dielectric increment presented below constitute support for this point of view.

The Tanford-Kirkwood theory of protein titration curves⁹ has recently been extended^{10,11} to allow calcula-

(1) This investigation was supported in part by Public Health Service Research Grant GM 11683 from the Division of General Medical Sciences.

(2) J. L. Oncley, *J. Amer. Chem. Soc.*, **60**, 1115 (1938).

(3) S. Takashima, *ibid.*, **78**, 541 (1956).

(4) W. Goebel and H. Vogel, *Z. Naturforsch.*, **19b**, 292 (1964).

(5) M. Hanss and R. Banerjee, *Biopolymers*, **5**, 879 (1967).

(6) J. G. Kirkwood and J. B. Shumaker, *Proc. Nat. Acad. Sci. U. S.*, **38**, 855 (1952).

(7) S. Takashima, *J. Phys. Chem.*, **69**, 2281 (1965).

(8) R. Lumry and R. H. Yue, *J. Phys. Chem.*, **69**, 1162 (1965).

(9) C. Tanford and J. G. Kirkwood, *J. Amer. Chem. Soc.*, **79**, 5333 (1957).

(10) W. H. Orttung, *J. Phys. Chem.*, **72**, 4058 (1968).

(11) W. H. Orttung, *ibid.*, **72**, 4066 (1968).

tion of the site occupation averages required by the Kirkwood-Shumaker theory, and site coordinates may now be estimated from three-dimensional structural models of proteins such as hemoglobin.¹² This approach has yielded a detailed interpretation of the titration curve of hemoglobin¹³ and is applied to the problem of the dielectric constant in the present paper.

Theoretical Relationships

If the environment of solvent and solute molecules is assumed to be a real spherical cavity of molecular size in a uniform dielectric,¹⁴ then

$$D - 1 = \frac{4\pi}{3} \left(\frac{3D}{2D + 1} \right) \sum_j N_j (\alpha_{j\alpha\alpha}^0 + \langle \mu_{j\alpha} \mu_{j\alpha} \rangle_0 / kT) \quad (1)$$

where D is the dielectric constant of the solution, $\alpha_{j\alpha\alpha}^0$ and $\mu_{j\alpha}$ are the electrostatic polarizability tensor and dipole moment of a molecule of type j as it exists in the solution,¹⁵ and N_j is the number of molecules of type j per milliliter. The average is over all rotational and internal coordinates describing the dipole moment of the molecule in the limit of zero applied field. The convention $j = 1, 2$ for solvent and solute is used below. In the Onsager theory,¹⁵ as applied to a globular protein

$$\mu_\alpha = \frac{2D + 1}{2D + D_p} \left[\frac{D_p + 2}{3} \mu_{v\alpha} + \mu_{e\alpha} \right] \quad (2)$$

where D_p is the effective dielectric constant of the protein, $\mu_{v\alpha}$ is the vacuum dipole moment of the molecule if all proton binding site charges were removed, and

$$\mu_{e\alpha} = \sum_{l=1}^{n_{st}} (e_l + \epsilon x_l) R_{l\alpha} \quad (3)$$

is the embedded dipole moment arising from the n_{st} proton binding sites.¹⁰

If we introduce

$$a_j = \left(\frac{3D}{2D + 1} \right) (\alpha_{j\alpha\alpha}^0 kT + \langle \mu_{j\alpha} \mu_{j\alpha} \rangle_0) \quad (4)$$

then, to a good approximation at low solute concentration

$$\frac{\Delta D}{g} = \frac{4\pi}{3kT} \left(\frac{\partial N_1}{\partial g} a_1 + \frac{\partial N_2}{\partial g} a_2 \right) \quad (5)$$

from which we may deduce that

$$a_2 = \frac{3kT}{4\pi} \frac{M_2}{N_A} \left[1000 \left(\frac{\Delta D}{g} \right) + \bar{v}_2 (D_0 - 1) \right] \quad (6)$$

in the limit of low protein concentration, where M_2 is the molecular weight of the solute, N_A is Avogadro's number, \bar{v}_2 is the partial specific volume of the solute, and D_0 is the dielectric constant of the solvent. If $\alpha_{2\alpha\alpha}^0$ is negligible, then eq 4 and 6 allow estimation of $\langle \mu_{2\alpha} \mu_{2\alpha} \rangle_0$ from the data.

The theoretical prediction of a_2 is similarly given in

terms of

$$\langle \mu_{\alpha} \mu_{\alpha} \rangle_0 = \langle \mu_{\alpha} \rangle_0 \langle \mu_{\alpha} \rangle_0 + \Delta(\mu_{\alpha} \mu_{\alpha}) \quad (7)$$

where the subscript $j = 2$ is not explicitly shown, and it has been assumed that $\alpha_{2\alpha\alpha}^0$ is negligible. $\Delta(\mu_{\alpha} \mu_{\alpha})$ is the fluctuation contribution to $\langle \mu_{\alpha} \mu_{\alpha} \rangle_0$.¹⁰ From eq 2

$$\langle \mu_{\alpha} \rangle_0 = \frac{2D + 1}{2D + D_p} \left[\frac{D_p + 2}{3} \langle \mu_{v\alpha} \rangle + \langle \mu_{e\alpha} \rangle \right] \quad (8)$$

If fluctuations of $\mu_{v\alpha}$ are negligible, then we also have

$$\Delta(\mu_{\alpha} \mu_{\alpha}) = \left(\frac{2D + 1}{2D + D_p} \right)^2 \Delta(\mu_{e\alpha} \mu_{e\alpha}) \quad (9)$$

The theoretical prediction therefore requires the calculation of $\langle \mu_{v\alpha} \rangle_0$, $\langle \mu_{e\alpha} \rangle_0$, and $\Delta(\mu_{e\alpha} \mu_{e\alpha})$. The method by which these quantities are evaluated below has been described.^{10,11}

Input Parameters for the Calculation. The model of horse oxy hemoglobin from which the site coordinates were obtained has been described.¹³ The same model was used to estimate the center of mass and intrinsic dipole moment. The computer-generated coordinates of all nonhydrogen atoms were used to calculate the center of mass. The masses of hydrogen atoms were combined with the masses of the atoms binding them. The center of mass was then calculated to be at $z = -1.52 \text{ \AA}$ in the crystal related coordinate system, $123 = xyz = c^*ab$. The intrinsic dipole moment was calculated on the assumption that only the planar peptide groups make a net contribution. Using a dipole magnitude of 3.7 D oriented at 57° to the CN bond,⁶ dipole moment magnitudes of 87 and 80 D were obtained for the α_1 and β_1 chains. The vector components for the α_1 and β_1 chains were $(\mu_x, \mu_y, \mu_z) = (-62, 59, -12)$ and $(77, 23, -2)$, respectively. The net moment of the tetramer was directed along the z axis, with $\mu_z = -28$ D. The intrinsic pK 's, site depth, protein dielectric constant, and masking inference were obtained by fitting the titration curve.¹³

To obtain site coordinates for deoxy hemoglobin, the α and β chains were rotated as rigid units.¹⁷ The center of mass shifted to $z = -1.51 \text{ \AA}$, and the net dipole moment due to the planar peptides changed to $\mu_z = -15$ D. The three sites, Arg FG4 α , Arg C6 β , and His FG4 β were also assumed to be unmasked in the deoxy structure.¹³

To represent met hemoglobin, sites were introduced at the iron atoms having zero charge with no proton

(12) M. F. Perutz, *J. Mol. Biol.*, **13**, 646 (1965).

(13) W. H. Orttung, *J. Amer. Chem. Soc.*, **91**, 162 (1969); *Nature*, in press.

(14) L. Onsager, *J. Amer. Chem. Soc.*, **58**, 1486 (1936).

(15) The convention for Greek subscripts is the following. If a subscript appears twice in the same symbol or in a product of symbols, summation over that index is applied.

(16) D. A. Brant and P. J. Flory, *J. Amer. Chem. Soc.*, **87**, 2791 (1965).

(17) H. Muirhead, J. M. Cox, L. Mazzarella, and M. F. Perutz, *J. Mol. Biol.*, **28**, 117 (1967).

bound. A pK of 8.7 (suggested by spectrophotometric titration data¹⁸) was tried in a first calculation, and the sites were found to be fully occupied up to pH 9. In a second calculation, the sites were treated as histidine residues (intrinsic pK of 6.0¹³) and the apparent pK resulting from the calculation was about 7.8. It is thus clear that an intrinsic pK of about 7.0 should give an apparent pK of about 8.7 for these sites. Unfortunately, however, the available computer programs handle only singly excited distributions,^{10,11} while such a calculation would require consideration of multiply excited distributions. The best representation of met hemoglobin is therefore the first calculation (pK_{int} of 8.7), which would only be expected to be correct up to a pH of about 6.5 at which the $FeOH_2^+$ site begins titrating. The calculated titration curve between pH 4.5 and 6.5 is almost identical with, but slightly higher than, the calculated best fit for horse oxyhemoglobin.¹³

A representation of human oxy hemoglobin was obtained by removing His E13 β , His 20 β , Asp E13 β , Glu B2 β , and Glu H3 β and adding His Na2 β .¹⁹ The conversion of Arg G18 β to His was not made because Arg G18 β had already been assumed to be masked in the horse oxy hemoglobin titration calculations.¹³ All other sites and their coordinates were assumed to be the same as in horse oxy hemoglobin. The calculated titration curve is shown in Figure 1. The shift of the isoionic pH by almost 0.2 unit is in the same direction as the experimentally observed shift of 0.4 unit.²⁰

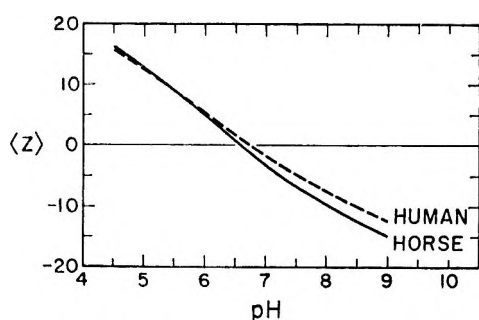


Figure 1. Comparison of the theoretical curves of horse and human oxy hemoglobin at zero ionic strength. The curve for horse hemoglobin is the best fit of the data obtained previously.¹³

Calculations

Detailed theoretical results for horse oxy hemoglobin are presented in Figures 2-6. The parameters used in the calculations were the same ones that gave the best fit of the individual site average approximation to the titration curve.¹³ The large difference between the group and individual site average approximations in Figure 2 emphasizes the importance of variations among sites of a given type. In Figure 3 it is seen that site variations are not as important in the fluctuation moment contribution. The group average calculation gives lower results than the individual site average

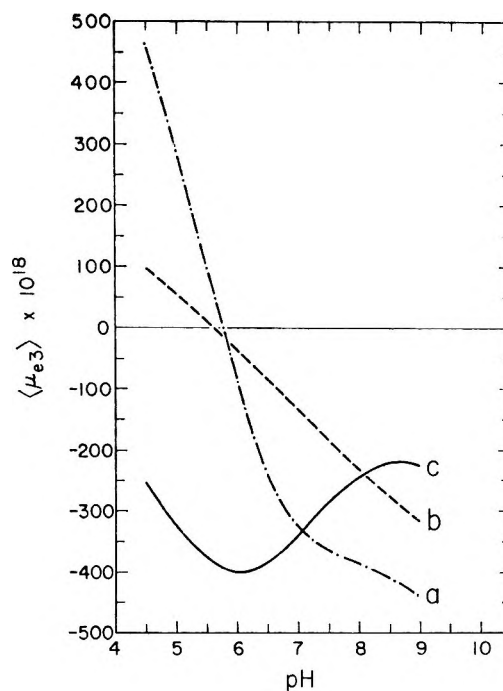


Figure 2. Theoretical mean embedded dipole moment of horse oxy hemoglobin due to the charges on proton binding sites: a, independent site approximation; b, group average approximation; c, individual site average approximation. The parameters used in the calculation gave the best fit of the titration curve.¹³

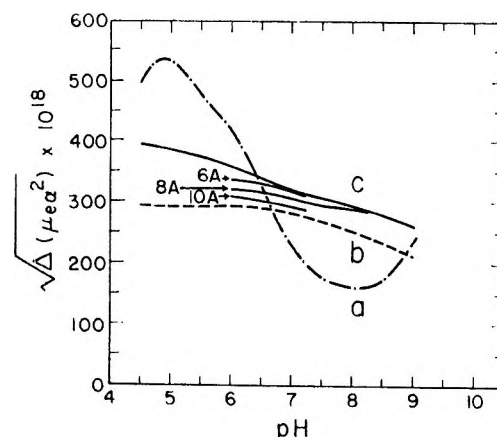


Figure 3. Theoretical rms embedded fluctuation dipole moment magnitude of horse oxy hemoglobin due to the charges on proton binding sites. The labels of curves a-c are the same as in Figure 2. The effect of including correlation averages for sites within 6, 8, and 10 Å of each other are also shown for limited pH intervals.

approximation. This difference is expected because the group average approximation includes a measure of the correlations between sites of the same type.¹⁰ The effect of including correlations in the individual

(18) P. George and G. Hanania, *Biochem. J.*, **55**, 236 (1953).

(19) "Atlas of Protein Sequence and Structure 1967-68," M. O. Dayhoff and R. V. Eck, Ed., The National Biomedical Research Foundation, Silver Spring, Md., 1968.

(20) C. Tanford and Y. Nozaki, *J. Biol. Chem.*, **241**, 2832 (1966).

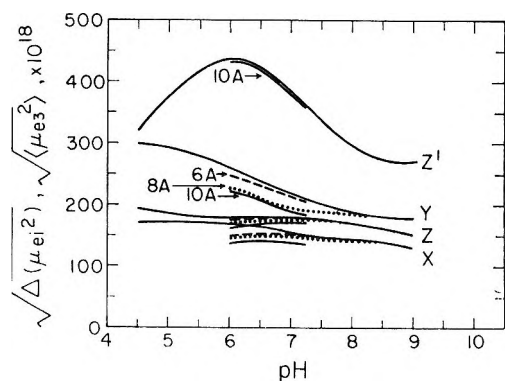


Figure 4. Theoretical rms principal values of the mean square fluctuation moment ellipsoid of horse oxy hemoglobin due to the charges on proton binding sites according to the individual site average approximation. The labels X, Y associate the curves with the closest axes x (c^*), y (a). Z' includes the mean embedded moment contribution of the site charges. The effect of including correlation averages for sites within 6, 8, and 10 Å of each other is shown for limited pH intervals.

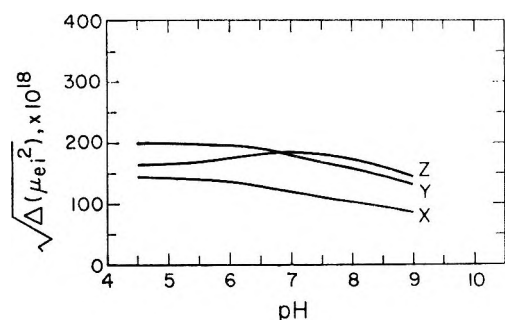


Figure 5. The curves are analogous to those of Figure 4, except that the group average calculation has been used.

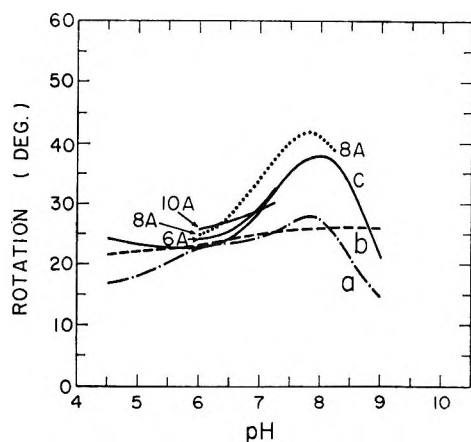


Figure 6. Theoretical rotation of the major axis labeled Y in Figures 4 and 5 from the y (a) axis toward the x (c^*) axis. The labels of curves a-c are the same as in Figures 2 and 3. The effect of including correlation averages for sites within 6, 8, and 10 Å of each other is also shown for limited pH intervals.

site average approximation is also shown in Figure 3. Correlations between sites separated by more than 10 Å are expected to be of importance,^{11,13} but such calcu-

lations would require an excessively long time on our present IBM 7040 computer. The anisotropy of the fluctuation moment is shown in Figure 4 for the individual site average and in Figure 5 for the group average approximation. It is clear that correlations have the strongest depressing effect on the fluctuations parallel to the long ($\sim a^*$) axis of the molecule. The rotation of the largest principal value in the xy (or xc) plane is shown in Figure 6. This result shows that the alignment of a protein in an electric field may vary considerably with pH. It will be shown that the anisotropy effects of Figures 4-6 are of considerable importance in the interpretation of the Kerr effect of hemoglobin.²¹

Figures 7 and 8 show the mean moment and fluctuation moment due to the bound protons and their sites for the various hemoglobin species that are closely related to horse oxy hemoglobin. The variations in the mean moment are much greater than the variations in the fluctuation moment. Additional details, of interest for Kerr effect interpretation, are shown in Table I. Figure 9 shows the root mean square moments obtained from eq 7-9. These values represent the most realistic calculations that could be performed at the present time. Deviations from the data could arise from several sources, including (1) neglect of correlations, (2) inaccuracies in the site coordinates, and (3) contributions to $\mu_{\nu\alpha}$ in addition to that of the peptide units. It should also be remembered that the calculations are for zero ionic strength.

Comparison with Data

Horse Oxy Hemoglobin. The experimental value of $\Delta D/g$ at 25° is 0.33 per g/l. at the isoionic pH (6.7-

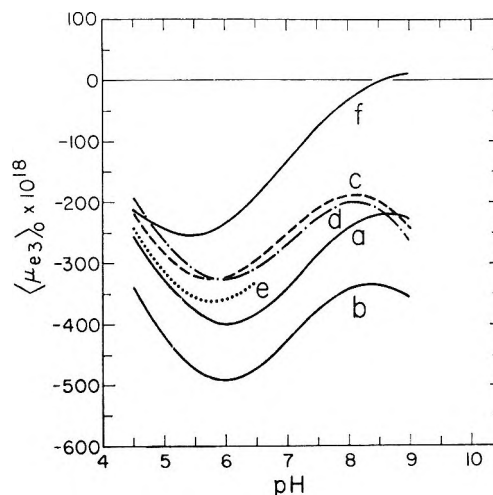


Figure 7. Theoretical mean embedded dipole moment due to the charges on proton binding sites: a, horse oxy hemoglobin, best fit of the titration curve; b, best fit (a), with Lys E9 α ; c, best fit (a), with FG4 α , C6 β , and FG4 β unmasked; d, same as (c), but with deoxy coordinates; e, met hemoglobin; f, human oxy hemoglobin.

(21) W. H. Orttung, to be published.

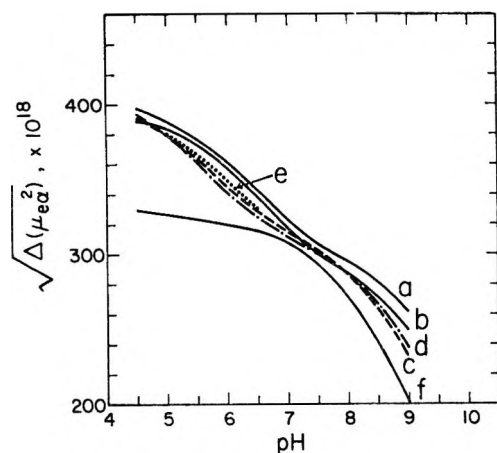


Figure 8. Theoretical rms embedded fluctuation dipole moment magnitude due to the charges on proton binding sites. The curves are labeled as in Figure 7 and do not include the effect of correlations.

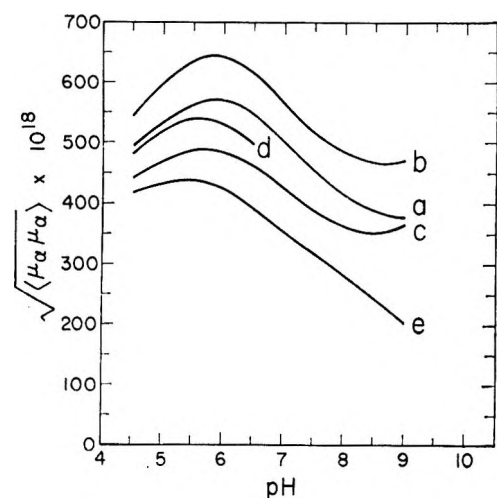


Figure 9. Theoretical estimates of the rms dipole moments of hemoglobin species; a, horse oxy hemoglobin, corresponding to the best fit of the titration curve; b, best fit (a), with Lys E9 α ; c, horse deoxy hemoglobin; d, horse met hemoglobin; e, human oxy hemoglobin. None of the curves includes the effect of correlations.

6.8).^{2,5} If $M_2 = 64,500$, $\bar{v}_2 = 0.75$ cc/g, and $D_0 = 78.4$, then from eq 6, $a_2 = 4.1 \times 10^{-31}$. If the polarizability term of eq 4 is negligible with respect to the dipole term, we obtain $(\langle \mu_{\alpha}^2 \rangle_0)^{1/2} = 523$ D. To obtain a comparative value from the theoretical results, two complicating factors must be considered: (1) correlations have not been fully considered in the calculations; and (2) in any given molecule, residues B5 α may be either Phe or Tyr and residues E9 α may be either Lys (slow component) or Gln (fast component).¹⁹ To bracket the correlation problem, we may first consider the individual site average calculation with no correlations (and Gln at E9 α). Using $D_p = 4$ and pH 6.75 in eq 7-9, $(\langle \mu_{\alpha}^2 \rangle_0)^{1/2} = 526$ D. If we substitute the

Table I: Theoretical Embedded Dipole Moment Averages for the Bound Protons and Their Sites of Hemoglobin Modifications at pH 7

Calculation ^a	Corr radius, Å	$\langle \mu_{e\alpha} \rangle_0 \times 10^{18}$	$\Delta(\mu_{e\alpha}\mu_{e\beta}) \times 10^{18}$			
			$\alpha\beta = 11$	$\alpha\beta = 22$	$\alpha\beta = 33$	$\alpha\beta = 12$
(a)	0	-340	29,641	41,597	33,144	9,493
	6		28,735	40,272	32,940	9,638
	8		27,780	33,760	32,380	7,451
	10		23,263	32,137	30,444	6,988
(b)	17,338	28,828	33,377	6,898
(c)	0	-251	30,625	35,956	32,394	10,095
(d)	0	-269	27,178	35,430	34,202	6,856
(e)	0	-426	29,519	37,951	33,231	8,723
(f)	0	-282	27,999	36,912	32,702	9,805
(g)	0	-133	28,963	33,837	31,494	8,605

^a The configurations for the various calculations were as follows: (a) best fit of the horse oxy hemoglobin titration curve, using the individual site average approximation; (b) same as (a), but using the group average approximation; (c) same as (a), with sites FG4 α , C6 β , and FG4 β unmasked; (d) same as (c), with subunits rotated to the deoxy position;¹⁷ (e) same as (a), with both E9 α sites Lys rather than Gln; (f) same as (a), but positive charge on the Fe atoms, approximating met hemoglobin; (g) sequence modification of (a) to approximate human oxy hemoglobin.

group average approximation for the fluctuation contribution, $\Delta(\mu_{e\alpha}^2)$, the above becomes 501 D, suggesting that correlations depress the theoretical moment by about 25 D.

The B5 α substitution is probably not of importance for dielectric properties since neither residue bears a charge at neutral pH. The E9 α substitution should be quite important, however, since Lys bears a positive charge and Gln is uncharged at neutral pH. Four molecular species should exist in solution having 0, 1, 1, and 2 Lys E9 α groups. The molecules having only one Lys E9 α do not have a twofold electric symmetry axis, and could not be subjected to calculations because of computer time considerations. From the individual site average calculation with no correlations and two Lys E9 α , we obtain $(\langle \mu_{\alpha}^2 \rangle_0)^{1/2} = 592$ D.

According to our model, the coordinates of Lys E9 α_1 relative to the center of mass are $(x, y, z) = (23, 20, -15)$ Å, corresponding to an embedded dipole moment, $e r_{\alpha}$, of (111, 94, -72) D. As may be seen from Figure 7, the change in the embedded dipole moment upon adding two Lys E9 α residues is only -85 D rather than the $2 \times -72 = -144$ D that would result by simply adding the sites without affecting other charge binding equilibria. If the above observation is used as a correction factor, the change in embedded moment upon adding one Lys E9 α may be taken as (65, 56, -43) D. If the change in the fluctuation moment is assumed to be negligible, then we obtain the estimate $(\langle \mu_{\alpha}^2 \rangle_0)^{1/2} = 545$ D for the species containing only one Lys

E9 α , ignoring correlation effects in the individual site calculation. If Lys and Gln are present in equal amounts, the relative concentrations of the 0, 1, 2 Lys species will be $1/4$, $1/2$, $1/4$, respectively. A weighted average of the above moments (526, 545, and 592 D) then gives 552 D. If correlations reduce this value by 25 D, as suggested above, we obtain a theoretical estimate of 527 D, in surprisingly good agreement with the "experimental" value of 523 D.

Other Modifications. The experimental dielectric increments suggest that horse met,⁴ deoxy,⁵ and oxy hemoglobin have essentially identical rms dipole moments, but that human oxy hemoglobin is 5–10% lower.⁵ The theoretical comparison shown in Figure 9 predicts that human oxy should be about 30% lower and that horse met and deoxy should be about 10 and 20% lower than horse oxy hemoglobin. The pH dependence of met hemoglobin is also predicted to be negative, in disagreement with the available data on fairly concentrated solutions (30–40 g/l.).⁴ An explanation for these discrepancies is not apparent at this time. It is possible that structural differences occur which were not recognized by the theoretical calculations.

Discussion

The calculations presented in this paper suggest that it is possible to achieve a detailed molecular interpretation of the dielectric properties of protein solutions. To pursue the subject further, it will be necessary to have more extensive experimental results, particularly including pH dependence. The availability of more reliable structural information will also help to remove some of the uncertainties in the present analysis, and the use of larger computers should allow the effect of correlations between the proton binding sites to be considered in a more satisfactory way.

The original objective of these calculations was to provide a basis for a molecular interpretation of Kerr effect optical dispersion data on hemoglobin.²² The Kerr effect is more difficult to interpret than the dielectric constant since it depends on both optical and electrostatic parameters. However, it also has a greater potential as a method for studying protein structure in solution. The results presented here provide a necessary input for the Kerr effect analysis.²¹

(22) W. H. Orttung, *J. Amer. Chem. Soc.*, **87**, 924 (1965).

A Nuclear Magnetic Resonance Study of the Association of Porphyrins in Chloroform Solution. Mesoporphyrin IX Dimethyl Ester and Its Nickel Chelate

by Daryl A. Doughty and C. W. Dwiggin, Jr.

*Bureau of Mines, Bartlesville Petroleum Research Center, U. S. Department of the Interior,
Bartlesville, Oklahoma (Received August 26, 1968)*

The proton nmr spectra of chloroform solutions of mesoporphyrin IX dimethyl ester and its nickel chelate exhibit an appreciable concentration dependence, all peaks shifting downfield upon dilution. This dilution shift is greater for the nickel chelate. The spectra of both porphyrins exhibit additional fine structure at higher concentrations. These results are interpreted in terms of porphyrin association with equilibrium between monomer and dimer forms. In the dimer two porphyrin molecules are stacked one above the other with the planes of the molecules parallel and separated by 10.0 Å in the mesoporphyrin and 7.9 Å in the chelate. In the nickel chelate, association is enhanced by the slight affinity of the nickel for further coordination. The fine structure can be accounted for by a lateral displacement of one molecule in the dimer relative to the other. This displacement is caused by steric interference of the longer side chains. No attempt was made to calculate the magnitude of the displacement for either porphyrin.

Introduction

During an investigation of metalloporphyrins contained in petroleums, a proton nmr study of mesoporphyrin IX dimethyl ester and its nickel and vanadyl chelates was undertaken. Preliminary work soon

established the impracticability of using high-resolution nmr on the vanadyl chelate. The broadening of the peaks in the spectra of this chelate, an effect due to the strong paramagnetism of the vanadyl complex,¹ pro-

(1) D. Kivelson and S.-K. Lee, *J. Chem. Phys.*, **41**, 1896 (1964).

hibited interpretation. Therefore, the remainder of this paper is confined to the mesoporphyrin and its nickel chelate.

The nmr spectra of chloroform solutions of both porphyrins exhibit an appreciable concentration dependence,² that of the nickel chelate being more pronounced. A definitive study of the concentration dependence of chloroform solution spectra of coproporphyrin tetramethyl esters has been reported.³ Abraham, *et al.*, explained the concentration dependence of coproporphyrins in terms of a monomer-dimer association, the dimer consisting of two porphyrin molecules stacked one above the other with the planes of the porphyrin rings parallel. The concentration effect in the nmr spectra of mesoporphyrin IX dimethyl ester and the influence of the nickel in enhancing this effect for the nickel chelate is the main interest of this paper.

Experimental Section

Solutions of the mesoporphyrin IX dimethyl ester and its nickel chelate were prepared in CDCl_3 with tetramethylsilane as an internal reference. The CDCl_3 was stored over calcium oxide to remove phosgene and filtered prior to use.⁴ Concentrations of the solutions ranged from 0.01061 (mole fraction) to 0.00025 for the mesoporphyrin and from 0.0122 to 0.00038 for the nickel chelate. The spectra were obtained with a Varian⁵ DP-60 spectrometer. Sample temperature was approximately 30°. Accuracy of peak location was assured by bracketing each peak or group of peaks in the spectra by two side bands using two audio oscillators and a Hewlett-Packard Model 523C electronic counter. Individual chemical shift measurements are estimated to be accurate to ± 0.01 ppm. The values shown in Table I are the average of two measurements at each concentration.

Results

As shown in Table I, all peaks in the nmr spectra of mesoporphyrin IX dimethyl ester and its nickel chelate shift to low field upon dilution in chloroform solution. The shift to low field upon dilution is greater for the nickel chelate. The amount of shift is greatest in each porphyrin for the *meso* hydrogens and least for the methoxyl hydrogens in the ester side chains.

The peaks of the chelate spectra are located upfield compared with the corresponding peaks in the mesoporphyrin spectra.⁶ (The methoxyl hydrogens, isolated from direct ring effects by the long side chain, are an exception.)

At high concentration, several of the peaks in the spectra of both porphyrins exhibit fine structure not due to spin-spin coupling. This fine structure disappears upon dilution. In the mesoporphyrin spectra, the β -methyl peak is a 2:2 doublet. In the chelate spectra, the β -methyl peak is a 1:1:2 triplet, and the *meso* peak is a 1:1:1:1 quadruplet. The shift values given

Table I: Proton Chemical Shifts^a as a Function of Concentration in CDCl_3 in Mole Fraction

Concn	β -Methyl	Methoxyl	CH_2CH_2^-	CH_3CO_2^- CH_2CH_2^-	<i>Meso</i>
Mesoporphyrin IX Dimethyl Ester					
0.01061	3.440	3.620	3.890	4.220	9.825
0.01002	3.435	3.600	3.890	4.235	9.830
0.00902	3.465	3.620	3.915	4.270	9.865
0.00803	3.490	3.625	3.945	4.290	9.895
0.00703	3.510	3.630	3.930	4.290	9.895
0.00603	3.510	3.625	3.965	4.315	9.915
0.00533	3.535	3.640	3.980	4.320	9.930
0.00503	3.535	3.640	3.975	4.320	9.945
0.00453	3.545	3.640	3.990	4.350	9.955
0.00403	3.560	3.650	4.010	4.365	9.970
0.00332	3.570	3.640	4.020	4.375	9.985
0.00266	3.590	3.650	4.025	4.390	9.995
0.00202	3.595	3.650	4.045	4.400	10.030
0.00165	3.610	3.650	4.070	4.425	10.040
0.00135	3.610	3.640	4.050	4.405	10.045
0.00101	3.625	3.655	4.070	4.425	10.055
0.00082	3.620	3.640	4.080	4.440	10.065
0.00068	3.635	3.660	4.085	4.440	10.070
0.00050	3.625	3.650	4.095	4.440	10.080
0.00034	3.640	3.655	4.100	4.450	10.080
0.00025	3.635	3.650	4.080	4.440	10.090
Ni Mesoporphyrin IX Dimethyl Ester					
0.01220	3.225	3.625	3.645	3.985	9.390
0.01100	3.260	3.645	3.690	4.020	9.420
0.01010	3.255	3.635	3.700	4.025	9.420
0.00915	3.275	3.640	3.705	4.045	9.450
0.00824	3.280	3.645	3.720	4.050	9.450
0.00733	3.320	3.650	3.750	4.100	9.520
0.00613	3.335	3.660	3.755	4.110	9.545
0.00505	3.355	3.660	3.780	4.135	9.560
0.00414	3.360	3.660	3.795	4.140	9.590
0.00307	3.390	3.655	3.830	4.175	9.640
0.00254	3.395	3.660	3.840	4.185	9.645
0.00207	3.440	3.685	3.880	4.230	9.705
0.00155	3.435	3.670	3.870	4.225	9.705
0.00127	3.450	3.680	3.880	4.225	9.715
0.00103	3.460	3.685	3.900	4.250	9.725
0.00077	3.473	3.680	3.900	4.250	9.740
0.00062	3.465	3.680	3.905	4.255	9.745
0.00038	3.490	3.695	3.925	4.275	9.770

^a All chemical shifts are measured in ppm below TMS.

in Table I for these multiplets are the mean shifts obtained by weighting the shift of each component of a multiplet with its relative abundance in the multiplet.

Before considering any specific solute association, the chemical shift data must be corrected for general solu-

(2) *Cf.* R. J. Abraham, P. A. Burbidge, A. H. Jackson, and G. W. Kenner, *Proc. Chem. Soc.*, 134 (1963).

(3) R. J. Abraham, P. A. Burbidge, A. H. Jackson, and D. B. Macdonald, *J. Chem. Soc., B*, 620 (1966).

(4) A. H. Corwin, "Proceedings of the Fifth World Petroleum Congress," Section V, New York, N. Y., June 1959, p 119.

(5) Reference to trade names is made for identification only, and does not imply endorsement by the Bureau of Mines.

(6) *Cf.* W. S. Caughey and W. S. Koski, *Biochemistry*, 1, 923 (1962).

Table II: Chemical Shift of CHCl_3^a Peak as a Function of Porphyrin Concentration in CDCl_3

Mesoporphyrin IX dimethyl ester Concn	δ_a	Ni mesoporphyrin IX dimethyl ester Concn	δ_a
0.00823	7.158	0.00853	7.165
0.00631	7.178	0.00719	7.185
0.00521	7.188	0.00506	7.200
0.00371	7.210	0.00380	7.217
0.00186	7.238	0.00254	7.230
0.00093	7.244	0.00127	7.245
0.00046	7.255	0.00064	7.255
		0.00047	7.253

^a Residual CHCl_3 in the available CDCl_3 .

tion effects. These effects are shifting of the internal reference peak upon dilution, change in bulk susceptibility of the solution upon dilution, and random averaging of the porphyrin ring current over the sample volume. The study of coproporphyrins³ showed that the first two effects may be neglected for solutions of porphyrins in chloroform (the correction being 0.01 ppm or less for the concentration range in question) and that the correction for the last effect is best obtained by subtracting the chloroform concentration shift ($\delta_a - \delta_\infty$) at any concentration from the observed porphyrin chemical shift at that concentration. The variation of chloroform chemical shift with porphyrin concentration is given in Table II. The corrected data for the nickel chelate showing the dilution shift due only to solute association are plotted in Figure 1.

Assuming the monomer-dimer association to account for the concentration dependence of the nmr spectra of mesoporphyrin and its nickel chelate, the observed

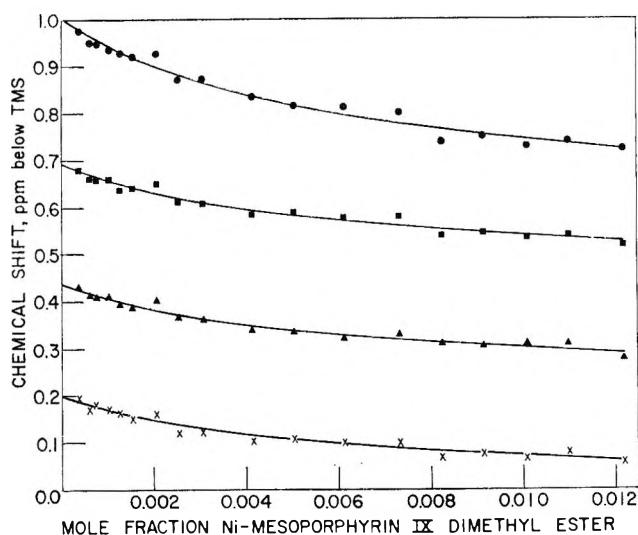


Figure 1. The chemical shifts of nickel mesoporphyrin IX dimethyl ester vs. concentration in chloroform: ●, *meso* protons (−8.80 ppm); ■, $\text{CH}_3\text{CO}_2\text{CH}_2\text{CH}_2-$ (−3.60 ppm); ▲, CH_3CH_2- (−3.50 ppm); ×, β -methyl protons (−3.30 ppm). The solid curves shown are computed for $K = 61.6$ and the monomer and dimer shifts given in Table III.

chemical shift of the porphyrin in solution is given by³

$$\delta = \delta_1 + (\delta_2 - \delta_1) [1 + \frac{1}{4}aK - (1 + 8aK)^{1/2}/4aK] \quad (1)$$

where δ_1 and δ_2 are the chemical shifts of the monomer and dimer, respectively, K is the equilibrium constant, and a is the porphyrin concentration in mole fraction.

Using a least-squares computer program, this relationship was fitted to the corrected data for both porphyrins. Values for the three unknown parameters giving a best fit were obtained. The value obtained for K was 30.9 for the mesoporphyrin and 61.6 for the nickel chelate. The corresponding monomer and dimer shifts are given in Table III.

The degree to which the protons on one ring of the dimer are shielded by the ring current of the second ring may be calculated from existing theory.⁷ The graph of Johnson and Bovey on the benzene ring-current field, giving shielding values as a function of position about the benzene ring, may be adjusted for the porphyrin ring current in the mesoporphyrin by multiplying by 0.88 to account for the larger ring radius and the increased number of π electrons.⁸ The ring current for the chelate is apparently reduced by incorporation of the nickel as shown by the occurrence of peaks in the chelate spectra at higher field compared with corresponding peaks in the mesoporphyrin spectra. The amount of reduction in the ring current may be found by comparing the *meso* hydrogen monomer shifts of the chelate and the mesoporphyrin after first correcting the shift values for that fraction due solely to the bond hybridization of the protons which is the same for both porphyrins. This fraction is best given by the shift for a close olefinic analog of the *meso* hydrogens in the absence of a circulating field (5.87 ppm⁷). When this fraction is subtracted from the monomer shifts of the *meso* hydrogens, the shift due to the ring current of the chelate is approximately 7% less than that of the mesoporphyrin. This gives a correction factor of 0.82 by which to adjust the benzene field for the nickel chelate ring current. Using the monomer-dimer shifts ($\delta_2 - \delta_1$) in Table III as the shielding values experienced by the protons on one ring from the ring-current field of the second ring, it is possible to determine the separation of the two porphyrin rings in the dimer. The best fit for the mesoporphyrin is obtained for a separation of 10.0 Å. The estimated monomer-dimer shifts at this separation were 0.38 ppm for the *meso* hydrogens and 0.23 ppm for both the β -methyl and α -methylenic hydrogens. These compare favorably with the observed values of 0.44 and 0.27 ppm. (The last is an average of the three observed values for the β -methyl and the α -methylenic hydrogens.) The best fit for the nickel chelate is ob-

(7) C. E. Johnson, Jr., and F. A. Bovey, *J. Chem. Phys.*, **29**, 1012 (1958).

(8) R. J. Abraham, *Mol. Phys.*, **4**, 145 (1961).

Table III: Extrapolated Monomer and Dimer Shifts

	β -Methyl	CH_2CH_2^-	$\begin{matrix} \text{CH}_2\text{CO}_2 \\ \text{CH}_2\text{CH}_2^- \end{matrix}$	<i>Meso</i>
	(a) Infinite Dilution (Monomer) Chemical Shift δ_1			
Mesoporphyrin IX dimethyl ester	3.647	4.100	4.458	10.095
Ni mesoporphyrin IX dimethyl ester	3.500	3.938	4.293	9.805
	(b) Shift to High Field of Dimer Compared with Monomer ($\delta_2 - \delta_1$)			
Mesoporphyrin IX dimethyl ester	-0.237	-0.262	-0.299	-0.437
Ni mesoporphyrin IX dimethyl ester	-0.309	-0.325	-0.364	-0.621

tained for a separation of 7.9 Å. The estimated monomer-dimer shifts were 0.56 and 0.34 ppm, respectively, for the *meso* and for the β -methyl and α -methylenic hydrogens. These compare favorably with the observed values of 0.62 and 0.33 ppm. (Again, the last is an average.)

Discussion

The results show that the observed concentration dependence in the nmr spectra of mesoporphyrin IX dimethyl ester and its nickel chelate in chloroform solution is adequately accounted for by the monomer-dimer association. The possibility of further association, *i.e.*, trimer, etc., is present, especially at the higher concentrations.³ This would not modify the vertical stacking of the porphyrin molecules in the complex, however, the additional molecules merely adding above or below the dimer. The gain in understanding derived from accounting for the possibility of higher order complexes in the quantitative interpretation is not commensurate with the resulting increase in complications. The dimer complex by itself adequately accounts for the observed dilution shift of both the mesoporphyrin and its nickel chelate.

The association mechanism is probably an electrostatic interaction between the π -electron clouds of the two porphyrin rings.³ This effect is known to occur with other aromatic molecules in solution^{9,10} and appears to be a general characteristic of aromatic molecules unless masked by more pronounced competing mechanisms.

That the association is enhanced by the presence of the nickel is apparent from the more pronounced dilution shift of the chelate and the decreased separation of the porphyrin rings in the chelate dimer. However, the vertical stacking of the porphyrin rings in the dimer is apparently not affected by the presence of the nickel because the same complex model gives good results for both porphyrins. Therefore, the effect of the nickel is apparently different from that of other metals such as iron and magnesium in metalloporphyrins and chlorophylls which form much stronger complexes in solution.^{11,12} These complexes are formed by further co-

ordination between the metal in the center of the ring and electron-donating groups on the porphyrin side chains, clearly leading to a different structure for the complex. No evidence for further coordination of the nickel chelates of mesoporphyrins has been found, but under favorable conditions donor ligands can coordinate to nickel chelated in other porphyrins.¹¹ It is therefore possible that nickel has a slight affinity for further coordination even when chelated with mesoporphyrin. In the chelate dimer, the primary association mechanism is the electrostatic interaction which stacks the porphyrin molecules one above the other. The π -electron cloud of one porphyrin molecule could therefore be in a position to serve as an electron-donating ligand to the nickel in the other porphyrin molecule of the dimer. Even though the separation of the two molecules is larger in the dimer than that of other coordination complexes,¹² the weak nature of the electrostatic interaction would require only a small assist from this weak coordination to show a noticeable enhancement.

The fine structure exhibited by some of the peaks in the spectra of both porphyrins is undoubtedly connected to the association since it disappears upon dilution. This fine structure can be accounted for by a lateral displacement of the centers of the two porphyrin rings in the dimer.³ No attempt was made to calculate the magnitude of the displacement for either the mesoporphyrin or the chelate. This displacement is caused by steric interference of the longer porphyrin side chains. There is increased fine structure in the nickel chelate spectra because of the decreased separation of the rings in this dimer. This decreased separation necessitates a greater lateral displacement for steric accommodation with a concomitant greater degree of magnetic non-equivalence of different substituent locations in the chelate dimer.

(9) S. C. Chan, M. P. Schweizer, P. O. P. Tao, and G. K. Helmkamp, *J. Amer. Chem. Soc.*, **86**, 4182 (1964).

(10) J. N. Murrell and V. M. S. Gil, *Trans. Faraday Soc.*, **61**, 402 (1965).

(11) J. E. Falk, "Porphyrins and Metalloporphyrins," Elsevier, Amsterdam, 1964, Chapter 3.

(12) G. L. Closs, J. J. Katz, F. C. Pennington, M. R. Thomas, and H. H. Strain, *J. Amer. Chem. Soc.*, **85**, 3809 (1963).

The Anodic Oxidation of Saturated Hydrocarbons. A Mechanistic Study

by J. O'M. Bockris, E. Gileadi, and G. E. Stoner

The Electrochemistry Laboratory, University of Pennsylvania, Philadelphia, Pennsylvania 19104 (Received June 12, 1968)

Determinations were made of the rate of electrochemical oxidation of propane, *n*-hexane, cyclohexane, and 2,2-dimethylbutane in concentrated phosphoric acid solutions at 80–150°. Transient values were recorded at fixed potentials upon introducing the reactant to solution. Steady-state rates were measured as a function of propane pressure, the activity of water, and the electric field gradient applied across the surface on which the reaction occurred. The Tafel slope is F/RT in the low-rate section of the rate-potential relation. The order of reaction with respect to hydrocarbon is one; that for water is zero. The rate at constant field gradient as a function of time passes through a maximum at about $t = 5$ sec. At constant potential, the rate of oxidation to CO_2 is propane > 2,2-dimethylbutane > *n*-hexane > cyclohexane. At potentials of more than 0.48 V on the hydrogen scale, the rate of oxidation at 80–130° decreases anomalously with increasing field. For propane, at 135–150°, the rate undergoes inhibition at 0.48 V but continues to increase with an increase in field strength. Some 15 partial-mechanism hypotheses (suggested sequences up to and including the rate-determining step) are used to predict the kinetic behavior for which data exist. Large numbers of the sequences are excluded by the coefficient $\partial \log(\text{rate})/\partial(\text{electric field strength})$. Two (partial) mechanisms are consistent with the observations. Of these, that which is most consistent with energy considerations of the bonding involved is the most likely. It is, for a saturated hydrocarbon RH: $\text{RH} \rightleftharpoons \text{R}_{\text{ads}} + \text{H}^+ + \text{e}^-$ and $\text{R}_{\text{ads}} \xrightarrow{\text{rds}}$ organic radicals. The rate-determining step for the alternative possibility was also a chemical reaction. The hypothesis is applied to the interpretation of the $i-t$ transient. It yields a value for $\theta_{\text{C}_2\text{H}_5}$ (480 mV) of 0.3. The inhibition occurring above 0.48 V is shown to be consistent with data published elsewhere for the adsorption of H_2PO_4^- .

Introduction

The electrooxidation of saturated hydrocarbons has received considerable attention in the past decade because of their connection with the development of electrochemical energy-conversion devices. The majority of the attention and, hence research effort, has been devoted either to the measurement of adsorption by various anodic and cathodic transient techniques^{1–6} or to the technological aspects of actual fuel cell systems.^{7–14} One factor contributing to lack of progress in the case of the latter is the absence of knowledge of the mechanism, in particular the rate-determining step, of these anodic hydrocarbon reactions under steady-state conditions.

The present work is concerned with the determination and interpretation of criteria relevant to the mechanism for the anodic oxidation of a series of saturated hydrocarbons at platinum electrocatalysts.

Experimental Section

1. *The Cell.* A special three-compartment cell was designed so as to allow its immersion in a thermostated bath which could be regulated from 80 to 150°. Figure 1 is a diagram of the cell. The reference and auxiliary electrodes have been described elsewhere.^{15,16}

The cap of the anode compartment, A, which contains the anode was replaced by a rotating-electrode assembly (described in another section) when hydrocarbon partial pressure measurements were made.

2. *Reagents Used.* The following reagents were used: Phosphoric Acid, Baker Analyzed reagent, 85

wt % H_3PO_4 ; Monsanto Phospholeum, concentrated 105% (76 wt % P_2O_5) phosphoric acid; hydrogen peroxide, Baker Analyzed reagent, 30 wt %; propane, Matheson CP grade, 99.5% minimum purity; *n*-hexane, Fisher Certified reagent, 99.94% minimum purity, bp 68.7°; cyclohexane, Fisher Certified reagent, 99.92% minimum purity, bp 81.4°; 2,2-dimethylbutane, City Chemical Corp., New York, N. Y., reagent grade,

- (1) S. Gilman, *J. Phys. Chem.*, **67**, 1898 (1963).
- (2) S. Gilman, *ibid.*, **66**, 2657 (1962).
- (3) S. Gilman, *ibid.*, **67**, 78 (1963).
- (4) S. B. Brummer, *ibid.*, **69**, 562 (1965).
- (5) S. B. Brummer, *ibid.*, **69**, 1363 (1965).
- (6) S. B. Brummer, J. I. Ford, and M. J. Turner, *ibid.*, **69**, 3424 (1965).
- (7) Progress Report No. 2, Contract No. DA-44-009-AMC-897(T), American Cyanamid Co., 1965.
- (8) Progress Report No. 3, Contract No. DA-44-009-AMC-897(T), American Cyanamid Co., 1966.
- (9) Progress Report No. 4, Contract No. DA-44-009-AMC-897(T), American Cyanamid Co., 1967.
- (10) Progress Report No. 1, Contract No. DAAK02-67-C-02.9, Engelhard Industries, 1967.
- (11) E. J. Cairns and D. I. Macdonald, *Electrochem. Technol.*, **2**, 65 (1964).
- (12) W. T. Grubb, *Nature*, **201**, 699 (1964).
- (13) W. T. Grubb and C. J. Micholske, *ibid.*, **201**, 287 (1964).
- (14) W. T. Grubb, *J. Electrochem. Soc.*, **111**, 1086 (1964).
- (15) Report No. 2, Contract No. DA-44-009-AMC-469(T), Electrochemistry Laboratory, University of Pennsylvania, Philadelphia, Pa., 1966.
- (16) Report No. 3, Contract No. DA-44-009-AMC-469(T), Electrochemistry Laboratory, University of Pennsylvania, Philadelphia, Pa., 1966.

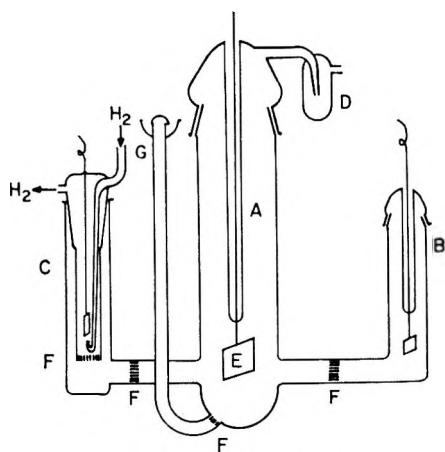


Figure 1. Diagram of the cell for studies in H_3PO_4 : A, working-electrode compartment; B, counterelectrode compartment; C, reference-electrode compartment; D, gas-outlet bubbler; E, working electrode; F, glass frits; G, gas inlet.

99.89% minimum purity; hydrogen, Matheson CP grade, 99.994% minimum purity.

3. *Rotating-Electrode Assembly.* For the determination of reaction orders with respect to hydrocarbon concentrations, a rotating-electrode assembly, shown in Figure 2, was used. The driving motor was a Bodine Electric Universal Motor Type NSE-12 (8800 rpm (maximum)). The speed of the motor was varied by a General Radio Variac speed control, Type 1701-AU. Electrical contact was made to the rotating electrode through a mercury seal in the cell cap. The mercury was in continuous contact with an inverted stainless steel cap which was Teflon coated on the side exposed to the atmosphere above the cell. This cap was connected with setscrews to the Teflon-coated rotating shaft which extended into the solution. The electrode was a platinum-plated 23 karat gold cylinder which was machine threaded to screw into the end of the stainless steel shaft, thus giving rigid physical and excellent electrical connections to the shaft. The rotating shaft could be raised from or lowered into the cell by three aluminum telescopic supports connecting the upper ball bearing housing and motor assembly to a solid-aluminum base plate which rested under the thermostated bath.

4. *Electrical Accessories.* The potentiostatic and galvanostatic circuitries have been described elsewhere.^{17,18}

5. *Constant-Temperature Bath.* The constant-temperature bath was a 1 ft \times 1.5 ft \times 0.75 in. porcelain tank containing 20 lb of A. H. Thomas No. 6407-J silicone fluid (bp 200°). The bath was heated by two A. H. Thomas No. 6147-G3 immersion knife-type heaters (500 W (maximum)) and were controlled through Superior Electric Powerstat Type 110 voltage regulators. One heater-regulator was controlled by a Brooks Instrument Brookstat proportional control

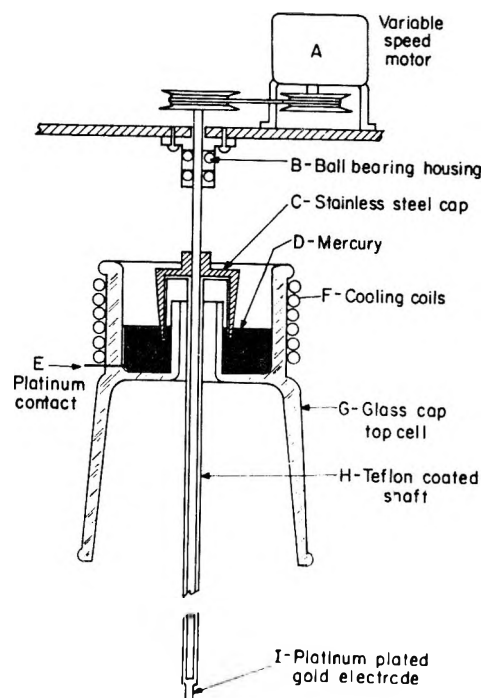


Figure 2. The rotating-electrode assembly.

thermoregulator, No. BS-1318, giving a bath-temperature control of $\pm 0.3^\circ$.

6. *Apparatus for Pretreating Reagent.* a. *Phosphoric Acid.* The phosphoric acid was refluxed at 150° for 12 hr after addition of 5 vol % of a 30% solution of hydrogen peroxide to destroy any undesirable organic matter. The excess water was then distilled off until the original concentration of phosphoric acid (before addition of H_2O_2) was obtained.

b. *Hydrocarbons.* Propane was passed through a solution of 10% KMnO_4 in 6 M NaOH and then through concentrated sulfuric acid to remove any traces of unsaturated hydrocarbons which may have existed as impurities more active than propane. The liquid hydrocarbons (*n*-hexane, cyclohexane, and 2,2-butadiene) were passed, as liquids, over Union Carbide molecular sieves, Type 3-A, which will adsorb unsaturates, water, hydrogen, and oxygen-containing organic species.

With the liquid hydrocarbons it was also necessary to vaporize them before passing them into the cell which was substantially above their boiling point, whereby the "hexanes," once vaporized, were maintained as gases by wrapping the connecting tubing between the vaporization flask and the bath with Briscoe Manufacturing No. 6148A flexible heating tapes.

c. *Presaturation.* All gases were passed through a series of presaturator liquid traps immersed in the bath containing phosphoric acid at the same concentration as that in the cell.

7. *Experimental Procedure.* The experimental pro-

(17) B. J. Piersma, Ph.D. Thesis, University of Pennsylvania, 1965.

(18) J. O'M. Bockris, H. Wroblowa, E. Gileadi, and B. J. Piersma, *Trans. Faraday Soc.*, 61, 2531 (1965).

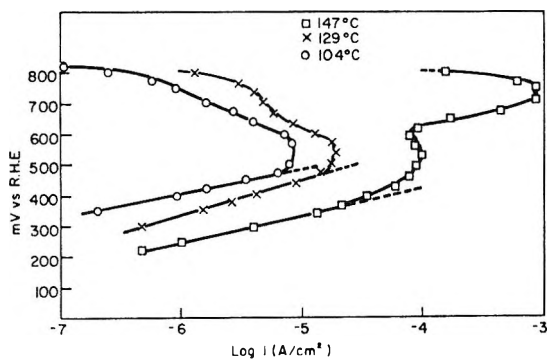


Figure 3. Current-potential behavior for the anodic oxidation of propane.

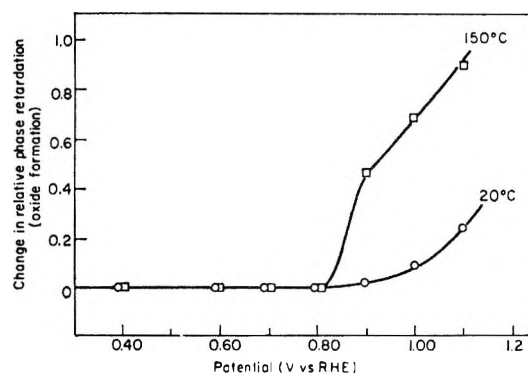


Figure 5. Ellipsometric data showing the potential of oxide formation on platinum in 85% H_3PO_4 .

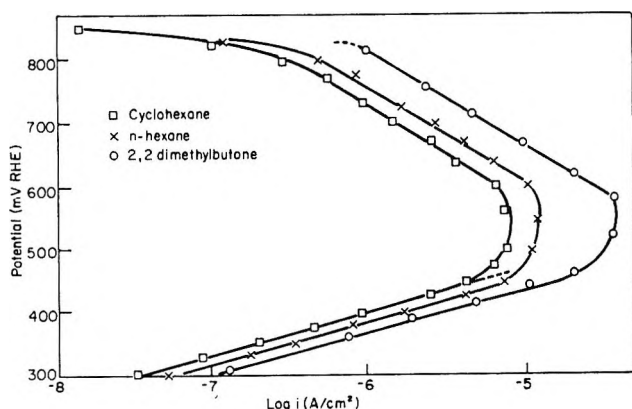


Figure 4. Current-potential behavior for the anodic oxidation of *n*-hexane, 2,2-dimethylbutane, and cyclohexane at 125°C.

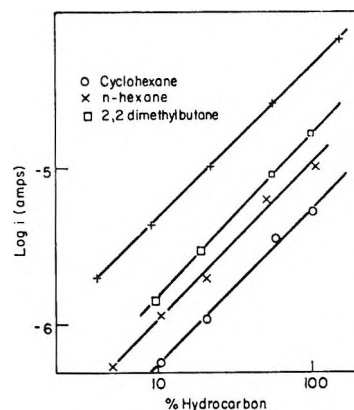


Figure 6. Reaction order with respect to hydrocarbon concentration for four hydrocarbons from 300 to 500 mV (reversible hydrogen electrode).

cedure for determining steady-state current-potential relations has been adequately described elsewhere.^{17,18} The determination of Faradaic efficiency by quantitative collection of CO_2 has also been described.¹⁷

Results

1. Current-Potential Behavior. The current-potential behavior for the four hydrocarbons (Figures 3 and 4) displays four characteristic regions. These regions are: (a) the region of linear V - $\log i$ behavior at potentials below 500 mV which exhibits a Tafel slope of $2.3RT/F$ at all temperatures in the range 100–150°; (b) the region of apparent passivation between 500 and 600 mV, occurring at all temperatures; (c) the region from 600 to 750 mV which depends on temperature as follows: (i) at temperatures from 100 to 125° there is a linear V - $\log i$ region with a negative Tafel slope of $-2.3(2RT/F)$; (ii) from 135 to 150° there is approximately one decade of linear V - $\log i$ behavior with an apparent Tafel slope of approximately $2.3(0.8RT/F)$ (this region is only exhibited by propane); and (iii) from 125 to 135° (for propane oxidation) there is a region in which the behavior is transitional between that of regions i and ii which does not display any linear V - $\log i$ behavior; and (d) above 750 mV for 135–150°

and 800 mV for 100–125°, a region of real passivation (this passivation region has been seen by Rao¹⁹ to be due to oxide formation (Figure 5)) in which the current-time behavior does not approach steady state but decreases to zero current.

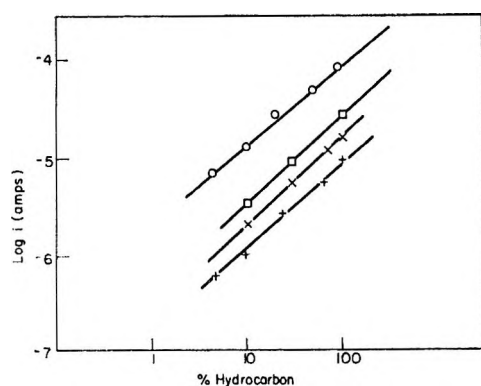
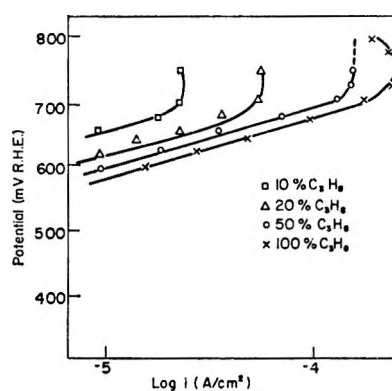
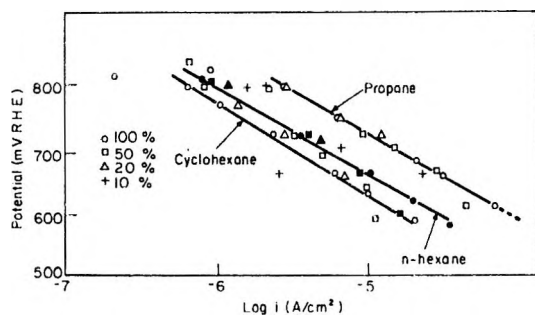
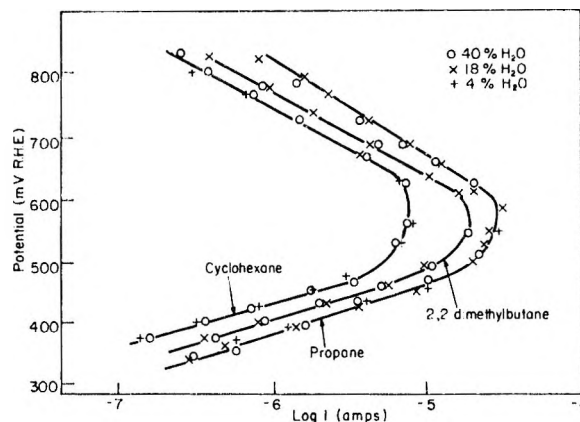
2. Reaction Order with Respect to a Hydrocarbon. The effect of hydrocarbon partial pressure on the rate of oxidation is as follows: (a) below 500 mV, the reaction is first order, as shown in Figure 6; (b) in the "quasi-passivation" region, the reaction is first order (Figure 7); (c) from 100 to 125° (or 150° for the hexanes), at 600–800 mV, the order is approximately zero (Figure 8) (for propane oxidation in this potential region and from 135 to 150°, dependence on propane concentrations is finite but small, *i.e.*, less than first order (Figure 9)); and (d) in the real passivation region, there is no observed pressure dependence.

3. Reaction Order with Respect to Water. The reaction rate is independent of water concentration from 49 to 4 mol % H_2O (Figure 10). In 85% H_3PO_4 , the pH values available in the literature are between -0.5

(19) "Phosphorus and Its Compounds," J. R. Van Wazer, Ed., Interscience Publishers, New York, N. Y., 1958.

Table I: Electrode Kinetic Parameters for Saturated Hydrocarbons at Platinum Electrodes in Phosphoric Acid from 280 to 500 mV (Reversible Hydrogen Electrode)

Hydrocarbon	i_0 , A/cm ² (geometric)	Q_{CO_2} , %	$(dV/d \ln i)_{P,T}$	$(di/dC_{H_2O})_{RH}$	$(d \ln i / d \ln P_{RH})_{H_2O}$
Propane (C ₃ H ₈)	7×10^{-9}	99 ± 2	RT/F	0	1
2,2-Dimethylbutane (C ₆ H ₁₄)	1.3×10^{-9}	89 ± 7	RT/F	0	1
<i>n</i> -Hexane (C ₆ H ₁₄)	0.6×10^{-9}	97 ± 5	RT/F	0	1
Cyclohexane (C ₆ H ₁₂)	0.13×10^{-9}	102 ± 5	RT/F	0	1

**Figure 7.** Reaction order with respect to hydrocarbon concentration from 500 to 600 mV (reversible hydrogen electrode).**Figure 9.** Concentration dependence for propane oxidation at 600–800 mV at 150°.**Figure 8.** Reaction order with respect to hydrocarbon concentration at 125° from 600 to 800 mV (reversible hydrogen electrode).**Figure 10.** Dependence on H₂O concentration in the range 40–4% H₂O for the anodic oxidation of hydrocarbons.

and +1.¹⁹ Such lack of precision and the difficulties encountered in systematically varying pH render determination of reaction order with respect to H⁺ impractical. The kinetic parameters and the results of the CO₂ determination are summarized in Table I.

4. *Transients.* The open-circuit potential was found to decrease upon introduction of a saturated hydrocarbon into the cell. (These transients do not occur when unsaturated hydrocarbon (*e.g.*, ethylene) is introduced.) A typical *V*-*i* transient is shown for propane in Figure 11. If, however, the same experiment is performed

while maintaining (potentiostating) the electrode at the original open-circuit value, one obtains anodic current-time transients characterized by Figures 12 and 13 for propane, *n*-hexane, and cyclohexane.

Discussion

1. *Preliminary Conclusions.* From the similar behavior of all the saturated hydrocarbons in terms of the kinetic parameters, the following conclusions can be drawn.

a. At potentials below 500 mV (reversible hydrogen electrode), the hydrocarbons are anodically oxidized

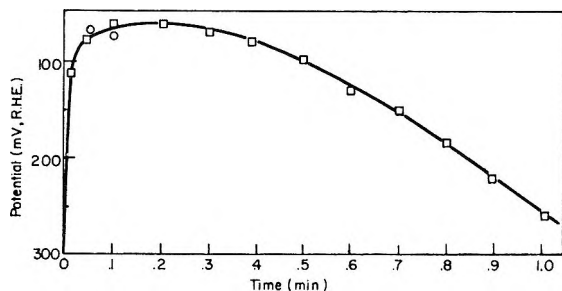


Figure 11. Initial potential-time transients for propane.

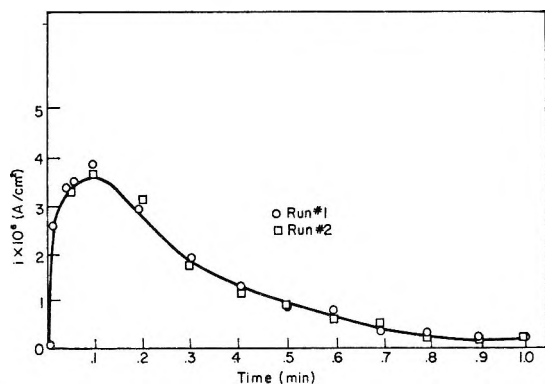


Figure 12. Initial current-time transients for propane.

(ca. 98%) to CO_2 through similar paths with the same rate-determining step.

b. The position of this step (from the beginning of the sequence) in the reaction sequence is the same for each of the hydrocarbons.

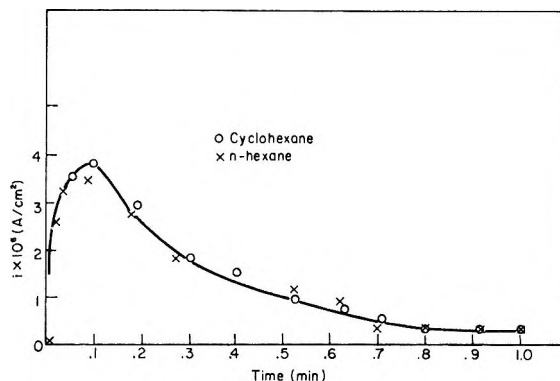
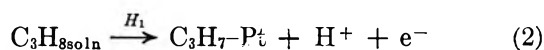
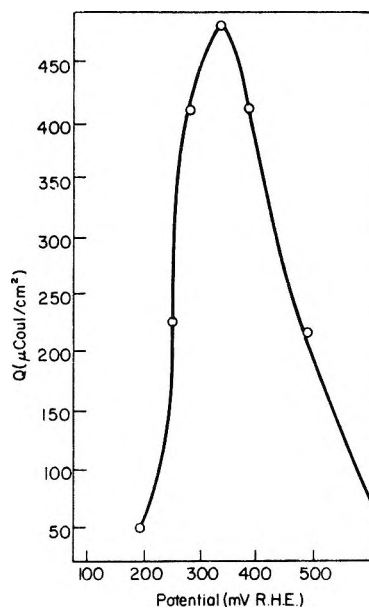
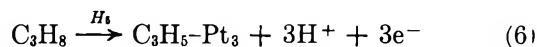
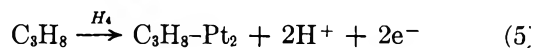
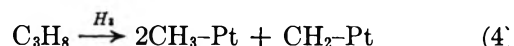
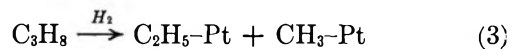
c. The anomalous Tafel behavior is characteristic of inhibition by some inhibiting species.

2. *Adsorption of Saturated Hydrocarbons.* The actual structure of adsorbed saturated hydrocarbons has not been determined from aqueous media, although Brummer^{5,6} has postulated the existence of three intermediates called CH-A, CH-B, and "O type" deduced from inflections on galvanostatic transient charging curves. The adsorption step from solution is hypothesized as a breaking up or severing of C-C bonds into fragments. The anodic charge (number of coulombs required to oxidize propane adsorbed on Pt in 85% H_3PO_4) as a function of potential is shown in Figure 14.

The adsorption of saturated hydrocarbons has been extensively studied from the gas phase, and in the cases of ethane,²⁰ *n*-pentane,²¹ cyclohexane,²¹ and 2,3-dimethylbutane,²¹ the initial adsorption step was found to be the dissociation of a single hydrogen atom, *i.e.*



It is possible to calculate the energies evolved for several theoretical adsorption reactions as follows

Figure 13. Initial current-time transients for *n*-hexane and cyclohexane.Figure 14. Anodic charging curve data for propane adsorption at 80° in 85% H_3PO_4 .

The following bond strengths were used: C-C, 83.1 kcal/mol; C-H, 106 kcal/mol;²² Pt-C, 44 kcal/mol;²² and Pt-H, 62 kcal/mol;²² and $\Delta H_{\text{ads}}(\text{H}_2\text{O}) = 20$ kcal/mol;²³ $I_{\text{H-H}^+} = 313$ kcal/mol; $S(\text{H}^+_{\text{g}} \rightarrow \text{H}^+_{\text{soln}}) = -263$ kcal/mol; and $\phi(\text{e}^-_{\text{g}} \rightarrow \text{e}^-_{\text{Pt}}) = -123$

(20) C. Kemball and H. S. Taylor, *J. Amer. Chem. Soc.*, **70**, 345 (1948).

(21) A. M. Galwey and C. Kemball, *Trans. Faraday Soc.*, **55**, 1959 (1959).

(22) C. A. Coulson, "Valence," Oxford University Press, London, 1961.

(23) J. O'M. Bockris, D. A. J. Swinkels, and M. Green, *J. Electrochem. Soc.*, **111**, 743 (1964).

Table II: Derived Kinetic Parameters for Propane Oxidation

Mechanism	$dV/d \ln i$			$(d \ln i/d \ln P_{C_3H_8})_{H_2O}$			$(d \ln i/d \ln C_{H_2O})_{RH}$		
	Low θ	Intermediate θ	High θ	Low θ	Intermediate θ	High θ	Low θ	Intermediate θ	High θ
Scheme i	$2RT/F$	1	0
Scheme ii	$2RT/3F$	0	$2RT/F$	1	$-1/2$	0	0	0	0
Scheme iii	RT/F	$-2RT/F$	0	1	$-1/2$	0	0	0	0
Scheme iv	RT/F	$-2RT/F$	0	1	$-1/2$	0	0	0	0
Scheme v	RT/F	RT/F	RT/F	1	$-\beta$	≈ 0	1	1	$1/n$
Scheme vi	$2RT/F$	$2RT/F$	$2RT/F$	0	$-1/2$	$-1/n$	1	1	$1/n$
Scheme vii	$2RT/F$	$2RT/F$	$2RT/F$	1	$-1/2$	0	0	0	0
Scheme viii	$2RT/3F$	$2RT/3F$	$2RT/3F$	1	$-1/2$	≈ 0	1	1	$1/n$
Scheme ix	RT/F	$2RT/3F$	RT/F	1	$1/2$	≈ 0	1	1	1
Scheme x	RT/F	1	1
Scheme xi	$2RT/F$	1	1
Scheme xii	$2RT/3F$	0	$2RT/F$	1	$-1/2$	≈ 0	1	1	1
Scheme xiii	RT/F	$-2RT/F$	0	1	$-1/2$	≈ 0	1	1	≈ 1
Scheme xiv	$2RT/3F$...	$2RT/3F$	1	...	≈ 0	1	...	$1/n$
Scheme xv	$RT/2F$	RT/F	0	1	$1/2$	≈ 0	1	1	≈ 1
Exptl (280-500 mV)		RT/F			1			0	

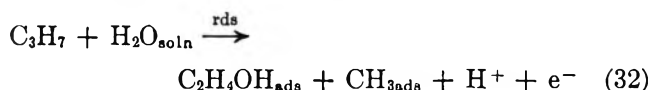
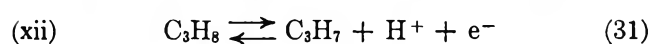
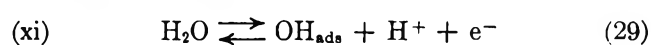
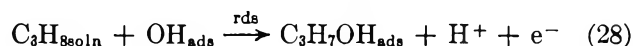
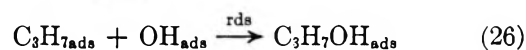
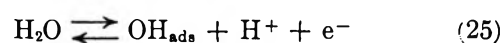
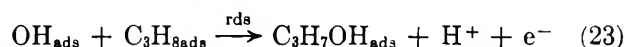
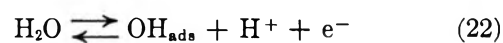
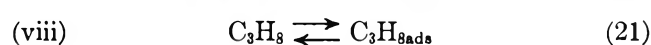
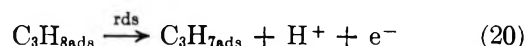
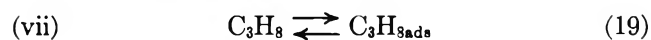
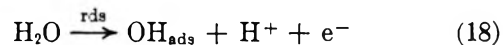
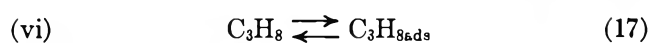
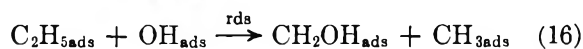
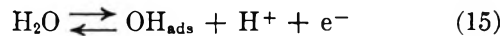
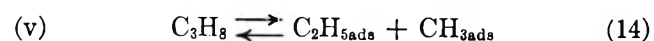
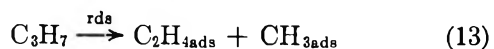
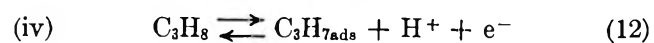
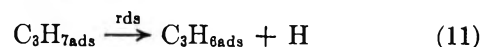
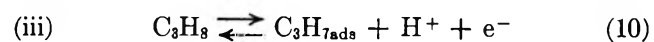
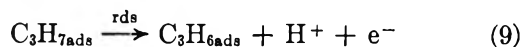
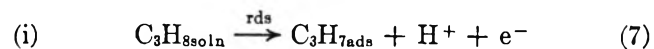
kcal/mol. From these values it follows that $H_1 = 5$ kcal/mol, $H_2 = 27$ kcal/mol, $H_3 = 82$ kcal/mol, $H_4 = 10$ kcal/mol, and $H_5 = 15$ kcal/mol.

From this approximate treatment, the results of the gas-phase work, and those of the transient studies, the step by which saturated hydrocarbons become adsorbed is probably as shown for propane in eq 2.

3. Mechanism of Electrooxidation at Low Potentials.

a. Possible Mechanisms. In the potential region 280–500 mV (reversible hydrogen electrode), no step may be rate determining which occurs during or after the third charge-transfer step, as under both Langmuir and Temkin conditions such a mechanism would display a Tafel slope less than or equal to $RT/2F$ and a reaction order with respect to propane which is fractional.²⁴ It is also known that OH is adsorbed in this potential range at fractions of coverage of $\theta < 0.1$.²⁴

With these limitations, the rate-determining step (rds) for propane may be sought among the following reaction sequences



(24) M. H. B. Rao, private communication.

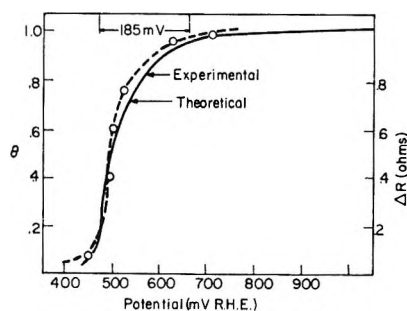
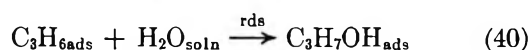
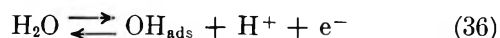
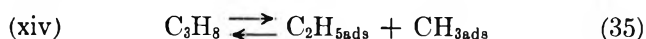
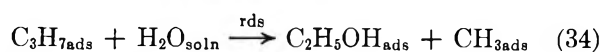


Figure 15. Theoretical plot of θ_s vs. V compared with experimental R - V curves.



The derived kinetic parameters for the 15 mechanisms considered above are given in Table II.

From Table II, consistency requires that the number of possible mechanisms can be reduced to either mechanism iii or iv, both under Langmuir conditions. Thus the rate-determining step is a chemical surface reaction breaking either C-C or C-H bonds. Using the above bond energies, it can be shown that the step involving the breaking of C-C bonds is favored by 5 kcal mol⁻¹. Scheme iv is also favored in view of the fact that a step forming adsorbed H is not likely at the potentials considered.

b. Mechanism of Hydrocarbon Oxidation at Higher Potentials. For mechanism iv, the predicted coverage-potential relation for the radical R (R = C₃H₇ for propane oxidation) should behave according to

$$\theta_R = kC_{RH}e^{VF/RT} \quad (41)$$

This exponential rise in θ_R should continue until either (i) the adsorbed radical reaches full coverage or (ii) another species S adsorbs and blocks a portion of the surface while the θ_R - V relation on the remaining part of the surface continues to increase with an increase of potential and reaches a limiting coverage on the unblocked portion of the surface. The coverage on the unblocked portion of the curve thus becomes independent of C_{RH} .

Case i is not valid, as the shape of Brummer's θ - V curve indicates that the coverage (per cm² (geometric)) decreases at higher potentials, nor would this hypothesis explain the experimentally obtained negative Tafel slope.

For case ii at sufficiently high potentials, the $\theta_{hydrocarbon}$ values would become independent of potential. Thus the rate on the available surface would become potential independent. The observed reaction rate would then be proportional to $1 - \theta_s$, where θ_s is the hypothetical anion adsorbed. This hypothesis has been applied to the i - v curves of Figures 3 and 4. The theoretical equation thus obtained is

$$1 - \theta_s = Ae^{-0.5VF/RT} \quad (42)$$

This equation is compared in Figure 15 with experimental measurements of phosphoric acid containing species by a thin film resistance method.^{25, 26} The experimental and theoretical θ_s - v curves are in good agreement.

At temperatures near to 150°, the inhibition effect is decreased as evidenced by the resumption of an increase in current with potential after 480 mV (Figure 3). Correspondingly, Borucka and Appelby²⁷ showed that phosphate inhibition of the oxygen reduction reaction was reduced at high temperatures (*e.g.*, above 120°). The final reduction of velocity at about 800 mV is due to the formation of oxide on Pt, as shown by the ellipsometric work of Rao (Figure 5).

c. Transients. The curves shown in Figures 12 and 13 may be described in terms of two consecutive processes. At first there is a delay connected with diffusion of reactant to the interface, after entry of gas to the solution commences. Thereafter, the current decrease represents the approach to steady state as the final θ_R approaches the value characteristic of the given potential, and the effect of the rapid adsorption reaction (eq 12) subsides.

A feasibility test of this model can be carried out in respect to the rising section as follows. Let it be further supposed that the reactant is transported to the neighborhood of the interface largely within bubbles of entering gas. These reach, but do not penetrate, the diffusion layer. The order of magnitude of the time for molecules to reach the electrode in significant quantities may be obtained from the equation for diffusion of dissolved gas across the diffusion layer of thickness δ , *i.e.*

$$\frac{\delta^2}{2D} \approx \tau \quad (43)$$

Using $D = 10^{-5}$ cm²/sec and $\delta \approx 0.01$ cm, a value of

(25) G. Stoner, Ph.D. Thesis, University of Pennsylvania, 1968.

(26) J. O'M. Bockris, B. D. Cahan, and G. Stoner, submitted for publication.

(27) H. Borucka and J. Appelby, Institute of Gas Technology, Chicago, Ill., private communication.

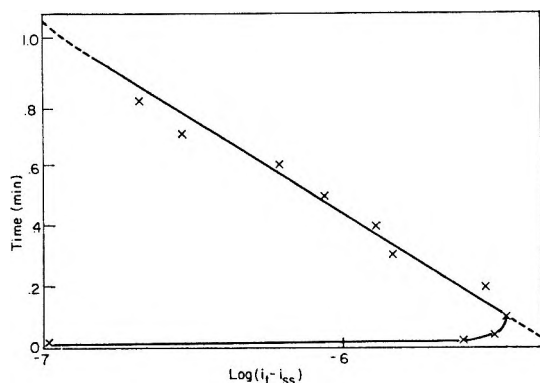


Figure 16. Plot of t against $\ln(i_t - i_r)$ for initial current-time transients.

$\tau \approx 5$ sec is obtained, in reasonable agreement with the time of the maximum on the current-time transient.

The fall of the current can be examined by considering the partial currents contributing to the transient after the maximum, when the rate-controlling diffusion which is described above can be assumed to have been replaced essentially by transiently rate-controlling adsorption. Then

$$i_t = i_{1,t} - i_{-1,t} + i_{r,t} \quad (44)$$

where $i_{1,t}$ and $i_{-1,t}$ are the respective forward and reverse reactions of eq 12 at a time corresponding to a changing coverage θ_t and $i_{r,t}$ is the current due to the steps after and including eq 13, at constant potential and time t .

It is assumed that C_{RH} , the concentration of the reactant in the double layer, varies negligibly with time after the maximum of the transient. The rate of change of coverage of R, $d\theta_R/dt$ is

$$\frac{d\theta_{R,t}}{dt} = k_1 C_{RH}(1 - \theta_{R,t}) - k_{-1}\theta_{R,t} - k_2\theta_{R,t} \quad (45)$$

where k_1 , k_{-1} , and k_2 are the rate constants for the adsorption, desorption, and rate-determining steps, respectively. Solving eq 45

$$\theta_{R,t} = \frac{K_1}{K_2}(1 - e^{-K_2 t}) \quad (46)$$

where $K_1 = k_1 C_{RH}$ and $K_2 = k_{-1} C_{RH} + k_2$. Now

$$F \frac{d\theta_R}{dt} = i_{1,t} - i_{-1,t} - A i_t' \quad (47)$$

where $0 < A_t < 1$, $A_{t=\infty} = 1$, and $i_{t=\infty}' = i_{ss}/19$ (where i_{ss} is the steady-state current density at $t = \infty$ and the 19 arises because there are 19 electrons more to be delivered to the electrode after the rate-determining step per act of over-all reaction). Hence, from eq 47

$$i_t - i_{r,t} = i_1 - i_{-1} \quad (48)$$

However

$$i_{1,t} - i_{-1,t} - A i_t' = F \frac{d\theta_{R,t}}{dt} \quad (49)$$

$$i_t - i_{r,t} = F \frac{d\theta_{R,t}}{dt} + A i_t' \quad (50)$$

and

$$i_t' = \frac{1}{19} i_{r,t} \quad (51)$$

therefore

$$i_t - (i_{r,t} + A i_t') = F \frac{d\theta_{R,t}}{dt} \quad (52)$$

However

$$A i_t' \ll i_{r,t} \quad (53)$$

therefore

$$i_t - i_{r,t} = F \frac{d\theta_{R,t}}{dt} \quad (54)$$

Differentiating eq 46

$$\frac{d\theta_{R,t}}{dt} = K_1 e^{-K_2 t} \quad (55)$$

and

$$i_t - i_{r,t} \approx F K_1 e^{-K_2 t} \quad (56)$$

This derivation predicts a linear t -log $(i_t - i_{r,t})$ region which is confirmed in Figure 16.

The area under the curve, extrapolated to zero time, thereby avoiding diffusional effects at $t < 5$ sec, is equal to about $100 \mu\text{C}/\text{cm}^2$. Using the roughness factor obtained by Piersma¹⁷ for platinized platinum at 300 mV (reversible hydrogen electrode) of 200, the coverage of singly adsorbed C_3H_7 is approximately

$$\begin{aligned} \theta_{\text{C}_3\text{H}_7}(300 \text{ mV}) &\approx \frac{100 \mu\text{C}/\text{cm}^2}{200 \times 210 \frac{\mu\text{C}/\text{cm}^2}{\text{monolayer}}} \\ &\approx 2 \times 10^{-3} \end{aligned} \quad (57)$$

Considering the predicted exponential rise in θ_R with potential, the coverage at 480 mV where departure from linear Tafel behavior occurs is

$$\begin{aligned} \theta_{\text{C}_3\text{H}_7} &\approx 2 \times 10^{-3} \times 10^{\frac{(480 - 300)F}{2.3RT}} \\ &\approx 0.3 \end{aligned} \quad (58)$$

The value for the maximum coverage (in terms of C_3H_7) from anodic charging curve data^{5,6} is 0.13 (on smooth Pt). The agreement is reasonable considering the methods used and the difference in surfaces studied.

Acknowledgment. Financial support for this work by U. S. Army Engineers Research and Development Laboratory, Fort Belvoir, Va., under Contract No. DA-44-009-AMC-469(T) is gratefully acknowledged. Discussion of the results with Dr. Maxine Savitz encouraged and aided the work. The authors also wish to thank Drs. H. Wroblowa, B. D. Cahan, and M. Genshaw for helpful discussions.

Hindered Rotation in N-Methylthiourea¹

by A. S. Tompa, R. D. Barefoot, and E. Price

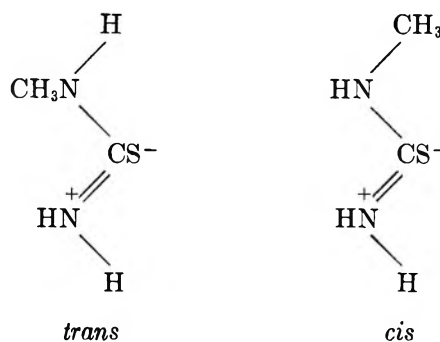
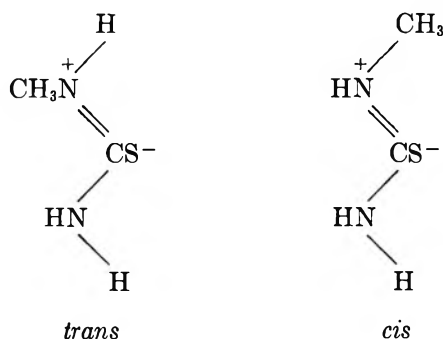
Naval Ordnance Research, Naval Ordnance Station, Indian Head, Maryland 20640 (Received September 28, 1967)

A study of the barrier to rotation about the carbon–nitrogen bond in N-methylthiourea in pyridine, acetonitrile-*d*₃, trifluoroacetic acid, methanol, water, and deuterium oxide was performed by the nmr technique. In these solvents it was observed that below 5° there were two methyl doublets of unequal intensity and coupling constants. The coupling constant of the high-field doublet was 0.5 Hz greater than that of the low-field doublet and was assigned to the *trans* isomer. From the ratio of the *trans* to *cis* areas equilibrium constants were calculated and were found to be solvent and temperature dependent. From the coalescence of the methyl doublets approximate activation energies were calculated and found to increase slightly as the polarity of the solvent increased.

Nuclear magnetic resonance studies of the rotational barrier about the central C–N bond in amides and thioamides have indicated that the energy barrier is greater than for a normal C–N bond because of electron delocalization.^{2–6} Furthermore, several authors have reported that the rotational barriers in thioamides are higher than for amides.^{4–8} However, the determination of kinetic parameters for the interconversion of geometrical isomers of amides and thioamides by nmr spectroscopy has been a controversial subject.^{6,9–11} Several authors have discussed and presented comparative results pertaining to the various nmr methods employed to obtain energy barriers to restricted rotation about the C–N bond in amides.^{5,9,12} In spite of the errors involved in comparing results obtained by the various nmr techniques, solvent and concentration effects seem apparent in these systems.^{10–15}

In connection with a research program in our laboratories, we have studied by the nmr technique the behavior of N-methylthiourea (MTU)¹⁶ and N-methylurea in a few nonpolar and polar solvents at various temperatures in order to determine whether hindered rotation is present in these molecules and whether any solvent interactions exist. The results and conclusions of these studies are given below.

There are two possible configurations of N-methylthiourea due to restricted rotation about the C–N bond



These two isomers (*cis* and *trans*) show a chemical shift difference between the methyl protons due to differences in shielding by the sulfur atom.

It was observed for N-methylthiourea in pyridine that below 6° there were two methyl doublets of un-

- (1) Presented before the Division of Physical Chemistry at the 153rd National Meeting of the American Chemical Society, Miami Beach, Fla., April 1967.
- (2) C. C. Lin and J. D. Swalen, *Rev. Mod. Phys.*, **31**, 841 (1959).
- (3) H. S. Gutowsky and C. H. Holm, *J. Chem. Phys.*, **25**, 1228 (1956).
- (4) A. Lowenstein, A. Melera, P. Rigny, and W. Walter, *J. Phys. Chem.*, **68**, 1597 (1964).
- (5) R. C. Neuman, Jr., and L. B. Young, *ibid.*, **69**, 2570 (1965).
- (6) R. C. Neuman, Jr., D. N. Roark, and V. Jonas, *J. Amer. Chem. Soc.*, **89**, 3412 (1967).
- (7) W. Walter and H. Maerten, *Ann. Chem.*, **669**, 66 (1963).
- (8) W. Walter, G. Maerten, and H. Rose, *ibid.*, **691**, 25 (1966).
- (9) A. Allerhand and H. S. Gutowsky, *J. Chem. Phys.*, **41**, 2115 (1964).
- (10) E. Lustig and W. B. Moniz, *Anal. Chem.*, **38**, 334R (1966).
- (11) A. Allerhand, H. S. Gutowsky, J. Jonas, and R. A. Meinzer, *J. Amer. Chem. Soc.*, **88**, 3185 (1966).
- (12) M. T. Rogers and J. C. Woodbrey, *J. Phys. Chem.*, **66**, 540 (1962).
- (13) A. G. Whittaker and S. Siegel, *J. Chem. Phys.*, **42**, 3320 (1965).
- (14) J. C. Woodbrey and M. T. Rogers, *J. Amer. Chem. Soc.*, **84**, 13 (1962).
- (15) E. Lustig, W. R. Benson, and N. Duy, *J. Org. Chem.*, **32**, 851 (1967).
- (16) Since the preparation of this article, T. H. Siddall and W. F. Stewart, *J. Org. Chem.*, **32**, 3261 (1967), have reported evidence of slow rotation of N-phenyl-N',N'-dimethylthiourea.

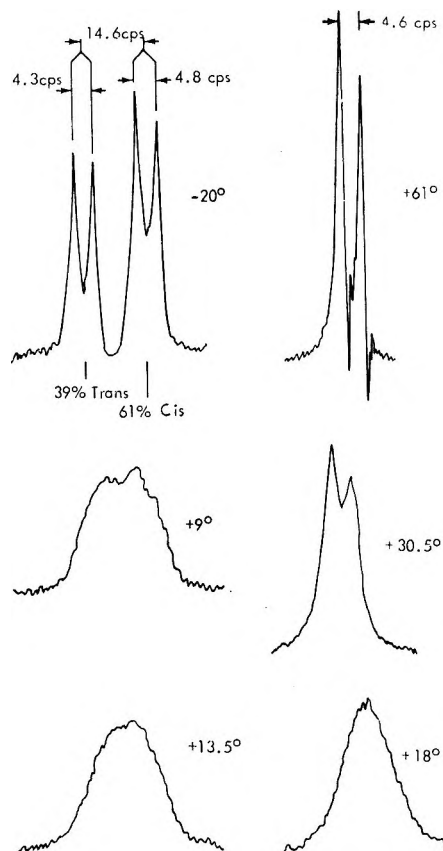


Figure 1. The nmr spectra of N-methyl protons in N-methylthiourea in pyridine at different temperatures.

equal intensity and coupling constants (Figure 1). At 14° in pyridine, a broad singlet was observed which split into a doublet above 25°. The doublet became very sharp as the temperature was raised to 61° and gave no indication that it would collapse to a singlet. However, in water the two doublets coalesced at approximately 21° to give one doublet which collapsed to a singlet at approximately 45°. These results indicated to us that there are two kinetic processes occurring in the hydroxylic solvents: (1) hindered rotation about the C-N bond and (2) proton exchange with the solvent.

As shown in Figure 1, the high-field doublet had a coupling constant of 4.8 Hz, which was 0.5 Hz greater than that of the low-field doublet. The low-field doublet was assigned to the *trans* isomer and the high-field doublet to the *cis* isomer. This assignment is based on the following two factors. First, molecular models indicate that the *trans* isomer is expected to be less favored than the *cis* form because of steric interaction between the *trans*-methyl and the *trans*-hydrogen. Therefore, one would expect to find two unequal methyl doublets in the pmr spectrum. Second, the methyl protons *cis* to the thiocarbonyl group are expected to appear more upfield than the methyl protons on the opposite side because of anisotropic diamagnetic shielding by the thiocarbonyl group.^{17,18} Chemical shift and coupling

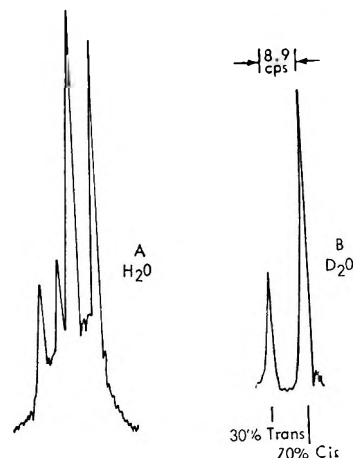


Figure 2. The nmr spectra of N-methyl protons in N-methylthiourea in H₂O and D₂O at 3°.

constant data in various solvents and at different temperatures are shown in Table I.

In deuterium oxide, the doublet due to spin-spin coupling disappeared because the protons on the nitrogen atoms were replaced by deuterium through proton exchange. Therefore, the methyl protons in N-methylthiourea gave two singlets of unequal intensity for each isomer. The spectrum of the N-methyl protons of N-methylthiourea in deuterium oxide at 3° is shown in Figure 2. These lines coalesced at a temperature of approximately 29°, whereas the two doublets in water coalesced at approximately 21°. These results give conclusive evidence that the unequal methyl doublets observed in water and the other solvents are due to the *trans* and *cis* isomers.

From the ratio of the areas of the methyl doublets, equilibrium constants, $K = [cis]/[trans]$, were calculated in pyridine and deuterium oxide. Results are listed in Table II. Between -30 and 5° in pyridine, the doublets were well resolved, but above 5° they began to overlap considerably and area ratios were difficult to obtain. In deuterium oxide, the area ratio of *cis* to *trans* remained constant between -3 and 20° and then became equal as the singlets began to merge.

On applying the method of least squares to the data in pyridine, we obtained the following results

$$\log K = -1.52 + (426/T) \quad (1)$$

The standard error of fit equals ± 0.006 log unit, $\Delta H^\circ = -1.95$ kcal, $\Delta S^\circ = -6.94$ eu, and $K_{298} = 0.81$. The only explanation that we offer concerning

(17) It is well known that the carbonyl group exhibits anisotropic diamagnetic shielding. The anisotropy is such that protons located approximately in line with the double bond are shifted downfield, while those located approximately below or above the double bond are shifted upfield; cf. L. M. Jackman, "Applications of Nuclear Magnetic Resonance Spectroscopy in Organic Chemistry," Pergamon Press Inc., New York, N. Y., 1959, p 124.

(18) H. W. Brown and D. P. Hollis, *J. Mol. Spectrosc.*, **13**, 305 (1964).

Table I: Nmr Chemical Shift Data for Methylthiourea in Various Solvents at 60 MHz

Solvent	Concn, M	Temp, °C	J_{LH,CH_3}	$J_{c-H,CH_3}^{b,c}$	δ^a			
					CH ₃		NH	NH ₂
Pyridine	4.05	-21	4.1	4.6	2.88	3.10	8.25	9.08 ^d
		-7	4.4	4.8	2.97	3.18	8.15	9.12
	1.57	-30	4.2	4.6	2.98	3.23
		2	4.0	4.6	2.92	3.15
Methanol	0.94	-21	4.2	4.8
Acetonitrile- <i>d</i> ₃	0.80	-24	4.4	4.9	2.68	2.87
Water	1.11	3	4.3	5.0	2.82	2.95
Trifluoroacetic acid	0.33	-11	1.0	2.0	2.91	2.96	6.92	7.43 ^d

^a Chemical shift, in ppm, relative to internal tetramethylsilane except in water where sodium 2,2-dimethyl-2-silapentane-5-sulfonate was used. ^b The high-field methyl resonance has been assigned to the methyl protons that are *cis* to the sulfur atom (see the text). ^c Average values of 4.3 ± 0.1 and 4.8 ± 0.2 , respectively, for *trans* and *cis* isomers were obtained in the various solvents in the range of -30 – 5° , with the exception of trifluoroacetic acid in which proton exchange occurs. ^d The area ratios are 2.0 (NH₂:NH) and 1.0 (CH₃:(NH₂ + NH)).

Table II: Equilibrium Constants for *trans*-to-*cis* Interconversion of N-Methylthiourea in Pyridine and Deuterium Oxide

Temp, °C	K ([<i>cis</i>]/[<i>trans</i>]) ^a
Pyridine	
-25	1.55
-20	1.46
-15	1.37
-10	1.28
-5	1.19
0	1.10
5	1.01
Deuterium Oxide	
-3	2.30
2	2.30
17	2.30
20	2.10

^a Area measurements were made with a planimeter.

Table III: Solvent Effects on the Chemical Shift^b of the Methyl Protons in N-Methylthiourea

Solvent	ϵ^a	Mol %	$\Delta\nu_\infty^b$
Pyridine	8.5	2.66	17.2
		11.20	14.5
		24.00	12.5
Trifluoroacetic acid	20.7	2.36	4.5
		10.50	4.2
		1.96	5.5
Acetone- <i>d</i> ₆	32.6	6.00	5.0
		3.60	11.3
Methanol	37.5	2.30	11.0
		4.00	11.6
Acetonitrile- <i>d</i> ₃	78.0	1.80	8.9
		2.80	8.4
D ₂ O			

^a Dielectric constants at 25.0°: "Handbook of Chemistry and Physics," 47th ed, Chemical Rubber Publishing Co., Cleveland, Ohio. ^b Chemical shift, in hertz, difference between methyl protons in the two isomers. Measurements were obtained in all solvents at -20 and -30° except in D₂O at -3° .

the larger ratio of the *cis* to *trans* isomer in deuterium oxide is that some types of hydrogen-bonded complex stabilize the *cis* isomer preferentially.

The only support that we have for such a complex is the observation that water gave approximately the same results as deuterium oxide, whereas methanol seemed to have shown higher values than pyridine and deuterated acetonitrile had lower values than pyridine. Gosavi, Agarwala, and Rao have reported a similar behavior of N-alkylthioureas in various solvents using infrared spectroscopy.¹⁹

From the separation between the two doublets, activation energies and frequency factors were calculated using the method of Gutowsky and Holm.³ The free energies of activation were computed according to the relationship given by Rogers and Woodbrey.¹² Values for E_A , ΔF^\ddagger , and $\log A$ ranged from 9 to 12 kcal/mol, 13.2 to 14.4 kcal/mol, and 8 to 10, respectively, in going from pyridine to deuterium oxide.

Inspection of the data in Table III reveals that the maximum value of the chemical shift, $\Delta\nu_\infty$, at low temperatures strongly depends on the solvent and also on the concentration in pyridine. These values seem to be real and to be constant between -10 and -30° , with no indication of increasing as observed in some cases by Whittaker and Siegel.¹³ These authors have indicated that changes in $\Delta\nu_\infty$ (the chemical shift between the methyl groups at which the internal rotation is negligible) with further lowering of the temperature arise because of the solvent or associative effects.

Experimental Section

N-Methylthiourea (Aldrich) was recrystallized from absolute ethanol-ethyl acetate. Deuterium oxide (99.8%), acetonitrile-*d*₃ (99.0%), and trifluoroacetic acid were obtained from NMR Specialties and were

(19) R. K. Gosavi, U. Agarwala, and C. N. R. Rao, *J. Amer. Chem. Soc.*, **89**, 235 (1967).

used without further purification. Pyridine (Malinckrodt) and methanol (Matheson, spectroquality reagent) were freshly distilled before use.

The nmr measurements were performed with a Varian DA-60-EL spectrometer equipped with a super-stabilizer. The chemical shifts were measured with a precision of 0.1 Hz by placing side bands on both sides of the signal. The side-band frequency was measured with a Hewlett-Packard Model 522-B electronic frequency counter. The temperature was kept constant to within $\pm 0.2^\circ$ by the use of a Leeds and Northrup

Azar H recorder-controller. The temperature was varied with dry nitrogen gas and the use of a Varian Model 4340 variable-temperature probe assembly and a Model V-4331-THR spinning-sample dewar probe insert.

Acknowledgment. This work was supported by the Foundational Research Program of the Bureau of Naval Weapons. We also wish to thank Dr. James U. Lowe, Jr., for supplying us with a recrystallized sample of N-methylthiourea.

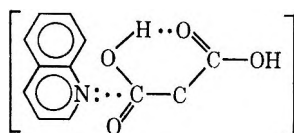
Further Studies on the Decarboxylation of *n*-Hexylmalonic Acid in Polar Solvents

by Louis Watts Clark

Department of Chemistry, Western Carolina University, Cullowhee, North Carolina 28723 (Received July 31, 1968)

Rate constants and activation parameters are reported for the decarboxylation of *n*-hexylmalonic acid in 12 polar liquids—1,3-propanediol, 1,2-propanediol, glycerol, 2,3-butanediol, 1-decanol, 1-octanol, 1-hexanol, *N,N*-dimethylaniline, *o*-toluidine, *N*-methylaniline, *o*-ethylaniline, and aniline. It is observed that the inductive effect of the *n*-hexyl group of the substrate causes an inversion of the order of increasing activation energy with increasing molecular weight of the members of the various homologous groups (glycols, alcohols, and amines). The average change in the enthalpy of activation per methylene group for the decarboxylation of *n*-hexylmalonic acid in the amines is compared with corresponding values previously reported for five other acids—malonic acid, oxanilic acid, oxalic acid, cinnamalmalonic acid, and benzylmalonic acid. The values obtained for all the compounds turn out to be exact multiples of the absolute magnitude of the value for malonic acid. A plot of ΔH^\ddagger vs. ΔS^\ddagger for the decarboxylation of *n*-hexylmalonic acid in each homologous group is linear, each line having a slope of 378°K or 105°C—the same temperature as the melting point of *n*-hexylmalonic acid. An interesting comparison is made between the data for the decarboxylation of *n*-hexylmalonic acid in alcohols and that for the solvolysis of methyl *p*-toluenesulfonate in alcohols reported by Hyne and Robertson. The melting point of *p*-toluenesulfonic acid is 105°—the same as the melting point of *n*-hexylmalonic acid. The isokinetic temperature for the solvolysis of the ester in alcohols is also 105°—the same as that for the decarboxylation of *n*-hexylmalonic acid in alcohols. Finally, the average change of the enthalpy of activation per methylene group on going from one alcohol to another is exactly the same for both reactions, namely, 947 cal.

Justification for continued investigation of the kinetics of the decarboxylation reaction lies in the potential of such studies to throw light on the mechanism and energetics of liquid-phase reactions. The rate-determining step in the decarboxylation of malonic acid in the presence of quinoline appears to be a nucleophilic attack by quinoline on the hydrogen-bond donating carboxyl group of malonic acid.¹ The electrophile is cleaved and the nucleophile escapes unscathed from



the collision. This mechanism apparently obtains in a large variety of decarboxylation reactions.² There appears to be no limit to the number of acids able to undergo cleavage nor to the number of nucleophiles capable of effecting it. Because of this generality of

mechanism, the study of this reaction cannot fail to yield greater understanding of the properties of chemical species in general. *n*-Hexylmalonic acid is a suitable compound for use in studying this reaction because it is easily purified and readily undergoes reaction in all sorts of polar liquids at moderate temperatures. The equation of the reaction is



The decarboxylation of *n*-hexylmalonic acid has been

(1) G. Fraenkel, R. L. Belford, and P. E. Yankwich, *J. Amer. Chem. Soc.*, **76**, 15 (1954).

(2) L. W. Clark, *J. Phys. Chem.*, **71**, 302 (1967), and previous papers in this series. [A reviewer has suggested that the alternative mechanism of nucleophilic attack by quinoline on the hydrogen-bond accepting carboxyl group is not ruled out by the data of ref 1 and 2. In addition, this reviewer stated, catalysis by this alternative mechanism is easily understood and is consistent with the effects of substituents on the decarboxylation of β -keto and unsaturated acids—*cf.* D. B. Bigley and J. C. Thurman, *J. Chem. Soc.*, **B**, 436 (1968)].

investigated previously in the molten state,³ in three glycols,³ and in two fatty acids.² In the study of the decarboxylation of *n*-hexylmalonic acid in the homologous fatty acids³ it was observed that at the melting point of the *n*-hexylmalonic acid (105°) the rate of reaction was independent of the nature of the solvent. Another way of stating this phenomenon is to say that the isokinetic temperature of the reaction series is equal to the melting point of the substrate. (The isokinetic temperature of a reaction series is the temperature at which all the reactions of the series have the same rate constant.⁴) A similar result was obtained in the case of several related compounds ranging in melting point from 105 to 210°. These intriguing results have prompted a continued intensive investigation of the decarboxylation of *n*-hexylmalonic acid in a large number of polar liquids, representing three homologous groups, in an attempt to ascertain whether or not a like relationship between melting points and chemical reactivity obtains in polar solvents other than fatty acids. The present paper reports results obtained in this laboratory on the decarboxylation of *n*-hexylmalonic acid in 12 polar liquids including representatives of three homologous groups: (1) alkanols (1-hexanol, 1-octanol, and 1-decanol); (2) glycols (1,3-propanediol, 1,2-propanediol, 2,3-butanediol, and glycerol); and (3) amines (aniline, *o*-toluidine, *N*-Methylaniline, *o*-ethylaniline, and dimethylaniline).

Experimental Section

Reagents. The *n*-hexylmalonic acid used in this research was obtained from Distillation Products Industries, Inc., Rochester, N. Y. After recrystallization from benzene its melting point (determined with the aid of a Mettler FP-1 melting point apparatus) was found to be 105.20°. The solvents were reagent grade and were freshly distilled at atmospheric pressure immediately before use.

Apparatus and Technique. Details of the apparatus and technique have been described previously.⁵ In each experiment a weighed sample of *n*-hexylmalonic acid was introduced in the usual manner into the reaction flask containing approximately 90 ml of solvent. The weight of sample (0.3361 g) was that required to furnish 40.00 ml of CO₂ at STP on complete reaction, calculated on the basis of the actual molar volume of CO₂ at STP, namely, 22,267 ml.

Results

At least two decarboxylation experiments were carried out in each solvent at each constant temperature selected. Each reaction was measured at three or four different temperatures over a 20° range. All the reactions gave good first-order kinetics over the greater portion of the reaction. Average rate constants, calculated in the usual manner from the slopes of the

Table I: Apparent First-Order Rate Constants for the Decarboxylation of *n*-Hexylmalonic Acid in Several Polar Liquids

Solvent	Temp, °C (cor)	$k \times 10^4, \text{sec}^{-1}$
1-Hexanol	110.07	2.20
	114.55	3.10
	122.45	5.65
1-Octanol	129.72	9.80
	110.07	2.30
	119.97	5.25
1-Decanol	130.00	11.84
	110.91	2.46
	121.13	6.15
1,3-Propanediol	125.56	9.21
	130.75	14.04
	110.27	1.68
1,2-Propanediol	115.17	2.71
	120.37	4.36
	130.02	10.17
2,3-Butanediol	119.12	3.49
	129.10	7.79
	139.02	16.94
Glycerol	110.60	1.64
	120.47	3.72
	125.27	5.40
Aniline	130.03	7.83
	120.00	3.65
	130.00	8.04
<i>o</i> -Toluidine	140.24	17.43
	110.63	3.41
	120.16	8.15
<i>N</i> -Methylaniline	130.47	20.04
	109.58	3.11
	119.25	8.91
<i>o</i> -Ethylaniline	130.03	27.13
	109.97	2.93
	120.07	7.86
<i>N,N</i> -Dimethylaniline	130.26	24.52
	109.77	3.02
	120.07	8.06
	130.16	20.35
	109.13	2.90
	119.35	9.07
	128.87	25.13

logarithmic plots, are shown in Table I. The parameters of the absolute reaction rate equation, based upon the data in Table I, are shown in Table II. Included for comparison are the data for the reaction in ethylene glycol obtained previously.

Discussion

It is of interest to compare the behavior of *n*-hexylmalonic acid in polar liquids with that of its parent compound, malonic acid, in related solvents. For this purpose data previously reported for the decarboxylation of malonic acid are collated in Tables III-V.

(3) L. W. Clark, *J. Phys. Chem.*, **67**, 2602 (1963).

(4) S. L. Friess, E. S. Lewis, and A. Weissberger. "Technique of Organic Chemistry," Vol. VIII, 2nd ed, Part I, Interscience Publishers, Inc., New York, N. Y., 1961, p 207.

(5) L. W. Clark, *J. Phys. Chem.*, **60**, 1150 (1956); **70**, 627 (1966).

A glance at the data in Table II reveals that an increase in the molecular weight of the solvent brings about an *increase* in the enthalpy of activation for the decarboxylation of *n*-hexylmalonic acid in the alkanols. However, in the case of the decarboxylation of malonic acid, the data in Table III reveal that the enthalpy of activation of the reaction *decreases* as the molecular weight of the alcohol increases.

If we consider the data in Table II for the decarboxylation of *n*-hexylmalonic acid in the three amines, aniline, and its *N*-substituted derivatives, again we dis-

Table II: Activation Parameters for the Decarboxylation of *n*-Hexylmalonic Acid in Several Polar Liquids

Solvent	ΔH^\ddagger , kcal/mol	ΔS^\ddagger , eu	$\Delta F^\ddagger_{105^\circ}$, kcal/mol
1,3-Propanediol	26.81	-6.39	29.21
1,2-Propanediol	24.71	-11.97	29.23
Glycerol	24.07	-13.64	29.23
2,3-Butanediol	23.71	-14.60	29.23
1-Decanol	26.60	-6.35	29.00
1-Octanol	24.72	-11.26	28.97
1-Hexanol	22.81	-16.34	28.99
<i>N,N</i> -Dimethylaniline	32.74	10.34	28.83
<i>o</i> -Toluidine	31.72	7.75	28.79
<i>N</i> -Methylaniline	28.57	-0.69	28.83
<i>o</i> -Ethylaniline	27.77	-2.66	28.78
Aniline	26.66	-5.68	28.81

Table III: Activation Parameters for the Decarboxylation of Malonic Acid in Alkanols^a

Solvent	ΔH^\ddagger , kcal/mol	ΔS^\ddagger , eu	$\Delta F^\ddagger_{105^\circ}$, kcal/mol
1-Butanol	27.2	-4.4	29.00
1-Hexanol	26.0	-7.6	29.10
2-Ethylhexanol-1	24.8	-10.7	29.05
Cyclohexanol	23.0	-15.0	29.12

^a L. W. Clark, *J. Phys. Chem.*, **64**, 508 (1960).

Table IV: Activation Parameters for the Decarboxylation of Malonic Acid in Several Aromatic Amines^a

Solvent	ΔH^\ddagger , kcal/mol	ΔS^\ddagger , eu	$\Delta F^\ddagger_{105^\circ}$, kcal/mol
Aniline	26.90	-4.46	28.72
<i>N</i> -Methylaniline	26.60	-5.32	28.72
<i>N</i> -Ethylaniline	26.00	-6.60	28.70
<i>N</i> -Propylaniline	25.70	-7.40	28.72
<i>N</i> -Butylaniline ^a	25.70	-7.50	28.76

^a L. W. Clark, *J. Phys. Chem.*, **62**, 79 (1958).

Table V: Activation Parameters for the Decarboxylation of Malonic Acid and of *n*-Hexylmalonic Acid in Fatty Acids^a

Solvent	<i>n</i> -Hexylmalonic acid (mp 105°)			Malonic acid (mp 135°)		
	ΔH^\ddagger , kcal/mol	ΔS^\ddagger , eu	$\Delta F^\ddagger_{105^\circ}$, kcal/mol	ΔH^\ddagger , kcal/mol	ΔS^\ddagger , eu	$\Delta F^\ddagger_{135^\circ}$, kcal/mol
Hexanoic acid	13.24	0.54	31.10	32.50	3.20	31.20
Octanoic acid	30.75	-1.00	31.14	34.83	8.90	31.19

^a Reference 2.

cover that an increase in the enthalpy of activation of the reaction accompanies an increase in the molecular weight of the solvent. For malonic acid, however, we note in Table IV that the enthalpy of activation *decreases* as the molecular weight of the amine increases for the reaction in aniline and its *N*-substituted derivatives.

In the case of the decarboxylation of malonic acid and of *n*-hexylmalonic acid in the two fatty acids, hexanoic acid and octanoic acid, the data in Table V reveal that for *n*-hexylmalonic acid there is a *decrease*, and for malonic acid an *increase* in the enthalpy of activation as the molecular weight of the acid increases.

The average change in ΔH^\ddagger per methylene group, for the decarboxylation of malonic acid and of *n*-hexylmalonic acid in these three homologous groups, calculated from the data in Tables II-V, are summarized in Table VI.

The data in Table VI clearly show that the alkyl moiety of *n*-hexylmalonic acid causes not only an inversion in the order of increasing activation energy with increasing molecular weight of the various homologous groups with respect to the parent malonic acid but also an inversion in absolute magnitude of the increasing activation energy on passing from the acids to the alcohols to the amines. For the reactions in the fatty acids, the average change in the enthalpy of activation per methylene group for the decarboxylation of malonic acid is large and positive; that for the decarboxylation of *n*-hexylmalonic acid in the same solvents is small and negative. In the amines the corresponding value is small and negative for malonic acid, whereas for *n*-hexylmalonic acid it is large and positive. The absolute magnitude of the change in ΔH^\ddagger per methylene group for the decarboxylation of malonic acid in the amines (300 cal) appears to be fundamentally related to the values for the other reactions listed. Those values are very nearly exact

Table VI: Average Change in the Enthalpy of Activation per Methylene Group for the Decarboxylation of Malonic Acid and of *n*-Hexylmalonic Acid in Fatty Acids, in Alcohols, and in Amines (Units: cal/methylene group)

Homologous group	Malonic acid	<i>n</i> -Hexylmalonic acid
Fatty Acids	1165	-245
Alkanols	-600	947
<i>N</i> -Substituted aniline derivatives	-300	2750

Table VII: Activation Parameters for the Decarboxylation of Several Acids in Aromatic Amines (Units: ΔH^\ddagger , kcal/mol; ΔS^\ddagger , eu)

	Oxalic acid ^a		Oxanilic acid ^b		Benzylmalonic acid ^c		Cinnamalmalonic acid ^d	
	ΔH^\ddagger	ΔS^\ddagger	ΔH^\ddagger	ΔS^\ddagger	ΔH^\ddagger	ΔS^\ddagger	ΔH^\ddagger	ΔS^\ddagger
Aniline	49.80	46.30			19.80	-21.64	23.80	-13.20
N-Methylaniline			35.50	8.25				
N,N-Dimethylaniline	37.60	15.30	32.40	+1.25	38.40	27.4	31.20	3.80

^a L. W. Clark, *J. Phys. Chem.*, **61**, 699 (1957). ^b L. W. Clark, *ibid.*, **66**, 1543 (1962). ^c L. W. Clark, *ibid.*, **70**, 627 (1966). ^d L. W. Clark, *ibid.*, **66**, 836 (1962).

Table VIII: Average Change in the Enthalpy of Activation per Methylene Group for the Decarboxylation of Several Acids in N-Substituted Aniline Derivatives (Units: cal/methylene group)

Group I		Group II	
Malonic acid	-300	<i>n</i> -Hexylmalonic acid	2750
Oxanilic acid	-3100	Cinnamalmalonic acid	7400
Oxalic acid	-6100	Benzylmalonic acid	9300

multiples of that for the decarboxylation of malonic acid in the amines. These multiples are: for the decarboxylation of malonic acid in alkanols, 2; for the decarboxylation of malonic acid in fatty acids, 4; for the decarboxylation of *n*-hexylmalonic acid in the fatty acids, 1; for the decarboxylation of *n*-hexylmalonic acid in alkanols, 3; for the decarboxylation of *n*-hexylmalonic acid in the amines, 9.

Kinetic data previously obtained for the decarboxylation of four additional acids in aniline and its N-substituted derivatives are brought together in Table VII for comparison. The average change in ΔH^\ddagger per methylene group for each of these reactions is shown in Table VIII along with corresponding data for malonic acid and *n*-hexylmalonic acid from Table VI. It will be observed in Table VIII that the six compounds for which comparable data are available fall into two groups—group I, compounds which experience a decrease in ΔH^\ddagger as the molecular weight of the amine increases, and group II, compounds which experience an increase in ΔH^\ddagger with increase in the molecular weight of the amine. Malonic acid, oxalic acid, and oxanilic acid belong to group I. The derivatives of malonic acid—*n*-hexylmalonic acid, cinnamalmalonic acid, and benzylmalonic acid—fall in group II. Of the six compounds listed, the one showing the greatest decrease in ΔH^\ddagger per methylene group, oxalic acid, is the one having the highest effective positive charge on the polarized carbonyl carbon atom which coordinates with the amine. The one showing the greatest increase, benzylmalonic acid, is the one having the lowest effective positive charge on the polarized carbonyl carbon atom. The only compound shown in Table VIII which experiences a relatively small change in ΔH^\ddagger with increase in the molecular weight of the amine is malonic acid (300 cal). All the other compounds

listed show comparatively larger changes in ΔH^\ddagger as the molecular weight of the amine increases. The absolute magnitude of the change in ΔH^\ddagger per methylene group for the decarboxylation of malonic acid in the amines appears to be fundamentally related to the values for the other reactions shown. Their values are very nearly exact multiples of that for malonic acid. These multiples are: for oxanilic acid, 10; for oxalic acid, 20; for *n*-hexylmalonic acid, 9; for cinnamalmalonic acid, 24; for benzylmalonic acid, 30. These results indicate that apparently the average change in ΔH^\ddagger per methylene group for the decarboxylation of malonic acid in N-substituted aniline derivatives (300 cal) represents the minimum energy associated with the electronic contribution of a methylene group in a molecule.

Isokinetic Temperatures. In the last column of Table II are recorded the calculated values of the free energy of activation at 105° (the melting point of *n*-hexylmalonic acid) for the decarboxylation of *n*-hexylmalonic acid in the various polar liquids. In the case of each of the various homologous groups (glycols, alcohols, amines) it will be observed that the free energy of activation for the reaction at the melting point of the substrate is fairly constant. This means that, as in the case of the reaction in fatty acids,² the isokinetic temperature for the decarboxylation of *n*-hexylmalonic acid in each of the various homologous series studied in this research coincides with its melting point. This fact is brought out perhaps more clearly by the plots in Figure 1. Lines I, II, and IV of Figure 1 show the plots for the decarboxylation of *n*-hexylmalonic acid in the glycols, alcohols, and amines, respectively, based upon the data in Table II. (Discussion of line III of Figure 1 will be postponed until later.) The three lines are parallel, and their slopes (determined by the method of least squares) are 104.5° (line I), 106.2° (line II), and 105.9° (line III), corresponding within experimental error to the melting point of *n*-hexylmalonic acid.

The data in the last columns of Tables III–V indicate that the isokinetic temperature for the decarboxylation of malonic acid in the various homologous series, acids, alcohols, amines, is equal to the melting point of the substrate, 408°K or 135°C. It

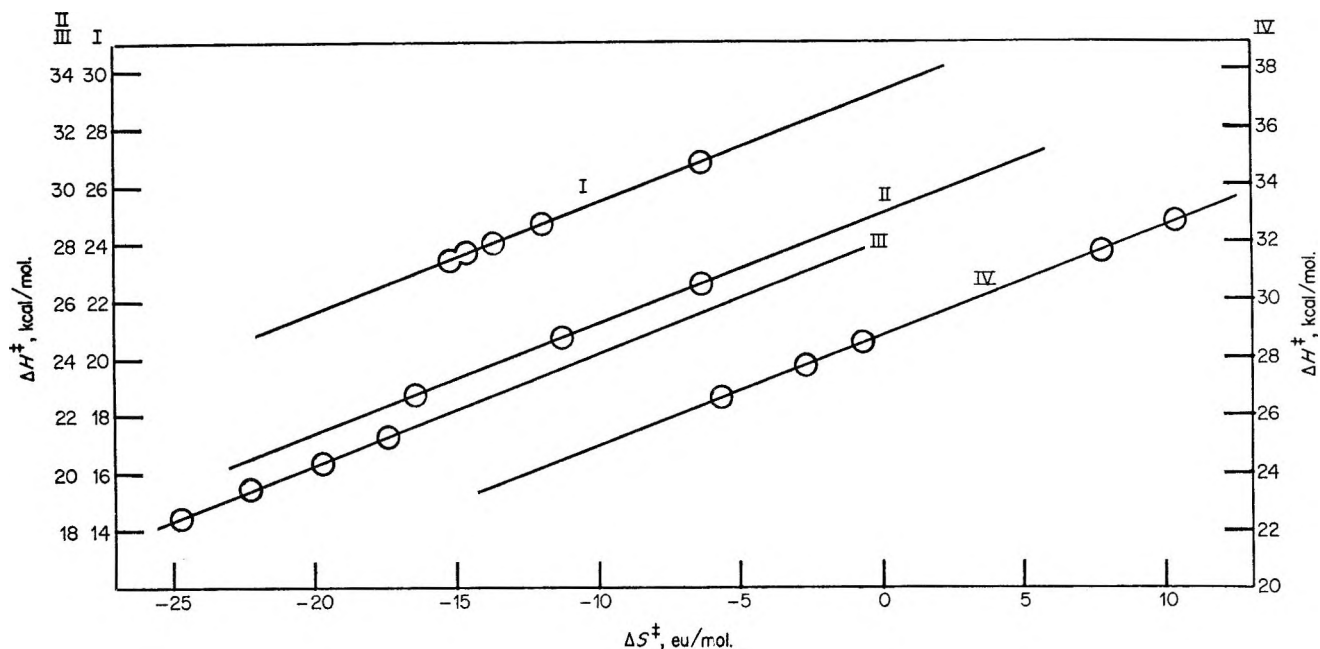
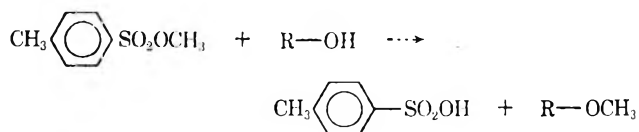


Figure 1. Lines I, II, and IV: Plot of enthalpy vs. entropy of activation for the decarboxylation of *n*-hexylmalonic acid in glycols, alcohols, and amines, from the data in Table II. Line III: The same plot for the solvolysis of methyl *p*-toluenesulfonate in alcohols, based upon the data in Table IX.

will be noted that, for each homologous group, the free energy of activation at the isokinetic temperature is approximately the same for both compounds, malonic acid and *n*-hexylmalonic acid.

Comparison of the Decarboxylation Reaction with Other S_N2 Reactions. Hyne and Robertson⁶ have studied the solvolysis of methyl *p*-toluenesulfonate in several alcohols, yielding *p*-toluenesulfonic acid plus ether



(It is an interesting coincidence that the melting point of *p*-toluenesulfonic acid is the same as that of *n*-hexylmalonic acid—105°.) The activation parameters for these solvolysis reactions, calculated by appropriate formulas^{7,8} from the reported *E* and log *PZ* values, are

$$\Delta H^\ddagger = E - RT \quad (1)$$

$$\Delta S^\ddagger = 2.303R \log PZ/T - 49.215 \quad (2)$$

shown in Table IX, and are plotted in line III of Figure 1. The last column of Table IX shows the free energy of activation for the reaction in the various alcohols at the melting point of the acid—105°. It will be seen that the $\Delta F^\ddagger_{105^\circ}$ values are fairly constant within experimental error. Also, the linear plot of the data (line III of Figure 1) is seen to be nearly parallel to the other three lines in the figure. (The slope of line III determined by the method of least squares is 385.2°K or 112.1°C. This result is intriguingly close to the

Table IX: Kinetic Data for the Solvolysis of Methyl *p*-Toluenesulfonate in Several Alcohols^a

Solvent	<i>E</i> , kcal/mol	Log <i>PZ</i>	ΔH^\ddagger , kcal/mol	ΔS^\ddagger , eu	$\Delta F^\ddagger_{105^\circ}$, kcal/mol
Methanol	21.987	9.494	21.307	-17.39	27.88
Ethanol	21.076	8.988	20.396	-19.71	27.84
1-Propanol	20.161	8.863	19.481	-22.26	27.90
1-Butanol	19.144	7.896	18.464	-24.71	27.83

^a Reference 6.

melting point of *p*-toluenesulfonic acid, suggesting that more careful experimental study might show an even better correlation.) The data in Table IX show that the enthalpy of activation of the solvolysis reaction *decreases* as the molecular weight of the solvent increases. In the case of the decarboxylation of *n*-hexylmalonic acid in alcohols (Table II) we have seen that ΔH^\ddagger *increases* as the molecular weight of the alcohol increases. The average change in ΔH^\ddagger *per methylene group*, however, is numerically the same for both reactions—947 cal/methylene group.

It is believed that these results demonstrate the utility of the study of the decarboxylation reaction in leading to a better understanding of nucleophilic bimolecular substitution reactions in solution.

Acknowledgement. Acknowledgment is made to the donors of the Petroleum Research Fund, administered by the American Chemical Society, for support.

(6) R. E. Robertson, *Can. J. Chem.*, **31**, 589 (1953); J. B. Hyne and R. E. Robertson, *ibid.*, **34**, 863 (1956).

(7) W. J. Moore, "Physical Chemistry," 3rd ed, Prentice-Hall, Inc., Englewood Cliffs, N. J. 1962, eq 8.27, p 927.

(8) G. W. Castellan, "Physical Chemistry," Addison-Wesley Publishing Co., Inc., Reading, Mass., 1964, eq 36, p 643.

NOTES

The Crystal and Molecular Structure of Tris(diethyldithiocarbamato)cobalt(III)

by Thomas Brennan and Ivan Bernal¹

Chemistry Department, State University of New York,
Stony Brook, New York 11790 (Received August 27, 1968)

Dithiocarbamates and their derivatives are extremely versatile substances which have been used, for example, in the treatment of alcoholism,² sarcoma cells,³ as possible protection against the lethal effects of X-rays,⁴ etc. A number of bis metal derivatives of dithiocarbamates have been studied in recent years⁵⁻⁹ in which the central metal ion is either fourfold coordinated (square planar or tetrahedral)^{5,6} or it is pentacoordinated because of dimerization.⁷⁻⁹ However, even though many tris derivatives are well characterized, no structural study is yet available on these substances. Since the recent discovery that *cis*-dithiolates give metal derivatives which exhibit trigonal prismatic coordination instead of the very common octahedral configuration, we thought it worthwhile to investigate some of the tris(dithiocarbamates) of the 3d transition metal ions. This note gives the results of the first structural study of a tris(dithiocarbamate) of a 3d transition metal ion.¹⁰

Deep green crystals of tris(diethyldithiocarbamato)cobalt(III) (hereafter referred to as $\text{Co}(\text{dtc})_3$) were grown from 1:1 benzene-ethanol solutions. Precession and Weissenberg photographs show that the crystals belong to the monoclinic system with the following cell dimensions: $a = 14.087$ (8) Å, $b = 10.308$ (4) Å, $c = 17.049$ (11) Å, and $\beta = 111.0$ (8)°. The volume of the unit cell is 2327 Å³. The observed extinctions, hkl ($h + k \neq 2n$) and $h0l$ ($l \neq 2n$) are consistent with the two space groups $C2/c$ and Cc . The experimental density of 1.43 (3) g/cm³ agrees well with the calculated value of 1.44 g/cm³ for four molecules in the unit cell. Assuming the space group to be $C2/c$, $\text{Co}(\text{dtc})_3$ is crystallographically required to possess a twofold symmetry axis with the Co atom occupying the 4e special positions of the space group. This assumption is confirmed by the satisfactory agreement ultimately obtained in the refinement of the structure.

Integrated intensity data (levels $h0l$ to $h11l$) from a crystal mounted along the b axis were collected by the multiple-film equiinclination Weissenberg technique using Zr-filtered Mo $K\alpha$ radiation. Data from integrated precession photographs of the levels $0kl$ to $4kl$, $h0l$ to $h3l$ and hhl were used to scale the main set of

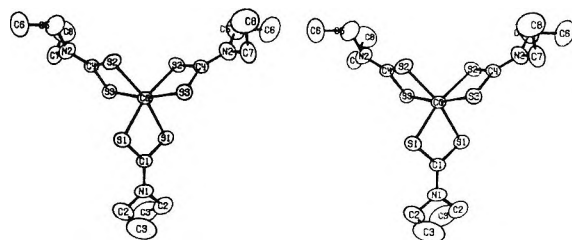


Figure 1. Molecular configuration of $\text{Co}(\text{dtc})_3$. The twofold axis passes through the Co, C(1) and N(1) atoms. This is a stereo pair which may conveniently be examined with a hand-held stereo viewer.

data. An intensity strip was used to estimate, visually, the Weissenberg data, while the scaling intensities were measured photometrically, using a Joyce-Loebl scanning microdensitometer. All the data were corrected for Lorentz-polarization factors. Standard methods were used to reduce the intensity data to $F(\text{obsd})$ values.

The structure was solved using Patterson, least-squares, and Fourier methods. Correction for anomalous dispersion was applied to cobalt and sulfur atoms, but no absorption or extinction corrections were made to the values of $F(\text{obsd})$. The crystal we used had the dimensions $0.45 \times 0.40 \times 0.20$ mm, which coupled with an absorption coefficient of 12.877 cm^{-1} (for Mo $K\alpha$ radiation) makes absorption a minor error in the values of our $F(\text{obsd})$ data. The current value of $R(F)$ for all nonhydrogen atoms, vibrating anisotropically, using 1183 nonzero reflections is 0.064.

In Table I we list the final coordinates of the atoms in the asymmetric unit. Figure 1 is a stereoscopic draw-

- (1) Department of Chemistry, Brookhaven National Laboratory, Upton, N. Y. 11973.
- (2) J. Hald, E. Jacobsen, and V. Larsen, *Acta Pharmacol. Toxicol.* **4**, 285 (1948).
- (3) A. K. Powell, *Brit. J. Cancer*, **8**, 529 (1954).
- (4) J. A. Cohen, O. Vos, and D. W. Bekkuun, "Advances in Radiobiology," G. C. Hevesy, Ed., Oliver & Boyd Ltd., Edinburgh, 1957, pp 134-144.
- (5) M. Bonamico, G. Dessy, C. Mariani, A. Vaciago, and L. Zambonelli, *Acta Crystallogr.*, **19**, 619 (1965).
- (6) H. P. Klug, *ibid.*, **21**, 536 (1966).
- (7) M. Bonamico, G. Dessy, A. Mugnoli, A. Vaciago, and L. Zambonelli, *ibid.*, **19**, 886 (1965).
- (8) M. Bonamico, G. Mazzone, A. Vaciago, and L. Zambonelli, *ibid.*, **19**, 898 (1965).
- (9) A. Domenicano, L. Torelli, A. Vaciago, and L. Zambonelli, *J. Chem. Soc., A*, 1351 (1968).
- (10) The List of Forthcoming Papers in *Acta Crystallogr.* (**B24**, 1968) indicates that Dr. S. Merlino of Pisa, Italy, has submitted to that journal a paper on the structure of $\text{Co}(\text{dtc})_3$. We sent our results to Dr. Merlino and he tells us that our results agree within experimental error with his. Also, he pointed out to us that, wherever relevant, the bonding parameters of our $\text{Co}(\text{dtc})_3$ agree very nicely with those of cobalt tris(ethyl xanthate), which he has just finished studying.

Table I: Fractional Coordinates and Anisotropic Thermal Parameters of the Atoms with Their Estimated Standard Deviations^a

Atom	X	Y	Z	β_{11}	β_{22}	β_{33}	β_{12}	β_{13}	β_{23}
Co	0000 (0)	2519 (1)	2500 (0)	46 (1)	53 (1)	27 (1)	0000 (0)	12 (1)	0000 (0)
S(1)	1001 (2)	0790 (2)	2508 (2)	59 (2)	68 (2)	36 (1)	12 (1)	11 (1)	-3 (1)
S(2)	1265 (2)	3995 (2)	2762 (2)	66 (2)	77 (2)	29 (1)	-22 (1)	17 (1)	-3 (1)
S(3)	0528 (2)	2782 (2)	3901 (1)	50 (1)	74 (2)	28 (1)	-6 (1)	12 (1)	4 (1)
N(1)	0000 (0)	-1424 (1)	2500 (0)	110 (15)	56 (13)	48 (7)	0000 (0)	-1 (7)	0000 (0)
N(2)	2058 (7)	4510 (7)	4415 (5)	62 (6)	97 (8)	32 (3)	-20 (5)	15 (4)	-3 (4)
C(1)	0000 (0)	-0149 (11)	2500 (0)	60 (9)	54 (5)	31 (5)	0000 (0)	10 (6)	0000 (0)
C(2)	0903 (13)	-2164 (14)	2514 (11)	96 (11)	98 (13)	75 (8)	34 (10)	9 (7)	1 (8)
C(3)	0823 (26)	-2644 (21)	1628 (17)	252 (31)	153 (22)	77 (11)	75 (11)	13 (14)	-11 (13)
C(4)	1405 (7)	3874 (7)	3808 (5)	43 (6)	56 (6)	28 (3)	-2 (4)	12 (3)	-3 (3)
C(5)	2676 (11)	5516 (14)	4230 (9)	79 (10)	147 (16)	55 (6)	-36 (10)	10 (16)	13 (8)
C(6)	3724 (11)	5515 (21)	4885 (13)	59 (11)	221 (28)	92 (11)	-3 (13)	16 (8)	44 (15)
C(7)	2064 (10)	4388 (12)	5274 (6)	67 (8)	130 (12)	23 (4)	-11 (7)	8 (4)	-7 (5)
C(8)	1550 (16)	5535 (19)	5537 (12)	137 (15)	182 (23)	74 (9)	38 (15)	49 (9)	-15 (11)

^a The anisotropic temperature factors are of the form $\exp[-(\beta_{11}h^2 + \beta_{22}k^2 + \beta_{33}l^2 + 2\beta_{12}hk + 2\beta_{13}hl + 2\beta_{23}kl)]$. The estimated standard deviations are in parenthesis. All values are $\times 10^4$.

ing of the molecule. The bond lengths and angles of the asymmetric unit, with their estimated standard deviations, are listed in Table II. The cobalt atom lies on a twofold axis, which bisects one of the two dithiocar-

Table II: Bond Lengths (ångströms) and Angles (degrees) with Standard Deviations

Co-S(1)	2.270 (3)	S(1)-Co-S(1)	76.5 (1)
Co-S(2)	2.268 (3)	S(2)-Co-S(3)	76.1 (1)
Co-S(3)	2.263 (3)	Co-S(1)-C(1)	86.3 (3)
S(1)-C(1)	1.706 (7)	Co-S(2)-C(4)	87.7 (3)
S(2)-C(4)	1.731 (8)	Co-S(3)-C(4)	88.2 (3)
S(3)-C(4)	1.718 (8)	S(1)-C(1)-S(1)	110.9 (3)
C(1)-N(1)	1.315 (15)	S(2)-C(4)-S(3)	108.1 (4)
C(4)-N(2)	1.303 (11)	S(1)-C(1)-N(1)	124.5 (3)
N(1)-C(2)	1.477 (15)	S(2)-C(4)-N(2)	125.7 (6)
N(2)-C(5)	1.455 (14)	S(3)-C(4)-N(2)	126.3 (6)
N(2)-C(7)	1.466 (12)	C(1)-N(1)-C(2)	121.1 (7)
C(2)-C(3)	1.556 (29)	C(4)-N(2)-C(5)	119.9 (8)
C(5)-C(6)	1.516 (19)	C(4)-N(2)-C(7)	120.7 (7)
C(7)-C(8)	1.533 (12)	C(1)-N(1)-C(1)	117.8 (8)
S(1)···S(1)	2.811 (5) ^a	C(5)-N(2)-C(7)	118.6 (8)
S(2)···S(3)	2.791 (3) ^a	N(1)-C(2)-C(3)	111.9 (13)
		N(2)-C(5)-C(6)	110.1 (10)
		N(2)-C(7)-C(8)	112.6 (11)

^a These are not intended to imply bonding. We give them for the sake of completeness since inquiries about such distances have been made by interested parties.

bamate ligands. The atoms in a second dithiocarbamate ligand all lie in general positions, but in turn they generate a third dithiocarbamate ligand by the action of the twofold axis. This symmetry relationship is shown in Figure 1 *via* the fact that the atoms in question have the same indices, *i.e.*, S(1), etc. . . . It is easy to see in Figure 1 that the geometry of the six sulfur atoms surrounding the cobalt is quite distorted from that of a regular octahedron, as demonstrated by the S(3)-Co-S(3) and S(1)-Co-S(2) angles of 166.21 (12)° and 166.51 (9)°. This distortion from a perfect octahedron is due primarily to the constraint imposed on the geometry of the molecule by the rigid nature of the dithiocarbamate ligands and by the size of the "bite" angles at the metal, which in this case are S(1)-Co-S(1) = 76.50 (14)° and S(2)-Co-S(3) = 76.05 (10)°.

Although there are no other structural studies of tris(dithiocarbamates) available for comparison with our results, it is of interest to compare the bond lengths and angles in Co(dtc)₃ with those of dithiocarbamate complexes of first row transition metals. Table III lists representative first row metal dithiocarbamates, ionic radii of the metal ion, and the observed bond lengths. In each case the S-C, C-N, and N-C (alkyl) bond lengths are in close agreement. However, there is

Table III: Comparison of Bond Distances in Various Dialkyldithiocarbamates

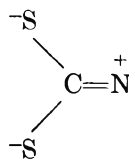
Compd	Ionic radii of metal, ^a Å	Bond distances, Å				Ref
		M-S ^b	S-C	C=N	N-C	
Fe(CO) ₂ [S ₂ CN(CH ₂) ₅] ₂	0.64	2.313	1.71	1.32	1.48	c
Co ^{III} [S ₂ CN(C ₂ H ₅) ₂] ₃	0.63	2.267	1.718	1.309	1.466	d
Ni ^{II} [S ₂ CN(C ₂ H ₅) ₂] ₂	0.69	2.201	1.707	1.33	1.48	e
Cu ^{II} [S ₂ CN(C ₂ H ₅) ₂] ₂	0.72	2.312	1.717	1.34	1.47	f
Zn ^{II} [S ₂ CN(CH ₃) ₂] ₂	0.74	2.362	1.722	1.32	1.473	g

^a "The Handbook of Chemistry and Physics," 45th ed, Chemical Rubber Publishing Co., Cleveland, Ohio, 1964. ^b Bond lengths are average values for M-S bond lengths only; nonbridging M-S values were averaged. ^c J. S. Ricci and I. Bernal, to be submitted for publication. ^d This work. ^e Reference 5. ^f Reference 7. ^g Reference 6.

a significant variation in the metal-sulfur (M-S) bond lengths. Other factors being equal, one might expect the M-S distances to vary as the ionic radii of the central metal ion. The iron and cobalt complexes, which are octahedral and isoelectronic, behave in the expected manner. That is, the Fe-S bond is longer than the Co-S bond. The fact that the difference in their bond length is not equal to the difference in ionic radii is probably accounted for by, among other factors, the difference in charge of the central metal ion.

Judging from the ionic radii of Ni(II), Cu(II), and Zn(II), one would expect all of their corresponding M-S bond lengths to be larger than either those of Co or Fe compounds. However, this is not the case. This apparent discrepancy can be resolved by considering the type of coordination of each complex. Both the Fe and the Co are sixfold coordinated, even though they are not both tris(dithiocarbamates). On the other hand, the Ni, Cu, and Zn complexes are essentially fourfold-coordinated. In the case of Ni the accepted values for fourfold-coordinated Ni-S bond lengths are 2.1-2.3 Å, while 2.4-2.6 Å seems to be the correct range for six-fold-coordinated Ni-S complexes.¹¹ Similarly, six-coordinated Cu(II) and Zn(II) complexes have M-S bonds which are 0.2-0.3 Å larger than the corresponding distances in fourfold-coordinated complexes. Thus if 0.25 Å is added to the M-S bond lengths of the fourfold-coordinated complexes, a good correlation is obtained between ionic radii and the corresponding M-S bond length.

The C-N bond distances, 1.303 and 1.315 Å, imply a high degree of double-bond character, indicating that there is a sizable contribution of the canonical structure



This is further evidenced by the identical (within experimental error) C-S distances, by the very nearly trigonal sp^2 angles around the nitrogens, which range from 117.78 to 121.11°, and by the virtual planarity of the two independent sets of CoS_2CN fragments.¹² The best least-squares molecular planes and the distances (in ångströms) of the atoms from these planes are: (1) the plane through Co, S(2), S(3), C(4), and N(2) ($9.331x - 7.638y - 2.091z - 2.447 = 0$) Co, 0.0003; S(2), -0.0010; S(3), -0.0010; C(4), 0.0029; N(2), 0.0010; (2) the plane through Co, S(1), S(1), C(1), and N(1) ($-1.338x - 1.765y + 1.608z + 4.019 = 0$). Since Co, C(1), and N(1) are on the same twofold axis, these atoms together with S(1) and the S(1) generated by operation of the twofold axis are exactly planar.

A final remark concerning the structure of $\text{Co}(\text{dte})_3$

pertains to the positions of the hydrogen atoms of the ethyl chains. Although Figure 1 does not show the aliphatic hydrogens, it is clear from the stereochemistry of the carbon atoms that the two alkyl chains are so situated as to minimize contacts of the hydrogens for both the $-\text{CH}_2-$ and the $-\text{CH}_3$ groups with those of the adjacent $-\text{CH}_2\text{CH}_3$ chain.

Acknowledgments. Research was supported in part by Grant No. 2035-A3 of the Petroleum Research Fund and by the U. S. Atomic Energy Commission. We also wish to thank Professor Stefano Merlino of Pisa for his helpful remarks and comments embodied in ref 10.

(11) J. S. Ricci and I. Bernal, to be submitted for publication.

(12) A. Lopez-Castro and M. S. Trutter, *J. Chem. Soc.*, 1309 (1933).

A Reinvestigation of the Dielectric Constant of Water and Its Temperature Coefficient

by Robert L. Kay,¹ G. A. Vidulich, and Krishnahadi S. Pribadi

Chemistry Department, Mellon Institute of Carnegie-Mellon University, Pittsburgh, Pennsylvania 15213
(Received September 10, 1968)

The dielectric constant of pure water between 0 and 40° was recently investigated² by a bridge method using fully shielded and guarded cells³ especially designed for the measurements. The results were shown to be in excellent agreement with two previous determinations by different methods^{4,5} both as to absolute value and temperature coefficient. At about the same time, Rusche and Good,^{6,7} reported results for water using the same type of capacitance bridge and a cell based on the design of Vidulich and Kay.³ A comparison of their results with our own indicates excellent agreement in the temperature coefficient but an absolute value about 0.16 unit higher.

Since the dielectric constant of water is of some importance, we have investigated the possible sources of this discrepancy rather carefully. Contrary to the statement by Rusche and Good,⁶ our cells were com-

(1) To whom all correspondence should be addressed.

(2) G. A. Vidulich, D. F. Evans, and R. L. Kay, *J. Phys. Chem.*, **71**, 656 (1967).

(3) G. A. Vidulich and R. L. Kay, *Rev. Sci. Instrum.*, **37**, 1662 (1966).

(4) W. L. Lees, Ph.D. Thesis, Harvard University, 1949.

(5) B. B. Owen, R. C. Miller, C. E. Milner, and H. L. Cogan, *J. Phys. Chem.*, **65**, 2065 (1961).

(6) E. W. Rusche and W. B. Good, *J. Chem. Phys.*, **45**, 4667 (1963).

(7) E. W. Rusche, Jr., Ph.D. Dissertation, New Mexico State University, 1966.

pletely shielded on the outside by a conducting surface layer of silver.³ Also, we have employed cells with gold alloy film electrodes in place of pure platinum and found no difference in the results. As was pointed out in earlier results,² the limiting factor which determined the accuracy of our data was the possibility of incomplete shielding between the cell leads due to the fact that the lead to the guarded electrode could "see" the high-voltage electrode through the very narrow guard gap. Vidulich⁸ investigated this possibility thoroughly, both experimentally and theoretically, and concluded that the correction for this effect would increase the dielectric constant by no more than 0.03 unit. We have recently confirmed this result by enclosing the lead to the guarded electrode in a glass tube that was completely covered with a grounded layer of silver paint. Three different cells gave dielectric constants for water at 25° that differed from our previous value² by no more than 0.01 unit.

We believe the most serious source of error in determining the absolute dielectric constant of a highly conducting solvent such as water by a bridge method lies in the correction required to compensate for the capacitance associated with the resistance networks used to balance the conductance of the dielectric cell. Although in our previous measurements² we used water of extremely low specific conductance, $K_0 < 10^{-7}$ mho cm^{-1} , an auxiliary "wye" resistance network was required to extend the conductance range of the General Radio Type 1615-A capacitance bridge. The capacitance associated with this network was measured by an iteration procedure with the assumption that the capacitance associated with the full-scale resistance network in the bridge was -2.5×10^{-3} pF, a value which was verified by capacitance measurements on water of varying conductance.² This negative correction seems to have been ignored by Rusche and Good.⁹ An analysis of their auxiliary resistance network indicated a correction of -0.06 unit at most should be made to their dielectric constants if the effective capacitance associated with their bridge conductance network was close to our own, as is most likely the case. The remaining difference between our results (0.10 unit in ϵ) could possibly be attributed to errors resulting from the necessity of placing their cell on the 0.01 tap in order to balance the high conductance with their auxiliary megohm resistor. This magnified all errors by 100 and could easily account for a difference of 0.10 in ϵ .

In order to avoid the problem of evaluating the errors associated with the conductance network and the use of the multiplying taps, we have designed a conductance network with an extended range up to 10^3 μmhos which has a greatly reduced associated capacitance that can be easily reduced to zero within the detectability of the bridge by using very small trimming capacitances or inductances. It consists essentially of a type CRT-12A Gertsch ratio transformer in series with a 1- or a 10-K

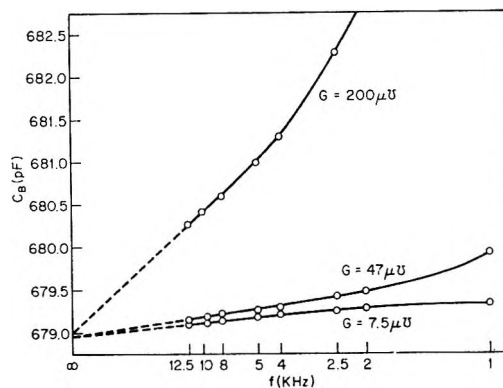


Figure 1. The frequency dependence of the cell capacitance is shown as a function of $1/f^{1/2}$ at various cell conductances.

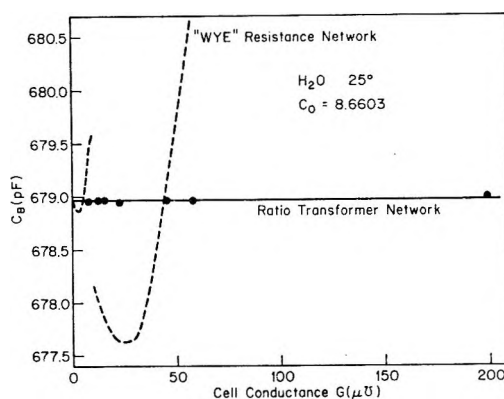


Figure 2. The measured cell capacitance is shown after correction for electrode polarization but with no correction for the capacitance associated with the bridge conductance balancing networks: ---, "wye" resistance network; ●, ratio transformer network.

metal film resistor and has been described in detail elsewhere.¹⁰ The network was tested by measuring the capacitance of water at 25° in a fully guarded and shielded cell³ with the center lead completely shielded and with gold-film electrodes. The normal electrode polarization was eliminated by an extrapolation to infinite frequency on a $1/f^{1/2}$ plot as shown in Figure 1. At frequencies above 12.5 kHz, lead and bridge inductance errors become significant. The extrapolated values are plotted in Figure 2 as a function of the cell conductance. The dashed curve indicates how the measured capacitance would vary if our previous "wye" resistance network was used to balance the conductance and if no correction was made for the associated capacitance. The discontinuity at 10 μmhos is the result of placing the cell on the 0.1 tap in order to extend the range of the conductance network. At a conductance of 10 μmhos (specific conductance, 0.1 μmho) a correction of 0.1% is necessary and a correction of about the same magni-

(8) G. A. Vidulich, Ph.D. Thesis, Brown University, 1964.

(9) W. B. Good, 1967, private communication.

(10) R. L. Kay and K. S. Pribadi, *Rev. Sci. Instrum.*, in press.

tude was required using the resistance network designed by Rusche and Good.¹¹ On the other hand, our ratio transformer network is capable of reproducing the cell capacitance to within better than 0.01% without any correction at conductances as high as 200 μmhos (specific conductance, 2 μmhos).

The resulting capacitance of 678.97 pF results in a dielectric constant of water at 25.00° of 78.40 ± 0.005 in excellent agreement with our previous value² of 78.41. Owing to the precision with which this value has been obtained, without the necessity of making any corrections, we have adjusted our data at other temperatures² and proposed for the dielectric constant of water

$$\log \epsilon_{\text{H}_2\text{O}} = 1.94409 - 1.991 \times 10^{-3}T \quad (1)$$

where T is in degrees Centigrade. This gives $\partial\epsilon_{\text{H}_2\text{O}}/\partial T = -4.585 \times 10^{-3}\epsilon_{\text{H}_2\text{O}}$, in excellent agreement with $-4.587 \times 10^{-3}\epsilon_{\text{H}_2\text{O}}$ obtained from the data of Rusche and Good,⁷ the logarithmic plot of their data being completely linear and preferable to their quadratic equation. It should also be pointed out that our present data at all temperatures are now identical with those of Lees⁴ to better than 0.01 unit. Significantly, Lees was able to completely compensate for the capacitance associated with his conductance network, as is the case with our measurements, by using a tungsten lamp whose resistance was varied by changing the dc current through the filament. Lees determined the constant capacitance of such a conductance network by using a cell of variable geometry. This fact and the excellent agreement with our data adds considerable weight to the reliability of Lees' data at higher pressures. The data of Owen, *et al.*,⁵ are only 0.02 unit lower than our own at 0° and 0.05 lower at 40°.

Acknowledgment. This work was supported by Contract No. 14-01-0001-1729 with the Office of Saline Water, U. S. Department of the Interior. We are indebted to Professors Good and Rusche for supplying us with the detailed information concerning their measurements.

(11) Reference 7, p 78.

Photochemical Reactions of Fluorescein

Dyes with H_2O_2 ¹

by Karl J. Youtsey and L. I. Grossweiner

Physics Department, Illinois Institute of Technology, Chicago, Illinois 60616 (Received September 23, 1968)

Hydrogen peroxide is expected to be a product in dye-sensitized autooxidations. The precursor HO_2 can be formed either by the reaction of the sensitizer triplet state (D_t) with oxygen ($\text{D}_t + \text{O}_2 \rightarrow \text{D}_{\text{oxld}} + \text{HO}_2$) or

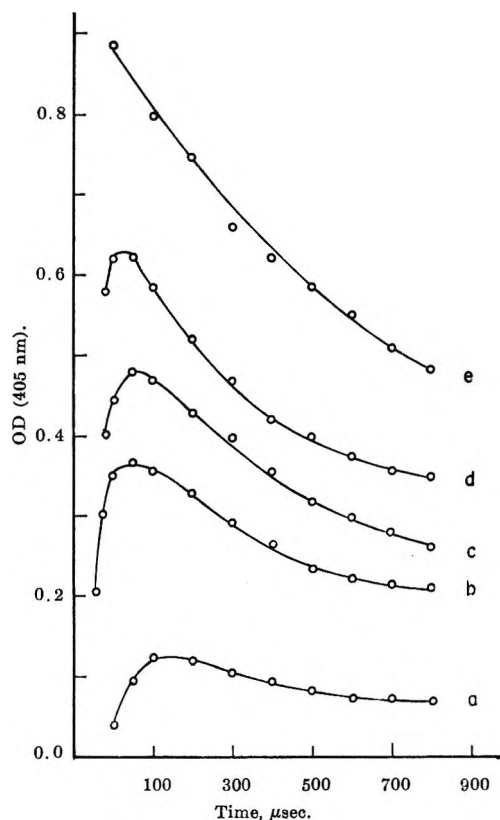


Figure 1. Growth and decay of erythrosin semiquinone in the presence of hydrogen peroxide after flash photolysis of a 5 μM deaerated solution at pH 9.3. H_2O_2 concentrations (μM): (a) 2, (b) 5, (c) 7, (d) 9, (e) 15.

indirectly *via* the reaction of the excited sensitizer with an oxidizable substrate ($\text{D}_t + \text{QH}_2 \rightarrow \text{D}_{\text{red}} + \text{QH}\cdot$), followed by oxidation of the reduced dye intermediate ($\text{D}_{\text{red}} + \text{O}_2 \rightarrow \text{D} + \text{HO}_2$). In the case of the fluorescein dyes, evidence for the first mechanism derives from the identification of H_2O_2 after aerobic photobleaching of concentrated fluorescein or eosin aqueous solutions.² The reduction of triplet eosin by aromatics has been studied by flash photolysis,^{3,4} while the oxidation of eosin semiquinone by oxygen was demonstrated with pulse radiolysis.⁵ The object of this work is to obtain information on the role of accumulated H_2O_2 in sensitized autooxidation reactions by studying the flash photolysis of deaerated dye- H_2O_2 solutions. The apparatus and procedures are similar to those described in ref 4.

The irradiation of a deaerated dye solution containing H_2O_2 with a green light flash (460–600 nm) produces a

(1) Supported by the U. S. Public Health Service on Grant No. GM-10038 from the National Institute of General Medical Sciences.

(2) Y. Usui, K. Itoh, and M. Koizumi, *Bull. Chem. Soc. Jap.*, **38**, 1015 (1965).

(3) L. I. Grossweiner, *J. Chem. Phys.*, **34**, 1411 (1961).

(4) J. Chrysochoos and L. I. Grossweiner, *Photochem. Photobiol.*, **8**, 193 (1968).

(5) J. Chrysochoos, J. Ovadia, and L. I. Grossweiner, *J. Phys. Chem.*, **71**, 1629 (1967).

Table I: Rate Constants for the First-Order and Second-Order Decay Processes of the Triplet Dye and the Reactions of Triplet Dye and the Dye Semiquinone with Hydrogen Peroxide

Dye	Rate constant ^a				
	D _t + H ₂ O ₂	D _{red} + H ₂ O ₂	D _t → D ^b	D _t + D _t	D _t + D
Fluorescein (pH 12.0)	...	8.8 × 10 ⁴	50 ^d	1.1 × 10 ^{9d}	1 × 10 ^{8d}
Dibromofluorescein (pH 9.3)	7.8 × 10 ⁴	4.9 × 10 ³	1500	3.0 × 10 ^{9c}	2.4 × 10 ⁸
Eosin (pH 9.3)	2.4 × 10 ⁴	1.9 × 10 ⁴	540 ^e	1.2 × 10 ^{9c}	3.7 × 10 ^{8e}
Erythrosin (pH 9.3)	3.3 × 10 ⁴	1.2 × 10 ⁶	5200	6.0 × 10 ^{9c}	2.2 × 10 ⁸

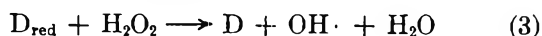
^a Units are l./mol-sec unless indicated otherwise. ^b Units in this column are sec⁻¹. ^c The results obtained in this work are expressed in terms of the unknown triplet molar absorbance at 600 mμ. ^d Reference 6. ^e V. Kasche and L. Lindqvist, *Photochem. Photobiol.*, **4**, 923 (1965).

broad, strong absorption in the blue region which grows in and decays more rapidly at higher H₂O₂ concentrations. Typical data for erythrosin are shown in Figure 1. The flash spectra show that the transient bands correspond with the dianionic forms of the semiquinone for the case of fluorescein,⁶ eosin,³ and erythrosin.⁷ Kinetic measurements in the red region, where only the dye triplet states absorb, indicate that the triplet lifetime decreases with increasing H₂O₂ concentration. It is concluded that H₂O₂ both reduces the dye in its triplet state and oxidizes the corresponding semiquinone. The over-all reactions can be described as



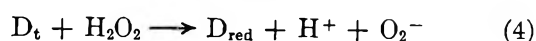
Measurements of the pseudo-first-order rates of triplet and semiquinone decay at H₂O₂ concentrations up to 50 mM led to the rate constants in Table I. The first-order and second-order triplet quenching rate constants obtained in this work and taken from the literature are given in Table I also.

The low rate constants are typical of noncatalyzed redox reactions involving H₂O₂. It is probable that reaction 2 proceeds *via* a slow Fenton-type process



followed by the well-known OH, HO₂, H₂O₂ radical chain.⁸ The energetics of reaction 3 can be estimated with the redox potentials given by Baxendale⁹ and taking the reversible polarographic half-wave potential of the dye as approximately equal to the redox potential of the couple D, H⁺/D_{red}. The calculation for the case of eosin based on $E_{1/2} = -1.03$ V (pH 10 *vs.* sce)¹⁰ gives $\Delta F'$ (pH 10) ~ -30 kcal/mol at 50% conversion of H₂O₂.

Reaction 1 demonstrates the ability of dye triplet states to act as electron acceptors. It probably takes place in two stages with the intermediate slow step



noting that pK_a of HO₂ is 4.5.¹¹ The energetics can be estimated for eosin, as in the above case, taking the

phosphorescence energy of 40 kcal/mol¹² as approximately the free energy change of D_t → D. It is found that $\Delta F'$ (pH 10) ~ -3 kcal/mol at 50% conversion of H₂O₂. Thus both the reduction (eq 4) and the oxidation (eq 3) are energetically feasible reactions.

Permanent bleaching of the dye after several light flashes was observed except in the case of fluorescein, where the triplet yield was very low. A possible explanation is the oxidation of the dye by OH formed in reaction 3, which has been shown to be fast.^{5,7} These results indicate that H₂O₂ should attain a steady-state concentration in dye-sensitized autooxidations not involving the excited singlet oxygen mechanism, in which H₂O₂ is not an intermediate, when it will compete with oxygen and the substrate for triplet dye in the initial act.

(6) L. Lindqvist, *Ark. Kemi*, **16**, 79 (1960).

(7) P. Cordier and L. I. Grossweiner, *J. Phys. Chem.*, **72**, 2018 (1968).

(8) F. Haber and R. Willstätter, *Ber. Bunsenges Phys. Chem.*, **648**, 2844 (1931).

(9) J. H. Baxendale, *Radiat. Res. Supp.*, **4**, 114 (1964).

(10) T. Tani and S. I. Kikuchi, *Rep. Inst. Ind. Sci. Univ. Tokyo*, **18**, 1 (1968).

(11) G. Czapski and L. M. Dorfman, *J. Phys. Chem.*, **68**, 1169 (1964).

(12) C. A. Parker and C. G. Hatchard, *Trans. Faraday Soc.*, **57**, 1894 (1961).

Vibrational Spectra of the Hydrogen

Dihalide Ions. V. BrHBr⁻ at 20°K

by J. C. Evans and G. Y-S. Lo

Chemical Physics Research Laboratory, The Dow Chemical Company, Midland, Michigan 48640 (Received September 12, 1968)

The previous paper in this series¹ contains a major printing error; the wave number scale was omitted from all the infrared absorption spectra. This missing scale,

(-) J. C. Evans and G. Y-S. Lo, *J. Phys. Chem.*, **71**, 3942 (1967).

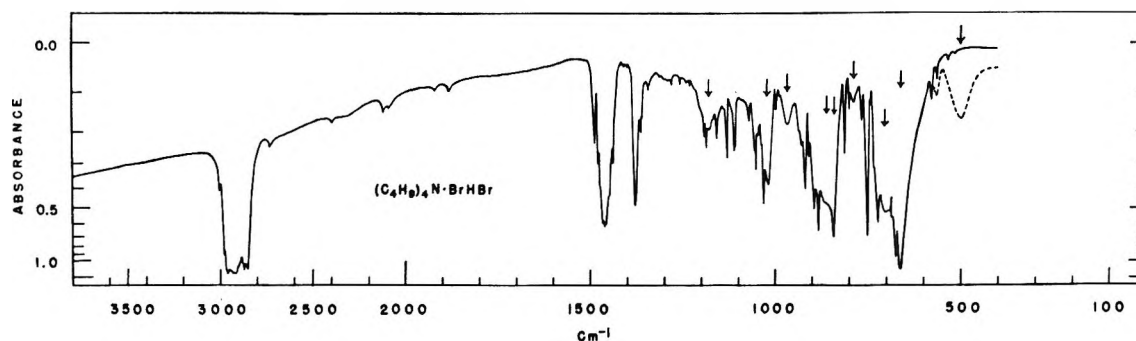


Figure 1. The infrared absorption spectrum of a Nujol mull of tetrabutylammonium protium dibromide at 20°K. The dotted curve shows the 500-cm⁻¹ region at approximately 273°K. Arrows signify bands assigned to the anion.

which is the same for all the spectra reproduced, is given in Figure 1. The figure also includes new data which clarify further the nature of the broad, complex absorption region between 1300 and 500 cm⁻¹ characteristic of the type II salts which are believed to contain symmetrical hydrogen bonds. The salt, tetrabutylammonium protium dibromide, which showed the best defined structure in this broad absorption region was examined at temperatures down to 20°K using a Cryo-tip refrigerator (Air Products and Chemicals, Inc.) with a Perkin-Elmer Model 225 spectrometer.² Bands which were broad at 100°K are resolved into well-defined peaks at 20°K.

The general interpretation advanced previously is confirmed. The main features are readily assigned to $\nu_3 \pm n\nu_1$, where ν_3 and ν_1 are the antisymmetric and the symmetric stretching modes, respectively, of the BrHBr⁻ ion. The band near 500 cm⁻¹ assigned previously on inconclusive evidence to the difference tone $\nu_3 - \nu_1$ disappears completely before 20°K is reached; the four most prominent features indicated by arrows in Figure 1 are $\nu_3 + n\nu_1$, where $n = 0, 1, 2, \text{ or } 3$. Superimposed on this main band progression are two others, $\nu_3 + m\nu_L$ and $\nu_3 + \nu_1 + m\nu_L$, where ν_L is about 40 cm⁻¹ and $m = 1, 2, \text{ or } 3$. ν_L is presumably a lattice mode. The absorption features and their assignments (cm⁻¹) are summarized thus: $\nu_3 - \nu_1$, 494; ν_3 , 663 s; $\nu_3 + \nu_L$, 704 m, sh; $\nu_3 + 2\nu_L$, ~750 obsc; $\nu_3 + 3\nu_L$, 790 w; $\nu_3 + \nu_1$, 842 m; $\nu_3 + \nu_1 + \nu_L$, ~880 w, sh; $\nu_3 + \nu_1 + 2\nu_L$, ~930 w, obsc; $\nu_3 + \nu_1 + 3\nu_L$, 968 w; $\nu_3 + 2\nu_1$, 1020 mw; $\nu_3 + 3\nu_1$, ~1185 w, where s indicates strong; m, medium; sh, shoulder; and w, weak; obsc indicates that overlapping cation absorption bands partially obscure the band and makes the choice of band center uncertain.

This interpretation of the spectrum of HBr₂⁻ in terms of $\nu_3 + n\nu_1$ is essentially similar to that generally accepted for the symmetrical HF₂⁻ ion³ for which ν_1 is much larger; the band progression $\nu_3 + n\nu_1$ is widely spaced and is not obscured by the band broadening, which has been shown by matrix-isolation experiments^{4,5} to arise from coupling between identical ions.

It is interesting to note that if the Stepanov energy level scheme for the hydrogen bond^{6,7} is assumed to apply, we may conclude from the observed values of $\nu_3 - \nu_1$ and $\nu_3 + \nu_1$, which yield values of 168 and 179 cm⁻¹ for ν_1 in the ground and first excited levels of ν_3 , respectively, that the hydrogen bond is stronger in the first excited level.

(2) We are indebted to Dr. S. T. King for his assistance in obtaining these low-temperature spectra.

(3) G. L. Cote and H. W. Thompson, *Proc. Roy. Soc.*, **A210**, 206 (1951).

(4) J. A. Ketelaar, C. Haas, and J. Vander Elsken, *J. Chem. Phys.*, **24**, 624 (1956); **30**, 336 (1959).

(5) J. A. Salthouse and T. C. Waddington, *ibid.*, **48**, 5274 (1968).

(6) B. I. Stepanov, *Zh. Fiz. Khim.*, **19**, 507 (1945).

(7) N. Sheppard, Proceedings of the Hydrogen Bonding Symposium, Ljubljana, D. Hadzi, Ed., Pergamon Press Inc., New York, N. Y., 1959.

Two-Bond, Carbon-Proton Coupling in Halogenated Ethylenes^{1a}

by Frank J. Weigert^{1b} and John D. Roberts

Contribution No. 3685 from the Gates and Crellin Laboratories of Chemistry, California Institute of Technology, Pasadena, California 91109 (Received May 21, 1968)

The large differences between the two-bond, carbon-proton couplings in *cis*- and *trans*-disubstituted ethylenes have been difficult to account for.² As an aid to additional clarification of this problem, we have determined two-bond coupling constants of several halogenated ethylenes which are presented in Table I. The predicted ¹³C spectrum of vinyl chloride was found to be sensitive to the relative signs of the carbon-proton coupling constants. The polyhaloethylenes exhibited first-order spectra and double resonance was required to obtain the relative signs. Sample spectra of *cis*-dichloroethylene using the indor technique³ are shown

(1) (a) Supported in part by the National Science Foundation; (b) National Science Foundation Predoctoral Fellow, 1965-1968.

(2) N. Muller, *J. Chem. Phys.*, **37**, 2729 (1963).

(3) E. B. Baker, *ibid.*, **37**, 911 (1963), performed the reverse experiment, observing protons while irradiating at the ¹³C frequencies.

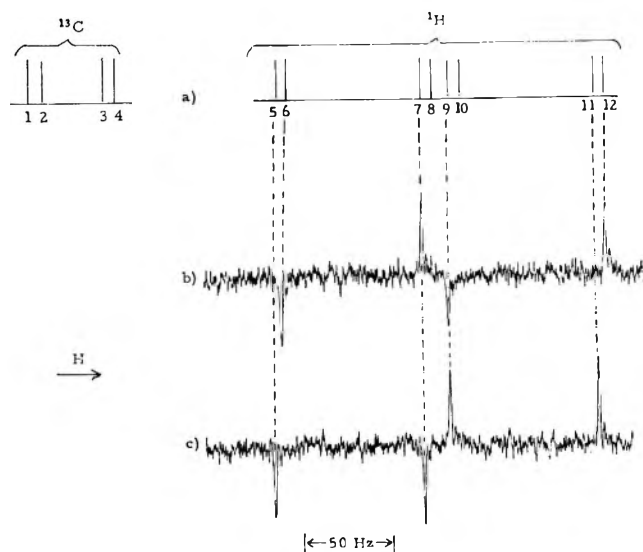


Figure 1. Indor spectra of *cis*-dichloroethylene, time averaged for 17 scans through the proton spectrum: (a) schematic ^{13}C and ^1H single-resonance spectrum; (b) indor double-resonance spectrum obtained observing at the frequency of ^{13}C , line 2; (c) same as b only observing at the frequency of ^{13}C , line 1.

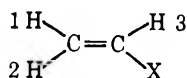
in Figure 1. Either spectrum is sufficient to show that the signs of all three coupling constants are the same. The line width of each half of the "doublet" of the ^{13}C spectrum of *trans*-dichloroethylene is 0.5 Hz, suggesting that the two-bond coupling is less than 0.3 Hz. Differences arising from solvent effects may explain the 0.8-Hz coupling found for this compound by Govil⁴ using homonuclear tickling techniques.

Table I: Two-Bond, Carbon-Proton Coupling in Halogen-Substituted Ethylenes

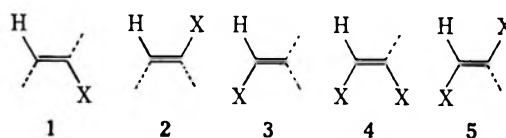
Compd	Proton	J_{CCH} , Hz	
		Obsd	Predicted
Ethylene ^a		-2.4	
Vinyl bromide ^{b,c}	1	7.5	
	2	-8.5	
	3	5.8	
Vinyl chloride ^c	1	7.1	
	2	-8.3	
	3	6.8	
<i>cis</i> -Dibromoethylene		14.7	15.7
<i>trans</i> -Dibromoethylene		-0.4	1.4
Tribromoethylene		[7.8]	9.6
<i>cis</i> -Dichloroethylene		15.4	16.3
<i>trans</i> -Dichloroethylene		<0.3	0.9
1,1-Dichloroethylene		<0.6	1.2
Trichloroethylene		[8.9]	10.4

^a R. M. Lynden-Bell and N. Sheppard, *Proc. Roy. Soc.*, **A269**, 385 (1962). ^b R. M. Lynden-Bell, *Mol. Phys.*, **6**, 537 (1963).

^c The protons are numbered as shown



It has now been found that the problems presented by the variations in the two-bond, carbon-proton coupling constants in the polyhaloethylenes can be reduced to simpler terms, namely, substituent effects in the individual vinyl halides. The general formula for calculating the coupling constant in polyhaloethylenes is $J = J_0 + \sum_i (J_i - J_0)$, where J_0 is the two-bond coupling in ethylene and the J_i are the appropriate coupling constants of structures 1-3. On this basis the two-bond coupling in *cis*-disubstituted compounds with arrangement 4 is interpretable as the result of the large and positive substituent effects arising from structures 1 and 3 so that a large, positive two-bond coupling would be expected (and is observed). On the other hand, the *trans* isomers (5) would have contributions of types 2



and 3 with opposite signs and smaller over-all two-bond couplings. The coupling in *gem*-disubstituted compounds should also be small because the contributions from 1 and 2 are of opposite sign. The trisubstituted compounds will be expected to show the net substituent effects contributed by 1-3.

Several calculated values of the two-bond, carbon-proton coupling constants obtained by this simple additivity postulate for various vinyl halides are given in Table I. Changes in bond angles and/or long-range s-bond order or orbital-orbital polarizability effects may account for part or all of the small deviations from additivity, but it seems clear the major influence on the two-bond coupling can be rationalized by additivity of substituent effects in the monosubstituted compounds.⁵

The remaining problem is how to interpret the couplings in the monosubstituted vinyl compounds themselves. The two-bond, carbon-proton coupling in situations like 3 may be understood in terms of the molecular orbital theory developed by Pople and Bothner-By for proton-proton coupling.⁶ A positive substituent effect was shown to be associated with the withdrawal of σ electrons from the $-\text{CH}_2-$ fragment by an electronegative substituent. Because of differences in symmetry, the arrangements corresponding to 1 and 2 cannot be treated in the same simple manner.



(4) G. Govil, *J. Chem. Soc.*, **A**, 1420 (1967).

(5) Similar results and conclusions about substituent effects on $J^{13}\text{CCH}$ couplings to those reached in this paper were arrived at several years ago by Professors R. J. Kurland and P. C. Lauterbur (private communication).

(6) J. A. Pople and A. A. Bothner-By, *J. Chem. Phys.*, **42**, 1339 (1965).

The Thermal Conductivity of Aqueous Solutions of Alkali Hydroxides

by Zdenek Losenicky

Department of Physics, Faculty of Mechanical Engineering,
Technical University, Prague, Czechoslovakia

Accepted and Transmitted by The Faraday Society
(June 5, 1967)

Previous studies have been made of the concentration dependence of the thermal conductivity coefficient, λ , of liquid electrolytes.¹⁻⁷ For example, it was concluded by Riedel^{1,2} that the molar concentration dependence of λ of aqueous solutions of salts and acids is linear and that λ of an aqueous solution of NaOH is independent of concentration in the high-concentration range. It was logical, therefore, to study thoroughly the whole group of alkali hydroxides.

The comparative steady-state method of coaxial cylinders was used. The system, which is partly based upon that described by Filippov,^{8,9} is represented schematically in Figure 1. The thin annular space (0.8 mm wide) between quartz-glass coaxial cylinders (0.2 mm thick) was filled with the liquid specimen. The inner cylindrical space was filled with mercury and was heated by coaxial constantan wire placed in a ceramic bicapillary (1.5 mm in diameter). The tem-

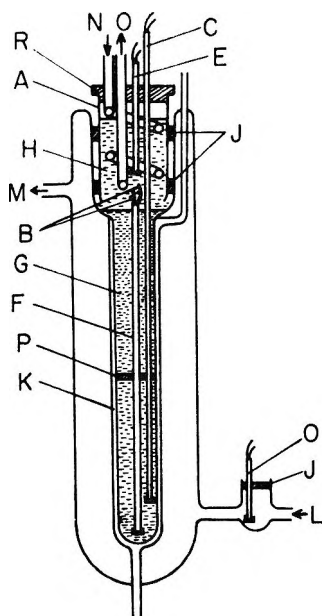


Figure 1. Schematic representation of the system used: A, cooler; B, heavy leads to the heating wire; C, D, four bicapillaries with thermocouples equally spaced at 90° (C, hot junctions; D, cold junctions); E, thermocouple of cooler; F, heater; G, heated space filled with mercury; H, oil; J, sealing rings; K, liquid specimen; L, from the main ultrathermostat; M, to the main ultrathermostat; N, from the ultrathermostat of the cooler; P, centering ring, R, cover.

perature difference between the mercury and the cooling liquid was measured with thermocouples placed in ceramic bicapillaries (1.0 mm in diameter).

Filippov used the formula $\varepsilon/U^2 = a + (b/\lambda)$, where ε is the measured thermal electromotive force and U is the voltage across the heating wire. Constants a and b were determined experimentally by using two different liquids of known λ . According to our measurements an error in λ of up to several per cent is produced by heat losses dependent upon the axial heat flow from the heated space. These heat losses were excluded by using the cooler (A) by means of which any temperature difference between the mercury and the oil layer was eliminated. If, as in the present experiment, the value of U is kept constant (with a maximum deviation of 0.05%), then the above-mentioned Filippov's formula gives the relation $\alpha = \lambda(\varepsilon - \beta)$. From this our λ 's were calculated. Constants α and β were determined by using toluene, mercury, water, aniline, and ethyl alcohol whose λ 's are well known to within $\pm 1\%$.¹⁰⁻¹⁵ The calculation of α and β was based upon the method of least squares.

The thermocouple circuit consisted of four copper-constantan thermocouples connected in series, and the thermal emf, ε , produced was measured with a potentiometer, the error being $\pm 1 \mu\text{V}$. The cooling liquid was supplied by Höppler's ultrathermostats ($\pm 0.01^\circ$ error). The maximum radial temperature difference in the layer of liquid specimen was about 2° , so that the convection condition $\text{Pr.Gr} < 600$ was satisfied for all the liquid specimens used. The temperature shocks (sharp increases in temperature) due to the ultrathermostat were within 0.02° . The heat exchange between the cooling system and its surroundings was minimized by the use of an insulating layer of cotton wool. This permitted a simple choice of electric current in the heating system of the ultrathermostat which would give a time interval between two consecutive shocks of about 60 min. Thermal equilibrium was reached after about

- (1) L. Riedel, *Chem. Ing. Tech.*, **23**, 59 (1951).
- (2) L. Riedel, *ibid.*, **22**, 54 (1950).
- (3) L. P. Filippov, *Vestnik. Mos. Univ.*, **6**, 59 (1954).
- (4) A. F. Kapustinskii and I. I. Ruzavin, *Zh. Fiz. Khim.*, **29**, 2222 (1955).
- (5) A. F. Kapustinskii and I. I. Ruzavin, *ibid.*, **30**, 548 (1956).
- (6) N. B. Vargaftik and J. P. Osminin, *Teploenergetika*, **7**, 11 (1956).
- (7) F. G. Eldarov, *Zh. Fiz. Khim.*, **10**, 2443 (1958).
- (8) L. P. Filippov and V. M. Ivanov, *Teploenergetika*, **8**, 68 (1961).
- (9) L. P. Filippov, *Inzh. Fiz. Zh. Akad. Nauk Belorussk. SSR*, **11**, 55 (1961).
- (10) B. P. Nikolski, "Handbuch des Chemikers," VEB Verlag Technik, Berlin, 1956.
- (11) C. D. Hodgman, Ed., "Handbook of Chemistry and Physics," 30th ed, Chemical Rubber Publishing Co., Cleveland, Ohio, 1961.
- (12) C. L. Mantell, "Engineering Materials Handbook," McGraw-Hill Book Co., Inc., New York, N. Y., 1957.
- (13) F. Henning, "Warmetechnische Richtwerke," VDI Verlag GMBH, Berlin, 1938.
- (14) N. B. Vargaftik, "Spravochnik po Teplo-Fizicheskim Svoistvam Gazov i Zhidkosti," Fizmatgiz, Moscow, 1963.
- (15) L. P. Filippov, *Vestn. Mosk. Univ.*, **3**, 61 (1960).

Table I

C, M	$\lambda, \text{kcal m}^{-1} \text{hr}^{-1} \text{deg}^{-1}$	C, M	$\lambda, \text{kcal m}^{-1} \text{hr}^{-1} \text{deg}^{-1}$
LiOH		NaOH	
1.97	0.547	1.36	0.546
2.65	0.547	3.95	0.567
4.15	0.565	5.50	0.572
KOH		8.60	0.572
1.50	0.542	11.8	0.570
3.00	0.546	13.1	0.564
4.15	0.527	15.0	0.554
6.10	0.523	16.4	0.541
8.80	0.514	RbOH	
10.1	0.510	1.30	0.524
12.6	0.498	2.50	0.512
16.1	0.477	4.45	0.492
CsOH		5.55	0.481
1.20	0.518	7.30	0.465
2.01	0.507	9.10	0.436
3.60	0.484	9.75	0.427
5.20	0.456	11.8	0.404
6.60	0.439	13.6	0.383
8.05	0.413	14.9	0.370
9.00	0.394		
10.6	0.360		
11.8	0.334		
13.2	0.311		

20 min. Thus each experiment could be carried out within two consecutive shocks, the influence of which was thus avoided. The limiting error of measurements is then less than 2%, which includes the error in calibration by liquids mentioned above.

Alkali hydroxides were obtained from the Spolana Co., Czechoslovakia. The following purities were guaranteed: NaOH and KOH, assay not less than 99.5%, carbonates less than 0.5%; RbOH and CsOH, assay not less than 99.0%, carbonates less than 1.0%; and LiOH, assay not less than 98.0%, carbonates less than 2.0%. The experimental results at 38.0° are given in Table I and Figure 2. The possible increase in

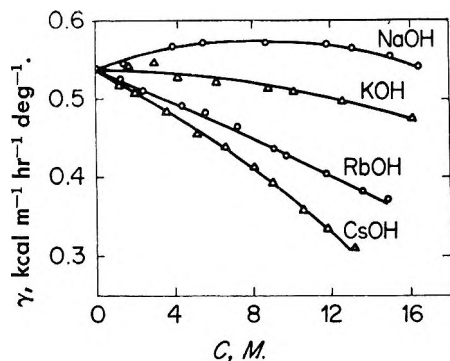


Figure 2. Thermal conductivity of aqueous solutions of alkali hydroxides at 38.0°.

Table II

	λ (calcd), $\text{kcal m}^{-1} \text{hr}^{-1} \text{deg}^{-1}$			
	NaOH	KOH	RbOH	CsOH
a_2	7.60×10^{-3}	-7.19×10^{-4}	-1.02×10^{-2}	-1.38×10^{-3}
a_3	-4.49×10^{-4}	-1.98×10^{-4}	-8.23×10^{-5}	-2.65×10^{-4}

concentration of carbonates was checked after each experiment and it was always less than 50% of the value guaranteed by the manufacturer. The effect of concentration on λ was expressed by the empirical relationship

$$\lambda = a_1 + Ca_2 + C^2a_3 \quad (1)$$

where λ is given in $\text{kcal m}^{-1} \text{hr}^{-1} \text{deg}^{-1}$, a_1 is the thermal conductivity of water at the same temperature ($0.538 \text{ kcal m}^{-1} \text{hr}^{-1} \text{deg}^{-1}$ at 38.0°), and C is the molar concentration. The calculation of constants a_2 and a_3 was based upon the method of least squares and the values obtained are given in Table II.

Riedel's measurements of NaOH^{1,2} seem to indicate that constants a_2 and a_3 are independent of the temperature. Our experimental values for different temperatures are given in Table III, and we further introduce λ 's calculated from eq 1, where constants a_2 and a_3 are supposed to be independent of the temperature and a_1 is the thermal conductivity of water at the respective temperatures. The deviations are always smaller than 3% and so eq 1 seems to be usable over a fairly wide range of temperatures.

The given experimental values proved that λ for alkali hydroxides is not a linear function of concentration and that λ for the NaOH solution is not independent of concentration in the high-concentration range.

Table III

	NaOH		KOH		
	$\lambda, \text{kcal m}^{-1} \text{hr}^{-1} \text{deg}^{-1}$	0.611	0.612	0.523	0.548
$\lambda(\text{exptl}), \text{kcal m}^{-1} \text{hr}^{-1} \text{deg}^{-1}$	0.620	0.601	0.515	0.556	0.500
Temp, °C	93.0	93.0	5.0	93.0	5.0
C, M	6.10	10.1	6.20	11.2	4.05
	RbOH		CsOH		
	$\lambda, \text{kcal m}^{-1} \text{hr}^{-1} \text{deg}^{-1}$	0.480	0.434	0.408	0.438
$\lambda(\text{exptl}), \text{kcal m}^{-1} \text{hr}^{-1} \text{deg}^{-1}$	0.482	0.439	0.412	0.429	
Temp, °C	93.0	5.0	93.0	5.0	
C, M	9.2	5.50	10.5	3.70	

A Proton Magnetic Resonance Solute-Solute Correlation. Solvent Interactions with the Sulfhydryl Proton^{1a}

by Sheldon H. Marcus^{1b} and Sidney I. Miller^{1c}

Department of Chemistry, Illinois Institute of Technology,
Chicago, Illinois 60616 (Received June 25, 1968)

Substituent effects of,² self-association in,³⁻⁵ and donor bonding to thiols⁶⁻⁸ have been examined by pmr studies of the SH function. In this paper, we report a useful solute-solute correlation ($r = 0.977$) of the pmr chemical shifts (in hertz) at infinite dilution (δ^0) of *n*-butanethiol with those of thiophenol in 18 solvents (Table I, Figure 1). The number of solvents is given by *N*.

$$\delta^0(\text{C}_6\text{H}_5\text{SH}) = 2.00\delta^0(n\text{-C}_4\text{H}_9\text{SH}) - 58.5 \quad (N = 18) \quad (1)$$

The effect of medium on pmr spectra is complex. If this is reflected in the behavior of a solute-solvent pair, it is shown even more forcibly for different solutes in several solvents. Since 1960, five solvent contributions to δ_{obsd} , have been postulated and discussed, bulk

$$\delta_{\text{obsd}} = \delta_b + \delta_w + \delta_a + \delta_E + \delta_s^i \quad (2)$$

susceptibility (δ_b), dispersion (δ_w), anisotropy (δ_a), electric field (δ_E), and specific interactions (δ_s^1 , δ_s^2 , etc.). Despite numerous attacks (we cite only a few) on the problem of identifying and assessing the component terms of eq 2, success has been limited at best.⁹⁻¹⁴ It is of some interest therefore that regularities in the solvent effects on δ do turn up occasionally, e.g., in the form of eq 1.

Table I: Sulfhydryl Chemical Shifts at Infinite Dilution in Organic Solvents (in hertz) from TMS

Code	Solvent	$-\delta^0(\text{C}_6\text{H}_5\text{SH})$	$-\delta^0(n\text{-C}_4\text{H}_9\text{SH})$
1	CCl ₄	195.4	64.7
2	C ₆ H ₁₂	188.7	62.1
3	CH ₃ CN	239.4	92.4
4	CHCl ₃	207.7	79.6
5	CH ₂ Cl ₂	213.1	81.3
6	CH ₃ OH	250.2	95.7
7	(CH ₃) ₂ CO	256.7	98.9
8	C ₂ H ₅ OH	247.9	89.1
9	(C ₂ H ₅) ₂ O	229.4	80.9
10	C ₆ H ₅ NO ₂	226.5	84.9
11	C ₆ H ₅ CH ₃	178.4	59.9
12	C ₆ H ₆	179.7	62.5
13	C ₆ H ₅ Br	196.1	71.9
14	C ₆ H ₅ Cl	192.2	68.3
15	C ₆ H ₅ CF ₃	186.4	64.4
16	C ₆ H ₅ OCH ₃	198.7	70.7
17	C ₆ H ₅ F	189.0	65.9
18	C ₆ H ₅ C(CH ₃) ₃	174.6	57.7

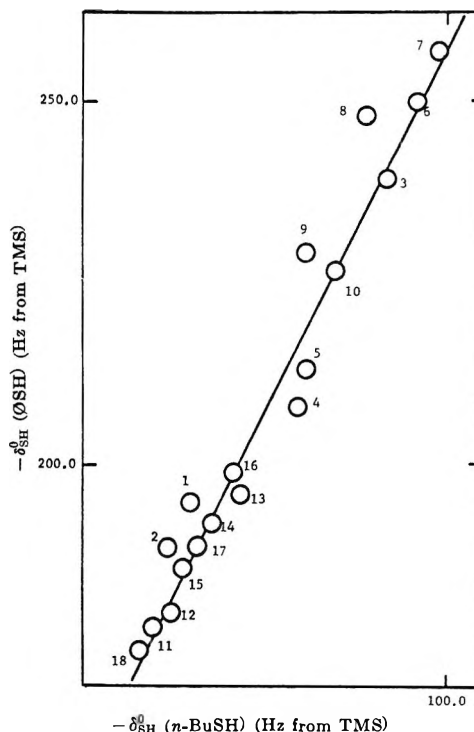


Figure 1. Relation between δ_{SH}^0 values of thiophenol and *n*-butanethiol in various solvents.

There have been several reports of solute-solute relations. These are obtained when the spectral parameters of two solutes in a series of solvents can be correlated:¹² the NH infrared stretching frequencies of pyrrole and aniline are linearly related,¹⁵ the OH infrared stretching frequencies and pmr δ 's of phenol-base adducts are likewise related.¹⁶ There do appear to be

(1) (a) Research supported in part by National Institutes of Health Grant GM07021 and abstracted in part from the Ph.D. thesis of S. H. M.; (b) National Science Foundation Fellow, 1961-1965; (c) author to whom inquiries should be addressed.

(2) S. H. Marcus and S. I. Miller, *J. Phys. Chem.*, **68**, 331 (1964).

(3) S. H. Marcus and S. I. Miller, *J. Amer. Chem. Soc.*, **88**, 3791 (1966).

(4) C. R. Kanekar, G. Govil, C. L. Khetrapal, and M. M. Dhingre, *Proc. Indian Acad. Sci.*, **A65**, 265 (1967).

(5) M-M. Rousselot, *Compt. Rend.*, **262**, 26 (1966).

(6) R. Mathur, S. M. Wang, and N. C. Li, *J. Phys. Chem.*, **68**, 214 (1964); R. Mathur, E. D. Becker, R. B. Bradley, and N. C. Li, *ibid.*, **67**, 2190 (1963).

(7) M-M. Rousselot and M. Martin, *Compt. Rend.*, **262**, 1445 (1966); M-M. Rousselot, *ibid.*, **263**, 649 (1966).

(8) E. Goldberg and S. I. Miller, unpublished data.

(9) A. D. Buckingham, T. Schaeffer, and W. G. Schneider, *J. Chem. Phys.*, **32**, 1227 (1960).

(10) H. M. Hutton and T. Schaeffer, *Can. J. Chem.*, **45**, 1111 (1967).

(11) H. J. Friedrich, *Z. Naturforsch.*, **20**, 1021 (1965).

(12) P. Jouve, *Ann. Phys.*, **1**, 1 (1966).

(13) I. D. Kuntz, Jr., and M. D. Johnston, Jr., *J. Amer. Chem. Soc.*, **89**, 6008 (1967).

(14) R. C. Fort, Jr., and T. R. Lindstrom, *Tetrahedron*, **23**, 3227 (1967).

(15) L. J. Bellamy, H. E. Hallam, and R. L. Williams, *Trans Faraday Soc.*, **54**, 1120 (1958).

(16) D. P. Eymann and R. S. Drago, *J. Amer. Chem. Soc.*, **88**, 1617 (1966); K. F. Purcell and R. S. Drago, *ibid.*, **89**, 2874 (1967).

far fewer pmr solute-solute correlations. From literature data or plots we can derive the following

$$\delta^0(\text{C}_6\text{H}_5\text{C}\equiv\text{CH}) = 1.05\delta^0(\text{ClCH}_2\text{C}\equiv\text{CH}) + \text{constant} \quad (N = 11) \quad (3)^{17}$$

$$\delta^0(\text{C}_6\text{H}_5\text{COC}\equiv\text{CH}) = 1.5\delta^0(\text{ClCH}_2\text{C}\equiv\text{CH}) + \text{constant} \quad (N = 11) \quad (4)^{17}$$

$$\delta^0(\text{C}_6\text{H}_5\text{C}\equiv\text{CH}) = 1.0\delta^0(\text{ClC}(\text{CH}_3)_2\text{C}\equiv\text{CH}) + \text{constant} \quad (N = 31) \quad (5)^{12}$$

$$\delta^0(\text{CCl}_3\text{H}) = 0.75\delta^0(\text{C}_6\text{H}_5\text{C}\equiv\text{CH}) + \text{constant} \quad (N = 31) \quad (6)^{12}$$

$$\delta^0\left(\begin{array}{c} \text{H} \\ | \\ \text{---} \text{C} \text{---} \text{F} \\ / \quad \backslash \\ \text{---} \quad \text{---} \\ | \quad | \\ \text{t-Bu} \quad \text{---} \end{array}\right) = 1.18\delta^0\left(\begin{array}{c} \text{F} \\ | \\ \text{---} \text{C} \text{---} \text{H} \\ / \quad \backslash \\ \text{---} \quad \text{---} \\ | \quad | \\ \text{t-Bu} \quad \text{---} \end{array}\right) + \text{constant} \quad (N = 10) \quad (7)^{18}$$

$$\delta^0(\text{C}_6\text{H}_5\text{SH}) = 1.7\delta^0(\text{C}_6\text{H}_5\text{C}\equiv\text{CH}) + \text{constant} \quad (N = 6) \quad (8)$$

Equation 7 is one of five rather similar plots given by Eliel and Martin for 3- and 4-*t*-butylcyclohexyl halides.¹⁸ We have found that our thiol chemical shifts correlate with those of certain ethynyl protons^{12,17} and have given eq 8 as an example. In addition, Suhr has obtained a fair correlation for the aryl proton chemical shifts (center of gravity) of 4-chloroaniline and 4-nitroaniline.¹⁹ Undoubtedly many other such correlations could be derived from published data.

These derived linear relations provide a compact means to store and to predict δ^0 . Moreover, a relation such as eq 1 can be used to estimate the normally inaccessible value δ_1^0 of any solute in itself as solvent. For one can first measure δ_2^0 for a second solute in a series of solvents, among them the first solute, and then apply an equation such as eq 1.

A few comments on the solvent effects should serve to illustrate the theoretical problems. With respect to the thiols, though they do self-associate,³ this is not an issue in this work, since we are dealing with infinite-dilution shifts of isolated molecules. At the sulfhydryl group, one or more solvent molecules presumably take up some average orientation. Now, the usual hydrogen bonding by dipolar sites deshields a proton, *e.g.*, in thiols.³ In the case of magnetically anisotropic solvent molecules of cylindrical electronic distribution, the anisotropy effect depends on whether the solute molecule interacts with the end or side of the cylinder.⁹ For orientation to the end, as might be the case with the SH on nitrogen of acetonitrile or the π electrons of benzene, the thiol proton would be shielded; for orientation to the side of the cylinder, as to an electronega-

tive substituent of benzene, the thiol proton would be deshielded. These solvent factors are best discussed with reference to cyclohexane (Table I, Figure 1).

In aromatic solvents with no electronegative atoms, *e.g.*, benzene and toluene, the dominant solute-solvent interaction appears to be hydrogen bonding to the π system. In these cases, the magnetic anisotropy effect shields the thiol proton, and δ^0 (SH) is upfield from cyclohexane. The usual deshielding effect of hydrogen bonding is apparently overwhelmed here. The aliphatic chloro-, nitrogen-, and oxygen-containing solvents are known to be hydrogen bonding. All of them shift δ^0 (SH) downfield from cyclohexane, more or less to the extent expected from their hydrogen-bonding power. In the absence of a dominant factor, one must resort to an appropriate "mix" of the major factors to account for the observed δ^0 in solvents such as trifluoromethylbenzene, nitrobenzene, and acetone.

The preceding notions about the trends in δ^0_{obsd} are not really satisfying. Any view of donor to acceptor strength should, of course, be associated with an equilibrium constant or possibly an enthalpy.⁶ French workers have used δ^0 as a measure of solvent donor power to several thiols but without justification.⁷ Eyman and Drago have studied phenol-donor adducts in an "indifferent" medium and found that $\delta(\text{complex})$ is proportional to the enthalpy of the reaction.¹⁶ Finally, there is the interesting dependence of $\delta^0(\text{C}_6\text{H}_5\text{C}\equiv\text{CH})$ or $\delta^0(\text{RSH})$ on the temperature, T .^{7,12}

In an attempt to clarify these problems and perhaps provide a rationale for the correlations 1 and 3-8, we devised the following "interaction" model. We suppose that the chemical shift $\delta(M)$ of a monomeric species is the same for a species M in the gas phase and in a solvent S. When M has fully interacted with n molecules of S, the chemical shift of the species MS_n is taken to be $\delta(\text{MS}_n)$. Incidentally, the fact that δ^0 for thiols changes only slightly from the gas phase to solution in cyclohexane⁵ suggests that the idea of a gas-like solute is not unrealistic. Following a standard approach,^{3,6} we take

$$[M_0]\delta_{\text{obsd}} = [M]\delta(M) + [\text{MS}_n]\delta(\text{MS}_n) \quad (9)$$

and

$$K = [\text{MS}_n]/[M][S]^n \quad (10)$$

or

$$\delta_{\text{obsd}} = \{\delta(M) + K[S]^n\delta(\text{MS}_n)\}[M]/[M_0] \quad (11)$$

For any given solvent, in the range $[M_0] \rightarrow 0$, we define

$$s \equiv d\delta_{\text{obsd}}/d[M] = \{\delta(M) + K[S]^n\delta(\text{MS}_n)\}/[M_0] \quad (12)$$

(17) J. V. Hatton and R. E. Richards, *Trans. Faraday Soc.*, **57**, 28 (1961).

(18) E. L. Eliel and R. J. L. Martin, *J. Amer. Chem. Soc.*, **90**, 689 (1968).

(19) H. Suhr, *Mol. Phys.*, **6**, 153 (1963).

If $s \leq 0$, K is negative, and the model is not applicable! If $s > 0$, K is positive, and we obtain the limiting expressions

$$\delta_{\text{obsd}} \simeq \delta(M) \quad (\text{for small } K) \quad (13)$$

$$\delta_{\text{obsd}} \simeq K[S]^n \delta(MS_n) \quad (\text{for large } K) \quad (14)$$

Experimentally, it is found that the sign of s may be either positive or negative. In dilution plots of $\delta(C_3H_7SH)$, s is positive for carbon tetrachloride or cyclohexane, and *ca.* zero for chloroform.⁷ Dilution plots $\delta(CH_2)$ of *p*-nitrobenzyl and benzyl chlorides in carbon tetrachloride²⁰ have negative and positive s values, respectively.

Consider the two limiting cases with $s > 0$. We find eq 13 interesting but unrealistic. Here, δ^0 of a solute is solvent independent.

If the model leading to eq 14 is correct, then it follows that the magnitude of δ^0 can reflect donor strength, since it is proportional to K . Note that this proportionality differs from those in which a pmr shift or an infrared frequency are linear in $\log K$ or in (free) energy.¹⁶ In the context of the solute-solute relation, *e.g.* eq 1, eq 14 requires a parallelism in K_1 and K_2 or $\log K_1 \propto \log K_2$. One can now consider eq 1 in the same way that one deals with linear free energy correlations; in particular, the slope of eq 1 may be regarded as the relative sensitivity of the solutes to interaction with the solvent. *Heretofore, the parallel of δ^0 with K had not been demonstrated, and the proportionality of δ^0_1 to δ^0_2 had not been rationalized!*

We wish to emphasize that although our interaction model fits certain systems, there are a number of probing questions one can raise. Some have to do with the fact that the model is deficient in detail: the several terms or contributions in eq 2 are ignored; the microstructure (shape, size, and conformation) of solute and solvent are disregarded; the electronic environment of the interaction site is not described, etc. Finally, correlations reported by others, *e.g.*, $\delta^0 \propto T^7$,¹² or $\delta(MS_n) \propto \Delta H$,¹⁶ do not follow from eq 14 and even appear to be incompatible with it, in view of the nonlinear dependence of K upon T and ΔH upon K .

The other kinds of criticism of eq 14 are more specific. Even though the interaction mechanism is unspecified, it nevertheless seems strange that the linear correlations, eq 1 and 3-8, include a broad range of solvents from the "weak" (nonpolar) hexane to the "strong" (polar) methanol (Table I). Even if some sort of acceptor-donor interaction could be envisioned between solute and solvent, as in the system of eq 1, there are solute pairs, *e.g.*, the alkyl halides of eq 7, whose protons can hardly be cast in the role of acceptors. There are, of course, many sets of δ^0 data which appear to be unrelated and do not give acceptable linear correlations, *e.g.*, $\delta(C_6H_5SH)$ vs. $\delta(4-t\text{-butylchlorocyclohexane-1-}H)$,¹⁸ $\delta(C_6H_5SH)$ vs. $\delta(CH_3CN)$,⁹ $\delta(CH_4)$ vs. $\delta(CH_3CN)$,⁹ etc.

Of course, the model cannot accommodate those strong donors in which the gaslike monomer is a fiction, and the dilution shift reflects association equilibria among several polymers.

An infinite-dilution shift is a complex quantity, whose origins are poorly understood. It is surprising, therefore, that certain solute pairs, *e.g.*, arylthiol-alkylthiol, propargyl chloride-phenylacetylene, and chloroform-phenylacetylene, evoke a parallel response from a diverse group of solvents. These derived correlations could be useful on an empirical level. Beyond this, the interaction model which leads to eq 14 is admittedly flawed and limited, but it does provide a rationale for some of the observations.

Experimental Section

Details of the experimental procedure with thiols have been given previously.^{2,3} The thiol spectra were obtained on a Varian A-60 nmr spectrometer operating at 60 MHz. Tetramethylsilane (TMS) was used as an internal reference. Values of δ^0 were obtained by extrapolation from values at three concentrations in the range of low thiol concentration ($<3 M$). As indicated elsewhere each value is the mean of at least three scans.^{2,3} The dilution curve approaches linearity in this concentration range so that the extrapolation to δ^0 is straightforward.³

(20) T. Yokoyama, G. Wiley, and S. I. Miller, unpublished data.

Nuclear Magnetic Resonance Spectra

of Some Indole Salts

by John F. Sebastian,

Department of Chemistry, Miami University, Oxford, Ohio 45056

Manfred G. Reinecke,

Department of Chemistry, Texas Christian University, Fort Worth, Texas 76129

and Harry W. Johnson, Jr.

Department of Chemistry, University of California, Riverside, California 92502 (Received July 1, 1968)

In a recent paper, the nmr spectra of phenyllithium and phenylmagnesium bromide were reported.¹ It was noted that the hydrogens *ortho* to the carbon-metal bond were considerably deshielded with respect to benzene. These results were attributed largely to paramagnetic contributions and not to electron-density effects. By assuming that the shift of the *para* hydrogen in C_6H_5Li and C_6H_5MgBr was solely a result of

(1) G. Fraenkel, D. G. Adams, and R. R. Dean, *J. Phys. Chem.*, **72**, 944 (1968).

paramagnetic contributions, it was possible to calculate $\Delta\chi$ from the point-anisotropy approximation,² eq 1.

$$\Delta\sigma = (\Delta\chi/3R^3)(1 - 3\cos^2\theta) \quad (1)$$

The value thus obtained for $\Delta\chi$ was used to calculate the shifts for the *ortho* and *meta* hydrogens. The calculated shifts were in good agreement with the observed shifts. In this note we wish to report an nmr investigation of indole, 2,5-dimethylindole, and their lithium, sodium, potassium, and Grignard derivatives (all in tetrahydrofuran solvent) which supports and extends the above-mentioned results.

Hückel molecular orbital calculations³ suggest that the π -electron density on each of the carbon atoms of the indolyl anion is higher than on the corresponding atoms of indole. On this basis only, one would expect all of the protons attached to the carbon atoms to be shielded upon formation of the anion.⁴ This is in fact *not* observed for the 2- and 7-protons, which are deshielded by 0.3 and 0.1 ppm, respectively (see Table I).^{3,5} The chemical shifts of the 2- and 3-protons of indole and its anion and 2,5-dimethylindole and its anion were obtained by first-order analysis and have been reported elsewhere.^{3,5} If the point-anisotropy approximation *and* the value of $\Delta\chi$ obtained for phenyllithium (the magnetic dipole is directed along the symmetry axis;¹ the corresponding axis in the indolyl anion is axis *y* in Figure 1) is used, the direction of the shifts is correctly predicted not only for the 2- and 7- but also for the 3- and 4-protons (Table I). However, the 6-proton shift is now predicted in the wrong direction.

In pyridine the largest positive component of the susceptibility tensor of the nitrogen atom lies in the nuclear plane and is perpendicular to the symmetry axis of the molecule⁶ (the corresponding axis in the indolyl anion is axis *x* in Figure 1). Taking the magnetic dipole to be directed along the *x* axis⁷ and assuming that the downfield shift of the *ortho* protons in phenyllithium arises primarily from anisotropic effects, it is possible to determine $(\Delta\chi)_x$ from eq 1. The shifts calculated using $(\Delta\chi)_x$ and the point-anisotropy approximation are given in Table I. Again, the predicted shift for the 6-proton is in the wrong direction. *These results suggest that for the 6-proton, electron density or other effects are more important than paramagnetic con-*

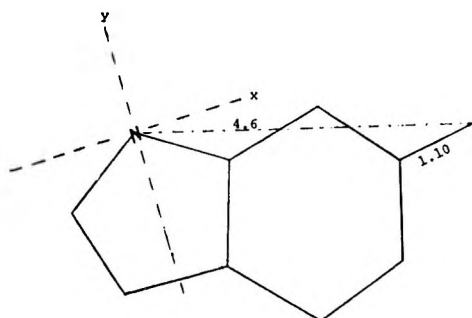


Figure 1. The geometry in the indolyl anion.

Table I: Differences, Observed and Calculated, between the Proton Resonances of Indole and 2,5-Dimethylindole and Their Respective Salts

Proton	Difference in proton resonance, ppm		
	Obsd	Calcd ^c	
		Axis <i>y</i> ^d	Axis <i>x</i> ^e
2-H	-0.29 ± 0.05 ^a	-0.69	-0.72
3-H	0.071 ± 0.04 ^a	0.33	0.062
4-H	0.10 ± 0.04 ^b	0.17	0.032
6-H	0.25 ± 0.06 ^b	-0.073	-0.081
7-H	-0.12 ± 0.09 ^b	-0.34	-0.32

^a The average of the MgBr⁺, Li⁺, Na⁺, and K⁺ salts of the indolyl anion. ^b The average of the MgBr⁺, Li⁺, Na⁺, and K⁺ salts of the 2,5-dimethylindolyl anion. ^c Calculated from eq 1. ^d The magnetic dipole taken along the *y* axis (Figure 1). ^e The magnetic dipole taken along the *x* axis (Figure 1).

tributions calculated from the point-anisotropy approximation.

The relatively poor agreement of the calculated and observed shifts of the 2- and 7-protons may be attributed in part to extensive solvent-solute interactions between indole and tetrahydrofuran.^{3,8} Other sources of error include the value chosen for $\Delta\chi$ (which is probably slightly different for two electrons in the nitrogen sp^2 orbital than in the carbon sp^2 orbital¹), the electron density, the ring current, and the association and aggregation effects.^{1,3} The indole geometry used for the point-anisotropy calculations is given in ref 9 and Figure 1.

(2) H. M. McConnell, *J. Chem. Phys.*, **27**, 226 (1957).

(3) J. F. Sebastian, Ph.D. Thesis, University of California, Riverside, Calif., 1965.

(4) G. Fraenkel, R. E. Carter, A. McLachlan, and J. H. Richards, *J. Amer. Chem. Soc.*, **82**, 5846 (1960).

(5) M. G. Reinecke, H. W. Johnson, and J. F. Sebastian, *Tetrahedron Lett.*, 1183 (1963).

(6) V. M. S. Gil and J. N. Murrell, *Trans. Faraday Soc.*, **60**, 248 (1964).

(7) The authors thank a referee for this suggestion.

(8) M. G. Reinecke, H. W. Johnson, Jr., and J. F. Sebastian, *Chem. Ind. (London)*, 151 (1964).

(9) I. L. Karle, K. Britts, and P. Gum, *Acta Crystallogr.*, **17**, 496 (1964).

The Photolysis of Ammonia at 2062 Å in the Presence of Ethylene

by U. Schurath, P. Tiedemann, and
R. N. Schindler

*Institut für Physikalische Chemie, Universität Bonn and
Kernforschungsanlage Jülich, Jülich, Germany
(Received August 23, 1968)*

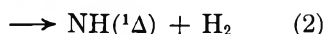
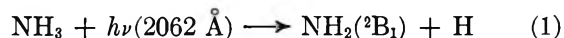
Since Warburg's first paper on the photodecomposition of ammonia¹ nearly 60 years ago, this system has

(1) E. Warburg, *Akad. Ber.*, 746 (1911).

repeatedly been the subject of studies in the liquid as well as in the gas phase. Nitrogen and hydrogen were the only products detected in static systems. From the rate of formation of these two gases under various conditions, rate expressions were developed to describe the decomposition of irradiated ammonia. More recently the intermediates NH_2 and NH were detected in flow systems, in flash photolysis experiments, and by esr measurements.² Also, molecular elimination of hydrogen from ammonia was demonstrated to be a primary step in the vacuum uv photolysis.³ In this study the photolysis of ammonia was carried out at 2062 Å in the presence of a scavenger which transformed the primary fragments into stable characteristic products. It was hoped that a quantitative determination of these products would allow evaluation of the primary quantum yield of decomposition.

The absorption spectrum of ammonia in the region 2200–1600 Å shows overlapping diffuse bands with a maximum around 1870 Å. Spectroscopic considerations indicate that the upper state causing the predissociations observed in the region around 1900 Å is a singlet.⁴

Consequently, (1) and (2) are the only primary processes energetically allowed in the photolysis of ammonia with 2062-Å radiation.



Since process 2 occurs with a quantum yield of <0.005 at 2062 Å, the photolysis of ammonia at this wavelength is considered a well defined system to study reactions of the primary species from step 1.

Results are reported for the photolysis of ammonia in the presence of ethylene. The additive is transparent at 2062 Å. Ethylene is known to be a very efficient H atom scavenger. Ethyl radicals are formed while other reactions of H atoms are suppressed. Under these conditions ethylamine, butane and hydrazine are the predominant products.

Experimental Section

Photolyses were carried out in a quartz vessel of ca. 220-ml volume attached to a standard vacuum line. An NH_3 pressure of 40 torr was chosen in most of the runs to obtain total absorption of the incident radiation within the cell. The pressure of the additive was varied between 0.2 and 28 torr. After irradiation the noncondensable gases were measured and analyzed by mass spectrometry. The condensable material was transferred for gas chromatographic analysis. Hydrazine was determined colorimetrically⁵ in separate runs. Gas chromatographic separation of the hydrocarbons was achieved on silica gel. The amines were separated on KOH-treated Chromosorb W with polyethylene glycol 1000 as stationary phase. The use of carbon-14

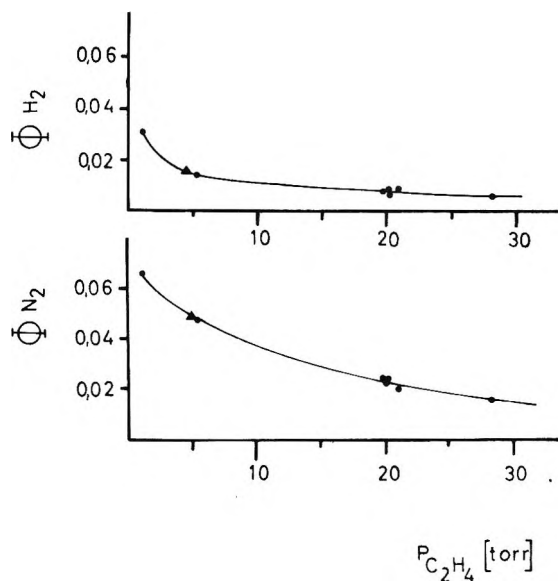


Figure 1. Quantum yields of noncondensable gases as a function of ethylene pressure: ●, $p(\text{NH}_3) = 37.5$ torr; ▲, $p(\text{NH}_3) = 202.4$ torr, $p(\text{C}_2\text{H}_4) = 28.6$ torr.

labeled ethylene combined with a flow-counter facilitated the calibration and permitted the precise determination of products even at very low conversion. Since the flow-counter is insensitive to NH_3 the analysis of the amines, especially of ethylamine, was possible which is otherwise difficult to carry out. The following products were determined quantitatively: H_2 , N_2 , N_2H_4 , C_2H_6 , C_4H_{10} , $\text{C}_2\text{H}_5\text{NH}_2$, $\text{C}_4\text{H}_9\text{NH}_2$, $\text{C}_2\text{H}_4(\text{NH}_2)_2$, plus an unidentified substance, formed with a quantum yield of $0.006/n$, n being the number of C atoms per molecule of the product.

The total amount of scavenger used up per irradiation was measured in separate runs. The scatter in these determinations was about 1%. However, the sum of the ^{14}C activity of the individual products agreed with this value to only 91%. It is suggested that products are formed which elude gas chromatographic detection.

Irradiations were carried out with a microwave-powered iodine lamp,⁶ its light being passed through a quartz cell of 1-cm path length filled with water to obtain monochromatic 2062-Å radiation. Actinometry was performed using HBr at a pressure of 60 torr with the initial quantum yield of H_2 production taken as unity.⁷

(2) For references, see J. G. Calvert and J. N. Pitts, Jr., "Photochemistry," John Wiley and Sons, Inc., New York, N. Y., 1966, p 203.

(3) J. R. McNesby and H. Okabe, *Advan. in Photochem.*, **3**, 157 (1964).

(4) G. Herzberg, "Molecular Spectra and Molecular Structure" Part III, D. van Nostrand Co., Princeton, N. J., 1966, p 465.

(5) G. Watt and C. Crisp, *Anal. Chem.*, **24**, 2006 (1952).

(6) P. Harteck, R. R. Reeves, and B. A. Thompson, *Z. Naturforsch.*, **19a**, 2 (1964).

(7) E. Warburg, *Berlin Akad. Ber.*, 300 (1918).

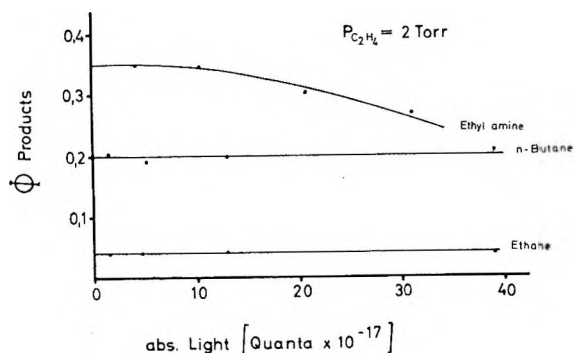


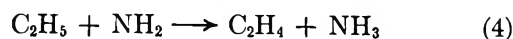
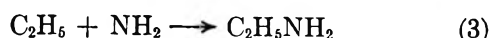
Figure 2. Product formation in the photolysis of ammonia in the presence of ethylene; light intensity: 4.33×10^{15} quanta/sec.

Results and Discussion

To establish the relative probabilities of processes 1 and 2, the quantum yields of noncondensable gases were studied as a function of C_2H_4 pressure (Figure 1).⁸ Hydrogen generated in process 2 is not scavenged by C_2H_4 . Thus the quantum yield for H_2 formation in the presence of excess C_2H_4 is a direct measure of the occurrence of process 2. As shown in Figure 1, $\phi(H_2)$ reaches a value of about 0.005 at $p_{NH_3}/p_{C_2H_4} = 1.4$. The yield shows little dependence on the total pressure if the ratio $p_{NH_3}/p_{C_2H_4}$ is kept constant. $\phi(2) \leq 0.003$ was also obtained in the photolysis of ND_3 in the presence of excess propane.⁹

In the following section the fate of the H atoms and NH_2 radicals produced in (1) in the presence of C_2H_4 will be discussed. Preliminary experiments demonstrated that at pressures above 1.5 torr C_2H_4 (at 40 torr of NH_3), butane and ethane formation reaches a plateau indicating almost complete scavenging of the H atoms. Therefore, the following experiments were carried out in the presence of 5% C_2H_4 at a total pressure of 42 torr. The quantum yields as a function of radiation dose are shown in Figure 2 for the products C_2H_6 , C_4H_{10} , and $C_2H_5NH_2$. For a dose of 4×10^{17} quanta absorbed the ammonia conversion was 0.15%.

The yields of all products observed are listed in Table I. A full accounting was attempted for all H atoms (measured as C_2H_5 radicals) and all NH_2 radicals generated by irradiation. Butane and ethane are formed by recombination and disproportionation of two ethyl radicals. The latter reaction produces C_2H_4 , which is indicated by the negative value for the corresponding yield in Table I. Formation of ethylamine results primarily from reactions between NH_2 and C_2H_5 radicals.



Reaction 4 will be discussed later. Also, NH_2 radicals attack C_2H_4 forming $C_2H_4NH_2$ which is the precursor of ethylenediamine and butylamine (see below).

By determining the number of ethyl radicals incorporated in the individual products, a total quantum yield of 0.85 was obtained for the formation of H atoms in the photolysis. However, the determination of the total amount of scavenger used up in the reaction indicated a quantum yield of 0.91 for ethylene consumption. The difference of 8 unaccounted C_2H_4 molecules per 100 quanta absorbed is beyond experimental error. It is suggested that products are formed which elude gas chromatographic detection, but should be considered in the material balance. Thus the experimental value of 0.85 would be a lower limit for the H-atom yield in the photolysis of ammonia. Furthermore, reaction 4 needs to be considered. This process cannot be directly observed in our system. No information is available on the relative rates of disproportionation and recombination of NH_2 radicals. Stief and de Carlo discussed the rather high value of 2.8 for N_2H_3 radicals.¹⁰ Corresponding values for the cross reactions between alkyl and amino radicals also have not been reported. From the NH_3 photolysis in the presence of C_3H_8 a value of 0.21 ± 0.07 is derived for the reactions between NH_2 and $i-C_3H_7$.⁹ If this value is of the same order for the cross combination in our system, step (4) should consume C_2H_5 radicals with a yield of about 0.08.

The fate of the amino radicals produced in (1) is more difficult to assess. NH_2 radicals are recovered in hydrazine, ethylamine, butylamine, and ethylenediamine. These four products account for an NH_2 quantum yield of 0.52. Also, nitrogen is formed with a yield of 0.06. Stoichiometry requires that at least two NH_2 radicals are consumed for the formation of one N_2

Table I: Products in the Photolysis of NH_3 at 2062 Å in the Presence of C_2H_4 [$p(NH_3) = 40$ torr, $p(C_2H_4) = 2$ torr, Intensity: 4.33×10^{15} quanta/sec]

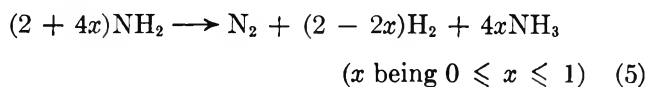
Products	Quantum yield	C_2H_5 consumed	C_2H_4 consumed	NH_2 consumed
Butane	0.20	0.40
Ethane	0.04	0.08	-0.04	...
Ethylamine	0.35	0.35	...	0.35
Butylamine	0.015	0.015	0.015	0.015
Ethylenediamine	0.004	...	0.004	0.008
Hydrazine	0.075	0.15
Nitrogen	0.06	0.12-0.36
Not identified	...	0.003
		0.85	-0.02	0.64-0.88

(8) With no ethylene added, integrated quantum yields of $\phi(H_2) = 0.48$ and $\phi(N_2) = 0.15$ were found in the photolysis at an NH_3 pressure of 37.5 torr. The yields show a slight dependence on irradiation time.

(9) W. E. Groth, U. Schurath, and R. N. Schindler, *J. Phys. Chem.*, **72**, 3914 (1968).

(10) L. J. Stief and V. J. de Carlo, *J. Chem. Phys.*, **44**, 4638 (1966).

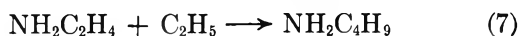
molecule. Thus the total yield of NH_2 radicals determined by product analysis corresponds to $\phi(\text{NH}_2) = 0.64$. This value again is only a lower limit since reaction 4 is not included and N_2 formation very probably involves more than two NH_2 radicals per N_2 molecule formed. In fact a maximum of 6 NH_2 radicals may be used up per N_2 molecule formed



Equation 5 holds only if no radicals other than NH_2 are involved in N_2 formation. Contributions from reactions of ethyl radicals will be of minor importance since the C_2H_6 yield is well accounted for by disproportionation of C_2H_5 radicals.¹¹

Only a tentative evaluation of the primary quantum yield of ammonia decomposition can be given since the ratio of the rate constants K_3/K_4 and the mechanism of nitrogen formation are not known. On the basis of the discussion given above this study leads to a value for ethyl radicals corresponding to an H-atom yield of 0.93 and to an NH_2 yield of 0.72–0.96. Both results are lower than the expected quantum yield of unity for (1). They are, however, in good agreement with $\phi(\text{HD}) = 0.94$ observed in the photolysis of ND_3 at 2062 Å in the presence of 620 torr of propane.⁹

In a series of runs the light intensity was reduced to $1/49$ of the normal value. The results are given in Table II. The yields of alkanes remain constant whereas the quantum yield of ethylamine is reduced. No hexane formation was observed although it would have been detected if formed with a quantum yield $\geq 3 \times 10^{-3}$. Thus the attack of C_2H_5 on C_2H_4 can be neglected in our system. However, an attack of NH_2 on C_2H_4 is postulated. This is supported by the reduced yield of ethylamine and hydrazine and the higher yield of butylamine and ethylenediamine among the products.



The relative rate of ethylamine to butylamine for-

mation is 23 for the high-intensity runs compared with 4.5 in the photolysis at low intensity. Furthermore, a qualitative agreement exists between the change in the rate of hydrazine formation and the production of ethylamine and butylamine, respectively. Steady-state calculations indicate that N_2H_4 should decrease by a factor of approximately 0.3 in irradiations at low intensity, which is in agreement with our findings.

Acknowledgment. The authors wish to thank Professor W. Groth for his stimulating interest and helpful discussions.

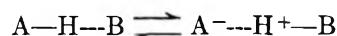
(11) J. A. Kerr and F. A. Trotman-Dickenson, *Progr. Reactor Kinetics*, 1, 105 (1961).

The Dielectric Properties of Pyridine Complexes with Dichloro- and Trichloroacetic Acids

by S. R. Gough and A. H. Price¹

Edward Davies Chemical Laboratory, University College of Wales, Aberystwyth, Great Britain (Received July 22, 1968)

Dielectric investigations of 1:1 acid-base complexes in the microwave region of the spectrum yield information on the stability of the complex and its dipole moment (hence ionic character) and may provide information on the proton-jumping process in the equilibrium between the hydrogen-bonded and the ionic forms



Complexes involving acetic acid and monochloroacetic acid with pyridine exist predominantly in the hydrogen-bonded form, while the trichloroacetic acid-pyridine complex is ionic.² Dielectric studies up to 1.8 GHz show that these complexes behave as rigid structures and gave no evidence of any proton-jumping process. The dichloroacetic acid complex presents a possible intermediate case where the proton jumping may occur in the microwave region. The results reported here are an investigation of the dielectric properties (in the solid state and in benzene solution) of the dichloroacetic acid-pyridine complex at frequencies up to 8.5 GHz and an extension of the data² on the trichloroacetic acid complex up to 36 GHz.

Experimental Section

The dichloroacetic acid was purified by fractional distillation under reduced pressure. The fraction boiling

Table II: Product Formation at Reduced Intensity (8.83×10^{13} quanta/sec)

Products	Quantum yields	C_2H_5 consumed
Butane	0.20	0.40
Ethane	0.045	0.09
Ethylamine	0.28	0.28
Butylamine	0.06	0.06
Hydrazine	0.025	...
Not identified		0.01
		0.84

(1) All correspondence should be sent to this author.

(2) M. Davies and L. Sobczyk, *J. Chem. Soc.*, 3000 (1962).

at 88–89° (10–11 mm of pressure) was collected. Analar grade trichloroacetic acid was crystallized from chloroform and was stored over phosphorus pentoxide. Both the benzene and pyridine were dried and fractionally distilled. The specific conductance of the benzene used ranged from 10^{-12} to 10^{-13} ohm $^{-1}$ cm $^{-1}$.

Benzene was used as a solvent and measurements were made at 20°. Solutions were prepared in a drybox and care was taken to exclude moisture from the measuring cells. In all cases 1:1 molar ratio of the acid to base was maintained.

Solid complexes were prepared by precipitation from concentrated benzene solution containing a 1:1 molar ratio of the acid and base. The dichloroacetic acid-pyridine complex was hygroscopic. Suitably shaped solid samples were prepared for insertion into the dielectric cells by pressing the powdered solid in specially manufactured dies.

Permittivity (ϵ') and dielectric loss factor (ϵ'') were measured in the frequency range 5 Hz–320 kHz using a Thompson bridge³ with calibrated dielectric cells. Over the frequency range 250 MHz–8.5 GHz, standing wave techniques were used for measurement⁴ with the sample contained within the wave guide. At 36 GHz dielectric loss factors were determined by direct measurement of the attenuation produced by the introduction of a known length of dielectric into the appropriate waveguide.⁵

Table I: Permittivity (ϵ') of the Solid Complex

Complex	Frequency range	Temp, °C	ϵ'
Dichloroacetic acid	250 MHz–8.5 GHz	20 –180	4.4 ± 0.2 3.8 ± 0.2
Trichloroacetic acid	1 GHz–8.5 GHz	20 –180	3.7 ± 0.2 3.4 ± 0.2

Results and Discussion

Solid Complexes. The permittivity of solid samples of the pyridine complexes with dichloro- and with trichloroacetic acids are shown in Table I. Assuming additivity of the electronic polarizability of the components of the complex a square of the refractive index of 2.2 is calculated for both complexes. This is much lower than the permittivity of the solid complexes and indicates a large atomic polarization probably associated with proton transfer between the covalent and ionic forms. Such a high atomic polarization would not be expected if complex formation resulted in only a stretching of the carboxylic O–H bond.⁶

Low-Frequency (5 Hz–320 kHz) Results on Solutions. The dielectric loss factor for the complex at any one concentration with the range 0.01–0.40 M is propor-

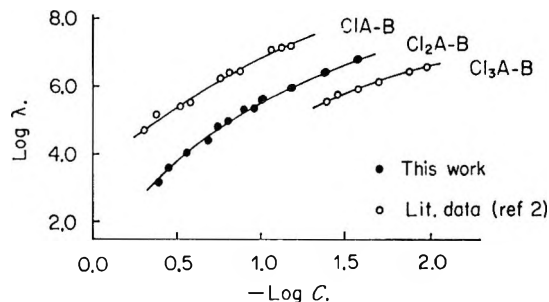


Figure 1. Log λ -log C plots for substituted acetic acid-pyridine complexes in benzene solution (20°).

tional to the frequency of measurement and is entirely due to ionic conduction. The equivalent conductance

$$\lambda = \frac{10^3 \kappa}{C} = \frac{\epsilon'' f}{1.80 \times 10^9 C}$$

(where κ is the specific conductance, C is the molar concentration, and f is the measuring frequency, in hertz) of these solutions is shown in Figure 1, together with the results of Davies and Sobczyk for the mono- and trichloroacetic acid complexes. The results for the dichloroacetic acid complex fall within the regular pattern observed for the other substituted acetic acid complexes.² The ionic conductance arises from, at most, the dissociation of about 10^{-7} part of the solute.

The dipole moment of the complex is calculated from the concentration variation of the solution static permittivity (ϵ_0) and refractive index (n) using the Guggenheim equation.⁷ The results are shown in Figure 2 where $\Delta = (\epsilon_0 - n^2) - (\epsilon_1 - n_1^2)$ (the subscript 1 refers to the solvent) is plotted against the molar con-

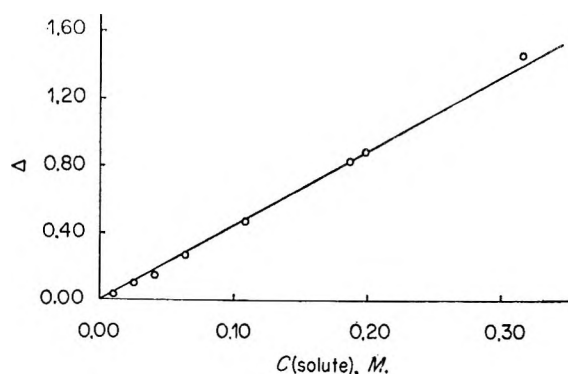


Figure 2. Guggenheim plot for dichloroacetic acid-pyridine complex in benzene solution.

- (3) A. M. Thompson, *Proc. Inst. Elec. Engrs. (London)*, **B103**, 1 (1956).
- (4) S. Roberts and A. von Hippel, *J. Appl. Phys.*, **17**, 611 (1946); G. Williams, *J. Phys. Chem.*, **63**, 534 (1959).
- (5) H. Kramer, *Z. Physik*, **157**, 134 (1959).
- (6) J. W. Smith, *J. Chim. Phys.*, **61**, 125 (1964).
- (7) E. A. Guggenheim, *Trans. Faraday Soc.*, **45**, 714 (1949).

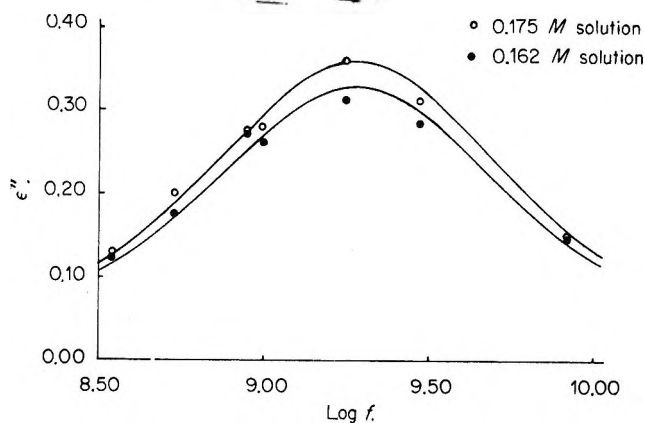


Figure 3. Variation of the dielectric loss factor (ϵ'') with frequency for dichloroacetic acid-pyridine complex in benzene solution. The solid line follows the Debye equation with $\epsilon''_m = 0.36$ and $\tau = 83 \times 10^{-12}$ sec for the 0.175 *M* solution and $\epsilon''_m = 0.31$ and $\tau = 83 \times 10^{-12}$ sec for the 0.162 *M* solution.

centration of the complex. The slope of the graph (strictly as $C \rightarrow 0$) is proportional to the square of the solute dipole moment and gives a value of 6.00 D for the dichloroacetic-pyridine complex.

High-Frequency (250 MHz-36 GHz) Results on Solutions. In liquids the dispersion of the orientation polarization occurs at microwave frequencies and the variation of the associated dielectric loss factor follows the Debye equation

$$\epsilon'' = (\epsilon_0 - \epsilon_\infty) \frac{\omega\tau}{1 + \omega^2\tau^2}$$

where ϵ_0 is the permittivity at low (or zero) frequency, ϵ_∞ is the permittivity at frequencies just beyond where the orientation polarization ceases to contribute, $\omega (= 2\pi f)$ is the angular frequency, and τ is the relaxation time of the polar species. The absorption maximum ($\epsilon''_m = (\epsilon_0 - \epsilon_\infty)/2$) is proportional to the

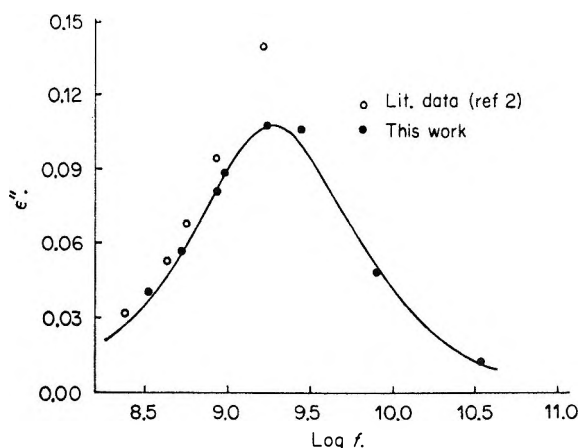


Figure 4. Dielectric absorption of trichloroacetic acid-pyridine complex in benzene solution. The solid line follows the Debye equation with $\epsilon''_m = 0.108$ and $\tau = 83 \times 10^{-12}$ sec.

square of the dipole moment of the relaxing species. The experimental results for the dichloroacetic acid-pyridine complex (complex concentration, 0.175 and 0.162 *M*) are shown in Figure 3. The experimental results are adequately described by a single relaxation time. There is no evidence of a second relaxation process which would be expected if proton jumping occurred at microwave frequencies. The observed relaxation time (83×10^{-12} sec) is a reasonable value for the relaxation time of a rigid species but is very much higher than the relaxation time of about 55×10^{-12} sec expected by interpolation of the results of Davies and Sobczyk.² It is also larger than the relaxation time of 65×10^{-12} sec reported for the trichloroacetic acid-pyridine complex. Consequently dielectric loss factor measurements on the trichloroacetic acid complex were repeated and extended over a much wider frequency range. These results are shown in Figure 4 together with the original data.² The revised relaxation time of 83×10^{-12} sec is identical with the relaxation time of the dichloroacetic acid complex. The increased volume expected on replacing the dichloroacetic acid by the larger trichloroacetic acid is probably offset by a closer approach of the components in the more ionic trichloroacetic acid complex. No satisfactory explanation is available for the large difference between the relaxation time of the dichloroacetic acid complex and the value of 46×10^{-12} sec reported for the monochloroacetic acid complex.²

The dipole moment may be calculated from the maximum dielectric loss factor ($\epsilon''_m = (\epsilon_0 - \epsilon_\infty)/2$) using the Onsager equation as applied to dilute solutions⁸

$$\mu^2 = \frac{(\epsilon_0 - \epsilon_\infty)(2\epsilon_1 + \epsilon_{\infty 2})^2 3kT}{\epsilon_1^2(\epsilon_{\infty 2} + 2)^2 4\pi N_2}$$

where the subscripts 1 and 2 refer to the pure solvent and to the pure solute, respectively; N_2 is the number of solute molecules per cubic centimeter; and $\epsilon_{\infty 2}$ is the pure solute permittivity at frequencies where only the atomic and electronic polarizations are significant. The permittivity of the solute in the pure state (Table I) gives an adequate representation of $\epsilon_{\infty 2}$. The dipole moment of the dichloroacetic acid complex is thus 5.45 ± 0.10 D. This is lower than the 6.00 D calculated from static permittivity measurements. The difference between these dipole moments arises from the neglect of the atomic polarization contribution in the calculation from the static permittivity data.

A dipole moment of 4.17 D is calculated for the dichloroacetic acid complex using the bond moments and configuration shown in Figure 5. Free rotation is assumed about the C_1-C_2 bond (a similar model assuming free rotation yields a calculated dipole moment

(8) L. Onsager, *J. Amer. Chem. Soc.*, **58**, 1486 (1936).

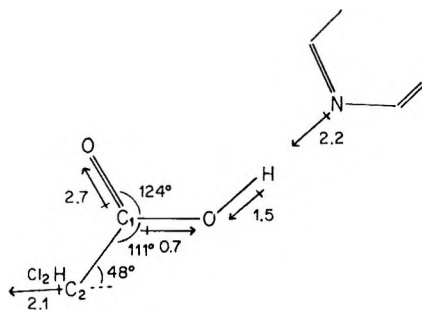


Figure 5. Bond moments and assumed configuration for the dichloroacetic acid-pyridine complex.

of 2.4 D for ethyl dichloroacetate; the literature value is 2.63 D⁹). Complex formation leads to increased polarity in the O—H—N bond. The dipole moment of

the complex (5.45 D) is reproduced if the moment of the (O—H—N) group is increased from 3.7 to 5.1 D. With an OH bond length of 1.02 Å in the complex,² this leads to an effective charge of 2.8×10^{-10} esu at the O and H centers. In the free acid the effective charge at the O and H centers (separation, 0.96 Å) is 1.57×10^{-10} esu. Thus complex formation nearly doubles the "ionicity" of the OH bond. This result is not unreasonable in view of the approximations involved in the group moment calculations and the neglect of polarizability effects. They suffice, however, to establish the qualitative conclusion that the proton remains predominantly attached to the oxygen atom rather than to the nitrogen atom.

(9) A. L. McClellan, "Tables of Experimental Dipole Moments," W. H. Freeman and Co., San Francisco, Calif., 1963.

COMMUNICATIONS TO THE EDITOR

Charge Distribution in Some Alkanes and Their Mass Spectra

Sir: In the past 15 years several papers¹⁻⁵ have appeared discussing the possibility of predicting the fragmentation pattern of organic ion-molecules on the basis of a proposal by Lennard-Jones and Hall,¹ who supposed the probability of fragmentation to be larger for those bonds where the density of the net positive charge is larger. Some authors³⁻⁵ have pointed out that such a proposal appears to be inconsistent with the experimental results, on the basis of a comparison of the mass spectra of *n*-alkanes (which show a pronounced maximum at C₃, sometimes C₄, fragments) with their calculated net positive charge distributions (which have a maximum at the center of the molecule). Surprisingly enough, these authors do not seem to take into account what seems to us a primary question, *i.e.*, to what extent does the distribution of the ions collected by the mass spectrometer reproduce that originating from the first fragmentation of the parent ion, thus accepting a sort of unjustified identification between mass spectrum and fragmentation pattern. More recently, Lorquet⁶ makes the still more surprising statement that the Lennard-Jones and Hall hypothesis (which, he says, does not hold for *n*-alkanes, due to a "too evenly distributed charge") is experimentally verified in the mass spectra of branched alkanes. He supports his statement by the mass spectra of five hydrocarbons.

It should be pointed out, however, that all the alkanes considered by this last author have such a formula as to give C₃ or C₄ fragments on fission of the most highly charged bond, *i.e.*, those fragments which are in any case the most abundant. In fact, an inspection of the mass spectra of two branched alkanes of larger size⁶ and of their net positive charge distributions (Figure 1), calculated by us for comparison (by the same method as Lorquet's), shows the following facts: (1) the only feature which clearly distinguishes these spectra from those of the *n*-alkanes with the same number of C atoms is the higher abundance of the ions C_{*n*-6} and C_{*n*-8}; (2) fragments which cannot originate by a single fragmentation (*i.e.*, those ranging from C₇ to C₁₂ for the first compound and from C₉ to C₁₆ for the second one) are roughly as abundant as in the spectra of the normal alkanes with the same number of C atoms. From these observations we must conclude that the shape of the spectra is largely determined by refragmentation phenomena; as a consequence, the well-known "weakness" of the tertiary bonds is observable only through

(1) J. Lennard-Jones and G. G. Hall, *Trans. Faraday Soc.*, **48**, 581 (1952).

(2) R. Thompson, Conference on Applied Mass Spectrometry, Institute of Petroleum, London, 1953, p 154.

(3) N. D. Coggeshall, *J. Chem. Phys.*, **30**, 593 (1959).

(4) K. Fueki and K. Hirota, *Nippon Kagaku Zasshi*, **81**, 212 (1960).

(5) J. C. Lorquet, *Mol. Phys.*, **9**, 101 (1965).

(6) The spectra were obtained from those of American Petroleum Institute Project 44, Carnegie Institute of Technology, Pittsburgh, Pa., by normalizing to 100 the sum of the abundances of all the ions.

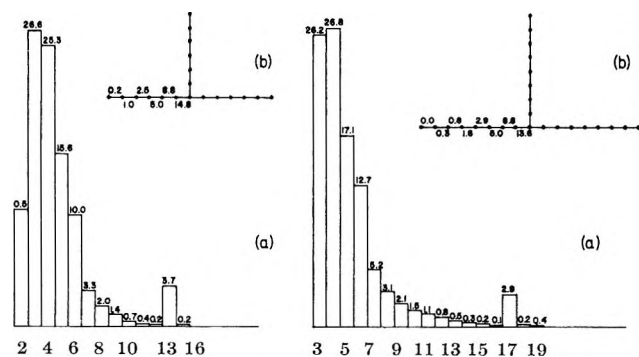


Figure 1. (a) Histograms representing mass spectra. The abscissa gives the number of C atoms of the fragment. (b) Schematic representation of the percentage distribution of the net positive charge on C-C bonds.

the very small peaks corresponding to the large (secondary) fragments. Owing to this situation, it is not admissible to test any theoretical prediction by means of so simple and direct a comparison with mass spectra as done by Lorquet and others. On the other hand, an accurate interpretation of the mass spectra, which takes into account the contribution of refragmentation, is not at all a simple problem; therefore we must more generally conclude that *ordinary* mass spectrometry is an experimental technique not suitable for the measurement of fragmentation patterns.⁷

Some information may be obtained by several other means. Preliminary results obtained by us by measurements of the products of liquid radiolysis of *n*-alkanes seem, for instance, to indicate a substantially flat fragmentation pattern, except for the first bond, which appears to have a lower fragmentation probability.

(7) We are very glad to ascertain that a substantial agreement on the interpretation of the mass spectra has been reached (see the Lorquet and Hirota communications in this issue). It is our opinion that such an agreement was not at all apparent in the papers available until a few months ago. We feel that our ideas were perhaps not clearly enough explained on two topics and they must be briefly clarified.

(a) When we state that refragmentation largely determined the *ordinary* mass spectra of the alkanes, we mean also those of low or medium molecular weight. See, for instance, the mass spectra of 3-methylpentane and of 4-methylheptane (V. Santoro and G. Spadaccini, *Ric. Sci.*, **38**, XI (1968)).

(b) We believe that, at present, the problem of predicting the fragmentation pattern of an ion-molecule is still open. The attempt to correlate fragmentation patterns to charge distributions has not yet proved to be satisfactory. Everybody knows that another most interesting approach has been developed by Rosenstock and co-workers (H. M. Rosenstock, M. B. Wallenstein, A. L. Wahrhaftig, and H. Eyring, *Proc. Nat. Acad. Sci. U. S.*, **38**, 667 (1952)), and the following papers), the so-called "quasi-equilibrium theory." Recently, Spiteller and coworkers (G. Spiteller and M. Spiteller-Friedmann, *Ann. Chem.*, **690**, 1 (1965)), and the following papers) have suggested another quite different kind of approach. A serious difficulty to test any theoretical prediction is the scarcity of really reliable experimental information about fragmentation patterns.

ISTITUTO DI FISICA SUPERIORE
UNIVERSITY OF NAPLES
NAPLES, ITALY

VITTORIA SANTORO
GIULIO SPADACCINI

RECEIVED JULY 22, 1968

Reply to "Charge Distribution in Some Alkanes and Their Mass Spectra"

Sir: From the previous communication by Santoro and Spadaccini, it appears that there is some misunderstanding concerning our early paper,¹ presumably due to overconciseness. More recent papers apparently did not come to the attention of these authors. However, since the point raised by them was only briefly dealt with in these latter papers,^{2,3} a restatement of our present position may therefore be appropriate.

It is obvious that a meaningful comparison between the charge density diagram of a molecular ion and the observed mass spectrum can only be made in those cases where secondary dissociations do not play a dominant role. This can be achieved by lowering the energy of the impinging electrons, *i.e.*, lowering the internal energy of the molecular ion. This is the reason why in the case of branched alkanes, our paper¹ includes spectra taken with low-energy electrons. Moreover, for the molecular ions we have studied, further decomposition is probably not very important (in contradistinction to the case of the *n*-alkanes) because the primary dissociation gives rather stable C₃ and C₄ ions, as noted by Santoro and Spadaccini.

It is clear that, for larger branched alkanes, such as those studied by the latter authors, secondary dissociation becomes important, and a direct comparison with the spectra taken at electron energies around 50 eV has little significance. This is the reason why such compounds were not studied in ref 1.

In the case of the *n*-alkanes, the mass spectrum observed at 50 eV is indeed "the initial fragmentation pattern strongly distorted by further secondary, tertiary, etc., unimolecular decompositions of the initially formed ions."^{2,3} However, the recent experimental technique developed by Spiteller and Spiteller-Friedmann⁴ which consists of recording the mass spectrum at low energies of the electrons together with a low temperature of the ion source, eliminates this complication. The mass spectrum is then the image of the initial fragmentation, and can be explained by a random dissociation of the CC bonds of the molecular ion, in agreement with the calculated charge distribution. Meyerson⁵ and Stevenson and Schissler² independently arrived at the same conclusion. The agreement is also good in the

(1) J. C. Lorquet, *Mol. Phys.*, **9**, 101 (1965).

(2) J. C. Lorquet in "Advances in Mass Spectrometry," W. L. Mead, Ed., The Institute of Petroleum, London, 1966. See especially the comment by D. P. Stevenson, p 448 ff.

(3) J. C. Lorquet, *Mém. Soc. Roy. Sci. Liège*, **XVI**, 30 (1968).

(4) G. Spiteller and M. Spiteller-Friedmann, *Liebigs Ann. Chem.*, **690**, 1 (1965).

(5) S. Meyerson, *J. Chem. Phys.*, **42**, 2181 (1961).

case of field-ionization experiments, because secondary dissociation is not important.⁶

There are other factors which make difficult a direct comparison between the electronic charge distribution calculated for the molecular ion in its ground state and the experimental mass spectrum. Excited states of the molecular ion, as well as autoionizing states of the neutral molecule, certainly play an important role, even if it is assumed that most of them decay radiationlessly into the ground state of the molecular ion.^{7,8}

Another important factor is the rearrangement undergone by the electronic structure of the ion during the dissociation process, which we believe to be of crucial importance.⁹ This factor can be studied by constructing the potential energy hypersurface of the molecular ion¹⁰ or by cruder methods.¹¹

Photoionization experiments and the Spitteller technique are probably the best available methods to determine the initial fragmentation pattern of a molecular ion. The processes involved in radiolysis experiments in the liquid phase seem to us to require a far more complicated analysis than those occurring in the ion source of a mass spectrometer.

Finally, it should be noticed that Lennard-Jones and Hall never proposed that there should be a direct relationship between the probability of fragmentation and the positive charge distribution. Quoting Hall: "I would like to add that the simple theory of mass spectra which has been attributed to Lennard-Jones and myself was not, in fact, one that we proposed. It may have been suggested by our calculations, but it was not contained in our paper. It is too simple to expect the ground state of the parent ion to be the only relevant factor."¹²

(6) J. C. Lorquet and G. G. Hall, *Mol. Phys.*, **9**, 29 (1965).

(7) J. C. Lorquet, *ibid.*, **10**, 493 (1966).

(8) F. Fiquet-Fayard and P. M. Guyon, *ibid.*, **11**, 17 (1966).

(9) J. C. Lorquet, A. J. Lorquet, and J. C. Leclerc in "Advances in Mass Spectrometry," Vol. IV, The Institute of Petroleum, London, 1968, p 569.

(10) J. C. Leclerc and J. C. Lorquet, *J. Phys. Chem.*, **71**, 787 (1967).

(11) J. C. Lorquet, *Mol. Phys.*, **10**, 489 (1966).

(12) J. D. Waldron, Ed., "Advances in Mass Spectrometry," Pergamon Press, London, 1959, p 306.

INSTITUT DE CHIMIE
UNIVERSITÉ DE LIÈGE
LIÈGE, BELGIUM

J. C. LORQUET

RECEIVED SEPTEMBER 9, 1968

Comment on the Paper "Charge Distribution in Some Alkanes and Their Mass Spectra"

Sir: The general conclusion in the Santoro-Spadaccini (SS) communication on ordinary mass spectrometry is

true in some respects, but rather seems to be due to a perfect misunderstanding about the present stage of investigation, which assumes the hypothesis that primary scission probability of the skeletal bond of alkanes is in proportion to the charge density in the highest occupied level of their molecular orbitals.

For instance, the contribution of the "refragmentation" was already concluded to be important in the cases of large alkanes,¹ and taking it into consideration, comparison of theory with experiment was carried in our paper on cyclododecane.² According to this paper, when the ionizing voltage V_i was decreased sufficiently low, C_6 fragments became maximum, instead of C_3 fragments in the ordinary mass spectra.³ Similar results were obtained recently on normal hexadecane,⁴ in whose spectra the maximum shifted to the central groups at low V_i . Figure 1 is a part of the unpublished data, from which Figure 1 of ref 4 was drawn. Similar results can be obtained from the data on *n*-triacontane $C_{30}H_{62}$ reported by Remberg, *et al.*⁵ Since excess energy of the primary fragments is too small to produce refragmentation in such cases, the above results may be expected from the standpoint of the theory, based on the hypothesis, because it predicts that the maximum probability of primary scission of *n*-alkanes lies at or nearly at the central bond of the chain.

A similar tendency of the effect of V_i on the spectra

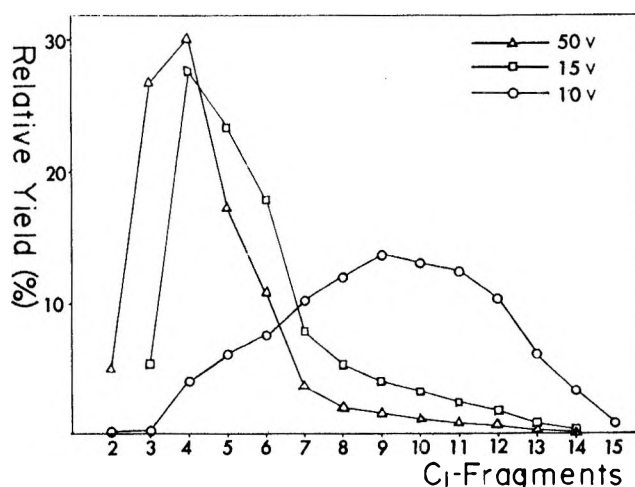


Figure 1. Percentage yield of fragments of normal hexadecane vs. carbon number of the fragments; ionization voltages are not corrected with a standard gas.

(1) K. Fueki and K. Hirota, *Nippon Kagaku Zasshi*, **81**, 212 (1960).

(2) K. Hirota and Y. Niwa, *J. Phys. Chem.*, **72**, 5 (1968); *Tetrahedron Letters*, 5757 (1966).

(3) The last column of Table III in ref 1 shows the calculated values.

(4) Y. Niwa and K. Hirota, *Bull. Chem. Soc. Jap.*, **41**, 1746 (1968).

(5) G. Remberg, E. Remberg, M. Spitteller-Friedmann, and G. Spitteller, *Org. Mass Spectrosc.*, **1**, 87 (1968).

of large branched alkanes can be concluded by the data of Remberg, *et al.* The discrepancy found by Santoro and Spadaccini on large branched alkanes, therefore, is not significant. Considering this situation, their conclusion has to be restricted within the mass spectra measured at ordinary conditions.

In order to minimize confusion which might occur in future discussions, it might be noted that to cite the above hypothesis as a proposal by Lennard-Jones and Hall is not proper, because Hall himself said⁶ that he did not even suggest such a hypothesis, when Thompson proposed it on octane.

(6) Discussion of the following papers: (a) R. Thompson, "Conference on Mass Spectrometry," Institute of Petroleum, London, 1953, p 154; (b) G. G. Hall, *Bull. Soc. Chem. Belges*, **73**, 305 (1964).

DEPARTMENT OF CHEMISTRY
FACULTY OF SCIENCE
OSAKA UNIVERSITY
TOYONAKA, OSAKA, JAPAN

KOZO HIROTA
YOSHIO NIWA
MASAO YAMAMOTO

RECEIVED SEPTEMBER 23, 1968

Recoil Tritium Reactions with Methylsilanes

Sir: While detailed and thorough studies have been made of the reactions of recoil tritium atoms with many hydrocarbons and with other carbon-skeletal molecules, relatively few experiments have been reported for such reactions with molecules containing other skeletal atoms.¹⁻⁴ Consequently, we initiated a study of the energetic reactions of tritium with the methyl derivatives of silicon, germanium, and tin.^{5,6} As our work was in progress, we learned of earlier experiments (1962) on methylsilanes, whose details have now been published.⁷ Since we find important quantitative discrepancies with this work and draw some qualitatively different conclusions, we are reporting here a brief description of our experiments with tetramethyl- and trimethylsilane. Further details, including those for the germanium and tin compounds, will be published shortly.

By analogy with similar hydrocarbon systems, the following tritiated products should be expected in hot reactions of tritium with a methylsilane (RCH_3): HT, CH_3T , RCH_2T , and RT. Each of these products was observed for each of the systems mono-, tri-, and tetramethylsilane, together with some additional products of less certain identity.⁷ In addition to the hydrocarbon analogy, two further conclusions were drawn from these experiments by the authors:⁷ (a) the total reactivity of silane systems is much higher than that of the analogous hydrocarbons; and (b) oxygen scavenger has relatively little effect on the yields from the reac-

tions with the methylsilanes. The minor effect of C_2 on yields and the excess reactivity were recorded for all three methylsilanes, with the latter almost entirely contributed by very much higher yields of HT than in reactions with the corresponding hydrocarbons. These higher yields were attributed for mono- and trimethylsilane to an expected relatively greater ease of abstraction of H from weak Si-H bonds.⁸

Our experiments with tetramethyl- and trimethylsilane also showed the same four products, HT, CH_3T , RCH_2T , and RT, with reasonable agreement on yields, except for that of HT. However, in both systems, we have found (a) a very substantial effect of O_2 on the HT yields and (b) no unusually high yield of HT, or total reactivity of the methylsilanes *vs.* hydrocarbons. The data on the O_2 -scavenger effect with tetramethylsilane are shown in Figure 1. In one set of our samples, more heavily irradiated than the other, we observed substantial depletion of O_2 during irradiation, accompanied by an increase in HT yield and the appearance of additional labeled products, not found in the well-scavenged samples. The agreement between our poorly scavenged samples and the earlier experiments is reasonable, especially when differences in irradiation conditions are considered.⁹

We have also carried out experiments under constant moderator conditions (excess N_2) in order to compare directly the reactivity toward hydrogen abstraction of methyl C-H groups in $(\text{CH}_3)_4\text{Si}$ and $(\text{CH}_3)_4\text{C}$. From these experiments, we have found that the yield of HT from $(\text{CH}_3)_4\text{Si}$ is only 0.8 as large as from $(\text{CH}_3)_4\text{C}$ under comparable conditions. This observation implies that the methyl C-H bond in the former is slightly stronger than in the latter,^{10,11} consistent with greater

(1) R. Wolfgang, *Progr. Reaction Kinetics*, **3**, 97 (1965).

(2) R. Wolfgang, *Ann. Rev. Phys. Chem.*, **16**, 15 (1965).

(3) F. Schmidt-Bleek and F. S. Rowland, *Angew. Chem., Intern. Ed. Engl.*, **3**, 769 (1964).

(4) T. Tominaga and F. S. Rowland, *J. Phys. Chem.*, **72**, 1399 (1968).

(5) Recoil tritium reactions with silanes have been reported by G. Cetini, *et al.*, *J. Chem. Phys.*, **46**, 89 (1967); *Atti Acad. Sci. Torino: Classe Sci. Fis., Mat. Nat.*, **97**, 1137 (1963).

(6) Reactions of energetic silicon atoms with silanes have been reported by P. P. Gasper, B. D. Pate, and W. Eckelman, *J. Amer. Chem. Soc.*, **88**, 3878 (1966).

(7) J. Witkin and R. Wolfgang, *J. Phys. Chem.*, **72**, 2631 (1968).

(8) The bond strength of Si-H bonds is frequently cited to be ~ 70 kcal/mol, in comparison to 99 kcal/mol for comparable C-H bonds. However, experimental measurements with silanes show wide variations, and a value of SiH₃-H of 94 ± 3 kcal/mol is quoted in N. J. Friswell and B. J. Gowenlock, *Advan. Free Radical Chem.*, **1**, 39 (1965).

(9) The two most prominent additional products are $\text{C}_2\text{H}_2\text{T}$ and $\text{C}_2\text{H}_4\text{T}$. The latter elutes in almost the same position as the tentatively identified $(\text{CH}_3)_2\text{SiHT}$ in the earlier experiments. A yield of $(\text{CH}_3)_2\text{SiHT}$ has been undetectable in all of our tetramethylsilane experiments.

(10) J. W. Root, W. Breckenridge, and F. S. Rowland, *J. Chem. Phys.*, **43**, 3694 (1965).

(11) E. Tachikawa and F. S. Rowland, *J. Amer. Chem. Soc.*, **90**, 4767 (1968).

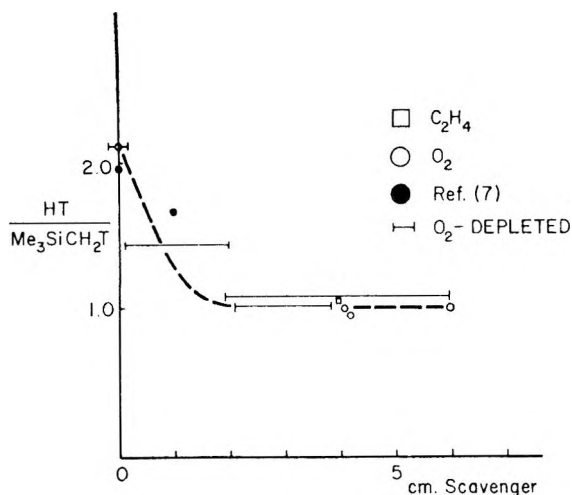


Figure 1. Scavenger effect on abstraction of H from $(\text{CH}_3)_4\text{Si}$ by recoil tritium: ●, ref 7; ○, O_2 ; |—|, O_2 -depleted; □, C_2H_4 .

donation of electrons to the CH_3 groups from a central Si atom than from a central C atom.

Detailed comparison of the total reactivity of $(\text{CH}_3)_4\text{C}$ and $(\text{CH}_3)_4\text{Si}$ requires knowledge of the fractional decomposition of the substitution products formed by replacement of H or CH_3 by T.¹⁻³ Such decompositions are substantially suppressed in liquid-phase experiments, and the total reactivities of $(\text{CH}_3)_4\text{C}$ and $(\text{CH}_3)_4\text{Si}$ appear to be approximately equal, with the former perhaps 10% larger. Our conclusion is that tetramethylsilane behaves very similarly to hydrocarbons, both with respect to reactivity and in sensitivity toward O_2 scavenger.

The experiments with trimethylsilane show, just as

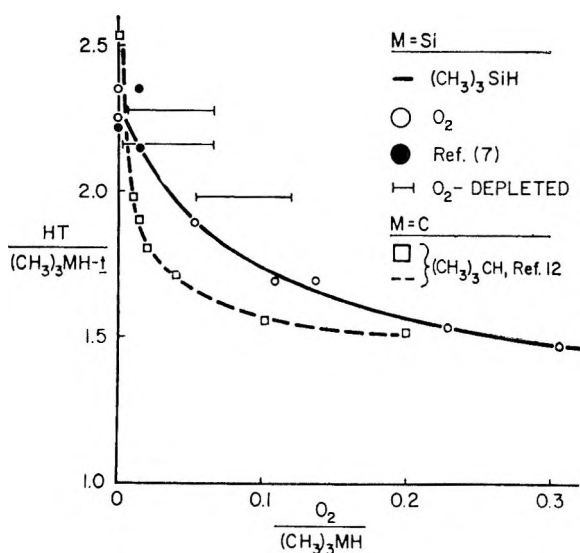


Figure 2. Scavenger effect on abstraction of H from $(\text{CH}_3)_3\text{SiH}$ by recoil tritium: ●, ref 7; ○, O_2 ; |—|, O_2 -depleted; —, $(\text{CH}_3)_3\text{SiH}$; □ and ---, $(\text{CH}_3)_3\text{CH}$, ref 12.

with isobutane,^{1,12} a decrease in HT yield with O_2 scavenger, as shown in Figure 2. With $(\text{CH}_3)_3\text{SiH}$, abstraction from Si-H should be much easier because of the tertiary nature of the Si atom and might also be much easier if Si-H bonds are in general substantially weaker than C-H bonds. However, the total reactivity toward abstraction is not very different ($\pm 15\%$) for $(\text{CH}_3)_3\text{CH}$ and $(\text{CH}_3)_3\text{SiH}$, suggesting that abstraction from tertiary C-H is quite similar to that from tertiary Si-H bonds. We therefore conclude, from the absence of any large difference in reactivity between Si-H and C-H, that the concept that Si-H bonds are much weaker than C-H bonds should be reexamined. Since abstraction from the CH_3 positions is definitely different for $(\text{CH}_3)_4\text{C}$ vs. $(\text{CH}_3)_4\text{Si}$, more accurate comparisons of C-H and Si-H will be done in experiments with partially deuterated methylsilanes such as CH_3SiD_3 and $(\text{CH}_3)_3\text{SiD}$.

(12) A. Rosenberg, Ph.D. Thesis, Yale University, 1964.

(13) This research has been supported by AEC Contract No. AT-(11-1)-34, Agreement No. 126.

DEPARTMENT OF CHEMISTRY¹³
UNIVERSITY OF CALIFORNIA
IRVINE, CALIFORNIA 92664

T. TOMINAGA
A. HOSAKA
F. S. ROWLAND

RECEIVED SEPTEMBER 25, 1968

"Electrocapillary Curves" of Solid Metals Measured by Extensometer Instrument

Sir: Although electrocapillary curves and the point of zero charge (pzc) have been extensively and accurately determined for mercury in various electrolytes, no comparable technique has heretofore been available for solid metal electrodes. Knowledge of the point of zero charge is important in the interpretation of electrochemical kinetics^{1,2} and other surface phenomena, but many of the techniques used to determine the pzc of solid metal electrodes suffer in some respect, by being indirect, experimentally difficult, of limited applicability, or uncertain in interpretation.^{3,4} A new extensometer instrument which directly measures change in length of a ribbon or wire due to changes in

(1) P. Delahay, "Double Layer and Electrode Kinetics," Interscience Publishers, New York, N. Y., 1965.

(2) L. I. Antropov, "Kinetics of Electrode Processes and Null Points of Metals," Council of Scientific & Industrial Research, New Delhi, India, 1960.

(3) B. E. Conway in "Electrochemistry," J. A. Friend and F. Gutmann, Ed. (1st Australian Conference on Electrochemistry, 1953), Pergamon Press, New York, N. Y., 1965, p 789.

(4) E. Gileadi, "Electrosorption," Plenum Press, New York, N. Y., 1967, p 87.

interfacial tension with electrolytes and which can be used to determine the *pzc* is described herein.⁵

The force on a wire or ribbon (a thin ribbon is used in the present instrument) can be expressed by

$$F = \sigma A + \gamma P \quad (1)$$

and the change in force by

$$dF = Ad\sigma + Pd\gamma \quad (2)$$

where F is the force on the ribbon, σ is the bulk tensile stress, A is the cross-sectional area, γ is the interfacial tension, and P is the periphery. (The terms σdA and γdP can be shown to be negligibly small compared to $Ad\sigma$ and $Pd\gamma$.) By applying the force to the ribbon through a spring with a small spring constant compared to the stiffness of the ribbon, the change in force can be made very small for an elongation of the ribbon and, applying Hooke's law

$$d\gamma = -(A/P)d\sigma = -(AE/PL)dL \quad (3)$$

where E is the elastic modulus of the ribbon (handbook value) and L is the immersed length of the ribbon. Changes in interfacial tension with potential can be calculated from measured small deflections, ΔL , with eq 3.

The design of the extensometer is shown in Figure 1. The ribbon is mounted axially inside a glass tube; the lower end is attached to the glass tube through a Teflon plug and the upper end is attached to a quartz spindle and spring which are part of the extension measuring head. An aluminum bobbin mounted on the quartz spindle forms two capacitors with fixed plates mounted in the head. Small changes in the two capacitances due to extension of the ribbon are measured with an electronic capacitance sensor.

The most serious problem to overcome in the design is minimizing error due to thermal expansion, which gives a considerably larger $\Delta L/\text{deg}$ than is produced by changes in interfacial tension. The thermal expansion is minimized in the following ways. (1) Invar and quartz, each having low thermal expansion coefficients, are used for the ΔL measuring head above the ribbon out of the electrolyte. (2) The instrument is placed in a thermally insulating box and measurements are made after the thermal drift has decreased to a low value. (3) A potential sweep is used in the measurements at a rate that is rapid compared to the residual thermal drift. (4) The measurements are limited to metals, electrolytes, and potential ranges in which electrolysis current density and consequent Joule, reversible, and overpotential heating effects are minimum.

In operation the metal ribbon, the saturated calomel reference electrode, and the platinum screen counter-electrode shown in Figure 1 are connected to a potentiostat driven by a triangular wave potential sweep

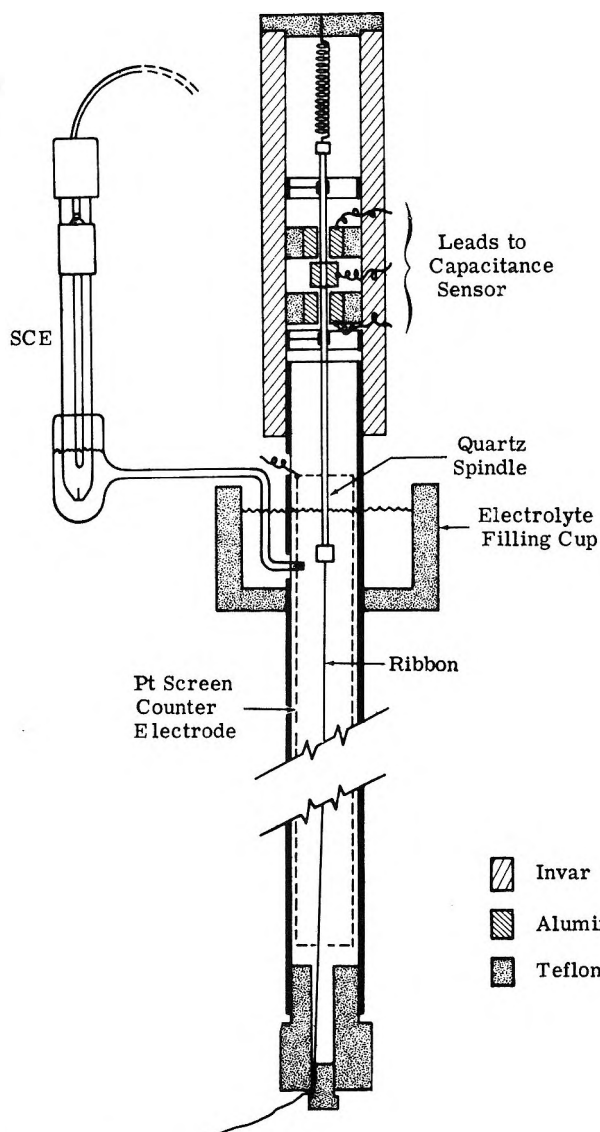


Figure 1. Design of extensometer.

generator. A potential sweep rate of at least 0.1 V/sec appears to give adequate resolution from thermal drift. Polarizing current and potential and ribbon deflection *vs.* potential are drawn on separate X - Y plotters.

The instrument is calibrated in respect to length changes of the ribbon by hanging weights on the bottom of the outer tube and measuring the stretch. The stretch is given by

$$\Delta L_t = \Delta w L_t / A_t E_t \quad (4)$$

where ΔL_t is the change in length of the tube, Δw is the weight added, L_t is the length of the tube from a support point near the upper end to the weight hanger near the lower end, A_t is the cross-sectional area of the tube, and E_t is the elastic modulus of the tube (handbook value). The stretch is transmitted through the ribbon to the capacitance sensor which reads out a

(5) T. R. Beck, presented to CITCE meeting, Detroit, Mich., Sept 25, 1968; full text in preparation.

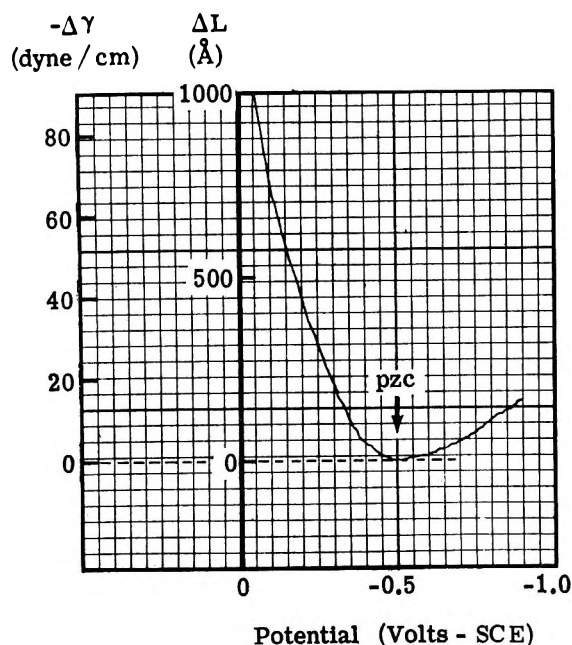


Figure 2. "Electrocapillary curve" for gold ribbon in 0.1 M KCl (sweep speed = 0.25 V/sec).

potential. The potential output was linear with w ; therefore, the deflection *vs.* potential plots on the X-Y plotter could be converted directly to $\Delta\gamma$ *vs.* potential by eq 3 using a constant scale factor.

A photograph of an X-Y plot of an "electrocapillary curve" for a gold ribbon is given in Figure 2, showing calibrations in terms of changes in length from eq 4 and in interfacial tension from eq 3. The similarity to electrocapillary curves for mercury may be noted. The value of the apparent pzc in Figure 2 is more negative (-0.25 V *vs.* s.c.e.) than the values of -0.1 to $+0.3$ V (s.c.e.) reported in the literature,^{6,7} but minima were observed in the preliminary experiments in the range of -0.4 to $+0.4$ V (s.c.e.) indicating that great care is required in purity of solutions and cleanliness of equipment.

In a more recent and more carefully controlled series of experiments with a platinum ribbon in 0.1 M K_2SO_4 in a glass tube, values of 0.15–0.25 V (s.c.e.) were found compared to 0.1–0.25 V reported.^{2,6} A second minimum in length of the ribbon was found at 1.75 V (s.c.e.) compared to an earlier reported value² of 1.50 V for the platinum oxide surface.

It is believed that the instrument shows promise as a new tool for studying surface phenomena, although limited to polycrystalline surfaces.

(6) A. N. Frumkin, *Svensk Kem. Tidskr.*, **77**, 300 (1965).

(7) T. N. Andersen, R. S. Perkin, and H. Eyring, *J. Amer. Chem. Soc.*, **86**, 4496 (1964).

SOLID STATE PHYSICS LABORATORY
BOEING SCIENTIFIC RESEARCH LABORATORIES
SEATTLE, WASHINGTON 98124

T. R. BECK

RECEIVED NOVEMBER 21, 1968

Electron Injection into Zinc Oxide¹

Sir: Various surface properties of the wide-band-gap semiconductor ZnO have been of considerable interest including dark catalysis² and photocatalysis,³ adsorption,⁴ charge-transfer adsorption,⁵ spin resonance,⁶ and oxidation-reduction processes.⁷ Zinc oxide single crystals are very suitable for the investigation of charge-transfer processes because of their behavior as an electrode⁸ and their commercial availability.⁹ Electron injection into wide-band-gap semiconductors from aqueous solutions of stable substances seems to be unknown.¹⁰ Previously the author and co-workers have reported¹¹ electron injection at room temperature from radical-type sorbed species that were generated by the hole oxidation of multiequivalent reducing agents.

We wish to report that we have found that the property of electron injection can be correlated with the oxidation potential of the substance. Specifically, reductants with high oxidation potentials (Latimer's¹² convention, the more positive the oxidation potential the stronger the reducing agent) inject electrons while those with low potentials do not inject. We found that aquochromium(III) ($E^\circ = 0.4$), aquoeuropium(II) ($E^\circ = 0.4$), aquovanadium(II) ($E^\circ = 0.3$), ethylenediaminecobalt(II) ($E^\circ = 0.3$), dithionite ion ($E^\circ = 0.1$), and aquotitanium(III) ($E^\circ = -0.1$) inject in contrast to the weaker reducing agents such as hexamminecobalt(II) ($E^\circ = -0.1$), (ethylenediaminetetraacetic acid)iron(II) ($E^\circ = -0.1$), hexacyanoiron(II)¹³ ($E^\circ = -0.4$), aquoiron(II) ($E^\circ = -0.7$), *o*-phenanthrolineiron(II) ($E^\circ = -1.1$), and aquomanganese(II)

(1) Part of the research was performed for the Jet Propulsion Laboratory, California Institute of Technology, sponsored by the National Aeronautics and Space Administration under Contract NAS 7-100, and part of the research was supported by Stanford Research Institute.

(2) G. Natta in "Catalysis," Vol. 3, P. H. Emmett, Ed., Reinhold Publishing Corp., New York, N. Y., 1955.

(3) M. C. Markam, J. C. Kuriacose, J. DeMarco, and C. Giaquinto, *J. Phys. Chem.*, **66**, 932 (1962); T. S. Nagarjunan and J. G. Calvert, *ibid.*, **68**, 17 (1964); T. Freund, *J. Catal.*, **3**, 289 (1964); J. G. Calvert, K. Theurer, G. T. Rankin, and W. M. MacNevin, *J. Amer. Chem. Soc.*, **76**, 2575 (1954); S. R. Morrison and T. Freund, *J. Chem. Phys.*, **47**, 1543 (1967).

(4) V. Kesavulu and H. A. Taylor, *J. Phys. Chem.*, **66**, 54 (1962); M. J. D. Low, *J. Amer. Chem. Soc.*, **87**, 7 (1965).

(5) H. Saltsburg and D. P. Snowden, *J. Phys. Chem.*, **68**, 2734 (1964).

(6) R. J. Kokes, *ibid.*, **66**, 99 (1962); K. S. Sancier and T. Freund, *J. Catal.*, **3**, 293 (1964).

(7) G. Oster and M. Yamamoto, *J. Phys. Chem.*, **70**, 3033 (1966).

(8) J. F. Dewald, *Bell Systems Tech. J.*, **39**, 615 (1960); W. P. Gomes, T. Freund, and S. R. Morrison, *J. Electrochem. Soc.*, **115**, 818 (1968); T. Freund and S. R. Morrison, *Surface Sci.*, **9**, 119 (1968).

(9) Minnesota Mining and Manufacturing Co., St. Paul, Minn.

(10) P. J. Boddy, *J. Electrochem. Soc.*, **115**, 199 (1968); P. J. Boddy, D. Kahng, and Y. S. Chen, submitted for publication.

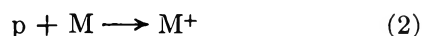
(11) T. Freund, W. P. Gomes, and S. R. Morrison, IV International Congress on Catalysis, Moscow, June 1968.

(12) Standard acid potentials for unit activity reductant, oxidant, and hydrogen ion.

(13) T. Freund and S. R. Morrison, *Surface Sci.*, **9**, 119 (1968).

($E^\circ = -1.5$). Clearly a high oxidation potential is not sufficient since the 8-equiv reducing agent borohydride ion ($E^\circ = 0.5$)¹⁴ and the 2-equiv formic acid ($E^\circ = 0.2$) do not inject. It is also clear that mono-equivalency is not a requirement for electron injection since $S_2O_4^{2-}$ ($E^\circ = 0.1$) injects. Borohydride ion does not inject electrons into other semiconductors¹⁰ including $KTaO_3$, TiO_2 , and Ta_2O_5 . The correlation with oxidation potential may be expected to fail for multi-equivalent reductants since the oxidation potential for the oxidation of the first equivalent of a multiequivalent reductant may be very low. The lack of reducing activity of borohydride ion is not surprising since its reactions¹⁵ with aqueous oxidants are often slow.

Electron injection, eq 1, can be distinguished from the other possible mechanism for an anodic current, *i.e.*, hole capture, eq 2. In these two equations



M is the reducing agent, e is an electron in the conduction band, and p is a hole in the valence band. For a wide-band-gap n-type semiconductor, such as ZnO, an anodic current in the dark can be taken as evidence of electron injection since holes are virtually absent without band-gap illumination. In terms of the band model, electron injection will occur from an adsorbed species when its electronic energy level is above the bottom of conduction band at the surface or when the temperature is sufficiently high to provide the activation energy for the transition of an electron from the surface level to the bottom of the conduction band.

The results of preliminary experiments, given below, are consistent with the assignment of electronic energy levels for injecting reductants at fixed energies that are about equal to or above the bottom of the ZnO conduction band at the surface. The increase of the injection current with stirring indicated that the electron-transfer step is fast compared to mass transport in solution; such a result is consistent with a small or zero energy barrier for the transition of an electron from the reductant level to the bottom of the conduction band at the surface. The lack of dependence of the injection current on applied voltage and the lack of dependence of the Helmholtz voltage (determined from capacitance-voltage measurements) on reductant concentration are consistent with fixed levels since movement of adsorbate levels might be expected to change the current. The lack of dependence of current on the concentration of the oxidized form of the reductant and the increase of injection current with increasing concentration of reductant are consistent with the postulated location

of adsorbate levels since high empty levels would not be expected to capture electrons and the current should increase with an increasing number of filled levels.

SOLID STATE CATALYSIS LABORATORY
STANFORD RESEARCH INSTITUTE
MENLO PARK, CALIFORNIA 94025

THOMAS FREUND

RECEIVED NOVEMBER 13, 1968

Study of the Energetics of Ion-Molecule Reactions by Pulsed Ion Cyclotron Double Resonance

Sir: From the start, workers studying gas-phase ion-molecule reactions have been concerned with obtaining the dependence of the reaction rate constants on the ion kinetic energy since such information would be of great value in assessing the importance of various possible reaction mechanisms. Unfortunately, it has been very difficult or impossible to produce mono-energetic ions in the range below 3 eV which is the range of greatest interest.

Recently it has been demonstrated that ion cyclotron double resonance spectroscopy (ICDR) is a useful tool for the study of ion-molecule reactions.¹⁻⁵ Reactant ions are irradiated by a radiofrequency electric field applied at their cyclotron frequency, thereby increasing their kinetic energy. Any variation in the rate of formation of a product ion due to the increase in the kinetic energy of the reactant ion is observed by a marginal oscillator detector which operates at the cyclotron frequency of the product ion. This directly demonstrates the connection between the reactant and product ions. Unfortunately, evaluation of reaction rates as a function of ion kinetic energy in this type of experiment is very difficult since the reactant ions are being irradiated while reacting, and consequently have a significant spread of kinetic energies.

This communication describes a pulsed ICDR method for the production of reactant ions of known kinetic energies. The ions are produced by an electron beam which is pulsed on for a period of approximately 100 μ sec and immediately after are irradiated by a radio-frequency electric field pulse as shown in Figure 1a. The ion kinetic energy is determined by the relationship⁶ $E_{ion} = e^2 E_2^2 t^2 / 8m$, where m is the mass of the ion,

(1) L. R. Anders, J. L. Beauchamp, R. C. Dunbar, and J. D. Baldeschwieler, *J. Chem. Phys.*, **45**, 1062 (1966).

(2) J. L. Beauchamp, L. R. Anders, and J. D. Baldeschwieler, *J. Amer. Chem. Soc.*, **89**, 4569 (1967).

(3) J. D. Baldeschwieler, *Science*, **159**, 263 (1968).

(4) J. L. Beauchamp and S. E. Buttrill, Jr., *J. Chem. Phys.*, **48**, 1783 (1968).

(5) J. M. S. Henis, *J. Amer. Chem. Soc.*, **90**, 844 (1968).

(6) J. L. Beauchamp, *J. Chem. Phys.*, **46**, 1231 (1967).

(14) W. H. Stockmayer, D. W. Rice, and C. C. Stephenson, *J. Amer. Chem. Soc.*, **77**, 1980 (1955).

(15) T. Freund, *J. Inorg. Nucl. Chem.*, **9**, 246 (1959); *J. Amer. Chem. Soc.*, **84**, 873, 2678 (1962).

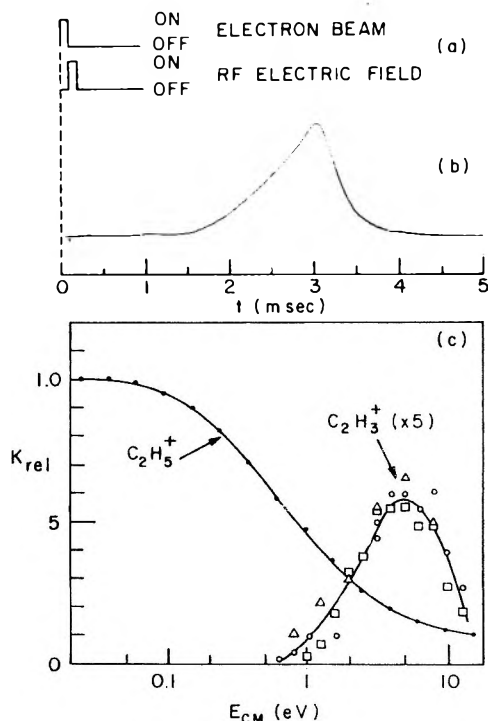


Figure 1. (a) Electron beam and radiofrequency electric field pulse sequence for the production and irradiation of reactant ions. (b) Typical $C_2H_5^+$ signal obtained after the pulse sequence in (a) at a magnetic field strength of 14.5 kG and a drift electric field of 0.54 V/cm. Since the distance from the electron beam to the resonance region of the cell is 5 cm and the length of the resonance region is 5 cm, it is calculated that the ions will reach the resonance region 1.5 msec and leave 3 msec after the electron beam pulse. The signal has a rather complex form since the power absorption by the ions is proportional not only to their number but also to the length of time that they have been exposed to the observing radiofrequency field. (c) Relative rate of production of $C_2H_5^+$ and $C_2H_3^+$ as a function of CH_3^+ energy in the center of mass coordinates.

t is the length of time the radiofrequency field is applied, and E_2 is the peak strength of the radiofrequency field. In this experiment $t = 100 \mu\text{sec}$ and E_2 was varied from 0.7 to 0.01 V/cm to give an E_{ion} ranging from thermal to about 20 eV. The ions then drift through the reso-

nance cell over a period of 3 msec during which time they react with neutral molecules to form product ions which are detected by a marginal oscillator, which has a response time of 0.1 msec. A typical signal obtained after averaging 10,000 times in a signal averager is shown in Figure 1b. The experiment was performed at a pressure of 10^{-6} Torr so that only about 10% of the reactant ions would collide with neutral molecules. Under these conditions the reaction rate is directly proportional to the signal intensity.

The reactions of CH_3^+ with methane to form $C_2H_5^+$ and $C_2H_3^+$ were selected as specific examples of this method and Figure 1c is a plot of the relative rates of formation of the two product ions obtained as a function of the center of mass energy. If ground-state heats of formation are employed, it is found that the reaction forming $C_2H_5^+$ is 0.9 eV exothermic and the reaction forming $C_2H_3^+$ is 1.6 eV endothermic. The decrease in the rate of formation of $C_2H_5^+$ with increasing energy is not surprising if one recalls the arguments of phase space theory as applied to ion-molecule reactions. As the energy in the system increases, more channels for reaction become available and the exothermicity of the reaction becomes a smaller proportion of the total energy in the system. Hence the rate for that reaction will decrease.⁷⁻⁹ At the same time the rates for other processes such as nonreactive collisions and endothermic reactions will increase. The reaction to form $C_2H_3^+$ illustrates the latter process. The threshold for the formation of $C_2H_3^+$ is slightly lower than predicted due to the presence of internally excited CH_3^+ produced by the electron beam. More experimental results and a more detailed discussion will be presented later.

(7) J. C. Light, *J. Chem. Phys.*, **40**, 3221 (1964).

(8) F. A. Wolf, *ibid.*, **44**, 1619 (1966).

(9) R. DeVogelaere and M. Boudart, *ibid.*, **23**, 1236 (1955).

(10) Deceased, Jan 10, 1969.

CHEMISTRY DEPARTMENT
SCIENTIFIC LABORATORY
FORD MOTOR COMPANY
DEARBORN, MICHIGAN 48121

L. R. ANDERS¹⁰

RECEIVED NOVEMBER 20, 1968